The Dissertation Committee for In Sung Kim certifies that this is the approved version of the following dissertation:

Use of CFRP to Provide Continuity in Existing Reinforced Concrete Members Subjected to Extreme Loads

Committee:

_____

James O. Jirsa, Supervisor

_____

Oguzhan Bayrak, Co-Supervisor

_____

Michael D. Engelhardt

_____

Harovel G. Wheat

_____

Sharon L. Wood

Use of CFRP to Provide Continuity in Existing Reinforced Concrete Members Subjected to Extreme Loads

by

In Sung Kim, B.S., M.S.E.

Dissertation

Presented to the Faculty of the Graduate School of

The University of Texas at Austin

in Partial Fulfillment

of the Requirements

for the Degree of

Doctor of Philosophy

The University of Texas at Austin

August 2008

Dedication

To My Parents

Acknowledgements

Finally, I would like to thank my parents, Soon Hee Kim and Yeo Keun Kim, as well as other members who have provided care, physical and emotional.

July 24, 2008

Use of CFRP to Provide Continuity in Existing Reinforced Concrete

Members Subjected to Extreme Loads

Publication No. _____

In Sung Kim, Ph.D.

The University of Texas at Austin, 2008

Supervisor: James O. Jirsa

Co-Supervisor: Oguzhan Bayrak

A special problem in many reinforced concrete structures built in the 1970's and earlier is the lack of continuity between elements. Continuity is a characteristic of structures essential to preventing collapse. Therefore, in extreme loading conditions such as loss of a column support due to terrorist attack or if earthquake or other extreme actions occur, the structures could be vulnerable to collapse. The study reported here focused on two structural discontinuities in existing reinforced concrete structures,

discontinuity in bottom reinforcement in beams (horizontal discontinuity) and poorly detailed lap splices in columns (vertical discontinuity).

The objective of this study was to develop rehabilitation methods using CFRP to provide continuity of reinforcement in existing structures. To develop the rehabilitation methods, two separate experimental studies were conducted using beam and column specimens. CFRP materials were applied to the bottom or side face of a beam and anchored using CFRP anchors or U-wraps to provide horizontal continuity in bottom reinforcement and tested under dynamic loading. After CFRP rehabilitation, the ductility of the bottom reinforcement and large rotational capacity of the beam were realized. CFRP materials were also applied to the lap splice region in square and rectangular columns which exhibited a brittle splice failure as-built. After rehabilitating the columns using CFRP jackets and anchors, the failure mode changed from a brittle splice failure to yield of column reinforcement, and the strength and deformation capacity were improved under both monotonic and cyclic loading. Based on the results of beam and column tests, design guidelines for CFRP rehabilitation were proposed.

Horizontal and vertical continuities can be provided through the use of CFRP for rehabilitating existing reinforced concrete structures that were designed prior to the introduction of codes that require continuous reinforcement along members and between adjacent members. The vulnerability of such structures to collapse can be reduced through rehabilitation.

Table of Contents

xv

List of Tables

List of Figures

CHAPTER 1

Introduction

1.1 CONTINUITY IN REINFORCED CONCRETE STRUCTURES

A special problem in many reinforced concrete structures built in the 1970's and earlier is the lack of continuity between elements. Continuity is a characteristic of structures essential to preventing progressive collapse. Therefore, in extreme loading conditions such as loss of a column support due to terrorist attack or if earthquake or other extreme actions occur, the structures could be vulnerable to progressive collapse. A progressive collapse is defined as the spread of local damage, from an initiating event from element to element resulting, eventually, in the collapse of an entire structure or a disproportionately large part of it; also known as disproportionate collapse (*Best Practice for Reducing the Potential for Progressive Collapse in Buildings, NIST, 2007*). To prevent progressive collapse, continuity needs to be reinforced so that tension due to extreme loading can be carried along a member under either axial or flexural actions.

Continuity in members of new structures is discussed in ASCE 7-05 *(Minimum Design load for Buildings and Other Structures, ASCE, 2005).* According to the document, local damage in the structure shall not extend disproportionately to the remaining portion of the structure. Damage is limited by providing sufficient continuity and redundancy, or energy-dissipating capacity, or a combination thereof, in the members of the structure. The document clearly expresses the requirement for continuity in structural members although specific methods to achieve continuity are not discussed.

The ACI Building Code for new construction (ACI 318-08) requires that members of a structure shall be tied together to improve integrity of the overall structure through appropriate detailing of reinforcement. It also requires continuity of the reinforcement in perimeter beams.

1

Continuity in a structural member is also discussed in *Progressive Collapse Analysis and Design Guidelines for New Federal Office Buildings and Major Modernization Projects, (GSA, 2003)*. One of the recommended characteristics for a robust structure and a low probability of progressive collapse is the use of detailing to provide structural continuity and ductility in reinforced concrete structures. The guidelines indicate correct detailing of connections to provide beam-to-beam continuity across a column. The document also recommends that existing structures undergoing modernization should be upgraded to new construction requirements. To meet this requirement, existing structure rehabilitated to limit progressive collapse should have the same level of continuity in the members as a new structure designed to limit progressive collapse.

The study reported here focused on two structural discontinuities in existing reinforced concrete structures, discontinuity in bottom reinforcement in beams and poorly detailed lap splices in columns. When the central column is removed in Figure 1.1, the force carried by the column needs to be transferred through the beams or the columns above the removed column to other columns to prevent progressive collapse of the structure. The load carried by the column that is removed can be supported by catenary action of the continuous beams and/or transferred upward to stories that have not been damaged through the column above the removed column. These alternate load paths require tensile capacity in the beams and columns. The tensile capacity of the members needs to be developed in the steel reinforcement in the beams and columns. Where discontinuities exist, the tensile capacity of the reinforcement can not be developed.

Typical beam details of reinforced concrete structures in ACI 315-74 (*Manual of Standard Practice for Detailing Reinforced Concrete Structures, ACI, 1974)* are shown in Figure 1.2 (ACI 315-74 was based on ACI 318-71.). Continuity of the reinforcement in the beams can be provided by either continuous bottom reinforcement or a combination of top and bottom reinforcement that is contained within closed transverse reinforcement. However, the bottom reinforcement is not continuous (Figure 1.2) and typically little or

no transverse reinforcement is provided in the overlap region of the top and bottom reinforcement. Therefore, horizontal discontinuities exist in the beams.

Typical column details in ACI 315-74 are shown in Figure 1.3. The lap splices in longitudinal reinforcement were based on compression loads only and the length of those splices and the amount of transverse reinforcement are inadequate if the column is subjected to tension. Although ACI 315-74 recommends 30 times the bar diameter of longitudinal reinforcement for length of lap splices, ACI 318-63 allows using 24 times the bar diameter for length of lap splices in compression (GR 60 reinforcement). In addition, only two transverse ties are provided in the lap splice region in Figure 1.3. Therefore, the longitudinal reinforcement can not develop tension when a column is removed because of the short lap slice length and insufficient transverse reinforcement, and a vertical discontinuity may exist in the columns above the removed column.
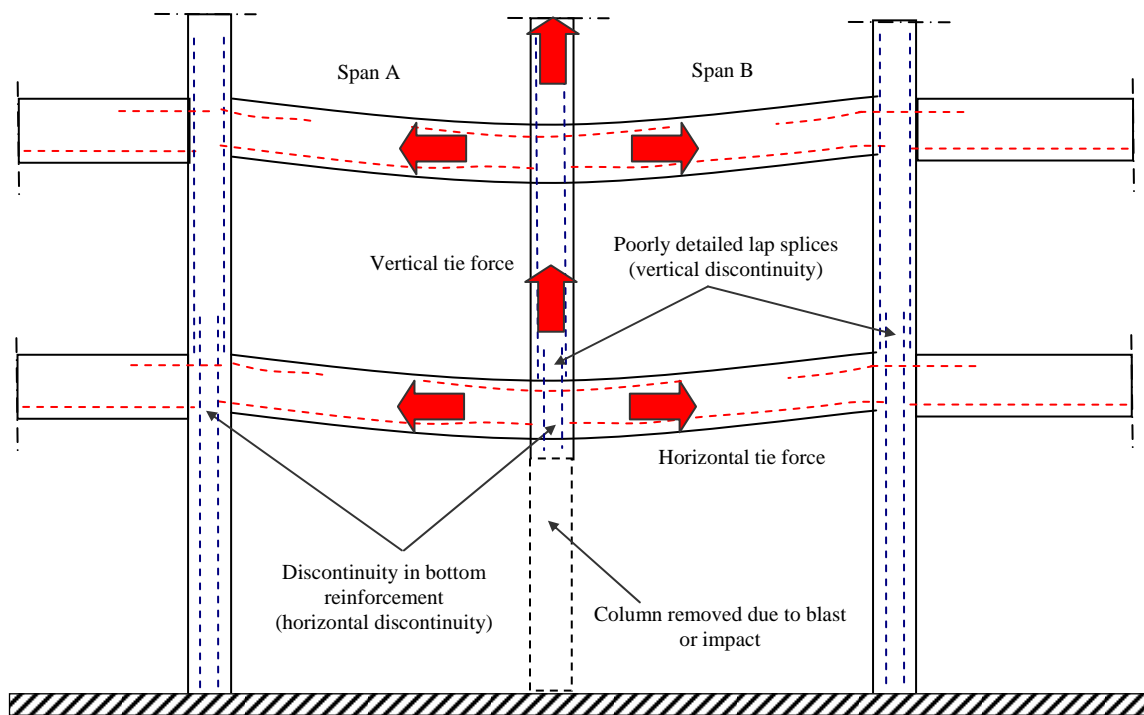
Figure 1.1   Discontinuities in exiting reinforced concrete structures

3
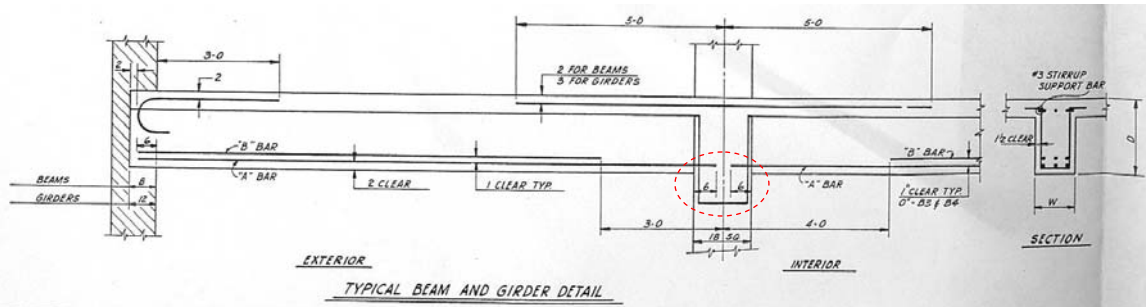
Figure 1.2 Discontinuity in bottom reinforcement (horizontal discontinuity),
ACI 315-74
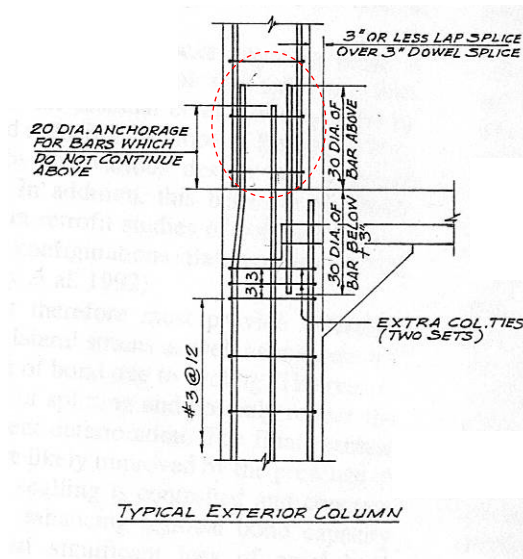
Figure 1.3 Poorly detailed lap splices of longitudinal reinforcement
(vertical discontinuity), ACI 315-74

1.2 OBJECTIVE

The use of Carbon Fiber Reinforced Polymer (CFRP) materials may provide a solution for rehabilitating structures with discontinuities in the reinforcement (Figure 1.4). The objective of this study is to develop rehabilitation methods using CFRP to provide continuity in existing reinforced concrete structures vulnerable to progressive collapse.

4

In this study, CFRP materials were applied to the bottom or side faces of a beam to provide horizontal continuity in the bottom reinforcement and tested under dynamic loading. Beam rehabilitation methods are discussed in Chapter 3. CFRP materials were also applied to the lap splice region in a column so that the tensile strength and ductility of the lap spliced longitudinal bars could be realized thereby providing vertical continuity. This column rehabilitation method is discussed in Chapter 4. Based on the test results of the rehabilitated beams and columns, design guidelines for CFRP rehabilitation are proposed in Chapter 5.
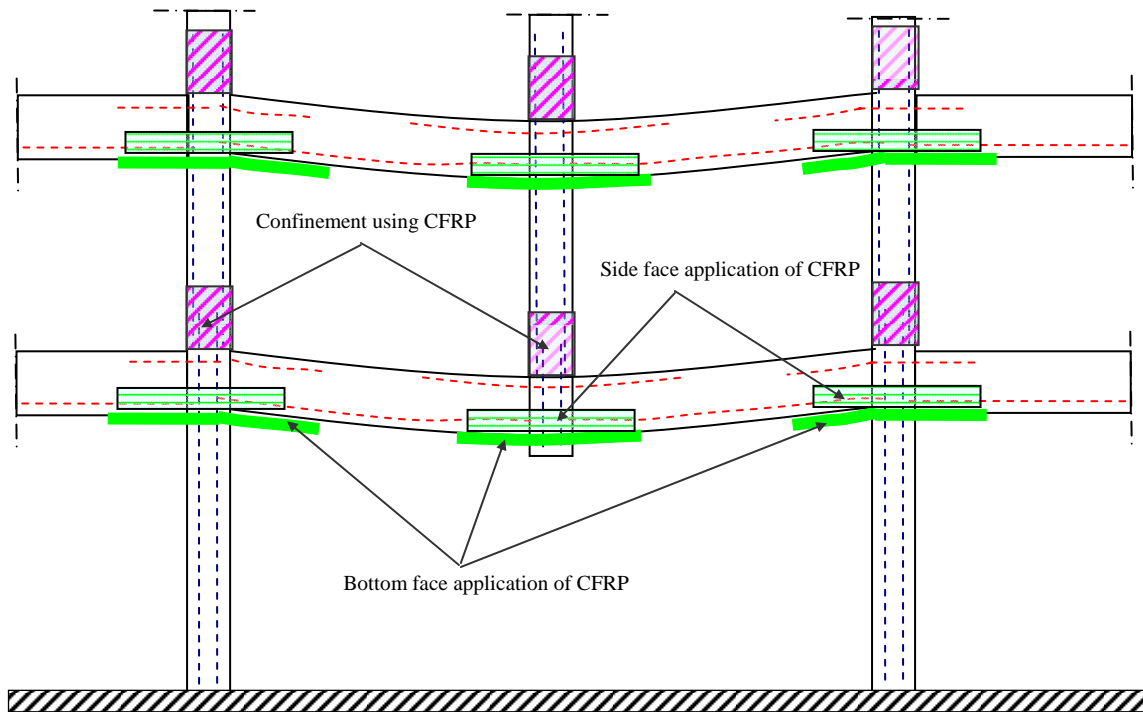
Figure 1.4   Application of CFRP to provide continuity

CHAPTER 2

Background

2.1 ANCHORAGE METHODS OF CFRP

When CFRP sheets are used in flexural strengthening of reinforced concrete structures, delamination (debonding) of CFRP from the concrete surface due to loss of adhesion at the interface is a primary failure mode if no additional anchors are provided (Figure 2.1). Delamination mechanisms of CFRP sheets without anchorage have been studied by Teng et al. (2002), Toutanji et al. (2006) and Bonacci et al. (2001). In addition, ACI 440 (2002) provides equations for estimating bond strength of CFRP. However, in this study, the expected failure mode of the CFRP sheets is fracture through the use of supplementary anchorage (Figure 2.2). Although delamination occurred, the final failure mode of CFRP sheet was fracture of CFRP sheet because the CFRP sheet is held in the concrete by the anchorage. Efficient use of the material can be achieved if the ultimate strength of CFRP is realized. When delamination occurs it has not been possible to mobilize more than 50% of the tensile strength of the CFRP sheet if no supplementary anchorage is provided.

Figure 2.1   Delamination of CFRP sheet

Supplementary anchors
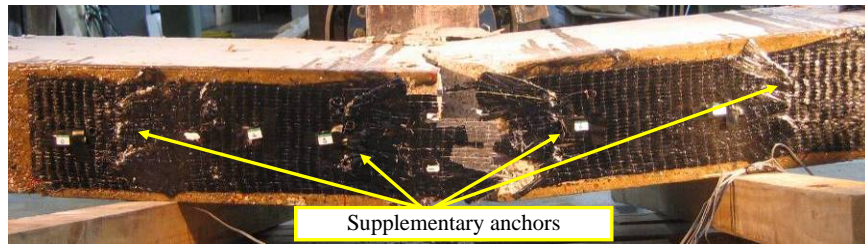
Figure 2.2   Fracture of anchored CFRP sheet

Anchorage methods for CFRP sheets in reinforced concrete structures have been studied by several researchers. The use of mechanical fasteners was studied by Lamanna (2002, Figure 2.3) and U-anchors (embedding CFRP into preformed grooves) were studied by Khalifa (1999, Figure 2.4). Premature failure of the anchorage before the CFRP sheet developed the full strength was observed using these methods and the application of the anchorage was relatively complicated because of the differences between the properties of the CFRP sheets and the anchorage system.

Figure 2.3   Anchorage of CFRP using mechanical fasteners (Lamanna, 2002)
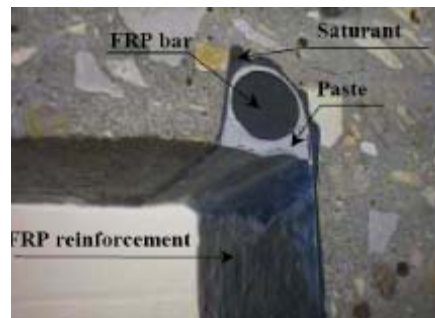
Figure 2.4   Anchorage of CFRP using U-anchor, (Khalifa, 1999)

The study reported herein focused on the use of CFRP anchors or U-wraps or a combination of the two to provide anchorage for CFRP sheets. The anchorage methods were relatively simple and easy to apply to existing reinforced concrete structures.

A CFRP anchor consists of a roll of CFRP sheet inserted into the concrete and splayed out over the CFRP sheet in a fan shape (Figure 2.5). Early use of CFRP anchors is reported by Kobayashi et al. (2001). Kobayashi investigated application of CFRP anchors to a CFRP wrapped column with wing walls (Figure 2.6). The wing walls prevent wrapping the CFRP sheets around the column continuously. The CFRP anchor can provide continuity of the CFRP sheet through the wing wall. Kobayashi investigated the stress transfer mechanisms of CFRP anchors and factors that influence the capacity of CFRP anchor. Kobayashi found that:

- Angle of the fan shape needs to be less than 90 degree (Figure 2.6).
- Radius of the fan shape needs to be more than 150 mm (Figure 2.6).
- Spacing of the anchors in the direction perpendicular to the main sheet needs to be less than 200 mm (Figure 2.6). .
- Overlapping of the fan portion of CFRP anchors needs to be more than 10 mm (Figure 2.6).
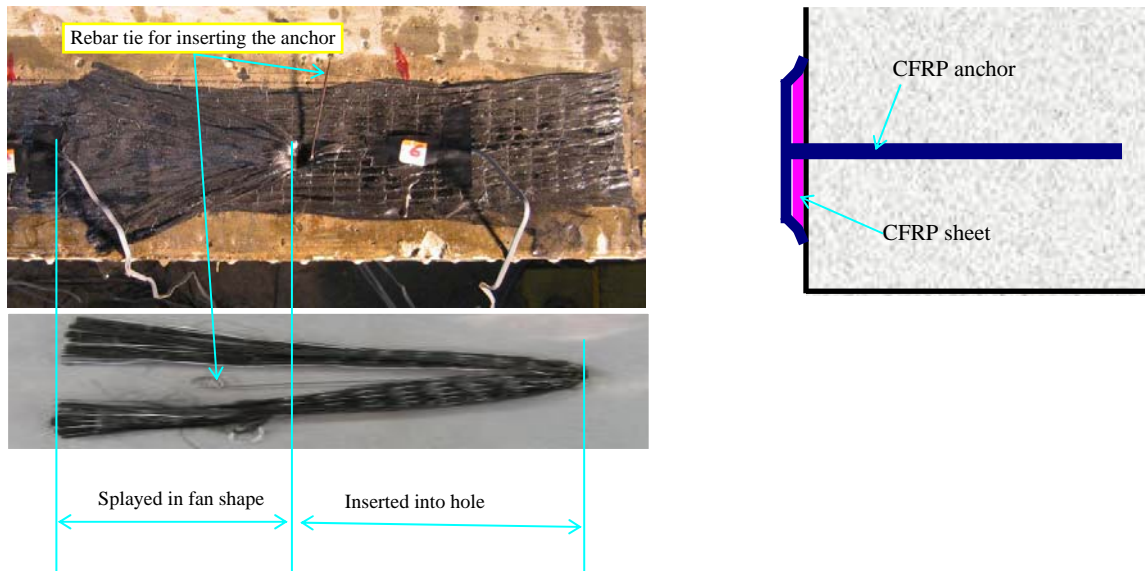
Figure 2.5   *CFRP anchor*

8
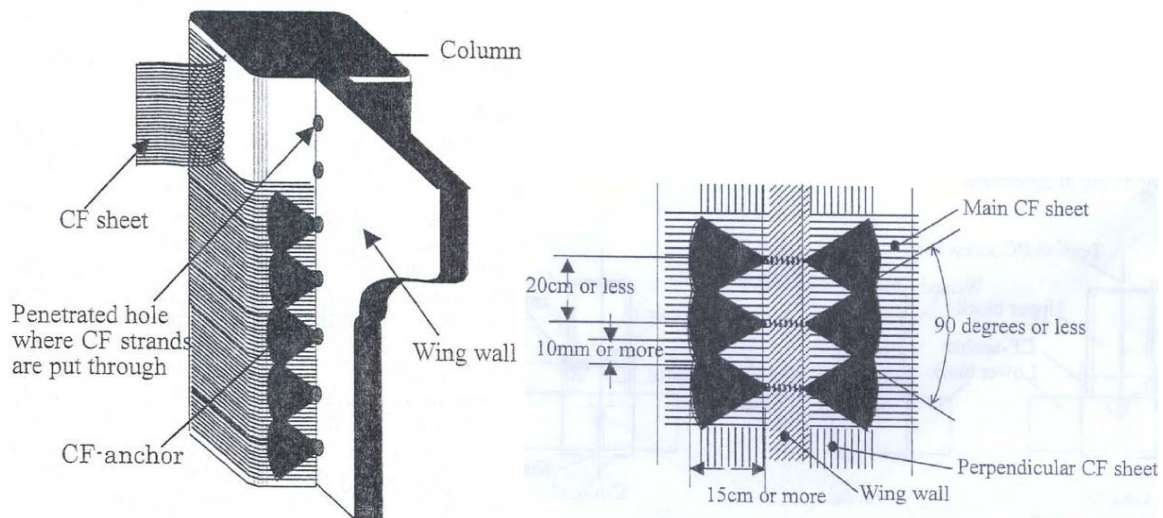
Figure 2.6   CFRP anchors for CFRP wrapping the column with wing wall,
(Kobayashi et. al,. 2001)

Further research on the capacity of CFRP anchors was conducted by Ozdemir and Akyuz (2005). They investigated the effects of concrete compressive strength, anchorage depth, size of anchor hole, and width of CFRP sheet per anchor on the tensile capacity of anchors. Ozdemir and Akyuz found that:

- Three failure modes were observed depending on the embedment depth, h.
    - Shallow concrete cone failure, $h \leq 50$ mm
    - Cone-bond failure, 70 mm $\leq h \leq 100$ mm
    - Rupture of CFRP sheet, $h = 150$ mm
- Compressive strength of the concrete did not affect the tensile capacity of the CFRP anchor if its embedment depth was less than 50 mm. However, as embedment depth increased, the effect of concrete compressive strength became more significant.
- As embedment depth increased, tensile capacity of the CFRP anchor also increased linearly until the depth reached an effective bond length of 100 mm. Beyond this length the tensile capacity did not increase.

- The diameter of the anchor hole did not have a significant effect on the tensile capacity of the CFRP anchor.
- The tensile capacity of the CFRP anchor increased with an increase in the amount of CFRP materials, but the increase was not proportional to the increase in the material.

Ozedmir and Akyuz also suggested equations (Equations 2-1 and 2-2) for predicting tensile capacity of CFRP anchors. These equations were based on their experimental study and a cone-bond failure model proposed by Cook et al. (1998). Ozedmir and Akyuz found that the concrete cone depth, h_c, in which shallow cone failure occurs, is 50 mm for all embedment length of the anchors. Equation 2-1 represents tensile capacity of an anchor when shallow cone failure occurs ($h \leq 50$ mm). Equation 2-2 represents tensile capacity of an anchor when shallow cone is followed by a slip through the remaining part in failure (cone-bond failure, $h > 50$ mm).
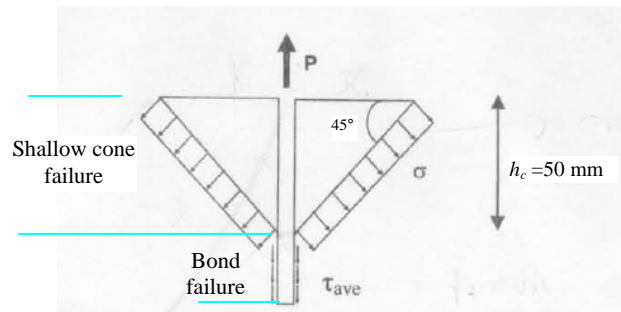
Figure 2.7   *Stress distribution along the embedment depth of CFRP anchor*
(Ozedmir and Akyuz, 2005)

$$P_n = 0.33\sqrt{f_c} \times h \times (d + h) \times \pi \qquad h \leq 50\,mm \qquad \textbf{\textit{Equation 2-1}}$$

$$P_n = 0.33\sqrt{f_c} \times h_c \times (d + h_c) \times \pi + \tau_{avg} \times \pi \times d \times (h - h_c) \quad h > 50\,mm \quad \textbf{\textit{Equation 2-2}}$$

P_n : tensile strength of CFRP anchor, N

f_c : compressive strength of concrete, MPa

d : hole diameter, mm

h : embedment depth of CFRP anchor, mm

h_c : concrete cone depth, 50 mm

τ_{avg} : average bond stress of the concrete, $\tau_{avg} = 1.84\sqrt{f_c}\,\dfrac{h_c}{\pi d}$ MPa, (Cook et al., 1998)

Equations 2-3 and 2-4 are modified versions of Equations 2-1 and 2-2 using US customary unit.

$$P_n = 4\sqrt{f_c} \times h \times (d+h) \times \pi \qquad h \leq 2\,in. \qquad \textit{Equation 2-3}$$

$$P_n = 4\sqrt{f_c} \times h_c \times (d+h_c) \times \pi + 22\sqrt{f_c} \times h_c \times (h-h_c) \quad h > 2\,in. \qquad \textit{Equation 2-4}$$

P_n : tensile strength of CFRP anchor, lb

f_c : compressive strength of concrete, psi

d : hole diameter, in.

h : embedment depth of CFRP anchor, in.

h_c : concrete cone depth, 2 in.

Based on above findings, Kim (2006) and Orton (2007) developed anchorage designs for CFRP anchors to anchor sheets to the bottom or side faces of reinforced concrete beams. The CFRP sheets with anchors in the test beams developed the tensile strength under static loading conditions. In Chapter 3, test results are presented on the performance of CFRP anchorage under dynamic loading to extend the application of the methods to rehabilitation of structure vulnerable to progressive collapse. A progressive collapse triggered by a blast where a column is suddenly removed results in dynamic loads and no reports were found in the literature on effects of loading rates on CFRP anchors.

Orton and Kim also studied CFRP U-wraps and a combination of CFRP anchors and U-wraps. CFRP U-wraps are sheets of CFRP attached transverse to the main CFRP

sheet for continuity (Figure 2.8). The CFRP sheets also developed the full tensile strength through the use of CFRP U-wraps or a combination of CFRP anchors and U-wraps. These anchorage methods are discussed in Chapter 3 and were also evaluated under a dynamic loading condition.

Figure 2.8   CFRP U-wrap

2.2   USE OF CFRP IN STRENGTHENING OF RC BEAMS UNDER DYNAMIC LOADING

Several researchers have investigated dynamic behavior of reinforced concrete beams strengthened using CFRP materials.

Jerome et al. (1996) experimentally investigated static and dynamic response of plain concrete beams externally reinforced with CFRP. CFRP materials were applied to the bottom and side faces of the plain concrete beams. The experimental results indicated that performance under static and dynamic loading of beams was improved after being reinforced with CFRP. In addition, they reported that the failure mode of the beams in a dynamic loading condition did not change from the failure mode in a static loading condition. The failure mode was shear failure of beam after delamination of CFRP from the concrete surface.

12

Cantwell et al. (1999) conducted similar research on CFRP strengthened plain concrete beams. They also found that the failure mode of the beams under static and dynamic loading was delamination of CFRP from the concrete surface although improvement in performance of the beams was observed after strengthening.

Erki et al. (1999) conducted a study on the behavior of reinforced concrete beams strengthened using CFRP under dynamic loading. The test beams were not plain concrete beams but reinforced concrete beams with continuous steel reinforcement. They reported that the test beams strengthened using CFRP performed well under dynamic loading although they showed less energy absorption than beams externally strengthened with steel plate. The failure mode of the test beams was delamination of CFRP. In addition, they recommended that use of additional anchorage for CFRP sheet would improve dynamic performance of the reinforced concrete beams.

In the previous studies, the dynamic behavior of concrete beams strengthened with CFRP was compared with static behavior. However, CFRP sheets were not anchored. In addition, only limited information about member behavior of CFRP strengthened beams failing under dynamic loading is available. Therefore, the study reported in this dissertation initially focused on the dynamic behavior of CFRP materials anchored using CFRP anchors and U-wraps and then was extended to investigation of member behavior of the CFRP strengthened beams under dynamic loading. These topics are discussed in Chapter 3.

2.3   REHABILITATION OF LAP SPLICED LONGITUDINAL BARS IN RC COLUMNS

Aboutaha et al. (1999) studied the effectiveness of rehabilitation methods using steel jackets with adhesive anchor bolts (Figure 2.9-b) and steel jackets with through rods (Figure 2.9-c) to repair damaged rectangular concrete columns. The columns were designed based on ACI 318 - 56 or 63 and had poorly detailed lap splices of longitudinal reinforcement. Lap splice failure occurred in the as-built columns and they showed poor strength and ductility. These columns were repaired using steel jacketing with adhesive anchor bolts or through rods. The test results indicated that the repair techniques improved strength and ductility. Although the columns repaired with steel jackets with through rods showed better performance than the columns repaired with adhesive anchor bolts, steel jackets with adhesive anchor bolts were effective in improving performance of the rectangular reinforced concrete columns. The adhesive anchor bolts restrained opening of splitting cracks in the splice region by improving the confining effects of steel jackets on splices not located near a corner of the jacket. CFRP anchors were intended to function in a similar manner in the rehabilitation using CFRP. In the study reported in this dissertation, CFRP jackets and CFRP anchors were used to repair and strengthen rectangular reinforced concrete columns with inadequate lap splices of longitudinal reinforcement. The design of the test columns and the test setup were based on the study of Aboutaha et al. Therefore, effectiveness of the rehabilitation methods using CFRP jackets and anchors could be compared with rehabilitation using steel jackets and adhesive anchor bolts.

a. Typical strengthened column

b. Details of steel jacket with anchor bolts

c. Details of steel jacket with through rods
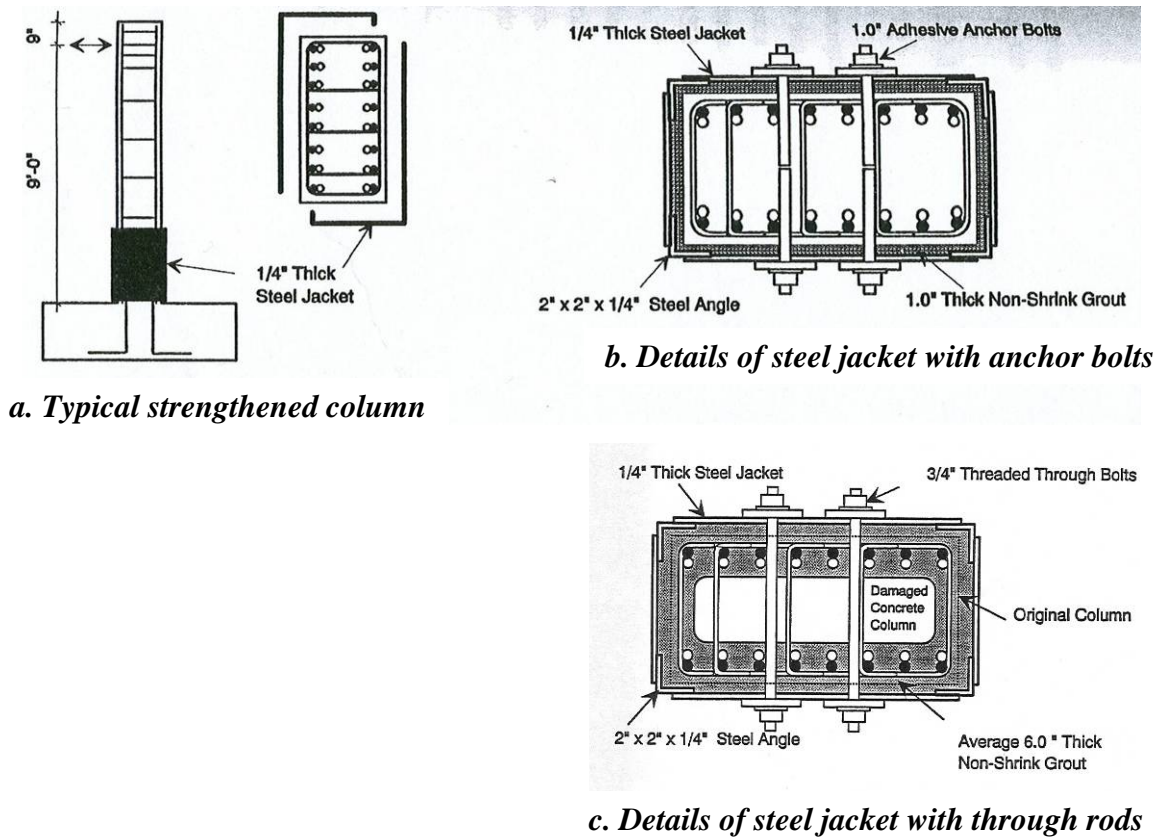
Figure 2.9   Repair of rectangular RC columns (Aboutaha et al., 1999)

Several researchers have investigated the use of fiber reinforced polymer materials to improve lap splice behavior in circular and rectangular reinforced concrete columns.

Elsanadedy et al. (2005) conducted an analytical study to predict the behavior of poor lap splices in circular bridge reinforced concrete columns retrofitted with FRP jackets and proposed a retrofit design criteria. Harries et al. (2006) experimentally investigated retrofit of poorly detailed lap splices in square reinforced concrete columns (18 in. x 18 in.) using CFRP jackets (Figure 2.10). Ghosh et al. (2007) also conducted an experimental study on rehabilitation of lap splices in circular and square columns (14 in. diameter, 12 in. x 12 in) using CFRP jackets (Figure 2.11). In above studies, all the

15

columns were strengthened to improve seismic performance and improvement of strength and deformation capacity was observed after strengthening. However, only circular or square columns were investigated in these studies. Rectangular columns were not investigated although CFRP jacketing of rectangular columns will not be as efficient as that of circular or square columns. In addition, the effectiveness of multiple layers of fiber reinforced jackets has been studied but the use of CFRP anchors has not been studied.

Harajli et al. (2008) experimentally investigated use of FRP jackets in seismic strengthening of lap splices in rectangular reinforced concrete columns (20 cm x 40 cm, Figure 2.12). The improvement in strength and deformation capacity was observed in the test columns after rehabilitation. However, the strengthened column was loaded in the long direction of section in which CFRP jackets would be more effective in confining the lap spliced region. Consequently, the loading in the long direction of column section was less critical than the loading in the short direction.

Previous studies have been limited to the rehabilitation of circular or square columns using FRP jackets. The rehabilitation of rectangular columns and effectiveness of CFRP anchors in the rehabilitation have not been studied.
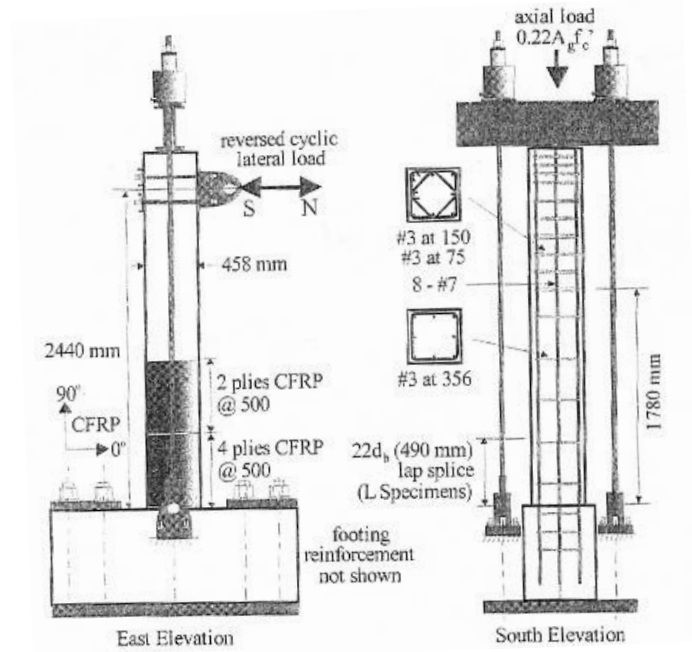
Figure 2.10   Square columns with poor lap splices, (Harries et al., 2006)
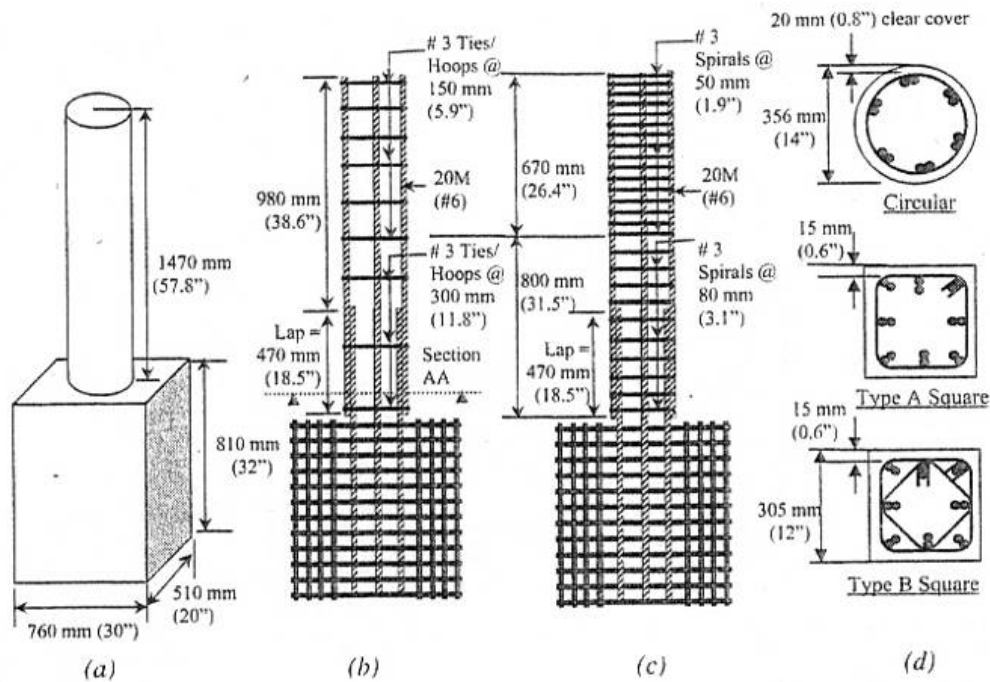
Figure 2.11   Square and circular columns with poor lap splices, (Ghosh et al., 2007)

Direction of loading
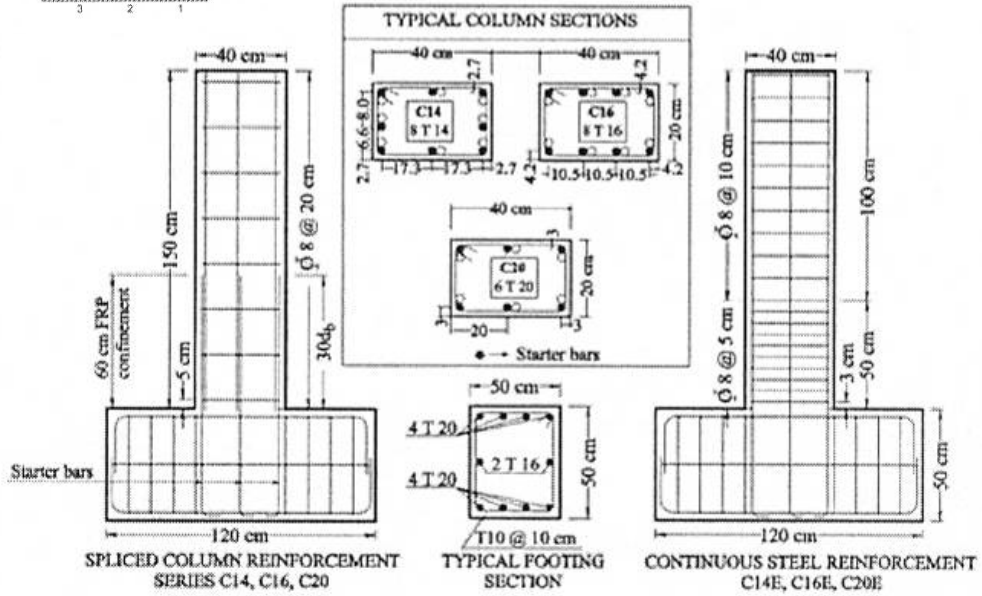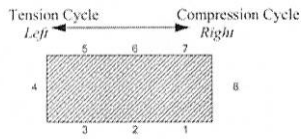
Figure 2.12 **Rectangular columns with poor lap splices, (Harajli et al., 2008)**

18

CHAPTER 3

Experimental Program – Rehabilitation of Poorly Detailed Reinforced Concrete Beams under Dynamic Loading

3.1 INTRODUCTION

The objective of this phase of the research program was to evaluate the performance of Carbon Fiber Reinforced Polymer (CFRP) sheets used to provide continuity in reinforced concrete structures under dynamic loading. High loading rates may occur in structures vulnerable to failure by progressive collapse when a column is suddenly removed due to extreme loads.

The basic rehabilitation technique for this program was installation of CFRP materials either on the bottom (Figure 3.1) or the sides (Figure 3.2) of the beam to provide continuity of bottom reinforcement. CFRP sheets were attached to the concrete surface by epoxy resin and by CFRP anchors or CFRP U-wraps to develop the full tensile capacity of the CFRP sheet after delamination. The rehabilitation technique was studied with different geometries and quantities of CFRP materials under static loading conditions and reported by Kim (2006) and Orton (2007). The CFRP fully developed the ultimate tensile strength under the static loading using CFRP anchors and CFRP U-wraps to transfer force from the concrete to the CFRP sheet.

However, in the case where a column is suddenly removed, the reinforced concrete floor beams are subjected to a dynamic load. Under high load rates, the response of CFRP materials may differ from that under a static load. Therefore, the performance of CFRP rehabilitation techniques under the static loading condition needs to be verified under dynamic loading conditions. The verification of the rehabilitation technique was also recommended by the practicing engineering panel of this research program.

19

The specimens tested in this study had the same geometry and quantity of CFRP materials as the specimens tested under the static loading conditions.
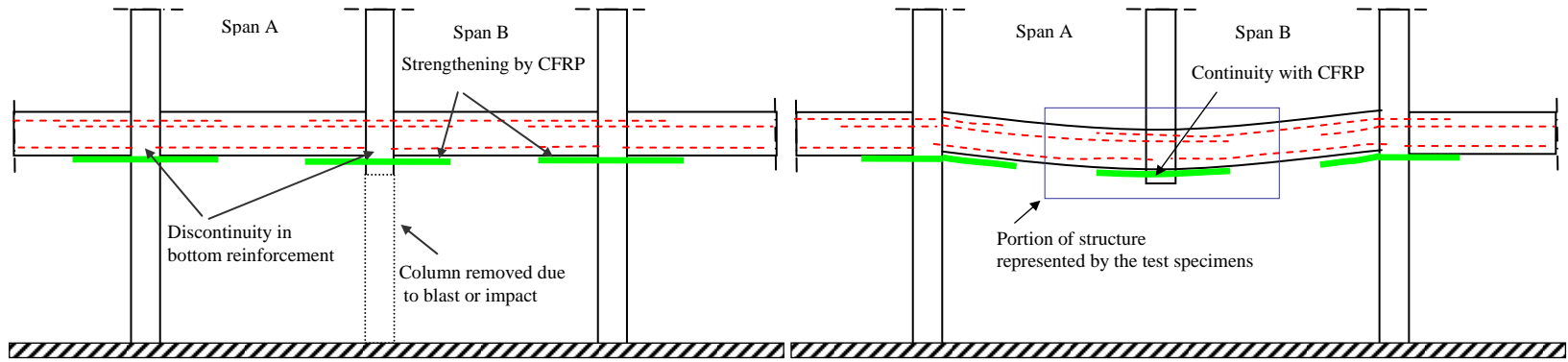
Figure 3.1 **Rehabilitation technique, CFRP on the bottom face of beam**
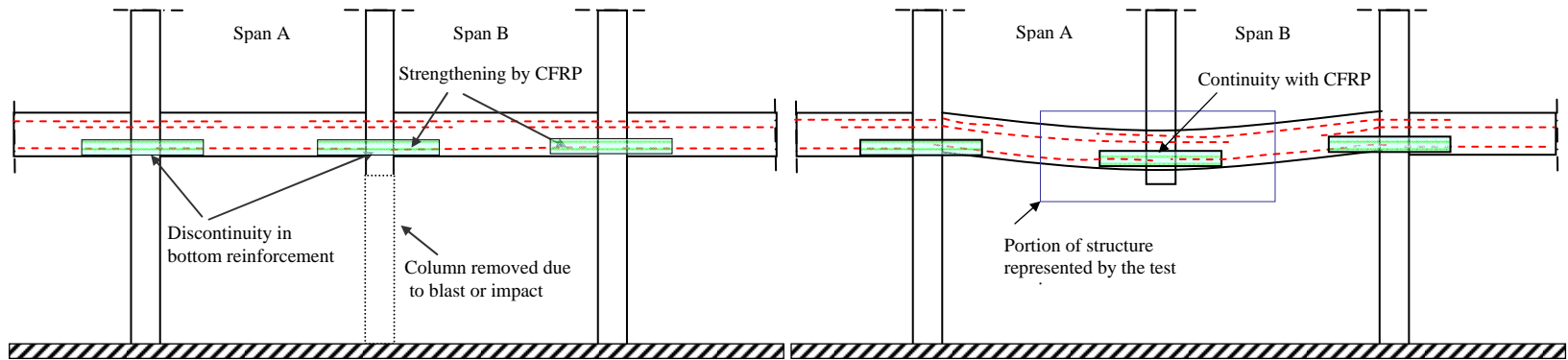
Figure 3.2 **Rehabilitation technique, CFRP on the sides of beam**

3.2   TEST SPECIMENS

Three types of reinforced concrete beams were tested in this study.   The dimensions and layout of longitudinal and transverse reinforcement of the beams tested are shown in Figure 3.3 (Type A), Figure 3.4 (Type B) and Figure 3.5 (Type C).   In all the beams, discontinuity in the bottom reinforcement existed at the middle and sufficient amount of transverse reinforcement was provided to prevent shear failure. The transverse reinforcement was placed symmetrically.

The purpose of testing Type A and B specimens was to observe effectiveness of the anchorage using CFRP anchors and U-wraps to develop the full tensile capacity of CFRP sheets. The bottom face of the Type A beam was flat while that of the Type B beam had a 2 in. height transition. This height transition was fabricated with a 1:4 slope ramp, which was installed after the beams were cast. The background of height transition ramp is discussed in Section 3.4.3. A 1 in. discontinuity in bottom beam reinforcement existed at the middle of both types of beams. The reentrant ends in Type A and B beams existed because the height of the beam was limited by size of the main supports in the test setup.

Type C beams represent a "proof-of-concept" test to verify that the CFRP rehabilitation would permit the discontinuous reinforcement to reach yielding and allow a flexural hinge to develop. A portion of a column was included at the mid-span of Type C beam. The 2 in. height transitions were also fabricated with a 1:4 slop ramp in the both side of Type C beam, which were installed after the specimens were cast. A hole was drilled through the column portion to connect the CFRP sheets through the column. A 3 in. discontinuity in the bottom beam reinforcement in the beam-column connection represented typical details of building designed under pre-1989 codes. The design of the Type C beam was based on the study by Orton (2007).

Fourteen beams, 9 Type A beams, 2 Type B beams and 3 Type C beams, were tested. Two of the Type-A specimens were rehabilitated by placing CFRP materials on

22

the side faces of the beam. CFRP materials were installed on the bottom face of the beams in the other eleven specimens.

204 in.

8 in.

East

#3 @ 3 in.   #3 @ 6 in.

West

12 in.

16 in.

1 in. discontinuity

Reinforcement, GR60
2-#3 top
2-#6 bottom

192 in.

Transverse reinforcement was placed symmetrically about mid-span.
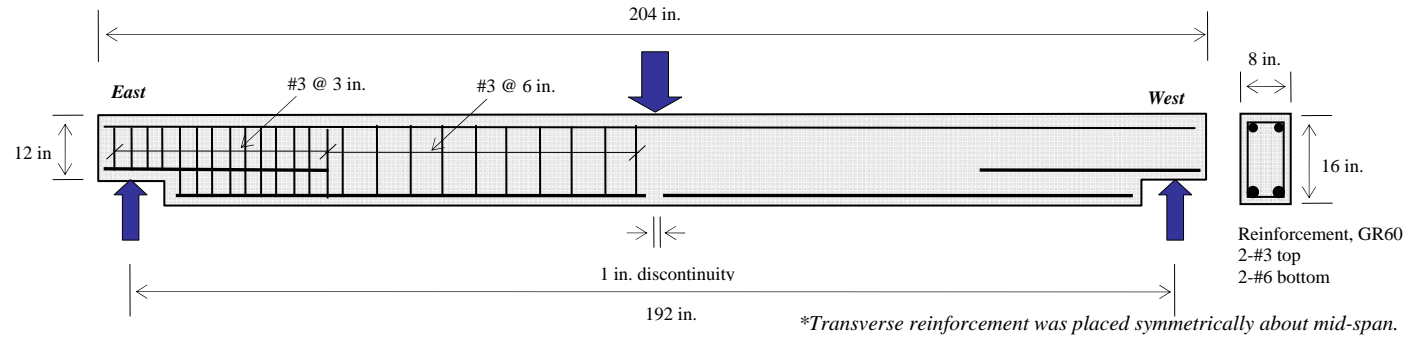
Figure 3.3   Type A specimen, flat bottom face

204 in.

8 in.

East

#3 @ 3 in.   #3 @ 6 in.

West

18 in.

16 in.

8 in.

2 in. height transition

Reinforcement, GR60
2-#3 top
2-#6 bottom

1 in. discontinuity

192 in.

Transverse reinforcement was placed symmetrically about mid-span.
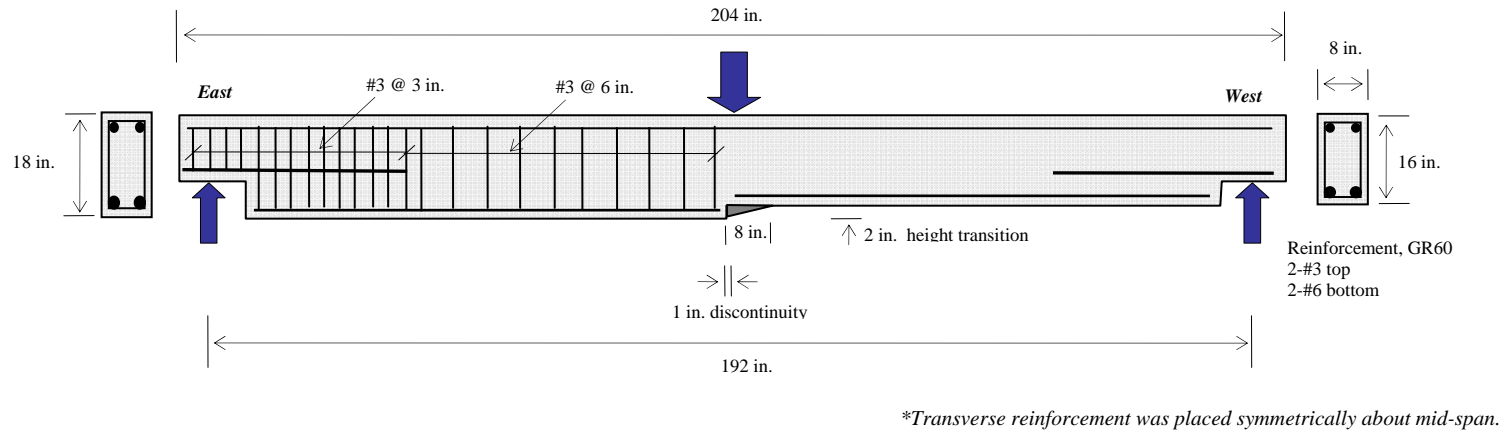
Figure 3.4   Type B specimen, height transition bottom face
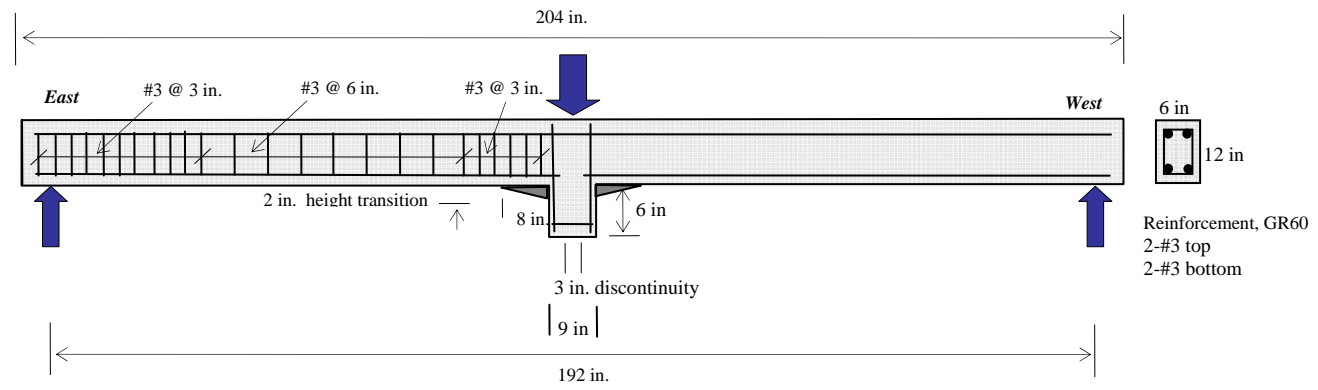
Figure 3.5   Type C specimen, column on bottom face

3.3 MATERIAL PROPERTIES

3.3.1 Concrete

Design compressive strength was 4,000 psi. The beams were fabricated from three different batches and the measured 28 day compressive strengths of concrete were 2,000 psi, 5,000 psi, and 6,000 psi. In the first cast, the compressive strength of the concrete was 2,000 psi due to supplier errors and the beams fabricated in this cast were tested to investigate the effect of concrete strength on CFRP rehabilitation although this was not a parameter that was intended in the test matrix. The measured compressive was used in calculating the static strength of the test beams.

3.3.2 Steel

The steel reinforcement used for longitudinal reinforcement was GR60. The #6 longitudinal bars used in Type A and Type B beams was designed to remain elastic during the test because the purpose of test was to observe behavior of CFRP materials. Strains measured in these bars were between 0.0002 and 0.0016 well below yield. The measured tensile yield strength of the #6 bars was between 63 ksi and 70 ksi.

The #3 longitudinal bars used in Type C beam were expected to yield and show plastic behavior during the test. The measured tensile yield strength of the #3 bars was 52 ksi and a stress-strain curve is shown in Figure 3.6.

3.3.3 CFRP

The CFRP material used in this experimental program was Tyfo® SCH-41 Composites with Tyfo® S Epoxy from FYFE Co. LLC.

The CFRP material was unidirectional material and had no tensile capacity in transverse direction of the fabric. The specified properties from the manufacturer are shown in Table 3.1. The typical test value of the ultimate tensile strength (143 ksi) was used in calculating the static strength of the test beams. The previous studies showed that

26

the measured properties of this CFRP material were consistent with the specified properties from the manufacturer (Kim, 2006; Orton, 2007).

The stress-strain curve of the CFRP material is shown in Figure 3.6. Although the CFRP has higher strength than the steel bar, the CFRP has a lower modulus than the steel bar. The CFRP has a linear stress-strain relationship up to fracture.
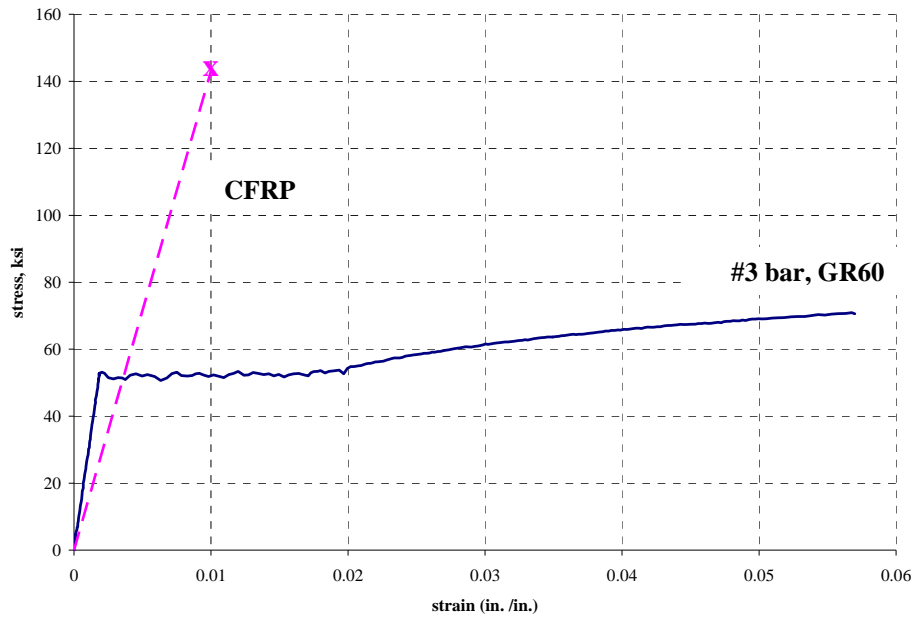
Figure 3.6   Strain-stress curves of steel and CFRP

Table 3.1 Material properties of CFRP suggested by manufacturer

Properties	Ultimate Tensile Strength	Elongation at Break	Tensile modulus	Laminate thickness
Typical Test Value	143 ksi	1.0 %	13,900 ksi	0.04 in.
Design Value	121 ksi	0.85 %	11,900 ksi	0.04 in.

No consideration has been given to fire effects on CFRP rehabilitation in this study. However, if the fire is of concern to designers and building owners, they may use

fire protection materials on CFRP strengthened reinforced concrete structures. Effectiveness of fire protection materials on CFRP has been studied by Nofal (2005), Chowdhury (2007), and Kodur (2007). They have found that the fire protection materials such as perlite mortar and ceramic fiber may protect CFRP for the required fire resistance rating for evacuation.

3.4 REHABILITATION METHODS

3.4.1 Test Variables

Static loading tests of the beams rehabilitated with different methods of using CFRP materials preceded this study. In the previous studies, focus was on finding efficient methods for anchoring CFRP materials to reinforced concrete structures. The anchorage methods selected for the dynamic loading test of Type A and B beams developed the ultimate tensile capacity of the CFRP under static loading conditions in the previous tests (Kim, 2006; Orton, 2007). Fracture of CFRP due to development of the ultimate strength was expected at the middle of the beams in the dynamic loading test (Figure 3.7). Failure modes of the beams were observed and strain in the CFRP was measured to study effectiveness of the anchorage method under dynamic loading. The static flexural strength of Type A and B beams was selected corresponding to an ultimate tensile strength of CFRP (143 ksi) and calculated using the equivalent rectangular stress block (ACI 318-08).

After verify that theses anchorage methods results in the CFRP reaching its ultimate strength under dynamic loading, the Type C beams were designed to develop ductility by yielding of the bottom reinforcement in the beam outside of the region that was strengthened (Figure 3.8). The strain in the steel reinforcement was measured to access non-linear response of the bottom reinforcement. The static flexural strength of Type C beams was selected corresponding to yielding of the bottom reinforcement at the ends of the region that was strengthened using CFRP where plastic hinges were expected.

29
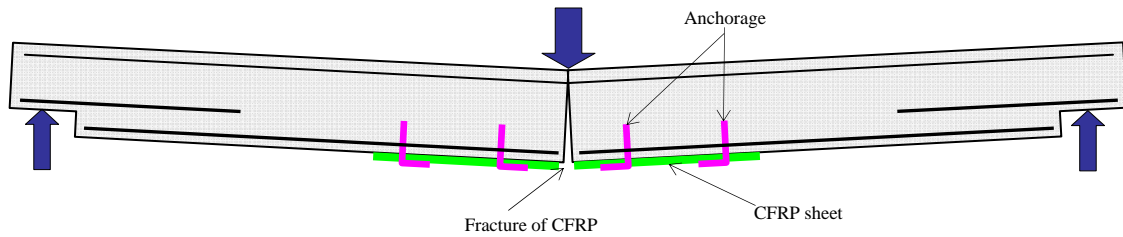
Figure 3.7   Test of Type A beam
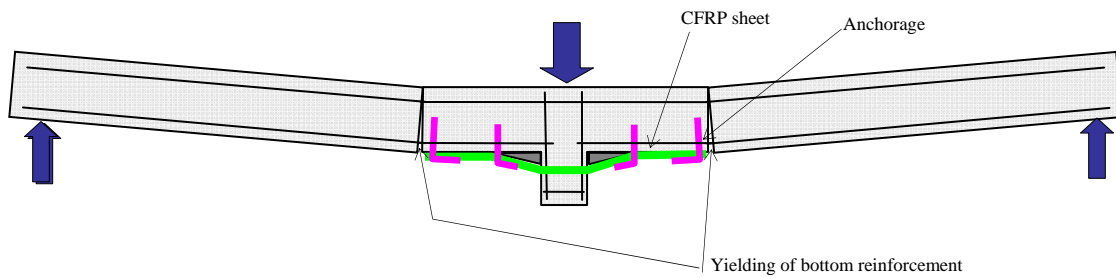
Figure 3.8   Test of Type C beam

The test variables for this experimental investigation are as follows: 1. Location of CFRP materials in a beam (bottom face or side faces); 2. Condition of bottom face (flat, height transition or column); 3. Type of anchorage (CFRP anchors or CFRP U-wrap); 4. Concrete strength; 5. Surface preparation; 6. Effect of overhead application.
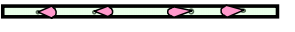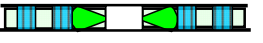
The bottom face application was used in more of the tests because it was indicated by the practicing engineering panel that CFRP materials are more easily applied on the bottom face in ordinary reinforced concrete structures. Side face application may be limited because the method requires flat side surfaces and many beam-column connections consist of columns that are wider than the beams.

In addition, this study focused on the use of the CFRP anchors rather than the use of the CFRP U-wraps because the anchorage method using CFRP anchors was a more efficient use of the materials than that of using CFRP U-wraps (Kim, 2006; Orton, 2007). Therefore, more variables were evaluated for the specimens with bottom face

30

application of the CFRP sheets anchored by the CFRP anchors. A summary of the test specimens and the test variables is shown in Table 3.2. In specimen notation, characteristics of a test beam are identified as follows:

- Type of beam: Type **A**, **B** or **C**
- Face where CFRP is applied to:
    - *BF*: Bottom face, Flat
    - *BH*: Bottom face, Height transition
    - *S*: Side face
    - *BC*: Bottom face with column
- Compressive strength of the concrete:
    - *2*: 2,000 psi
    - *5*: 5,000 psi
    - *6*: 6,000 psi
- Surface preparation
    - *S*: Sand blast
    - *N*: No surface preparation (separation)
    - *G*: Grind

Table 3.2   ***Summary of test variables***

Specimen Notation	Sketch	Location of CFRP	Condition of bottom face	Type of anchorage	Concrete strength	Surface preparation	Type of Specimen
A-BF-N-5S		Bottom face	Flat	None	5,000 psi	Sand-blast	Type-A
A-BF-A-2S					2,000 psi	Sand-blast	
A-BF-A-5S*				CFRP anchors	5,000 psi		
A-BF-A-2N					2,000 psi	Separation	
A-BF-1.3A-5N					5,000 psi		
A-BF-U-5S*				CFRP U-wraps	5,000 psi	Sand-blast	
A-BF-A/U-6G	Overhead application			CFRP anchors / CFRP U-wraps	6,000 psi	Grind	
B-BH-A-6S*			Height transition	CFRP anchors	6,000 psi	Sand-blast	Type-B
B-BH-U-6S				CFRP U-wraps	6,000 psi	Sand-blast	
A-S-A-6G*		Side face		CFRP anchors	6,000 psi	Grind	Type-A
A-S-AU-2S*				CFRP anchors and CFRP U-wrap	2,000 psi	Sand-blast	
C-BC-A-6G-01*		Bottom face	Height transition	CFRP anchors	6,000 psi	Grind	Type-C
C-BC-A-6G-02*				CFRP anchors	6,000 psi	Grind	
C-BC-U-6G*				CFRP U-wraps	6,000 psi	Grind	

*: Multiple impacts prior to failure, all others subjected to only one loading

A: Type A; *B*: Type B; *C*: Type C

BF: Bottom face, Flat; *BH*: Bottom face, Height transition; *S*: Side face; *BC*: Bottom face with column

A: CFRP Anchor; *U*: CFRP U-wrap

2: 2,000 psi; *5*: 5,000 psi; *6*: 6,000 psi

S: Sand blast; *N*: No surface preparation (separation); *G*: Grind

3.4.2   Components of CFRP Rehabilitation

The CFRP materials were used for 2 different purposes. First, they were used as a tensile element to provide continuity to the bottom reinforcement. The CFRP sheet shown in Figure 3.9 is attached solely by epoxy resin at the CFRP concrete interface for flexural continuity. Second, the CFRP materials were used as anchors to transfer forces from the CFRP sheet to the concrete substrate. Two types of the anchors were used; CFRP anchors and CFRP U-wraps. Installation procedures for CFRP materials to reinforced concrete beam are provided in Section 3.4.2.4.

3.4.2.1   CFRP Sheet

Two types of CFRP sheets, beam sheet and connection sheet, were used to provide continuity in the bottom reinforcement (Figure 3.9 and Figure 3.10). Beam sheet consists of a layer or layers of CFRP sheet applied to the flat bottom or side faces of the beam. In specimens with height transition, a strap of CFRP sheet was used to connect the sheets on each sides of the height difference. In the specimens with a column, a CFRP sheet connected the sheets on the bottom face of the beam in one bay to the sheet in the adjacent bay through a hole in the column. The ends of the connection sheet were spread out in a fan shape at the end of the transition ramp. The width of CFRP used in fabricating a connection sheet was 33 % more than that in the beam sheet being connected in all the specimens.

When beam sheets were used on side faces of a beam, the application was symmetrical on both sides.
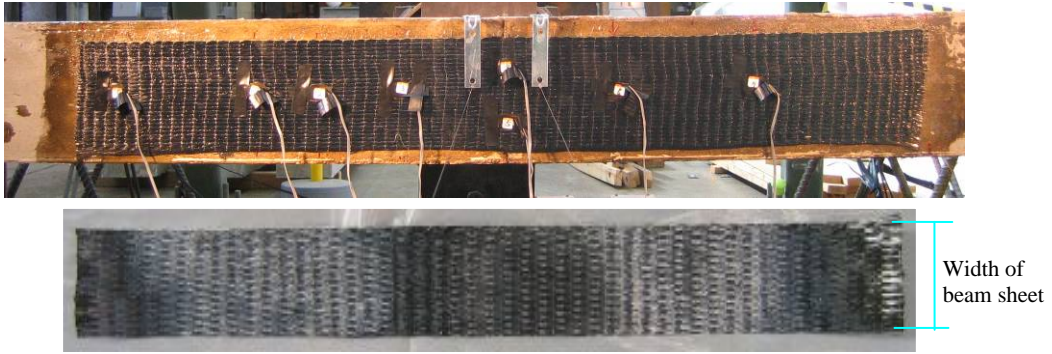
Width of
beam sheet

Figure 3.9   CFRP sheet, beam sheet

Beam sheet
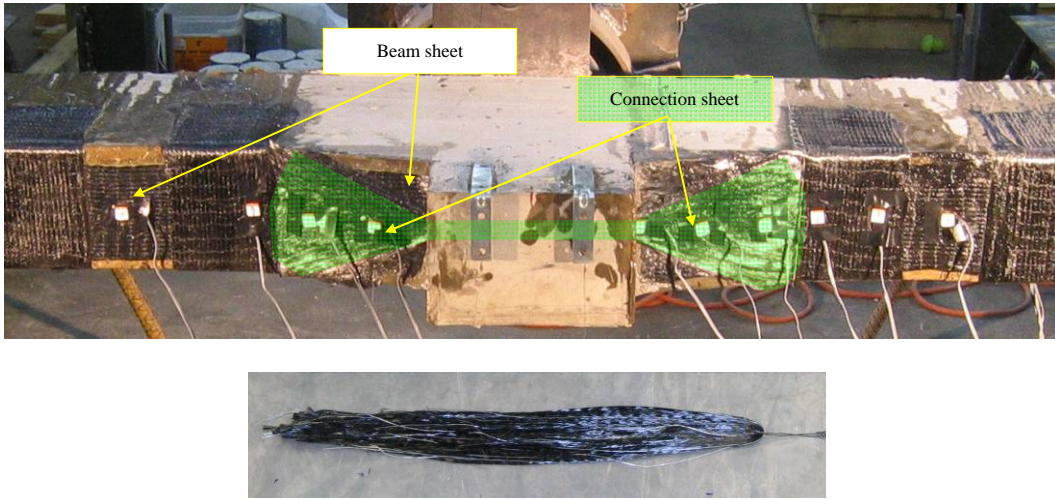
Connection sheet

Figure 3.10   CFRP sheet, Connection sheet

3.4.2.2 CFRP Anchor

A CFRP anchor consists of a roll of CFRP sheet inserted into the concrete and splayed out over the CFRP sheet (Figure 3.11). The width of CFRP used in fabricating a CFRP anchor depended on the strength of the CFRP sheet being anchored. Total width of a set of the CFRP anchors at an anchor point was either the same width as the main sheet or 33 % larger than the main sheet. Details of CFRP anchors in the test beams are provided later in this section. Examples of application of the CFRP anchors to the test beams are shown in Figure 3.12 and Figure 3.13 .

Figure 3.11   CFRP anchor

CFRP anchor

CFRP sheet, beam sheet
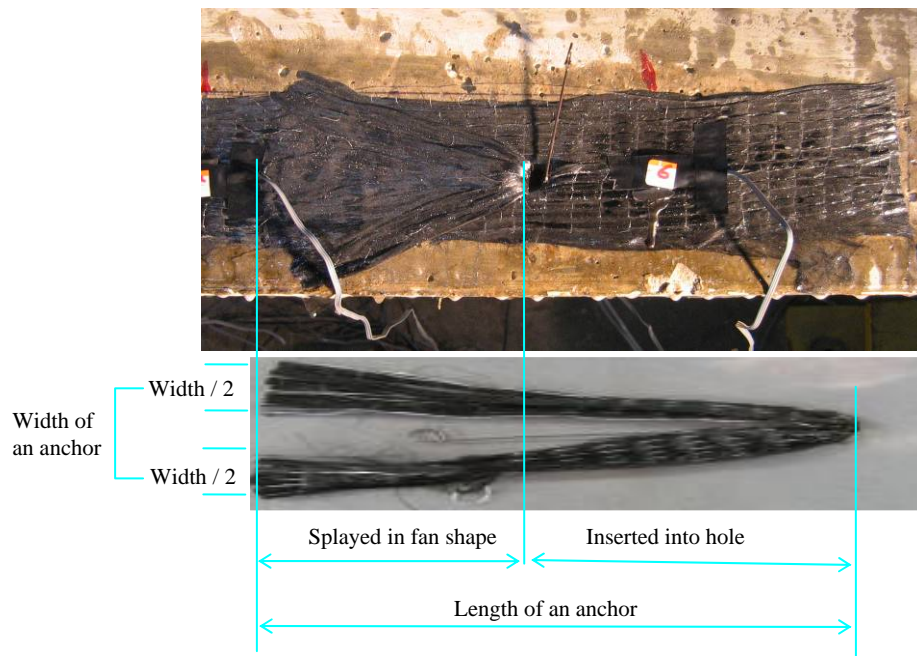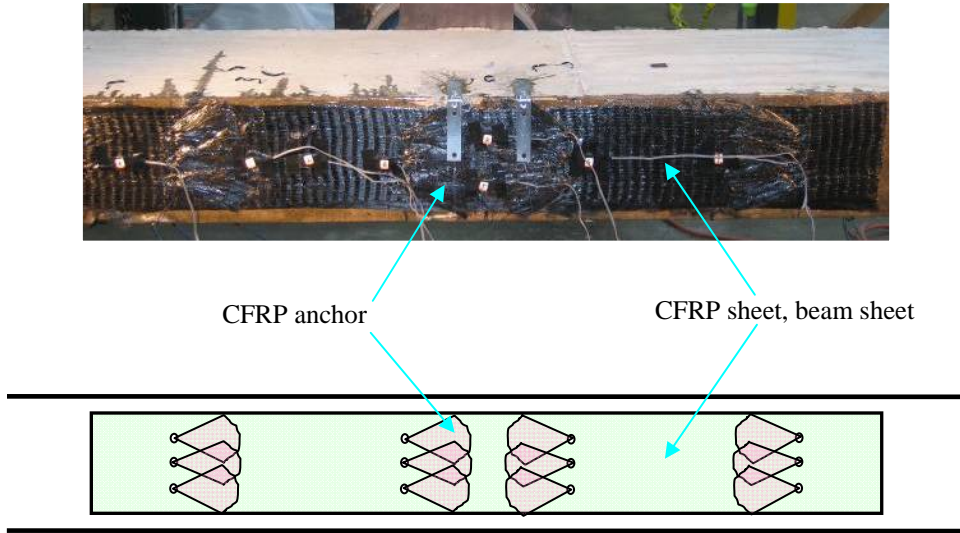
Figure 3.12   Layout of CFRP, Type A, bottom face

CFRP anchor

CFRP sheet. beam sheet
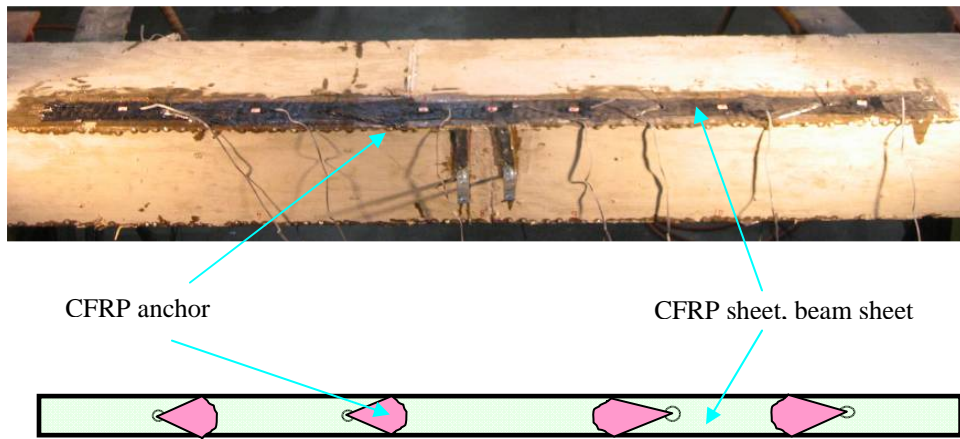
Figure 3.13   Layout of CFRP, Type A, side face

3.4.2.3 CFRP U-wrap

CFRP U-wraps were sheets of CFRP attached transverse to the main CFRP sheet (Figure 3.14). The width of a CFRP U-wrap was identical to the width of the main CFRP sheet. The width of CFRP U-wrap was 6 in. for Type A and B beams and 4.5 in. for Type C beam. The CFRP U-wrap was attached on the bottom face of the beam over the CFRP sheet and extended on each side of beam 9 in. (Type A or B beam) or 6 in. (Type C beam) from the bottom face of beam. Examples of application of the CFRP U-wraps to the test beams are shown in Figure 3.15 and Figure 3.16.

Figure 3.14   CFRP U-wrap

37

CFRP sheet. connection sheet   CFRP sheet, beam sheet   CFRP U-wrap

6 in.
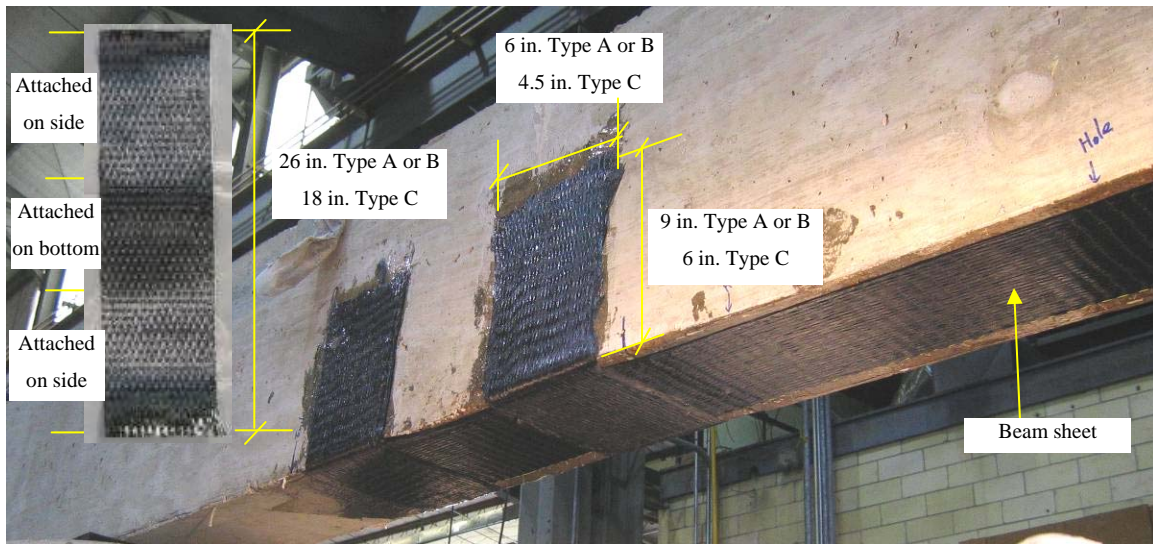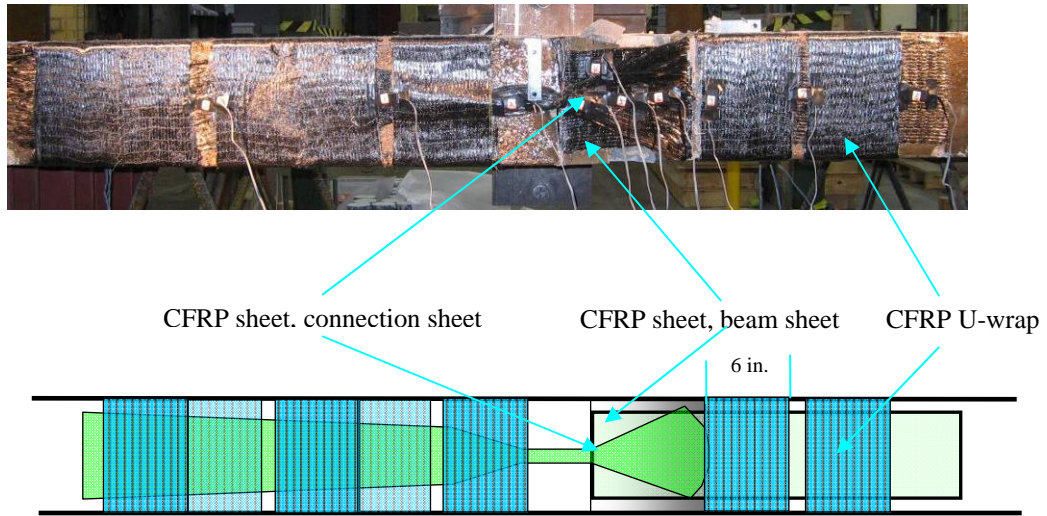
Figure 3.15   Layout of CFRP, Type B

6 in.

4.5 in.

CFRP sheet. Beam sheet   CFRP sheet. Connection sheet   CFRP U-warp

4.5 in.
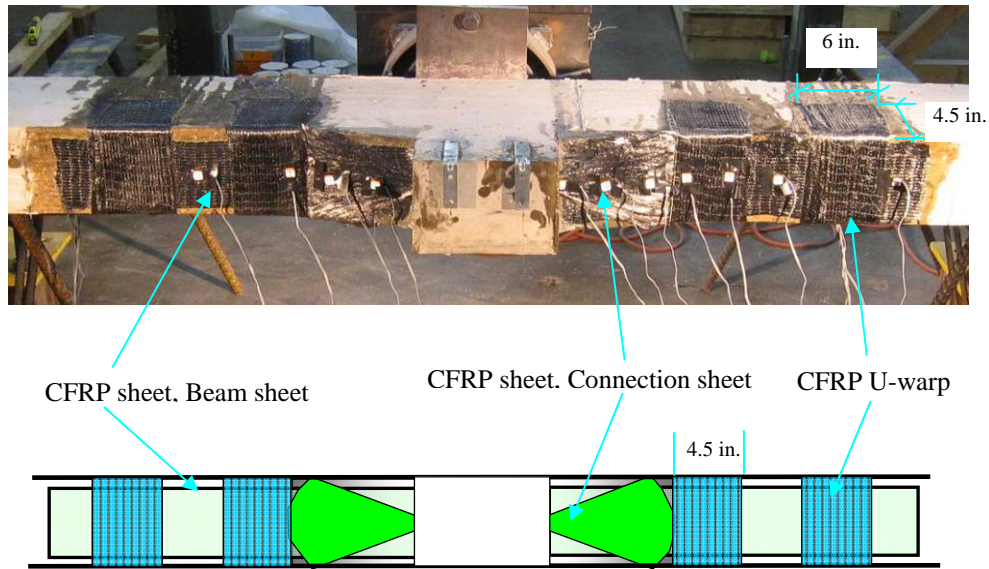
Figure 3.16   Layout of CFRP, Type C

38

3.4.3   Installation of CFRP to Reinforced Concrete Beams

3.4.3.1   *Surface Preparation*

The CFRP sheet was attached on three different surface conditions. The concrete surface of a test beam where CFRP sheet would be applied was either 1. sand-blasted, 2. ground or 3. separated using clear polyethylene wrap. A summary of the surface preparation of the test beams is shown in Table 3.2.

The sand-blasted and ground concrete surfaces to removed cement paste on the concrete surface are shown in Figure 3.17 and Figure 3.18. The concrete surface was prepared to meet the requirement for a minimum concrete surface profile (CSP) 3 as defined in the International Concrete Research Institute (ICRI) surface-profile-chips. In a previous study, Orton (2007) reported that sand-blasting and grinding were equally effective on preparation of the concrete surface for CFRP sheets. The surface of test beams except A-BF-A-2N and A-BF-1.3A-5N, were sand-blasted or ground.

In A-BF-A-2N and A-BF-1.3A-5N, clear polyethylene wrap was placed on the surface to eliminate bond between the CFRP sheet and the concrete (Figure 3.19). This polyethylene wrap separated the concrete surface from CFRP sheets and epoxy resin so there was no adhesion between the surface and the sheets. In this case, stress in the CFRP sheet was transferred to the concrete only by the CFRP anchors.

Before grinding

After grinding
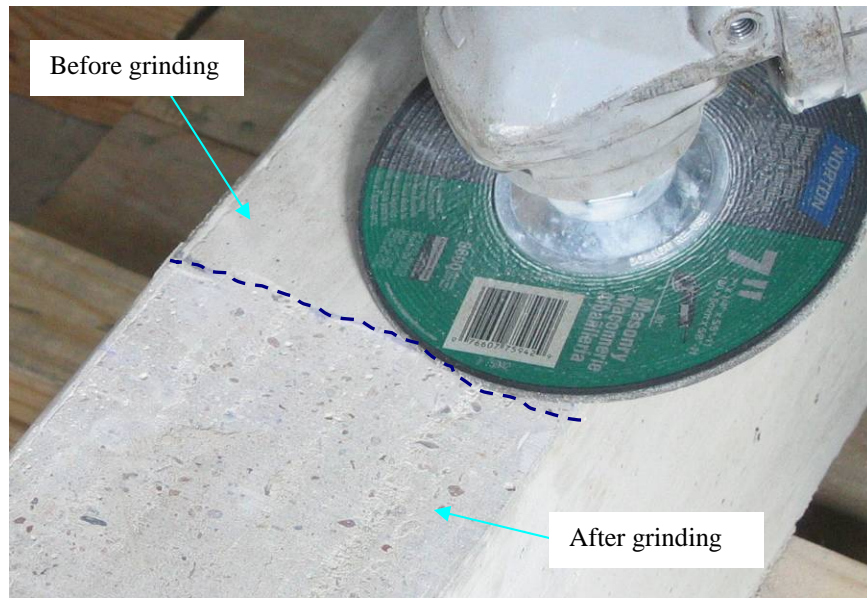
Figure 3.17   Preparation of concrete surface, grinding

After Sand-blasting

Before Sand-blasting
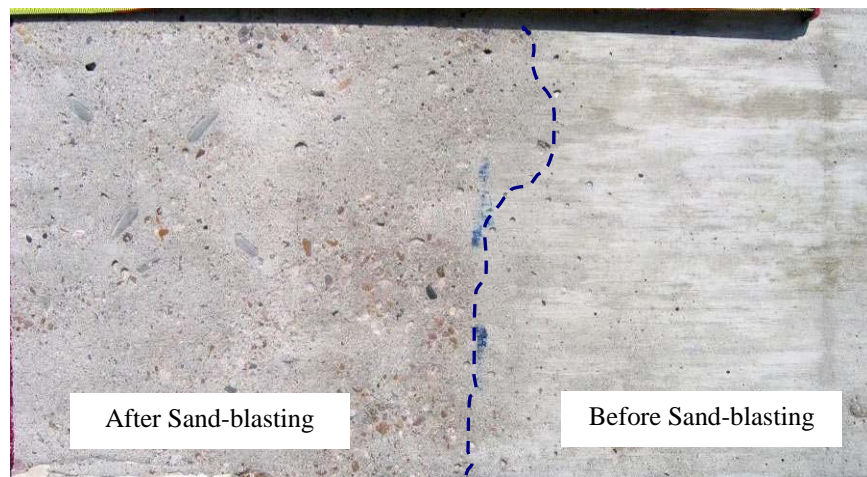
Figure 3.18   Preparation of concrete surface, sand-blasting
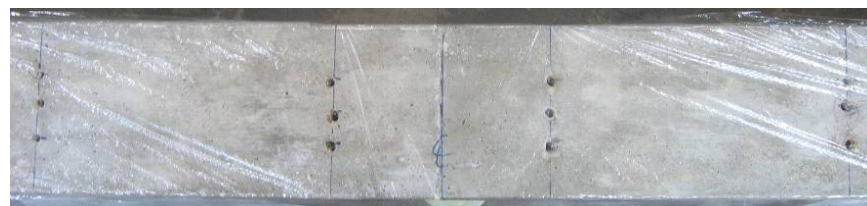
Figure 3.19   Preparation of concrete surface, separation

3.4.3.2 *Preparation of Holes for CFRP Anchors and Connection Sheets*

Holes were drilled in the concrete where CFRP anchors were applied. The holes were drilled with masonry drill bits with different diameters. An example of the anchor hole is shown in Figure 3.20. The diameter of drill bit was based on the width of CFRP per anchor and the size of holes in the test beams are provide in Section 3.4.4. The depth of the holes was 5.5 in. for the beams with the bottom face application of CFRP and 4 in. for the holes with the side face application.

In, Type C specimen, a 1 in. diameter hole was drilled through the column portion to pass a connection sheet from one side of beam to another (Figure 3.21). This hole was drilled before the height transition ramps were placed and located at 2 in. from the bottom face of the beam.

The edge of hole was ground to smooth perimeter transition of the CFRP anchor or connection sheet from the hole to the beam sheet. The holes were cleaned with compressed air.
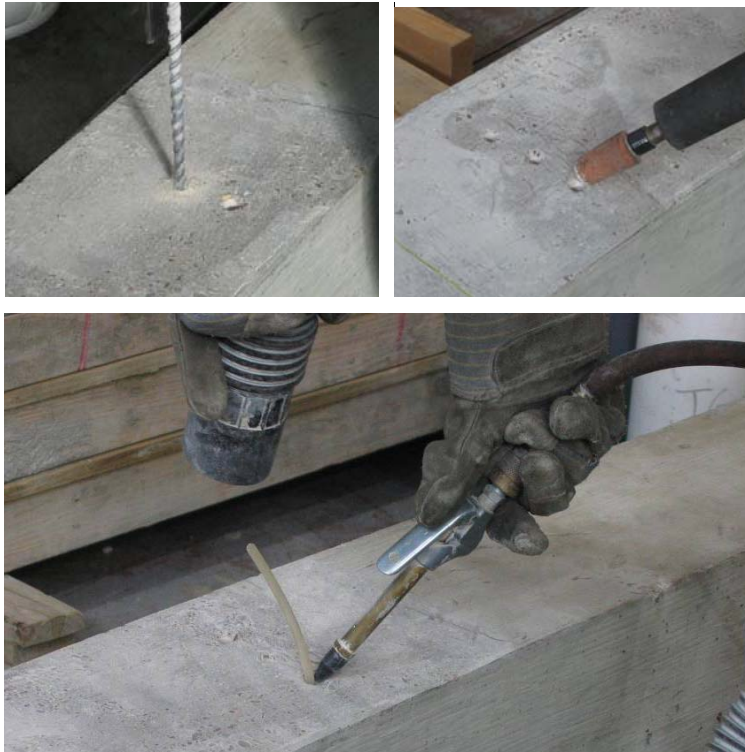
Figure 3.20   Preparation of holes for CFRP anchors

Figure 3.21   Preparation of a hole for connection sheet

3.4.3.3   Height Transition Ramp

A polymer mortar, Tyfo® P from FYFE Co. LLC, was used in fabricating the height transition ramp in Type B and Type C beams. The transition ramp was fabricated after the beam was cast. The transition ramp applied to Type C specimen is shown in Figure 3.22. Slope of the ramp was 1:4 (2 in.: 8 in.) for all the test beams. The various height and slope of height transition was studied by Orton (2007) and the 2 in. height and 1:4 slope ramp was reported as the most effective in fabricating height transition for CFRP sheets.
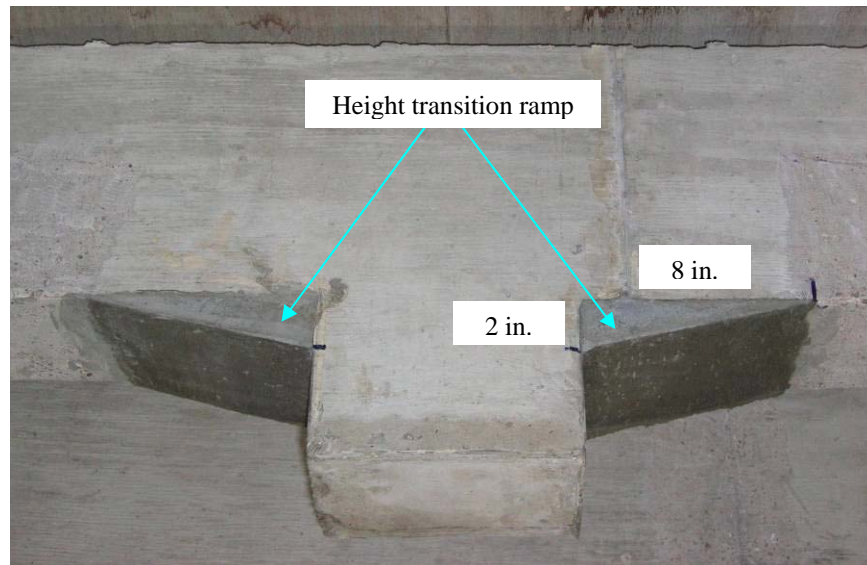
Figure 3.22   Height transition ramp

3.4.3.4   Installation Procedure of CFRP

After preparing the concrete surface, holes and transition ramps, CFRP materials were installed in reinforced concrete beams as follows:

1) Prepare epoxy resin (Figure 3.23)

2) Saturate the concrete surface and holes with the epoxy resin (Figure 3.24)

3) Saturate CFRP sheet with the epoxy resin and remove excess epoxy
   (Figure 3.25)

4) Place the CFRP sheet on the beam (Figure 3.26)

5) Saturate and place the CFRP U-wraps and anchors
   (Figure 3.27 and Figure 3.28)

6) Cure

In this section, overhead application of CFRP in A-BF-A/U-6G is presented. However, CFRP was applied to all the other beams in the direction of gravity. The test results indicated that the direction of application did not influence the performance of the rehabilitation.

Figure 3.23   Prepare epoxy resin

Figure 3.24   Saturate the concrete surface and holes with the epoxy resin

Figure 3.25   Saturate CFRP sheet with the epoxy resin and remove excess epoxy

Figure 3.26   Place the CFRP sheet on the beam

45

Figure 3.27   Saturate and place the CFRP U-wraps

Figure 3.28   Saturate and place the CFRP anchors

3.4.4 Application of CFRP to Test Beams

3.4.4.1 *Rehabilitation Using Bottom Face of Beam: Flat Bottom Face*

For all the beams rehabilitated on the flat bottom face, a CFRP sheet 6 in. wide x 48 in. long was attached. In A-BF-N-5S, no anchorage was provided so that this beam provided a reference to evaluate the efficiency of anchorage systems in the other beams (Figure 3.29).
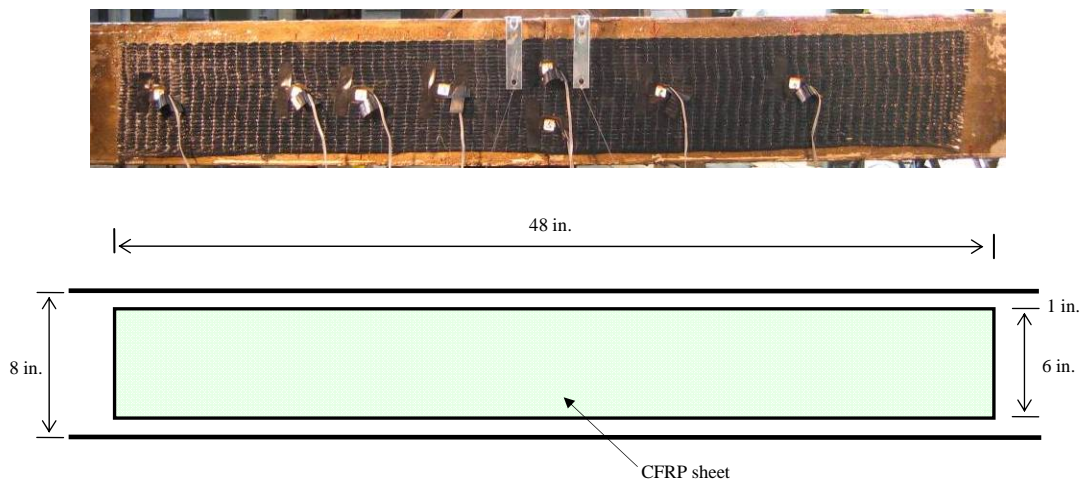
Figure 3.29   Rehabilitation using flat bottom face without CFRP anchors or U-wrap (A-BF-N-5S)

In A-BF-A-2S, A-BF-A-5S and A-BF-A-2N, a set of three CFRP anchors was fabricated using the same width as the CFRP sheet, 6 in. (2 in. per anchor). As shown in Figure 3.30, the length of the anchor was 9 in. with 5.5 in. of the anchor inserted into a 3/8 in.-diameter-hole drilled into concrete, and the rest of the anchor was spread out in a fan shape on the CFRP sheet. The anchor was inserted to 4 in. depth into the core of the concrete (interior of the first layer of the reinforcing steel). Twelve anchors were installed on the beams as indicated in Figure 3.31. In A-BF-1.3A-5N, the geometry of the CFRP

materials was the same as A-BF-A-2S, A-BF-A-5S and A-BF-A-2N except that 33 % more CFRP materials, 8 in. total, (2.7 in. per anchor) was provided for the CFRP anchors than for CFRP anchors in the other beams. The diameter of the anchor hole in A-BF-1.3A-5N was 1/2 in. and the depth was identical to the other beams, 5.5 in.
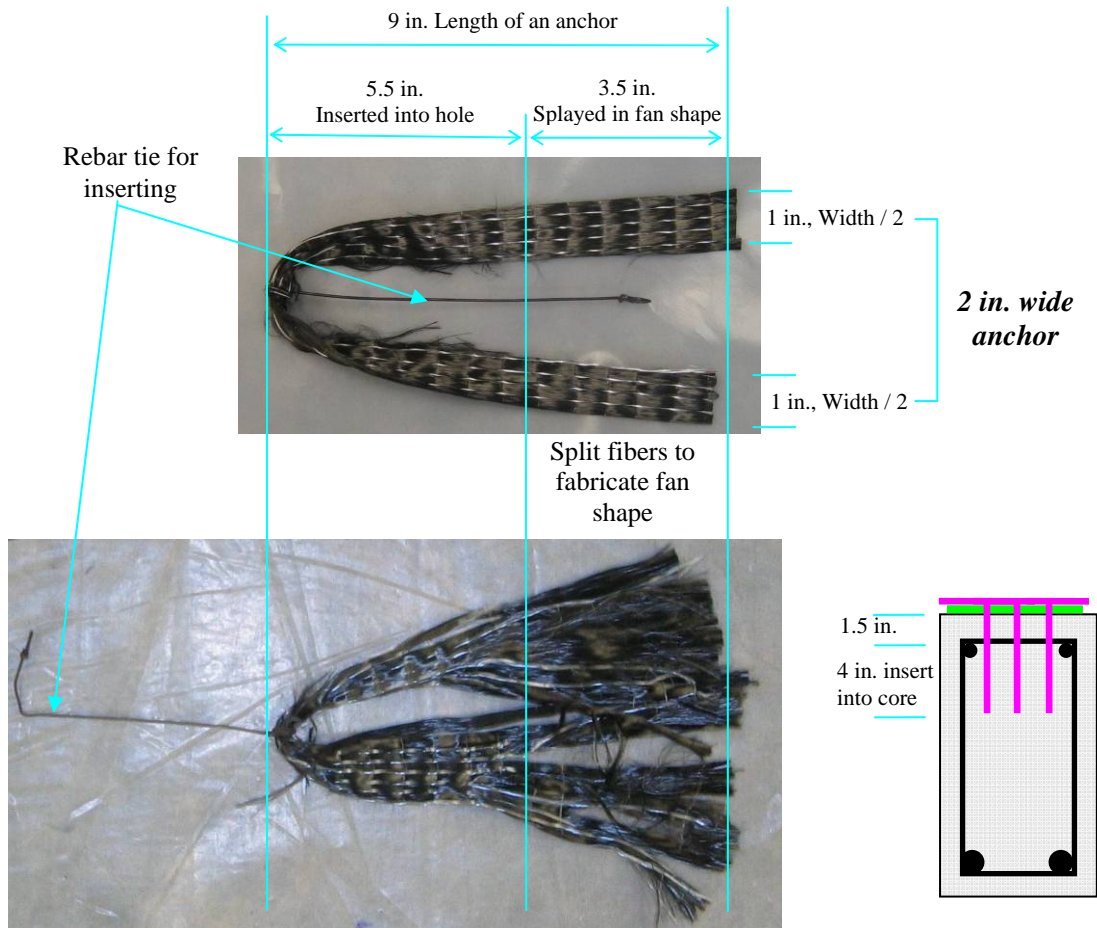
Figure 3.30   2 in. wide CFRP anchor used in A-BF-A-2S, A-BF-A-5S and A-BF-A-2N
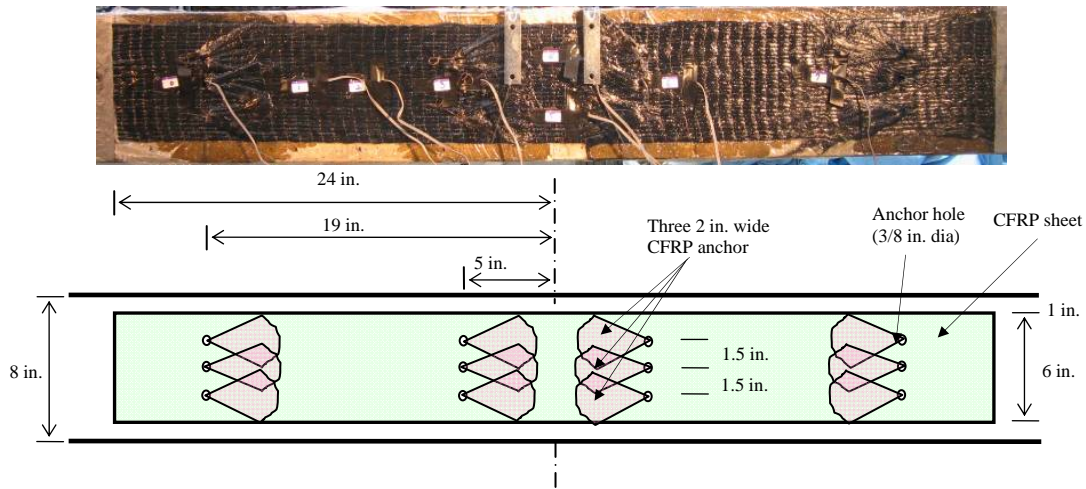
***Figure 3.31   Rehabilitation using flat bottom face with CFRP anchors
(A-BF-A-2S, A-BF-A-5S, A-BF-A-2N, A-BF-1.3A-5N)***

In A-BF-U-5S, CFRP U-wraps were installed for anchorage (Figure 3.32). Each CFRP U-wrap was the same width as the CFRP sheet, 6 in. and with a total length of 26 in. (Figure 3.14). The CFRP U-wraps were attached on the bottom of the beam over the CFRP sheet, and extended 9 in. on the each side of the beam from the bottom face of the beam. Four CFRP U-wraps were installed in a beam, two located at 2 in. from the center of specimen and the other two at 16 in. The center of CFRP U-wraps corresponded to location of the anchor holes at Type A beams with CFRP anchors.

In A-BF-A/U-6G, the CFRP U-wraps were installed on the left side of the beam, and the CFRP anchors were installed on the right side of the beam (Figure 3.33). The CFRP U-wraps and the CFRP anchors in the beam had the same geometry of CFRP materials as those in A-BF-U-5S and A-BF-A-2S. The CFRP materials in A-BF-A/U-6G were installed in an overhead direction while those in the other specimens were installed in a gravity direction. In the overhead application, fumed silica was added to the epoxy resin to increase viscosity. This specimen was tested to determine the effect of the application direction on the performance of the CFRP materials.

The dimensions of the CFRP sheet and the locations of the CFRP anchors were identical to those in a previous study, Orton (2007).

49
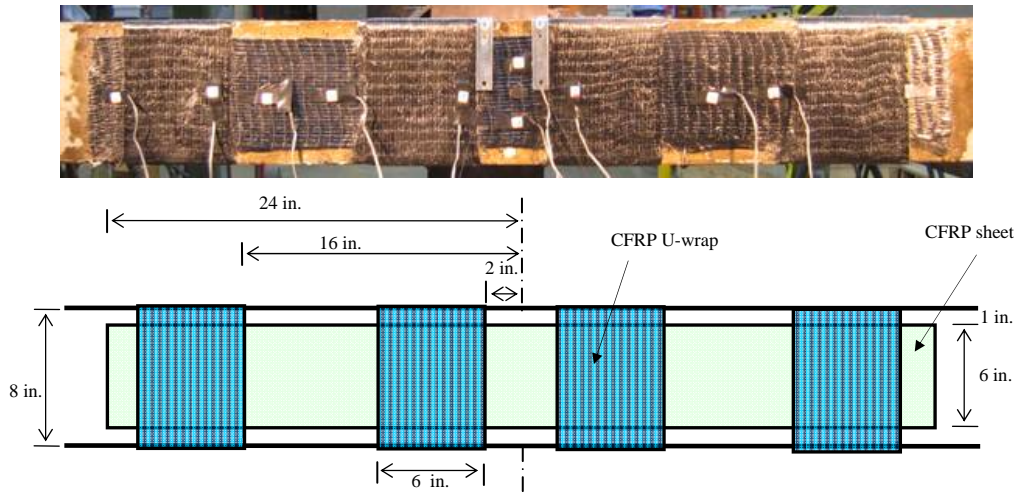
Figure 3.32   Rehabilitation using flat bottom face with CFRP U-wraps (A-BF-U-5S)
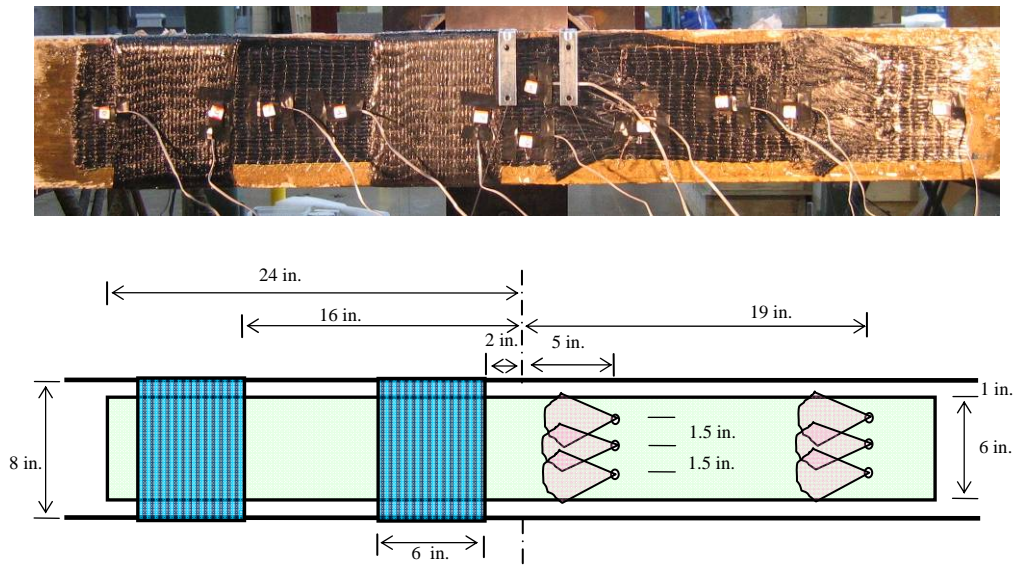
Figure 3.33   Rehabilitation using flat bottom face with CFRP U-wraps and anchors (A- BF-A/U-6G)

3.4.4.2 Rehabilitation Using Bottom Face of Beam: Height Transition Bottom Face

The beams with height transition (Type B) were tested after testing Type A beams and before testing Type C beams. Experimental investigation on Type B beams linked the tests of Type A beams (material test) to test of Type C beams (structural member test).

Type B beams were tested because a hole in a column, through which the sheets must pass to connect beams from adjacent bays, is not easily bored so that it is in the same plane as the bottom face of the beams. The geometry of such a beam column connection is shown in Figure 3.34 with the Type B test highlighted. In addition, these specimens were tested to investigate the effect of splices of CFRP sheets on the transition ramp. The CFRP sheets were applied to the bottom face of a beam (a beam sheet) up to the column face. The CFRP material passing through the hole in the column (a connection sheet) was spliced to the beam sheet on the height transition ramp.
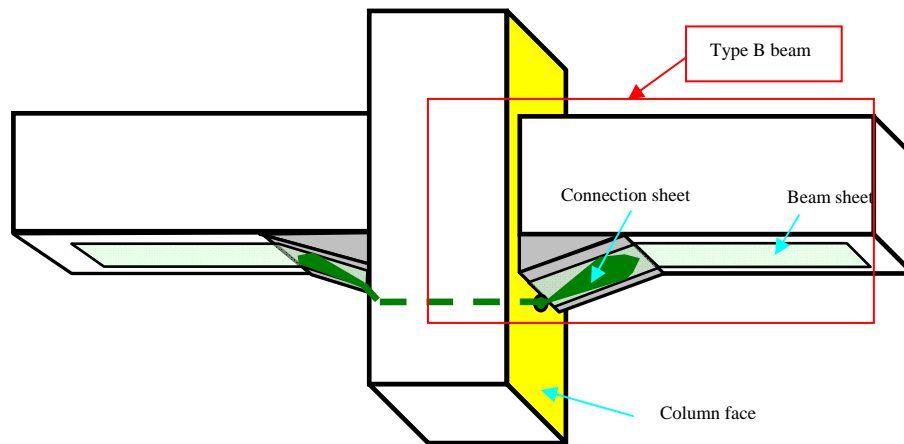
Figure 3.34   Geometry of a beam column connection with CFRP

The direction of the tension in the CFRP sheet changes at the bottom of the transition ramp. The first set of the anchors and the first U-wrap in Type B beams was located at the bottom of the transition ramp to provide equilibrium to the vertical component of tensile force occurred in the connection sheet (Figure 3.35). The anchor could provide this vertical force more effectively than U-wrap because the anchor might create a concentrated force at the point where the direction of the tension changes.

51

a. CFRP anchor

b. CFRP U-wrap
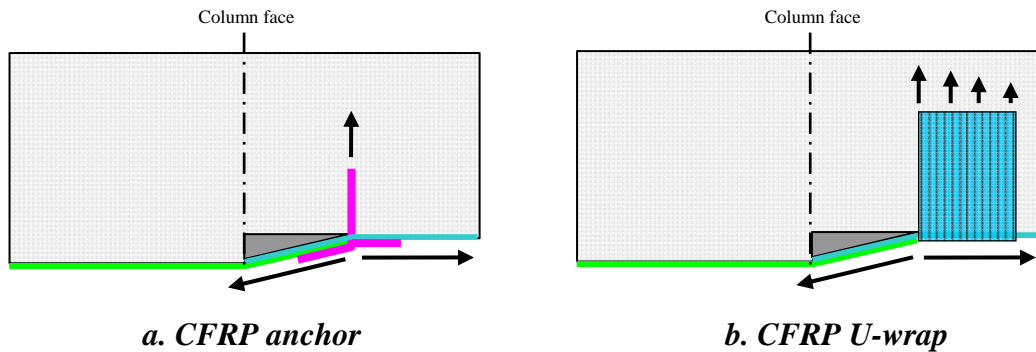
Figure 3.35   Anchorage at the bottom of the transition ramp

Layout of CFRP in Type B beams is shown in Figure 3.36 and Figure 3.37. To left side of the beams with a height transition, a connection sheet, 8 in. wide x 44 in., long was attached. Eight in. of the connection sheet was spread out in a fan shape and spliced over a beam sheet on the transition ramp. The rest of the connection sheet, 36 in., was anchored on left side of the beam. This portion of the connection sheet was anchored with CFRP U-wraps which provided more anchorage than the CFRP anchors or U-wraps on right side of the beam. The intent was to test CFRP materials on the right side of the beam only.   A beam sheet 6 in. wide x 26 in. long was attached to right side of B-BH-A-6S and a beam sheet 6 in. wide x 24 in. long was attached to right side of B-BH-U-6S. 33 % more CFRP was used in the connection sheet than the beam sheet because of a rapid shape change in the connection sheet at the column face (Orton, 2007).

In B-BH-A-6S, a set of three CFRP anchors was fabricated using the same width as the CFRP sheet, 6 in. (2 in. per anchor). The length of the anchor was 9 in. with 5.5 in. of the anchor inserted into a 3/8 in.-diameter-hole drilled into concrete, and the rest of the anchor was spread out in a fan shape on the CFRP sheet. The first set of the anchors at the bottom of the transition ramp was spread in two directions to provide the vertical force effectively. The anchor was same as that used in Type A beams (Figure 3.30). Six anchors were installed on the beams as indicated in Figure 3.36.

52
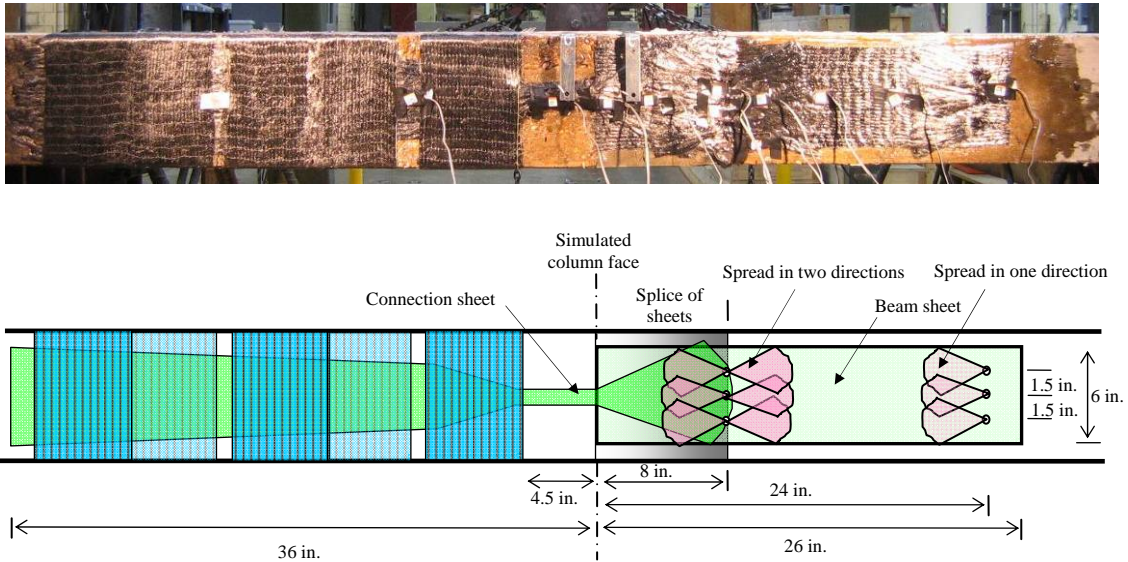
Figure 3.36   Rehabilitation using height transition bottom face with CFRP anchors (B- BH-A-6S)

In B-BH-U-6S, CFRP U-wraps were installed to anchor the beam sheet (Figure 3.37). The CFRP U-wrap was fabricated with the same width as the CFRP sheet, 6 in. and with a total length of 26 in. The CFRP U-wraps were attached on the bottom of the beam over the CFRP sheet, and extended 9 in. on the each side of the beam from the bottom face of the beam. Two CFRP U-wraps were installed in right side of the beam, and one of them was located at 8 in. from the center of specimen (at the bottom of the height transition ramp) and the other was located at 15 in.
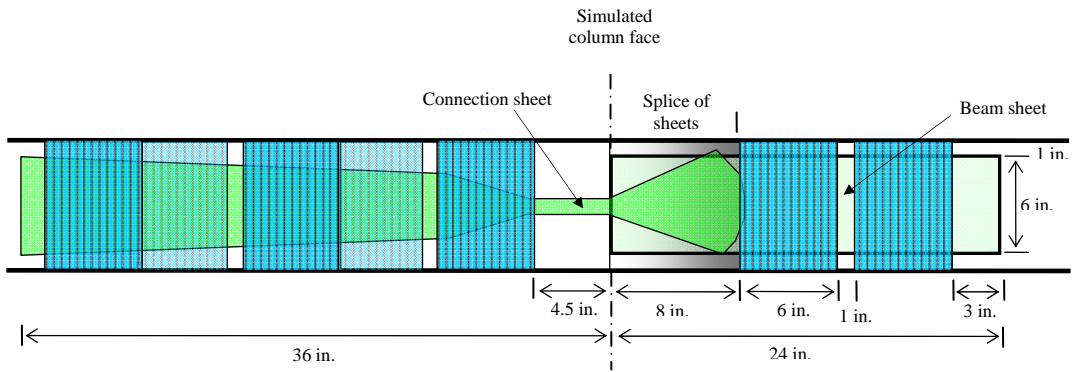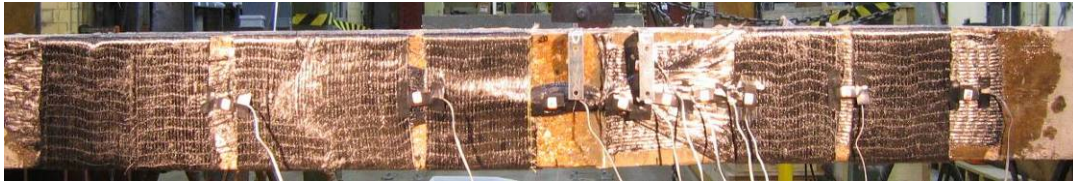
Figure 3.37   Rehabilitation using height transition bottom face with CFRP U-wraps (B- BH-U-6S)

3.4.4.3 Rehabilitation Using Side Faces of Beam

Two Type A beams (A-S-A-6G and A-S-AU-2S) were tested to investigate rehabilitation method using the side faces of the beams and column at a connection. Layout of CFRP in the beams rehabilitated on side faces is shown in Figure 3.38 and Figure 3.39.

For the beam rehabilitated on side faces, CFRP materials were installed on both sides. Two CFRP sheets 2.75 in. wide x 66 in. long were placed on top of one another on each side. The CFRP sheets in A-S-A-6G were anchored by the CFRP anchors only while those in A-S-AU-2S were anchored by a combination of the CFRP anchors and U-wraps. The geometry of CFRP in A-S-A-6G and A-S-AU-2S were the same except CFRP U-wraps were added to A-S-AU-2S.

The CFRP anchors were made using the same material contained in the two CFRP sheets (5.5 in.) that were attached to the beams. The length of the anchor was 9.5 in. with 4 in. of the anchor inserted in a 5/8 in. diameter hole drilled into the concrete, and the rest of anchor was spread out in a fan shape on the CFRP sheet for A-S-A-6G and on the CFRP U-wrap for A-S-AU-2S. Eight anchors (four on each side) were installed in the beam as shown in Figure 3.38 and Figure 3.39.

The CFRP U-wraps in A-S-AU-2S were made of the same 6 in. width of CFRP sheet with a total length of 26 in. Four CFRP U-wraps were attached to the beam over the CFRP sheet as shown in Figure 3.39.

55
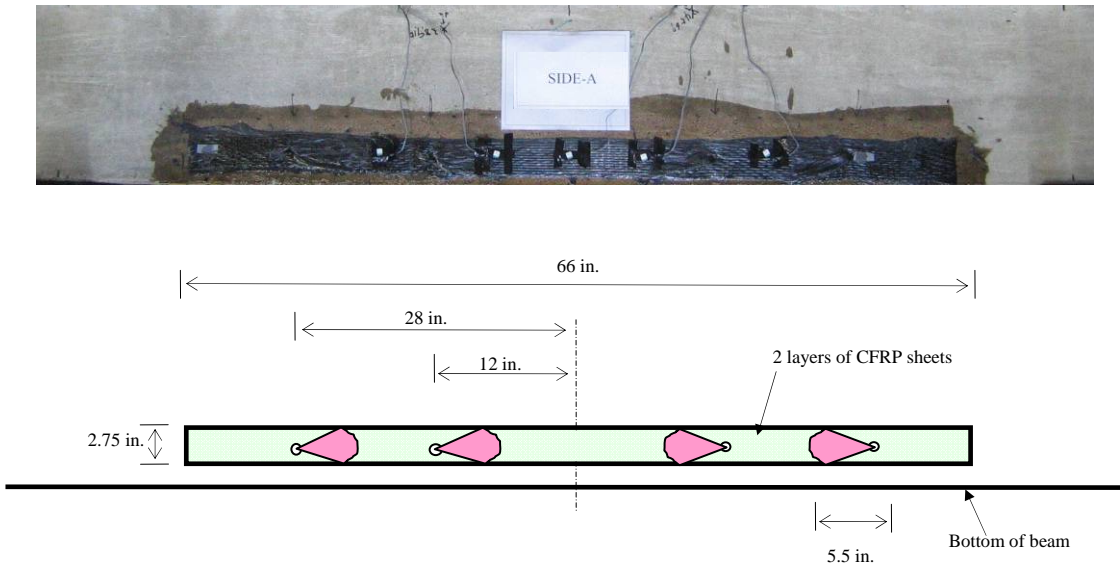
Figure 3.38   Rehabilitation using side faces with CFRP anchors

(A-S-A-6G)
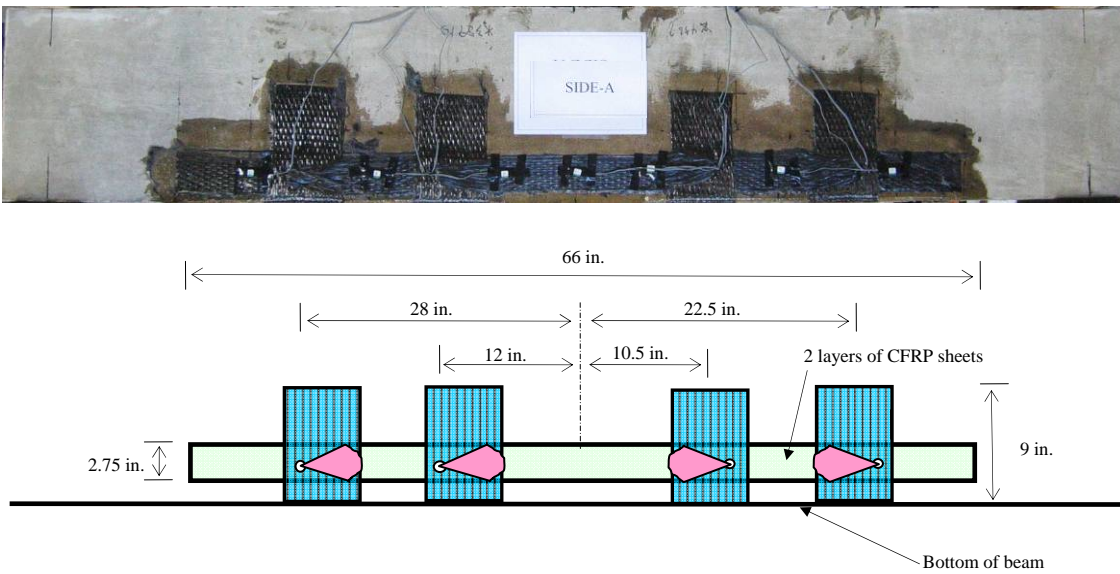
Figure 3.39   Rehabilitation using side faces with CFRP anchors and U-wraps

(A-S-AU-2S)

3.4.4.4 Rehabilitation of Beams with Column

Beams adjacent to a column (Type C) were tested to investigate the practical application of the rehabilitation methods using CFRP sheets, anchors and U-wraps. The geometry of a beam column connection and the rehabilitation represented by Type C beams is shown in Figure 3.40. Type C beams were symmetrical on both sides of the column. The CFRP beam sheets and connection sheet were spliced on the transition ramps. Strains in the bottom reinforcement were monitored to evaluate transfer of stress from the CFRP sheets to the bottom reinforcement.
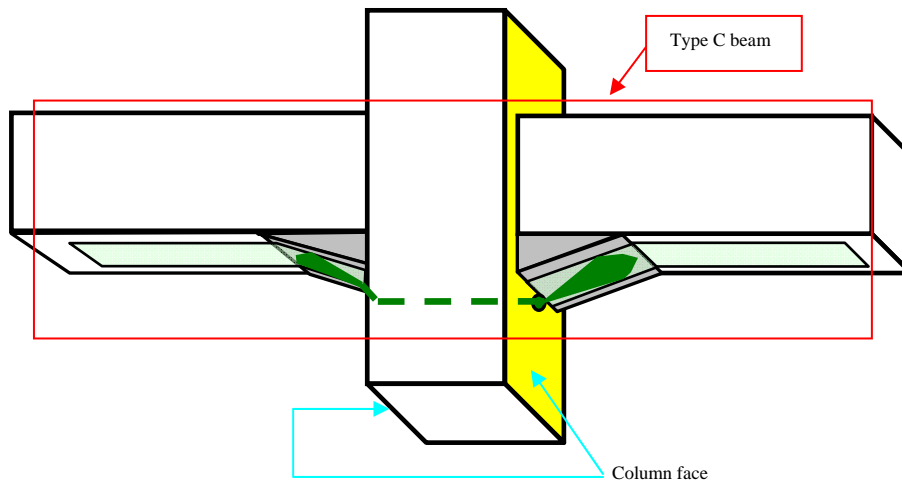
Figure 3.40   Geometry of a beam column connection with CFRP

Layout of CFRP in Type C beams is shown in Figure 3.41 to Figure 3.43. In the column portion and transition ramps of Type C beams, a connection sheet, 6 in. wide x 25 in., long was attached. 8 in. of the connection sheet was spread out in fan shape and spliced over a beam sheet on the height transition ramp in each side. The rest of the connection sheet, 9 in., passed through the column hole. A beam sheet 4.5 in. wide x 26 in. long was attached to each side of C-BC-A-6G-01, a beam sheet 4.5 in. wide x 15 in. long was attached to each side of C-BC-A-6G-02 and a beam sheet 4.5 in. wide x 24 in. long was attached to each side of C-BC-U-6G. 33 % more CFRP was used in the connection sheet than the beam sheet because a rapid change of the shape in the

57

connection sheet at the column faces (Orton, 2007). The beam sheets were designed to develop 56 % more tensile strength than the bottom reinforcement (2-#3). The calculation of the tensile capacity of the beam sheet and the bottom reinforcement are as follows:

$$T_b = 1.25 f_y A_s = 1.25 \times 60{,}000 \times (2 \times 0.11) = 16{,}500 \, lb \qquad \textbf{\textit{Equation 3-1}}$$

$$T_f = f_{fu} w_f t_f = 143{,}000 \times 4.5 \times 0.04 = 25{,}740 \, lb \qquad \textbf{\textit{Equation 3-2}}$$

$$T_f / T_b = 1.56 \qquad \textbf{\textit{Equation 3-3}}$$

T_b: *expected tensile strength of the bottom reinforcement, lb*

T_f: *tensile strength of CFRP sheet, lb*

f_y : yield strength of reinforcement, psi

$f_c^{'}$: compressive strength of concrete, psi

A_s: *area of longitudinal bars, in²*

f_{fu}: *tensile strength of CFRP, psi*

t_f: *thickness of CFRP sheet, in.*

w_f: *width of CFRP beam sheet, in.*

C-BC-A-6G-01 was designed based on a specimen studied in a previous study by Orton (2007). After C-BC-A-6G-01 was tested, length of the beam sheet was reduced based on the development length of #3 bottom reinforcement and then, fabricated C-BC-A-6G-02.

In C-BC-A-6G-01 and C-BC-A-6G-02, a set of two CFRP anchors was fabricated using the same width as the connection sheet, 6 in. (3 in. per anchor). The length of the anchor was 9 in. with 5.5 in. of the anchor inserted into a 1/2 in. diameter-hole drilled into concrete, and the rest of the anchor was spread out in a fan shape on the CFRP sheet. The location of the second set of anchors from the column face in C-BC-A-6G-01 and C-BC-A-6G-02 was different because length of CFRP sheet was different. The layout of CFRP anchors in those beams is shown in Figure 3.41 and Figure 3.42.
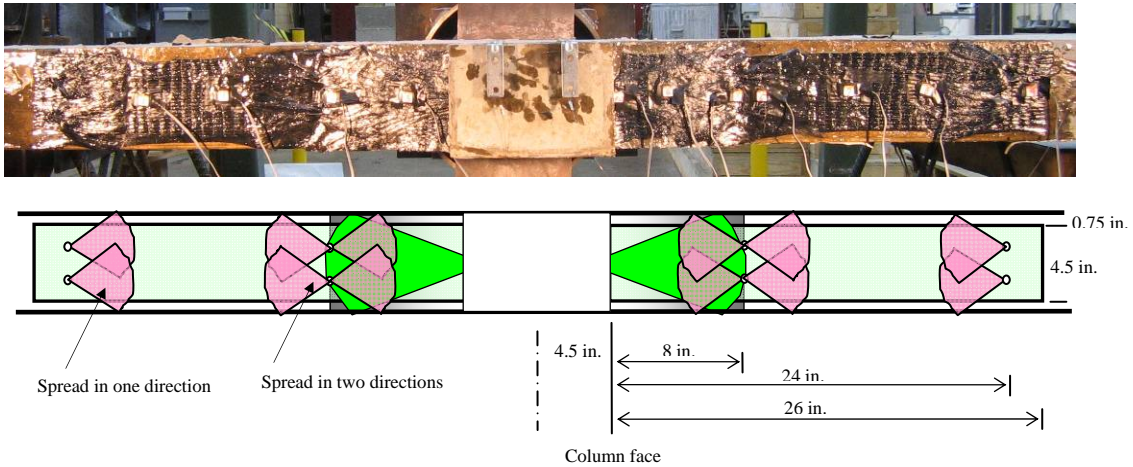
***Figure 3.41   Rehabilitation of beams with column using CFRP anchors
(C-BC-A-6G-01)***
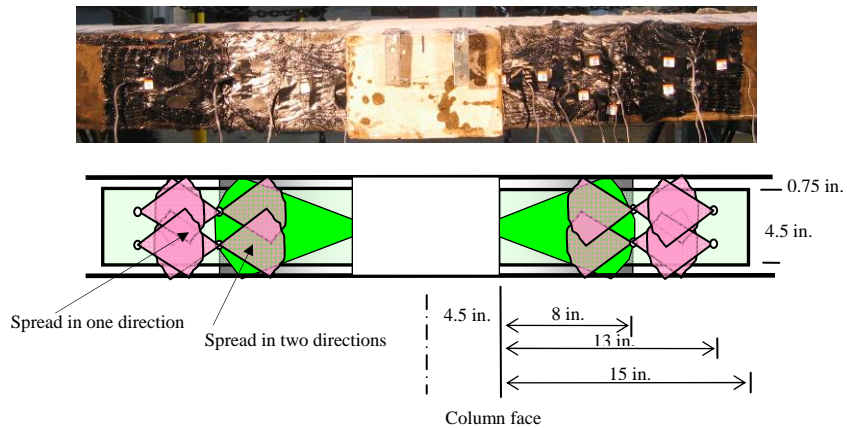
***Figure 3.42   Rehabilitation of beams with column using CFRP anchors
(C-BC-A-6G-02)***

In C-BC-U-6G, CFRP U-wraps were installed to anchor the beam sheet (Figure 3.43). The CFRP U-wrap was fabricated with the same width as the CFRP sheet, 4.5 in. and with a total length of 18 in. The CFRP U-wraps were attached on the bottom of the beam over the CFRP sheet, and extended 6 in. on the each side of the beam from the

59

bottom face of the beam (Figure 3.14). Two CFRP U-wraps were installed in each side of the beam, and one of them was located at 8 in. from the center of specimen (at the bottom of the transition ramp) and the other was located at 16.5 in.
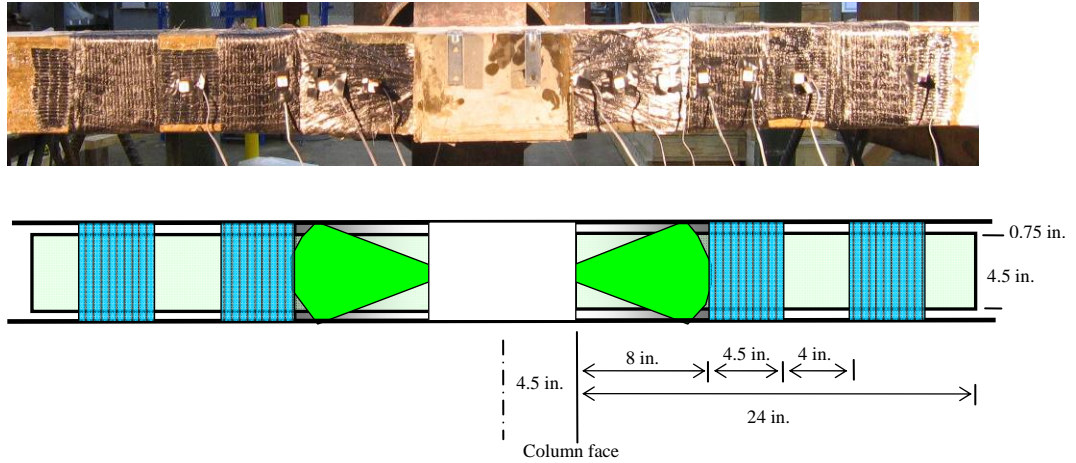
Figure 3.43   Rehabilitation of beams with column using CFRP U-wraps
(C-BC-U-6G)

3.5 TEST SETUP AND INSTRUMENTS

The overall test setup is shown below in Figure 3.44. The test setup was originally designed by Mitchell (2005) to test bridge barriers and then, modified to test beams for this study. A dynamic load with a 928 kg pendulum mass was applied to the middle of the beam, which was placed on its side for testing. Drop heights of the pendulum mass were varied with respect to the capacity of the specimens. The drop height was based on test results of a pilot test beam that had one #6 continuous bar at the bottom of the beam.

As shown in Figure 3.45, a test beam was supported horizontally and vertically at the ends of beam (main supports) and vertically at quarter points of beam from the ends (supplementary supports). The spacing of the main supports was 16 ft and that of the supplementary supports was 8 ft. At each support, two Teflon sheets were placed one over another underneath test beam to eliminate effect of friction in the direction of the applied load. A-BF-A-2S, A-BF-A-2N and A-S-AU-2S were tested without the supplementary supports.

Load cells were installed in front of the pendulum mass (200 kip capacity load cell) and at both horizontal supports (100 kip capacity load cell) to measure an applied load and reactions. Deflection at the middle of the specimen was measured with two linear motion transducers. Data acquisition rate of the tests was selected based on the natural frequency of the test beams and the duration of response. The natural frequency of the test specimen was about 20 Hz and the response duration in the pilot test was about 0.1 sec. The data acquisition rate selected was 2,000 Hz which was hundred times more than the natural frequency of the specimen and enable to plot 200 points during the response duration. Resolution of the instruments used in the tests was verified according to the data acquisition rate before the tests.

A normalization method using sinusoidal curve was used to normalize measured applied load and reactions caused by impact of the pendulum. The normalization method is introduced in Section 3.6.1.1 where the test results of the first specimen are presented.

61

Strain gages were installed on the CFRP materials and were distributed horizontally to measure development of tensile strains along the CFRP sheets. The layout of CFRP strain gages for each test beam is shown in the next section. Strain gages were also installed on the longitudinal steel reinforcement of the test beams. The layout of reinforcement strain gages for each type of test beam is shown in Figure 3.46.

The response duration of the test specimens to the pendulum mass impact was between 0.02 sec and 0.2 sec. It was about 0.1 sec if the specimens did not fail. Sasani (2007) reported that the response duration of structural members in an actual reinforced concrete building was about 0.1 sec when a column was removed due to explosion. Therefore, the test setup created similar loading rate which an actual structural member may experience in a case of a column removal.

Pendulum mass

Load cell

Linear motion
transducer

928 kg

Drop height of
pendulum mass

Linear motion
transducers

12 in.

CFRP on sides

Pendulum

Section at point of
impact

16 in.

CFRP on bottom

Pendulum
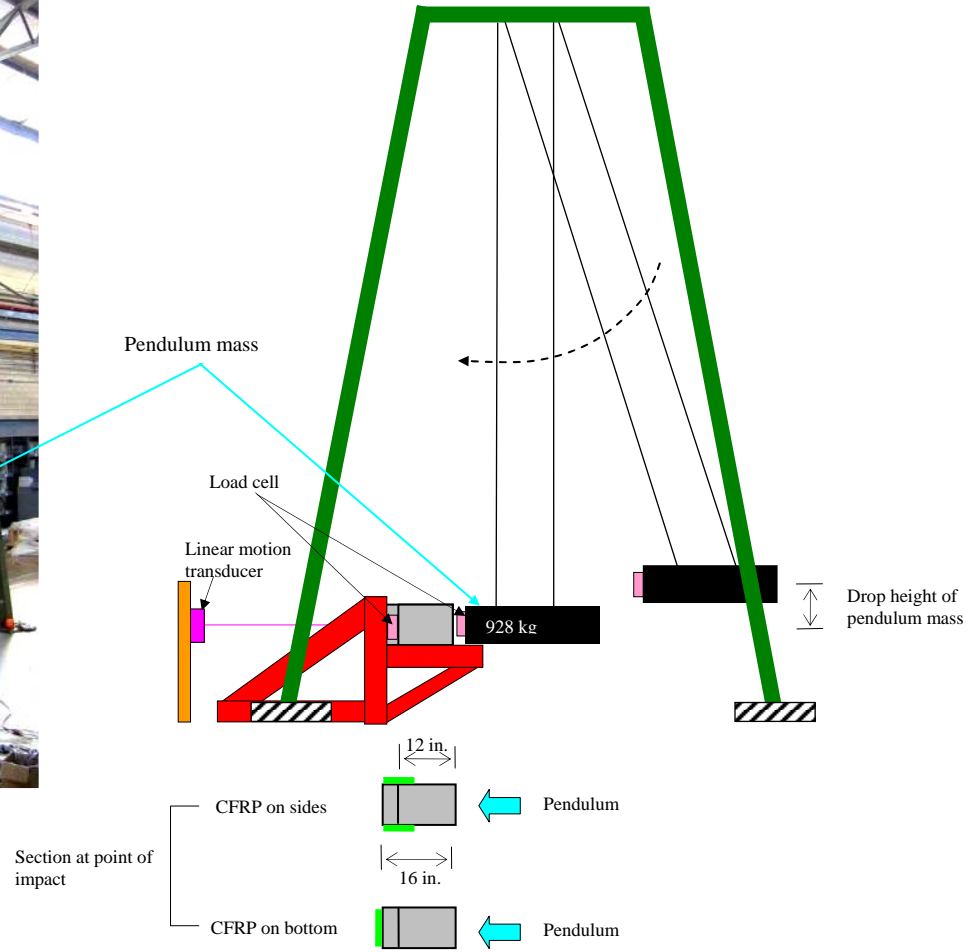
Figure 3.44   Test setup 1

Figure 3.45   Test setup 2

East Type A West

Reinforcement, GR60
2-#3 top
2-#6 bottom

15 in.
27 in.
39 in.

18 in.

East Type B West

Reinforcement, GR60
2-#3 top
2-#6 bottom

15 in.
27 in.
39 in.

East Type C West

Reinforcement, GR60
2-#3 top
2-#3 bottom

15 in.
27 in.
39 in.
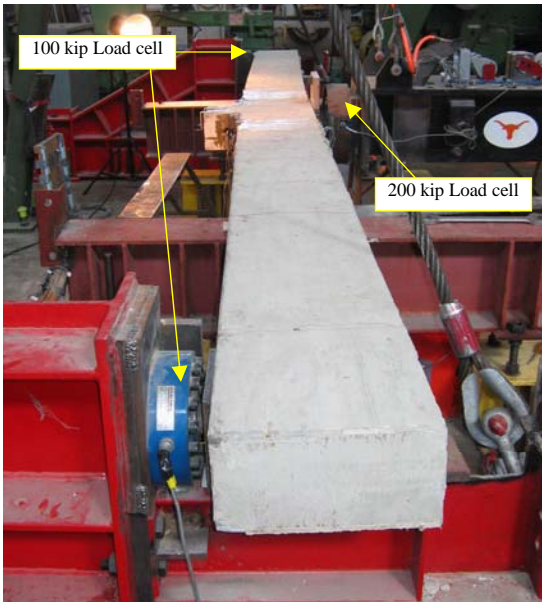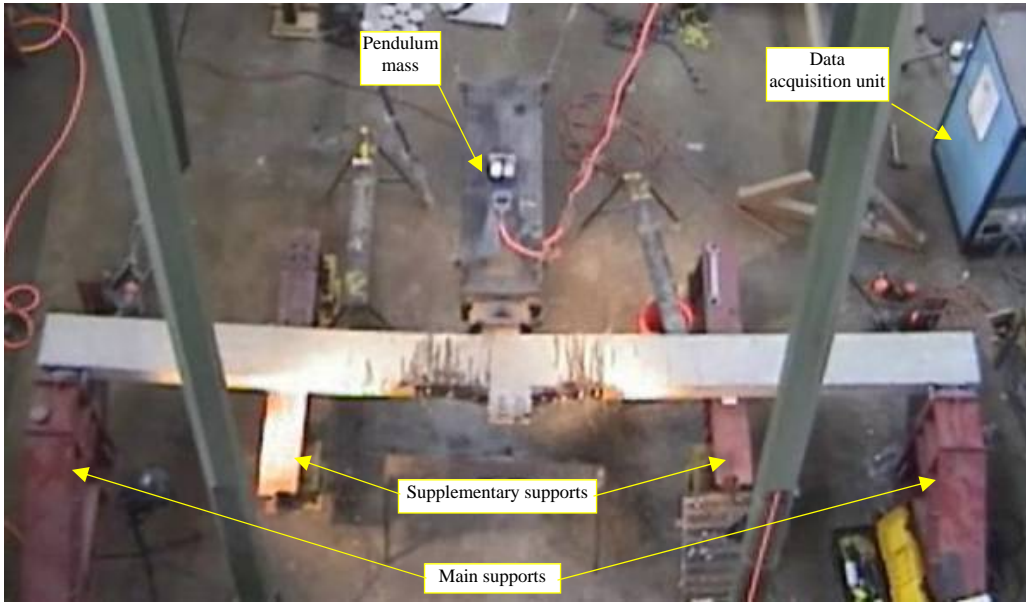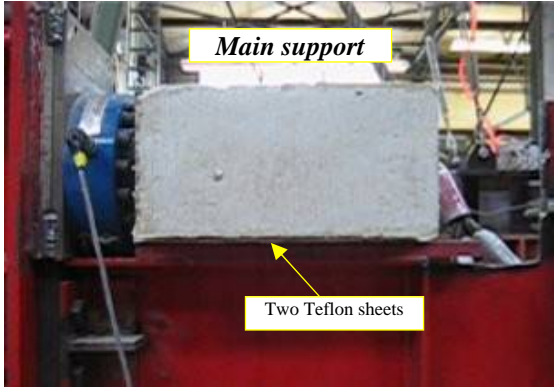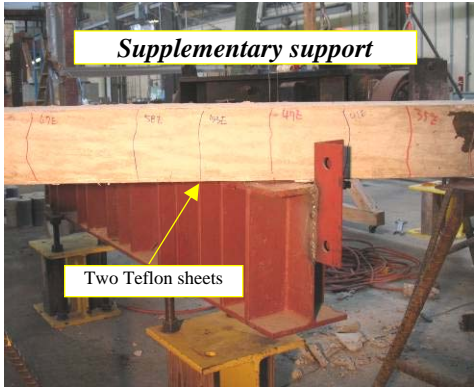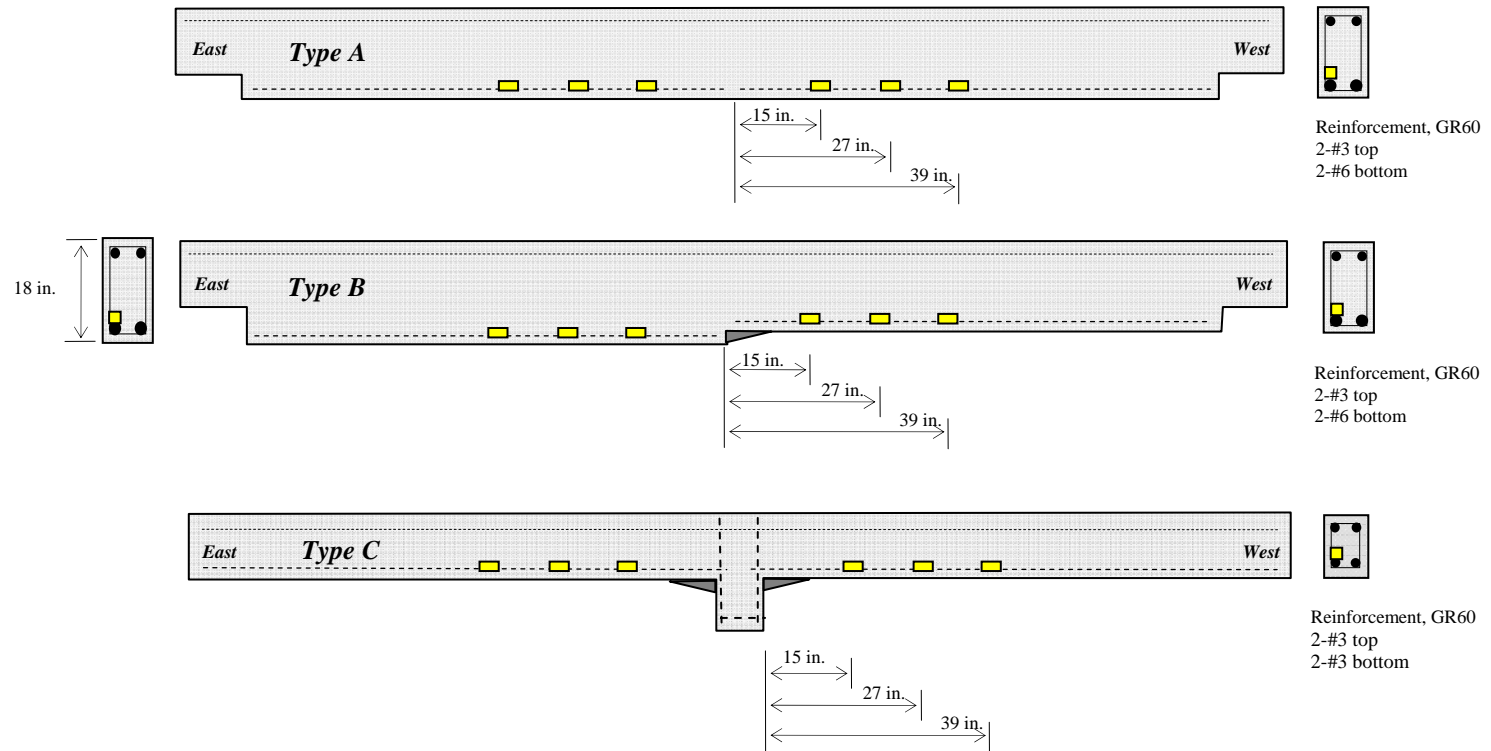
Figure 3.46   Layout of bar strain gages

3.6 **DYNAMIC TEST RESULTS AND COMPARISONS**

3.6.1 Rehabilitation Using Bottom Face of Beam: Flat Bottom Face

Test results of the rehabilitation discussed in Section 3.4.4.1 are presented in this section. Type A beams were tested and expected failure mode was fracture of the CFRP sheet. Failure mode, applied load, reactions and strains in the CFRP and the reinforcement are presented.

Multiple impacts were applied to A-BF-A-5S and A-BF-U-5S while only one impact was applied to the other beams with CFRP on the flat bottom face. In this section, the test results from the impact that failed these two beams are discussed. Additional test data for other loading are presented in Appendix A.

3.6.1.1 A-BF-N-5S

A-BF-N-5S was a Type A beam and CFRP was applied to the flat bottom face. This beam had 1 layer of the CFRP sheet and no additional anchorage. The surface of the bottom face was sand-blasted and the measured compressive strength of the concrete was 5,000 psi. Configuration of the beam is shown in Figure 3.47. The failure of A-BF-N-5S was delamination of the CFRP sheet form the concrete surface because no additional anchorage existed in this beam (Figure 3.48). The ultimate tensile strength of the CFRP was not realized because delamination occurred before the CFRP reached its capacity.
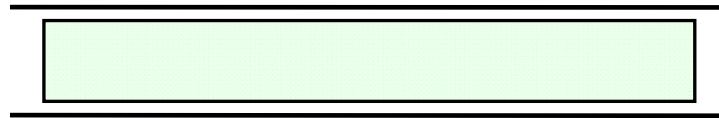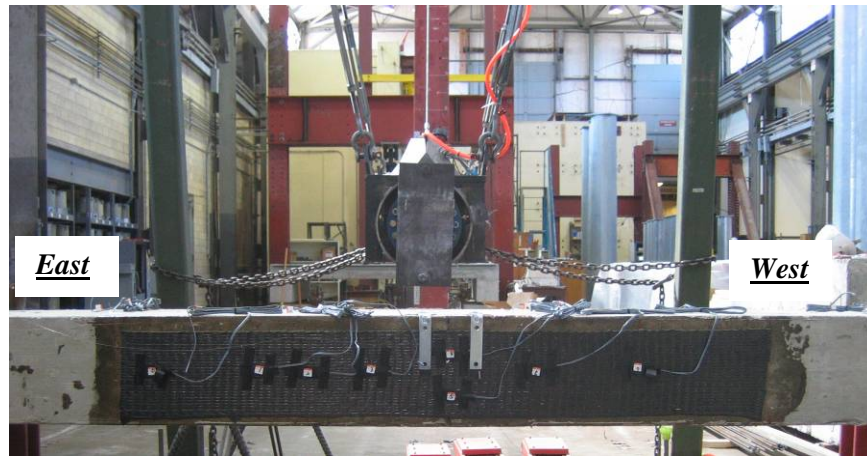
Figure 3.47   Configuration of A-BF-N-5S
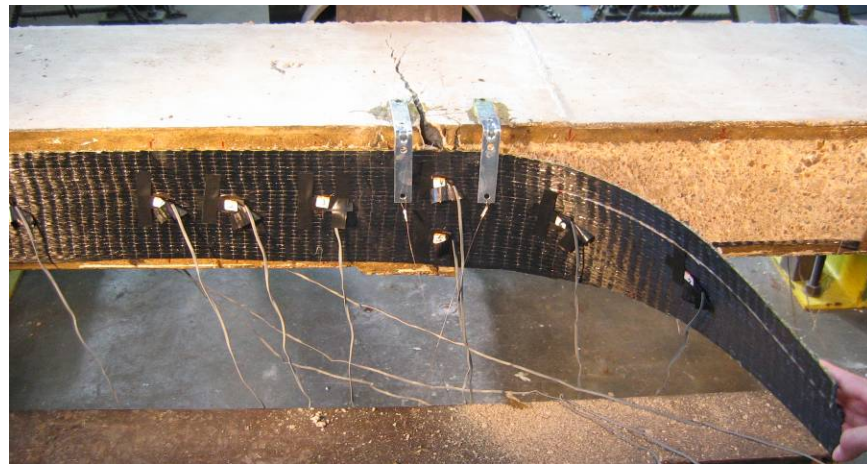
Figure 3.48   Failure of A-BF-N-5S, delamination

The measured applied load and reactions plotted in time domain are shown in Figure 3.49. Drop height of the pendulum mass in A-BF-N-5S was 3 in. and the duration of event was 0.026 sec. The duration of event was the duration from the time of contact of the pendulum mass with the beam to the time when the load cell in the pendulum mass and in the supports returned to zero. There was a delay in the response of the support

load cells after the time of the contact of the pendulum mass because the bearing locations of the beam did not contact perfectly with the support load cells. The delay was about 0.01 sec in the tests but the theoretical duration for the wave due to the impact reaching the supports, was about 0.0005 sec. Therefore, the delay was mainly due to the imperfect contact between the specimen and the supports. This delay was observed in all the other tests. The peak applied load was 36.8 kip and the peak reaction was 8.6 kip at the east support. Impulse of the applied load was 0.18 kip-sec while that of sum of the reactions was 0.11 kip-sec.
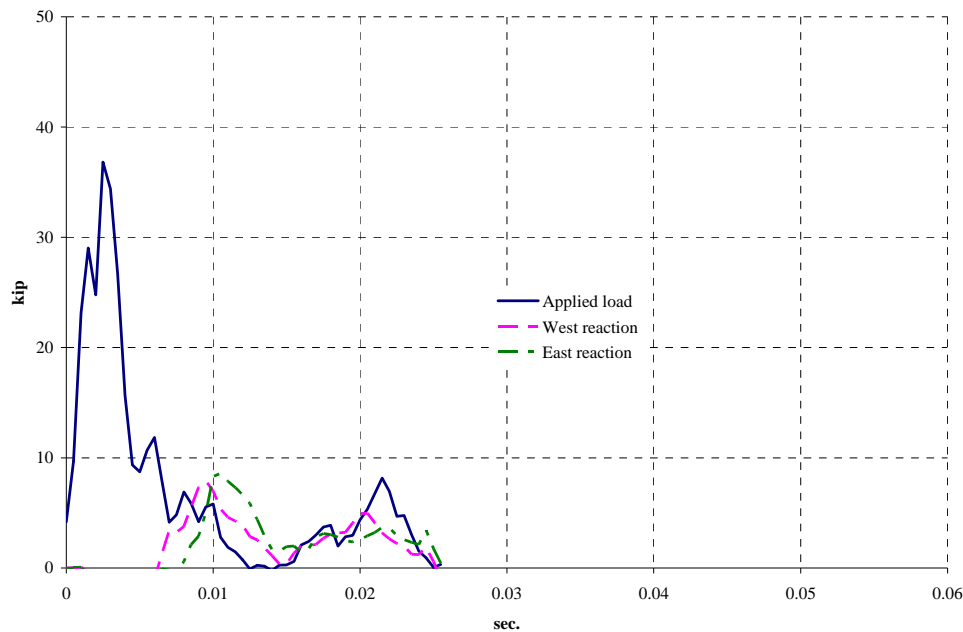
Figure 3.49   Measured applied load and reactions, A-BF-N-5S

The normalization of the measured load data was needed because the measured loads were not easy to compare with calculated static strength of the specimens. A half sine curve was selected to normalize the measured applied load and reactions because the load and displacement responses of a wood beam tested in the same pendulum test setup exhibited a response similar to a half sine curve as shown as Figure 3.50 (Orozco, 2006).

68

The wood beam behaved elastically during the impact test at a 6 in. drop height of the pendulum mass. The properties of the wood beam are shown in Table 3.3.

Table 3.3   Properties of the wood beam

Length	Total Weight	Calculated Stiffness (mid-span deflection vs center point loading)	Calculated Natural Frequency (mid-span deflection vs center point loading)
17 ft	347 lb	54,240 lb/ft	16 Hz

In Figure 3.50, the applied load measured in the pendulum load cell and normalized applied load using the half sine curve are plotted. The half period of the sine curve was equal to the response duration indicated by the pendulum load cell and the area under the curve was equal to the impulse of the measured applied load. The mid-span deflection measured by the linear motion transducer multiplied by calculated stiffness is also plotted in Figure 3.50. As shown in Figure 3.50, the half sine curve reflects response of the measured applied load and displacement. In Figure 3.51, sum of the measured reactions and normalized sum of the reactions are plotted. The normalized curve for sum of the reactions also reflects response of the measured reactions.
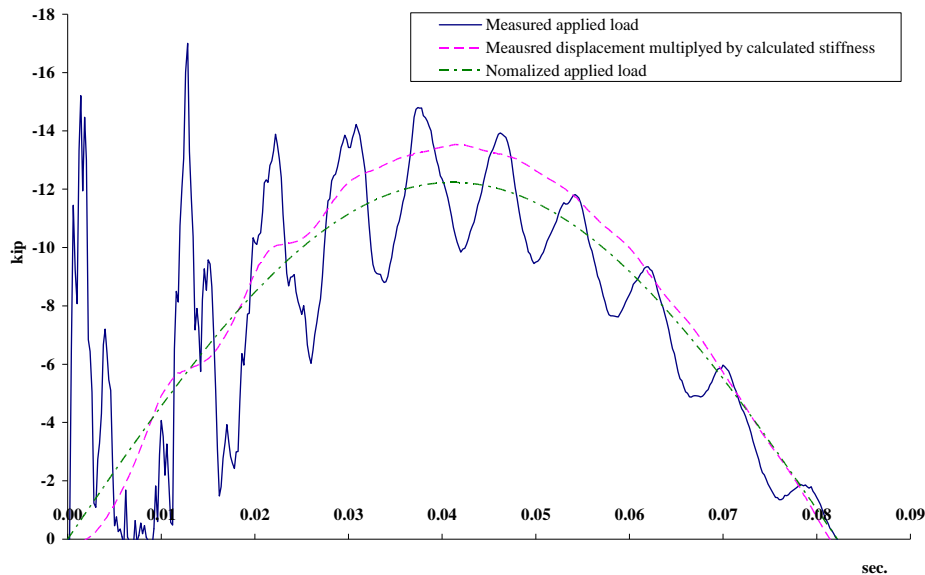
Figure 3.50   Measured and normalized applied load, wood beam test

69
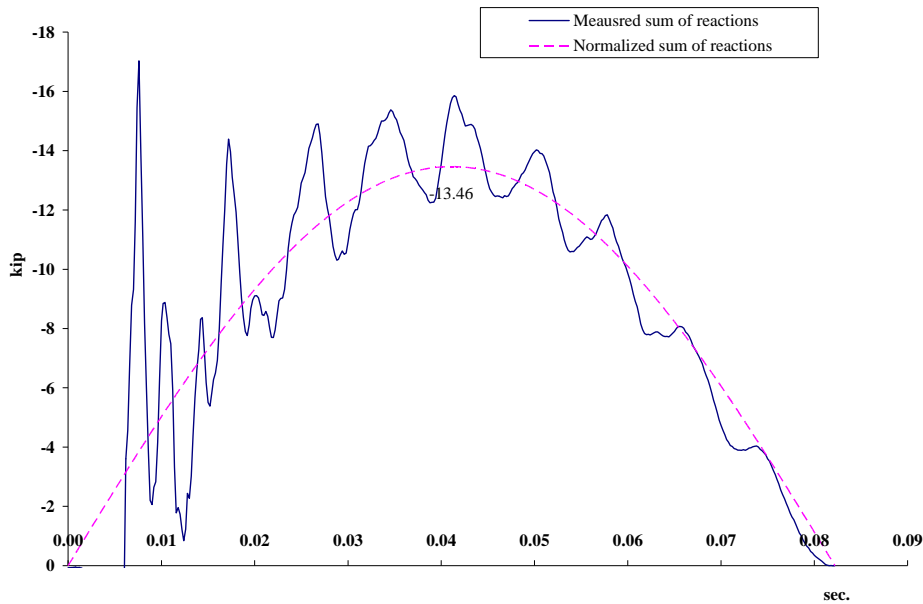
Figure 3.51   Measured and normalized sum of reactions, wood beam test

Because of difference in duration of response between the pendulum and reaction load cells, the duration for normalization (half period of the sine curve) needed to be selected. The duration of event (the duration from the time of contact of the pendulum mass with the beam to the time when the load cell in the pendulum mass and in the supports returned to zero) was selected for the normalization because the peak value in normalized curve reflects impulse and through the use of the same period sine curve, impulse of the applied load and sum of the reactions can be compared directly using the normalized curves.

The normalized curves of the applied load and sum of the reactions of A-BF-N-5S are shown in Figure 3.52. The peak normalized applied load was 11.3 kip and sum of the reactions was 6.9 kip. The peak normalized sum of reaction was 61 % of the peak normalized applied load. The ratio of the peak normalized sum of the reactions to applied load was same as the ratio of the impulse of sum of the reactions to that of the applied load because the normalized load was based on the measured impulse. This equivalence of the ratios was observed in all the other tests because the same normalization method

70

was used. The calculated strength of A-BF-N-5S corresponding to the delamination of the CFRP was 4.4 kip.
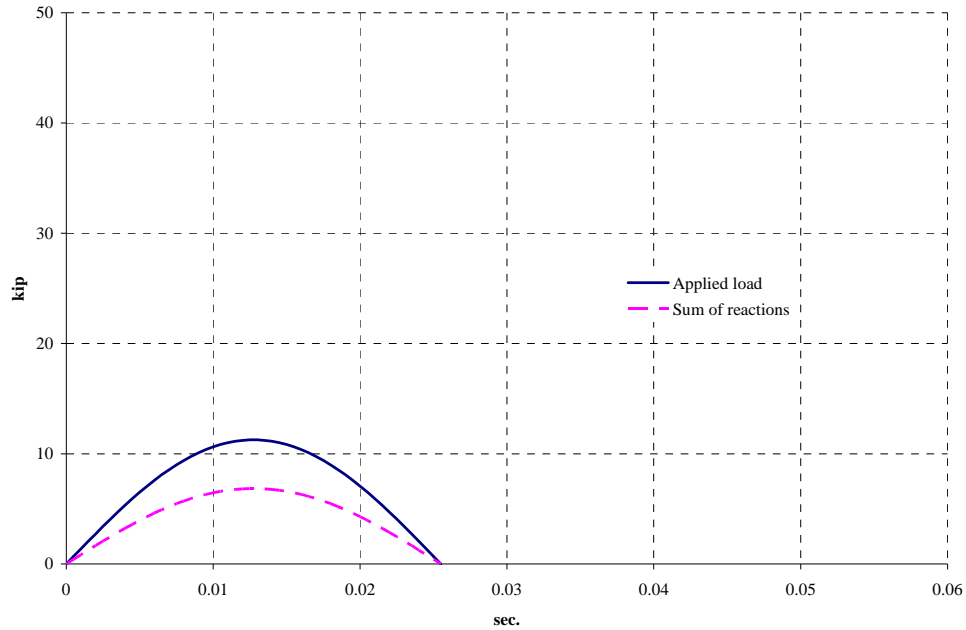
Figure 3.52   Normalized applied load and sum of reactions, A-BF-N-5S

The location of the strain gages installed in A-BF-N-5S and the maximum measured strain in each gage are shown in Figure 3.53. The maximum strain measured in A-BF-N-5S was 0.0042 at gage 4 and was 42 % of the ultimate tensile strain of the CFRP. From the horizontal distribution of strains in the CFRP sheet, the part of the CFRP sheet that developed the highest strain was where debonding failure occurred, the west side of beam. Strain rate of CFRP (maximum strain divided by the time to reach the strain) in this beam was 0.182 /sec. The strain response of gages 4, 6 and 7 in time domain is shown in Figure 3.54. These gages were installed where delamination occurred. Although the values of peak strain in these gages were similar, the gage close to the loading point, at the center of the beam, was strained earlier than the gages away from the loading point. This variation reflected propagation of the delamination from the center of the beam to the end of the CFRP sheet.

71

The location of steel strain gages from the center of the beam and maximum measured strain are also shown in Figure 3.53. The maximum strain measured in the #6 bars in A-BF-N-5S was 0.0006 which was about 1/3 of yield of the steel reinforcement.
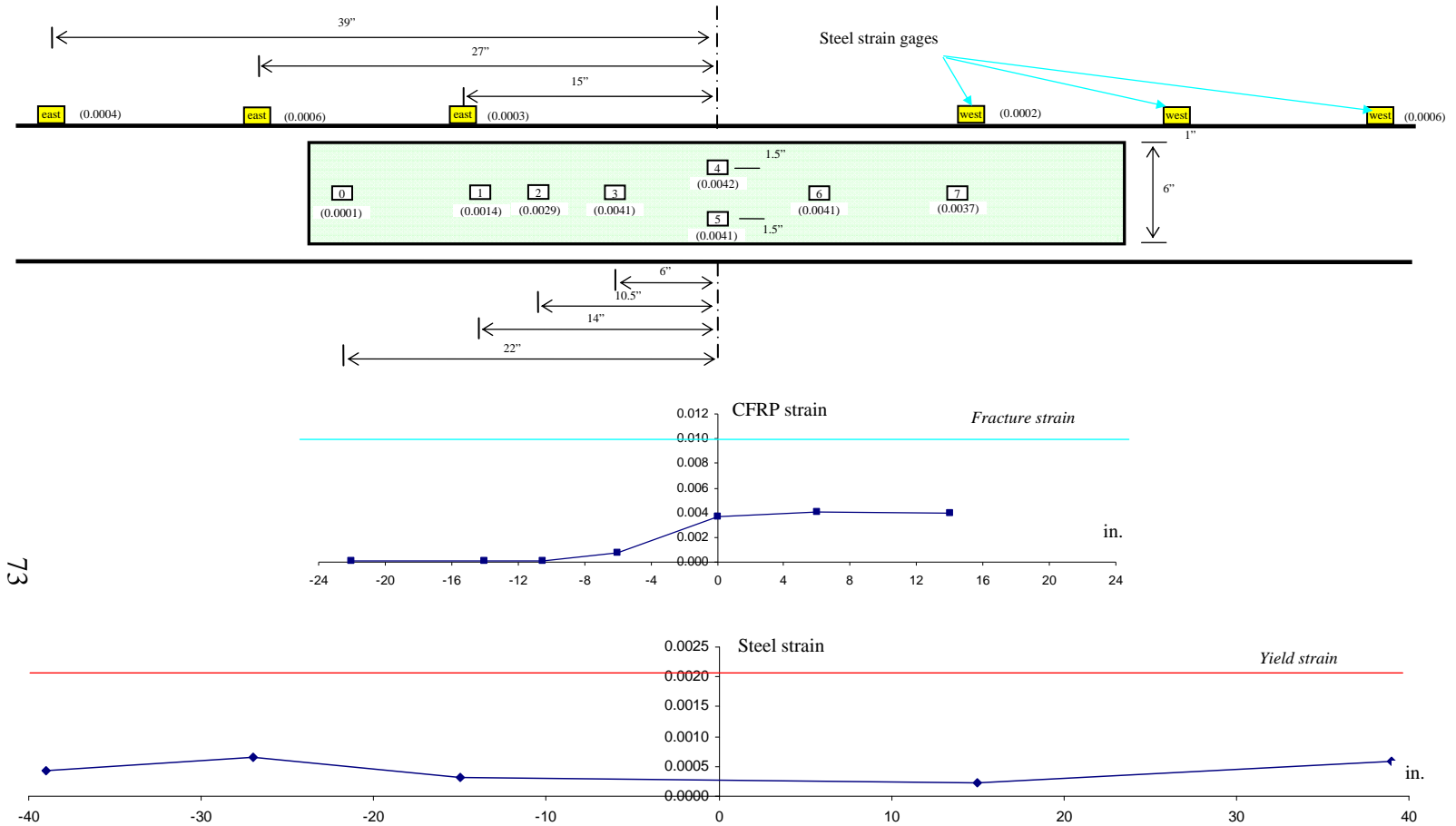
Figure 3.53   Location of strain gages and distribution of strain in CFRP and bar, A-BF-N-5S

73
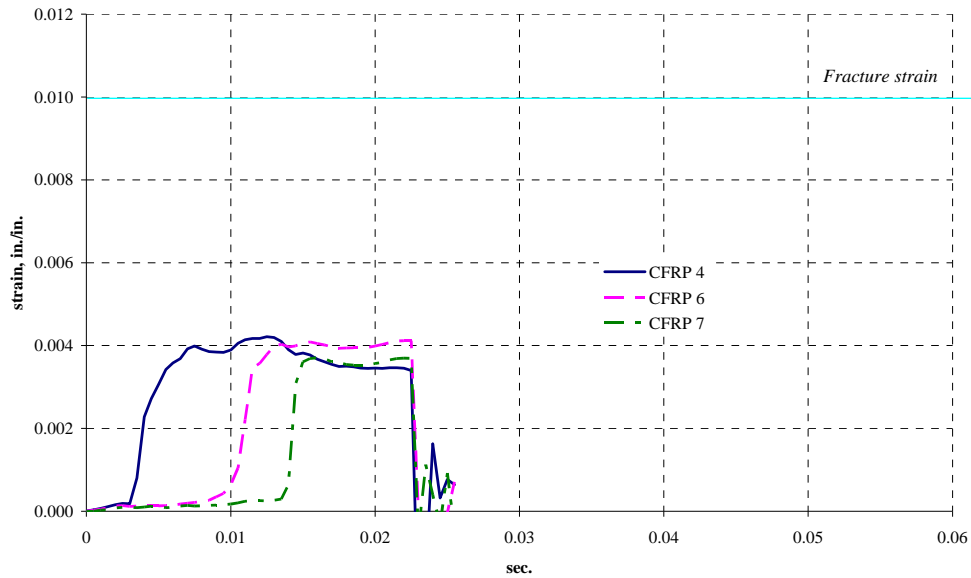
Figure 3.54   CFRP strain, A-BF-N-5S

3.6.1.2   A-BF-A-2S

A-BF-A-2S was a Type A beam with one layer of CFRP on the flat bottom face and CFRP anchors. The bottom face was sand-blasted. The measured compressive strength of the concrete was 2,000 psi. Configuration of the beam is shown in Figure 3.55. The failure mode of A-BF-A-2S was fracture of the CFRP sheet in the center of the beam (Figure 3.56).

The measured applied load and reactions are shown in Figure 3.57. Drop height of the pendulum mass in A-BF-A-2S was 3 in. and the duration of event was 0.033 sec. The peak applied load was 40.0 kip and the peak reaction was 9.4 kip at the west support. Impulse of the applied load was 0.21 kip-sec while that of sum of the reactions was 0.19 kip-sec.

The normalized applied load and sum of the reaction responses are shown in Figure 3.58.   The peak normalized applied load was 10.2 kip and sum of the reactions

74

was 8.9 kip (87 % of the peak normalized applied load). The calculated static strength of A-BF-A-2S was 10.5 kip and the peak normalized applied load was 97 % of the static strength.
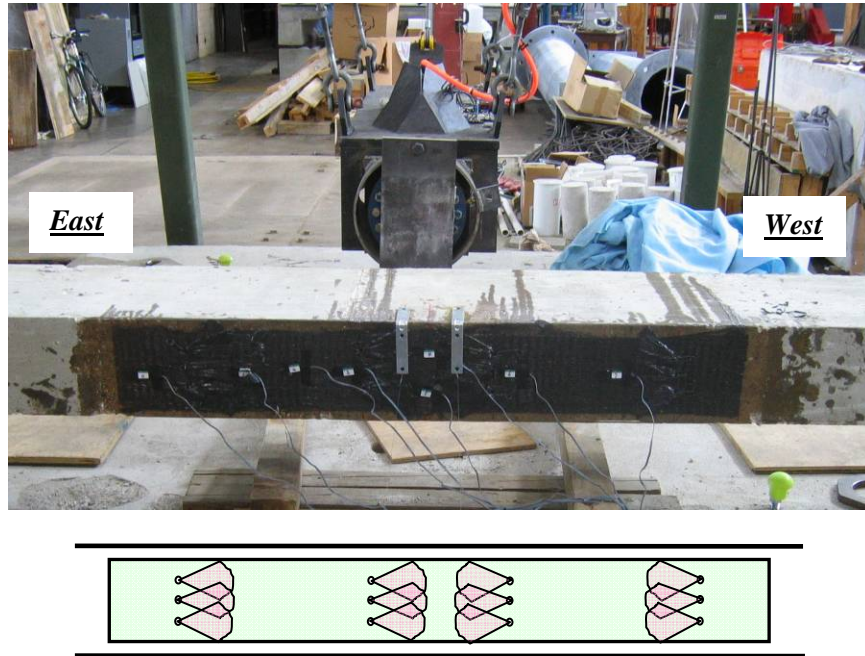
Figure 3.55   Configuration of A-BF-A-2S
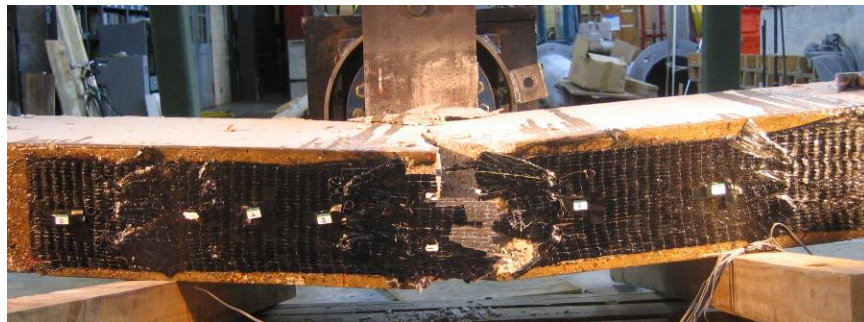
Figure 3.56   Failure of A-BF-A-2S, fracture of CFRP sheet
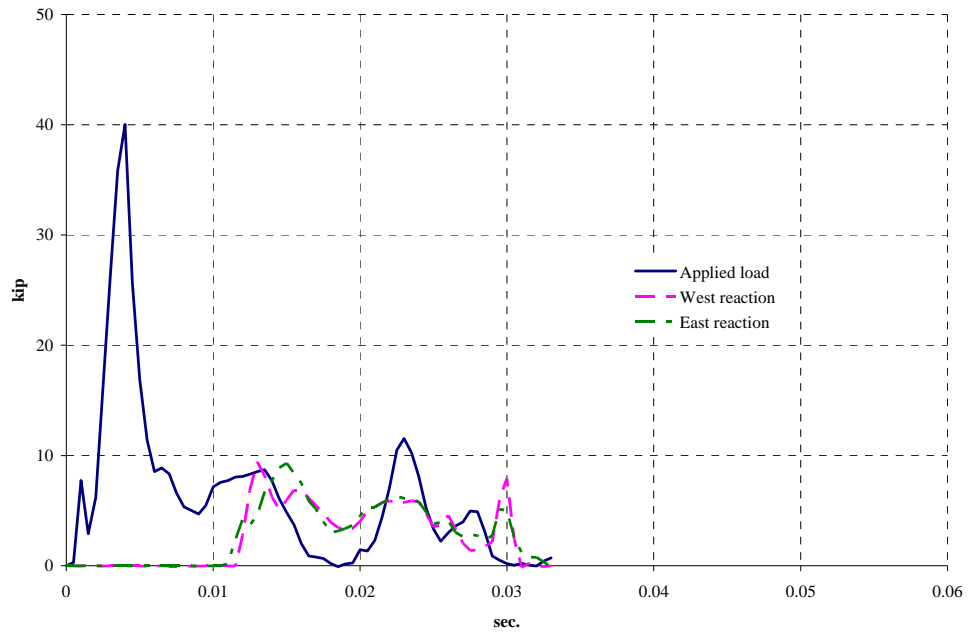
Figure 3.57   Measured applied load and reactions, A-BF-A-2S
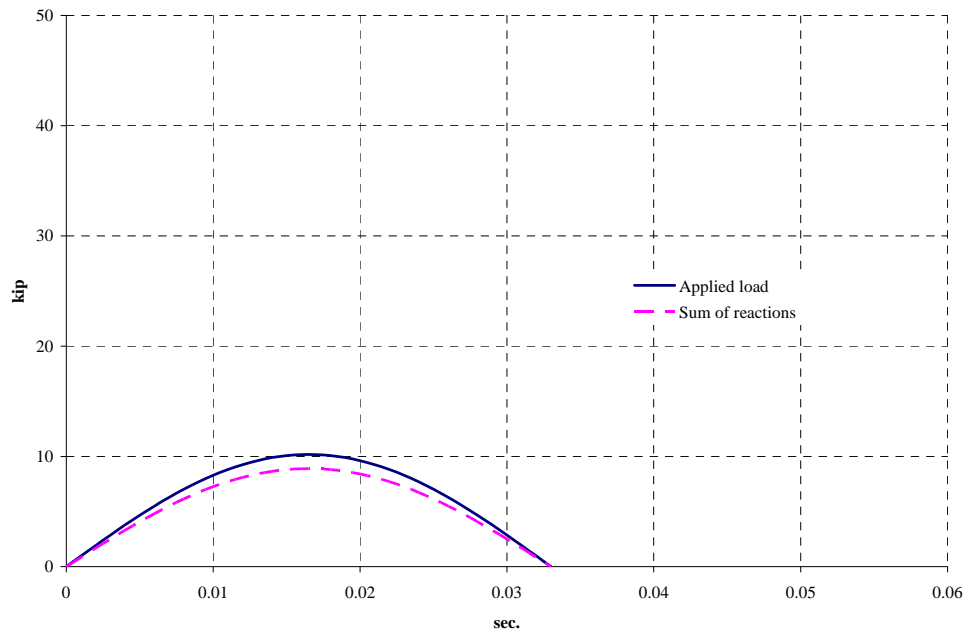
Figure 3.58   Normalized applied load and sum of reactions, A-BF-A-2S

76

The location of the strain gages installed in A-BF-A-2S and the maximum measured strain in each gage are shown in Figure 3.59. The maximum strain measured in A-BF-A-2S was 0.0112 at gage 4 (112 % of the ultimate tensile strain of the CFRP). From the horizontal distribution of strains in the CFRP sheet, a symmetric distribution of strains was observed in the beam. The highest strain occurred in the gage in the center of beam and strain decreased away from the center. Because of the CFRP anchors, delamination did not propagate. The maximum strain measured in gage 7 was 0.0015 (less than the 0.004 strain at which delamination occurred in A-BF-A-2S). Strain rate of CFRP (maximum strain divided by the time to reach the strain) was 0.467 /sec.

The strain response of gages 4, 6 and 7 in time domain is shown in Figure 3.60. The gage in the center (gage 4) reached higher strain than gages 6 and 7 located between the first and the second set of the CFRP anchors.

Strain gages were not installed on the #6 bars in this beam.
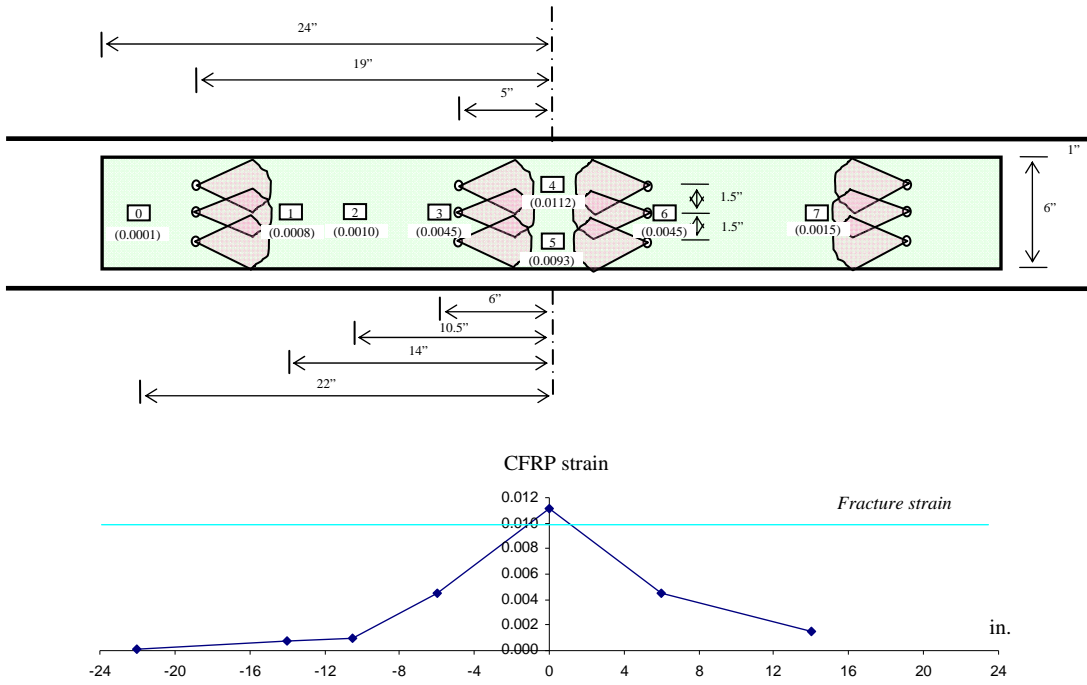
Figure 3.59   Location of strain gages and distribution of strain in CFRP, A-BF-A-2S
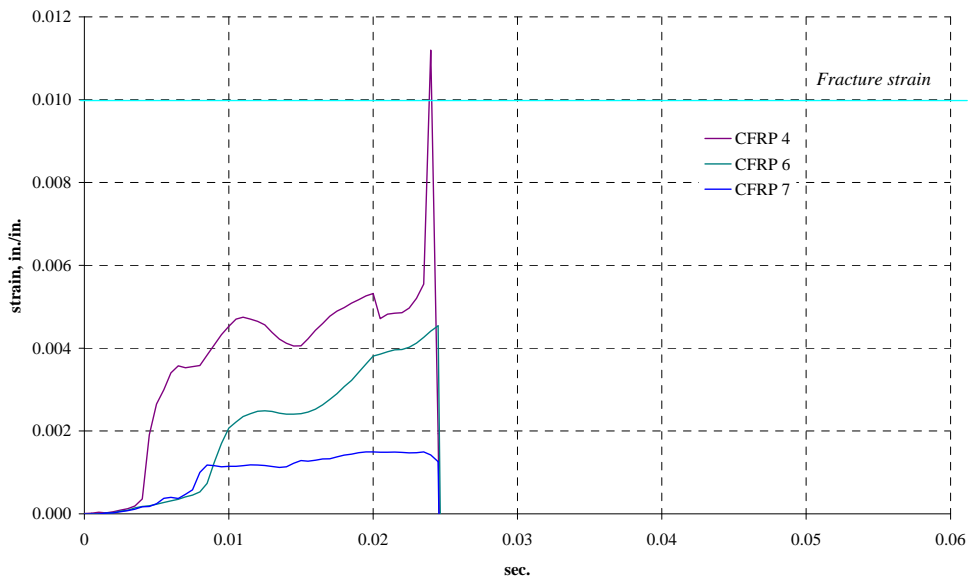
Figure 3.60   CFRP strain, A-BF-A-2S

3.6.1.3 A-BF-A-5S

A-BF-A-5S was a Type A beam with one layer of CFRP sheet and CFRP anchors. The surface of the bottom face was sand-blasted. The measured compressive strength of the concrete was 5,000 psi. Configuration of the beam is shown in Figure 3.61. The failure mode of A-BF-A-5S was fracture of the CFRP sheet in the center of the beam (Figure 3.62).

The measured applied load and reactions are shown in Figure 3.63 for loading to failure. Drop height of the pendulum mass was 4.5 in. when it failed and duration of event was 0.039 sec. The peak applied load was 47.4 kip and the peak reaction was 26.9 kip at the west support. Impulse of the applied load was 0.36 kip-sec while that of sum of the reactions was 0.30 kip-sec. Before the test with a 4.5 in. drop height of pendulum, loading with the pendulum at 1 in. and 3 in. drop heights was applied. The test results of these tests are provided in Appendix A.

The normalized curves of the applied load and sum of the reactions are shown in Figure 3.64. The peak normalized applied load was 14.5 kip and sum of the reactions was 12.0 kip (83 % of the peak normalized applied load). The calculated static strength of A-BF-A-5S was 11.0 kip and the peak normalized applied load was 132 % of the static strength.

Figure 3.61   Configuration of A-BF-A-5S
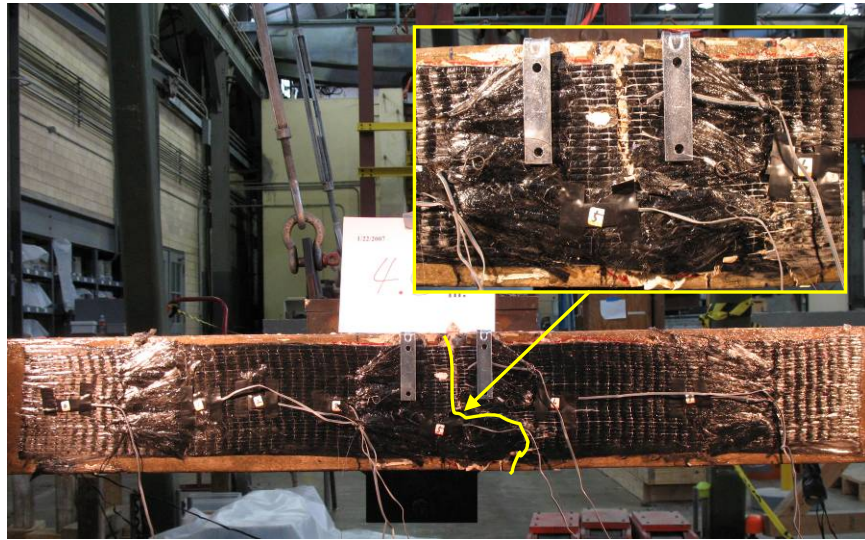
Figure 3.62   Failure of A-BF-A-5S, fracture of CFRP sheet

Figure 3.63   Measured applied load and reactions, A-BF-A-5S

Figure 3.64   Normalized applied load and sum of reactions, A-BF-A-5S

The location of the strain gages installed in A-BF-A-5S and the maximum measured strain in each gage are shown in Figure 3.65. The maximum measured strain was 0.0112 at gages 4 and 5 (112 % of the ultimate tensile strain of the CFRP). A symmetric horizontal distribution of strains was observed. The highest strain occurred in the gage in the center of beam and strain decreased away from the center. Strain rate of CFRP was 0.325 /sec. The strain response of gages 1, 3 and 4 with time is shown in Figure 3.66. The initial values of strain in the gages were not zero because of the previous impacts on this beam. The CFRP sheet in this beam delaminated under the earlier loading. Therefore, no time lag was observed between gages 1, 3 and 4.

The location of steel strain gages from the center of the beam and maximum measured strain are also shown in Figure 3.65. The maximum strain measured in the #6 bars in A-BF-A-5S was 0.0016 which was about 80 % of yield in of the steel reinforcement.

81
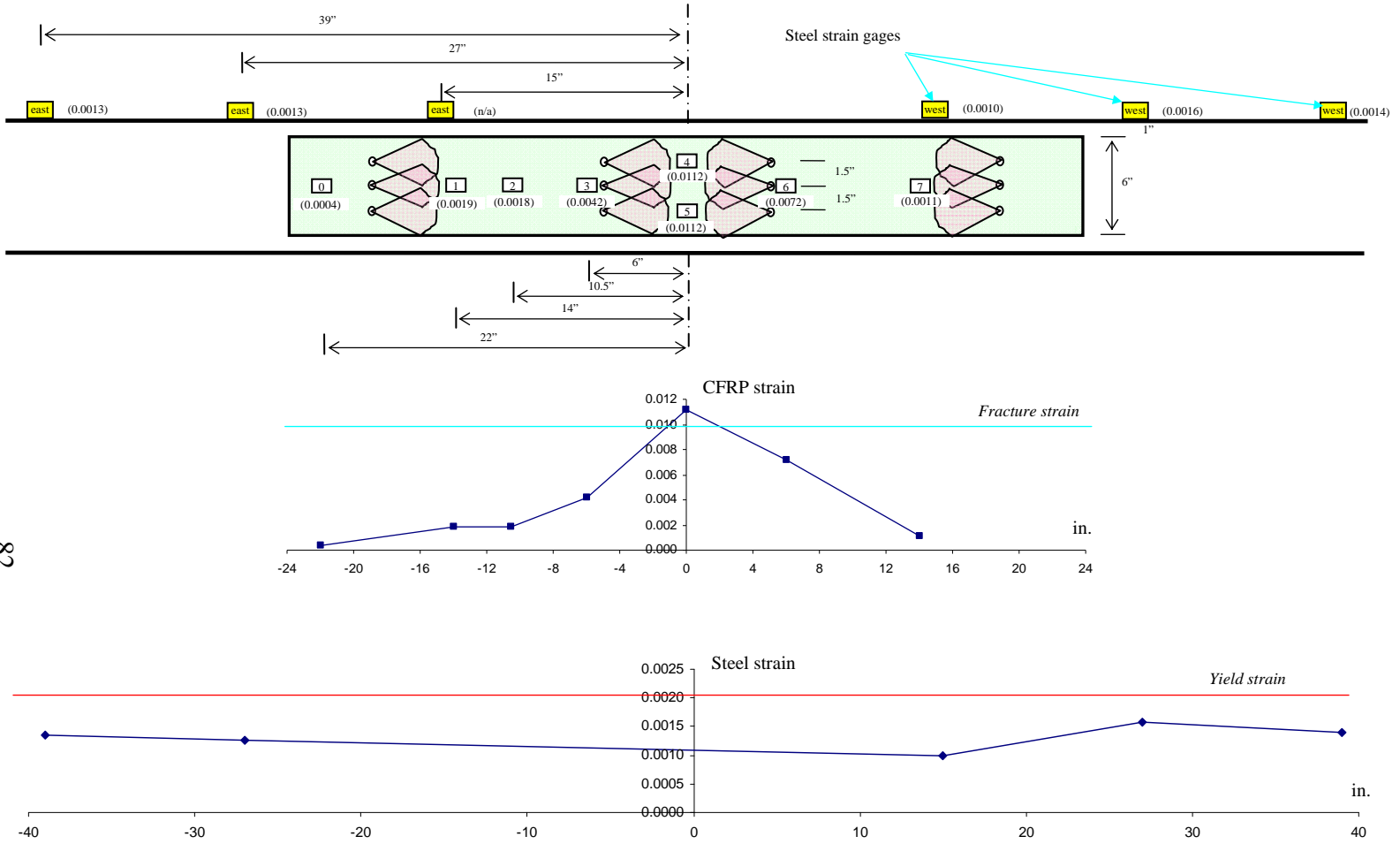
Figure 3.65   Location of strain gages and distribution of strain in CFRP and bar, A-BF-A-5S
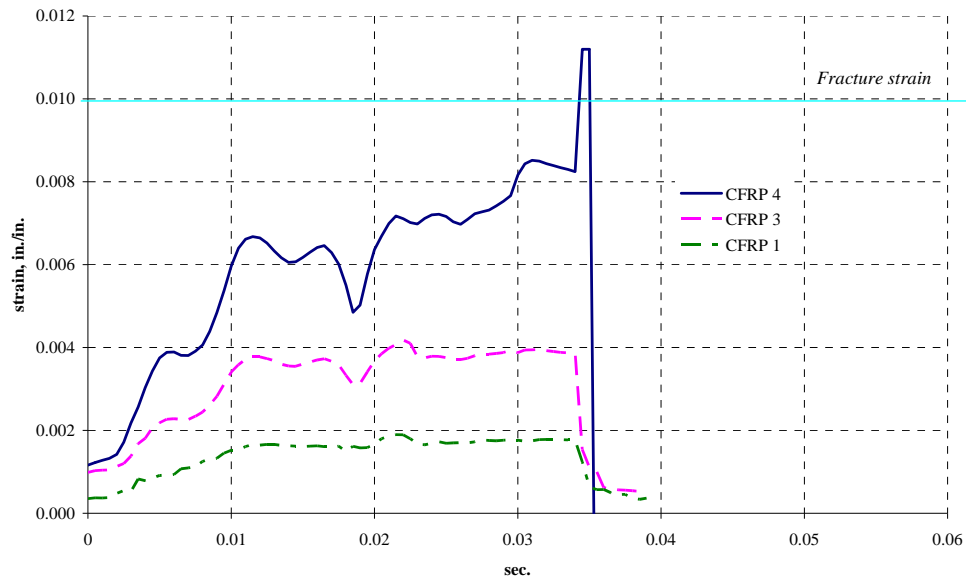
Figure 3.66   CFRP strain, A-BF-A-5S

3.6.1.4 A-BF-A-2N

A-BF-A-2N was a Type A beam with one layer of CFRP sheet and CFRP anchors. Clear polyethylene wrap was placed between the CFRP and the concrete surface. The measured compressive strength of the concrete was 2,000 psi. Configuration of the beam is shown in Figure 3.67. The failure mode of A-BF-A-2N was fracture of the CFRP anchors on the west side of the beam (Figure 3.68). The ultimate strength of the CFRP was not realized. The same width of CFRP material was used for the anchors as was in the CFRP sheet. The CFRP sheet did not reach ultimate strength with only anchors to transfer force form the CFRP sheet to the concrete.

The measured applied load and reactions are shown in Figure 3.63. Drop height of the pendulum mass was 3 in. and the duration of event was 0.055 sec. The peak applied load was 34.0 kip and the peak reaction was 11.5 kip at the east support. Impulse of the applied load was 0.35 kip-sec while that of sum of the reactions was 0.30 kip-sec.

The normalized applied load and sum of the reactions are shown in Figure 3.70. The peak normalized applied load was 10.1 kip and sum of the reactions was 8.7 kip (86 % of the peak normalized applied load).

The calculated static strength of A-BF-A-2N was 10.5 kip and the peak normalized applied load was 96 % of the static strength.
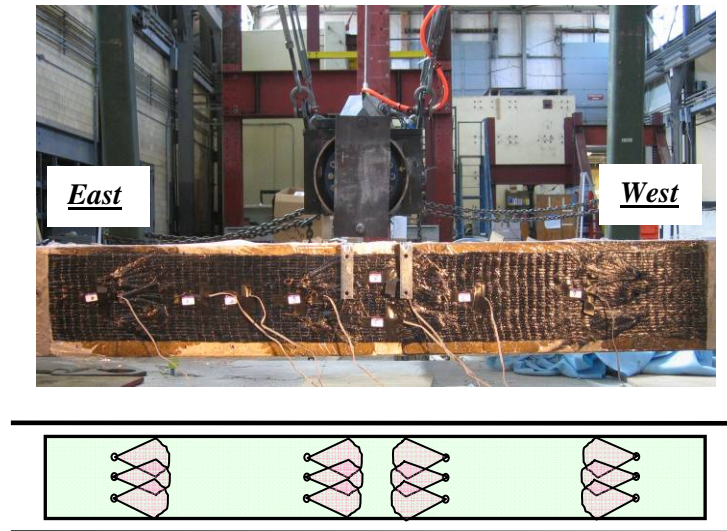
Figure 3.67   Configuration of A-BF-A-2N
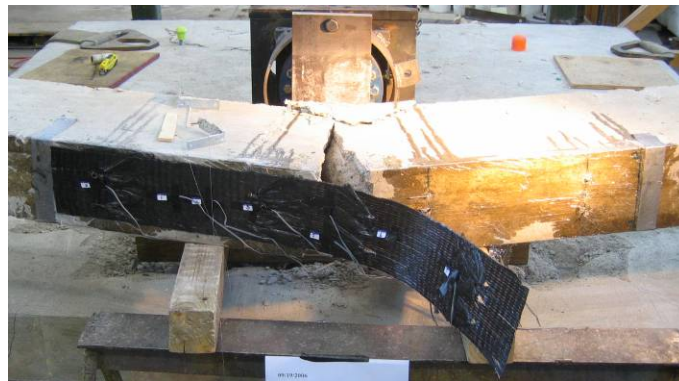
Figure 3.68   Failure of A-BF-A-2N, fracture of CFRP anchors

The location of the strain gages and the maximum measured strain in each gage are shown in Figure 3.71. The maximum strain measured in A-BF-A-2N was 0.0051 at gage 5 (51 % of the ultimate tensile strain of the CFRP). From the horizontal distribution of strains in the CFRP sheet, a symmetric distribution of strains was observed. The highest strain occurred in the gage in the center of beam and strain decreased away from the center. Strain rate of CFRP was 0.113 /sec.

The response of gages 5, 6 and 7 is shown in Figure 3.72. Since the CFRP sheet was not bonded to the concrete surface and was held by the CFRP anchors only using the polyethylene wrap, the time lag was not significant between gages 5, 6 and 7.

Strain gages were not installed on the #6 bars in this beam.
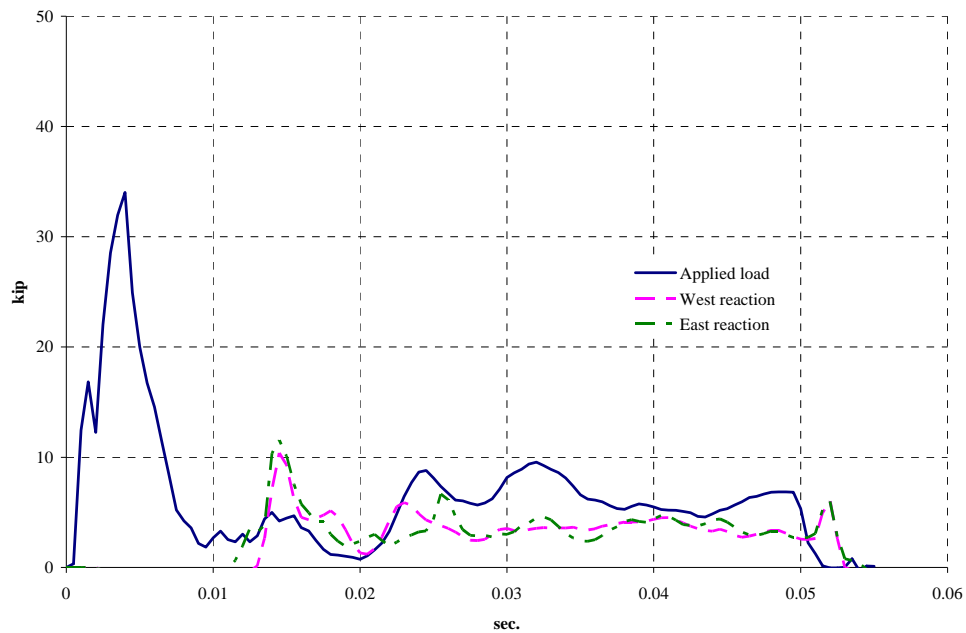
Figure 3.69   Measured applied load and reactions, A-BF-A-2N

85
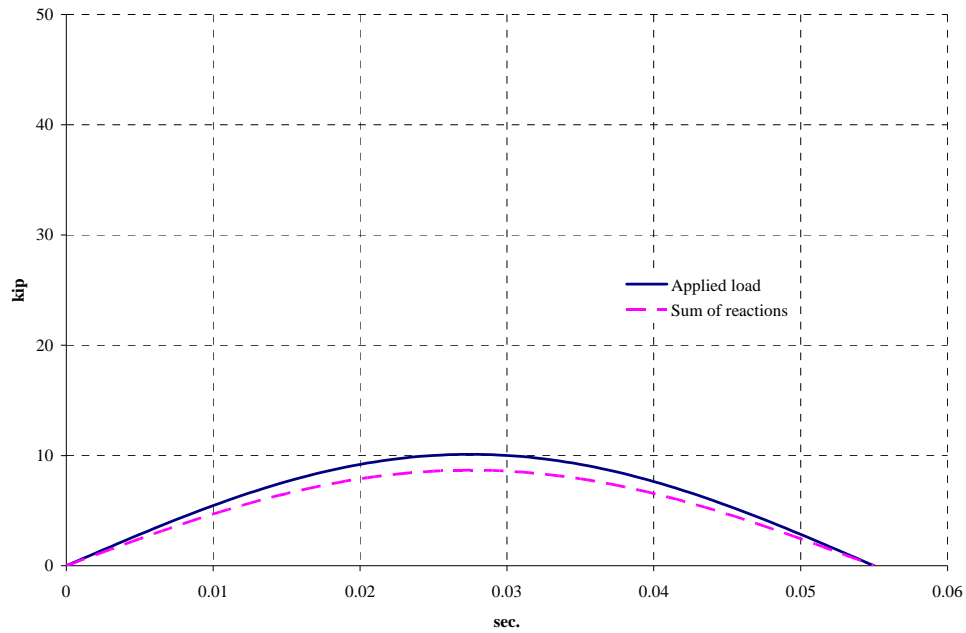
Figure 3.70   Normalized applied load and sum of reactions, A-BF-A-2N
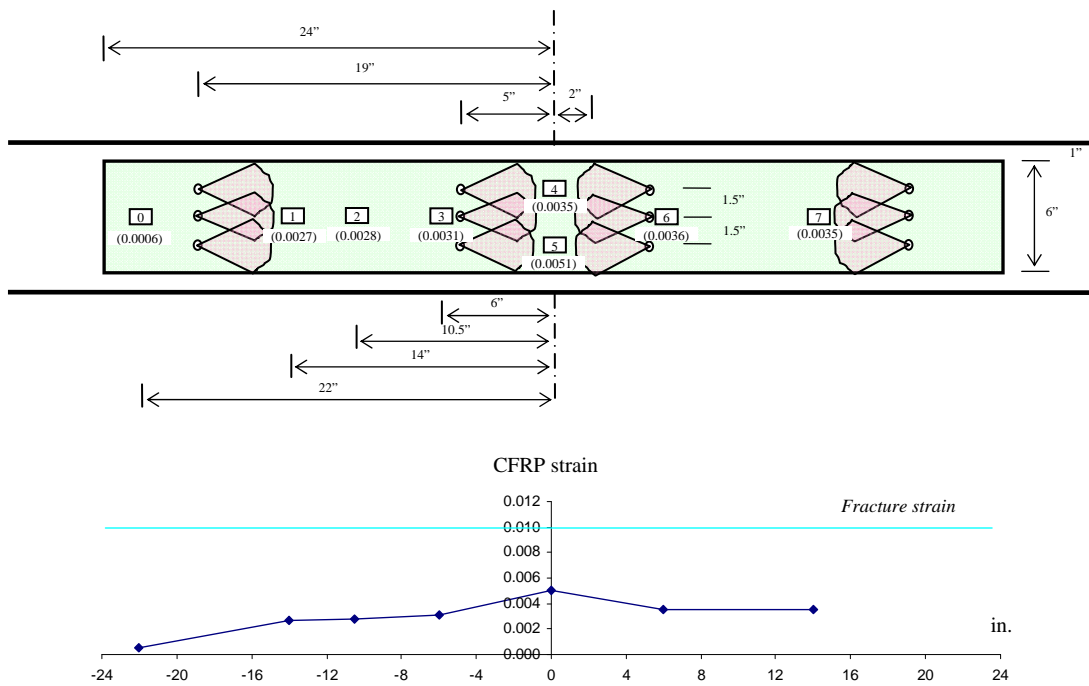
Figure 3.71   Location of strain gages and distribution of strain in CFRP, A-BF-A-2N

86
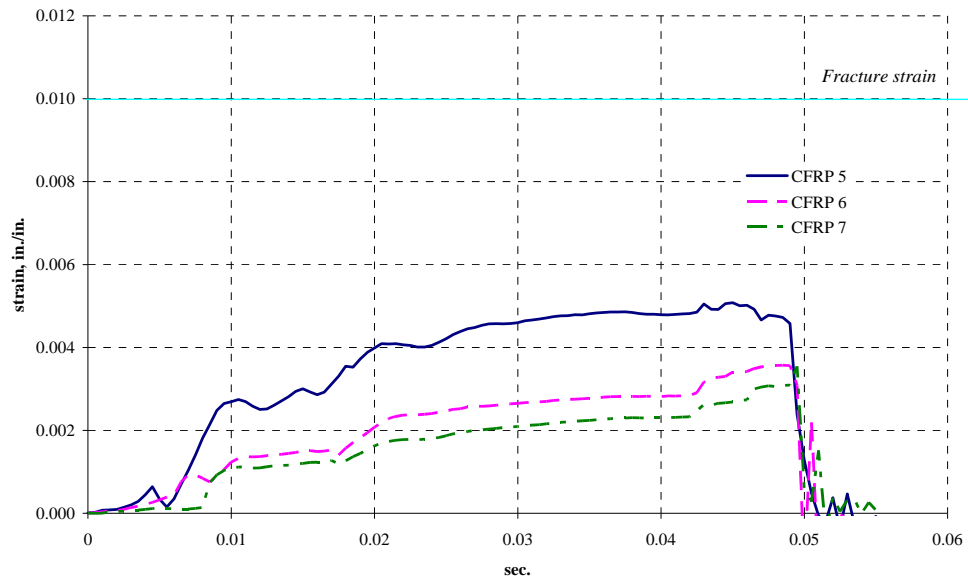
Figure 3.72　CFRP strain, A-BF-A-2N

3.6.1.5　A-BF-1.3A-5N

A-BF-1.3A-5N was a Type A beam with one layer of CFRP sheet and CFRP anchors. Thirty three percent more CFRP was used in fabricating one set of the anchors than the CFRP sheet. Clear polyethylene wrap was placed between the CFRP sheet and the concrete surface. The measured compressive strength of the concrete was 5,000 psi. This beam was damaged during moving and a crack occurred in the center. The crack was filled with the epoxy resin (Tyfo® S Epoxy), which was adhesive of the CFRP, before the application of the CFRP. Configuration of the beam is shown in Figure 3.73. The failure mode of A-BF-1.3A-5N was fracture of the CFRP sheet in the center of the beam (Figure 3.74). The ultimate tensile strength of the CFRP was realized using this anchorage method. The failure mode of this beam also involved splitting of the CFRP sheet and anchor.

East   West
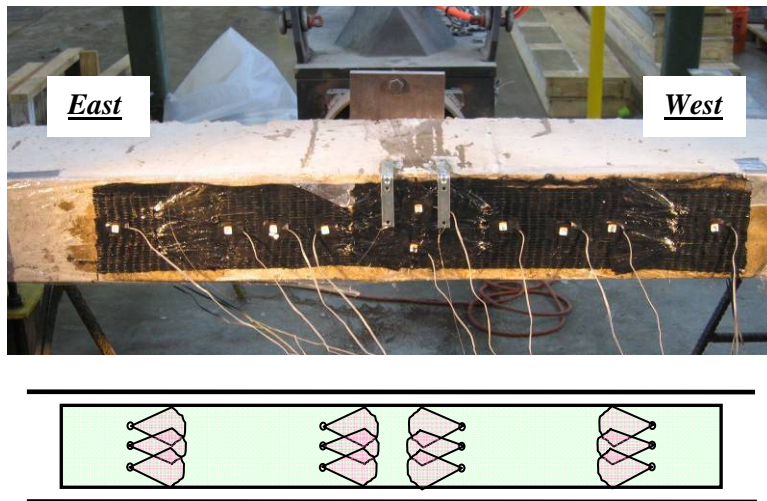
Figure 3.73   *Configuration of A-BF-1.3A-5N*

Fracture of CFRP sheet

Splitting of sheet and anchor
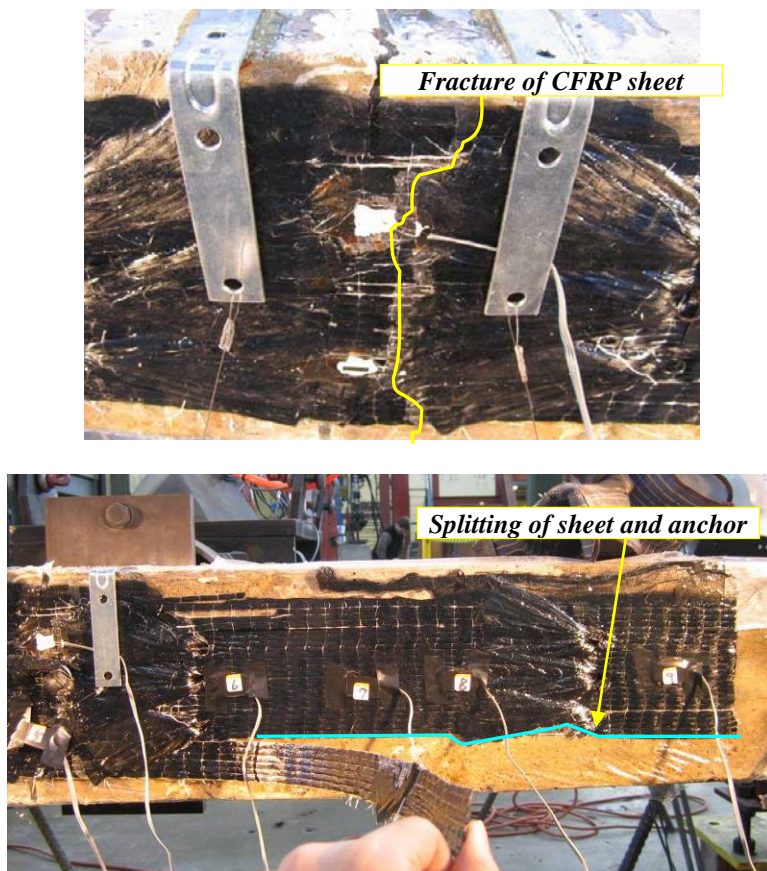
Figure 3.74   *Failure of A-BF-1.3A-5N, fracture of CFRP sheet*

The measured applied load and reactions plotted in time domain are shown in Figure 3.76. Drop height of the pendulum mass in A-BF-1.3A-5N was 3 in. and duration of event was 0.034 sec. The peak applied load was 34.9 kip and the peak reaction was 13.2 kip at the east support. Impulse of the applied load was 0.26 kip-sec while that of sum of the reactions was 0.20 kip-sec.

The normalized applied load and sum of the reactions are shown in Figure 3.76. The peak normalized applied load was 11.9 kip and sum of the reactions was 9.1 kip. The peak normalized sum of reaction was 77 % of the peak normalized applied load. The calculated static strength of A-BF-1.3A-5N was 11.0 kip and the peak normalized applied load was 108 % of the static strength.
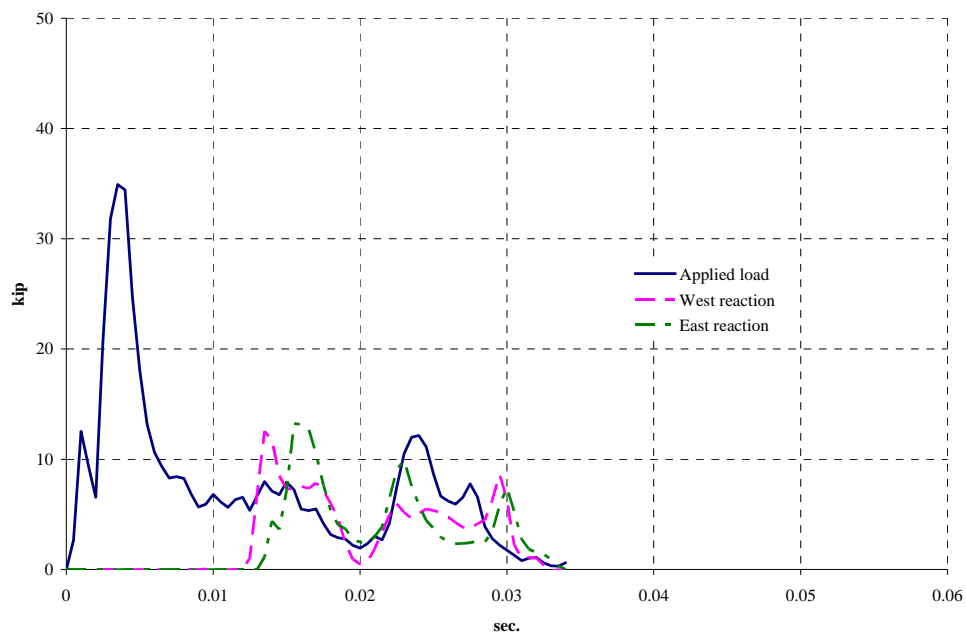
Figure 3.75   Measured applied load and reactions, A-BF-1.3A-5N
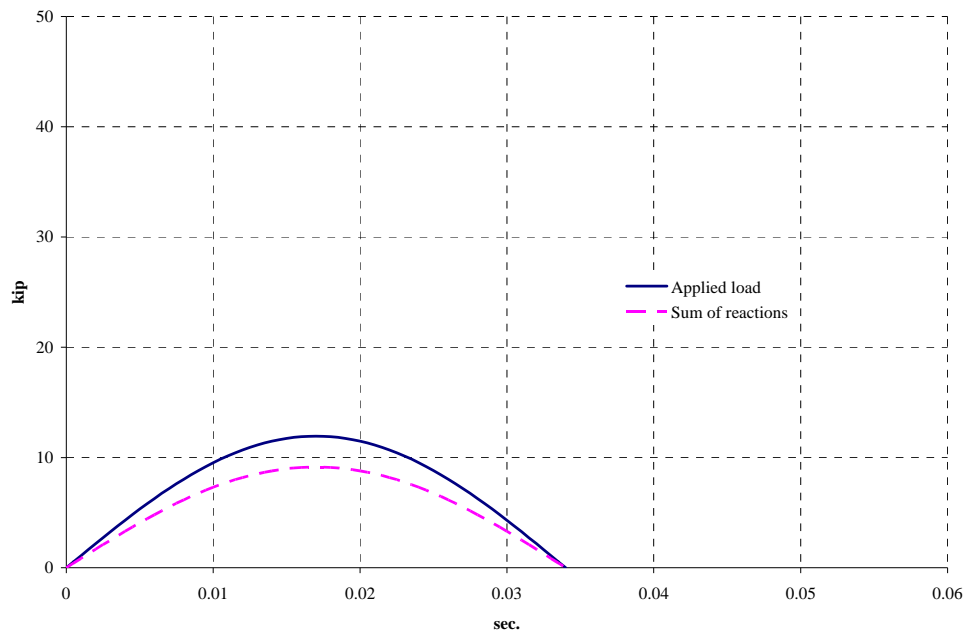
Figure 3.76   Normalized applied load and sum of reactions, A-BF-1.3A-5N

The location of the strain gages and the maximum measured strain in each gage are shown in Figure 3.77. The maximum measured strain was 0.0106 at gage 4 (106 % of the ultimate tensile strain of the CFRP). A symmetric horizontal distribution of strains was observed in the beam. The highest strain occurred in the gage in the center of beam and strain decreased away from the center. Strain rate of CFRP was 0.400 /sec. The strain response of gages 4, 6 and 8 is shown in Figure 3.78. The gage in the center (gage 4) reached higher strain than gage 6 and 8. There was a time lag between the responses of gage 4, 6, and 8.

The maximum strain measured in the #6 bars in A-BF-N-5S was 0.0010 which was about 50 % of yield of the steel reinforcement.
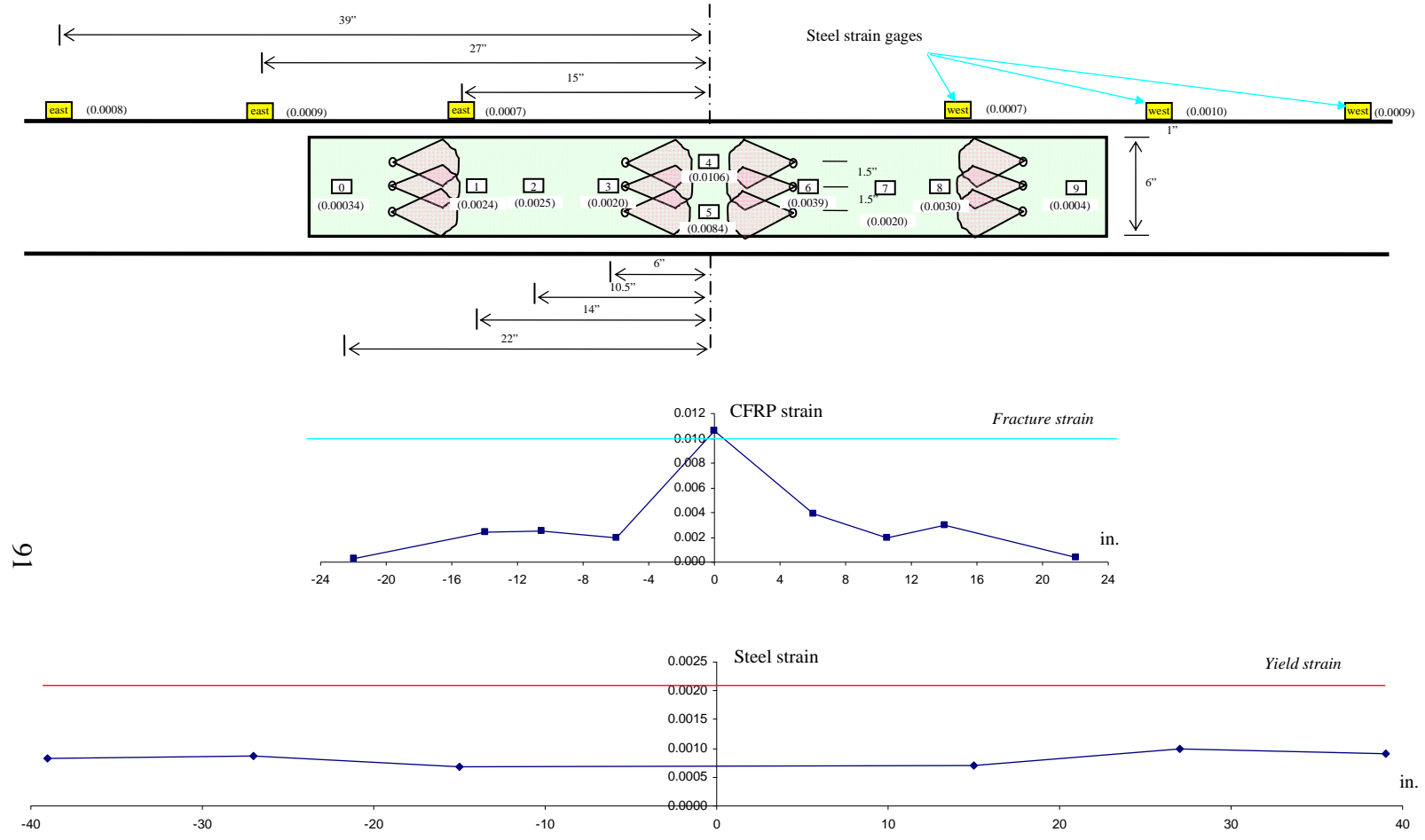
Figure 3.77   Location of strain gages and distribution of strain in CFRP and bars, A-BF-1.3A-5N
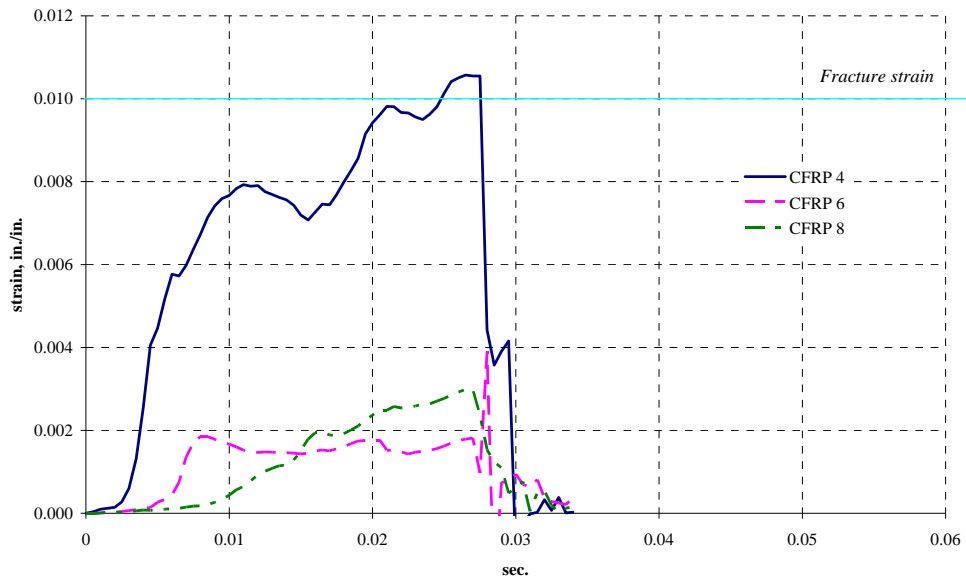
Figure 3.78   CFRP strain, A-BF-1.3A-5N

3.6.1.6   A-BF-U-5S

A-BF-U-5S was a Type A beam with one layer of CFRP sheet and CFRP U-wraps. The surface of the bottom face was sand-blasted. The measured compressive strength of the concrete was 5,000 psi. Configuration of the beam is shown in Figure 3.79. The failure mode of A-BF-U-5S was fracture of the CFRP sheet in the center of the beam (Figure 3.80).

The measured applied load and reactions are shown in Figure 3.81 for loading to failure. Drop height of the pendulum mass was 3 in. when it failed and the duration of event was 0.022 sec. The peak applied load was 28.8 kip and the peak reaction was 15.8 kip at the west support. Impulse of the applied load was 0.17 kip-sec while that of sum of the reactions was 0.07 kip-sec. Before the test with a 3 in. drop height of pendulum, loading with the pendulum at 1 in. and 1.5 in. drop heights was applied. Results of these tests are provided in Appendix A.

92

The normalized applied load and sum of the reactions are shown in Figure 3.82. The peak normalized applied load was 11.6 kip and sum of the reactions was 5.1 kip (44 % of the peak normalized applied load). The calculated static strength of A-BF-U-5S was 11.0 kip and the peak normalized applied load was 105 % of the static strength.
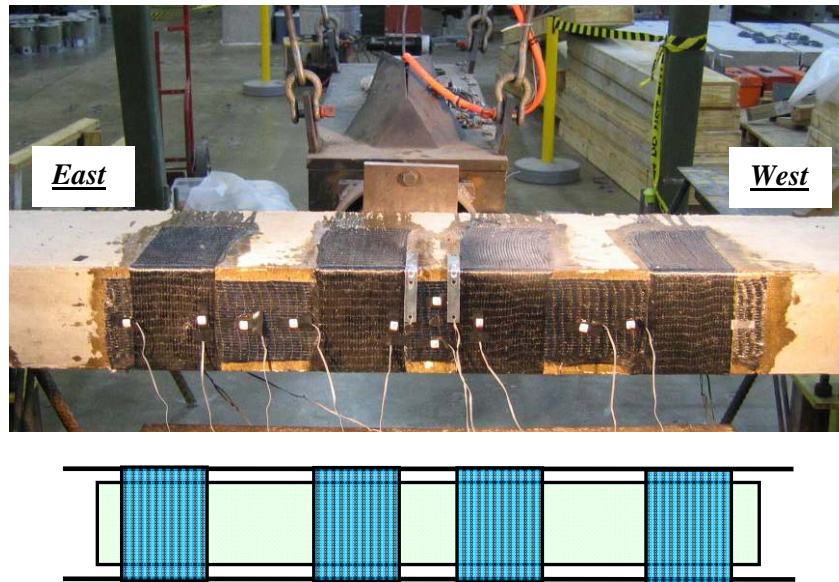
Figure 3.79   Configuration of A-BF-U-5S
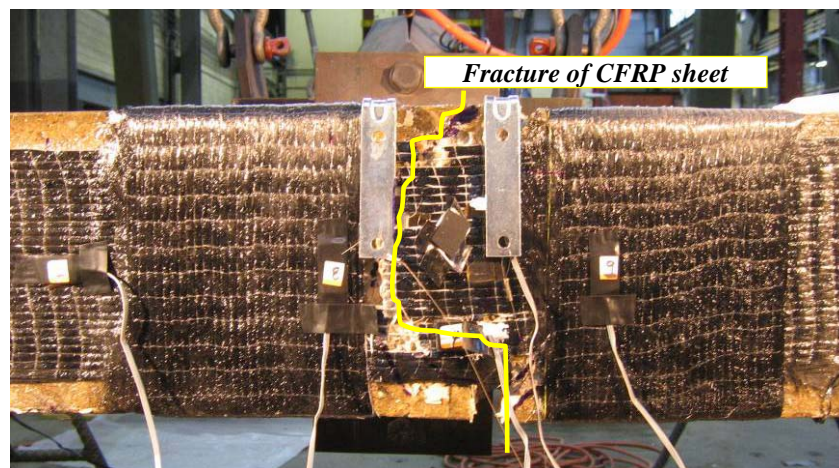
Figure 3.80   Failure of A-BF-U-5S, fracture of CFRP sheet
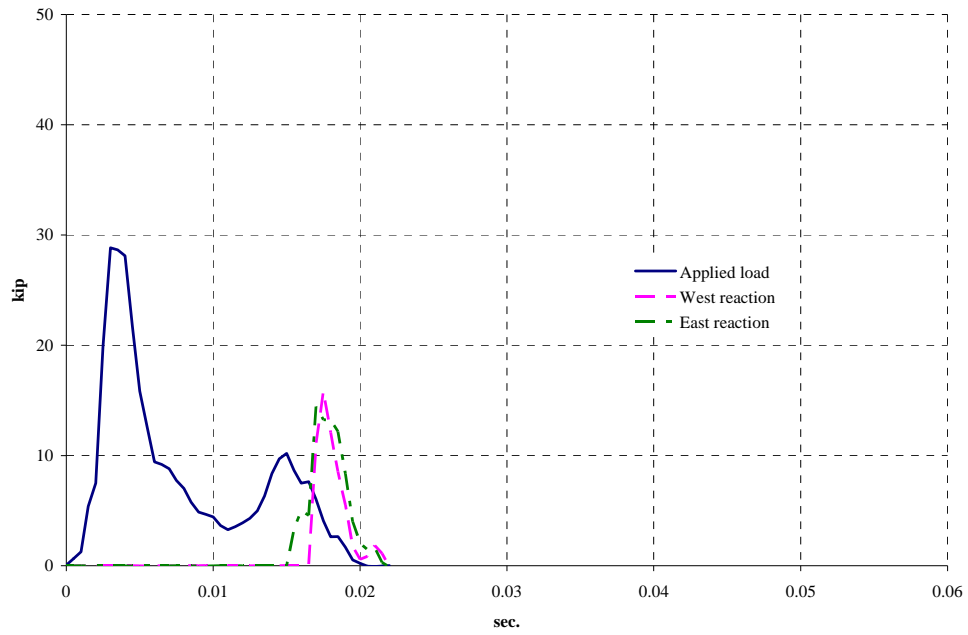
Figure 3.81   Measured applied load and reactions, A-BF-U-5S

Figure 3.82   Normalized applied load and sum of reactions, A-BF-U-5S

94

The location of the strain gages installed and the maximum measured strain in each gage are shown in Figure 3.83. The maximum strain measured in A-BF-U-5S was 0.0077 at gage 4 (77 % of the ultimate tensile strain of the CFRP). Although facture of CFRP sheet occurred, the measured strain did not reach the ultimate tensile strain because the gage failed before the strain reached the ultimate strain. A symmetric horizontal distribution of strains was observed. The highest strain occurred in the gage in the center of beam and strain decreased away from the center. The strains in gages beyond the first U-wrap from the center were relatively small compared with the strain in the center. Stress is concentrated on the portion of the CFRP sheet between the first sets of the U-wrap while stress is distributed along the entire CFRP sheet in the previous test beams with the CFRP anchors. Strain rate of was 0.264 /sec. The strain response of gages 2, 3 and 4 is shown in Figure 3.84. The initial values of strain in the gages were not zero because of the previous impacts on this beam.

Strain in the CFRP U-wraps was also measured. The peak strain measured in the strain gages on the CFRP U-wraps was 0.0018 (18 % of the ultimate tensile strain of the CFRP).

The maximum strain measured in the #6 bars in A-BF-U-5S was 0.0010 which was about 50 % of yield of the steel reinforcement.
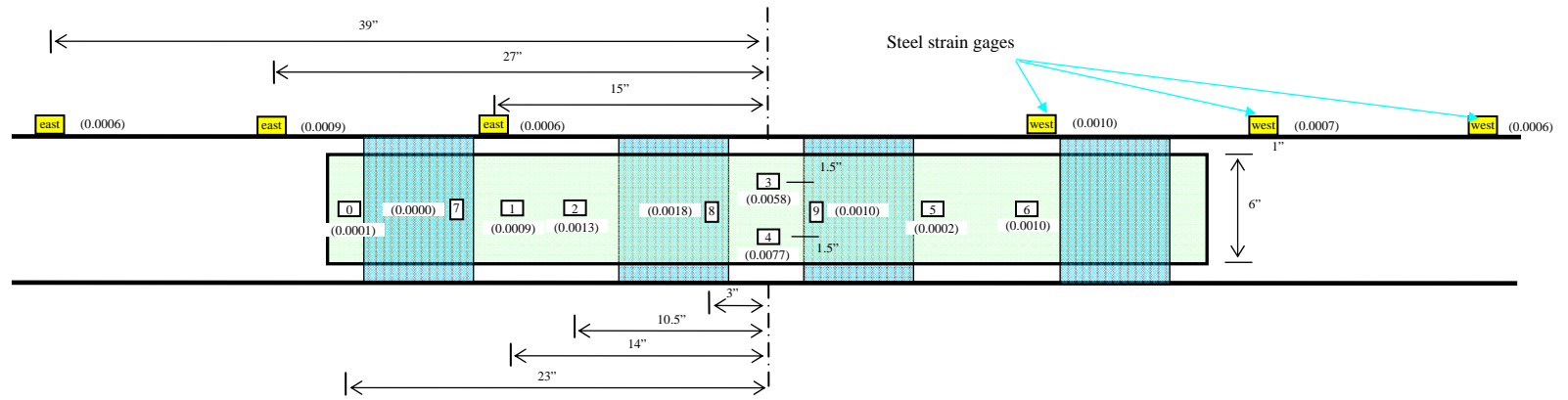
Figure 3.83   Location of strain gages and distribution of strain in CFRP and bars, A-BF-U-5S
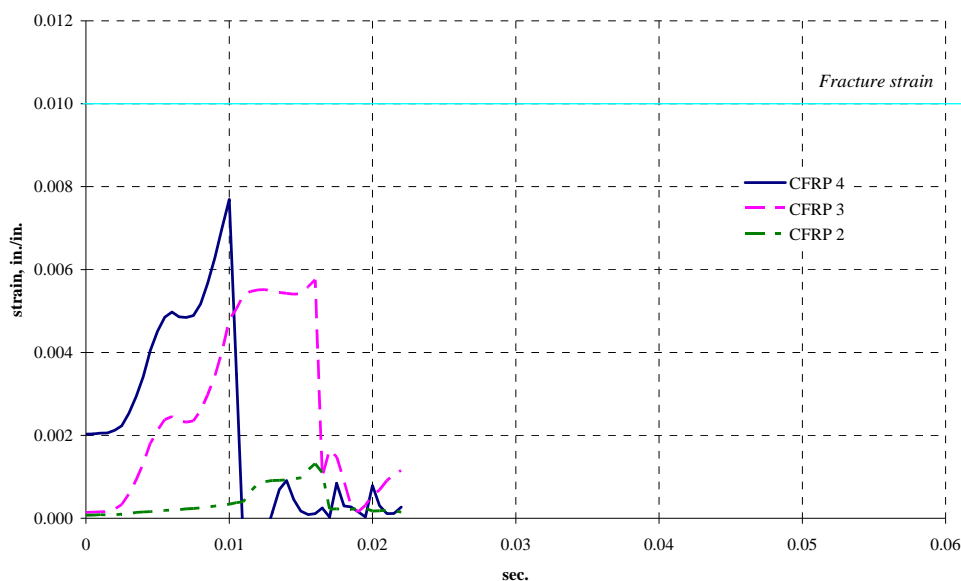
Figure 3.84 CFRP strain, A-BF-U-5S

3.6.1.7 A-BF-A/U-6G

A-BF-A/U-6G was a Type A beam with one layer of CFRP sheet, CFRP anchors (west side) and CFRP U-wraps (east side). The surface of the bottom face was ground. The measured compressive strength of the concrete was 6,000 psi. Configuration of the beam is shown in Figure 3.85. The failure mode of A-BF-A/U-6G was fracture of the CFRP sheet in the center of the beam (Figure 3.86).

The measured applied load and reactions are shown in Figure 3.87. Drop height of the pendulum mass was 3 in. and the duration of event was 0.022 sec. The peak applied load was 36.0 kip and the peak reaction was 12.5 kip at the east support. Impulse of the applied load was 0.16 kip-sec while that of sum of the reactions was 0.10 kip-sec.

The normalized applied load and sum of the reactions are shown in Figure 3.88. The peak normalized applied load was 11.3 kip and sum of the reactions was 6.9 kip (61 % of the peak normalized applied load). The calculated static strength of A-BF-A/U-6G was 11.1 kip and the peak normalized applied load was 102 % of the static strength.

97

Figure 3.85   Configuration of A-BF-A/U-6G
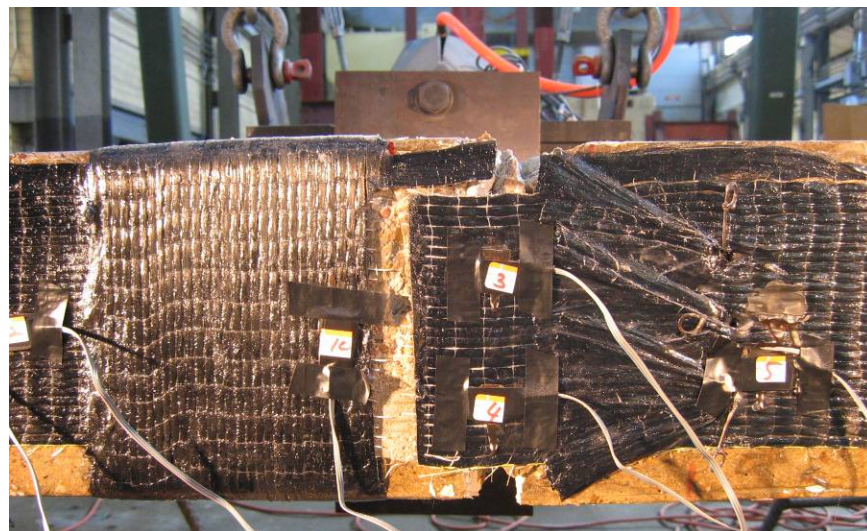
Figure 3.86   Failure of A-BF-A/U-6G, fracture of CFRP sheet

98
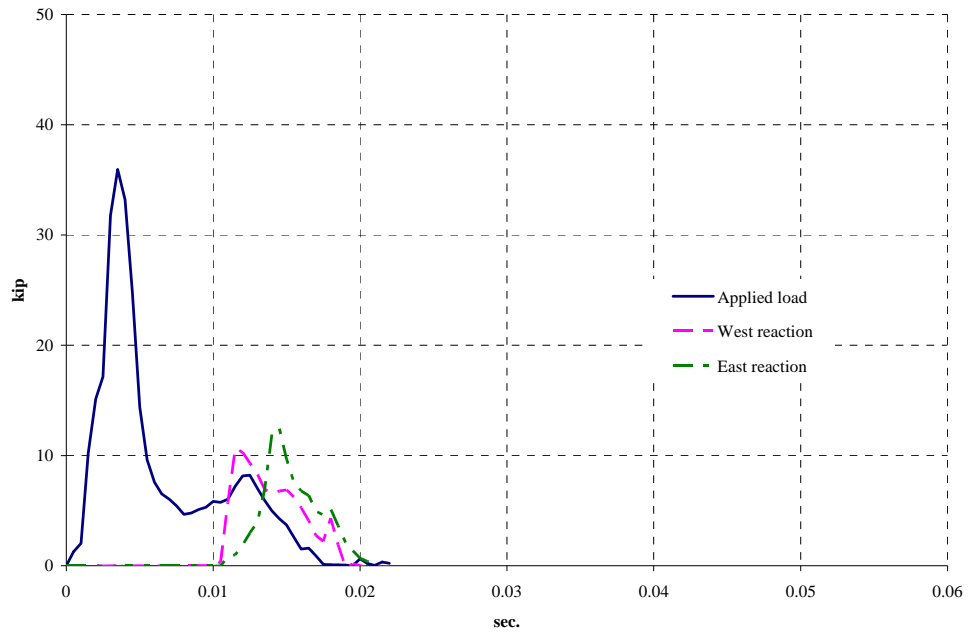
Figure 3.87   Measured applied load and reactions, A-BF-A/U-6G

Figure 3.88   Normalized applied load and sum of reactions, A-BF-A/U-6G

99

The location of the strain gages and the maximum measured strain in each gage are shown in Figure 3.89. The maximum measured strain was 0.0103 at gage 4 (103 % of the ultimate tensile strain of the CFRP). A symmetric horizontal distribution of strains was observed. The highest strain occurred in the gage in the center of beam and strain decreased away from the center. However, the strains in the gages beyond the first U-wrap or CFRP anchors from the center were relatively small compared with the measured strain in the center. Stress was concentrated on the portion of the CFRP sheet between the first set of anchors and U-wrap while stress was distributed along the CFRP sheet in the test beams with the CFRP anchors only. Strain rate of CFRP was 0.644 /sec. The strain response of gages 4, 5 and 7 is shown in Figure 3.90. The gage in the center (gage 4) reached higher strain than gage 5 and 7. There was a time lag between the responses of gage 4, 5 and 7.

Strain in the CFRP U-wraps was also measured. The peak strain measured in the gages on the CFRP U-wraps was 0.0008 (8 % of the ultimate tensile strain of the CFRP).

The maximum strain measured in the #6 bars in A-BF-U-5S was 0.0008 which was about 40 % of yield of the steel reinforcement.
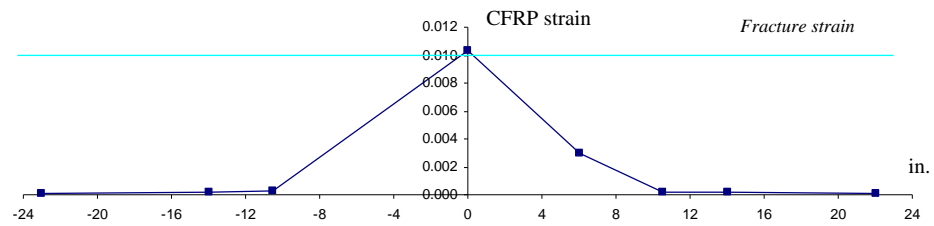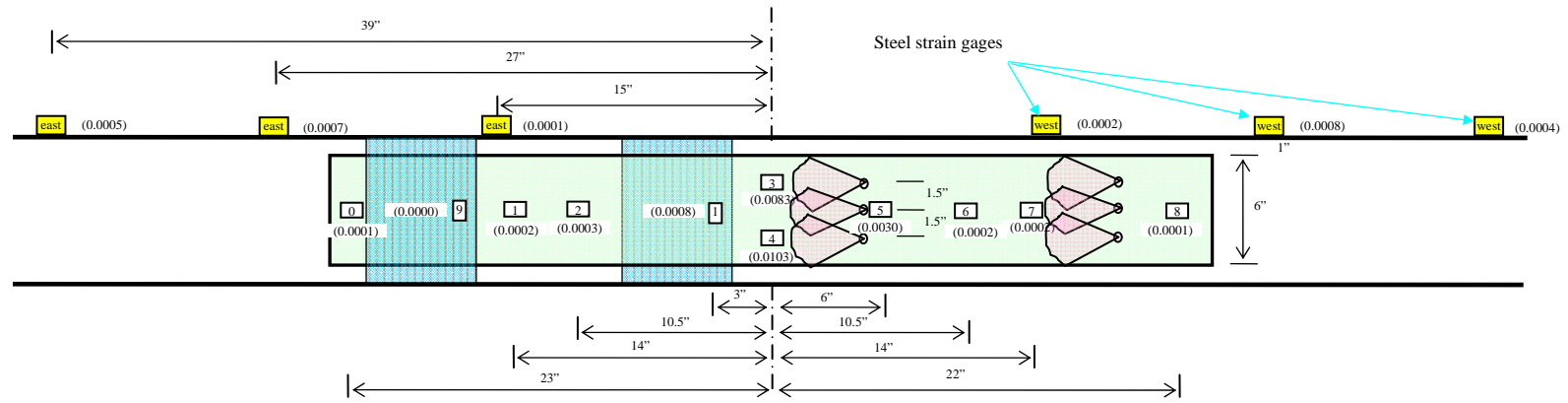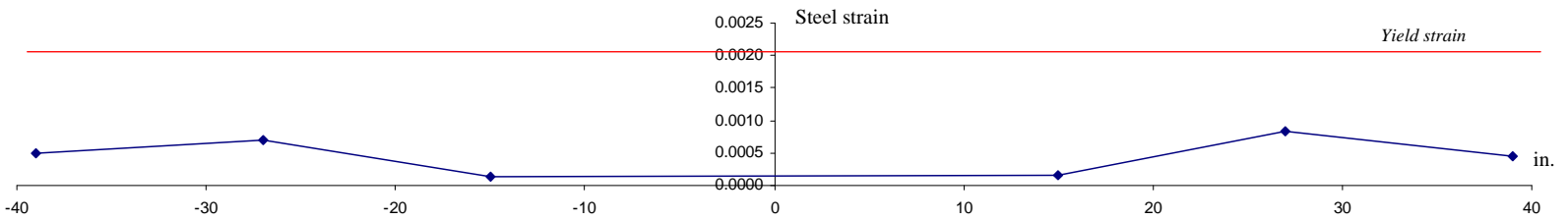
Figure 3.89   Location of strain gage and distribution of strain in CFRP and bars, A-BF-A/U-6G
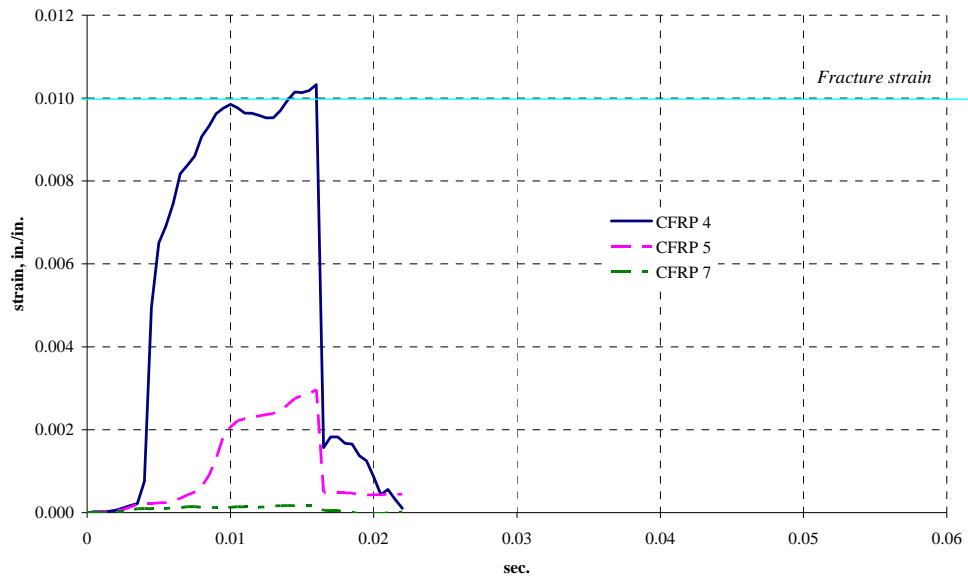
Figure 3.90   CFRP strain, A-BF-A/U-6G

3.6.1.8 Comparisons

3.6.1.8.1 Failure Modes of the Beams

The failure modes of the specimens with CFRP sheets the bottom face under dynamic loading were the same as those in static loading conditions (Orton, 2007). The observed failure modes were delamination of the CFRP sheet, fracture of the CFRP sheet, and anchorage failure. Specimens with the same geometry of the CFRP materials showed the same failure mode in both dynamic and static loading conditions.

The failure mode of A-BF-N-5S, for which no anchorage was provided, was delamination of the CFRP sheet. In this specimen, the measured maximum strain in the CFRP sheet was 42 % of the ultimate tensile strain. This result showed that less than half capacity of the CFRP sheet can be realized if this sheet was not anchored.

The failure mode of the specimens using the proper anchorage methods (A-BF-A-2S, A-BF-A-5S, A-BF-1.3A-2N, A-BF-U-5S and A-BF-A/U-6G) was the fracture of the CFRP sheet. That indicated the ultimate tensile strength of the sheet was reached. These results showed that the anchorage methods used to reach ultimate strength under static loading performed similarly under dynamic loading. As shown in Figure 3.91 and Figure 3.92, beams with the anchorage using the anchors or U-wraps failed by CFRP fracture under static loading.

The failure mode of A-BF-A-2N was anchorage failure, and the measured maximum strain was 51 % of the ultimate tensile strain. In this specimen, the stress in the CFRP sheet was transferred to the concrete only by the CFRP anchors because of the separation between the CFRP sheet and the concrete, and these anchors failed before the ultimate tensile strain of the CFRP sheet was realized. Therefore, to prevent the premature failure of the CFRP anchors, the width of the CFRP in theses anchors needed to be increased. The width of CFRP in the CFRP anchors was increased by 33 % in A-BF-1.3A-5N with respect to that in A-BF-A-2N, and consequently, the CFRP sheet in A-BF-1.3A-5N developed ultimate tensile strength.
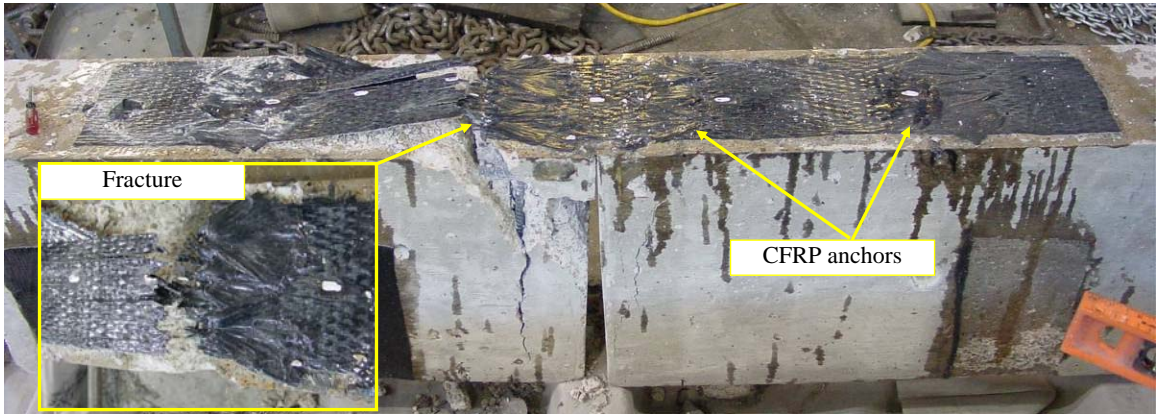
Figure 3.91   Static test, CFRP sheet and anchors, 100 % of the ultimate strength
(Orton, 2007)
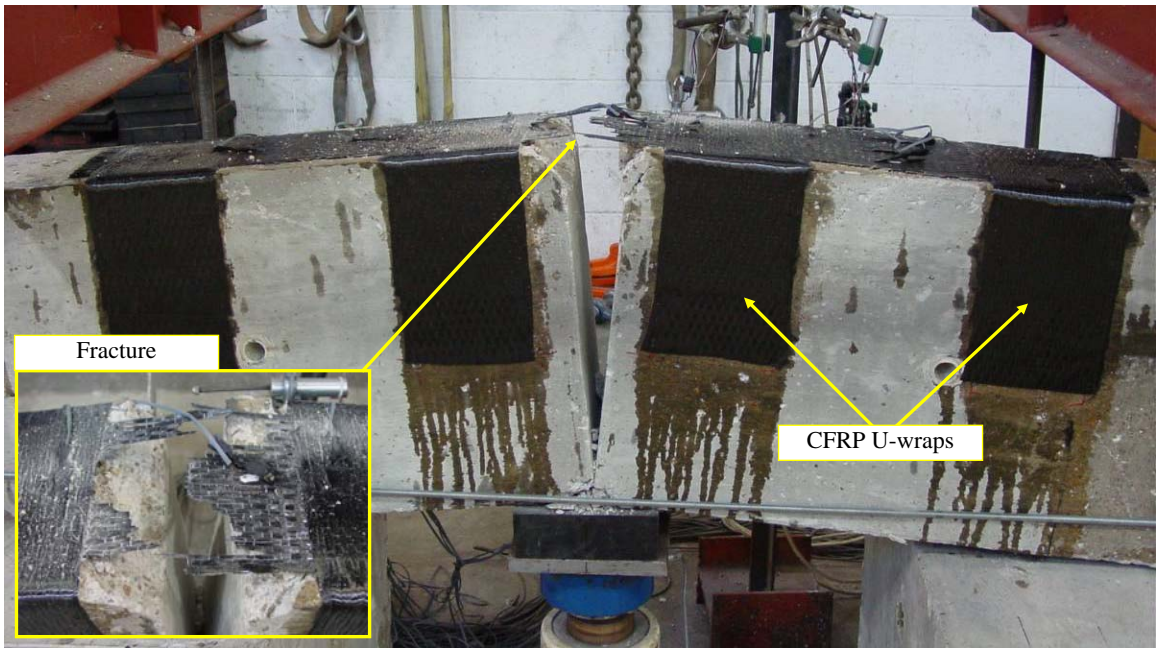
Figure 3.92   Static test, CFRP sheet and U-wraps, 93 % of the ultimate strength
(Orton, 2007)

104

3.6.1.8.2 Effect of Test Variables

In the beams rehabilitated using the flat bottom face of the beams, the following test variables were examined: type of anchorage (CFRP anchor or CFRP U-wrap), concrete strength, surface preparation and effect of overhead application. A summary of test results of the flat bottom face beams are provided in Table 3.4.

Table 3.4   *Comparison of the test results of the beams with flat bottom face*

Condition at the fracture of the CFRP sheet		Drop height	Peak applied load		Static strength	Impulse			Max. strain in bars
			Measured load	Normalized load		Applied load, A	Sum of reactions, R	Ratio, R/A	
A-BF-A-5S		4.5 in	47.4 kip	14.5 kip	11.0 kip	0.36 kip-sec	0.30 kip-sec	83%	0.0016
A-BF-U-5S		3 in.	28.8 kip	11.6 kip	11.0 kip	0.17 kip-sec	0.07 kip-sec	43%	0.0010
A-BF-A-2S		3 in.	40.0 kip	10.2 kip	10.5 kip	0.21 kip-sec	0.19 kip-sec	87%	
A-BF-1.3A-5N		3 in.	34.9 kip	11.9 kip	11.0 kip	0.26 kip-sec	0.20 kip-sec	77%	0.0010
A-BF-A/U-6G	Overhead application	3 in.	36.0 kip	11.3 kip	11.1 kip	0.16 kip-sec	0.10 kip-sec	61%	0.0008

Anchorage Types

A-BF-U-5S was compared with A-BF-A-5S to study the effect of anchorage type on dynamic performance of CFRP. The only difference between these two beams was type of anchorage. Both beams failed by fracture of the CFRP sheet and the CFRP sheet reached the ultimate tensile strength. These test results indicated that the anchorage method with the CFRP U-wraps was also an effective way of anchoring the CFRP sheets as CFRP anchors. However, A-BF-A-5S, which had the CFRP anchors, showed better performance than A-BF-U-5S, which had the U-wraps. The drop height of the pendulum mass at the fracture of the CFRP sheet was 4.5 in. for A-BF-A-5S while that of A-BF-U-5S was 3 in. It showed that more energy was required to fracture the CFRP sheet in A-BF-A-5S than that in A-BF-U-5S. Duration of event was 0.039 sec for A-BF-A-5S while was 0.022 sec for A-BF-U-5S. Longer time was required in A-BF-A-5S than in A-BF-U-

5S to fracture the CFRP sheet. In A-BF-A-5S, the ratio of the impulse of applied load to that of sum of the reactions at the fracture of CFRP sheet was 83 % while that in A-BF-U-5S was 44 %. More load was transferred to the support between the time of impact and fracture of the CFRP sheet in A-BF-A-5S than in A-BF-U-5S. The maximum measured strain in the steel reinforcement was high in A-BF-A-5S (0.0016) compared with that in A-BF-U-5S (0.001). Before the fracture of CFRP sheet, more stress was transferred to the steel reinforcement from the CFRP in A-BF-A-5S than in A-BF-U-5S. Stress concentration was noted in the portion of the CFRP sheet between the U-wraps while stress was distributed along the entire CFRP sheet when anchors were used.

Concrete Strength

Concrete strength has been considered a critical factor in the use of CFRP materials in common practice because the typical failure mode of CFRP materials is debonding of the CFRP from the concrete surface and the tensile strength of concrete effects the debonding mechanism. However, the results of this investigation indicated that the concrete strength is not a critical factor for realizing the full strength of the CFRP sheets when the sheets were properly anchored with CFRP anchors. The only difference between A-BF-A-5S and A-BF-A-2S was the compressive strength of the concrete. Although the compressive strength of concrete in A-BF-A-2S (2000 psi) was lower than that of A-BF-A-5S (5,000 psi), the CFRP sheet in both beams reached the ultimate tensile strength. The dynamic performance of A-BF-A-2S is also shown in Table 3.4.

Surface Preparation

Surface preparation also has been considered as a critical factor in the use of CFRP materials in common practice. A sand-blasted or ground concrete surface is recommended in common practice to achieve a proper surface preparation for applying CFRP. However, the results of this experimental investigation indicate that the use of CFRP anchors for anchoring CFRP sheets may reduce the cost of rehabilitation because the surface preparation may not be critical to realizing full strength of the CFRP sheets if

CFRP anchors are used. An anchorage with at least 33 % more CFRP for the anchors than in the sheets performed well. The CFRP sheet in A-BF-1.3A-5N reached the ultimate tensile strength although the bond between the concrete surface and the CFRP sheet was broken by the polyethylene wrap. The dynamic performance of this beam was not as good as A-BF-A-5S but similar to A-BF-U-5S.

Because this study focused on the application of the CFRP anchors, not as many variables were examined in the beams with CFRP U-wraps. The effects of the concrete strength and surface preparation were not evaluated for beams with U-wraps.

Overhead Application

The CFRP materials in A-BF-A/U-6G were installed in an overhead direction while those in the other specimens were installed in a gravity direction to study effect of the overhead application in dynamic performance of CFRP. The failure mode of this beam was fracture of the CFRP sheet and the dynamic performance was similar to A-BF-U-5S (Table 3.4). Therefore, the direction of CFRP application did not appear to effect the performance of CFRP.

The measured peak normalized load was close to the calculated static strength of the test beams because the beams behaved elastically until fracture of the CFRP sheet. If inelastic behavior occurred in the specimens the normalized load would be larger than the static strength because of the increase in the impulse during contact of the pendulum mass. As will be seen later, in the test of Type C beams, a large normalized load was observed compared with the static strength.

3.6.2 Rehabilitation Using Bottom Face of Beam: Height Transition Bottom Face

3.6.2.1 B-BH-A-6S

B-BH-A-6S was a Type B beam with one layer of beam sheet and CFRP anchors on the west side. The connection sheet was anchored with excess CFRP U-wraps on the east side to provide stronger anchorage than that on the west side. The test of this specimen focused on the lap spliced region of the beam and connection sheet. It also focused on behavior of the beam sheet and anchors on the west side. The surface of the bottom face was sand-blasted. The measured compressive strength of the concrete was 6,000 psi. Configuration of the beam is shown in Figure 3.93. The failure mode of B-BH-A-6S was fracture of the connection sheet in the center of the beam (Figure 3.94). The fracture occurred where fan shape spliced portion of the connection sheet merged into a strap.
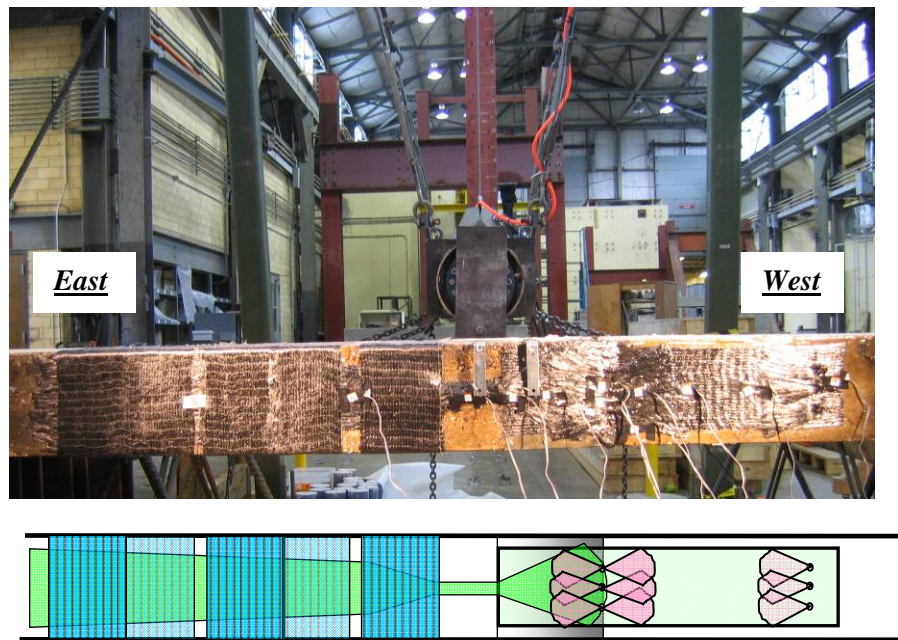
Figure 3.93   Configuration of B-BH-A-6S
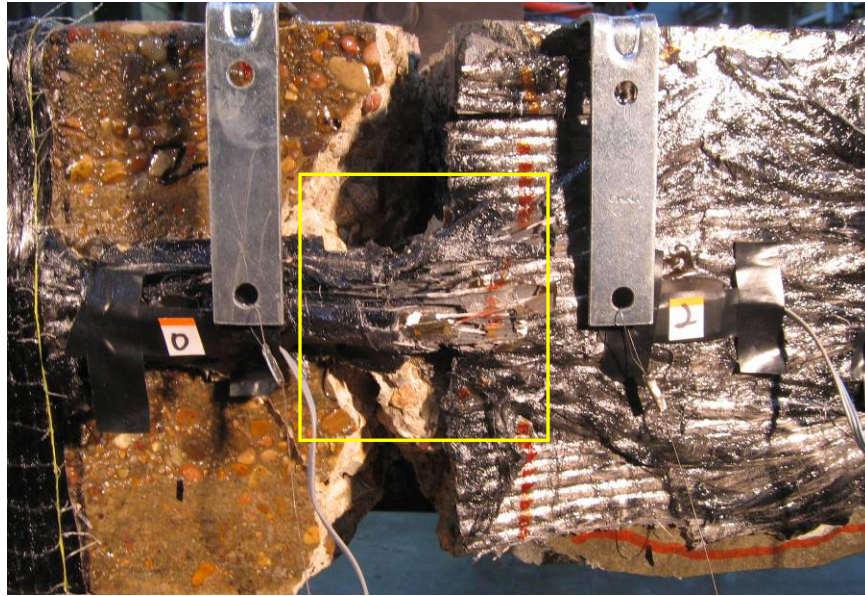
Figure 3.94   Failure of B-BH-A-6S, fracture of connection sheet

The measured applied load and reactions are shown in Figure 3.95 for loading to failure. Drop height of the pendulum mass was 3 in. and the duration of event was 0.023 sec. The peak applied load was 41.4 kip and the peak reaction was 16.1 kip at the west support. Impulse of the applied load was 0.16 kip-sec while that of sum of the reactions was 0.13 kip-sec. Before this test, this beam was tested with a 3 in. drop height initially but it did not fail. Results of the first 3 in. drop height test are provided in Appendix A.

The normalized applied load and sum of the reactions are shown in Figure 3.96. The peak normalized applied load was 10.1 kip and sum of the reactions was 8.2 kip (80 % of the peak normalized applied load). The calculated static strength of B-BH-A-6S was 11.1 kip and the peak normalized applied load was 91 % of the static strength.
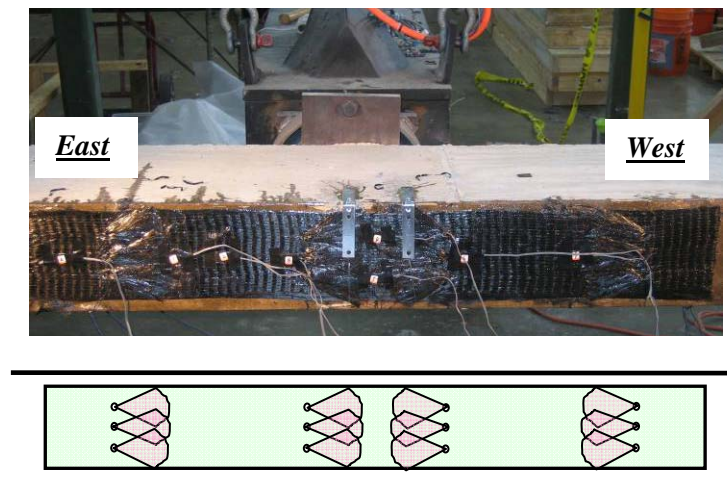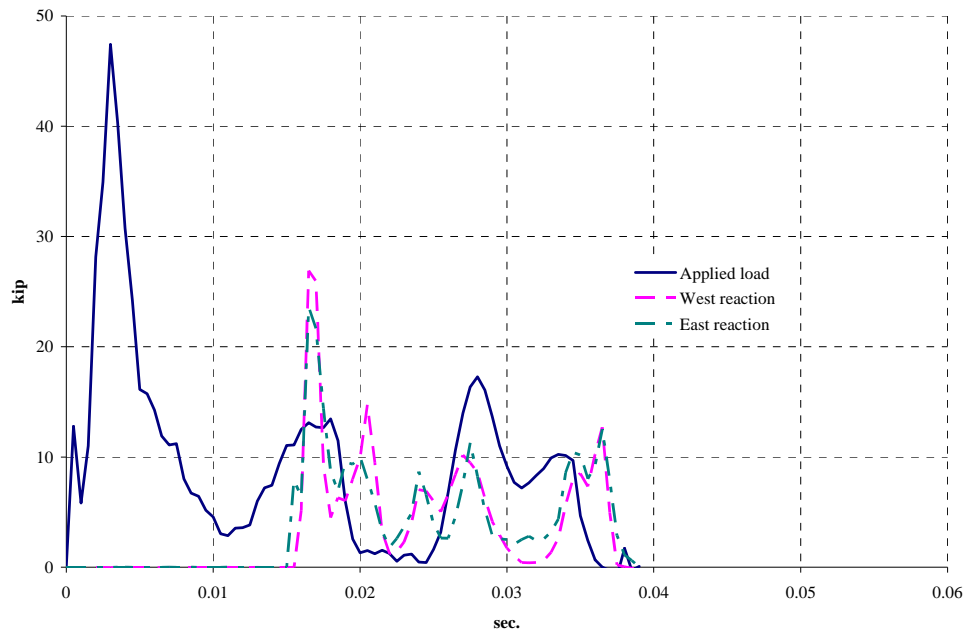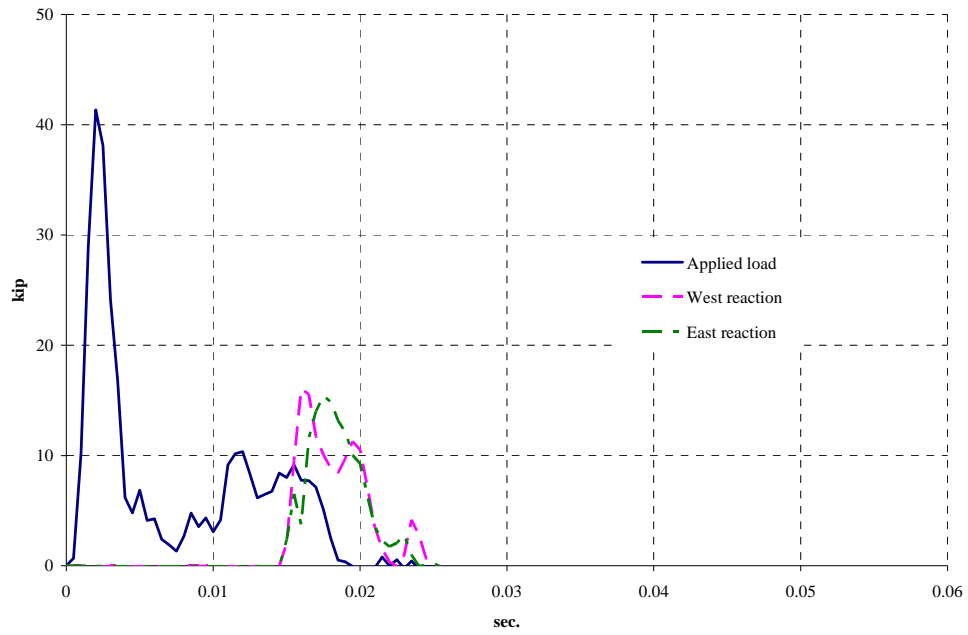
Figure 3.95   Measured applied load and reactions, B-BH-A-6S
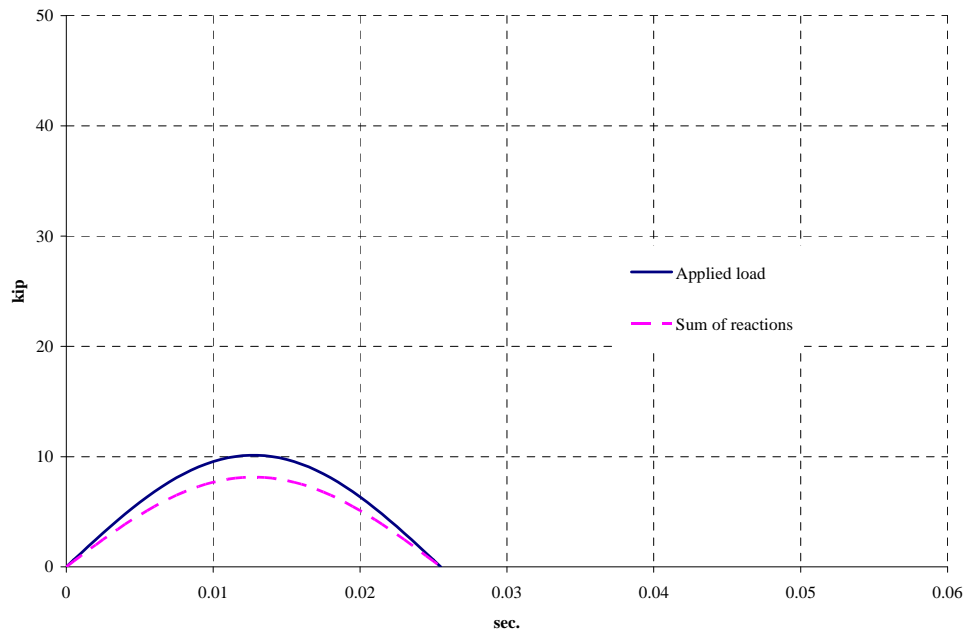
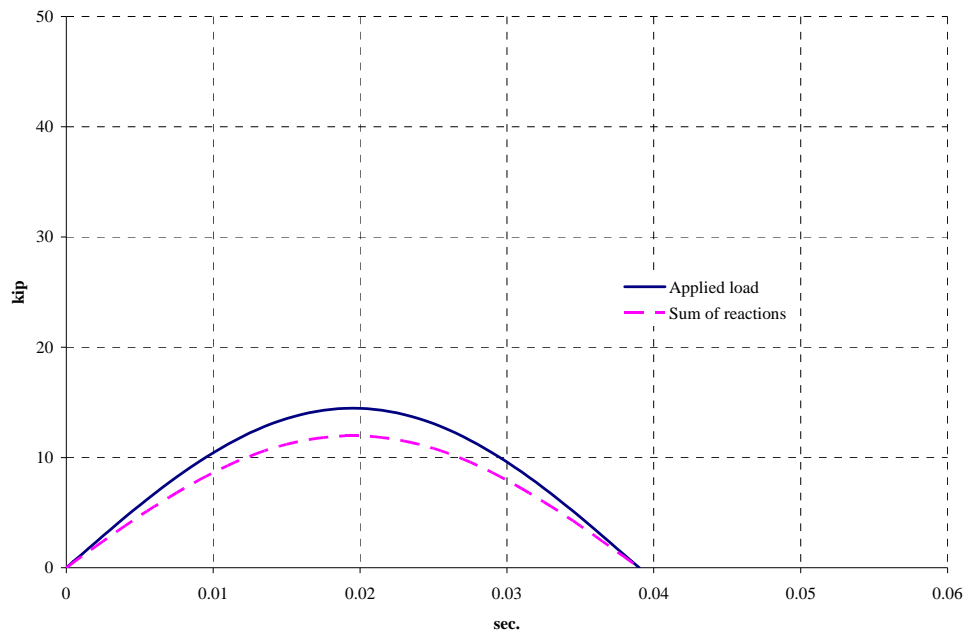*Figure 3.96   Normalized applied load and sum of reactions, B-BH-A-6S*

110

The location of the strain gages and the maximum measured strain in each gage are shown in Figure 3.97. The maximum strain measured was 0.0084 at gage 2 (84 % of the ultimate tensile strain of the CFRP). The peak strain did not reach the ultimate tensile strain because this gage was away from the location of fracture (gage 1 was inoperable). From the horizontal distribution of strains in the CFRP sheet, the highest strain occurred in the gage close to the center of beam and strain decreases in the gages away from the center. The solid line in the CFRP strain plot in Figure 3.97 was plotted connecting the measured strains and the dashed line was plotted using the expected ultimate strain where fracture occurred. Strain rate of CFRP was 0.400 /sec. The strain response of gages 2, 3, 7 and 8 in time domain is shown in Figure 3.98. The initial values of strain in the gages were not zero because of the previous impacts on this beam.

The maximum strain measured in the #6 bars in B-BH-A-6S was 0.0011 which was about 50 % of yield of the steel reinforcement.
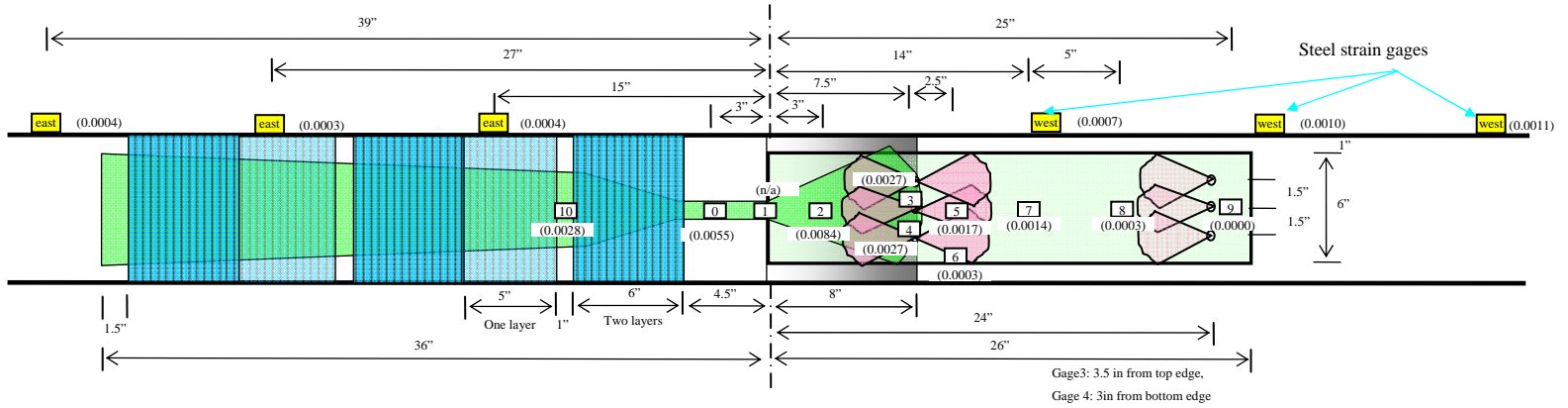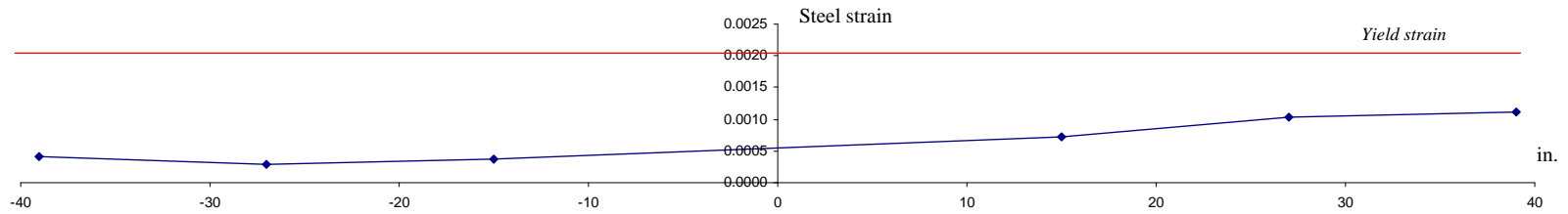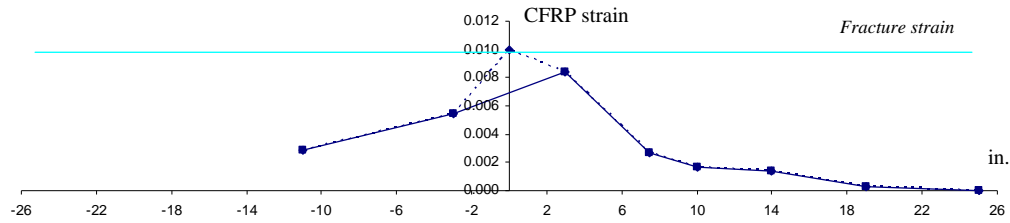
Figure 3.97 *Location of strain gages and distribution of strain in CFRP and bars, B-BH-A-6S*
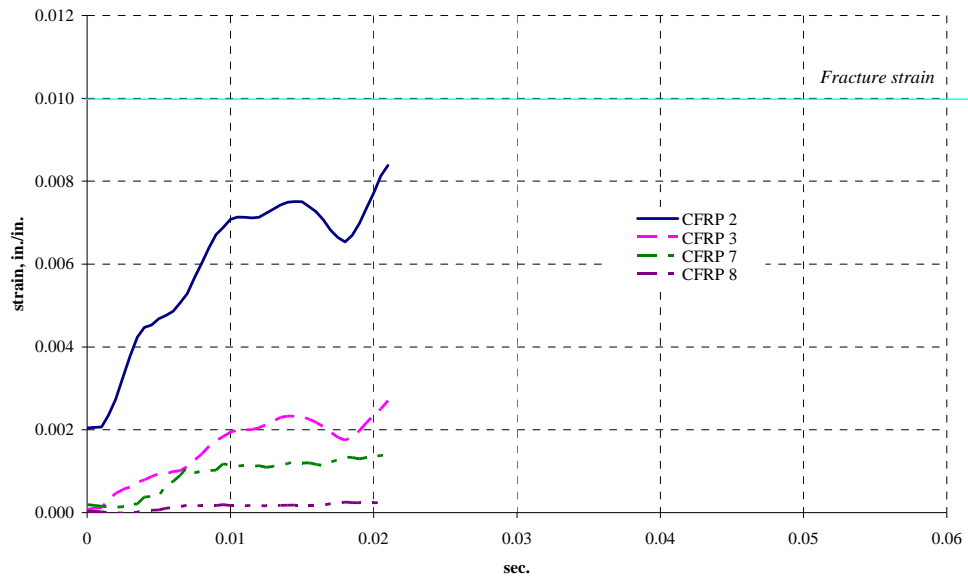
Figure 3.98   CFRP strain, B-BH-A-6S

3.6.2.2   B-BH-U-6S

B-BH-U-6S was a Type B with one layer of beam sheet and CFRP U-wraps on the west side. The connection sheet was anchored with excess CFRP U-wraps on the east side to provide stronger anchorage than that on the west side. The test of this specimen focused on the lap spliced region of the beam and connection sheets. It also focused on behavior of the beam sheet and CFRP U-wraps on the west side. The surface of the bottom face was sand-blasted. The measured compressive strength of the concrete was 6,000 psi. Configuration of the beam is shown in Figure 3.99. The failure mode of B-BH-U-6S was fracture of the beam sheet in the center of the beam (Figure 3.100). The fracture occurred where the lap splice ended.

The measured applied load and reactions are shown in Figure 3.101. Drop height of the pendulum mass was 3 in. and the duration of event was 0.025 sec. The peak

113

applied load was 45.5 kip and the peak reaction was 9.8 kip at the east support. Impulse of the applied load was 0.17 kip-sec while that of sum of the reactions was 0.09 kip-sec.

The normalized applied load and sum of the reactions are shown in Figure 3.102. The peak normalized applied load was 10.4 kip and sum of the reactions was 5.4 kip (52 % of the peak normalized applied load). The calculated static strength of B-BH-U-6S was 11.1 kip and the peak normalized applied load was 94% of the static strength.
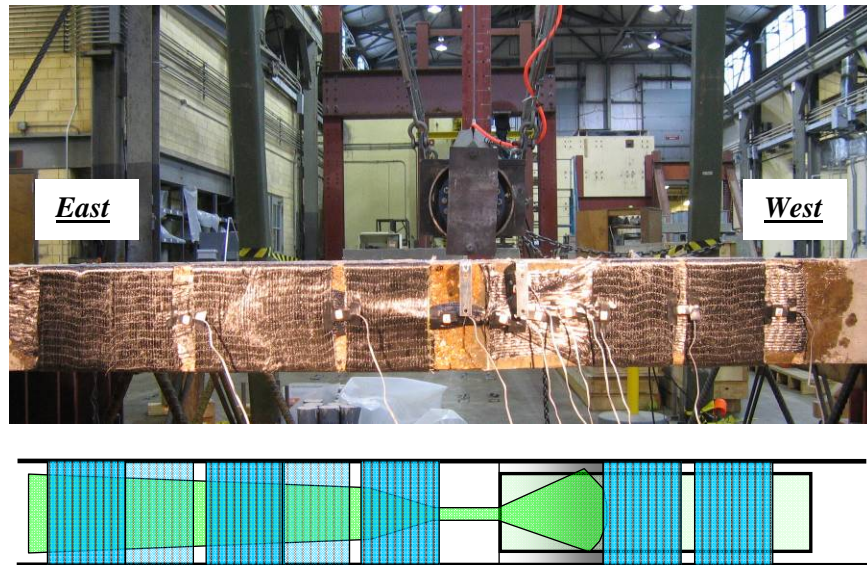
*Figure 3.99   Configuration of B-BH-U-6S*
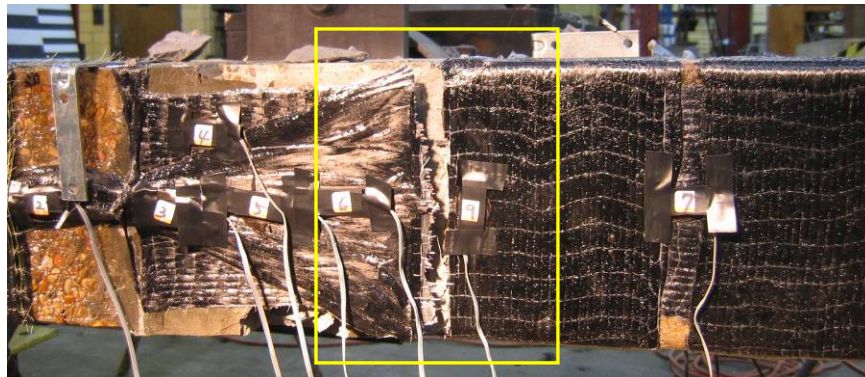

Figure 3.100   Failure of B-BH-U-6S, fracture of beam sheet

114
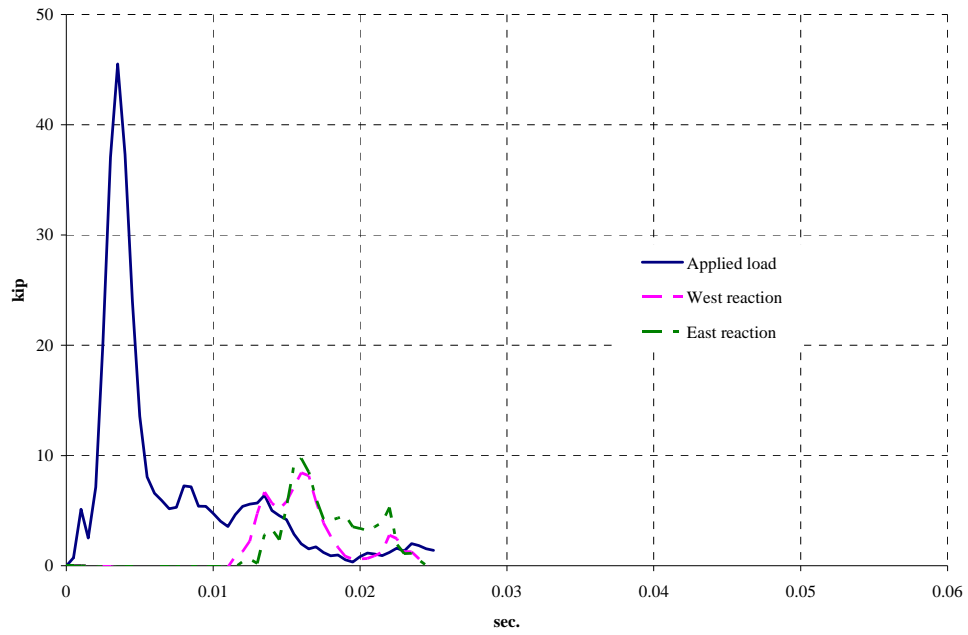
Figure 3.101   Measured applied load and reactions, B-BH-U-6S
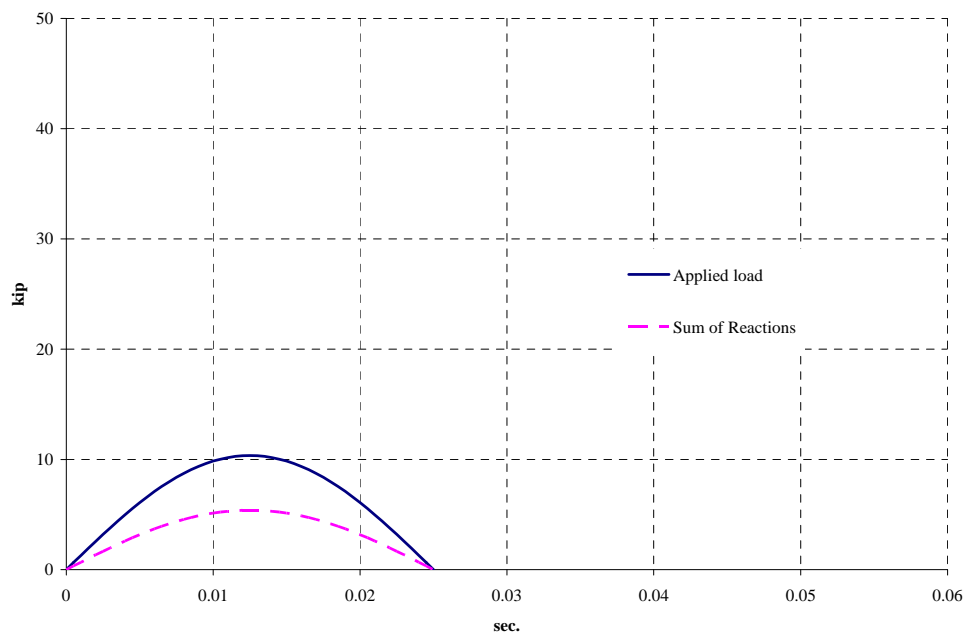
Figure 3.102   Normalized applied load and sum of reactions, B-BH-U-6S

115

The location of the strain gages installed and the maximum measured strain in each gage are shown in Figure 3.103. The maximum strain was 0.0060 at gage 2 (60 % of the ultimate tensile strain of the CFRP). The peak strain did not reach the ultimate tensile strain because this gage was away from the location of fracture. The highest strain occurred in the strap portion of the connection sheet (gage 2) and a similar level of strains was observed in the lap splice region (gage 3, 4 and 5). The solid line in the CFRP strain plot in Figure 3.103 was plotted connecting the measured strains and the dashed line was plotted using the expected ultimate strain where fracture occurred. Because of a rapid change of the quantity of the CFRP at the end of the lap splice on the beam sheet side (west), a high stress might occur at the location and create a weak link. Strain rate of CFRP was 0.750 /sec. The strain response of gages 2, 3, 6 and 7 is shown in Figure 3.104.

The maximum strain measured in the #6 bars in B-BH-U-6S was 0.0003 which was about 15 % of yield of the steel reinforcement.
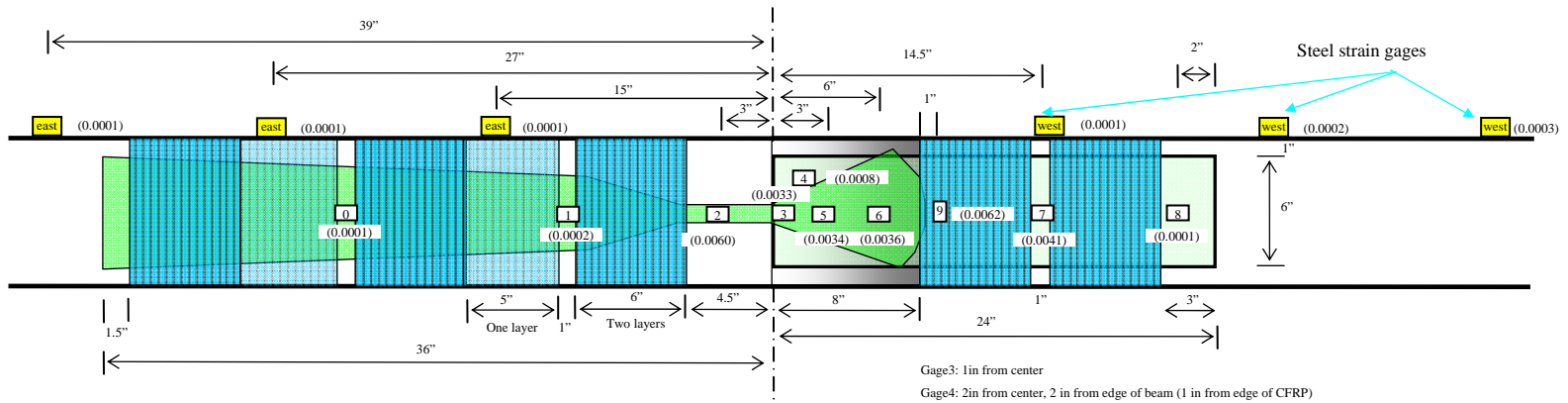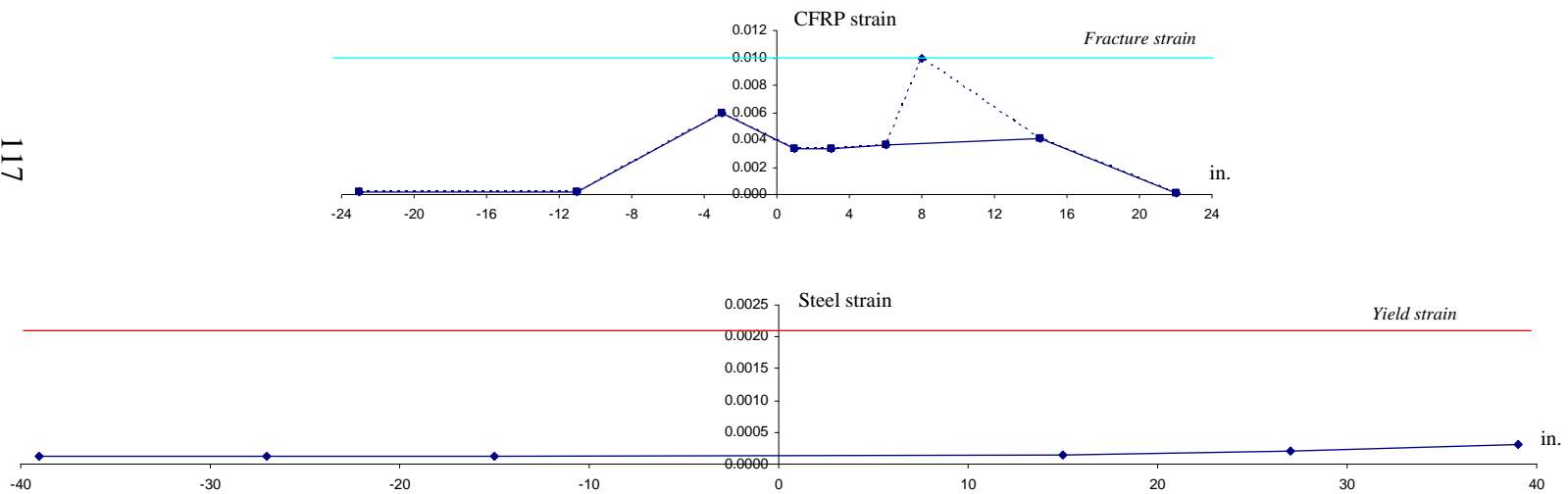
Figure 3.103   Location of strain gages and distribution of strain in CFRP and bars, B-BH-U-6S
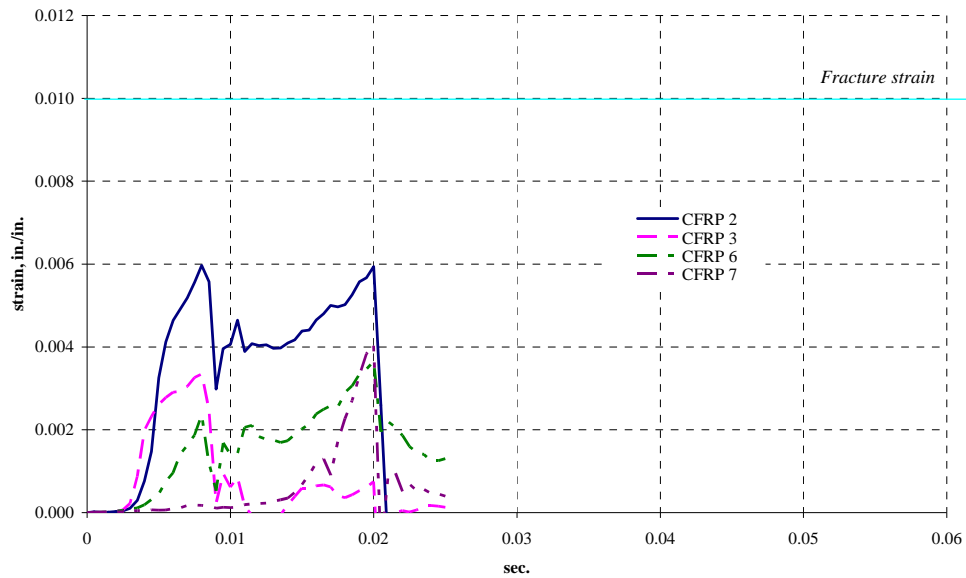
Figure 3.104   CFRP strain, B-BH-U-6S

3.6.2.3   Comparisons

In the beams with a height transition (B-BH-A-6G and B-BH-U-6G), the effectiveness of different anchorage methods (CFRP anchor or CFRP U-wrap) on dynamic performance of CFRP was examined. The only difference between these two beams was type of anchorage. Both beams failed by fracture of the CFRP sheet and the CFRP sheet reached the ultimate tensile strength. These results showed that the anchorage methods used to reach ultimate strength under static loading performed similarly under dynamic loading. As shown in Figure 3.105 and Figure 3.106, beams with the anchorage using the anchors or U-wraps failed by CFRP fracture under static loading.
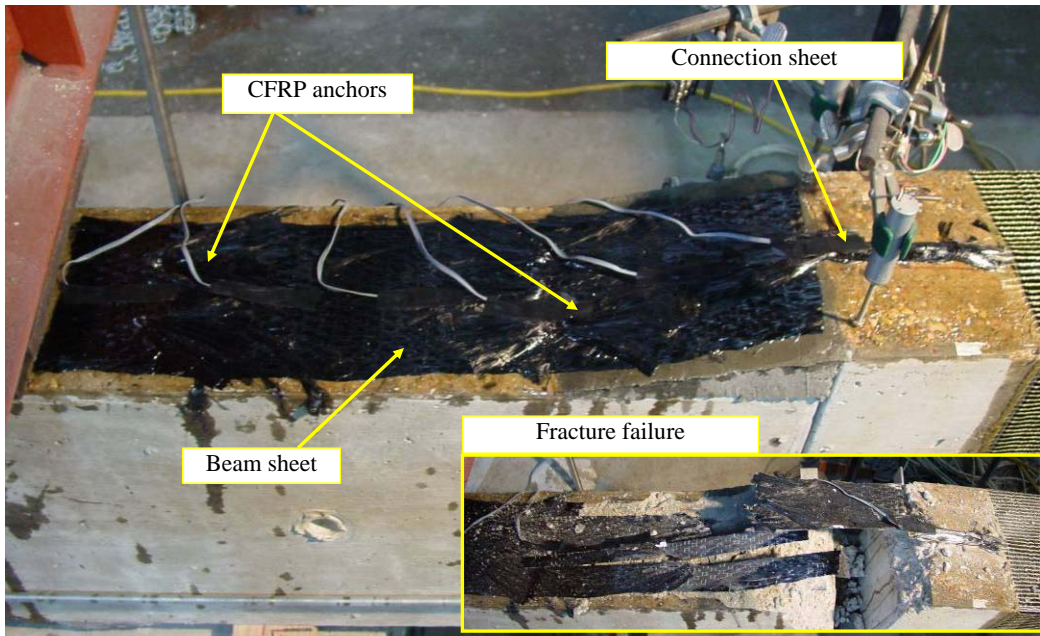
Figure 3.105   Static test, CFRP sheet and anchors, 105 % of the ultimate strength
(Orton, 2007)
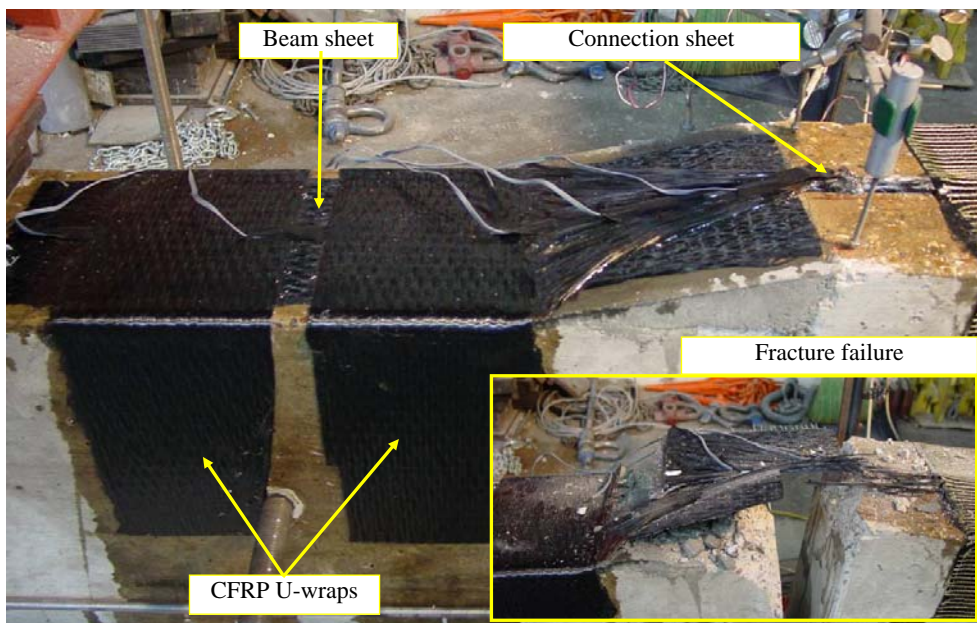
Figure 3.106   Static test, CFRP sheet and U-wraps, 89 % of the ultimate strength
(Orton, 2007)

The test results indicated that the anchorage method with the CFRP U-wraps was effective in anchoring the CFRP sheets as CFRP anchors. However, the connection sheet failed in B-BH-A-6G while the beam sheet failed in B-BH-U-6G because a smooth transition from the connection sheet to the beam sheet can be provided using CFRP anchors while a sudden change in quantity of CFRP sheet occurred at the bottom of the transition ramp when the CFRP U-wraps were used. In addition, B-BH-A-6G, which had CFRP anchors, showed better performance than B-BH-U-6G, which had U-wraps. The drop height of the pendulum mass at the fracture of the CFRP sheet was 3 in. for both beams. However, two impacts at 3 in. drop height were required for the failure of B-BH-A-6G while B-BH-U-6G failed after only one impact at the same drop height. It showed that more energy was required to fracture the CFRP sheet with anchors than with U-wraps. In B-BH-A-6G, the ratio of the impulse of applied load to that of sum of the reactions at the fracture of CFRP sheet was 80 % while that in B-BH-U-6G was 52 %. It indicated that more applied load was transferred to the support between the time of impact and fracture of the CFRP sheet in B-BH-A-6G than B-BH-U-6G. The maximum measured strain in the steel reinforcement was high in B-BH-A-6G (0.0011) compared with that in B-BH-U-6G (0.0003). Before the fracture of CFRP sheet, more stress was transferred to the steel reinforcement from the CFRP in B-BH-A-6G than in B-BH-U-6G. A summary of comparison of test results between two beams are shown in Table 3.5.

Peak normalized applied load was less than calculated static strength but still close to the strength.

Table 3.5   ***Comparison of the test results of the beams with height transition bottom face***

Condition at the fracture of the CFRP sheet		Drop height	Peak applied load		Static strength	Impulse			Max. strain in bars
			Measured load	Normalized load		Applied load, A	Sum of reactions, R	Ratio, R/A	
B-BH-A-6S		3 in	41.4 kip	10.1 kip	11.1 kip	0.16 kip-sec	0.13 kip-sec	80%	0.0011
B-BH-U-6S		3 in.	45.5 kip	10.4 kip	11.1 kip	0.17 kip-sec	0.09 kip-sec	52%	0.0003

3.6.3 Rehabilitation Using Side Faces of Beam

3.6.3.1 A-S-A-6G

A-S-A-6G was a Type A beam with two layers of CFRP sheet and CFRP anchors. The CFRP sheets and anchors were applied to both sides of the beam symmetrically. The surface of the side faces was ground. The measured compressive strength of the concrete was 6,000 psi. Configuration of the beam is shown in Figure 3.107. The failure mode of A-S-A-6G was fracture of the CFRP sheets in the center of the beam (Figure 3.108). The fracture occurred in the CFRP sheets on both sides.

The measured applied load and reactions are shown in Figure 3.109 for loading to failure. Drop height of the pendulum mass in A-S-A-6G was 12 in. when it failed and the duration of event was 0.020 sec. The peak applied load was 81.4 kip and the peak reaction was 17.0 kip at the west support. Impulse of the applied load was 0.23 kip-sec while that of sum of the reactions was 0.04 kip-sec. Before the test with a 12 in. drop height of pendulum, loading with the pendulum at 6 in. drop height was applied. Results of this test is provided in Appendix A.

The normalized applied load and sum of the reactions are shown in Figure 3.110. The peak normalized applied load was 18.4 kip and sum of the reactions was 3.0 kip (16 % of the peak normalized applied load). The calculated static strength of A-S-A-6G was 16.3 kip and the peak normalized applied load was 113 % of the static strength.

121
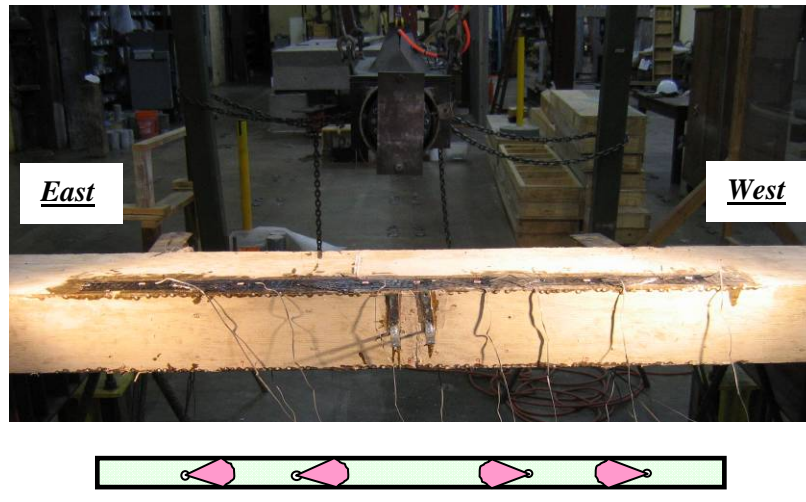
Figure 3.107   Configuration of A-S-A-6G

**Figure 3.108   Failure of A-S-A-6G, fracture of CFRP sheet**
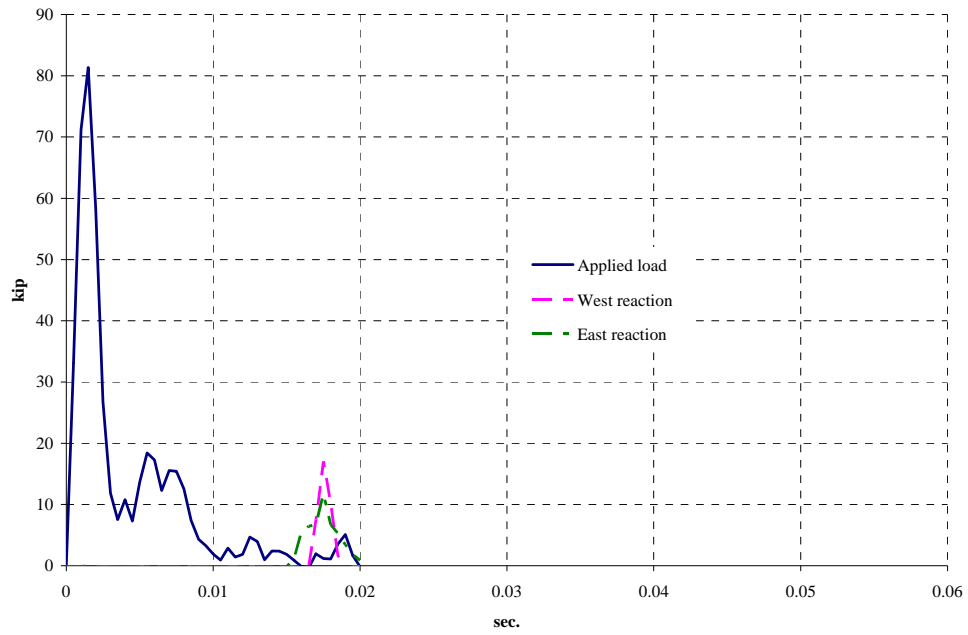
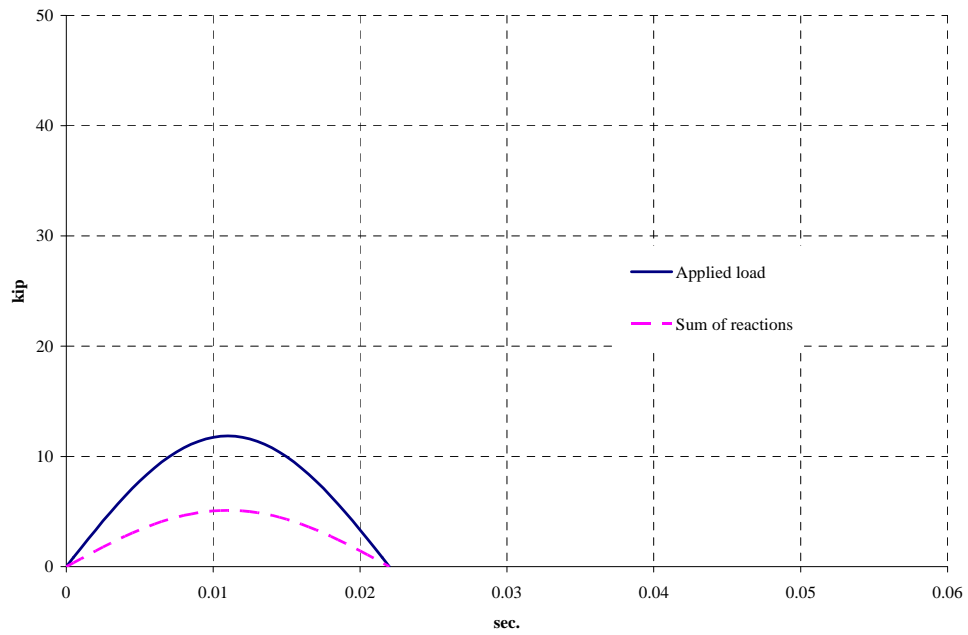*Figure 3.109   Measured applied load and reactions, A-S-A-6G*
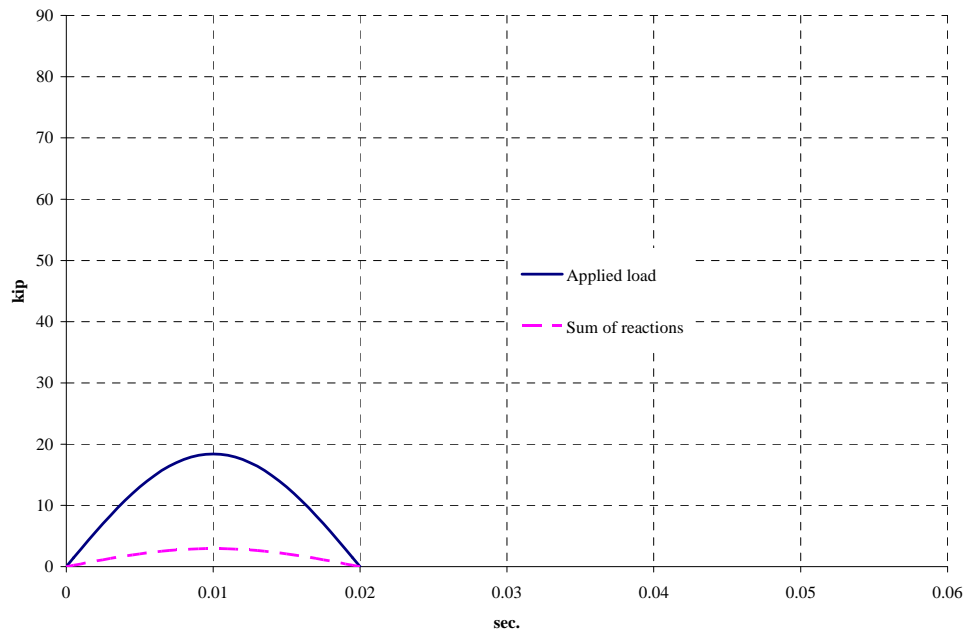
Figure 3.110   Normalized applied load and sum of reactions, A-S-A-6G

The location of the strain gages and the maximum measured strain in each gage are shown in Figure 3.111. The measured strains only on one side, top side, of the beam are shown in this figure. The maximum strain measured was 0.0098 at gage 2 (98 % of the ultimate tensile strain of the CFRP). Although facture of the CFRP sheet occurred, the measured strain did not reach the ultimate tensile strain because the location of fracture was not identical to that of the gage. A symmetric horizontal distribution of strains was observed. The highest strain occurred in the gage in front of the first anchor and strain decreased away from the center. Strain rate of CFRP this beam was 0.891 /sec. The strain response of gages 3, 4 and 5 is shown in Figure 3.112. The initial values of strain in the gages were not zero because of the previous impact on this beam.

The maximum strain measured in the #6 bars in A-S-A-6G was 0.0015 which was about 70 % of yield of the steel reinforcement.
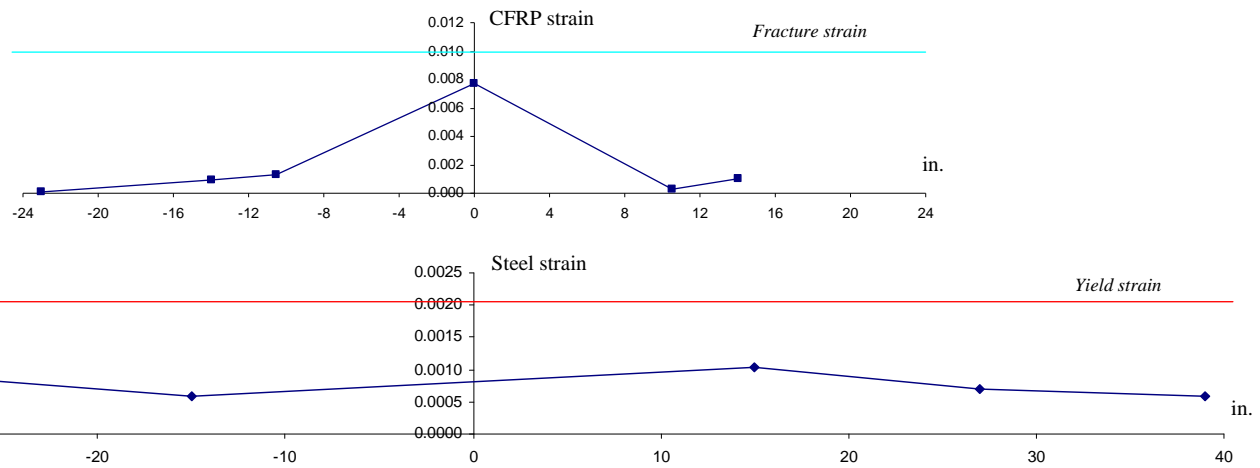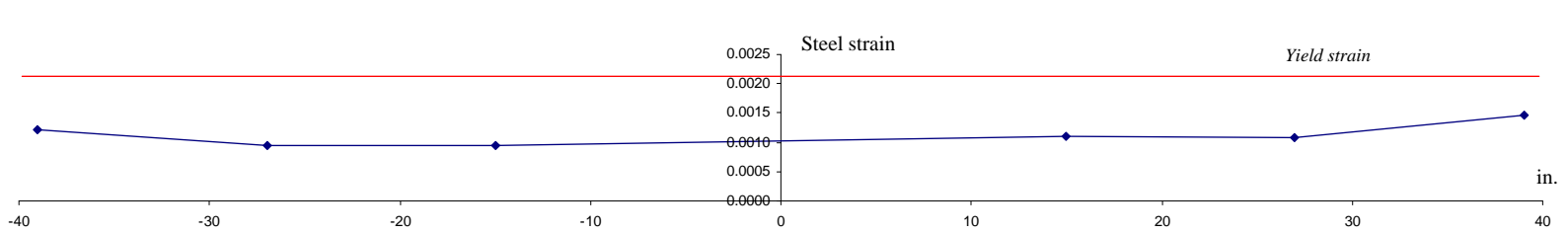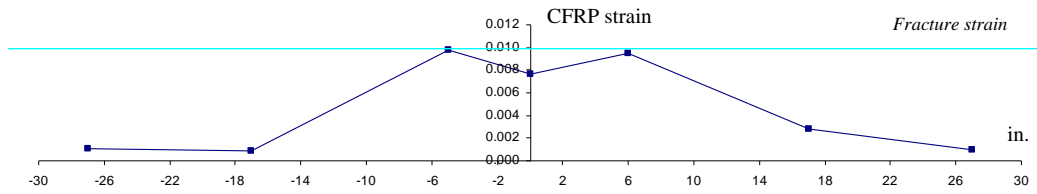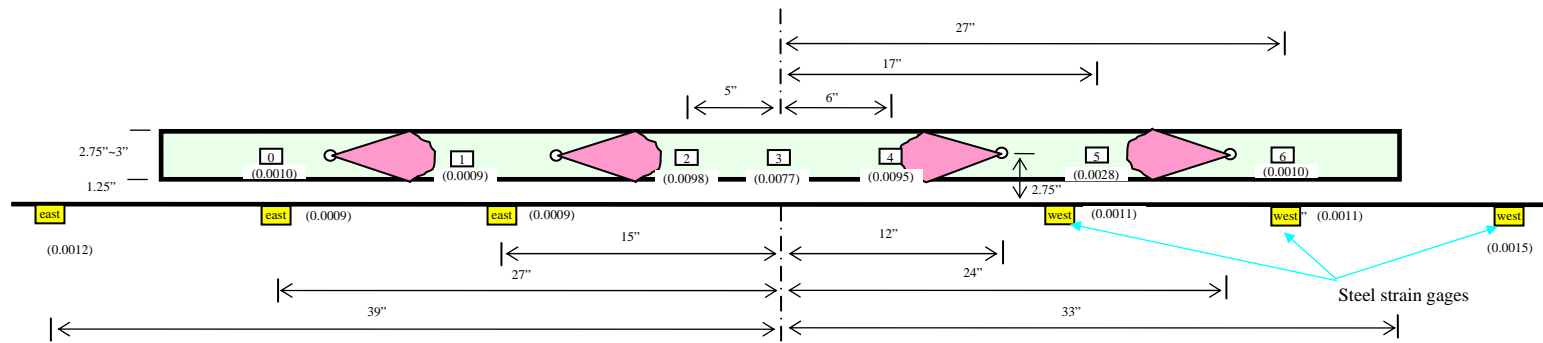
*Figure 3.111   Location of strain gages and distribution of strain in CFRP and bars, A-S-A-6G*
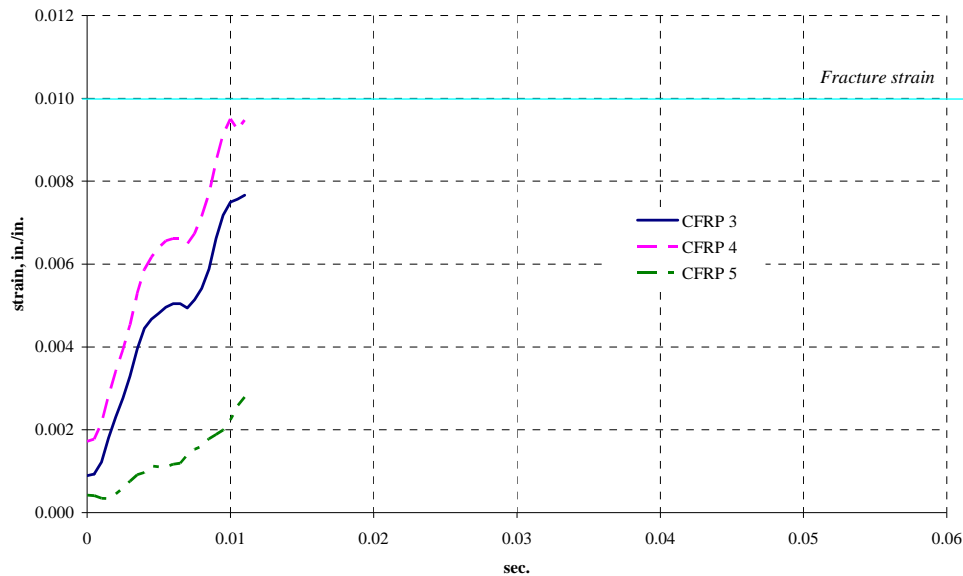
Figure 3.112   CFRP strain, A-S-A-6G

3.6.3.2   *A-S-AU-2S*

A-S-AU-2S was a Type A beam with two layers of the CFRP sheets and a combination of the CFRP anchors and U-wraps. The CFRP sheets, anchors and U-wraps were applied to both sides of the beam symmetrically. The surface of the side faces was sand-blasted. The measured compressive strength of the concrete was 2,000 psi. Configuration of the beam is shown in Figure 3.113. The failure mode of A-S-AU-2S was fracture of the CFRP sheets in the center of the beam (Figure 3.114). The fracture occurred in the CFRP sheets on both sides.

The measured applied load and reactions are shown in Figure 3.115 for loading to failure. Drop height of the pendulum mass was 12 in. when it failed and the duration of event was 0.031 sec. The peak applied load was 73.8 kip and the peak reaction was 16.9 kip at the east support. Impulse of the applied load was 0.24 kip-sec while that of sum of the reactions was 0.13 kip-sec. Before the test with a 12 in. drop height of pendulum,

126

loading with the pendulum at 6 in. drop height was applied. Result of this test is provided in Appendix A.

The normalized applied load and sum of the reactions are shown in Figure 3.116. The peak normalized applied load was 12.4 kip and sum of the reactions was 6.5 kip (53 % of the peak normalized applied load). The calculated static strength of A-S-AU-2S was 14.3 kip and the peak normalized applied load was 87 % of the static strength.
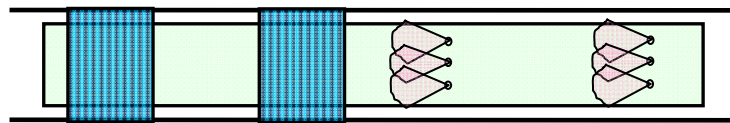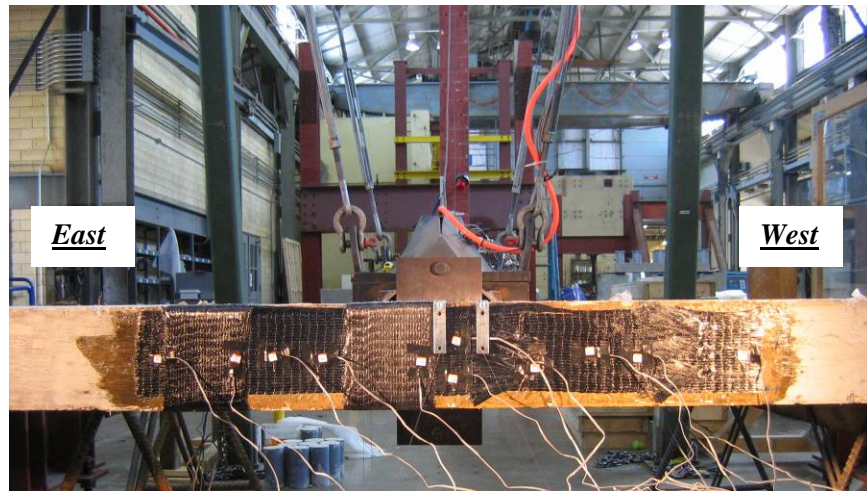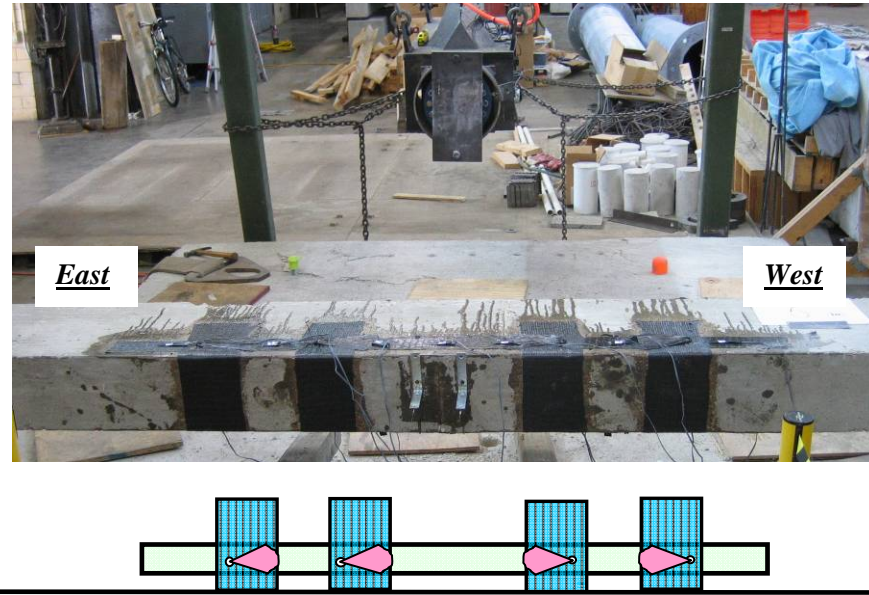

Figure 3.113   Configuration of A-S-AU-2S

*Figure 3.114   Failure of A-S-AU-2S, fracture of CFRP sheet*
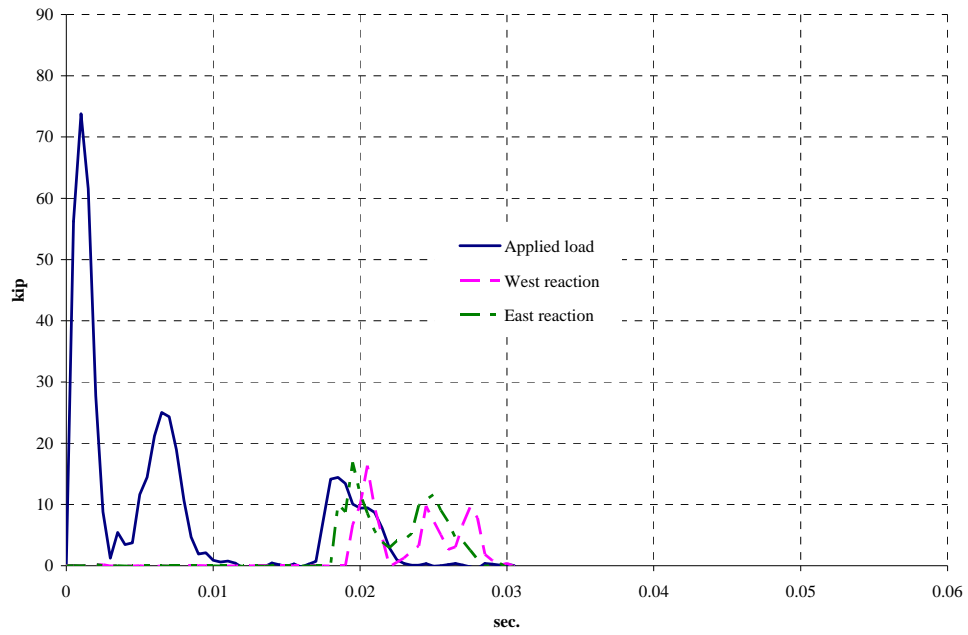
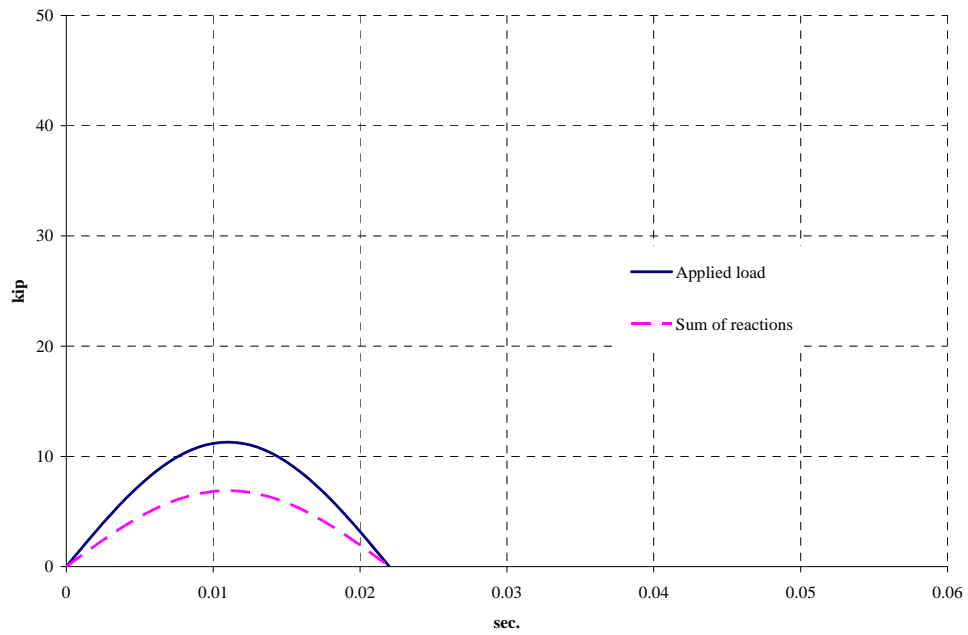*Figure 3.115   Measured applied load and reactions, A-S-AU-2S*
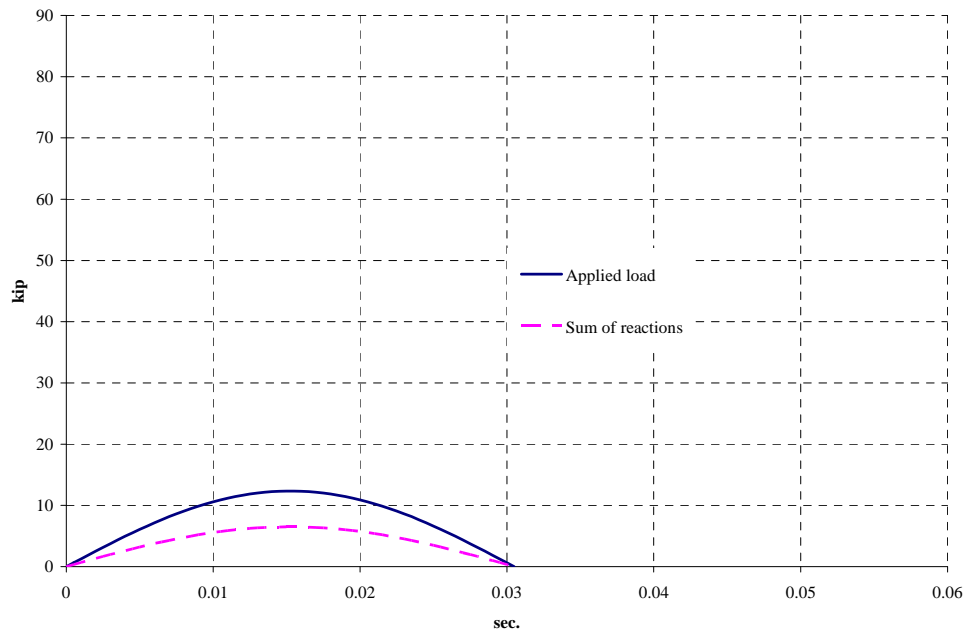
Figure 3.116   Normalized applied load and sum of reactions, A-S-AU-2S

128

The location of the strain gages and the maximum measured strain in each gage are shown in Figure 3.117. The measured strains on both top and bottom sides of the beam are shown in this figure. The maximum strain measured was 0.0110 at gage 2 (110 % of the ultimate tensile strain of the CFRP). The measured CFRP strain reached the ultimate tensile strain of the CFRP. A symmetric distribution of strains was observed. The highest strain occurred in the gages between the first CFRP anchors and strain decreased away from the center. The CFRP sheets on two sides showed similar strain distribution. Strain rate of CFRP was 0.423 /sec. The strain response of gages 10, 11 and 12 is shown in Figure 3.118. The initial values of strain in the gages were not zero because of the previous impact on this beam.

Strain gages were not installed in the #6 bars in this beam.

Bottom

Top
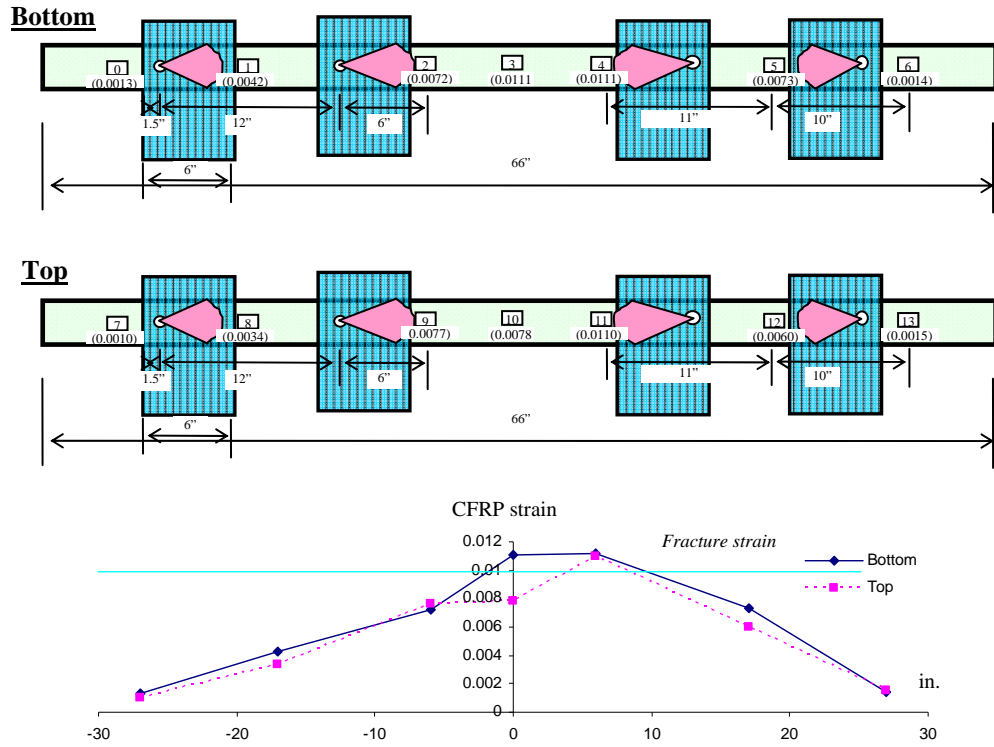
Figure 3.117   Location of strain gages and distribution of strain in CFRP, A-S-AU-2S
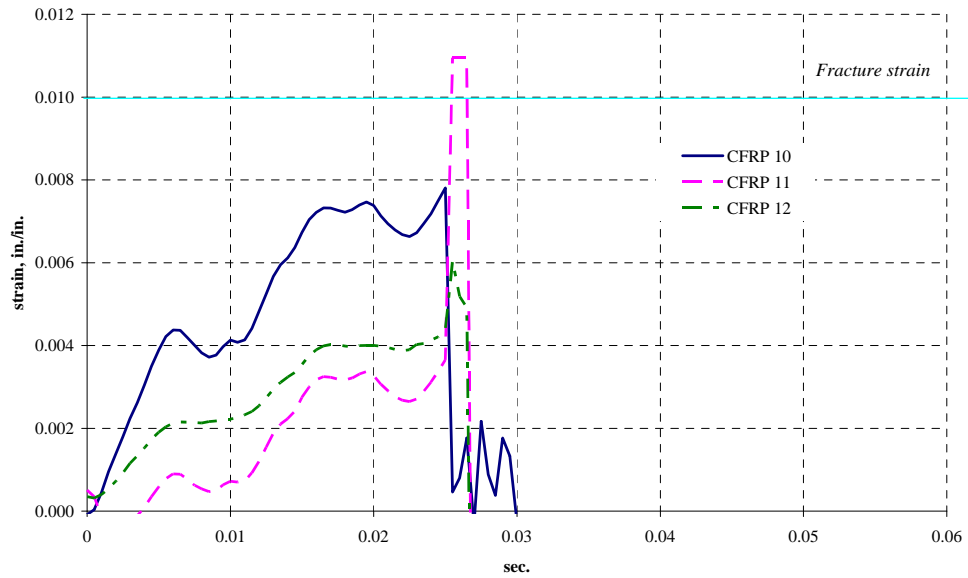
Figure 3.118   CFRP strain, A-S-AU-2S

130

3.6.3.3 Comparisons

Two specimens (A-S-A-6G and A-S-AU-2S) were tested with the side face strengthening. The failure mode of both specimens was fracture of the CFRP sheets, and this failure mode indicated that the ultimate strength of the CFRP sheets was realized in both specimens. The failure mode of A-S-A-6G under dynamic loading was different from that under static loading (concrete failure near the anchor holes, Figure 3.119) while the failure mode of A-S-AU-2S was the same as that under static loading (fracture of the CFRP sheet, Figure 3.120). In similar tests under static loading (Kim, 2006), the compressive strength was 3,500 psi. Because of the low compressive strength, the specimen loaded statically exhibited a failure in the concrete while the comparison specimen with 6,0000 psi concrete failed by fracture of the CFRP sheet under dynamic loading. In the case where the anchors only were used, the compressive strength of the concrete might affect the performance of the specimen. However, if a combination of the CFRP anchors and U-wraps was used, the ultimate strength of CFRP strength was realized in both static and dynamic loading conditions regardless of the compressive strength of the concrete. These results indicated that anchors combined with U-wraps were effective in anchoring the CFRP sheets applied to the side faces of reinforced concrete beams.
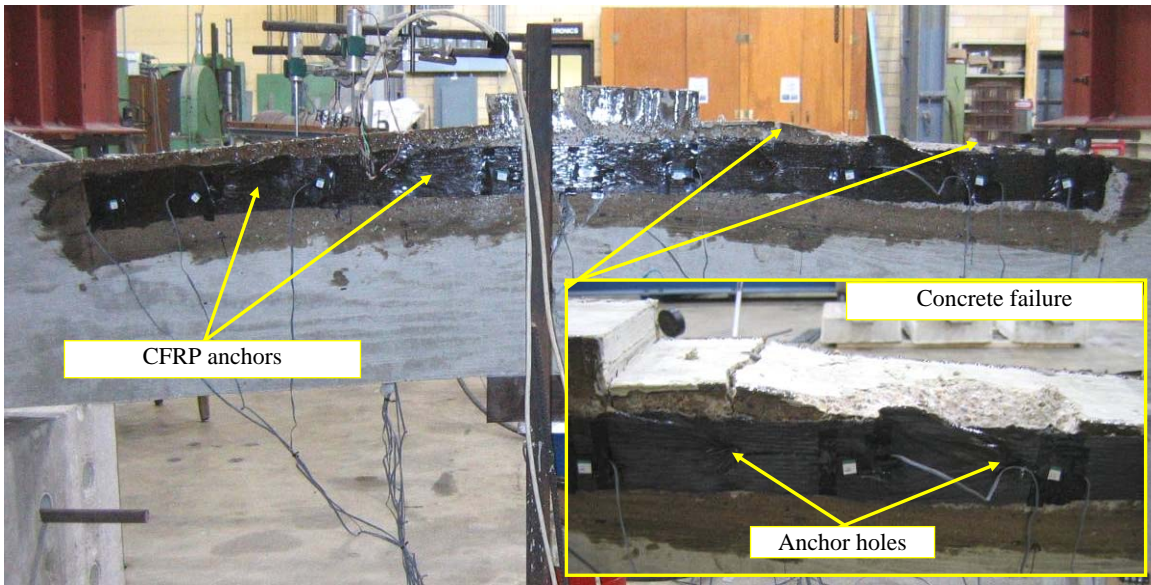
Figure 3.119 Static test, CFRP anchors, 81 % of the ultimate strength (Kim, 2006)
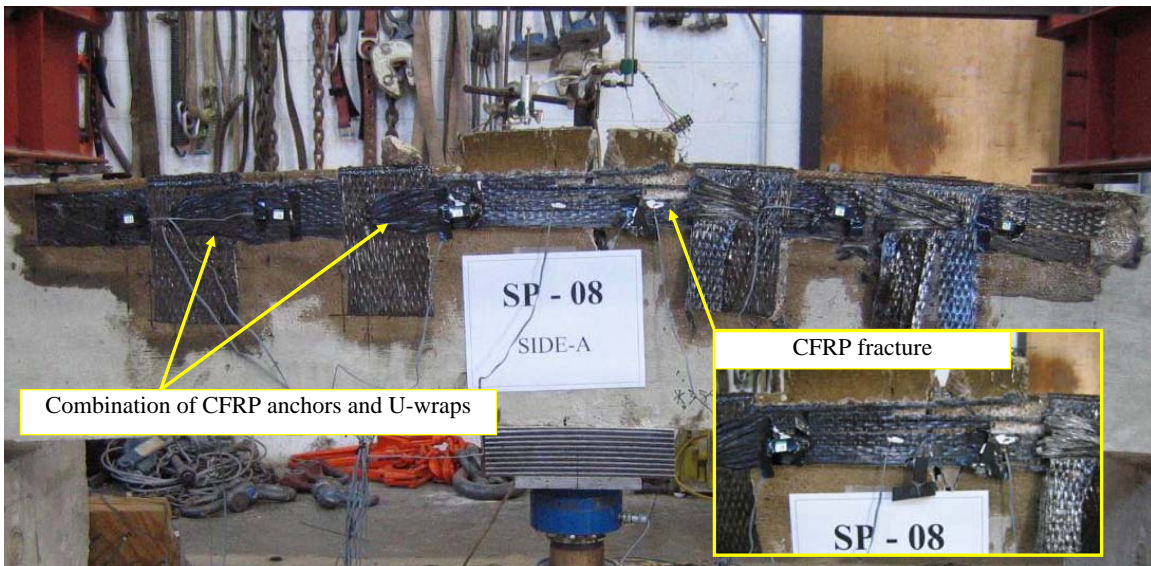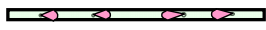
Figure 3.120 Static test, a combination of CFRP anchors and U-wraps,
100 % of the ultimate strength (Kim, 2006)

A-S-AU-2S showed better dynamic performance than A-S-A-6G although the drop height of the pendulum mass at the fracture of the CFRP sheet was 12 in. for both beams. In A-S-AU-2S, the ratio of the impulse of the applied load to that of sum of the reactions at fracture of CFRP sheet was 53 % while that in A-S-A-6G was 16 %. It indicated that more applied load was transferred to the support between the time of impact and fracture of the CFRP sheet. Strain in the steel reinforcement was not measured in A-S-AU-2S so it was not possible to compare the steel reinforcement strain. A summary of comparison of test results between two beams are shown in Table 3.6.

Table 3.6   *Comparison of the test results of the beams using side faces*

Condition at the fracture of the CFRP sheet		Drop height	Peak applied load		Static strength	Impulse			Max. strain in bars
			Measured load	Normalized load		Applied load, A	Sum of reactions, R	Ratio, R/A	
A-S-A-6G		12 in	81.4 kip	18.4 kip	16.3 kip	0.23 kip-sec	0.04 kip-sec	16%	0.0015
A-S-AU-2S		12 in.	73.8 kip	12.4 kip	14.3 kip	0.24 kip-sec	0.13 kip-sec	53%	

3.6.4 Rehabilitation of Beams with Column

3.6.4.1 *C-BC-A-6G-01*

C-BC-A-6G-01 was a Type C beam and CFRP was applied through the column at the bottom face. This beam had one layer of the beam sheet on the east and west side, and the sheet was anchored using the CFRP anchors. The connection sheet connected the beam sheets through the column hole and was lap spliced with the beam sheets on the transition ramps. The surface of the bottom face was ground. The measured compressive strength of the concrete was 6,000 psi. Configuration of the beam is shown in Figure 3.121.
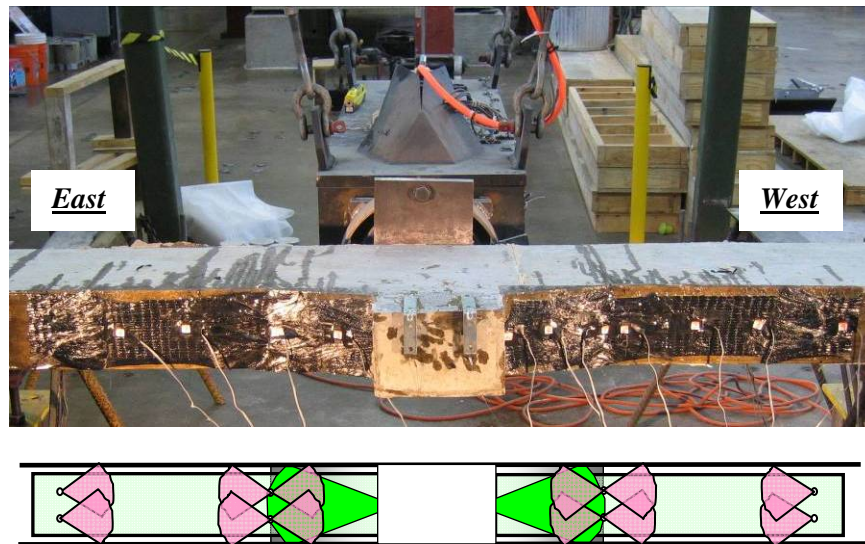
Figure 3.121   Configuration of C-BC-A-6G-01

C-BC-A-6G-01 was tested under the drop heights of 2 in., 3 in., 4.5 in., 9 in. and 12 in. At a 9 in. drop height, the steel yielded with large deflection and the concrete cracking. A 12 in. drop height, the beam sheet fractured. This beam was designed to develop yield of the steel reinforcement before fracture of CFRP. Large deformation capacity and yield of the reinforcement was observed before fracture of the CFRP.

Initially C-BC-A-6G-01 was exhibited stress well beyond yield of the steel reinforcement (Figure 3.122). Two large cracks occurred at the ends of the beam sheets and other cracks were evenly distributed over the beam where no CFRP was applied. The final failure mode of this beam was fracture of the beam sheet and CFRP anchors (Figure 3.123). The fracture occurred at the end of the lap splice of the beam and connection sheet on the west side. The ultimate tensile strength of the CFRP was realized.
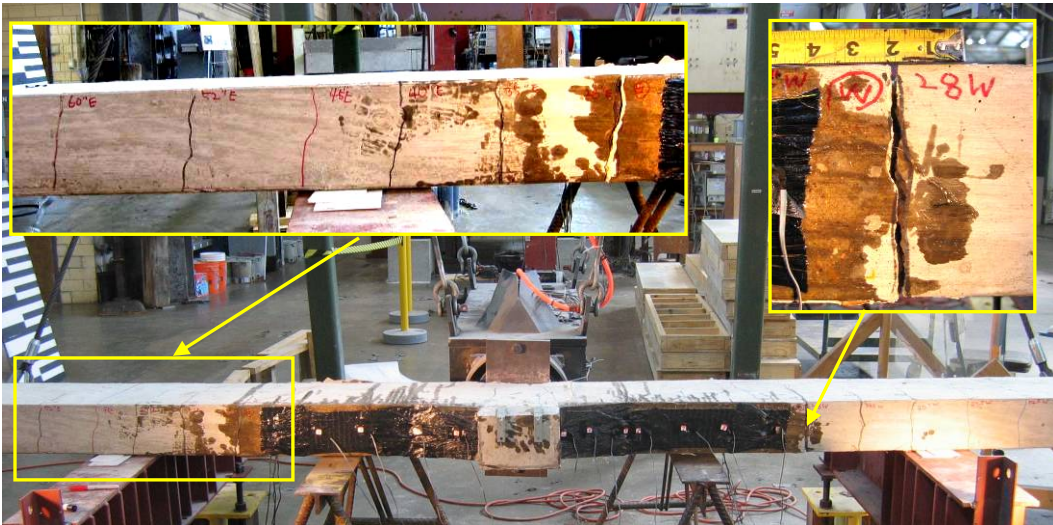
Figure 3.122   Failure of C-BC-A-6G-01, 9 in. (yield of steel reinforcement)

Figure 3.123   Failure of C-BC-A-6G-01, 12 in. (fracture of CFRP)

A summary of the applied loads and reactions are shown in Table 3.7. The results of the tests at different drop heights except 4.5 in. are presented in this section because

the results were similar to the previous test. Results of the test at 4.5 in. drop height are presented in Appendix A

The measured applied load and reactions are shown in Figure 3.124. The duration of event was relatively short in the test at 12 in. drop height (fracture of CFRP) comparing with that of the other tests (yield of steel reinforcement). The peak applied load and reactions are shown in Table 3.7. In addition, impulse of the applied load and sum of the reactions are shown in Table 3.7. The impulse and the duration of event increased as the drop height increased when the failure mode of the specimen was yield of the steel. However, they decreased when CFRP fracture occurred although the drop height is higher than the previous tests.

The normalized applied load and sum of the reactions are shown in Figure 3.125 and Figure 3.126. The peak normalized applied load and sum of the reactions and the ratio of the two are shown in Table 3.7. The ratio was relatively lower when CFRP fractured than when the steel yielded.

The calculated static strength of this beam was 4.2 kip and it was based on yield of the steel at the ends of the beam sheets (26 in. from the column face). The peak normalized load was considerably larger than the strength because of inelastic behavior of the beam during the impact. Therefore, the impulse during the impact did not represent the calculated strength of the beam.

Table 3.7   ***Summary of applied load and reactions, C-BC-A-6G-01***

(calculated static strength: 4.2 kip)

Drop height	Duration of event	Measured load			Measured impulse		Normalized load		
		Applied load	Reaction		Applied load	Sum of reactions	Peak applied load, A	Peak sum of reactions, R	Ratio, R/A
		Peak	Peak	Support					
2 in.	0.099 sec	18.4 kip	10.7 kip	West	0.44 kip- sec	0.34 kip- sec	7.0 kip	5.5 kip	78 %
3 in.	0.114 sec	18.8 kip	17.5 kip	West	0.51 kip- sec	0.41 kip- sec	7.0 kip	5.7 kip	81 %
4.5 in.	0.128 sec	31.5 kip	23.3 kip	West	0.59 kip-sec	0.50 kip-sec	7.2 kip	6.1 kip	84 %
9 in.	0.145 sec	43.9 kip	28.2 kip	West	0.74 kip- sec	0.65 kip- sec	8.1 kip	7.1 kip	87 %
12 in.	0.048 sec	60.0 kip	29.3 kip	West	0.30 kip- sec	0.20 kip- sec	10.0 kip	6.5 kip	65 %
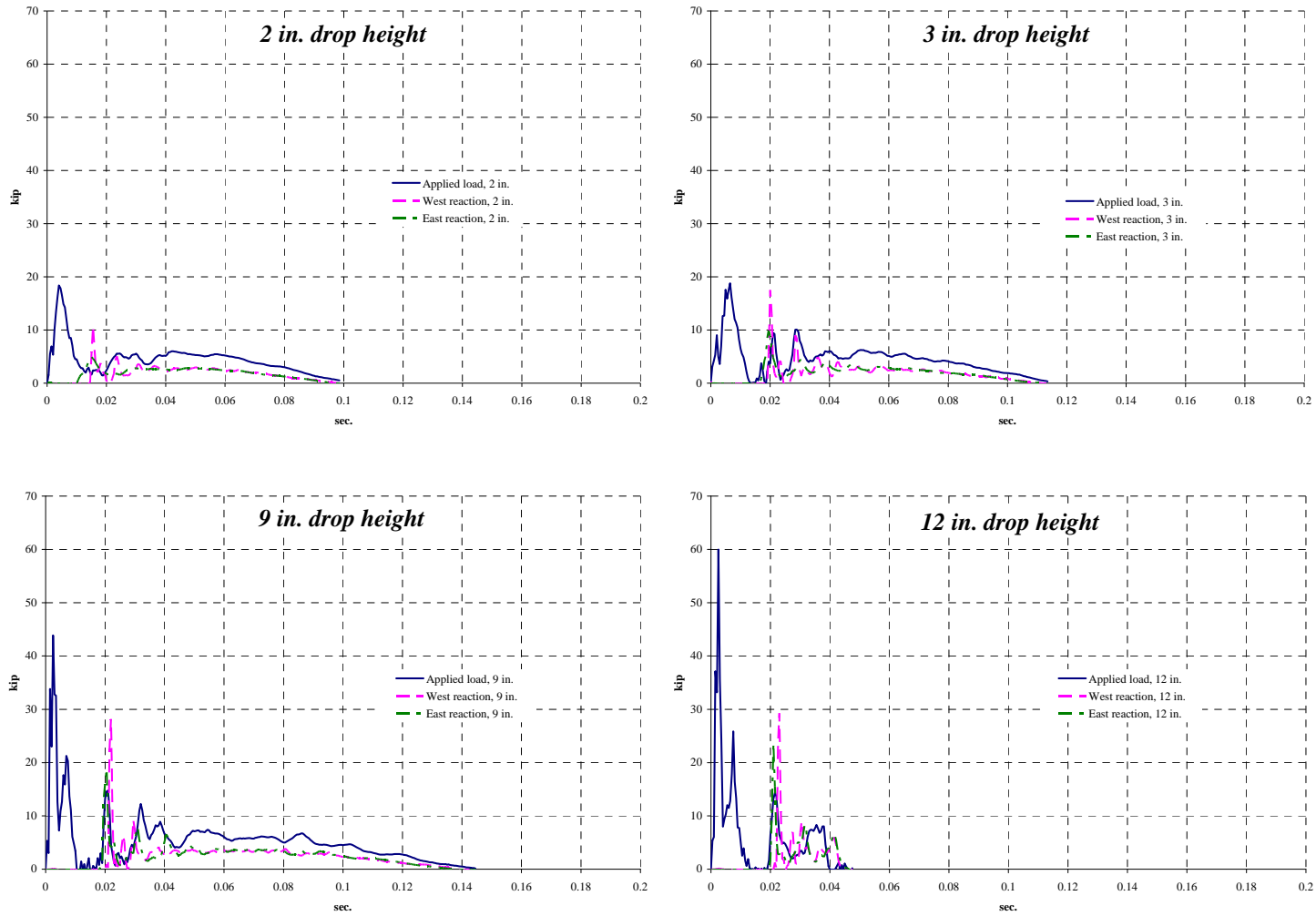
Figure 3.124   Measured applied load and reactions, C-BC-A-6G-01

138
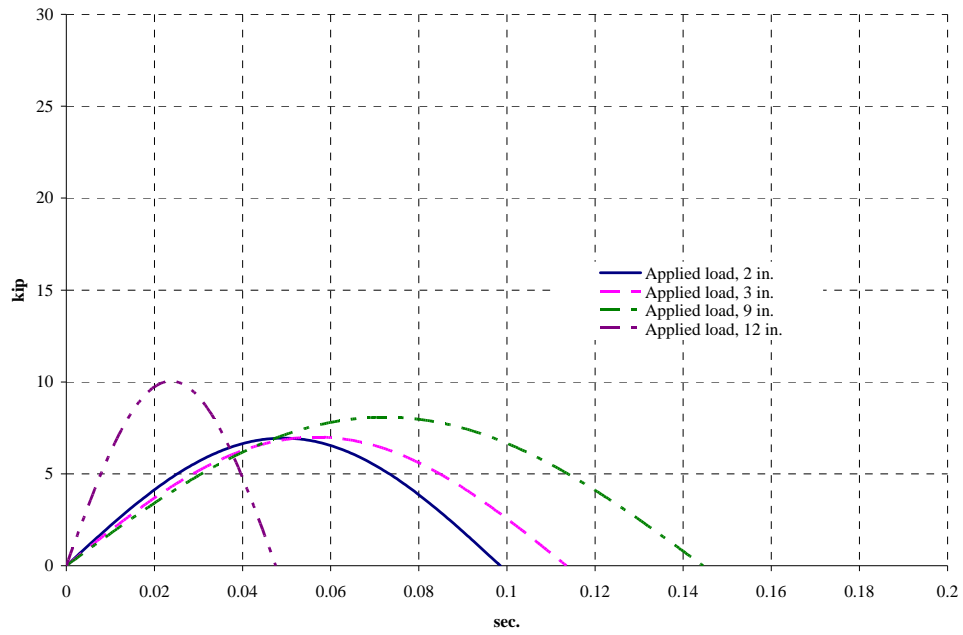
Figure 3.125   Normalized applied load, C-BC-A-6G-01
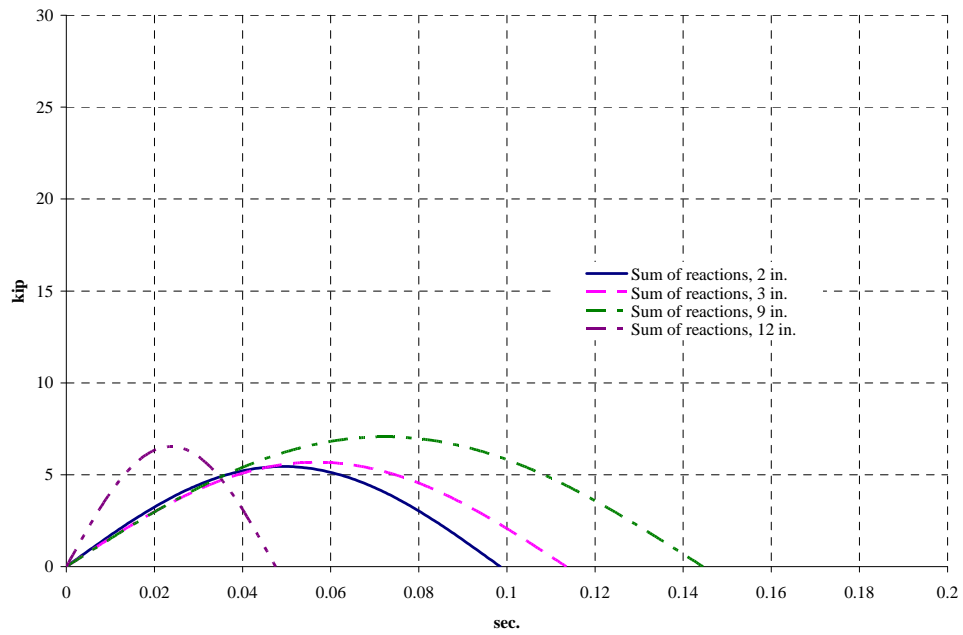
Figure 3.126   Normalized sum of reactions, C-BC-A-6G-01

139

Displacements at the column at different drop heights are plotted in Figure 3.127. The initial displacement was not zero for 3 in. and 9 in. drop height tests because of the permanent displacement after the previous tests. The shape of the measured displacement curves was similar to a half-period sine curve, and the peak displacement increased as the drop height of pendulum mass increased. The maximum displacement was 3.52 in. at a 9 in. drop height which was 1.8 % of the beam span length (16 ft). The displacement data for 12 in. drop height test is not shown in Figure 3.127 because it was not possible to determine the deflection at the instant the CFRP fractured
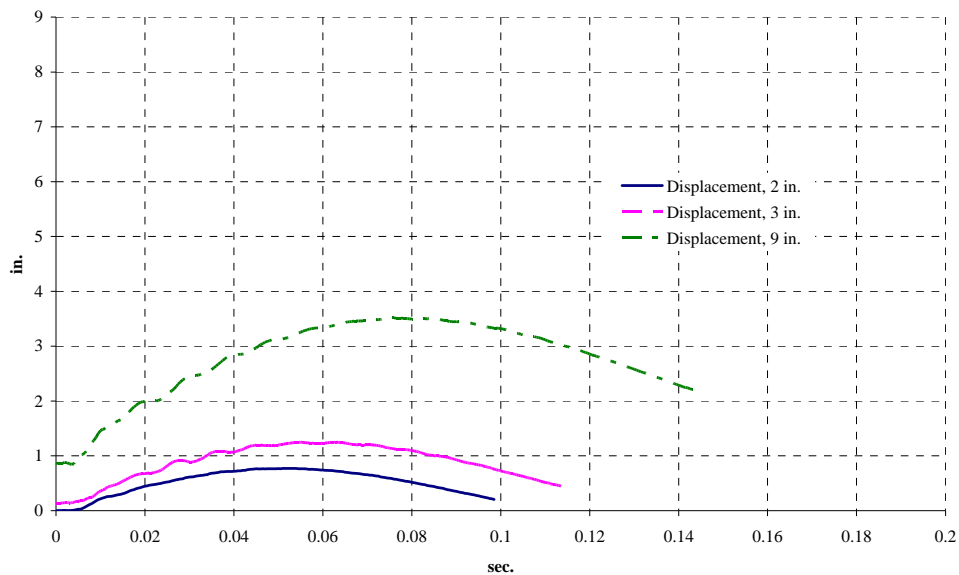
Figure 3.127   Displacement at the column, C-BC-A-6G-01

The location of the strain gages installed and the maximum measured strain are shown in Figure 3.128 and Figure 3.129. The strain data at a low drop height, 3 in., and a drop height for loading to failure, 12 in., are provided in this section. The strain distribution of the other tests is provided in Appendix A.

The maximum CFRP strain during the tests was 0.0064 at gage 10 (64 % of the ultimate tensile strain of the CFRP). The peak strain did not reach the ultimate tensile

140

strain because this gage was away from the location of fracture. From the horizontal distribution of strains in the CFRP sheet, the highest strain occurred in the gage close to the center of beam and strain decreased away from the center.

The responses of gage 10 at different drop heights are shown in Figure 3.130. The initial values of strain in the tests except the first test, 2 in. drop height, were not zero because of the previous impacts. The peak strain increased as the drop height increased.
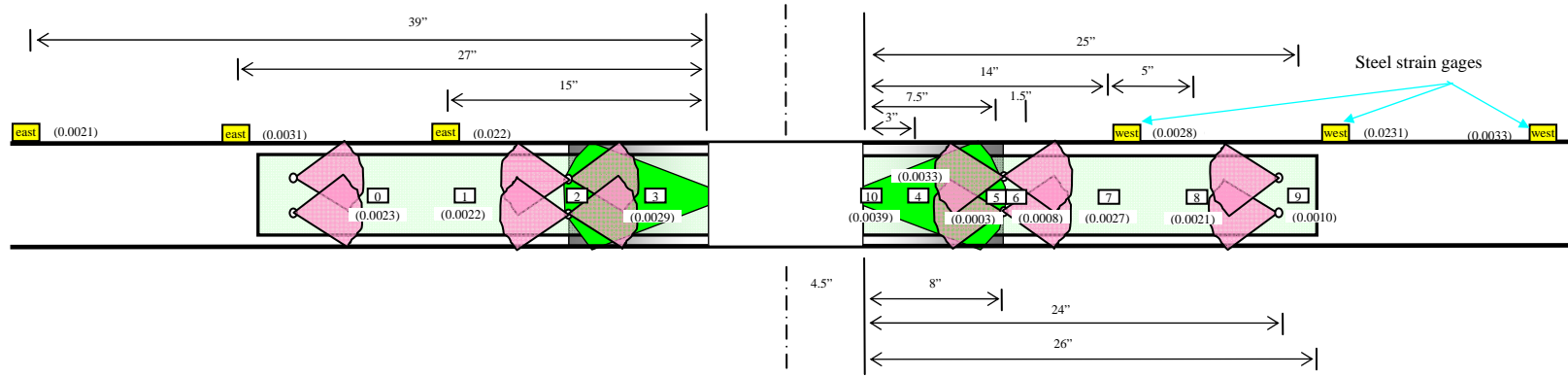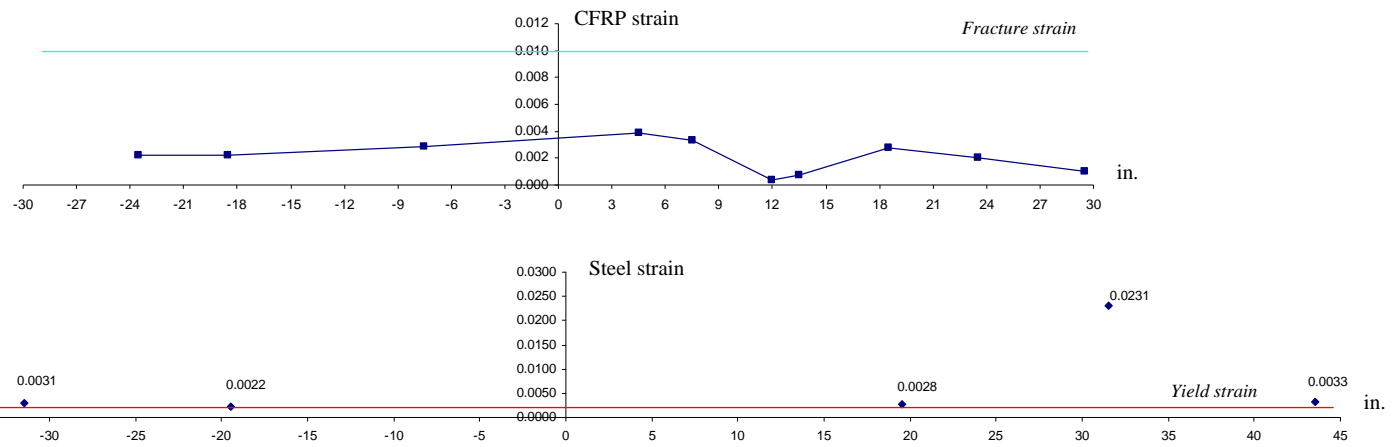
Figure 3.128 Location of strain gages and distribution of strain in CFRP and bars, C-BC-A-6G-01, 3 in.

142
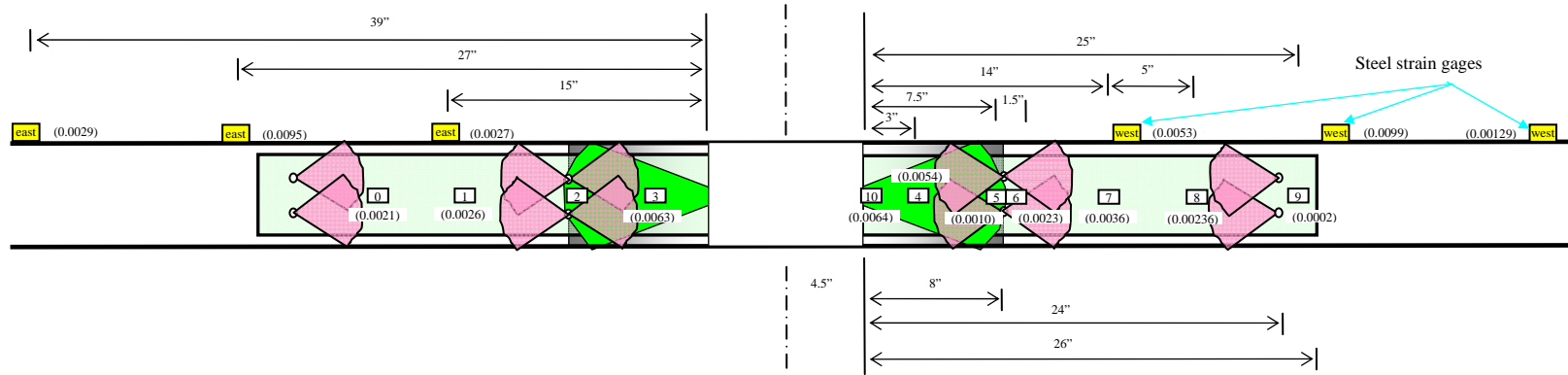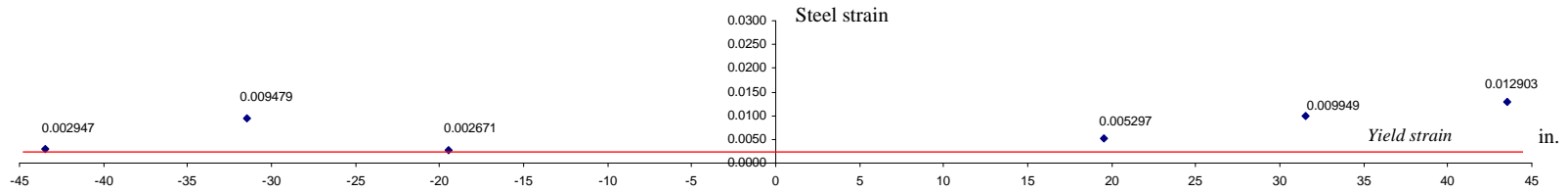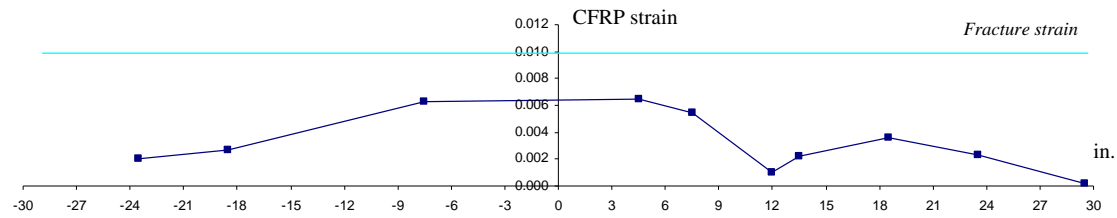
Figure 3.129   Location of strain gages and distribution of strain in CFRP, C-BC-A-6G-01, 12 in.

143
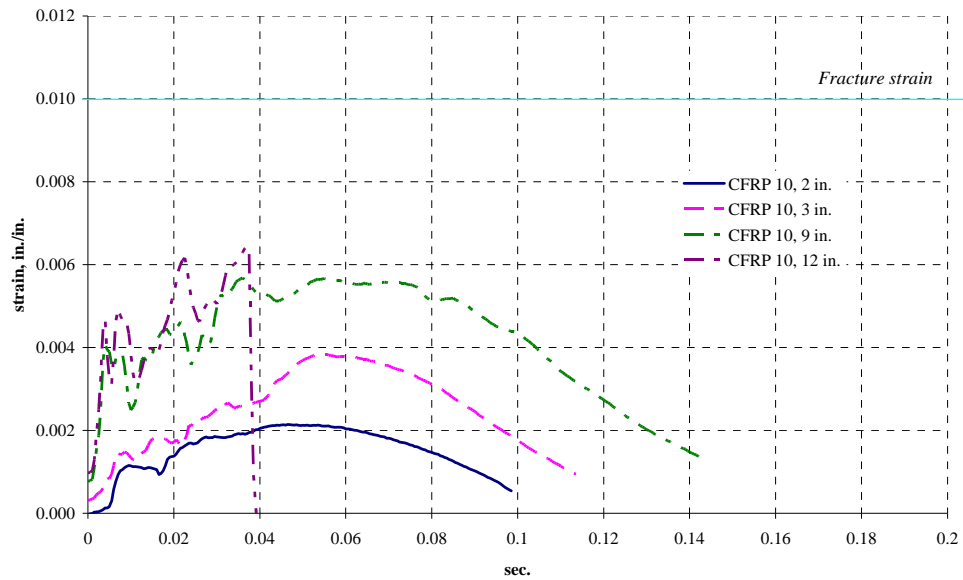
Figure 3.130   CFRP strain, C-BC-A-6G-01

The location of steel strain gages from the column face and maximum measured strain are also shown in Figure 3.128 and Figure 3.129. In the tests at 3 in. and 12 in. drop heights, all the measured strains in the #3 bars were larger than the yield strain of the steel reinforcement although they were away from the column faces. The largest bar strain was observed at location close to the ends of the CFRP material (26 in. from the column face) where large cracks existed. Steel strain gages (East-27 in. and West-27 in.) were installed at the points close to the location of the cracks. The responses of these gages at different drop heights were shown in Figure 3.131 and Figure 3.132. The bars started yielding from the first impact at a 2 in. drop height and showed large deformation when drop height increased. The peak measured strain was not proportional to the drop height because the strain depended on size, location and distribution of cracks in each impact.
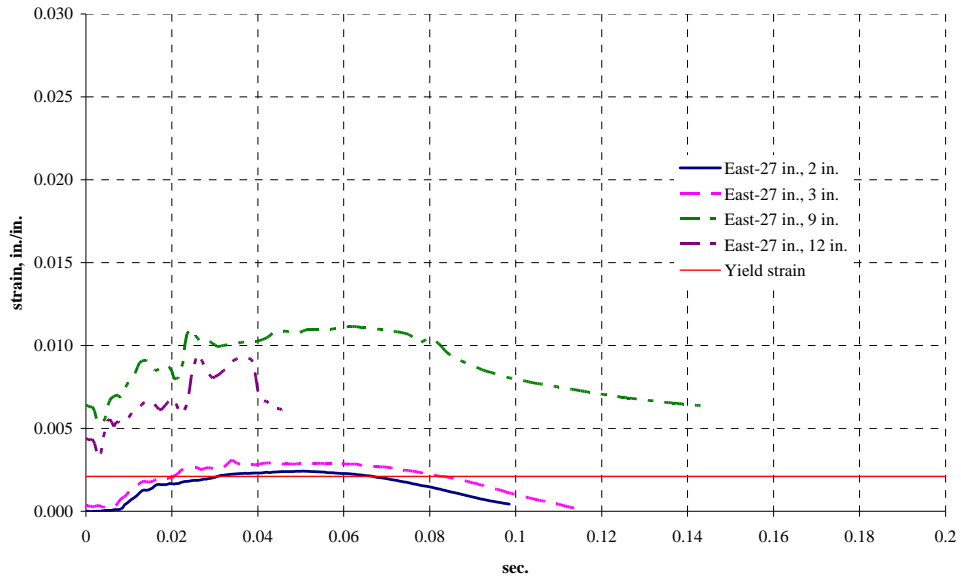
Figure 3.131   Steel reinforcement, east, C-BC-A-6G-01
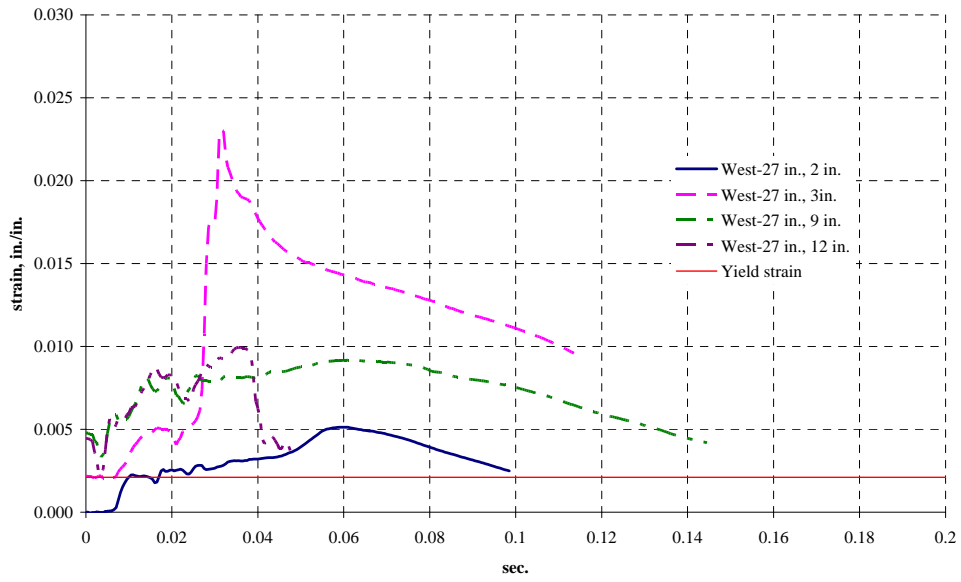
Figure 3.132   Steel reinforcement strain, west, C-BC-A-6G-01

145

3.6.4.2 C-BC-A-6G-02

C-BC-A-6G-02 was a Type C beam and CFRP was applied through the column at the bottom face. This beam had one layer of the beam sheet on the east and west side, and the sheet was anchored using the CFRP anchors. The connection sheet connected the beam sheets through the column hole and was lap spliced with the beam sheets on the transition ramps. The difference between this beam and C-BC-A-6G-01 was length of the beam sheet and location of the second set of the CFRP anchors. The length of the beam sheet was reduced based on the development length of a #3 bottom bar and the location of the second set of the anchors was also selected based on the development length. The distance from the column face to the second set of the anchors (13 in.) was longer than the development length of the #3 bar (11.6 in., ACI318-08 Section 12.2.2). Detailed geometry of the CFRP in this beam is shown in Figure 3.42. The surface of the bottom face was ground. The measured compressive strength of the concrete was 6,000 psi. Configuration of the beam is shown in Figure 3.133.
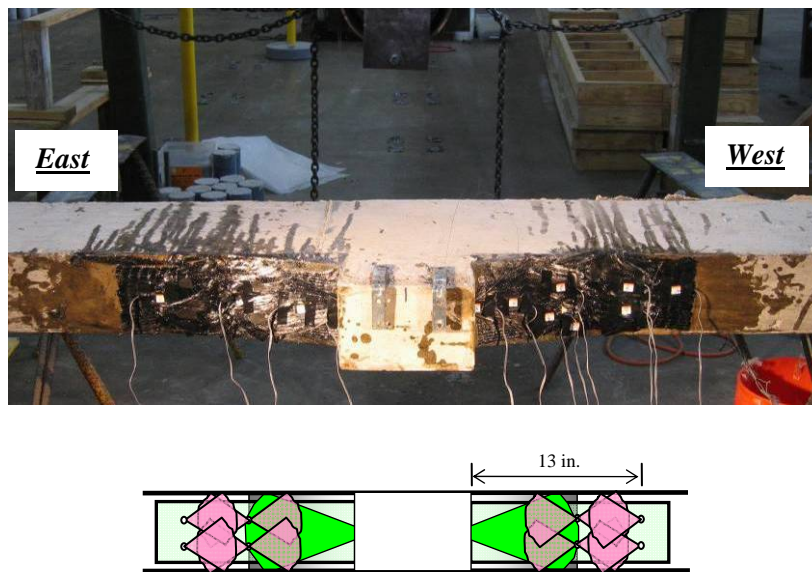
Figure 3.133   Configuration of C-BC-A-6G-02

146

C-BC-A-6G-02 was tested under the drop heights of 2 in., 3 in., 4.5 in., 9 in. and 12 in. At a 9 in. drop height, the steel yielded with large deflection and the concrete cracking. Two tests were conducted with a 12 in. drop height. In the first 12 in. test, concrete crushing and cover spalling were observed at the east end of the CFRP sheet. In the second 12 in. drop height test, the #3 bottom reinforcement fractured. This beam was designed to develop yield of the steel reinforcement before fracture of the CFRP. Large deformation capacity and yield of the reinforcement was observed, and the final failure mode was fracture of the steel reinforcement.

Initially C-BC-A-6G-02 was exhibited stress well beyond yield of the steel reinforcement (Figure 3.134). Two large cracks occurred at the ends of the beam sheets and other cracks were evenly distributed over the beam where no CFRP was applied.

The beam failed when the #3 bottom reinforcement fractured (Figure 3.135). The fracture occurred close to the east end of the beam sheet. The ultimate tensile strength of the steel reinforcement was realized.
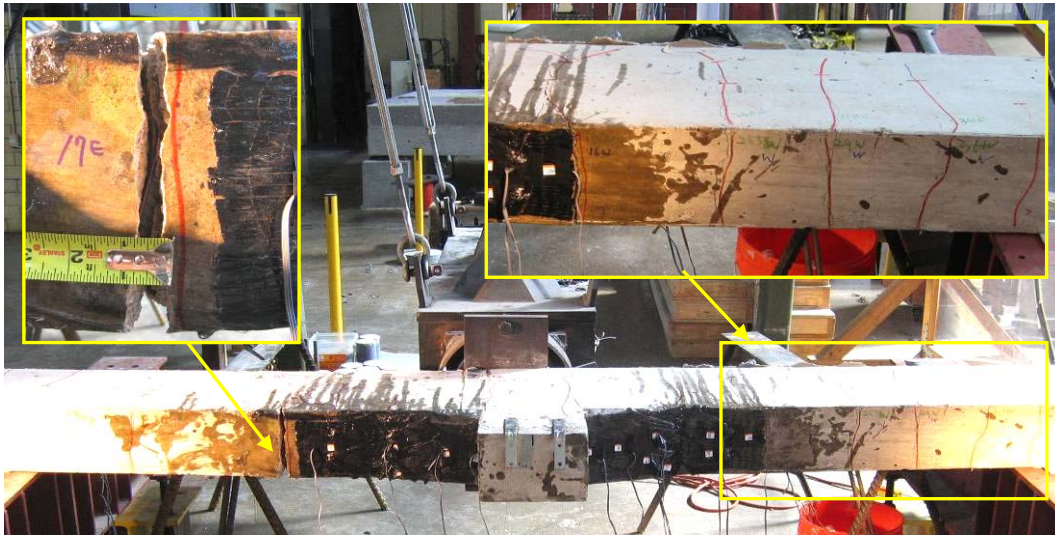
Figure 3.134   Failure of C-BC-A-6G-02, 9 in. (yield of steel reinforcement)

Figure 3.135   Failure of C-BC-A-6G-02, 12 in.-02 (fracture of steel reinforcement)

A summary of the applied loads and reactions are shown in Table 3.8. The beam was tested twice with a 12 in. drop height. In this section, the results of the tests at different drop heights except 4.5 in. and the first 12 in. are presented. Results of these tests are presented in Appendix A

The measured applied load and reactions are shown in Figure 3.136. The duration of event was relatively short in the test at a12 in. drop height (fracture of steel reinforcement) compared with that of the other tests (yield of steel reinforcement). The peak applied load and reactions are shown in Table 3.8. In addition, impulse of the

148

applied load and sum of the reactions are shown in Table 3.8. The impulse and the duration of event increased as the drop height increased when the failure mode of specimen was yield of the steel. However, they decreased when bar fracture occurred although the drop height was higher than the previous tests.

The normalized applied load and sum of the reactions are shown in Figure 3.137 and Figure 3.138. The peak normalized applied load and sum of the reactions and the ratio of the two are shown in Table 3.8. The ratio was relatively lower when steel reinforcement fractured than when it yielded.

The calculated static strength of this beam was 3.6 kip and it was based on yield of the steel reinforcement at the ends of the beam sheet (15 in. from the column face). The peak normalized load was considerably larger than the calculated strength because of inelastic behavior of the beam during the impact. Therefore, impulse during the impact did not represent the strength of the beam.

Table 3.8   *Summary of applied load and reactions, C-BC-A-6G-02*
(calculated static strength: 3.6 kip)

Drop height	Duration of event	Measured load			Measured impulse		Normalized load		
		Applied load	Reaction		Applied load	Sum of reactions	Peak applied load, A	Peak sum of reactions, R	Ratio, R/A
		Peak	Peak	Support					
2 in.	0.102 sec	25.8 kip	11.6 kip	West	0.31 kip- sec	0.33 kip- sec	4.8 kip	5.1 kip	105 %
3 in.	0.119 sec	29.0 kip	13.3 kip	West	0.38 kip- sec	0.40 kip- sec	5.0 kip	5.4 kip	107 %
4.5 in.	0.134 sec	32.8 kip	16.3 kip	West	0.46 kip- sec	0.50 kip- sec	5.4 kip	5.8 kip	108 %
9 in.	0.162 sec	52.0 kip	26.1 kip	West	0.59 kip- sec	0.63 kip- sec	5.7 kip	6.1 kip	107 %
12 in.-01	0.188 sec	52.9 kip	29.0 kip	West	0.84 kip- sec	0.71 kip- sec	7.1 kip	6.0 kip	85 %
12 in.-02	0.060 sec	62.7 kip	23.1 kip	West	0.37 kip- sec	0.20 kip- sec	9.8 kip	5.1 kip	52 %
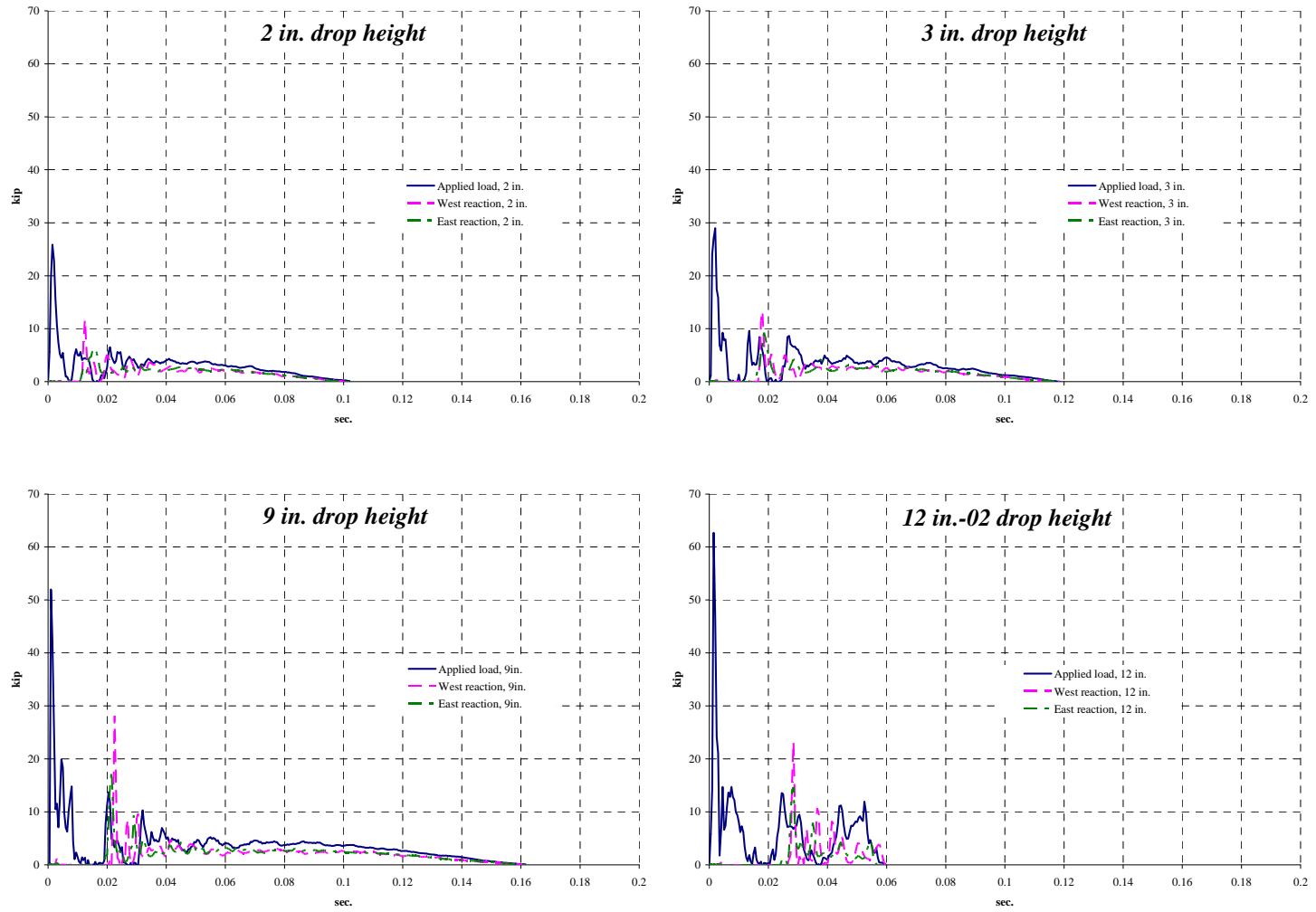
Figure 3.136   Measured applied load and reactions, C-BC-A-6G-02
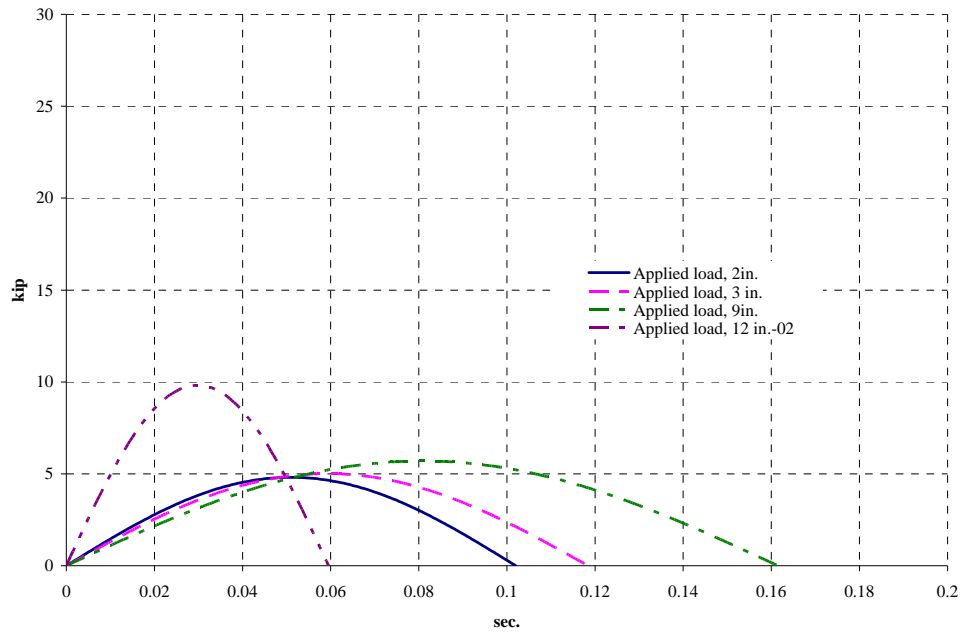
Figure 3.137   Normalized applied load, C-BC-A-6G-02
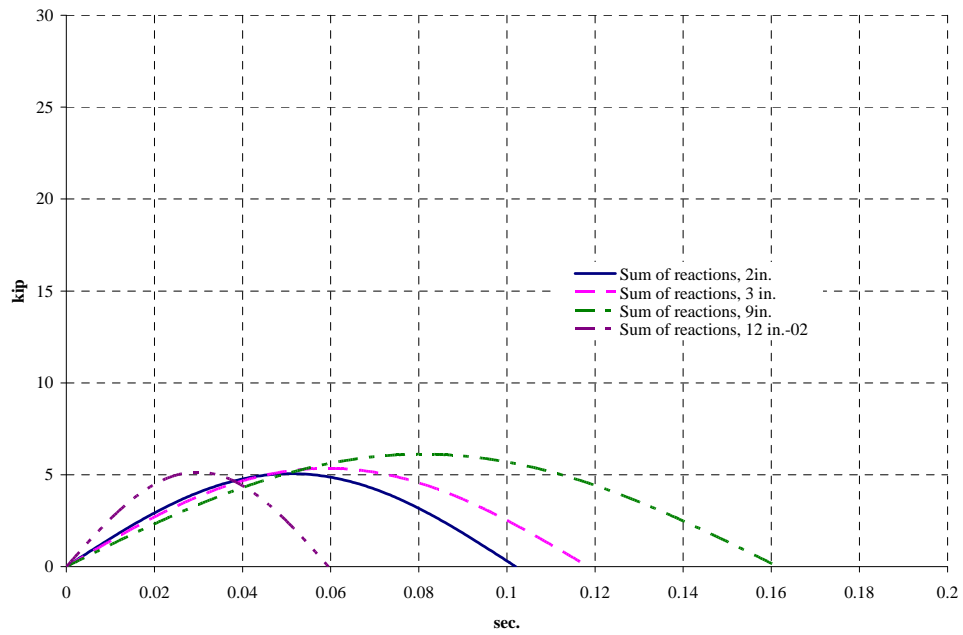
Figure 3.138   Normalized sum of reactions, C-BC-A-6G-02

151

Displacements at the column at different drop heights are plotted in Figure 3.139. The initial displacement was not zero for 3 in. and 9 in. drop height tests because of the permanent displacement after the previous tests. The shape of the measured displacement curves was similar to a half-period sine curve, and the peak displacement increased as the drop height of pendulum mass increased. The maximum displacement was 7.28 in. in the first 12 in. drop height test which was 3.8 % of the beam span length (16 ft). The displacement data for the second 12 in. drop height test is not shown in Figure 3.139 because it was not possible to determine the deflection at the instant the steel fractured.
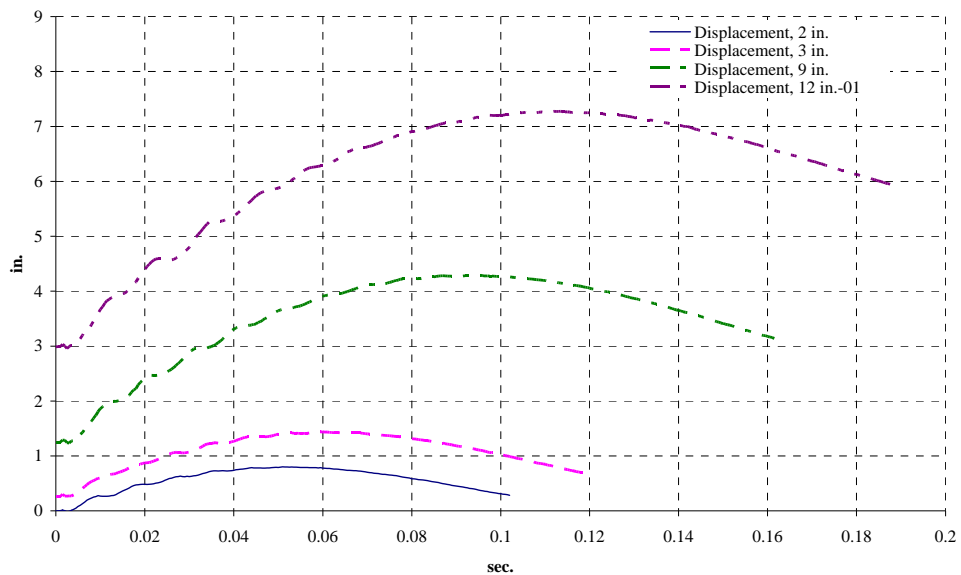
Figure 3.139   Displacement at the column, C-BC-A-6G-02

The location of the strain gages and the maximum measured strain in each gage are shown in Figure 3.140 and Figure 3.141. The strain data of 3 in. and the second 12 in. drop height tests are provided in this section. The strain distribution of the other tests is provided in Appendix A.

The maximum CFRP strain during the tests was 0.0059 at gage 4 (59 % of the ultimate tensile strain of the CFRP). The highest strain occurred in the gage close to the center of beam and strain decreased away from the center.

The response of gage 4 at different drop heights is shown in Figure 3.142. The initial values of strain in the tests except the first test, a 2 in. drop height, were not zero because of the previous impacts. The peak strain increased as the drop height increased.
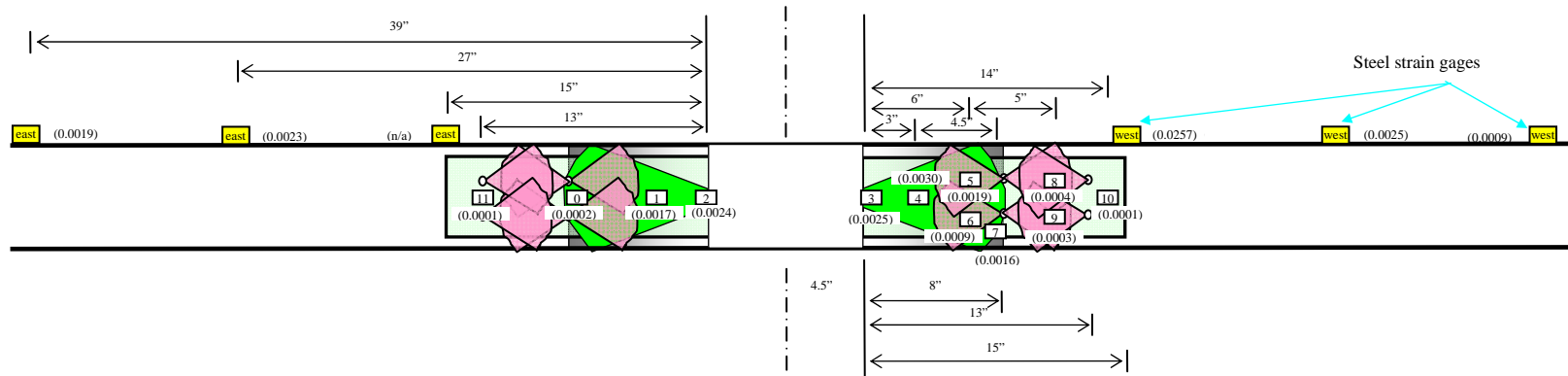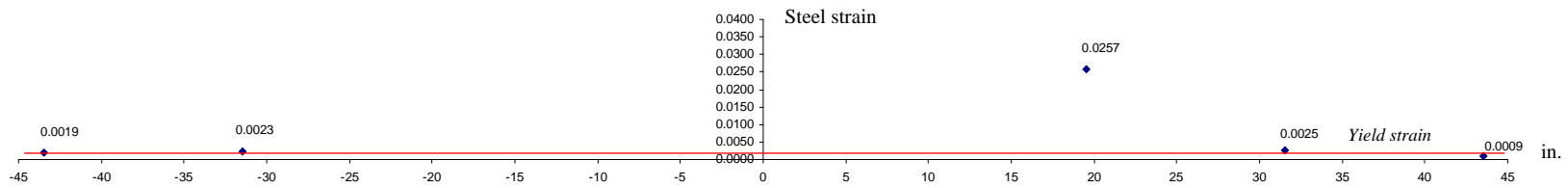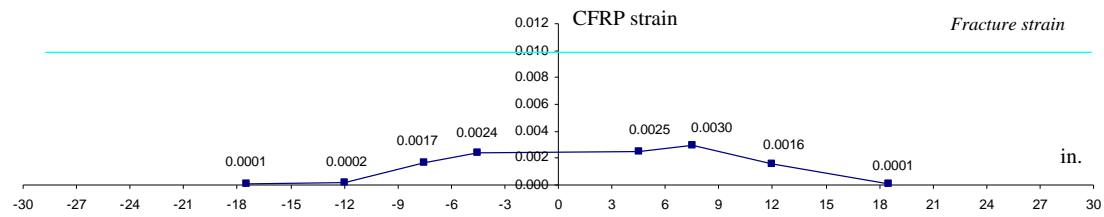
Figure 3.140   Location of strain gages and distribution of strain in CFRP and bars, C-BC-A-6G-02, 3 in.

154

east (0.0027)　　east (0.0032)　　(n/a)　　east　　14"　　6"　　5"　　Steel strain gages

39"

27"

15"

13"

west (0.0094)　　west (0.0032)　　(0.0029)　west

(0.0058)　5　　8
11　　0　　1　　2　　3　4　(0.0026)　(0.0009)　10
(0.0000)　(0.0003)　(0.0027)　(0.0036)　(0.0038)　6　(0.0000)
(0.0021)　7　(0.0003)
(0.0015)

4.5"　　8"

13"

15"

CFRP strain

Fracture strain

Steel strain

Yield strain

155
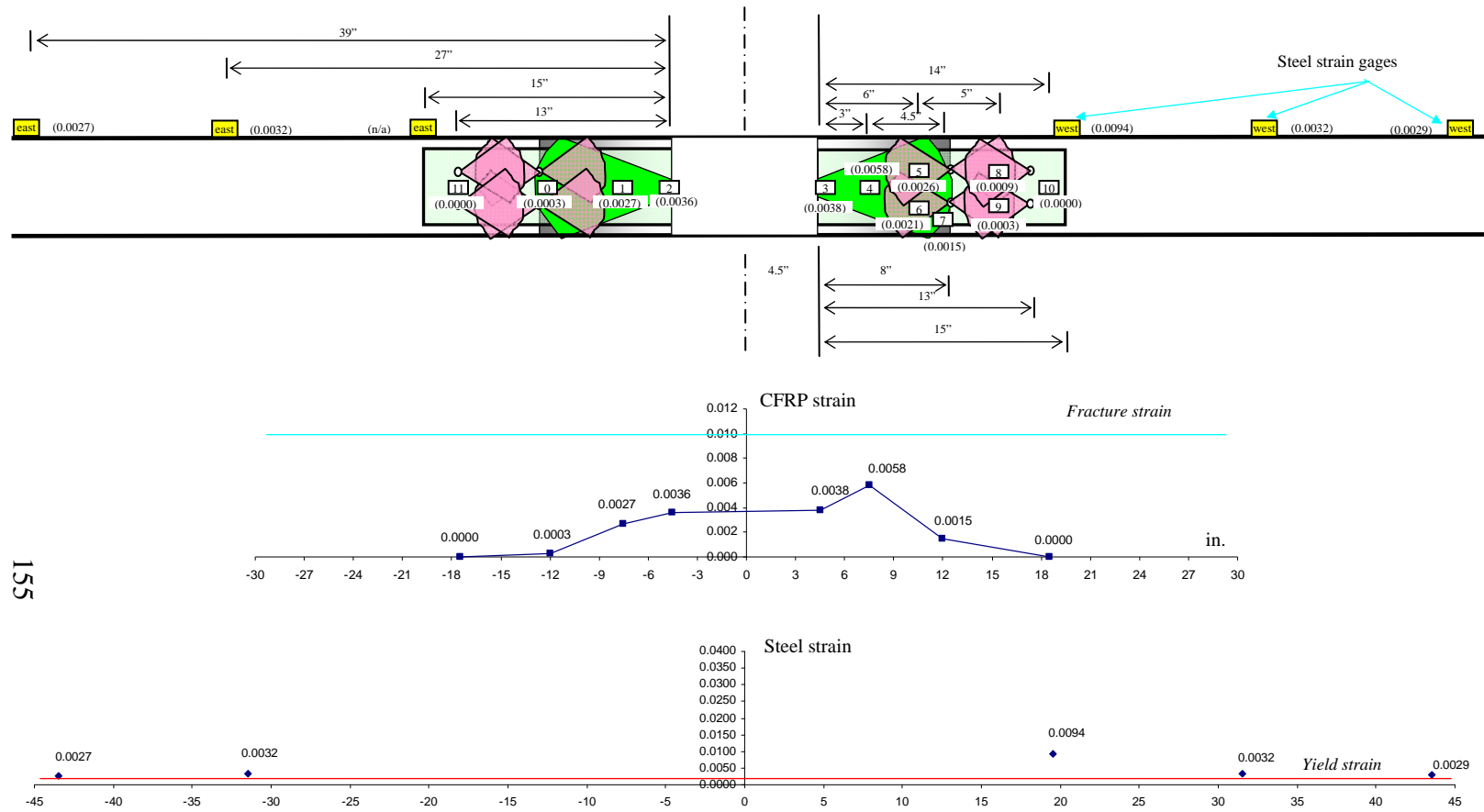
Figure 3.141　Location of strain gages and distribution of strain in CFRP and bars, C-BC-A-6G-02, 12 in.-02
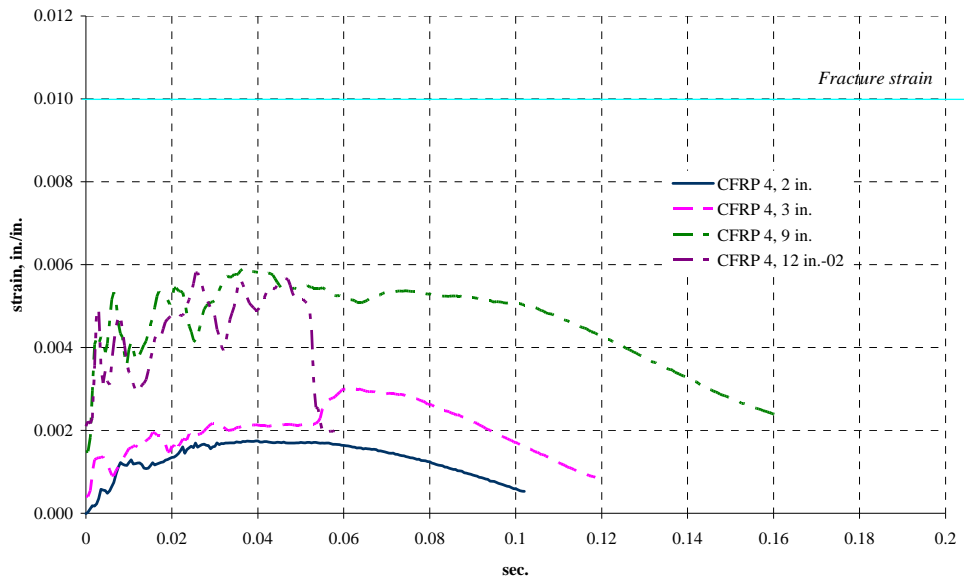
Figure 3.142   CFRP strain, C-BC-A-6G-02

The location of steel strain gages from the column face and maximum measured strain are also shown in Figure 3.140 and Figure 3.141. In the tests at 3 in. and 12 in. drop heights, most of the measured strains in the #3 bars were larger than the yield strain of the steel although they were away from the column faces. The largest bar strain was observed at a location close to the ends of CFRP material (15 in. from the column face) where a large crack existed. A steel strain gage (West-15 in.) was installed at the points close to the location of the crack. The responses of these gages at different drop heights were shown in Figure 3.143. The bars started yielding from the first impact at 2 in. drop height and showed large deformation when drop height increased. The peak measured strain was not proportional to the drop height because the strain depended on size, location and distribution of cracks in each impact.

156
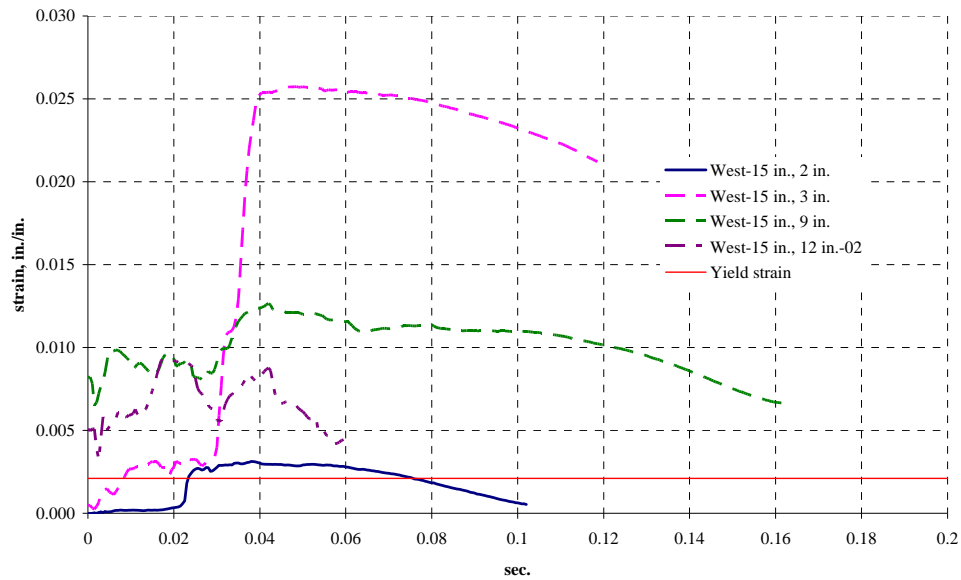
Figure 3.143   Steel reinforcement strain, west, C-BC-A-6G-02

3.6.4.3   C-BC-U-6G

C-BC-U-6G was a Type C beam and CFRP was applied through the column at the bottom face. This beam had one layer of the beam sheet on the east and west side, and the sheet was anchored using the CFRP U-wraps. The connection sheet connected the beam sheets through the column hole and was lap spliced with the beam sheets on the transition ramps. The difference between this beam and C-BC-A-6G-01 was type of anchorage. The surface of the bottom face was ground. The measured compressive strength of the concrete was 6,000 psi. Configuration of the beam is shown in Figure 3.144.

157
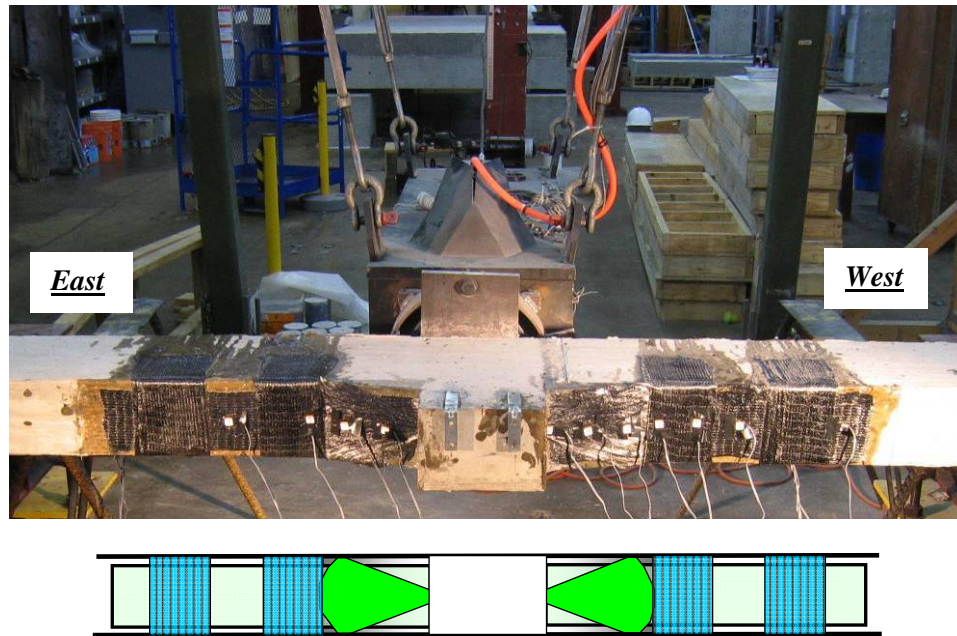
Figure 3.144   Configuration of , C-BC-U-6G

C-BC-U-6G was tested under the drop height of 2 in., 3 in. and 4.5 in. At a 3 in. drop height, the steel yielded with the concrete cracking. At a 4.5 in. drop height, the beam sheet fractured. This beam was designed to develop yield of the steel reinforcement before fracture of CFRP, and Large deformation capacity and yield of the steel reinforcement was observed before the fracture of CFRP.

Initially C-BC-U-6G exhibited stress wee beyond yield of the steel reinforcement (Figure 3.145). Two large cracks occurred at the ends of the beam sheets and other cracks were evenly distributed over the beam where no CFRP was applied.

The beam failed when the beam sheet fractured (Figure 3.146). The fracture occurred at the end of the lap splice of the beam and connection sheets on the east side. The ultimate tensile strength of the CFRP was realized.
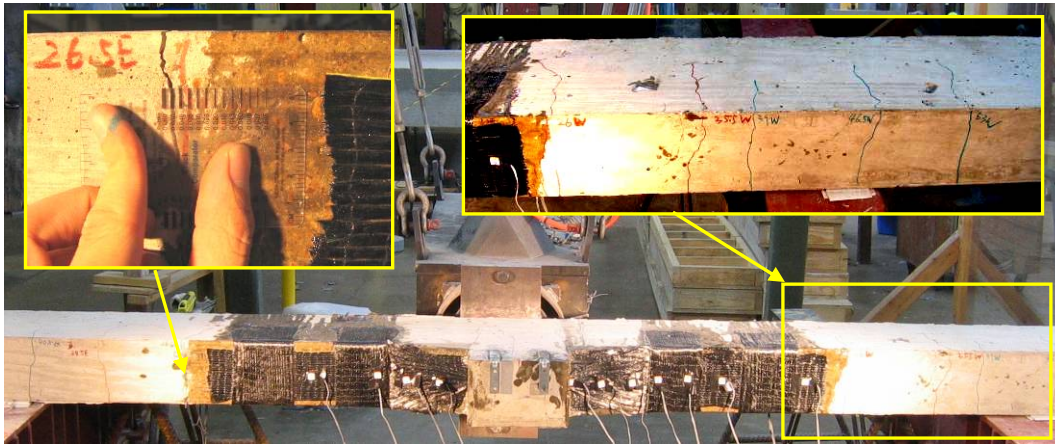
Figure 3.145   Failure of C-BC-U-6G, 3 in. (yield of steel reinforcement)
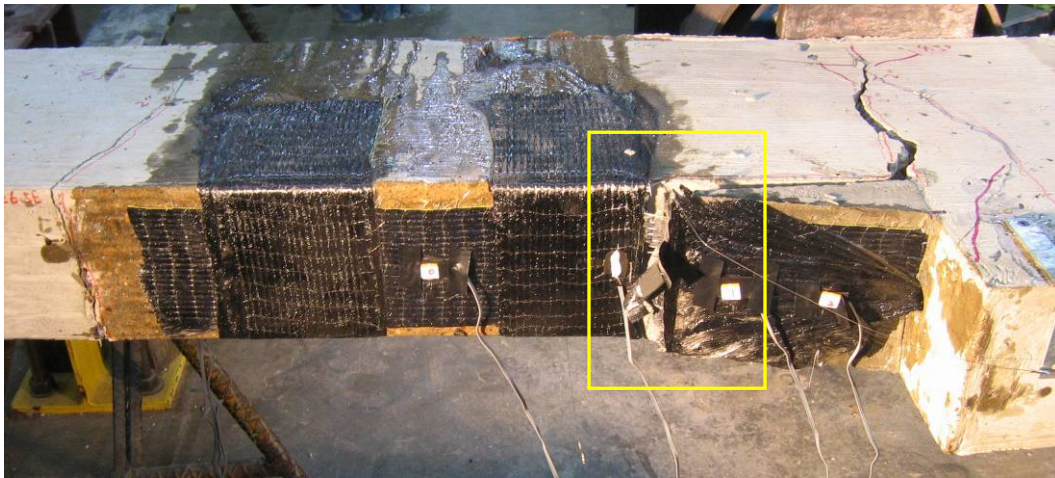
Figure 3.146   Failure of C-BC-U-6G, 4.5 in. (fracture of CFRP)

A summary of the applied load and reactions are shown in Table 3.9. The measured applied load and reactions plotted are shown in Figure 3.147. The duration of event was relatively short in the test at a 4.5 in. drop height (fracture of CFRP) compared with that of the other tests (yield of steel reinforcement).   The peak applied load and reactions are shown in Table 3.9. In addition, impulse of the applied load and sum of the reactions are shown in Table 3.9. The impulse and the duration of event increased as the drop height increased when the failure mode of specimen was yield of the steel.

159

However, they decreased when CFRP fracture occurred although the drop height is higher than the previous tests.

The normalized applied load and sum of the reactions are shown in Figure 3.148 and Figure 3.149. The peak normalized applied load and sum of the reactions and the ratio of two are shown in Table 3.9. The ratio was relatively lower when CFRP fractured than when the steel yielded.

The calculated static strength of this beam was 4.1 kip and it was based on yield of the steel at the ends of the CFRP sheet (24 in. from the column face). The peak normalized load was larger than the calculated strength because of inelastic behavior of the beam during the impact. Therefore, impulse during the impact did not represent the strength of the beam.

Table 3.9   Summary of applied load and reactions, C-BC-U-6G
(calculated static strength: 4.1 kip)

Drop height	Duration of event	Measured load			Measured impulse		Normalized load		
		Applied load	Reaction		Applied load	Sum of reactions	Peak applied load, A	Peak sum of reactions, R	Ratio, R/A
		Peak	Peak	Support					
2 in.	0.110 sec	21.9 kip	8.7 kip	West	0.34 kip- sec	0.33 kip- sec	4.9 kip	4.8 kip	98 %
3 in.	0.123 sec	22.8 kip	13.8 kip	West	0.41 kip- sec	0.42 kip- sec	5.2 kip	5.3 kip	102 %
4.5 in.	0.041 sec	30.8 kip	20.5 kip	West	0.18 kip- sec	0.14 kip- sec	6.8 kip	5.4 kip	79 %
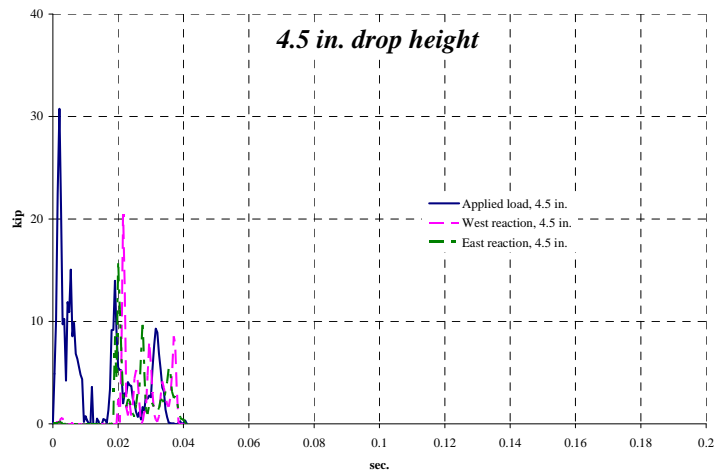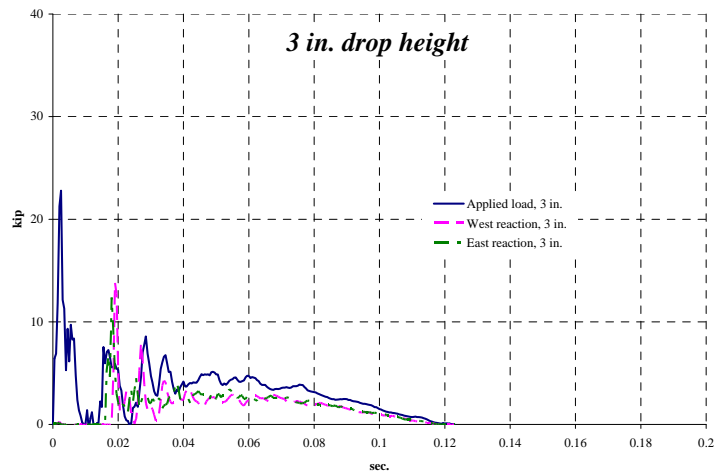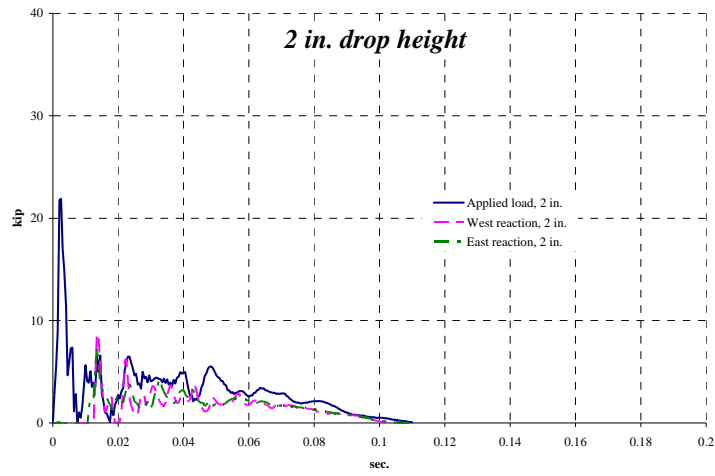
Figure 3.147   Measured applied load and reactions, C-BC-U-6G

161
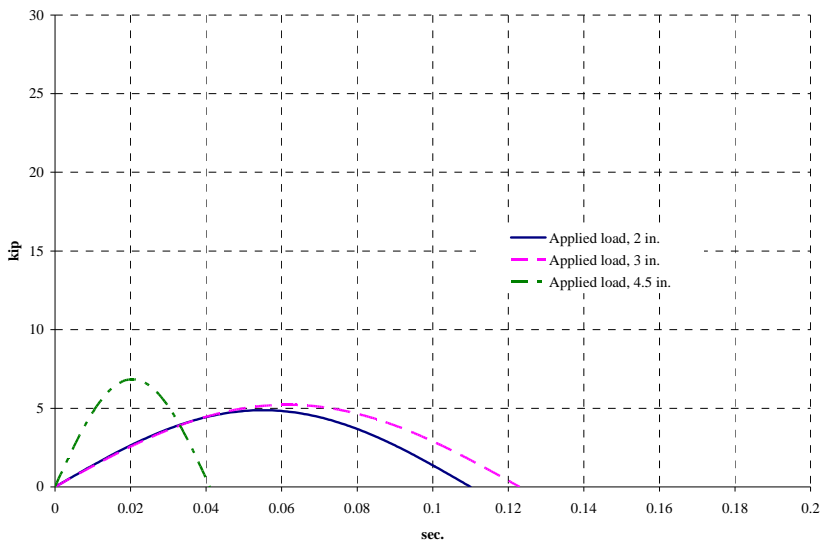
Figure 3.148   Normalized applied load, C-BC-U-6G
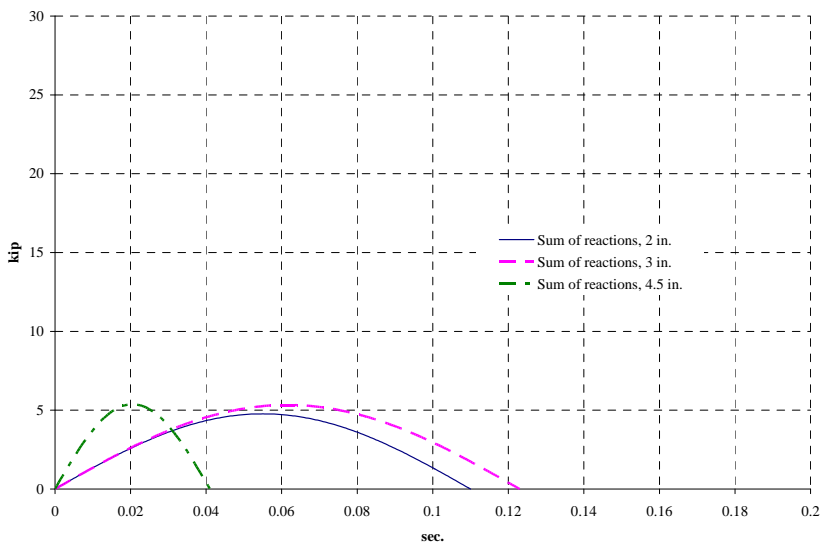
Figure 3.149   Normalized sum of reactions, C-BC-U-6G

162

Displacements at the column at different drop heights are plotted in Figure 3.150. The initial displacement was not zero for 3 in. drop height test because of the permanent displacement after the previous test. The shape of the measured displacement curves was similar to a half-period sine curve, and the peak displacement increased as the drop height of pendulum mass increased. The maximum displacement was 1.45 in. at a 3 in. drop height which was 0.8 % of the beam span length (16 ft). The displacement data for 4.5 in. drop height test is not shown in Figure 3.150 because it was not possible to determine the deflection at the instant the CFRP fractured.
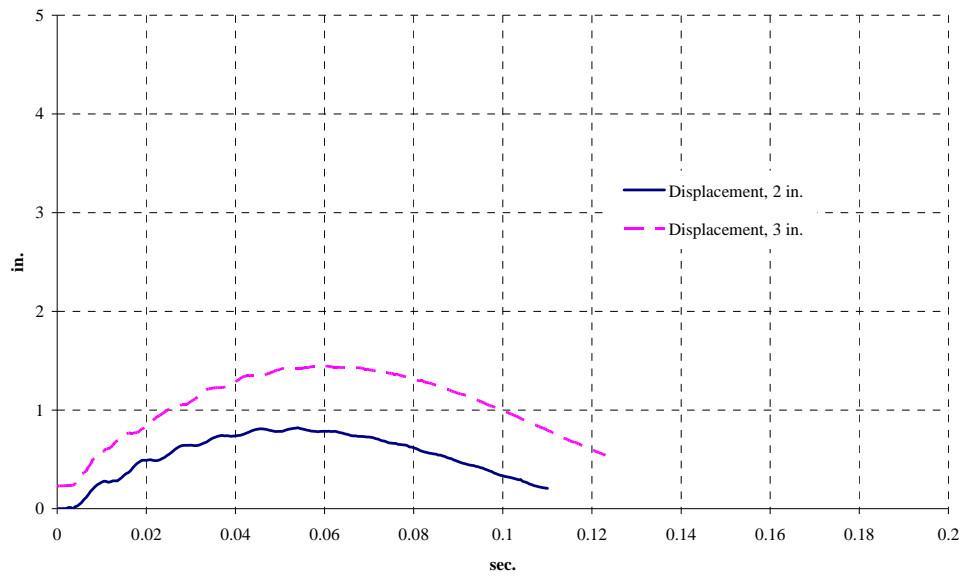
Figure 3.150   Displacement at the column, C-BC-U-6G

163

The location of the strain gages and the maximum measured strain in each gage are shown in Figure 3.151 and Figure 3.152. The strain data of 3 in. and 4.5 in. drop height tests are provided in this section. The strain distribution of 2 in. drop height test is provided in Appendix A.

The maximum CFRP strain measured in the beam sheets during the tests was 0.003 at gage 10 (30 % of the ultimate tensile strain of the CFRP). The peak strain did not reach the ultimate tensile strain because this strain gage was away from the location of fracture. From the horizontal distribution of strains in the CFRP sheet, the uniform distribution of strain was observed compared with the strain distribution in the beam sheets anchored with the CFRP anchors.

The response of gage 10 at different drop heights is shown in Figure 3.153. This gage was installed on the connection sheet. The initial values of strain in the tests except the first test, a 2 in. drop height, were not zero because of the previous impacts. The peak strain increased as the drop height increased. The response of gage 7, installed in the U-wrap at different drop heights is shown in Figure 3.154. The peak strain increased as the drop height increased and the maximum strain measured in the CFRP U-wrap was larger than that in the CFRP sheets.
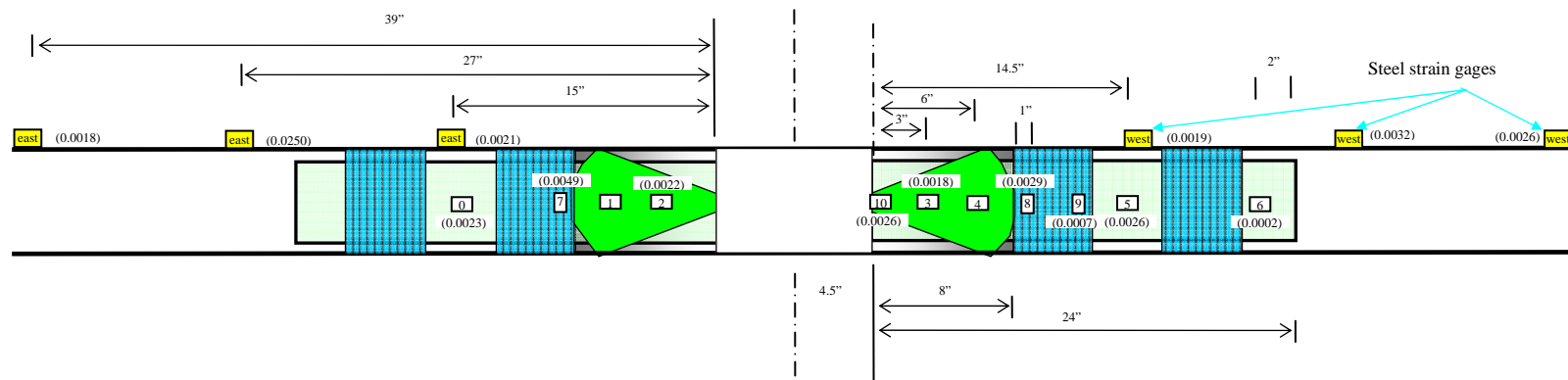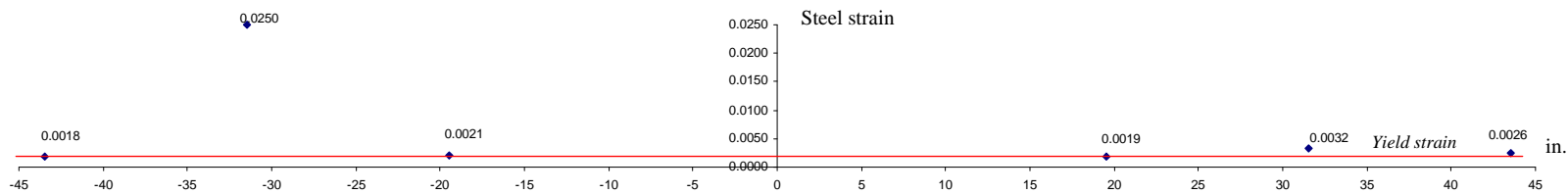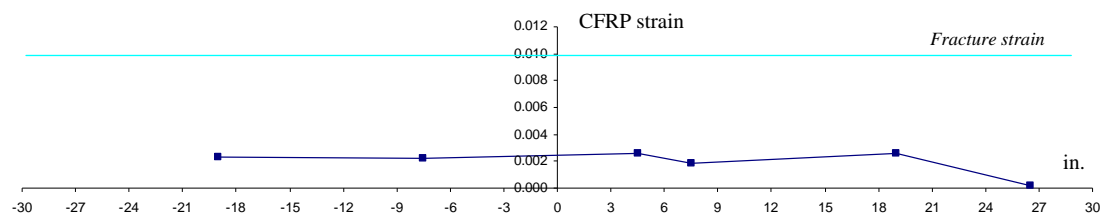
Figure 3.151   Location of strain gages and distribution of strain in CFRP and bars, C-BC-U-6G, 3 in.
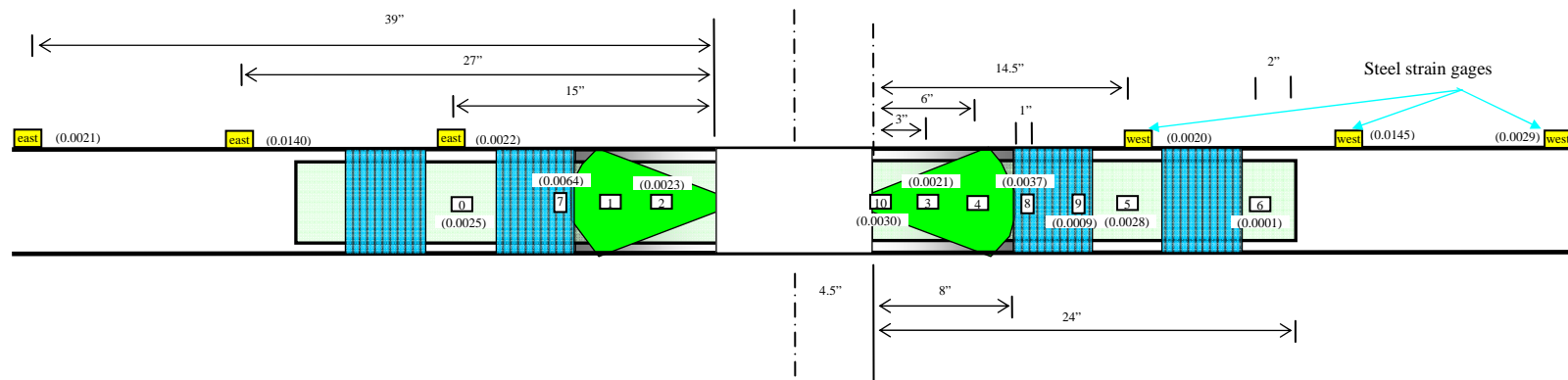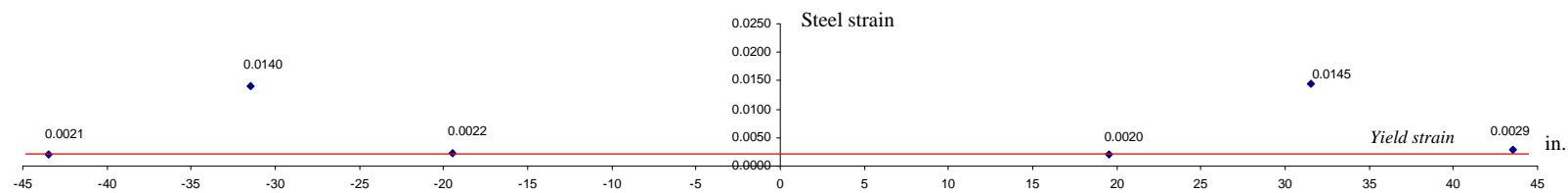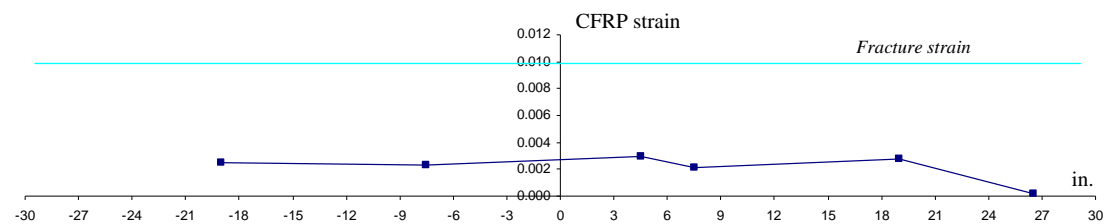
Figure 3.152 Location of strain gages and distribution of strain in CFRP and bars, C-BC-U-6G, 4.5 in.
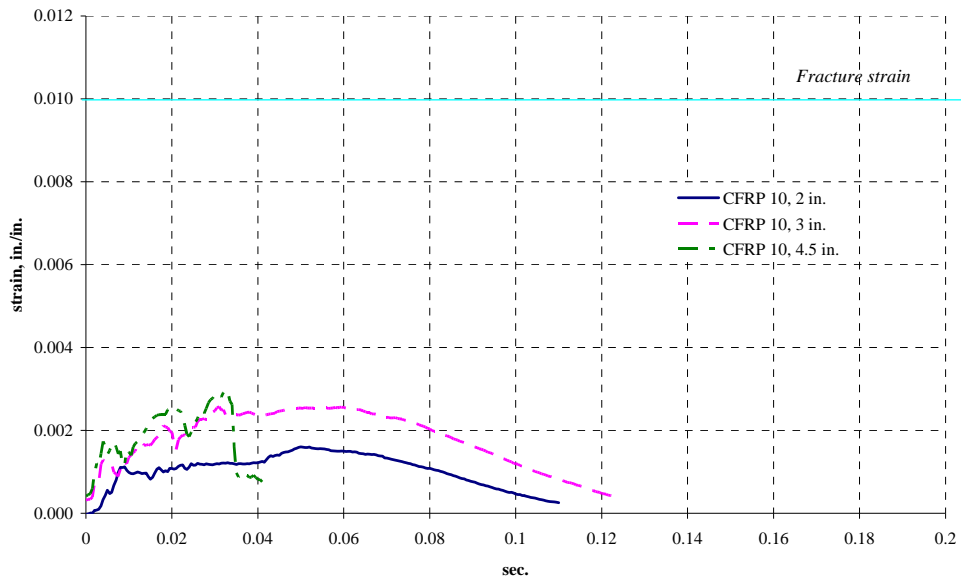
Figure 3.153   CFRP strain, CFRP sheet, C-BC-U-6G
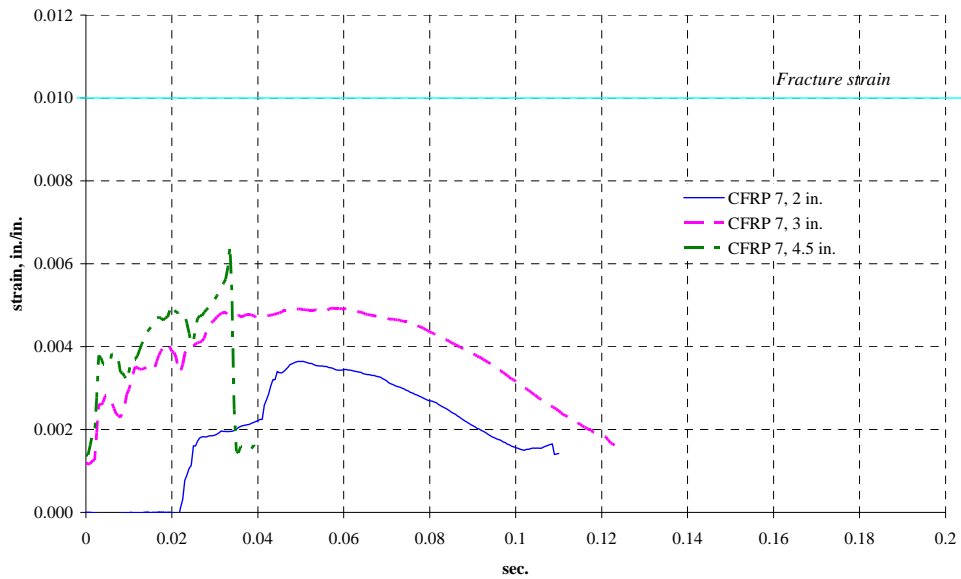
Figure 3.154   CFRP strain, CFRP U-wrap, C-BC-U-6G

167

The location of steel strain gages from the column face and maximum measured strain are also shown in Figure 3.151 and Figure 3.152. In the tests at 3 in. and 12 in. drop heights, most of the measured strains in the bars were larger than the yield strain of the steel although they were away from the center of beam. The largest bar strain was observed at location close to the ends of the beam sheet (24 in. from the column face) where large cracks existed. Steel strain gages (East-27 in. and West-27 in.) were installed at the points close to the location of the cracks. The responses of these strain gages at different drop heights were shown in Figure 3.155 and Figure 3.156. The bars started yielding from the first impact at 2 in. drop height and showed large deformation when drop height increased. The peak measured strain was not proportional to the drop height because the strain depended on size, location and distribution of cracks in each impact.
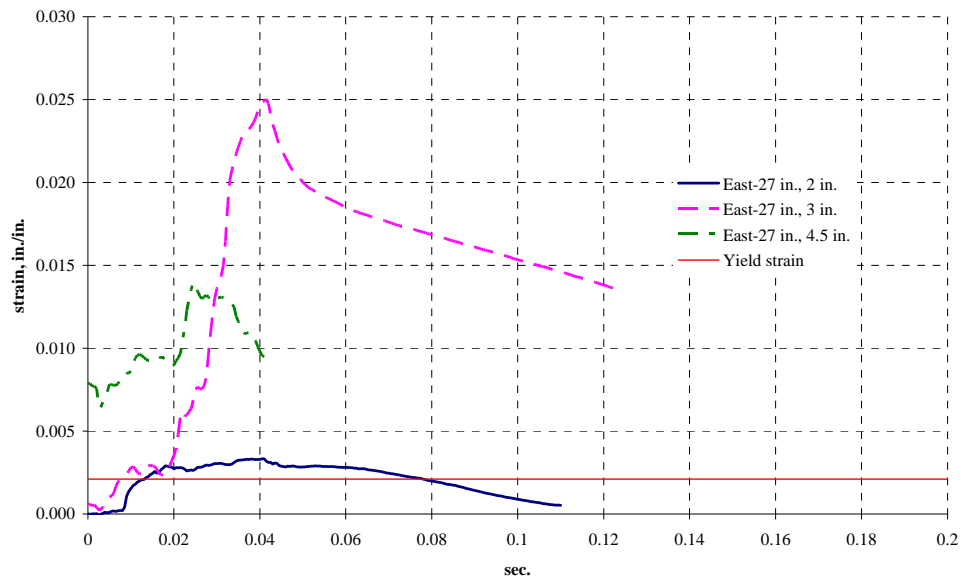
Figure 3.155   Steel reinforcement strain, east, C-BC-U-6G

168
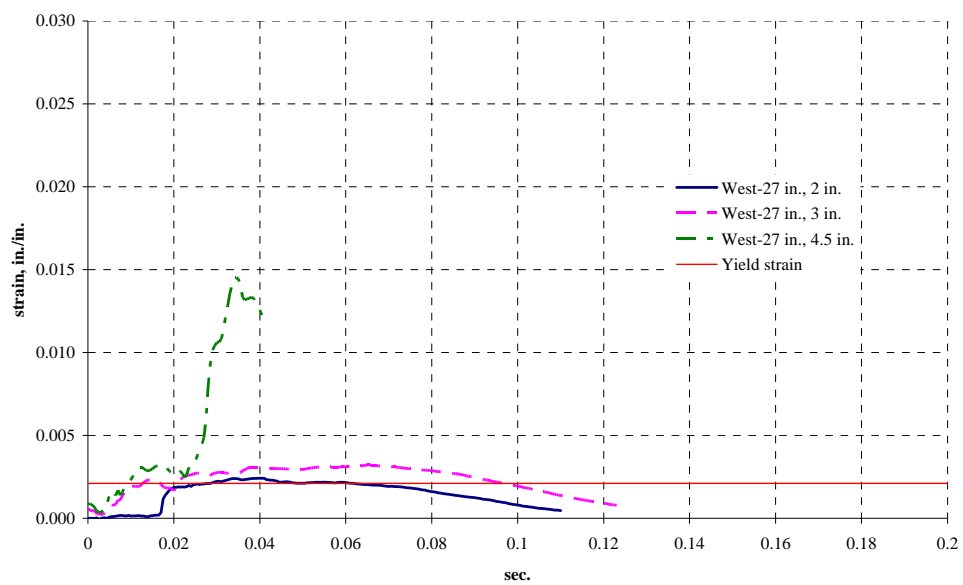
Figure 3.156   Steel reinforcement strain, west, C-BC-U-6G

169

3.6.4.4 Comparisons

The anchorage methods that produced the best response under dynamic loading were studied using Type A and Type B beams. In Type C beams, the effectiveness of the rehabilitation methods using the CFRP materials for providing continuity in the bottom steel reinforcement of the beam was evaluated. By providing continuity to the bottom reinforcement, it was anticipated that ductility in the steel reinforcement could be mobilized. Strain in the bottom reinforcement was measured and evaluated with respect to yield strain.

Three Type C beams, C-BC-A-6G-01, C-BC-A-6G-02 and C-BC-U-6G, were tested with multiple impacts by increasing the drop height of the pendulum mass until the beams failed. The drop heights were 2 in., 3 in., 4.5 in., 9 in. and 12 in. C-BC-A-6G-01 and C-BC-A-6G-02 failed at a 12 in. drop height while C-BC-U-6G failed at a 4.5 in. drop height. The failure mode of C-BC-A-6G-01 and C-BC-U-6G was fracture of the CFRP sheets while that of C-BC-A-6G-02 was fracture of the bottom steel reinforcement. Strain in the bottom steel reinforcement in all Type C beams showed more than 10 times yield strain during the loading before the failure occurred. The largest strain was observed at locations close to the ends of the CFRP sheets where large cracks occurred. Plastic hinges developed at these locations in all Type C beams indicating that continuity of the bottom reinforcement was provided by the rehabilitation methods used.

C-BC-U-6G was compared with C-BC-A-6G-01 to study the effect of anchorage type on dynamic performance of CFRP. Both beams failed by fracture of the CFRP sheet. Anchorage method with U-wraps was as effective as anchors. In addition, ductility was realized in the bottom steel reinforcement in both cases before the CFRP sheet failed. However, C-BC-A-6G-01 with anchors performed better than C-BC-U-6G with U-wraps. The drop height of the pendulum mass at fracture of the CFRP sheet was 12 in. with anchors and 4.5 in. with U-wraps. It showed that more energy was required to fracture the CFRP sheet with anchors. With anchors, the peak displacement at the column was 3.5 in. at a 9 in. drop height but with U-wrap, was only 1.5 in. at a 3 in. drop height. These test

results indicates that it is possible to achieve more deformation capacity of the beam using anchors rather than U-wraps. A summary and comparison of test results of the two beams is shown in Table 3.10.

The differences between C-BC-A-6G-01 and C-BC-A-6G-02 were the length of the beam sheet and the location of the second set of the CFRP anchors from the column face. In C-BC-A-6G-01, the length of the beam sheet and the location of the anchors were based on a previous study by Orton (2007). In C-BC-A-6G-02, the length was reduced and the location was adjusted based on a development length of #3 bars of 11.6 in. using ACI-318-08 section 12.2.2. In C-BC-A-6G-02, the length of reinforcement from the column face to the second set of the anchors was 13 in. which was slightly longer than the development length. The 3 in. embedded length in the column was ignored to determine the location of the anchors. The test results indicate that it is possible to provide continuity to the bottom reinforcement and to achieve ductility of the reinforcement if the length between the face of the column where discontinuity of the bottom reinforcement exists and the last set of CFRP anchors are longer than the code specified development length.
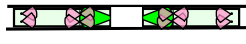
The location of the plastic hinges in C-BC-A-6G-02 was closer to the center of the beam than that in C-BC-A-6G-01 so the level of applied load required to develop plastic hinge was relatively low in C-BC-A-6G-02 compared with that in C-BC-A-6G-01. Therefore, in C-BC-A-6G-02, the bending moment at the plastic hinge location exceeded the rotational capacity before the CFRP sheet reached the ultimate tensile capacity, and the failure mode was the fracture of the steel reinforcement.

It is desirable to use a short length of CFRP sheet because it reduces quantity of materials used in rehabilitation and provides more ductility to the beam. More ductility can be achieved when plastic hinges are close to the column.

The peak normalized load in all Type C beams was larger than the calculated static strength and it represents that all Type C beams behaved inelastically during the test. The difference between the load and strength was the largest in C-BC-A-6G-02,

171

which showed the most significant inelastic behavior among 3 Type C beams, and the least in C-BC-U-6G.

Table 3.10   Comparison of the test results of the beams with column

		Failure mode	Drop height at failure	Peak applied load at failure		Static strength	Max. bar strain		Max. displacement before failure	
				Measured load	Normalized load		Strain	Drop height	Displacement	Drop height
C-BC-A-6G-01		Fracture of CFRP sheet	12 in.	60.0 kip	10 kip	4.2 kip	0.0231	3 in.	8.1 in.	9 in.
C-BC-A-6G-02		Fracture of bars	12 in.	62.7 kip	9.8 kip	3.1 kip	0.0257	3 in.	7.3 in.	12 in.
C-BC-U-6G		Fracture of CFRP sheet	4.5 in.	30.8 kip	6.8 kip	4.1 kip	0.0277	3 in.	1.5 in.	4.5 in.

3.7 SUMMARY OF BEHAVIOR

A summary of the dynamic test results is shown in Table 3.11 to 3.13. The test results of each beam in at the drop heights are summarized in these tables. Failure modes, measured and normalized peak applied load and reactions, impulse of applied load and sum of the reactions, strain in CFRP and bar, and displacement in the center of beam are presented in these tables.

The normalized applied load and sum of the reactions were calculated based on the duration of event and measured impulse. These data provide the characteristic of loading and dynamic response of the test beam. Strain and strain rate of the CFRP sheet was measured to observe dynamic performance of CFRP materials.

In Type A and B beams, failure mode and the peak strain in CFRP sheet indicates if the ultimate strain was realized under dynamic loading. Effectiveness of anchorage methods was evaluated using these specimens. In Type C beams, large strains of the reinforcement at location where plastic hinges were expected indicate if the ductility of the bottom steel reinforcement was realized. The development of large deformation in the steel reinforcement indicates that CFRP materials provide continuity to the bottom reinforcement successfully. The displacement at the column is only presented when the test beam did not fail at a particular drop height. This displacement data provides deformation capacity of the beam before it loses load carrying capacity.

Table 3.11   Summary of test results, rehabilitation using the flat bottom face
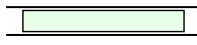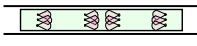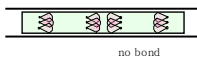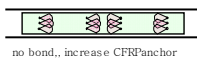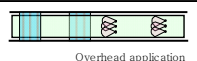
Beams	Drop height, in	Duration of event, sec	Failure mode	Peak load — Applied load Measured, kip	Applied load Nomalized, kip	Measured raction at one support, kip	Sum of reactions Measured, kip	Sum of reactions Nomalized, kip	Ratio of nomalized load (S/A)	impulse Applied load, kip-sec	Sum of reaction, kip sec	Ratio of impulse (S/A)	Peak CFRP atrain CFRP strain, ultimate strain=0.01	Time at peak strain, sec	Strain rate, strain/sec	Peak bar strain	Displacement Initial	Displacement Peak	Displacement Relative peak
A-BF-N-5S	3	0.026	Delamination	36.8	11.3	8.6 e	15.3	6.9	61%	0.183	0.111	61%	0.0041	0.023	0.182	0.0006	0.00		
A-BF-A-2S	3	0.033	Fracture of CFRP sheet	40.0	10.2	9.4 w	15.3	8.9	87%	0.214	0.187	87%	0.0112	0.024	0.467		0.00		
A-BF-A-5S	1	0.055		16.7	8.4	9.3 e	15.2	7.1	84%	0.293	0.247	84%	0.0015	0.026	0.059	0.0008	0.00	0.20	0.20
A-BF-A-5S	3	0.067		39.6	11.6	22.0 w	39.6	10.7	92%	0.495	0.455	92%	0.0063	0.030	0.210	0.0013	0.06	0.60	0.54
A-BF-A-5S	3	0.071		38.2	10.7	26.1 w	45.9	10.2	96%	0.483	0.462	96%	0.0070	0.031	0.230	0.0015	0.03	0.61	0.58
A-BF-A-5S	4.5	0.039	Fracture of CFRP sheet	47.4	14.5	26.9 w	50.4	12.0	83%	0.359	0.297	83%	0.0112	0.035	0.325	0.0016	0.10		
A-BF-A-2N (no bond)	3	0.055	Fracture of CFRP anchors	34.0	10.1	11.5 e	21.9	8.7	86%	0.354	0.304	86%	0.0051	0.045	0.113		0.00		
A-BF-1.3A-5N (no bond,, increase CFRPanchor)	3	0.034	Fracture of CFRP sheet	34.9	11.9	13.2 e	20.7	9.1	77%	0.258	0.198	77%	0.0106	0.027	0.400	0.0010	0.00		
A-BF-U-5S	1	0.064		13.6	5.9	12.1 w	21.1	5.6	94%	0.240	0.225	94%	0.0033	0.029	0.114	0.0008	0.00	0.21	0.21
A-BF-U-5S	1.5	0.069		21.7	7.2	13.4 w	25.4	7.2	101%	0.313	0.315	101%	0.0074	0.028	0.264	0.0009	0.06	0.48	0.42
A-BF-U-5S	3	0.022	Fracture of CFRP sheet	28.8	11.6	15.8 w	29.1	5.1	44%	0.166	0.072	43%	0.0077	0.010	0.770	0.0010	0.11		
A-BF-A/U-6G (Overhead application)	3	0.022	Fracture of CFRP sheet	36.0	11.3	12.5 e	19.3	6.9	61%	0.158	0.097	61%	0.0103	0.016	0.644	0.0008	0.00		

Table 3.12   Summary of test results, rehabilitation using the height transition bottom face

Beams	Drop height, in	Duration of event, sec	Failure mode	Applied load – Measured, kip	Applied load – Nomalized, kip	Measured raction at one support, kip		Sum of reactions – Measured, kip	Sum of reactions – Nomalized, kip	Ratio of nomalized load (S/A)	Applied load, kip-sec	Sum of reaction, kip sec	Ratio of impulse (S/A)	CFRP strain, ultimate strain=0.01	Time at peak strain, sec	Strain rate, strain/sec	Peak bar strain	Initial	Peak	Relative peak
B-BH-A-6S	3	0.067		45.9	8.8	13.3	e	21.2	10.0	113%	0.377	0.425	113%	0.0078	0.032	0.244	0.0009	0.00	0.58	0.58
	3	0.023	Fracture of CFRP sheet (column sheet)	41.4	10.1	16.1	w	27.0	8.2	80%	0.164	0.132	80%	0.0084	0.021	0.400	0.0011	0.10		
B-BH-U-6S	3	0.025	Fracture of CFRP sheet (beam sheet)	45.5	10.4	9.8	e	18.2	5.4	52%	0.165	0.086	52%	0.0060	0.008	0.750	0.0003	0.00		

Table 3.13   Summary of test results, rehabilitation using the side faces

Beams	Drop height, in	Duration of event, sec	Failure mode	Applied load – Measured, kip	Applied load – Nomalized, kip	Measured raction at one support, kip		Sum of reactions – Measured, kip	Sum of reactions – Nomalized, kip	Ratio of nomalized load (S/A)	Applied load, kip-sec	Sum of reaction, kip sec	Ratio of impulse (S/A)	CFRP strain, ultimate strain=0.01	Time at peak strain, sec	Strain rate, strain/sec	Peak bar strain	Initial	Peak	Relative peak
A-S-A-6G (on sides)	6	0.093		51.6	9.6	16.6	w	28.4	11.8	122%	0.567	0.693	122%	0.0082	0.047	0.174		0.00	1.26	1.26
	12	0.031	Fracture of CFRP sheet	73.8	12.4	16.9	e	24.9	6.5	53%	0.240	0.126	53%	0.0110	0.026	0.423		0.09		
A-S-AU-2S (on sides)	6	0.078		63.8	12.2	18.7	e	36.2	13.0	107%	0.603	0.642	107%	0.0093	0.036	0.258	0.0014	0.00	1.06	1.06
	12	0.020	Fracture of CFRP sheet	81.4	18.4	17.0	w	28.8	3.0	16%	0.234	0.038	16%	0.0098	0.011	0.891	0.0015	0.16		

Table 3.14   Summary of test results, rehabilitation using the bottom face with column

Beams		Drop height, in	Duration of event, sec	Failure mode	Peak load							impulse			Peak CFRP atrain			Peak bar strain	Displacement, in		
					Applied load		Measured raction at one support, kip		Sum of reactions		Ratio of nomalized load (S/A)	Applied load, kip-sec	Sum of reaction, kip sec	Ratio of impulse (S/A)	CFRP strain, ultimate strain=0.01	Time at peak strain, sec	Strain rate, strain/sec		Initial	Peak	Relative peak
					Measured, kip	Nomalized, kip			Measured, kip	Nomalized, kip											
C-BC-A-6G-01		2	0.099	Yield of bar	18.4	7.0	10.7	w	15.3	5.5	78%	0.436	0.342	78%	0.0023	0.047	0.049	0.0051	0.00	0.77	0.77
		3	0.114	Yield of bar	18.8	7.0	17.5	w	26.4	5.7	81%	0.506	0.411	81%	0.0039	0.054	0.072	0.0231	0.14	1.25	1.11
		4.5	0.128	Yield of bar	31.5	7.2	23.3	w	27.9	6.1	84%	0.589	0.497	84%	0.0047	0.055	0.085	0.0229	0.37	1.96	1.59
		9	0.145	Yield of bar	43.9	8.1	28.2	w	32.3	7.1	88%	0.744	0.650	87%	0.0057	0.057	0.100	0.0231	0.86	3.52	2.66
		12	0.048	Fracture of CFRP sheet (beam sheet)	60.0	10.0	29.3	w	32.2	6.5	65%	0.304	0.198	65%	0.0064	0.037	0.173	0.0129	0.33		
C-BC-A-6G-02		2	0.102	Yield of bar	25.8	4.8	11.6	w	13.3	5.1	105%	0.313	0.329	105%	0.0021	0.041	0.052	0.0031	0.00	0.80	0.80
		3	0.119	Yield of bar	29.0	5.0	13.3	w	19.9	5.4	107%	0.378	0.404	107%	0.0030	0.061	0.050	0.0257	0.26	1.44	1.18
		4.5	0.134	Yield of bar	32.8	5.4	16.3	w	26.4	5.8	108%	0.462	0.496	107%	0.0050	0.057	0.088	0.0150	0.64	2.32	1.68
		9	0.162	concrete crusing (comp)	52.0	5.7	26.1	w	32.4	6.1	107%	0.586	0.630	107%	0.0059	0.037	0.162	0.0126	1.25	4.29	3.04
		12	0.188	concrete crushing and conver spalling	52.9	7.1	29.0	w	51.9	6.0	85%	0.841	0.714	85%	0.0058	0.040	0.145	0.0086	2.99	7.28	4.29
		12	0.060	Fracture of bar	62.7	9.8	23.1	w	37.8	5.1	52%	0.372	0.195	52%	0.0058	0.026	0.227	0.0094			
C-BC-U-6G		2	0.110	Yield of bar	21.9	4.9	8.7	w	16.2	4.8	98%	0.341	0.334	98%	0.0024	0.040	0.060	0.0040	0.00	0.82	0.82
		3	0.123	Yield of bar	22.8	5.2	13.8	w	18.9	5.3	102%	0.409	0.417	102%	0.0026	0.027	0.096	0.0277	0.23	1.45	1.22
		4.5	0.041	Fracture of CFRP sheet (beam sheet)	30.8	6.8	20.5	w	23.4	5.4	79%	0.179	0.140	78%	0.0030	0.033	0.092	0.0146	0.55		

The major findings from the dynamic loading test are as follows;

1. It was possible to develop the ultimate strength of the CFRP sheets under strain rates greater than 0.1 /sec using CFRP anchors and/or CFRP U-wraps.

2. Anchorage methods with the CFRP anchors and/or U-wraps were tested under static loading and were found to be acceptable under dynamic loading as well.

3. The methods used to anchor CFRP sheets on either the bottom face or side faces of a reinforced concrete beam were acceptable.

4. Concrete strength, surface preparation and direction of application were not critical if the CFRP sheets were anchored by the CFRP anchors or U-wraps.

5. Although rapid changes in shape and quantity of CFRP existed due to the height transition, CFRP material passing through a column hole and lap splices of the beam and connection sheets, the CFRP sheet developed its ultimate tensile strength.

6. Anchored CFRP sheets successfully provided continuity to the bottom steel reinforcement. Ductility of the bottom reinforcement was realized and large rotations were observed.

7. The length of the CFRP sheet and location of CFRP anchors was based on development length of the bars for which continuity is required and was found to give satisfactory performance.

8. The beams with CFRP anchors required more energy to fracture CFRP sheet than with CFRP U-wraps.

The results of this study also indicate that it is possible to successfully provide continuity in the bottom steel reinforcement using the CFRP materials. The CFRP sheet anchored with proper anchorage methods effectively transferred stress from the CFRP to bottom reinforcement and the CFRP did not fail until the ductility of the bottom reinforcement and large rotational capacity of the section were realized.

This study focused on the behavior of CFRP materials in reinforced concrete beams in a high rate loading condition but this condition did not represent a real loading condition in the case where a column was suddenly removed. However, the rate of loading used in this study is comparable to that in the case of column removal (Sasani, 2007). The recommendations for the amplified factored load for static analysis regarding this case are provided in several design guidelines (GSA, 2003; DOD, 2005). If an engineer proportions CFRP sheets according to these recommendations, and anchors the sheets using the anchorage methods studied, an acceptable design should be achieved. The effects of a static load after the column removal were investigated by previous studies on the use of CFRP materials under static loading (Kim, 2006; Orton, 2007)

In this study, one type of CFRP material from a specific manufacturer was tested. Therefore, for the general use of other types of CFRP materials in this application, a qualification test method for evaluating performance of anchorage methods with CFRP anchors and U-wraps is needed. A qualification test method for CFRP anchors proposed in the research program is discussed in the next section.

3.8 **FUTURE RESEARCH: QUALIFICATION TEST FOR CFRP ANCHORS**

CFRP materials used in this study were supplied by a manufacturer and CFRP materials from other manufactures were not used. Typical material properties of a CFRP composite are provided by the manufacturer and delamination characteristic of CFRP sheets from the concrete has been studied based on the properties. However, information the effectiveness of CFRP anchors depending on their material properties is limited. Although the performance of CFRP anchors has received considerable attention, a reliable test method for qualifying of CFRP anchors in reinforced concrete structures does not exist. Therefore, development of a simple test method for evaluating effectiveness of CFRP anchors is necessary. This test will evaluate effectiveness of CFRP anchors without repeating different tests for different applications. In addition, this test method may be used in quality control of CFRP anchors. Although a test method for evaluating strength of lap spliced region of CFRP anchor and CFRP sheet (Figure 3.157) and a pull-out test method for a CFRP anchor installed into the concrete (Figure 3.158) exist (SR-CF 工法 研究會, SR-CF Construction Method Research Council, 2001), these test methods can not represent the load transfer mechanism from the CFRP sheets to the concrete through the CFRP anchors.
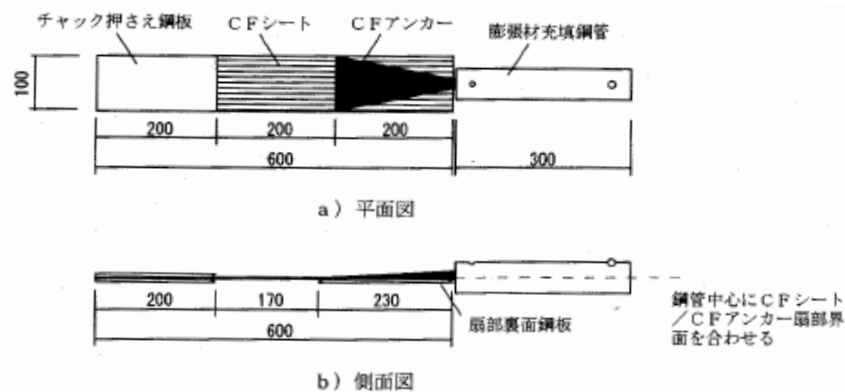
Figure 3.157   Test method for evaluating strength of lap spliced region CFRP anchor and CFRP sheet (SR-CF Construction Method Research Council, 2001)
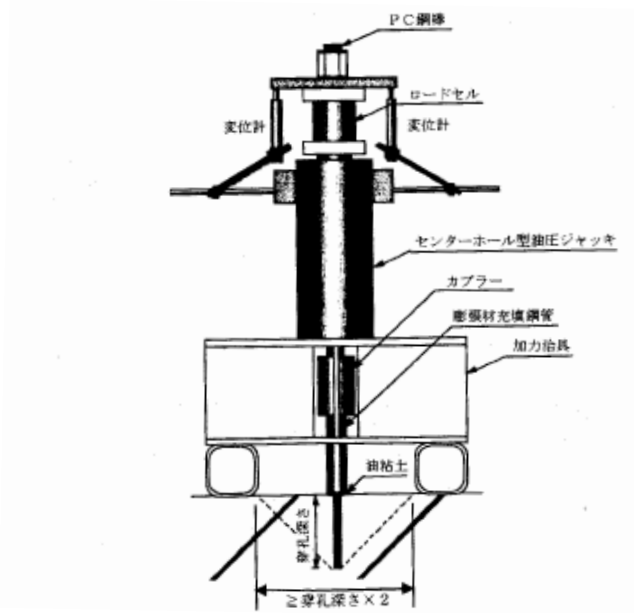
Figure 3.158 Pull-out test method for CFRP anchor (SR-CF 工法 研究會, 2001)

A test method, which is similar to Standard Test Method for Flexural Strength of Concrete Using Simple Beam with Center-Point Loading (ASTM C 293-07), was proposed during the study of CFRP rehabilitation. Preliminary tests were conducted using the standard concrete beam specimens according to ASTM C 293-07. CFRP sheets and anchors were applied to the bottom face of the beam which was tested under center-point loading (Figure 3.159). However, this test method did not provide reliable test results due to lack of shear strength in the beam. In some cases, it was possible to achieve a failure mode of the beam that was crack in the center and fracture of CFRP sheet (Figure 3.160-a) while in other cases, failure mode of the beam was shear failure before the CFRP sheet developed full tensile strength (Figure 3.160-b). Therefore, the test methods need to be improved to develop a reliable and simple test method for CFRP anchors. In addition, Details of test setup, specimen, and installation of CFRP need to be studied for a standard test method. Research on qualification test methods for CFRP anchors is continuing at the University of Texas at Austin.
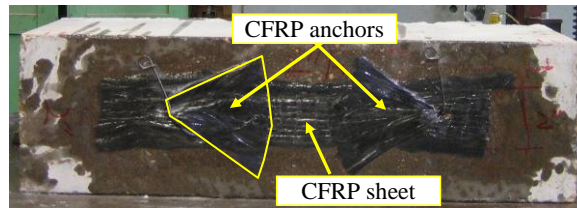
Figure 3.159 Proposed qualification test method for CFRP anchors
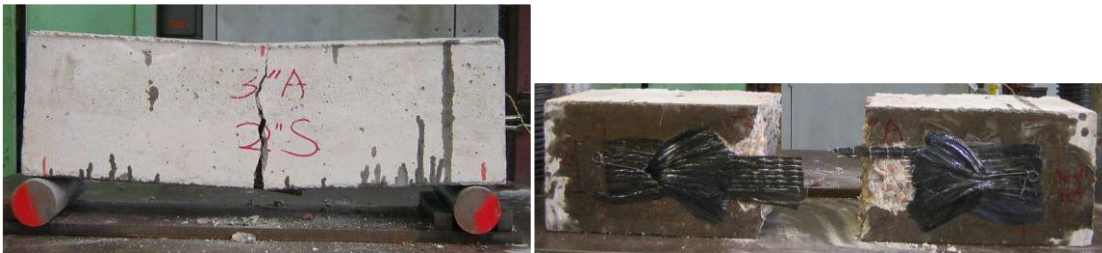
a. Fracture of CFRP sheet

b. Shear failure of the beam

Figure 3.160 Failure modes in the qualification test

181

CHAPTER 4

Experimental Program - Rehabilitation of Poorly Detailed Reinforced Concrete Columns

4.1 INTRODUCTION

In many reinforced concrete structures built in the 1970's and earlier, lap splices in column longitudinal reinforcement were based on compression loads only. The length of those splices and the amount of transverse reinforcement are inadequate if the lap splices are subjected to different types of loading or if ductility is needed. Locations of poorly detailed lap splices in the reinforced concrete structures are shown in Figure 4.1.
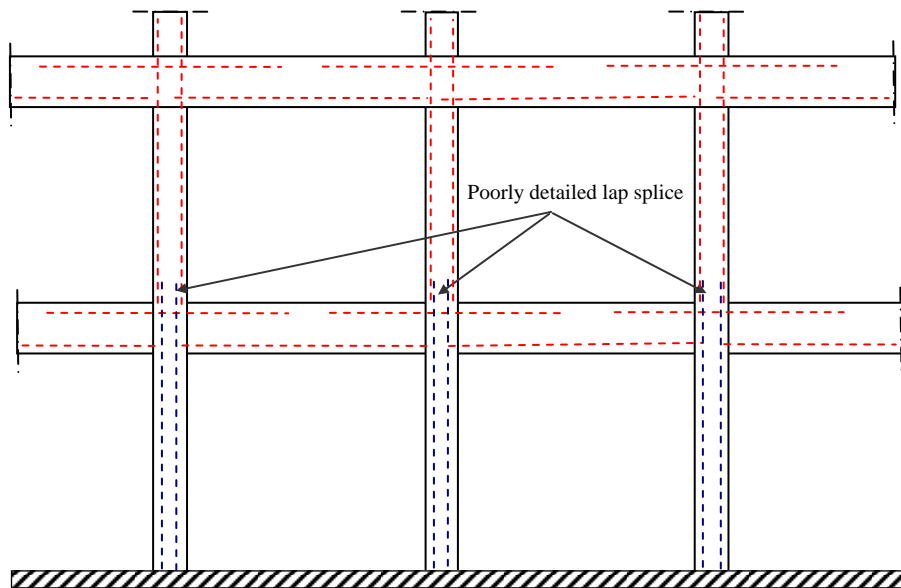
Figure 4.1   Location of poorly detailed lap splices

In extreme loading conditions such as loss of a column support due to terrorist attack or if earthquake or other extreme actions cause severe damage, the performance of the structure may be unsatisfactory. Jacketing of reinforced concrete columns using

182

CFRP may provide a solution for improving lap splice behavior. Use of CFRP jacketing in reinforced concrete columns to transfer tension through the splice region in the case of loss of a column support is shown in Figure 4.2.
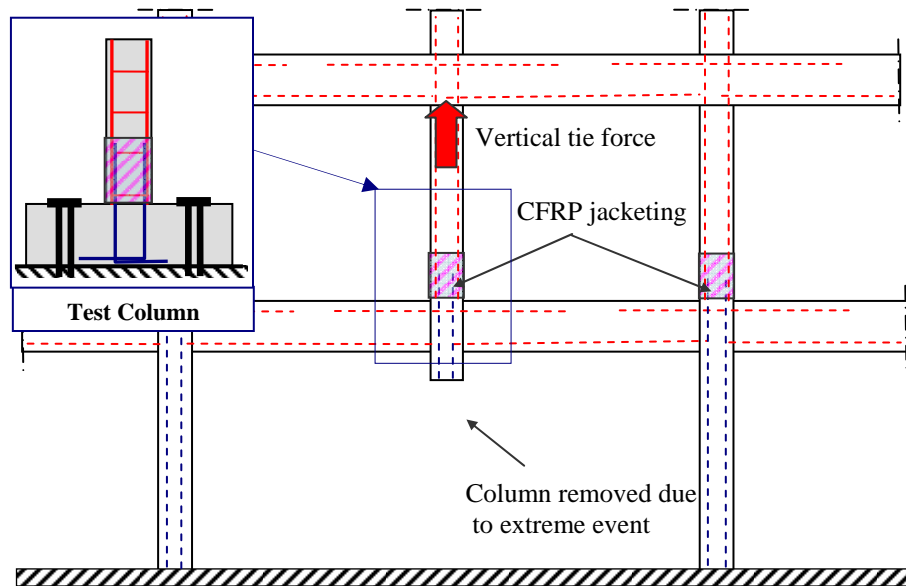
Figure 4.2   CFRP jacketing in splice region

However, CFRP jacketing of square and rectangular reinforced concrete columns (Figure 4.3-b) is not as efficient as it is for circular columns (Figure 4.3-a) because CFRP jackets can not confine a rectangular section as effectively as a circular section. Except for lap splices located at the corners of a square or rectangular column, splitting caused by lap splices of bars away from the corner will not be restrained by the CFRP jacketing. The effectiveness of CFRP jacketing in rectangular columns could be improved using CFRP anchors (Figure 4.3-c). The CFRP anchors cross the splitting crack that develops at the lap splices located away from a corner.

Direction of loading

CFRP jacket

a. Circular column section with CFRP

CFRP anchor

b. Rectangular column section with CFRP jacket

c. Rectangular column section with CFRP jackets and CFRP anchor
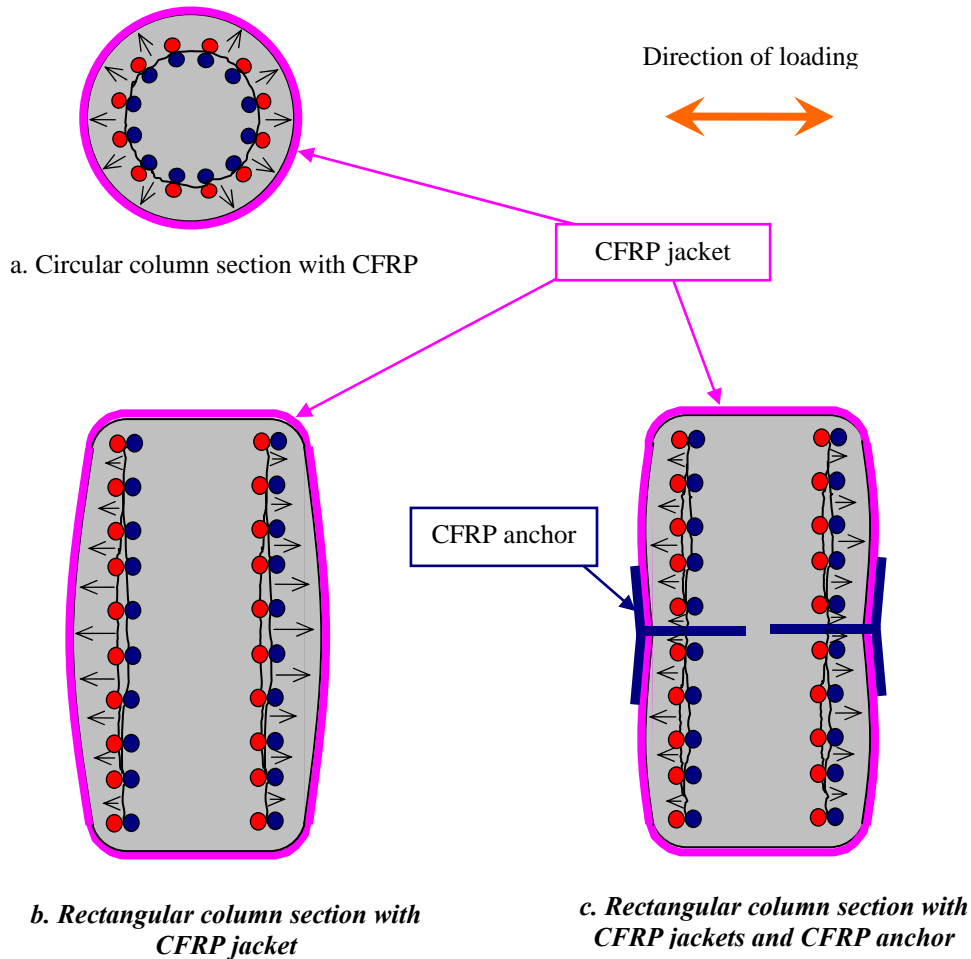
Figure 4.3   **Confinement effect of CFRP jackets and CFRP anchors**

Two alternative methods of loading, vertical loading (Figure 4.4-a) and lateral loading (Figure 4.4-b), were initially considered to apply tension to the lap splices. The lateral loading was selected for this study although the vertical loading could create a stress condition in the lap splices which was more similar to the condition when a column below the lap splices was removed. However, the lateral loading was selected because of following reasons. First, more than one test was possible using one column under the lateral loading because only one side of the lap splices was in tension when the lateral

load was applied and when the load was reversed, the other side was in tension. Therefore, more test variables could be evaluated using two sides of a column by applying the lateral loading in both directions. In this study, column specimens were tested under monotonic or cyclic lateral loading. Under monotonic loading, a column was tested in three different conditions: as-built, repair after loading to splice failure, and strengthening prior to loading. Under cyclic loading, different strengthening methods were evaluated using each side of a column. Details of the loading program are presented in Section 4.4.2. Second, under lateral loading, a drift ratio vs lateral load response of a column was obtained. This information provided a clear indication of performance of the column before and after rehabilitation and was easy to compare with test results from other studies with similar loading. Third, the test setup and specimens could be compared to those reported by Aboutaha (1994) in which steel jackets were used.

The difference in the stress condition of the lap splices under vertical loading and lateral loading was variable moment along the lap spliced region. The effect of the variable moment was studied by Ferguson and Krishnaswamy (1971). According to their study, the lap splice length can be decreased by multiplying the splice length by a factor, $\frac{1}{2}(1+k)$ and k is ratio of stresses at the ends of the lap spliced region $(0.5 \leq k \leq 1)$. In Figure 4.4-b, if bending moment at the bottom of the column is just at yield, the stress in the lap spliced bar at that point is f_y and the stress in the other lap spliced bar at the top of the splice is $\frac{L - L_s}{L} f_y$ ($k = \frac{L - L_s}{L}$). In our test program, k was equal to 0.78 (L=108 in. and L_s=24 in.) and the lap splice length could be reduced by 11%. Although less development length was required in a variable moment condition than in a constant moment condition, lateral loading was selected because the effect of the variable moment was small for the specimen dimensions selected.

Different approaches for strengthening and repairing inadequate lap splices in square and rectangular reinforced concrete columns using combinations of CFRP jackets

185

and CFRP anchors were studied. Three square columns (1-A-S8-M, 2-A-S8-M and 3-B-S10-M) and three rectangular columns (4-C-R20-M, 5-C-R20-C and 6-C-R20-C) were fabricated and rehabilitated using CFRP jackets only, CFRP anchors only, or by a combination of CFRP jackets and CFRP anchors. Both damaged and undamaged columns were strengthened and tested.
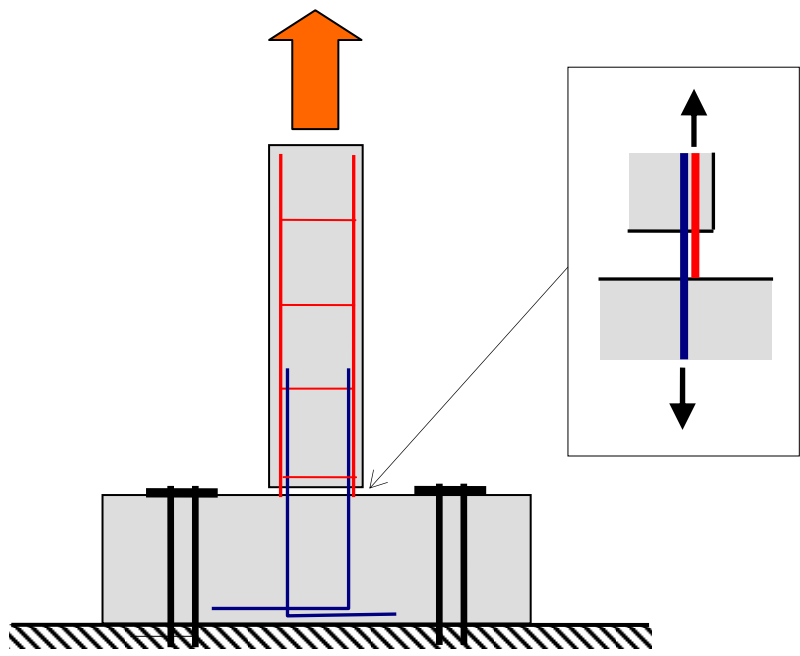
a. Vertical loading, no moment
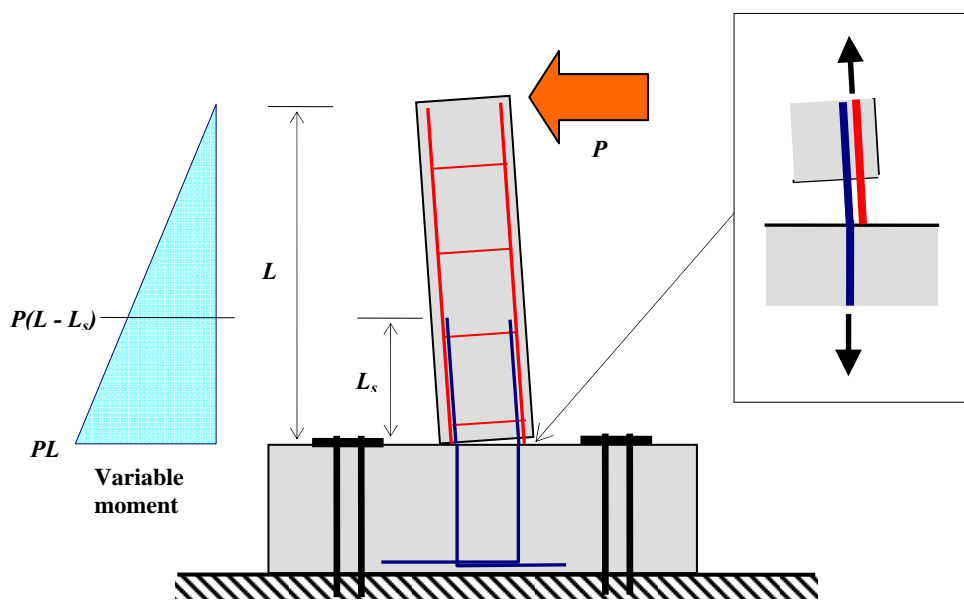
b. Lateral loading, no axial load

Figure 4.4   Vertical loading vs lateral loading

4.2   TEST VARIABLES

The test variables were as follows: 1. Section shape and number of lap splices; 2. Loading programs (monotonic or cyclic); 3. Rehabilitation methods (use of CFRP jackets and/or anchors, design method)

4.2.1   Test Specimens

The geometry and dimensions for the test specimens are provided in Figure 4.5. The longitudinal bars in the column and the bars from the footing were lap spliced above the construction joint between the column and the footing. All the spliced longitudinal bars were #8 and the length of the lap splices was 24 in. In the lap spliced region, transverse reinforcement was provided by #3 bars at 16 in. spacing with the first tie at 4 in. from the footing. Design of columns was based on provisions of the ACI 318-63.

Three types of reinforced concrete columns were fabricated. Dimensions of columns and details of transverse reinforcement are shown in Figure 4.5 and Figure 4.6. Six columns, two Type A (1-A-S8-M and 2-A-S8-M) with 8 splices, one Type B (3-B-S10-M) with 10 splices and three Type C (4-C-R20-M, 5-C-R20-C and 6-C-R20-C) with 20 splices, were tested. A summary of specimens is shown in Table 4.1. In specimen notation, characteristics of a test column are indicated as follows:

- Specimen number
- Type of column (Type **A**, **B** or **C**),
- Shape of section (**S**quare or **R**ectangle)
- Number of lap splices (**8**, **10** or **20** lap splices in a column)
- Type of loading (**M**onotonic or **C**yclic)

188

Table 4.1   Summary of test columns

Specimen	Section type	Size of specimen	Number of lap splices	Type of loading	Test condition	Compressive strength of concrete	Age on test day
1-A-S8-M	Type A	18 in. x 18 in. (Square)	8	Monotonic	As-built	5,300 psi	56 days
					Repair and strengthening	5,600 psi	79 days
2-A-S8-M	Type A	18 in. x 18 in. (Square)	8	Monotonic	As-built	4,700 psi	28 days
					Repair and strengthening	5,300 psi	47 days
3-B-S10-M	Type B	18 in. x 18 in. (Square)	10	Monotonic	As-built	4,200 psi	28 days
					Repair and strengthening	4,500 psi	39 days
4-C-R20-M	Type C	18 in. x 36 in. (Rectangle)	20	Monotonic	As-built	4,600 psi	53 days
					Repair and strengthening	4,600 psi	69 days
5-C-R20-C	Type C	18 in. x 36 in. (Rectangle)	20	Cyclic	Strengthening	5,600 psi	63 days
6-C-R20-C	Type C	18 in. x 36 in. (Rectangle)	20	Cyclic	Strengthening	5,600 psi	82 days

Specimen notation: A: Type A; **B:** Type B; **C:** Type C (Figure 4.5)

S: Square; **R:** Rectangle

8: 8 lap splices; **10:** 10 lap splices; **20:** 20 lap splices

M: Monotonic loading; **C:** Cyclic loading

Design compressive strength of concrete was 4,000 psi. The measured compressive strengths of concrete at the day of the test are shown in Table 4.1. Two columns were fabricated at the same time (3 castings: 1-A-S8-M and 2-A-S8-M; 3-B-S10-M and 4-C-R20-M; 5- C-S20-C and 6- C-R20-C). 2-A-S8-M was tested prior to 1-A-S8-M and the other columns were tested in the same order as the number of the

189

specimen   In Table 4.1, two values of compressive strengths are provided for 1-A-S8-M, 2-A-S8-M, 3-B-S10-M and 4-C-R20-M because these columns were tested as-built and after rehabilitation.

Grade 60 reinforcement was used for the longitudinal (#8) and transverse (#3) reinforcement. The measured tensile yield strength of longitudinal reinforcement was 63 ksi and that of transverse reinforcement was between 66 ksi and 74 ksi. A measured strain-stress curve of the longitudinal reinforcement (#8) is shown in Figure 4.7.

- **Longitudinal reinforcement: #8 GR60**
- **Ties: #3 @ 16 in. GR60**
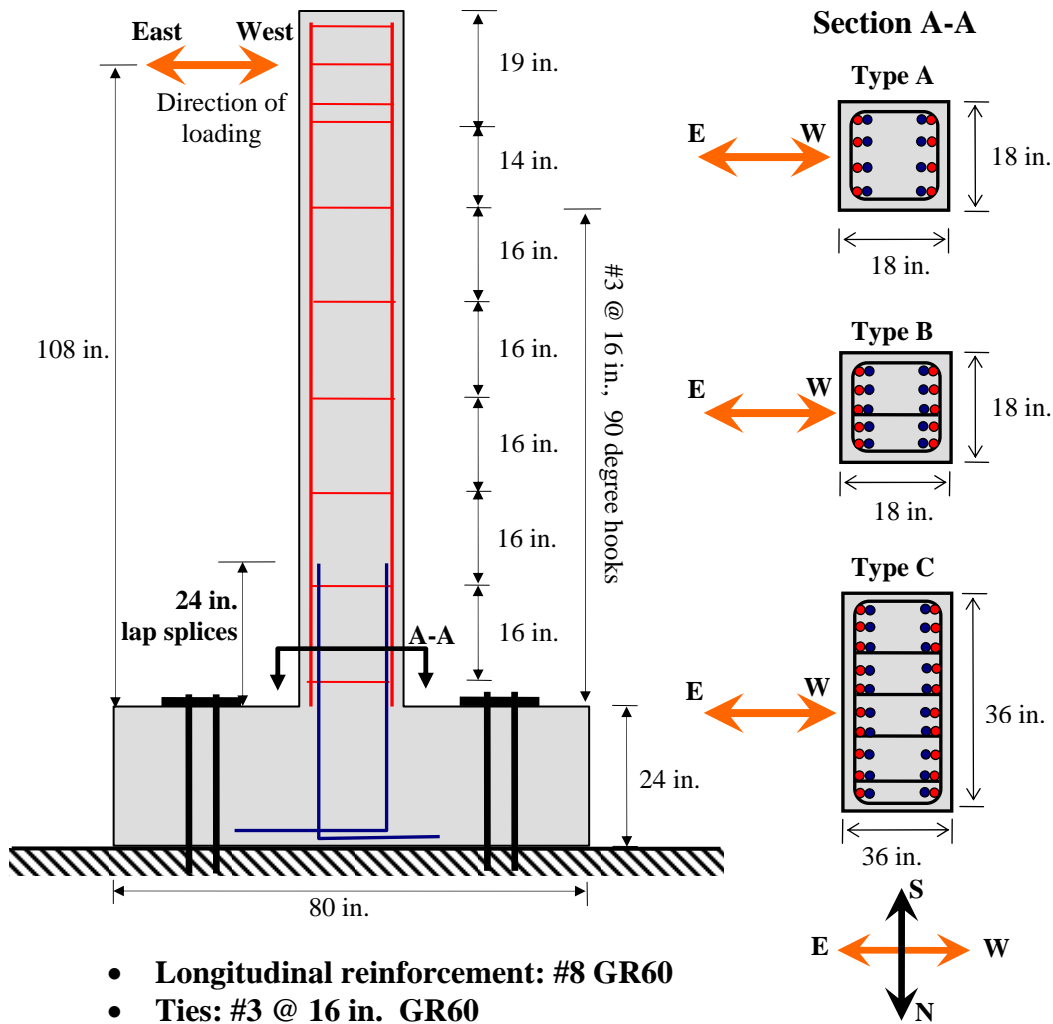
Figure 4.5   Geometry and dimensions for test specimens

190

Type A

18 in.

18 in.

Type B

18 in.

18 in.

Type C

36 in.

36 in.
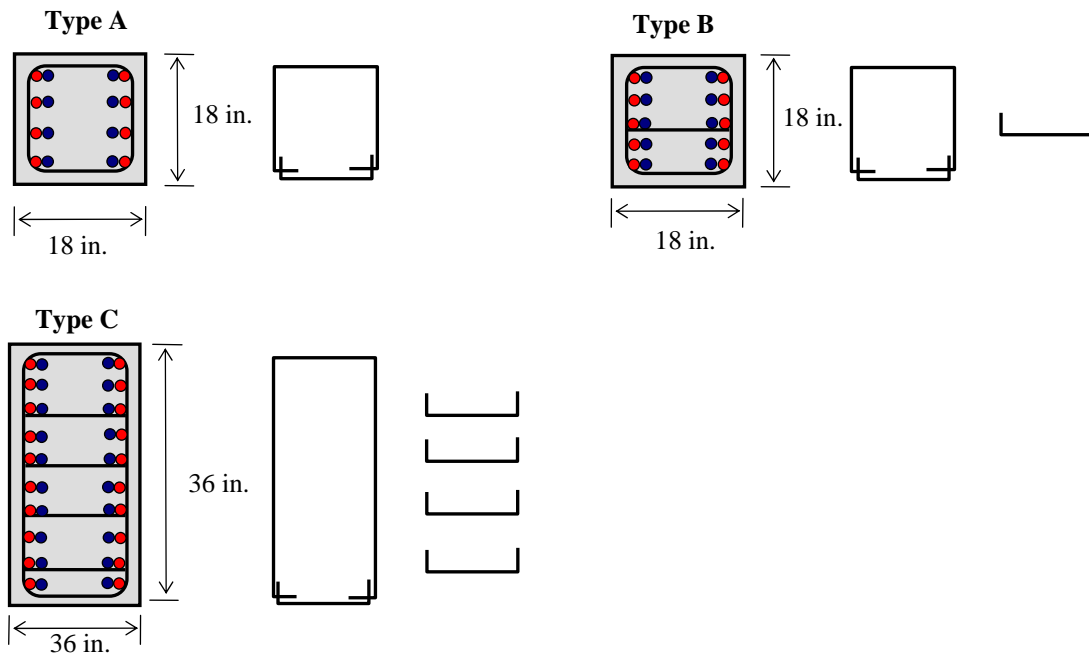
Figure 4.6   Transverse reinforcement details
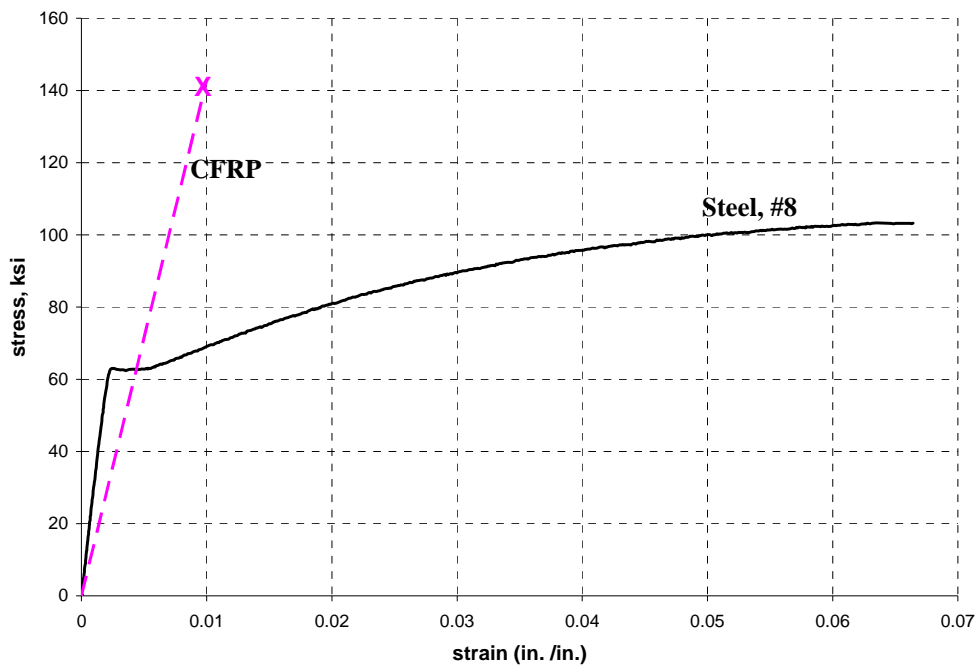
Figure 4.7   Strain-stress curves of steel and CFRP

191

4.2.2 Loading Program

Two types of lateral loading were applied to the columns. Monotonic loading was applied to 1-A-S8-M, 2-A-S8-M, 3-B-S10-M and 4-C-R20-M and cyclic loading was applied to 5-C-R20-C and 6-C-R20-C.

No axial load was applied to the columns. The dominant action of the bottom portion of the columns, lap spliced region, was flexure. To minimize the effect of shear on the failure mechanism, the columns were designed to have considerably higher nominal shear strength than flexural strength. The loading program is shown in Table 4.1.

Lateral applied load and displacement was measured at the load point. Drift ratio corresponds to the measured lateral displacement divided by the height of the loading location from the top of the footing (108 in.). Details of test setup are described in Section 4.4.

4.2.2.1 *Monotonic Loading Test*

In the columns tested under monotonic loading, two tests, as-built and after rehabilitation, were conducted on each column. First, a column was tested as-built. 1-A-S8-M, 2-A-S8-M, 3-B-S10-M and 4-C-R20-M were first loaded to determine the load and deformation capacity up to the point where the capacity of the splices on only one face of the column was reached (Figure 4.8-a). When a rapid drop of the load was observed, the loading was stopped in order to prevent severe damage to the splice region. The drift ratio at this point was about 1%.

After unloading, the column was repaired (damaged side during first loading) and strengthened (undamaged side) using CFRP materials. Rehabilitation details for each test column are discussed in Section 4.3. As part of the repair procedure of the side damaged in the as-built test, epoxy crack injection preceded application of the CFRP. HILTI CI 060 Crack Injection System was used to inject cracks. (Figure 4.8-b) The crack injection procedure recommended by the manufacturer was used and is introduced in Appendix B.1.

192

After rehabilitation, the column was loaded in the opposite direction of load in the first test (Figure 4.8-c). Under the second load, the bars in the face undamaged in the first test were in tension. After the column reached a drift of 2.3 % and the spliced bars in the undamaged side yielded, the load was reversed so that bars in the damaged side were subjected to tension (Figure 4.8-d). After the column reached a drift of about 6 % and the bars yielded, the direction of loading changed so the bars in the initially undamaged side were again subjected to tension (Figure 4.8-e). The column was loaded up to the stroke limit of the hydraulic actuator in this direction.

Using this test procedure, lap splices of bars in three different conditions were evaluated using one test column: (1) as-built, (2) repaired column after damage and (3) strengthened undamaged column.

4.2.2.2 Cyclic Loading Test

5-C-R20-C and 6-C-R20-C were tested under cyclic loading to assess of strength and deformation capacity of the splice after CFRP rehabilitation under seismic loading.

The loading history suggested by Krawinkler (1996) was selected for the cyclic loading test. Because 4-C-R20-M was tested under monotonic loading and was identical to 5-C-R20-C and 6-C-R20-C, the yield displacement was 1.3 in. and corresponded to a drift ratio of 1.2 %. The amplitude of cyclic loading was based on the yield displacement. The amplitude of displacement in the first 3 cycles was 50 % of the yield displacement and in the second 3 cycles was 75 % of the yield displacement. The amplitude of displacement in the third 3 cycles was the same as the yield displacement. After the yield displacement was reached, the incremental increase in displacement was equal to the yield displacement. Deflections increased up to the stroke limit of the hydraulic actuator. The cyclic loading histories for 5-C-R20-C and 6-C-R20-C are shown in Figure 4.9 and Figure 4.10.
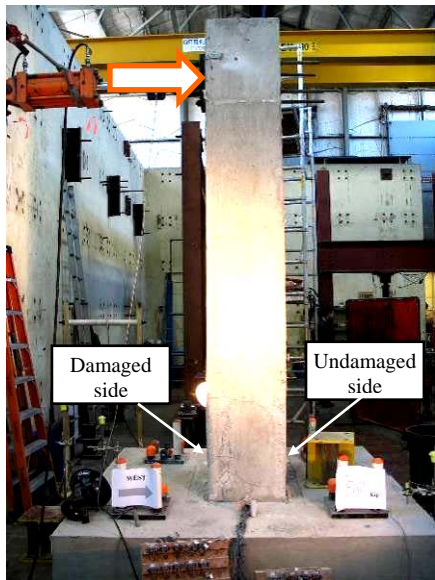
a. As-built test
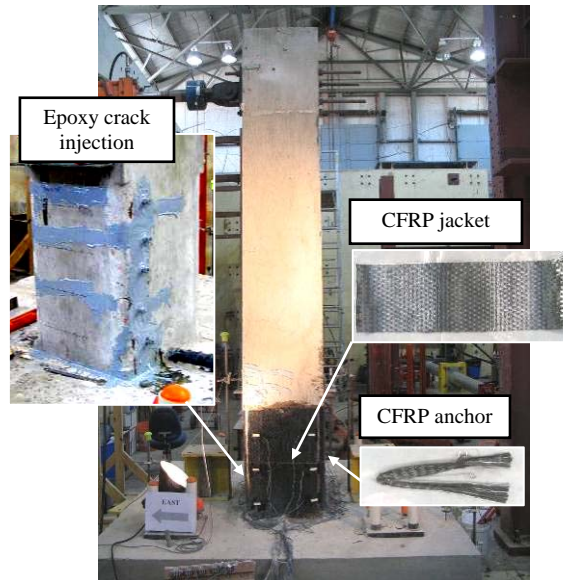
b. Repair and strengthening

c. Tension of undamaged side   *d. Tension of damaged side*   *e. Tension of initially undamaged side*

Figure 4.8   Monotonic loading test procedure
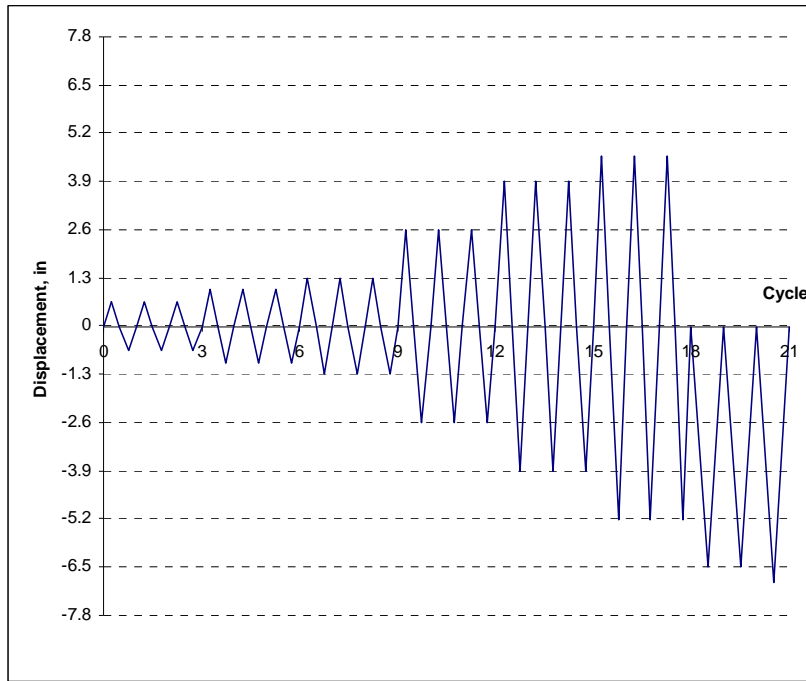
a. Displacement
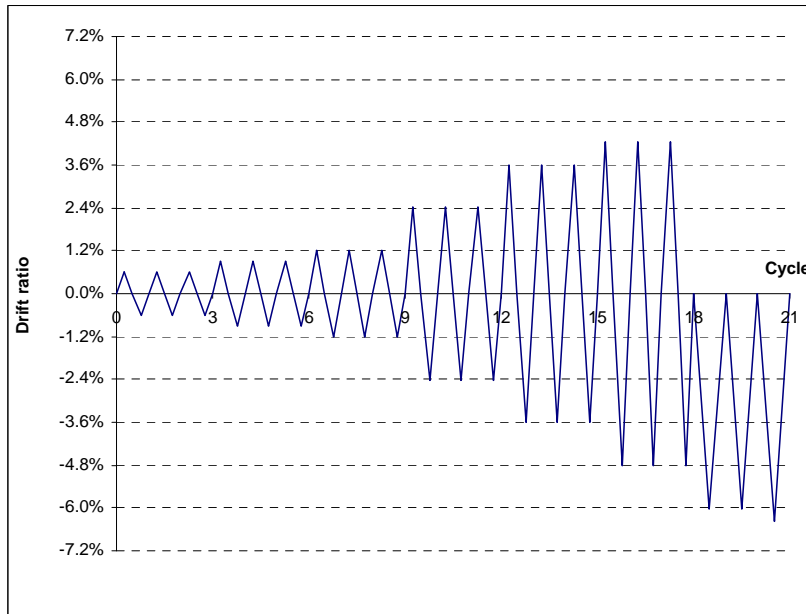
b. Drift ratio

Figure 4.9   Cyclic loading history of 5-C-R20-C

195
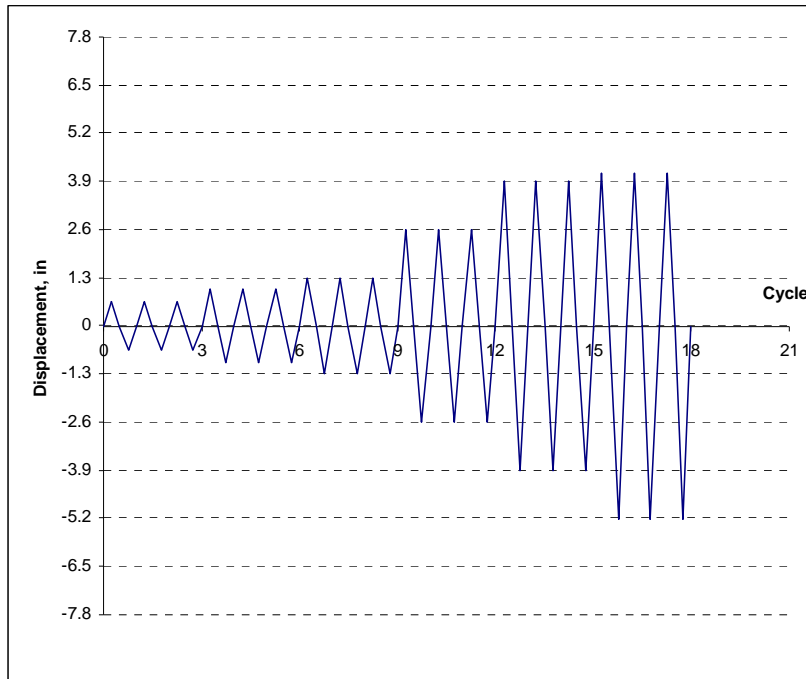
a. Displacement
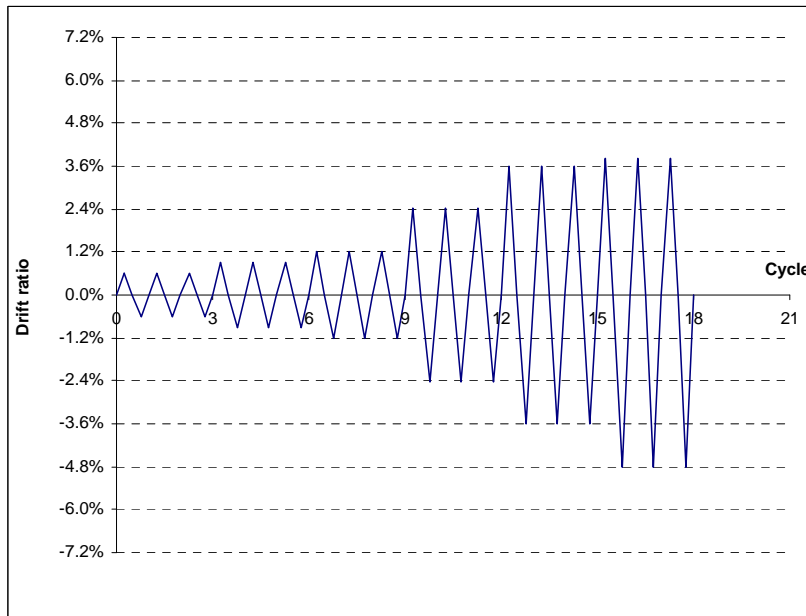
b. Drift ratio

Figure 4.10   Cyclic loading history of 6-C-R20-C

196

4.2.3   Rehabilitation Methods Using CFRP

4.2.3.1   Rehabilitation Design

Using CFRP materials, 1-A-S8-M, 2-A-S8-M, 3-B-S10-M and 4-C-R20-M were repaired and strengthened after the as-built column was tested, and 5-C-R20-C and 6-C-R20-C were strengthened in the as-built condition.

All strengthened and repaired tests had CFRP jackets except the west face of 6-C-R20-C. The number of CFRP anchors and width of CFRP material used in the anchors varied depending on the design method. In Table 4.2, details of the rehabilitation are given.

One layer of CFRP sheet was used to wrap in all the test columns as a jacketing element to provide confinement of the lap splices. The number of layers of CFRP in the jackets was not varied because the confinement effect of CFRP jackets on rectangular columns is limited to the corner bars and many researchers have investigated columns confined with multiple layers of CFRP. CFRP jackets with no anchor were used in 1-A-S8-M to study effectiveness of the CFRP jacket only. In contrast, a combination of CFRP jackets and CFRP anchors was used in the other columns. In 1-A-S8-M, 2-A-S8-M, 3-B-S10-M, 4-C-R20-M and 5-C-R20-C, CFRP jackets wrapped the entire section of the lap spliced region while on the east face of 6-C-R20-C, ends of the partial CFRP jackets were anchored. On west side of 6-C-R20-C, anchors only were provided. Layout of CFRP jackets in the test columns are described in Section 4.3.

When CFRP anchors were used, they were installed with the CFRP jackets except on the west side of 6-C-R20-C. The CFRP anchors were installed so at least one side of every lap spliced longitudinal bars was next to anchors. CFRP anchors were applied either in 2 (18 in. vertical spacing) or 4 rows (6 in. vertical spacing). Different numbers of rows of CFRP anchors were studied to determine whether the number of anchors could be reduced to save installation costs.

197

Table 4.2   Details of the rehabilitation

Specimen	Type of loading	Test conditions		CFRP jacket	CFRP anchors	No. of rows of CFRP anchors	No. of total CFRP anchors	Design of CFRP
1-A-S8-M	Monotonic	As-built						
		Repair and strengthening	Undamaged side (West)	x				
			Damaged side (East)	x				
2-A-S8-M	Monotonic	As-built						
		Repair and strengthening	Undamaged side (West)	x	x	4	4	Shear friction
			Damaged side (East)	x	x	4	4	Shear friction
3-B-S10-M	Monotonic	As-built						
		Repair and strengthening	Undamaged side (East)	x	x	4	8	Previous test
			Damaged side* (West)	x	x	4	8	Shear friction
4-C-R20-M	Monotonic	As-built						
		Repair and strengthening	Undamaged side (West)	x	x	2	8	Previous test
			Damaged side (East)	x	x	4	16	Previous test
5-C-R20-C	Cyclic	Strengthening	West	x	x	2	8	Previous test
			East	x	x	4	16	Previous test
6-C-R20-C	Cyclic	Strengthening	West		x	`4	20	Previous test
			East	x**	x	4	16	Previous test

* East side was damaged under monotonic loading except 3-B-S10-M.

**Partial jacket with anchors were used on the east side of 6-C-R20-C.

CFRP materials for rehabilitation of 2-A-S8-M and the west side of 3-B-S10-M were initially designed using shear friction as shown in Figure 4.11.
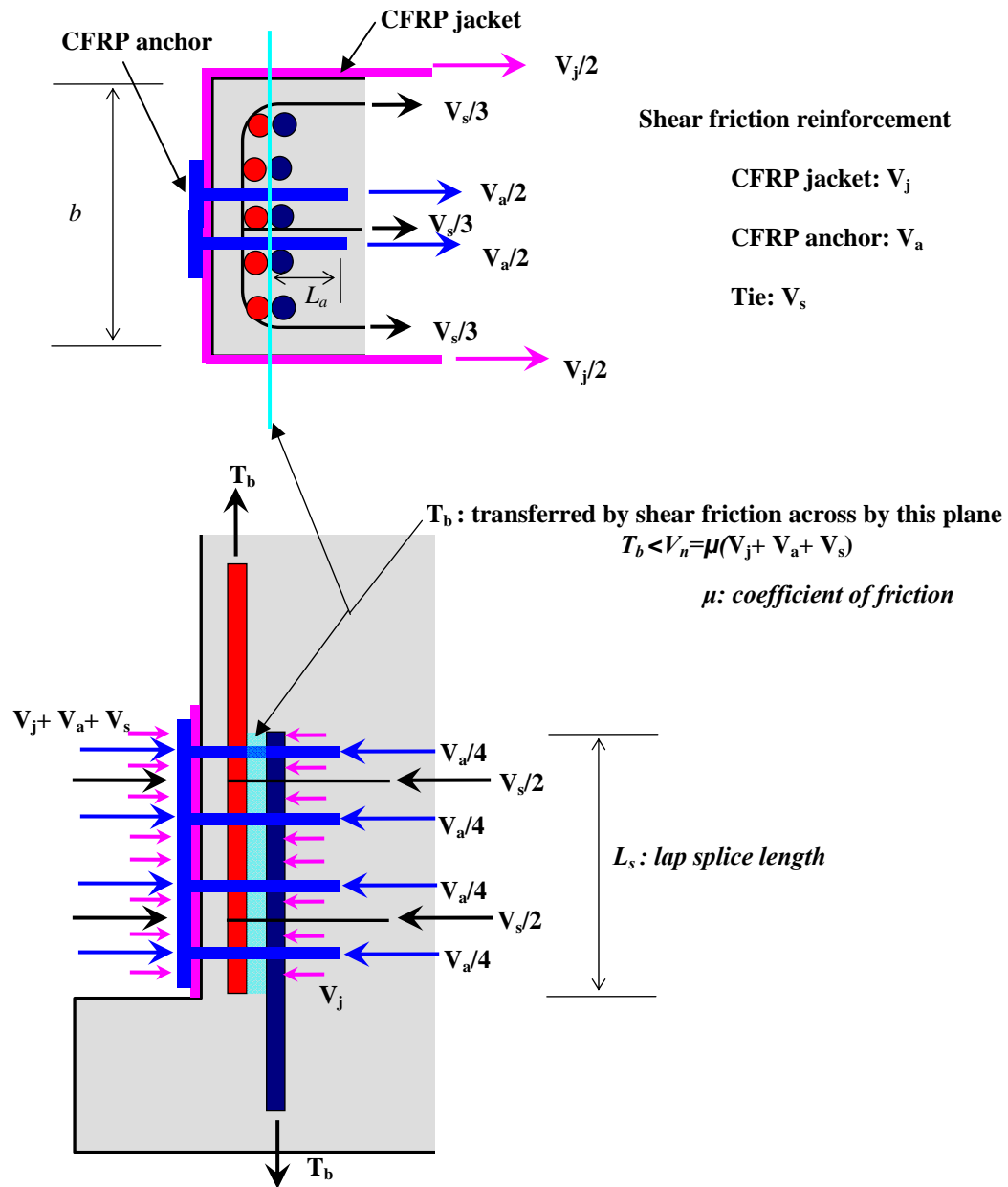
Figure 4.11   Shear friction mechanism, 3-B-S10-M

The total width of CFRP materials across the shear plane was calculated using the shear friction equation. The tensile force in the lap spliced bars was assumed to be transferred across a shear plane where splitting cracking was expected. A stress of 1.25 f_y assumed to account for the possibility of strain hardening. CFRP jackets, CFRP anchors and ties were assumed to contribute a force perpendicular to the shear plane. When calculating this force, it was assumed that only 1/3 of ultimate strength of CFRP can be developed. One third of the ultimate strain of CFRP was 0.0033 which was less than the delamination strain of CFRP (0.0040) but larger than the yield strain of steel (0.0021). After determining the total width of CFRP needed, the distribution of that material between the jacket and the anchors was determined. First, one layer of CFRP jacket with the same width as the lap splice length was used for jacketing. Second, vertical spacing of CFRP anchors in the lap spliced region was 6 in. Third, CFRP anchors were placed at the middle of the lap splices on at least one side of every lap spliced longitudinal bar except corner bars. Forth, the diameter and depth of the anchor hole was selected to prevent bond failure of a CFRP anchor. The diameter of the anchor and the hole was assumed to be the same. The preliminary design procedure and a design example for CFRP jackets and anchors using shear friction are described below.

Design Procedure

1. Calculate tensile force in the longitudinal bars, T_b and check T_b with the upper limit on shear-friction strength, $V_{n,max}$

$$T_b = 1.25 f_y A_s \qquad\qquad\text{\textit{Equation 4-1}}$$

$$V_{n,\max} = vbL_s \qquad\qquad\text{\textit{Equation 4-2}}$$

$$V_{n,\max} \geq T_b \qquad\qquad\text{\textit{Equation 4-3}}$$

T_b: expected tensile force in the longitudinal bars, lb

f_y : yield strength of reinforcement, psi

200

$f_c^{'}$: compressive strength of concrete, psi

A_s: area of longitudinal bars, in^2

$V_{n,max}$: upper limit on shear friction strength, lb(ACI 318-08,11.6.5)

v: maximum stress transferred by shear friction smaller of $0.2 f_c^{'}$ or 800 psi

(ACI 318-08, Section 11.6.5)

b: width of column

2. Determine the total effective width of CFRP anchors using one layer of CFRP jackets and $V_n > T_b$ (Assume 1/3 of f_{fu} is effective)

$$V_n = \mu(V_j + V_a + V_s) \geq T_b \qquad\qquad \textbf{\textit{Equation 4-4}}$$

$$V_j = (f_{fu}/3)t_f(2L_j) \qquad\qquad \textbf{\textit{Equation 4-5}}$$

$$V_a = n_a(f_{fu}/3)A_a \qquad\qquad \textbf{\textit{Equation 4-6}}$$

$$V_s = f_y A_{vf} \qquad\qquad \textbf{\textit{Equation 4-7}}$$

$$\frac{n_a A_a}{t_f} \geq \frac{1}{t_f}\frac{3}{f_{fu}}\left[\frac{T_b}{\mu} - (f_{fu}/3)t_f(2L_j) - f_y A_{vf}\right] \qquad \textbf{\textit{Equation 4-8}}$$

μ : coefficient of friction =1.4 (ACI 318-08,11.6.4.3)

V_n: nominal shear strength, lb

V_j: force perpendicular to shear plane contributed by CFRP jackets, lb

V_a: force perpendicular to shear plane contributed by CFRP anchors, lb

V_s: force perpendicular to shear plane contributed by transverse steel reinforcement, lb

f_{fu}: tensile strength of CFRP, psi

t_f: thickness of CFRP sheet, in.

L_j: width of CFRP jacket, in.

n_a: number of CFRP anchors

A_a: area of a CFRP anchor, in^2

A_{vf}: area of steel shear-friction reinforcement, in^2

$\dfrac{n_a A_a}{t_f}$: effective width of total CFRP anchors, in^2

3. Determine the number of CFRP anchors using the following detailing requirements

    - Vertical spacing of CFRP anchors in the lap spliced region: *6 in.*

    - Horizontal distribution of CFRP anchors: *at the middle of lap splices on at least one side of every lap spliced longitudinal bar except corner bars*

    - Diameter and depth of anchor hole to prevent bond failure of a CFRP anchor: (Equation 4-10 is discussed in Section 2.1)

$$(f_{fu}/3)A_a \leq P_n \qquad\qquad \textbf{\textit{Equation 4-9}}$$

$$P_n = 4\sqrt{f_c^{'}} \times h_c \times (d_h + h_c) \times \pi + 22\sqrt{f_c^{'}} \times h_c \times (L_a - h_c)$$

$$\textbf{\textit{Equation 4-10}}$$

      P_n : tensile strength of CFRP anchor, lb, Equation 2-3

      h_c : concrete cone depth, 2 in. (Ozdemir et al,. 2005)

      d_h: diameter of anchor hole, in.

      L_a: depth of anchor hole from the shear plane, in,. > 4 in. (Ozdemir et al,. 2005)

Design Example, the West face of 3-B-S10-M

1. Calculate tensile force in the longitudinal bars, T_b and check T_b with the upper limit on shear-friction strength, $V_{n,max}$

$$T_b = 1.25 f_y A_s = 1.25 \cdot 60{,}000 \cdot (5 \cdot 0.79) = 296{,}250 \ lb$$

$$V_{n,max} = vbL_s = 800 \cdot 18 \cdot 24 = 345{,}600 \ lb$$

$$V_{n,max} \geq T_b \qquad\qquad \textbf{O.K.}$$

A_s= 5-#8(5x0.79 in²)

b=18 in.

2. Determine the effective width of total CFRP anchors using one layer of CFRP jackets and $V_n > T_b$

$$V_n = \mu(V_j + V_a + V_s) \geq T_b$$

$$V_j = (f_{fu}/3)t_f(2L_j) = (143{,}000/3) \cdot 0.04 \cdot 24 = 91{,}520 \ lb$$

$$V_s = f_y A_{vf} = 60{,}000 \cdot (6 \cdot 0.11) = 39{,}600 \ lb$$

$$\frac{n_a A_a}{t_f} \geq \frac{1}{t_f}\frac{3}{f_{fu}}\left[\frac{T_b}{\mu} - (f_{fu}/3)t_f(2L_j) - f_y A_{vf}\right]$$

$$\frac{n_a A_a}{t_f} \geq \frac{1}{0.04}\frac{3}{143{,}000}\left[\frac{296{,}250}{1.4} - 91{,}520 - 396{,}000\right] = 42.2 \ in.$$

μ =1.4

f_{fu}=143,000 psi,

t_f= 0.04 in.

L_j = 24 in.

A_{vf} = 6x0.66 in², (6-#3 ties across the shear plane)

3. Determine the number of CFRP anchors using the detailing requirements

- Vertical distribution: *24 in./6 in. = 4 rows of anchors*

- Horizontal distribution: *2 columns of anchors*

- Total number of anchor, n_a= 4x2=*8 anchors*

$$\frac{42.2\ in}{8\ anchors}. = 5.275\ in.\ per\ anchor \rightarrow Use\ 5.5\ in.\ anchor$$

- Diameter and depth of anchor hole:

Try d_h=5/8 in. and L_a= 6 in. > 4 in.

$$(f_{fu}/3)A_a = (143,000/3)(0.04 \cdot 5.5) = 10,487\ lb$$

$$P_n = 4\sqrt{f_c'} \times h_c \times (d_h + h_c) \times \pi + 22\sqrt{f_c'} \times h_c \times (L_a - h_c)$$
$$= 4\sqrt{4,000} \times 2 \times (5/8 + 2) \times \pi + 22\sqrt{4,000} \times 2 \times (6 - 2) = 15,304\,lb$$

$$(f_{fu}/3)A_a \leq P_n \qquad\qquad\qquad \boldsymbol{O.K.}$$

The design procedure using shear friction was evaluated using data from the experimental program and a modified design guideline is proposed in Section 5.

The test results of 2-A-S8-M and the west side of 3-B-S10-M indicated that a reduced width of material could be used for the CFRP anchors in the rest of test columns to optimize the quantity of CFRP originally selected using shear friction. Columns with a fewer number of the anchors and less anchor area were tested to find an acceptable area for splice rehabilitation. Details of the CFRP materials used in each test column are discussed in Section 4.3.

4.2.3.2   Material Properties of CFRP

The CFRP material used in fabricating the CFRP jackets and CFRP anchors was Tyfo® SCH-41 Composite with Tyfo® S Epoxy from FYFE Co. LLC.

The CFRP material was unidirectional and had no tensile capacity transverse to the fiber. The specified properties from the manufacturer are shown in Table 4.3. Previous studies showed that the measured properties of this CFRP material were consistent with the specified properties from the manufacturer. (Kim, 2006; Orton, 2007)

A stress-strain curve of the CFRP material provided by the manufacturer is shown in Figure 4.7. Although the CFRP has higher strength than the Grade 60 reinforcement, the CFRP is less stiff than the reinforcement and has a linear strain-stress relationship up to fracture.

Table 4.3   Material properties of CFRP suggested by manufacturer

Properties	Ultimate Tensile Strength	Elongation at Break	Tensile modulus	Laminate thickness
Typical Test Value	143 ksi	1.0 %	13,900 ksi	0.04 in.
Design Value	121 ksi	0.85 %	11,900 ksi	0.04 in.

4.2.3.3   Advantages of Rehabilitation Methods Using CFRP

Rehabilitation methods using CFRP jackets and anchors are comparable to rehabilitation methods using steel jackets and anchor bolts. Advantages of rehabilitation methods of reinforced concrete columns using CFRP over steel are as follows. First, easy and rapid installation is possible through rehabilitation methods using CFRP materials compared with those using steel. CFRP sheets and devices for installing these materials are relatively light and small compared with steel plates requiring welding. Steel plate may be difficult to install and may require non-shrinking grout between the steel plate and concrete column. The time required for applying CFRP is shorter than for steel plates

because the application procedure is relatively simple. CFRP would appear to be more versatile than steel for rehabilitation of existing structures which have limited work space and speed of construction is important.

In addition, CFRP conforms to the shape of the column and does not result in any substantial change in column dimensions. If steel jackets and anchor bolts are used in rehabilitating reinforced concrete columns, the size of the column section increases due to thickness of the steel plates and grout, and the anchor bolts or nuts protrude from the column surface.(Figure 4.12-b) However, layers of CFRP jackets and CFRP anchors are thin and easy to cover after installation. (Figure 4.12-a)

Therefore, use of CFRP can be an effective and efficient solution for repair and strengthening existing reinforced concrete columns.
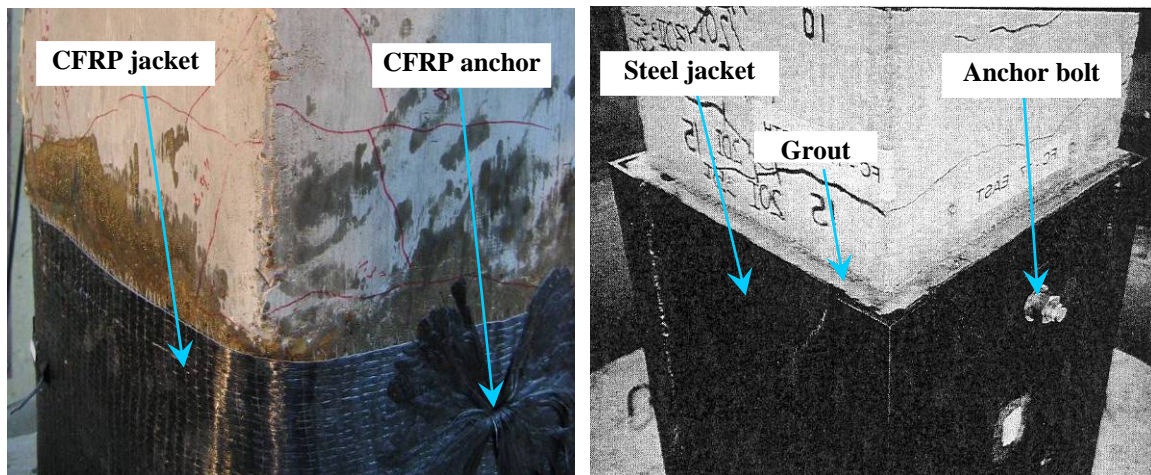
a. CFRP jackets with CFRP anchors   *b. Steel jackets with anchor bolts (Aboutaha, 1994)*

Figure 4.12   Change in column dimensions after rehabilitation

4.3 REHABILITATION OF TEST COLUMNS

4.3.1 Grouting of Cracks

In specimen 1-A-S8-M, 2-A-S8-M, 3-B-S10-M and 4-C-R20-M, crack injection preceded application of CFRP on the damaged side due to the as- built test. HILTI CI 060 Crack Injection System was used to inject cracks. Details of crack injection are described in Appendix B.1. In 5-C-R20-C and 6-C-R20-C, CFRP was applied to undamaged columns so crack injection was not necessary.

4.3.2 Preparation of Concrete Surface and Column Corners for CFRP Jackets

The concrete surface of all the test columns where CFRP would be applied was ground to remove cement paste. The concrete surface before and after grinding is shown in Figure 4.13. The concrete surface was prepared to meet the requirement for a minimum Concrete Surface Profile (CPS) 3 as defined in the International Concrete Research Institute (ICRI) surface-profile-chips. Based on the test results discussed in the previous section, the surface preparation may not be essential for the CFRP application. However, the column surface was ground to reduce the variables of the test program. In addition, grinding the concrete surface was relatively easy. Residual epoxy on the concrete surface due to crack injection was removed by grinding to expose the concrete surface.

The corners of all the test columns with CFRP jackets were also rounded to 2 in. radius to make a smooth transition of CFRP around a corner. The radius of the corner was selected based on a study by Johnson (2004). The rounded corner is shown in Figure 4.14.
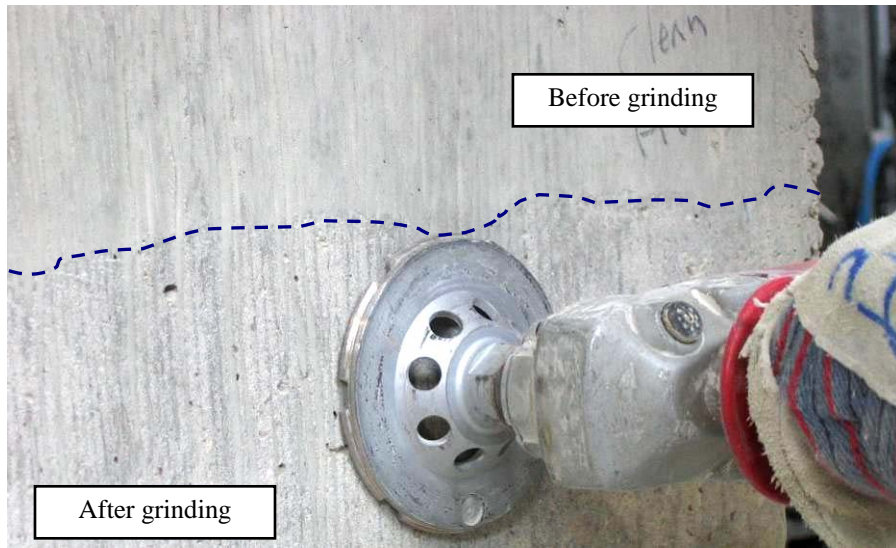
Figure 4.13   Concrete surface before and after grinding

Figure 4.14   Rounded corner

Before applying CFRP to a column, any needed anchor holes were drilled. The size and geometry of anchor holes varied depending on the number of the lap splices and the rehabilitation detail. Details of geometry of the anchor holes in each test column are described in Section 4.3.3 to 4.3.8 where the rehabilitation is discussed. Details of installation of the CFRP jackets and anchors are also described in Appendix B.2.

4.3.3   1-A-S8-M

1-A-S8-M was a Type A column with 8 splices. It was rehabilitated using only CFRP jackets and no CFRP anchors were used. It was tested under monotonic loading.

4.3.3.1   CFRP Jacket

Details of the CFRP jacket are shown in Figure 4.15. One layer of CFRP sheet was used in 1-A-S8-M as a jacketing element to provide confinement of the lap splices. Two CFRP sheets 12 in. wide x 80 in. long were used to confine the 24 in. lap spliced region. The CFRP jacket was applied to the column with a 2 in. gap from the top of the footing because of the irregularities in the column surface next to the footing. The CFRP sheet was overlapped by 5 in. on the north face of the column. The 2 in. gap was exposed in all the test columns and the same overlap was used in all the columns except 6-C-R20-C.
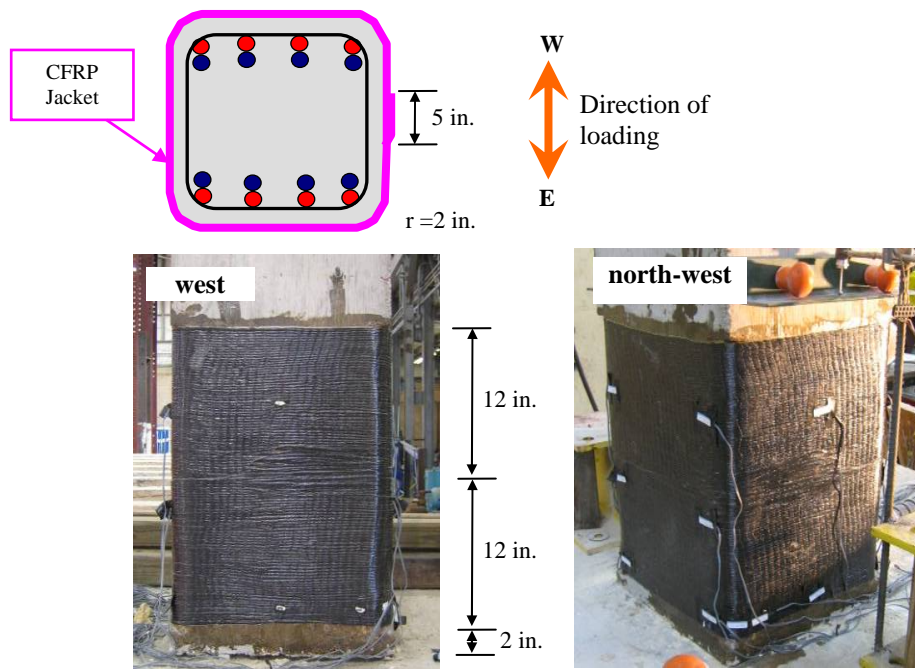
Figure 4.15   Layout of the CFRP jackets, 1-A-S8-M

4.3.4 2-A-S8-M

2-A-S8-M was a Type A column with 8 splices. It was rehabilitated using CFRP jackets and CFRP anchors. It was tested under monotonic loading.

4.3.4.1 Preparation of Holes for CFRP Anchors

A CFRP anchor requires a hole in the concrete for installation. Four holes were drilled on the east and the west face of 2-A-S8-M. The holes were drilled with a 3/4 in. diameter masonry drill bit in 9 in. depth, and they were cleaned with compressed air. The edge of the hole was ground to provide a smooth transition of the CFRP anchor from the hole to the CFRP jacket. In all the other test columns, the edge of anchor hole was prepared in the same way as 2-A-S8-M and the anchor holes were cleaned with compressed air. The anchor holes in 2-A-S8-M prior to installation of CFRP are shown in Figure 4.16.

Figure 4.16   Anchor holes in 2-A-S8-M

4.3.4.2   CFRP Jacket and CFRP Anchor

Details of the CFRP jacket and CFRP anchors are shown in Figure 4.17. One layer of CFRP sheet was used in 2-A-S8-M as a jacketing element to provide confinement of the lap splices. Two CFRP sheets 12 in. wide x 80 in. long were used to confine the 24 in. lap spliced region.

CFRP anchors consist of a roll of CFRP material inserted into a 9 in. deep hole drilled into the concrete. The inserted depth of the CFRP anchor from the expected plane of splitting cracking was 6 in. The inserted depth of the anchor holes in all the other columns was the same as 2-A-S8-M. The CFRP protruding from the hole was splayed out in a 6 in. radius over the CFRP jacket. The anchors were installed at the center of the column so at least one side of every lap spliced longitudinal bars was next to CFRP anchors or column ties. Four anchors were installed in both the damaged and undamaged sides of 2-A-S8-M (at 5 in., 11 in., 17 in. and 23 in. from the top of the footing). Clear spacing between the CFRP anchor and a lap splice bars was 1.25 in.

Figure 4.17   Layout of the CFRP jackets and CFRP anchors, 2-A-S8-M

212

The width of CFRP across the expected plane of splitting is shown in Figure 4.18. The width of the CFRP sheet used in fabricating an anchor was 7 in. and the width of the CFRP sheet used to fabricate the anchors in each side of 2-A-S8-M was 28 in. (7 in. x 4 pc). Total width of CFRP across the plane of splitting was 76 in. (CFRP jacket: 24 in. x 2 sides; CFRP anchor: 28 in.) The width of the CFRP anchors was selected using shear-friction equations discussed in Section 4.2.3.
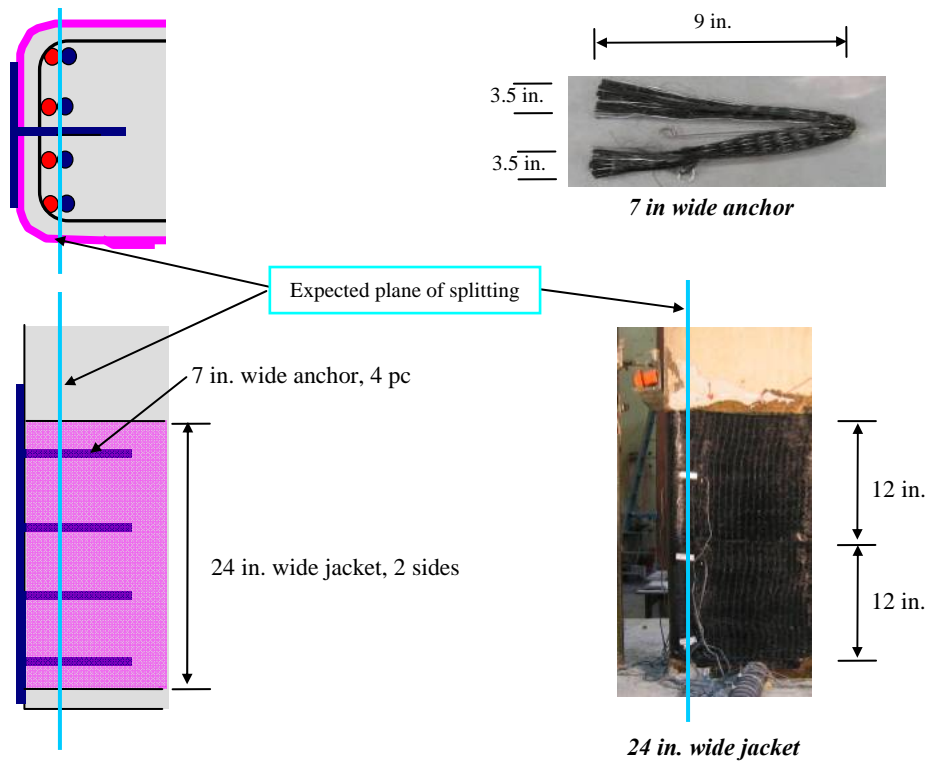
Figure 4.18   Width of CFRP across the expected plane of splitting

4.3.5   3-B-S10-M

3-B-S10-M was a Type B column with 10 splices. It was rehabilitated using CFRP jackets and CFRP anchors. It was tested under monotonic loading.

4.3.5.1 Preparation of Holes for CFRP Anchors

Eight holes were drilled on the east and west face of 3-B-S10-M. The holes were drilled with a 1/2 in. diameter masonry drill bit on the east face and a 5/8 in. bit on the west face. The anchors on the damaged face (west) of 3-B-S10-M were larger than those on the undamaged face (west). Therefore, the holes on the west face needed to be larger than those on the east face. The width of anchors on each face was determined through the shear friction equation and the results from the previous test. The calculated width using shear friction required a larger width of CFRP anchors than the previous test results. The larger width of CFRP was installed on the damaged face because strength of the face was expected be lower than the undamaged face. The anchor holes of 3-B-S10-M prior to installation of CFRP are shown in Figure 4.19.
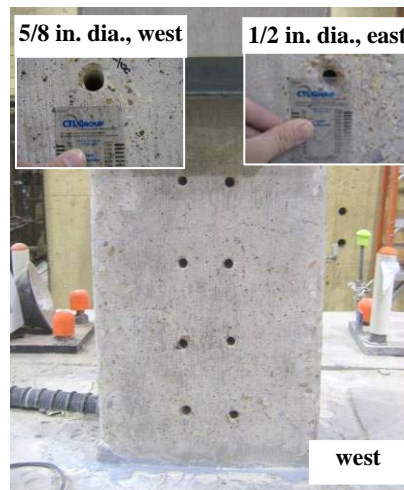
Figure 4.19   Anchor holes in 3-B-S10-M

4.3.5.2 *CFRP Jacket and CFRP Anchor*

Details of the CFRP jacket and CFRP anchors are shown in Figure 4.20. One layer of CFRP sheet was used in 3-B-S10-M as a jacketing element to provide confinement of the lap splices. Two CFRP sheets 12 in. wide x 80 in. long were used to confine the 24 in. lap spliced region.

The portion of CFRP anchor protruding from the hole was splayed out in 4 in. radius over the CFRP jacket. Eight anchors were applied to damaged and undamaged side in 3-B-S10-M. The anchors were installed in two columns so at least one side of every lap spliced longitudinal bars was next to the anchors except for the corner bars. Two anchors were installed in each row at 5 in., 11 in., 17 in. and 23 in. from the top of the footing. Clear spacing between the CFRP anchor and a lap splice bars was 0.91 in. on the east face and 0.84 in. on the west face.

The width of a CFRP sheet used in fabricating an anchor was 5.5 in. on the west face (damaged) and 3.5 in. on the east face (undamaged). The width of the CFRP anchors on the west face was 44 in. (5.5 in. x 8 pc) and on the east face was 28 in. (3.5 in x 8 pc). Total width of CFRP across the plane of splitting was 92 in. on the west face (CFRP jacket: 24 in. x 2 sides; CFRP anchor: 44 in.) and 76 in. (CFRP jacket: 24 in. x 2 sides; CFRP anchor: 28 in.) on the east face. The width of CFRP anchors on the west face was selected using the shear- friction mechanism and that on the east face was selected to provide the same width of CFRP anchors to 3-B-S10-M as 2-A-S8-M. The design method of deciding the width of the CFRP anchors on the west face is discussed in Section 4.2.3.
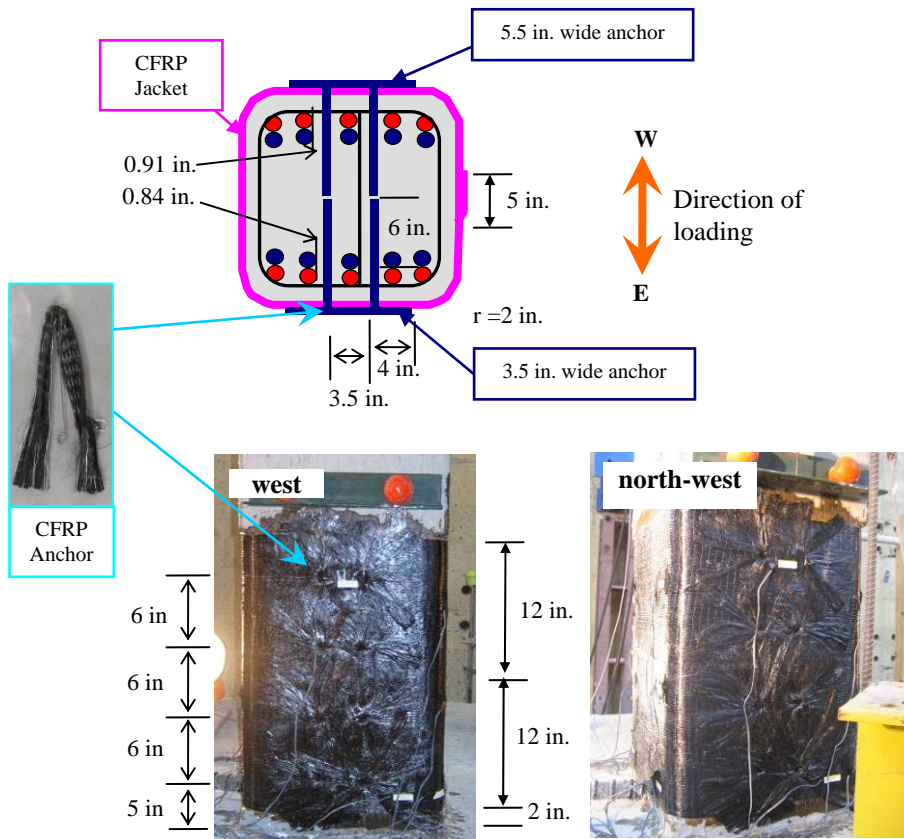
Figure 4.20   Layout of the CFRP jackets and CFRP anchors, 3-B-S10-M

4.3.6 4-C-R20-M

4-C-R20-M was a Type C column with 20 splices. It was rehabilitated using CFRP jackets and CFRP anchors. It was tested under monotonic loading.

4.3.6.1 Preparation of Holes for CFRP Anchors

Sixteen holes were drilled on the east face and eight holes were drilled on the west face of 4-C-R20-M. The holes were drilled with a 1/2 in. diameter masonry drill bit on the east face and a 3/4 in. bit on the west face in 9 in. depth. The total width of CFRP used in the anchors on the each side was the same but anchors on the damaged face (east) were ½ of the width of those on the undamaged face (west) because larger number of CFRP anchors was used on the damaged face where low strength was expected. Therefore, the holes on the west face needed to be larger than those on the east face. The anchor holes of 4-C-R20-M prior to installation of CFRP are shown in Figure 4.21.

Some honeycombing occurred in 4-C-R20-M due to lack of vibration during casting. The honeycombing in the lap spliced region was repaired using a patching polymer mortar (Tyfo® P from FYFE Co. LLC) after removing all loose materials. The surface of 4-C-R20-M after the repair is shown in Figure 4.21.
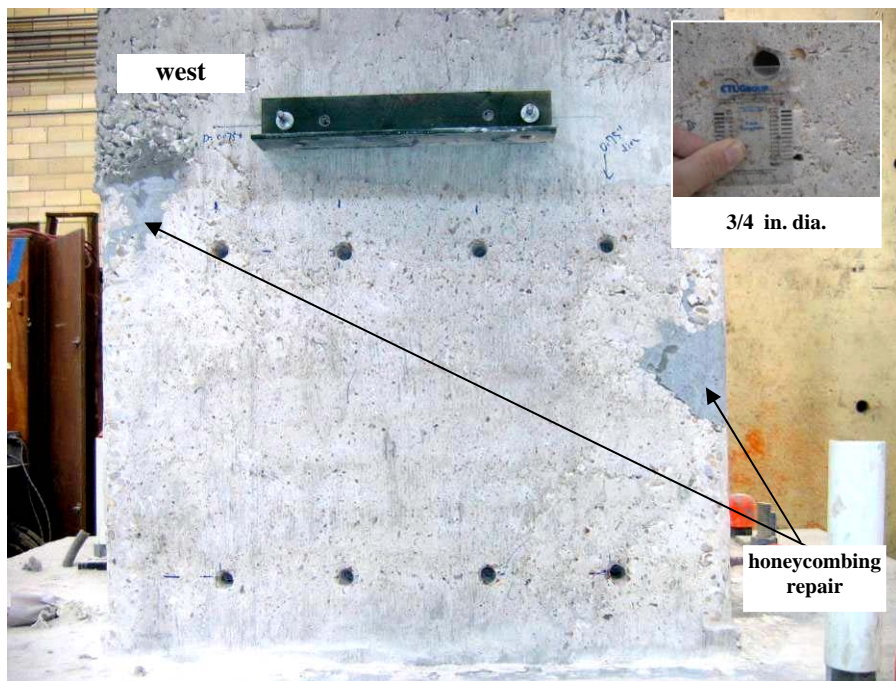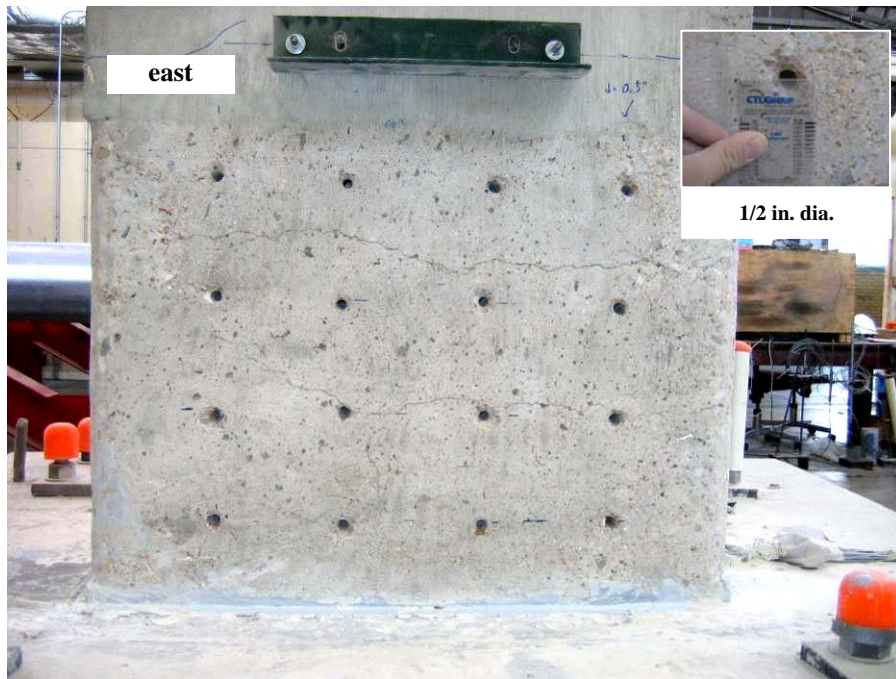
Figure 4.21   Anchor holes in 4-C-R20-M

218

4.3.6.2   CFRP Jacket and CFRP Anchor

Details of the CFRP jacket and CFRP anchors are shown in Figure 4.22. One layer of CFRP sheet was used in 4-C-R20-M as a jacketing element to provide confinement of the lap splices. Two CFRP sheets 12 in. wide x 116 in. long were used to confine the 24 in. lap spliced region.

The portion of CFRP anchor protruding from the hole was splayed out in a 4 in. radius over the CFRP jacket. The anchors were installed in four columns so at least one side of every lap spliced longitudinal bars was next to the anchors except for the corner bars. On the east face, four anchors were installed in each row at 5 in., 11 in., 17 in. and 23 in. from the top of the footing. On the west face, four anchors were installed in each row at 5 in. and 23 in. from the top of the footing. Clear spacing between the CFRP anchor and a lap splice bars was 1.0 in. on the east face and 0.875 in. on the west face.

The width of a CFRP sheet used in fabricating an anchor was 3.5 in. on the damaged face (east) and 7 in. on the undamaged face (west). However, the total width of CFRP in the anchors on each face was the same. The width of the CFRP anchors on the east face was 56 in. (3.5 in. x 16 pc) and on the west face was also 56 in. (7 in x 8 pc). Total width of CFRP across the plane of splitting was 104 in. on the east and the west face (CFRP jacket: 24 in. x 2 sides; CFRP anchor: 56 in.).

The width of CFRP was selected based on the test results of the west face of 3-B-S10-M. Four 3.5 in. or two 7 in. anchors were placed in a column of CFRP anchors so the total width of CFRP material in the anchors next to a lap spliced bars was 14 in.

219
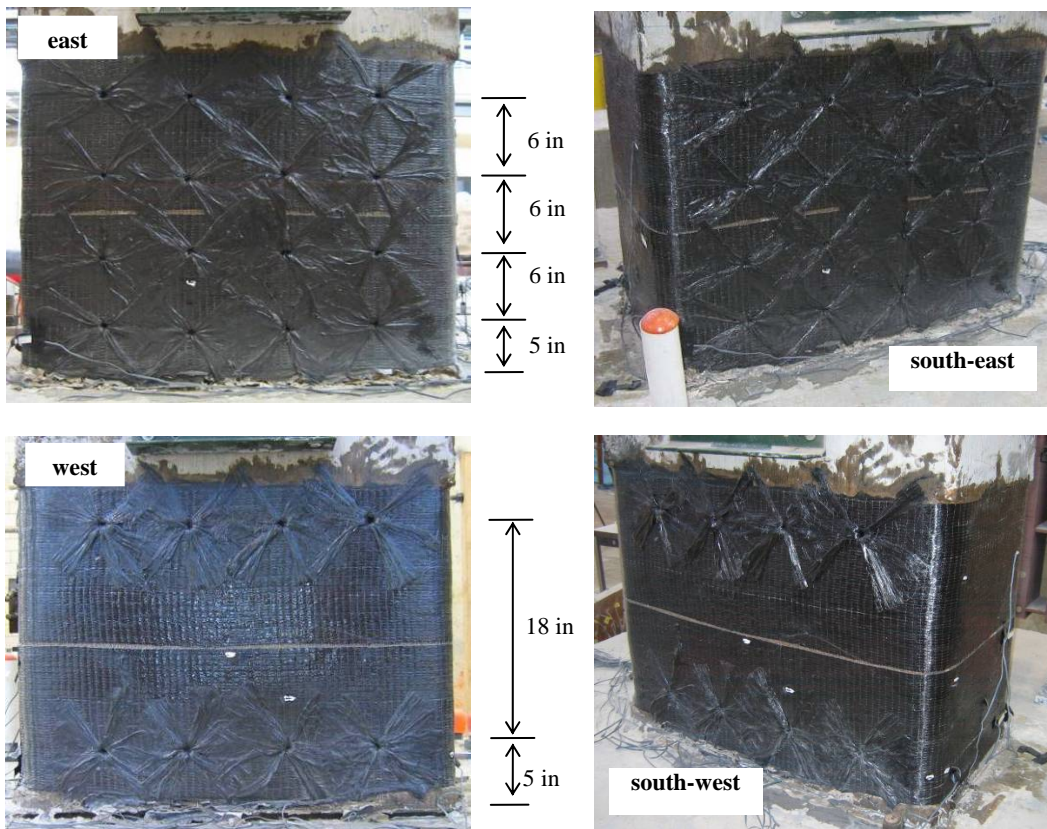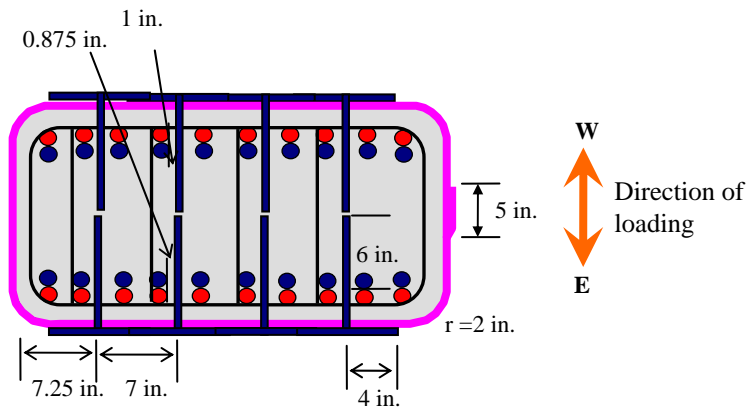
Figure 4.22   Layout of the CFRP jackets and CFRP anchors, 4-C-R20-M

4.3.7 5-C-R20-C

5-C-R20-C was a Type C column with 20 splices. It was rehabilitated using CFRP jackets and CFRP anchors. The specimen was tested under cyclic loading.

4.3.7.1 Preparation of Holes for CFRP Anchors

Size and depth of anchor holes in 5-C-R20-C was the same as those in 4-C-R20-M because the identical rehabilitation method was used. The anchor holes were prepared in the same way as those in 4-C-R20-M.

4.3.7.2 CFRP Jacket and CFRP Anchor

Details of the CFRP jacket and CFRP anchors are shown in Figure 4.23. The geometry of the CFRP jackets and anchors in 5-C-R20-C was identical to that in 4-C-R20-M except that the lowest row of CFRP anchors started 7 in. from the top of the footing. During casting, the bottom tie moved upward about 1 in. and it was located at level of the anchors. Therefore, the location of the anchors needed to change. The width of CFRP used in the rehabilitation of 5-C-R20-C was the same as those in 4-C-R20-M.
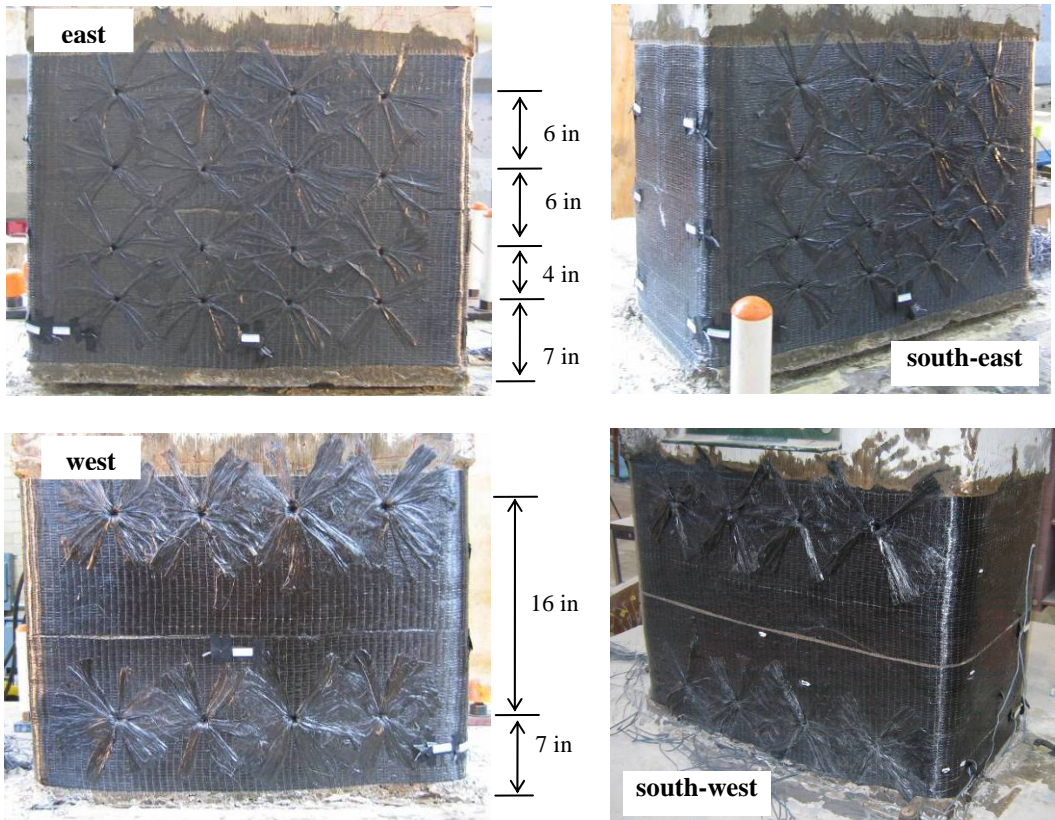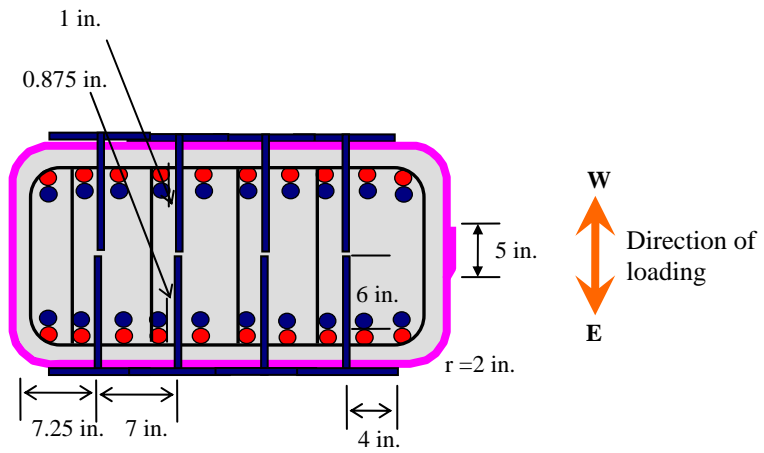
Figure 4.23   Layout of the CFRP jackets and CFRP anchors, 5-C-R20-C

4.3.8   6-C-R20-C

6-C-R20-C was a Type C column with 20 splices. It was rehabilitated using CFRP jackets and CFRP anchors on the east face and using only CFRP anchors on the west face. 6-C-R20-C reflected a column with walls as shown in Figure 4.24 and rehabilitation without removing the walls was desired. The walls may contribute to the strength of the lap splices because the walls may restrain opening of the splitting cracks at the wall. However, in this specimen, the walls were not fabricated to isolate the effect of the rehabilitation. The specimen was tested under cyclic loading.

4.3.8.1   *Preparation of Holes for CFRP Anchors*

Sixteen holes were drilled on the east face and twenty holes were drilled on the west face of 6-C-R20-C. The holes were drilled with a 1/2 in. diameter masonry drill bit on the east face and a 5/8 in. bit on the west face in 9 in. depth. In one anchor, a 3.5 in. wide CFRP sheet was used on the east side and a 5.2 in. wide CFRP sheet was used on the west side. Therefore, the holes on the west face needed to be larger than those on the east face. On the north and south face, 4 holes were drilled with 3/4 in. diameter in 6 in. depth to install 6 in. wide CFRP anchors to anchor the CFRP jackets. These holes are drilled at about a 45 degree angle. The anchor holes of 6-C-R20-C prior to installation of CFRP are shown in Figure 4.24.
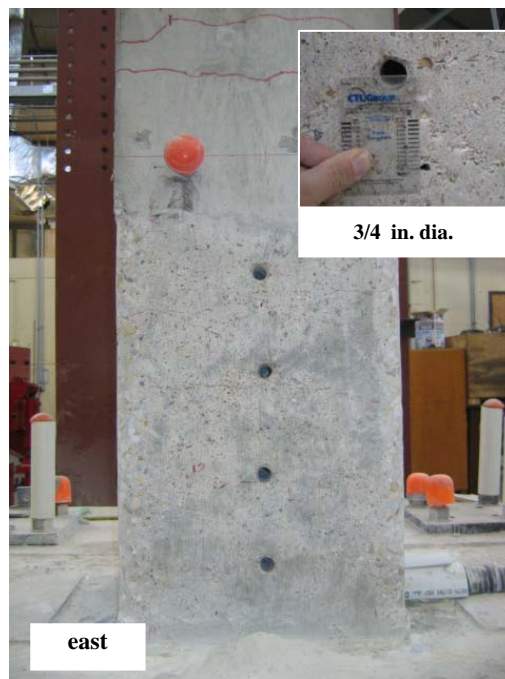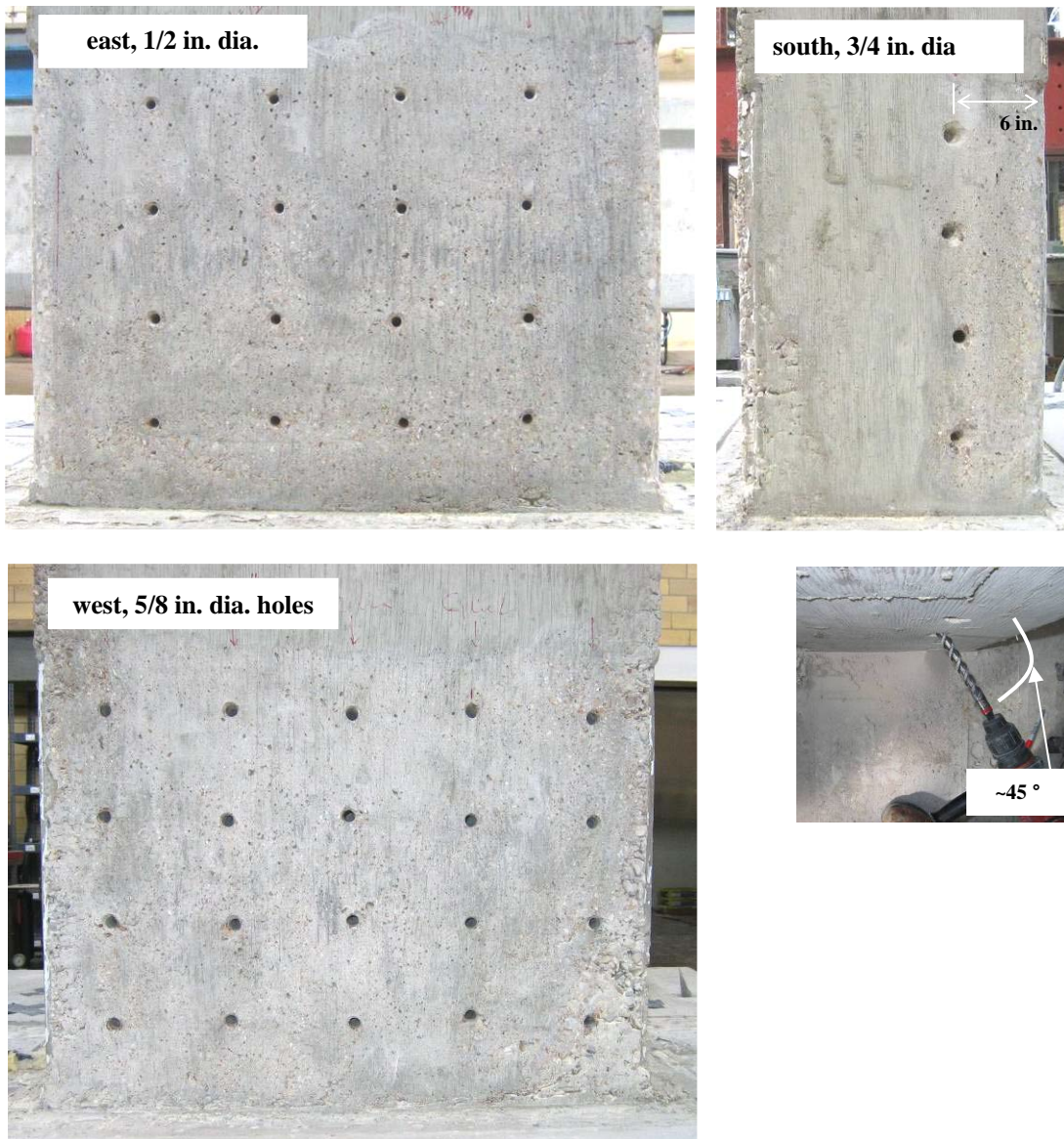
Figure 4.24   Anchor holes in 6-C-R20-C

4.3.8.2   CFRP Jacket and CFRP Anchor

Details of the CFRP jacket and CFRP anchors are shown in Figure 4.25. It was assumed that 12 in. wide walls existed on the north and south face and faced even with the west face of the column. Therefore, wrapped CFRP jackets could not be applied to

this column. The CFRP partial jackets covered the east face and 6 in. of the south and north face up to the wall. The short sides of the jacket were anchored by four 6 in. CFRP anchors (Partial CFRP jacket). One layer of CFRP sheet was used in 6-C-R20-C as a jacketing element to provide confinement of the lap splices. Two CFRP sheets 12 in. wide x 47 in. long were used to confine the 24 in. lap spliced region. The CFRP jacket was applied to the column with a 2 in. gap from the top of the footing because of irregularities in the column surface next to the footing.

On the west face, one layer of CFRP sheet was applied to the face before applying the anchors to provide a more uniform distribution of confining force from the anchors.

The portion of CFRP anchor protruding from the hole was splayed out in a 4 in. radius over the partial CFRP jacket on the east face and over the CFRP sheet on the west face. Sixteen anchors were applied on the east face and twenty anchors were applied on the west face in 6-C-R20-C. The anchors were installed in four columns on the east face and five columns on the west face so at least one side of every lap spliced longitudinal bars was next to anchors. Four anchors on the east face and five anchors on the west face were installed in each row at 5 in., 11 in., 17 in. and 23 in. from the top of the footing. Clear spacing between the CFRP anchor and a lap splice bars was 1.0 in. on the east face and 0.93 in. on the west face.
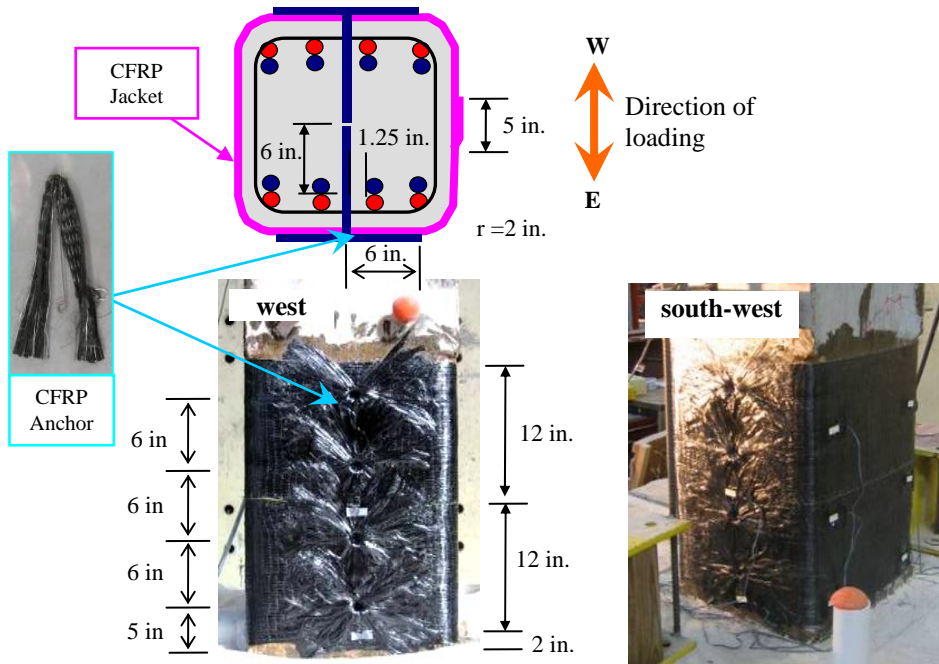
The width of a CFRP sheet used in fabricating an anchor was 3.5 in. on the east face and 5.2 in. on the west face. The width of the CFRP anchors in the east face was 56 in. (3.5 in. x 16 pc) and in the west face was also 104 in. (5.2 in x 20 pc). However, Total width of CFRP across the plane of splitting was the same on either face. It was 104 in. on the east (CFRP jacket: 24 in. x 2 sides; CFRP anchor: 56 in.) and west face (CFRP anchors: 104 in.). The width of CFRP on the east face was selected based on the test results of 4-C-R20-M and 5-C-R20-C.
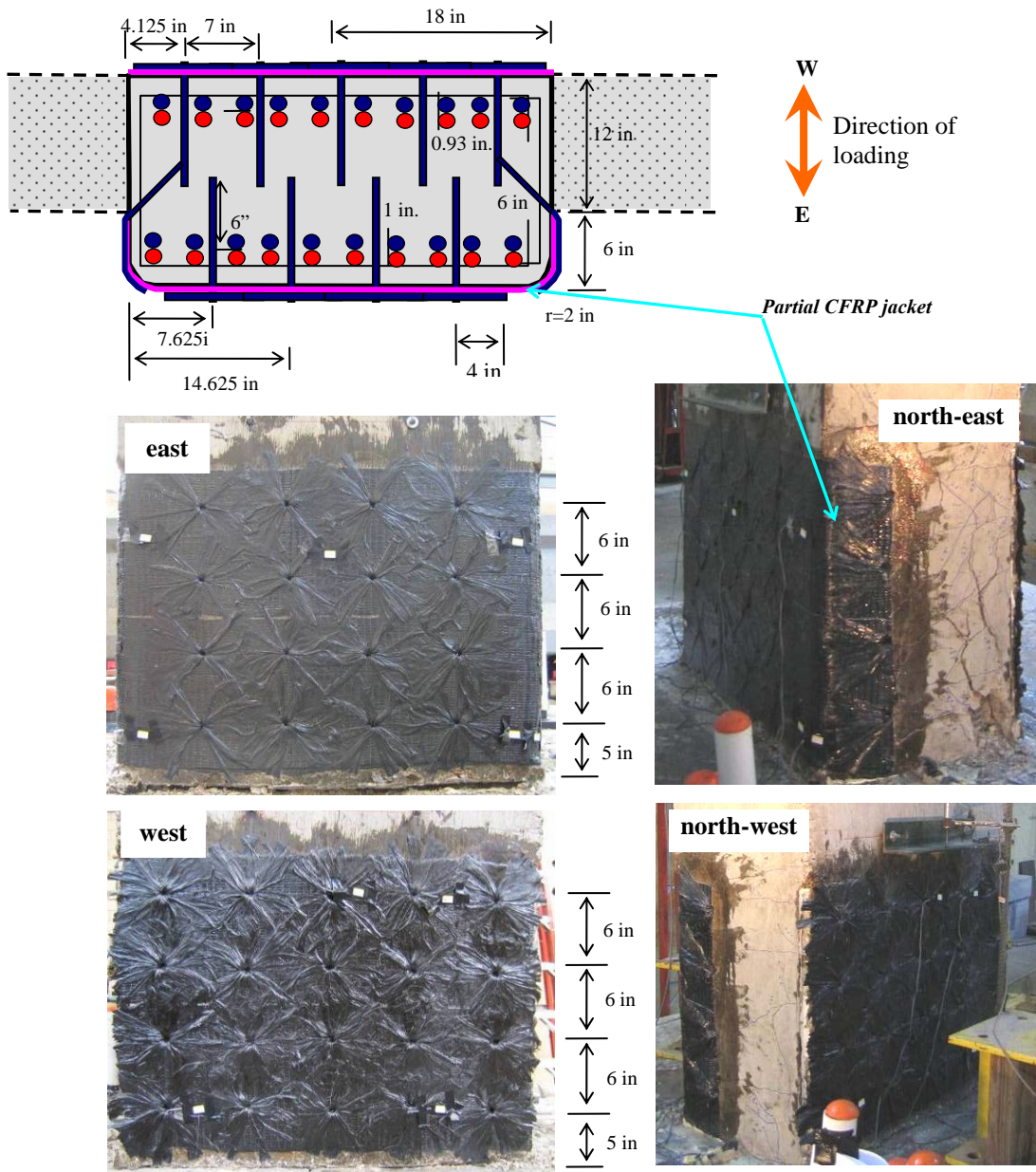
Figure 4.25   Layout of the CFRP jackets and CFRP anchors, 6-C-R20-C

4.3.9   Summary of Rehabilitation Methods

A summary of the rehabilitation of the test columns is shown in Table 4.4.

Two Type A (1-A-S8-M and 2-A-S8-M) with 8 splices, one Type B (3-B-S10-M) with 10 splices and three Type C (4-C-R20-M, 5-C-R20-C and 6-C-R20-C) with 20 splices specimens were tested under either monotonic or cyclic loading. Under monotonic loading, the column was initially tested as-built and tested again after being repaired and strengthened using CFRP materials. Under cyclic loading the column was strengthened in the as-built condition and tested. One layer of CFRP was used to jacket in all the test columns and CFRP anchors were installed in all columns except 1-A-S8-M. The total width of CFRP in the CFRP jackets and anchors was determined using the shear friction equation or modified using the results of the previous tests. The CFRP anchors were distributed so at least one side of every lap spliced longitudinal bars was next to the anchors. Depth and diameter of anchor holes were selected to avoid bond failure of a CFRP anchor. The effective width of CFRP jackets or anchors represents the width of CFRP sheet used in fabricating CFRP jackets or anchors across the plane of the splitting cracking (shear plane).

227

Table 4.4   *Summary of rehabilitation methods using CFRP*

Specimen	Test condition		CFRP Jacket		CFRP Anchor				Total Effective Width of CFRP
			No. of Layers	Effective Width	No. of Anchors	Width of a Anchor	Effective Width	Dia. of Hole	
1-A-S8-M	As-built								
	Repair and strengthening	Undamaged side (West)	1	48 in.					48 in.
		Damaged side (East)	1	48 in.					48 in.
2-A-S8-M	As-built								
	Repair and strengthening	Undamaged side (West)	1	48 in.	4	7 in.	28 in.	3/4 in.	76 in. (S.F.)
		Damaged side (East)	1	48 in.	4	7 in.	28 in.	3/4 in.	76 in. (S.F.)
3-B-S10-M	As-built								
	Repair and strengthening	Undamaged side (East)	1	48 in.	8	3.5 in.	28 in.	1/2 in.	76 in.
		Damaged side (West)	1	48 in.	8	5.5 in.	44 in.	5/8 in.	92 in. (S.F.)
4-C-R20-M	As-built								
	Repair and strengthening	Undamaged side (West)	1	48 in.	8	7 in.	56 in.	3/4 in.	104 in.
		Damaged side (East)	1	48 in.	16	3.5 in.	56 in.	1/2 in.	104 in.
5-C-R20-C	Strengthening	West	1	48 in.	8	7 in.	56 in.	3/4 in.	104 in.
		East	1	48 in.	16	3.5 in.	56 in.	1/2 in.	104 in.
6-C-R20-C	Strengthening	West			20	5.2 in.	104 in.	5/8 in.	104 in.
		East	1	48 in.	16	3.5 in.	56 in.	1/2 in.	104 in.

4.4   TEST SETUP AND INSTRUMENTS

The test setup and loading configuration are shown in Figure 4.26. The footing was fixed to a strong floor by threaded rods and lateral load was applied to the column at 108 in. from the top of the footing. The lateral load was applied using a 150 kip hydraulic actuator with 12 in. stroke. The load was measured using a 100 kip load cell.

The location of linear transducers is shown in Figure 4.27. Displacement at the load point was measured using two linear string transducers and was used in calculating the drift ratio of the column under the lateral loading. Drift ratio corresponds to measured displacement using these transducers divided by the height of the loading location from the top of the footing (108 in.). Two linear transducers were placed in the vertical direction at 30 in. from the top of the footing on the east and west faces of the column. Using these linear transducers, rotation of a section above the lap spliced region was measured to monitor slip of the lap spliced bars. Four linear transducers were placed at the footing to measure vertical and horizontal displacement of the footing. The footing displacement was small compared with the tip displacement of the column. Therefore, footing displacement was ignored and the measured displacement at the tip of the column was used as the lateral displacement of the column.

Strain gages were placed on longitudinal and transverse bars and on CFRP jackets. Layout of the strain gages is discussed in Section 4.5.

229
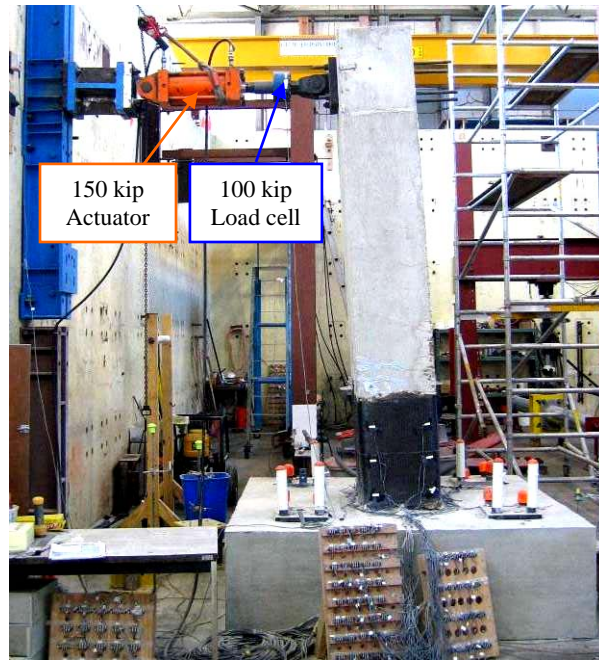
Figure 4.26   Test setup
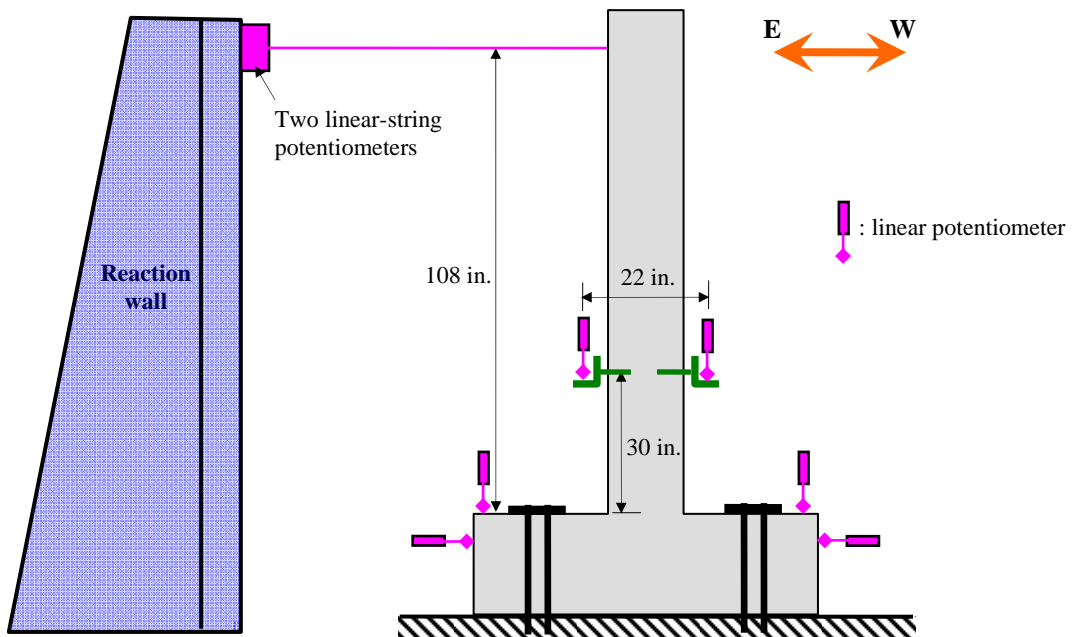
Figure 4.27   Location of linear transducers

230

4.5   TEST RESULTS AND COMPARISONS

For each of the tests, the drift ratio vs normalized lateral load and steel or CFRP strain vs load will be presented. The lateral load was normalized using the computed nominal strength of the column. The nominal strength was calculated using the design strength of concrete (4,000 psi) and steel (60 ksi). Under monotonic loading, a positive value of loading corresponds to the direction of loading in which the bars in the undamaged side were in tension while a negative value of loading corresponds to the direction of loading in which the bars in the damaged side were in tension (1-A-S8-M, 2-A-S8-M, 3-B-S10-M and 4-C-R20-M). Under cyclic loading, a positive value of loading corresponds to the direction of loading in which the bars in the west side were in tension while a negative value of loading corresponds to the direction of loading in which the bars in the east side were in tension (5-C-R20-C and 6-C-R20-C). The measured lateral displacement vs measured lateral load response for all tests is presented in Appendix C.

4.5.1   1-A-S8-M

A summary of the test results of 1-A-S8-M is shown in Table 4.5 in the end of this section.

4.5.1.1   Drift Ratio VS Normalized Lateral Load

Figure 4.28 shows drift ratio vs normalized lateral load response of 1-A-S8-M as-built and after rehabilitation. The actual yield strength ($P/P_n = 1.09$) and ultimate strength ($P/P_n = 1.72$) calculated based on measured strength of the concrete and reinforcement are also provided. The measured compressive strength of the concrete was 5,600 psi and the measured yield and ultimate strength of the reinforcement were 63 ksi and 106 ksi.

Although the nominal strength ($P/P_n = 1.14$) was reached in the as-built test, the load dropped once splitting of the concrete occurred at the splice. However, significant improvement of strength and deformation capacity was observed in 1-A-S8-M after rehabilitation with CFRP on both the damaged and undamaged sides of the column. The

231

strength increased by 13 % for the damaged side and by 18% for the undamaged side after rehabilitation compared with the as-built strength of this column. The drift ratio of 1-A-S8-M as-built was 1.1 % at the maximum load. The drift ratio corresponding to the peak strength was 1.9 % in the damaged side and 2.3 % in the undamaged side after rehabilitation. In both directions, there was a gradual reduction in strength beyond the peak load up to the stroke limit of the load actuator.
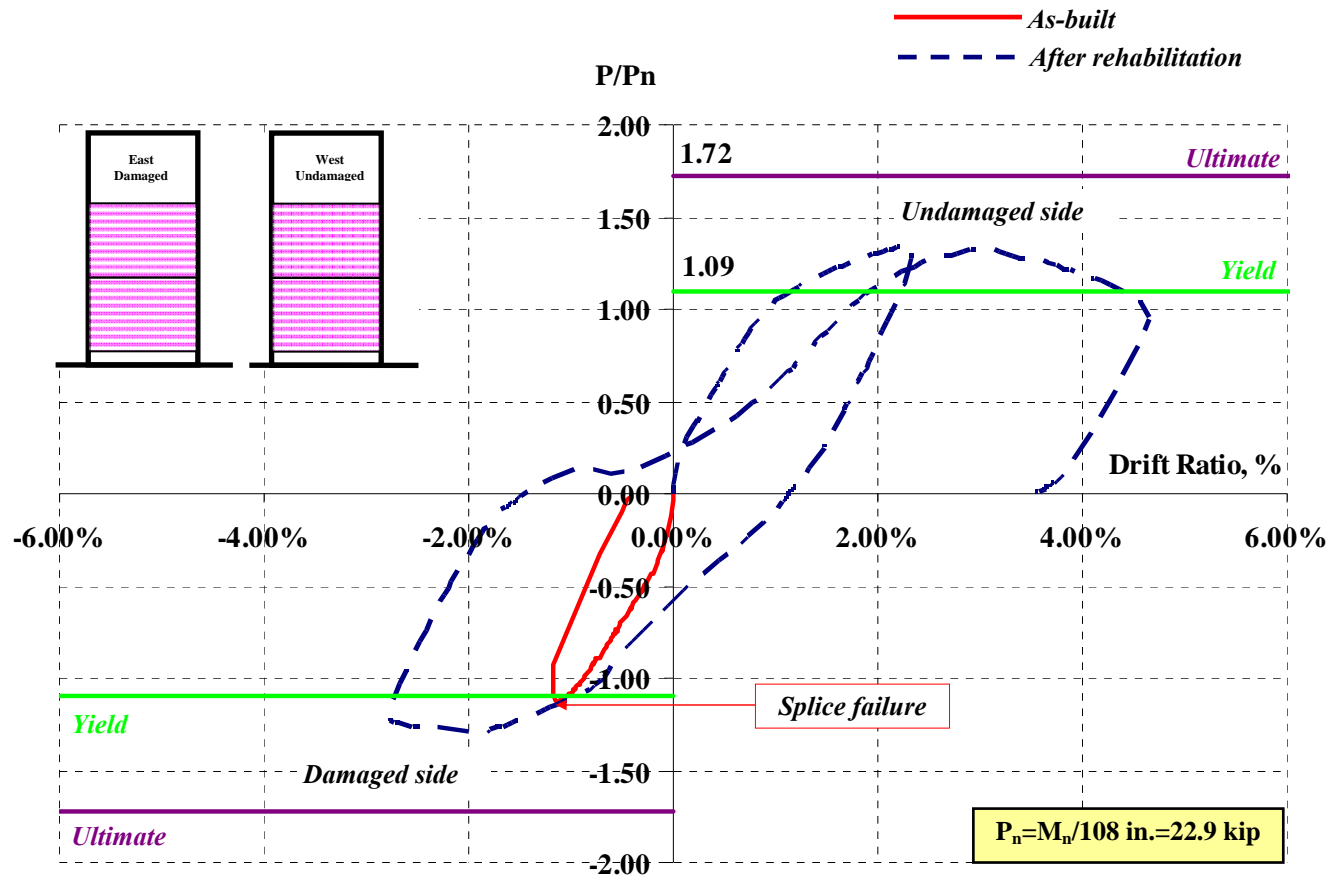
Figure 4.28 **Drift ratio vs normalized lateral load, 1-A-S8-M**

The failure mode of 1-A-S8-M as-built was a brittle splice failure (Figure 4.29). A sudden drop of load was observed at the peak load during the test of this column as-built (Figure 4.28). The use of the CFRP jackets effectively confined lap splices and changed the failure mode of 1-A-S8-M from a brittle splice failure to yielding of tension steel indicated by measured strains in the steel reinforcement presented in the next section.

Splitting crack due to splice failure

north

south-east
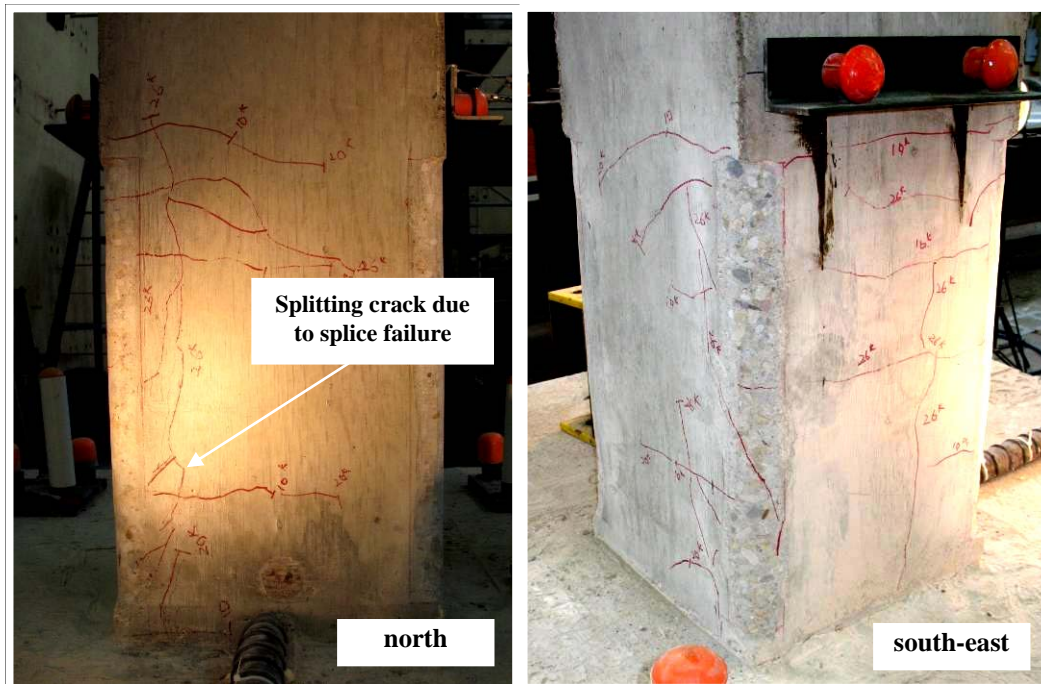
Figure 4.29   Splice failure of 1-A-S8-M, before rehabilitation

4.5.1.2   Steel Reinforcement Strain

Layout of steel reinforcement strain gages in 1-A-S8-M is shown in Figure 4.30. For all the columns, strain gages were installed on base bars (longitudinal bars extending from the footing), column bars (longitudinal bars starting at the top of the footing) and ties in the 24 in. lap spliced region. In Section 4.5, only strain data of the base bars are presented because maximum strain in the lap splice bars is expected to occur at the location of base bar strain gages. Strain data in ties are not presented in this section

because the data were not reliable. Strain gages in ties were not located at the cracked section. Additional strain data in the steel reinforcement including ties and column bars are presented in Appendix C.
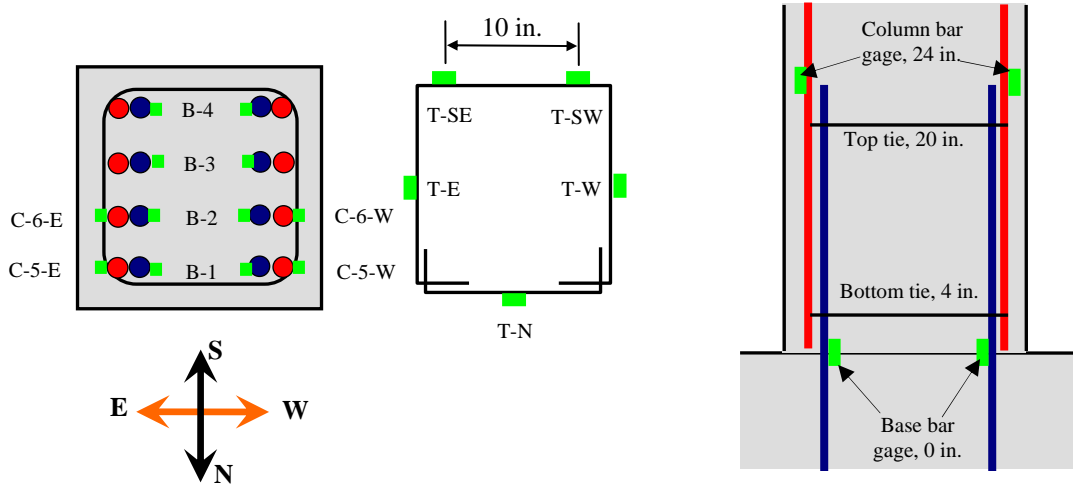
- **Base bar gages (B - # - Direction):** at the top of the footing
- **Column bar gages (C - # - Direction):** 24 in. from the top of the footing
- **Tie bar gages (T-Top or Bottom- Direction):**

  Top-tie at 20 in. from the top of the footing

  Bottom- tie at 4 in. from the top of the footing

Figure 4.30   Layout of steel reinforcement strain gages, 1-A-S8-M

4.5.1.2.1 Base Bar Strain, As-Built Test

Tensile strains in the base bars during the initial test are shown in Figure 4.31. Strain gages were installed on the base bars at the top of the footing. Although the bars yielded, the failure mode of 1-A-S8-M in the as-built test was a brittle splice failure that occurred before the column developed significant ductility. The bars developed a strain larger than the yield strain but the column section developed little rotational capacity.

235

Figure 4.31   Base bar strains, as-built test, 1-A-S8-M

4.5.1.2.2 Base Bar Strain, Test after Rehabilitation

Base bar strains during the test after rehabilitation are shown in Figure 4.32 and Figure 4.33.   The bars on the east face (damaged) of 1-A-S8-M were initially in compression while the bars on the west face (undamaged) of 1-A-S8-M were in tension. When the load was reversed the bars on the east face were in tension. All the bars yielded during tension loading. After the base bars reached large tensile strains, the strain gages on the bars were damaged during loading reversal. Therefore, strain hardening of the bars could not be observed although the lateral deformation of the column was significant and the measured lateral load reflected strain hardening of the bars.

236

Figure 4.32   Base bar strains, test after rehabilitation, east face, 1-A-S8-M

Figure 4.33   Base bar strains, test after rehabilitation, west face, 1-A-S8-M

237

4.5.1.3   CFRP Strain

The layout of strain gages on the CFRP jackets in 1-A-S8-M is shown in Figure 4.34. On the north and south face of 1-A-S8-M, six gages are installed on each face at the location where splitting cracking was expected. Gages NE-B, M and T and NW-B, M and T were installed at location where splitting cracking was expected on the north face, and gages SE-B, M and T and SW-B, M and T were installed at location where splitting cracking was expected on the south face. Strains in the CFRP jackets were measured at three levels on the north and south face (B: bottom, M: middle and T: top). Strain gages were also installed at the bottom corners on the south face to observe strain transition around the corners (E-C, SE-C, W-C and SW-C). Two strain gages were installed on the middle of the east (E-B and E-T) and west (W-B and W-T) face. The level of those gages corresponded to that of the top and bottom gages on the north and south faces.

 In this section, measured strains on the south face and at the corners of 1-A-S8-M are provided. Additional strain data are shown in Appendix C.

Strain vs lateral load for the strain gages at the location of expected splitting cracking is shown in Figure 4.35 and Figure 4.36. The maximum measured strain was between 0.0015 and 0.0025 (15 ~ 25 % of ultimate tensile strain of the CFRP) on the south-east side and between 0.0030 and 0.0045 (30 ~ 45 % of ultimate tensile strain of the CFRP) on the south-west side. The highest strain was observed in the gages closest to the footing which were the bottom strain gages. The strain reduced as the distance from the footing increased.

Strain vs lateral load for strain gages at the corners of 1-A-S8-M is shown in Figure 4.37 and Figure 4.38. From the data of the distribution of CFRP strains at the corners, a smooth transition of strains was observed around the corner. The measured strain in the gage at the corner on the east face (E-C) was close to that in the gage at the corner on the south face (SE-B). The measured strain in the gage at the corner on the west face (W-C) was close to that in the gage at the corner on the south face (SW-B). The

measured strain at the arc of the corners (SW-C and SE-C) also showed a similar response as the strains at the corners.

Figure 4.34   Layout of CFRP strain gages, 1-A-S8-M

239

Figure 4.35   CFRP strains at location of splitting cracking, south-east, 1-A-S8-M

Figure 4.36   CFRP strains at location of splitting cracking, south-west, 1-A-S8-M

Figure 4.37   CFRP strains at south-east corner, 1-A-S8-M

Figure 4.38   CFRP strains at south-west corner, 1-A-S8-M

241

Table 4.5   Summary of test results, *1-A-S8-M*

Face	Effective width of CFRP jackets	No. of CFRP anchors	Effective width of CFRP anchors	Total effective width of CFRP	Measured peak strength (Max. Load) P/P_n	Drift ratio at measured peak strength	Strain in CFRP jackets at location of splice cracking expected
East (As-built)					1.14*	1.1 %	
West (Undamaged)	48 in.			48 in.	1.34	2.3 %	0.0030 ~ 0.0045
East (Damaged)	48 in.			48 in.	1.29	1.9 %	0.0015~ 0.0025

*: splice failure

Computed: Nominal Strength (P_n): 22.9 kip;   Yield strength: 25.0 kip;   Ultimate Strength: 39.4 kip

4.5.2   2-A-S8-M

A summary of the test results of 2-A-S8-M is shown in Table 4.6 at the end of this section.

4.5.2.1   *Drift Ratio VS Normalized Lateral Load*

Figure 4.39 shows drift ratio vs normalized lateral load response of 2-A-S8-M as-built and after rehabilitation.   The actual yield strength ($P/P_n = 1.08$) and ultimate strength ($P/P_n = 1.71$) based on measured strength of the concrete and reinforcement are also provided.   The measured compressive strength of the concrete was 5,300 psi and the measured yield and ultimate strength of the reinforcement were 63 ksi and 106 ksi.

Although the nominal strength was realized in the as-built test ($P/P_n = 1.10$), the load dropped once splitting of the concrete occurred at the splice. However, significant improvement of strength and deformation capacity was observed in 2-A-S8-M after rehabilitation with CFRP on both the damaged and undamaged sides of the column. The

242

strength increased by 35 % for both the damaged and undamaged side after rehabilitation compared with the as-built strength. The drift ratio of 2-A-S8-M as-built was 1.1 % at the maximum load. The drift ratio corresponding to the peak strength was 4.5 % for the damaged side and 4.8 % for the undamaged side after rehabilitation. On the damaged side, there was a gradual reduction in strength up to the stroke limit of the load actuator while on undamaged side, no reduction of strength was observed.

The failure mode of 2-A-S8-M as-built was a brittle splice failure (Figure 4.40). A sudden drop of load was observed at the peak load during the test of this column as-built (Figure 4.39). The use of the CFRP jackets and anchors effectively confined lap splices and changed the failure mode of 2-A-S8-M from a brittle splice failure to yielding of tension steel indicated by measured strains in the steel reinforcement presented in the next section.
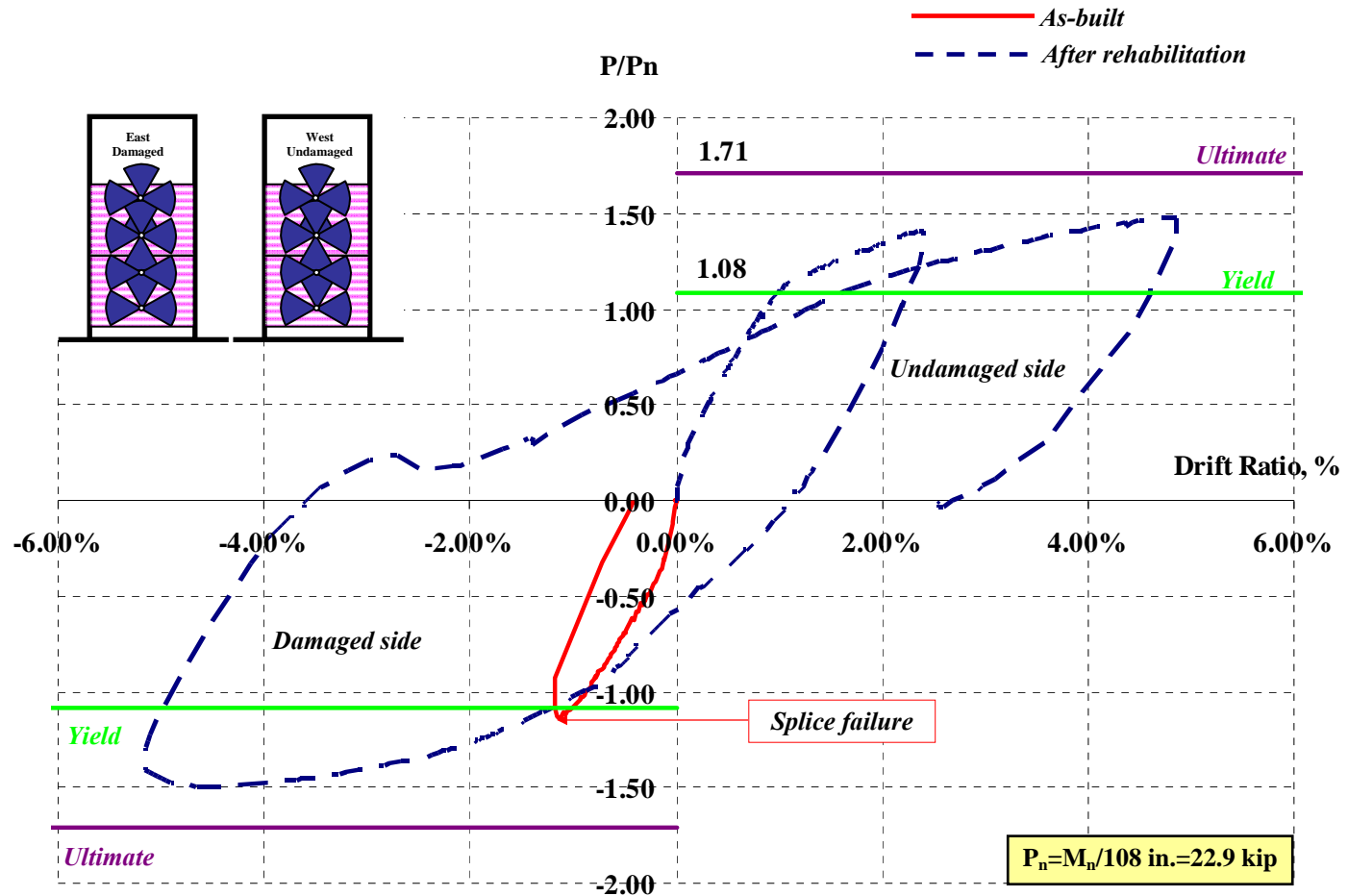
Figure 4.39   Drift ratio vs normalized lateral load, 2-A-S8-M

Figure 4.40   Splice failure of 2-A-S8-M before rehabilitation

4.5.2.2   Steel Reinforcement Strain

Layout of steel reinforcement strain gages in 2-A-S8-M is shown in Figure 4.41.
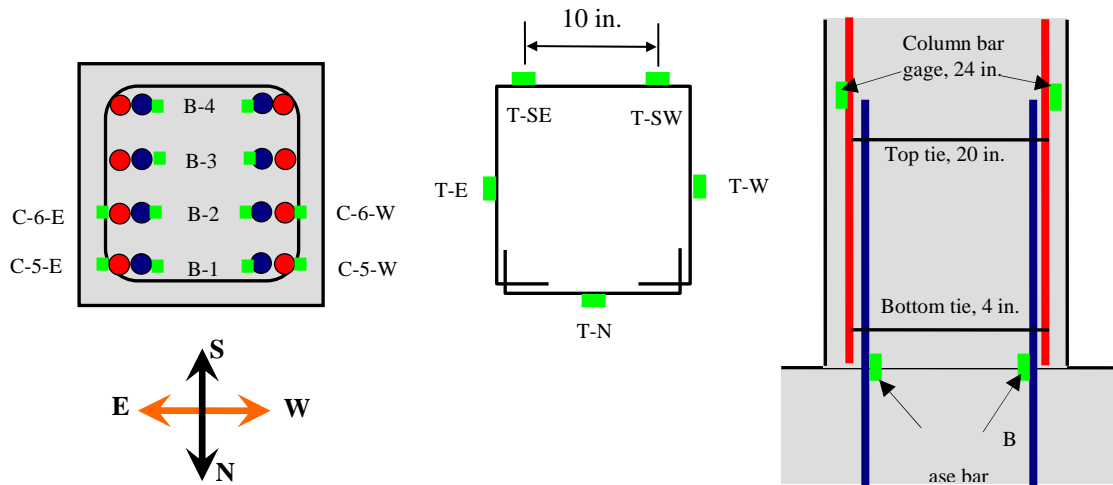
- **Base bar gages (B - # - Direction):** at the top of the footing
- **Column bar gages (C - # - Direction)**: 24 in. from the top of the footing
- **Tie bar gages (T-Top or Bottom- Direction):**

> **Top-**tie at 20 in. from the top of the footing
>
> **Bottom-** tie at 4 in. from the top of the footing

Figure 4.41   Layout of steel reinforcement strain gages, 2-A-S8-M

4.5.2.2.1 Base Bar Strain, As-Built Test

Tensile strains in the base bars during the initial test are shown in Figure 4.42. Strain gages were installed on the base bars at the same level as the top of the footing. The bars yielded although the failure mode of 2-A-S8-M in the as-built test was a brittle splice failure that occurred before the column developed significant ductility. The bars developed strains larger than the yield strain but the column section developed little rotational capacity.
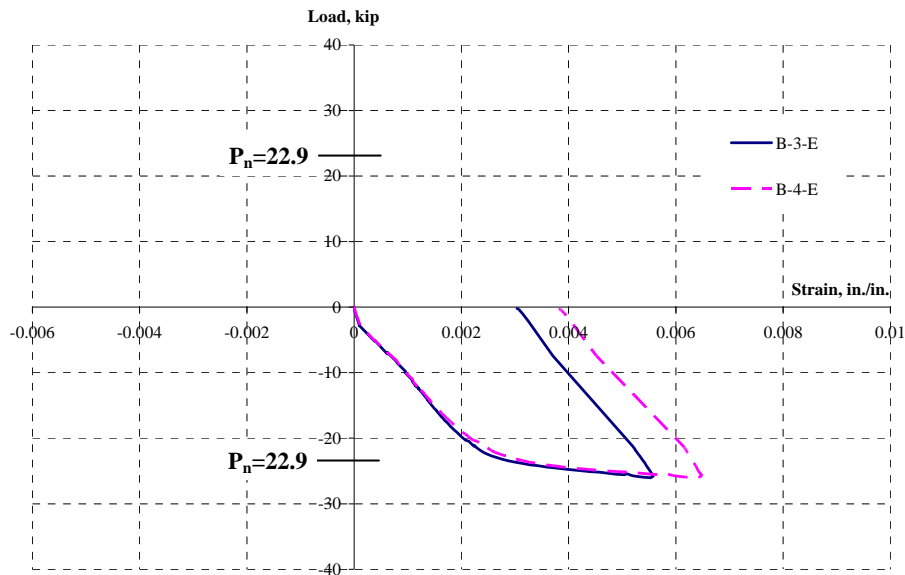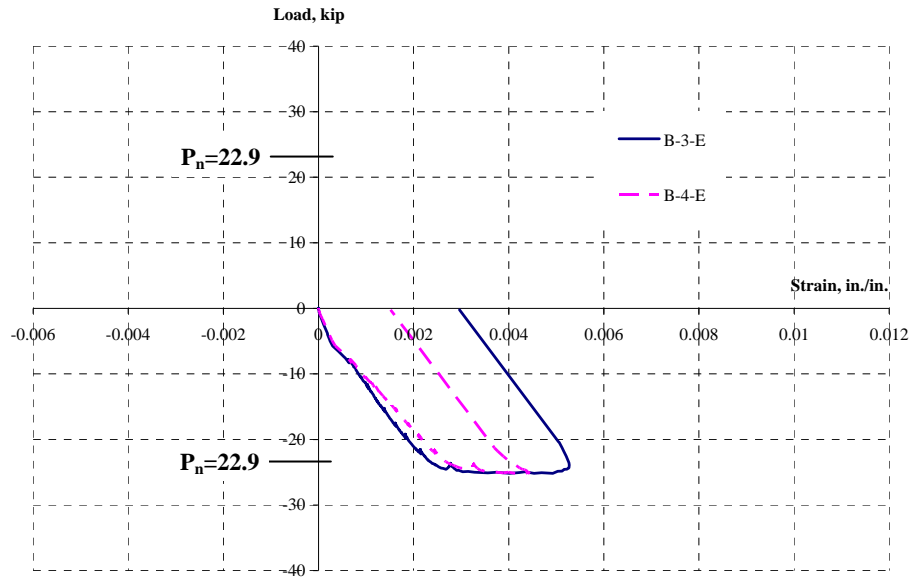
Figure 4.42   Base bar strains, as-built test, 2-A-S8-M

4.5.2.2.2 Base Bar Strain, Test after Rehabilitation

Base bar strains during the test after rehabilitation are shown in Figure 4.43 and Figure 4.44. The bars on the east face (damaged) of 2-A-S8-M were initially in compression while the bars on the west face (undamaged) of 2-A-S8-M were in tension. When the load was reversed, the bars on the east face were in tension. All the bars yielded during tension loading. After the base bars reached large tensile strains, the gages on the bars were damaged during loading reversal. Therefore, strain hardening of the bars could not be observed although the lateral deformation of the column was significant and the measured lateral load reflected strain hardening of the bars.
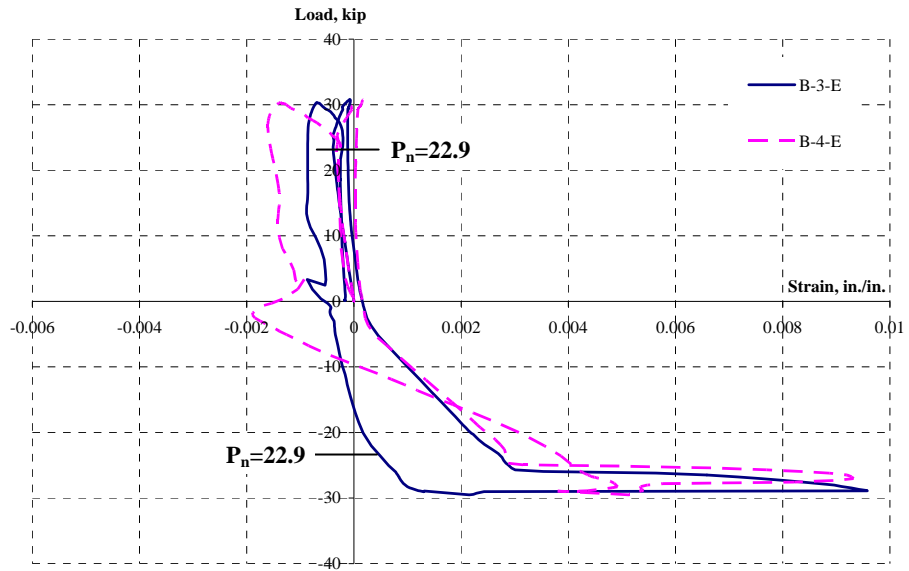
247
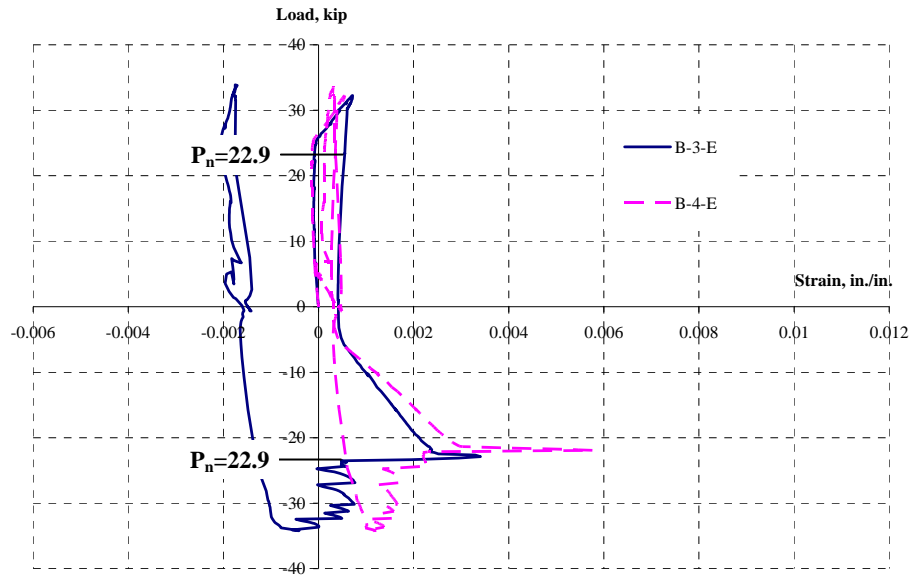
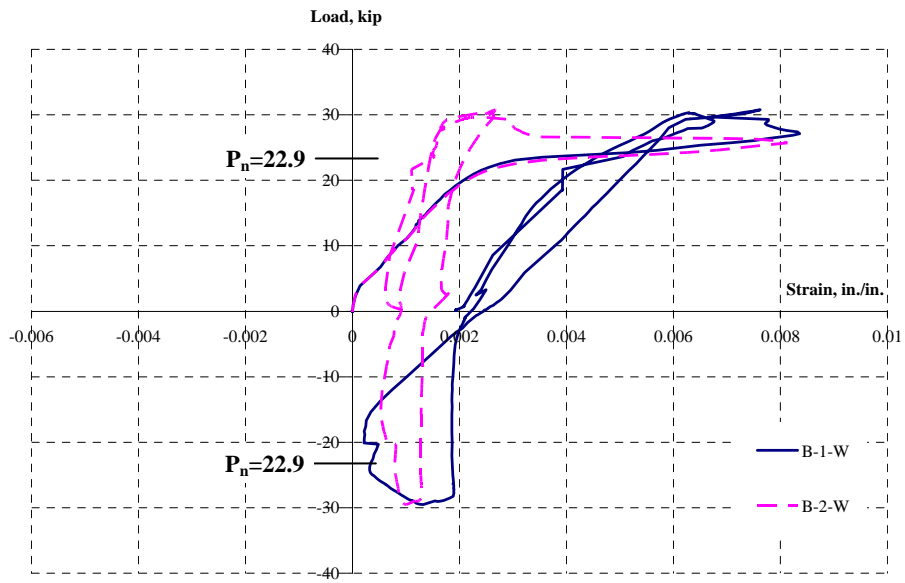*Figure 4.43   Base bar strains, test after rehabilitation, east face, 2-A-S8-M*
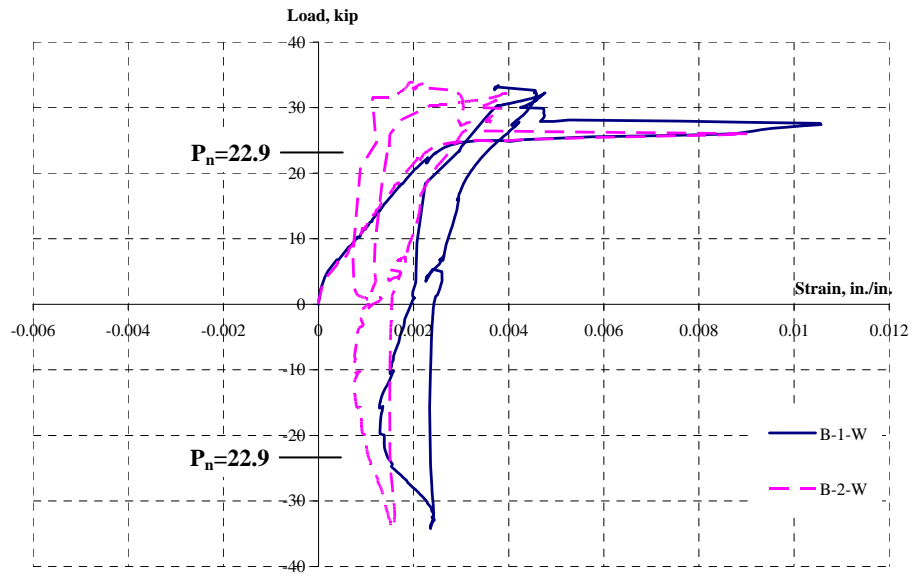
Figure 4.44   Base bar strains, test after rehabilitation, west face, 2-A-S8-M

248

4.5.2.3 CFRP Strain

The layout of strain gages on the CFRP jackets in 2-A-S8-M is shown in Figure 4.45. On the north and south face of 2-A-S8-M, six gages are installed on each face at the location where splitting cracking was expected. Gages NE-B, M and T and NW-B, M and T were installed at location where splitting cracking was expected on the north face, and gages SE-B, M and T and SW-B, M and T were installed at location where splitting cracking was expected on the south face. Strain in CFRP jackets were measured at three levels on the north and south face (B: bottom, M: middle and T: top). No strain gages were installed at the corners of 2-A-S8-M. Two strain gages were installed on the middle of the east (E-B and E-T) and west (W-B and W-T) face in the CFRP jackets.

In this section, measured strains on the south face of 2-A-S8-M are provided. Additional strain data are shown in Appendix C.

Strain vs lateral load for strain gages at the location of splitting cracking expected is shown in Figure 4.46 and Figure 4.47. The maximum measured strain was between 0.0020 and 0.0030 (20 ~ 30 % of ultimate tensile strain of the CFRP) on the south-east side and between 0.0015 and 0.0035 (15 ~ 35 % of ultimate tensile strain of the CFRP) on the south-west side. In the south-west side, the highest strain was observed in the gage closest to the footing which was the bottom gage (SW-B) while the highest strain was observed in the top gage in the south-east side (SE-T). Strains of the corners in 2-A-S8-M were not measured.
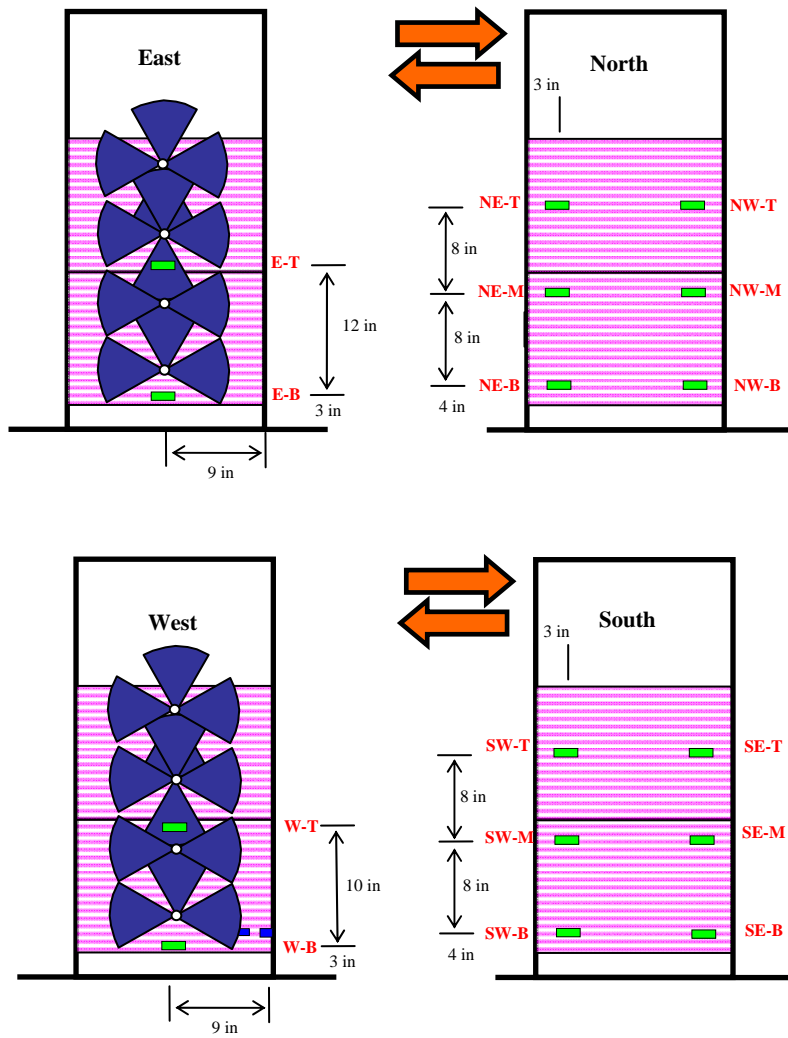
- **E-T, E-B, W-T and W-B were placed on CFRP jackets.**
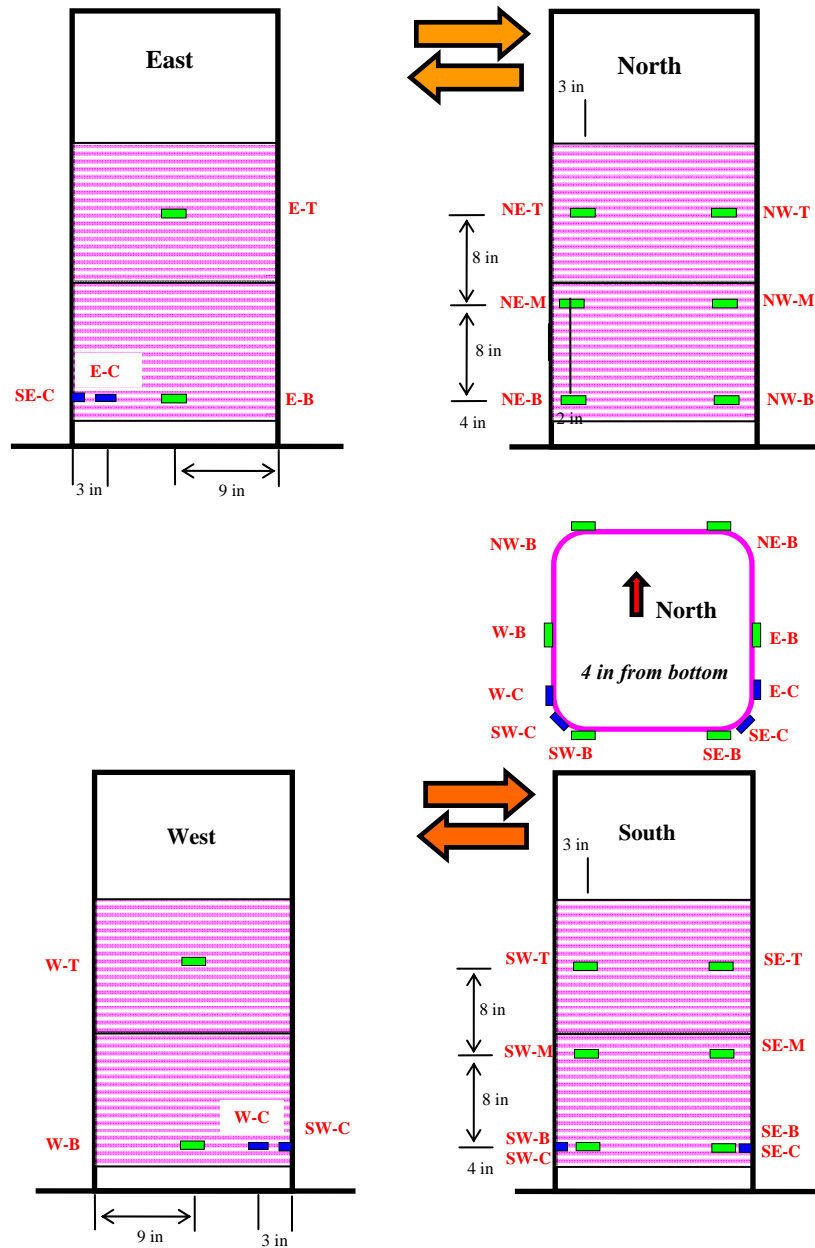
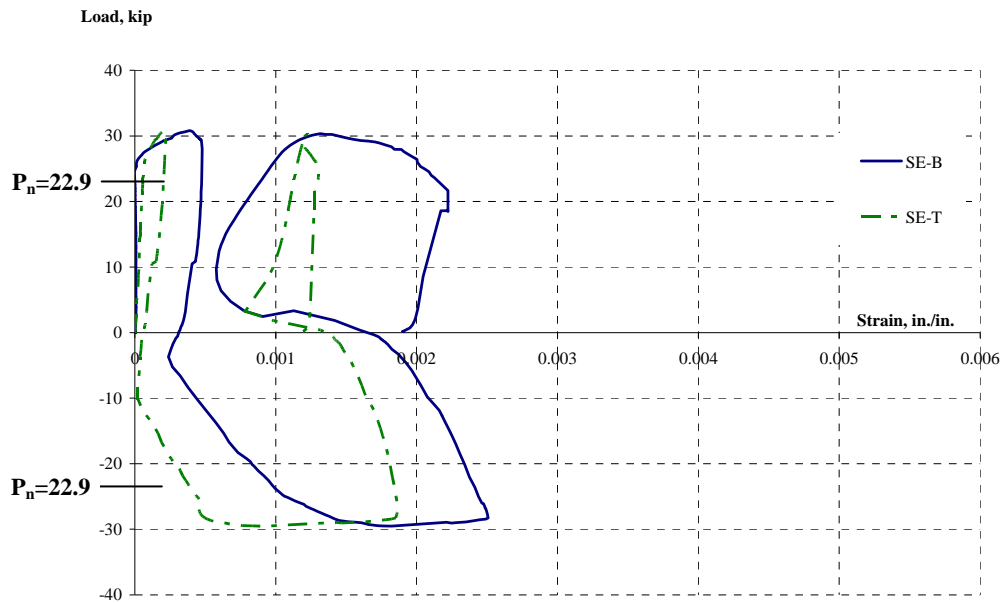**Figure 4.45   Layout of CFRP strain gages, 2-A-S8-M**
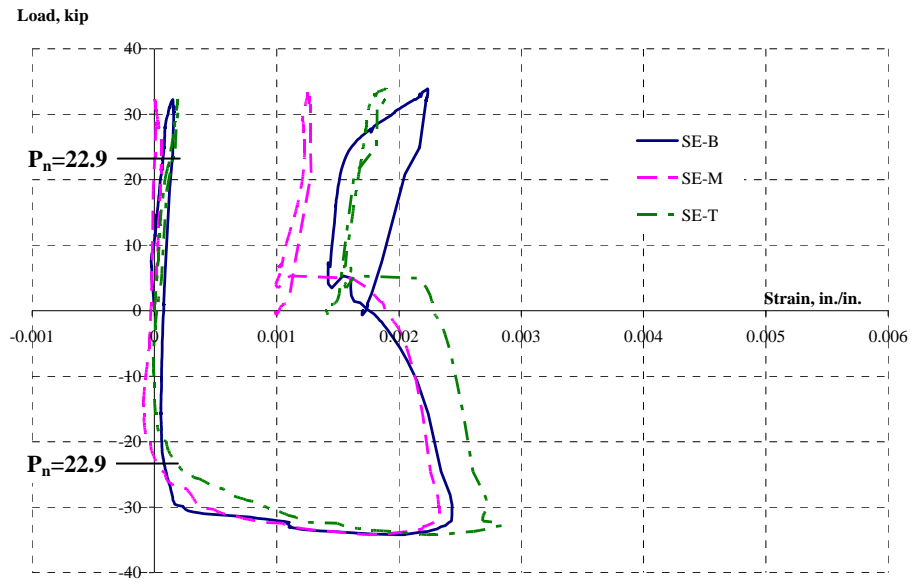
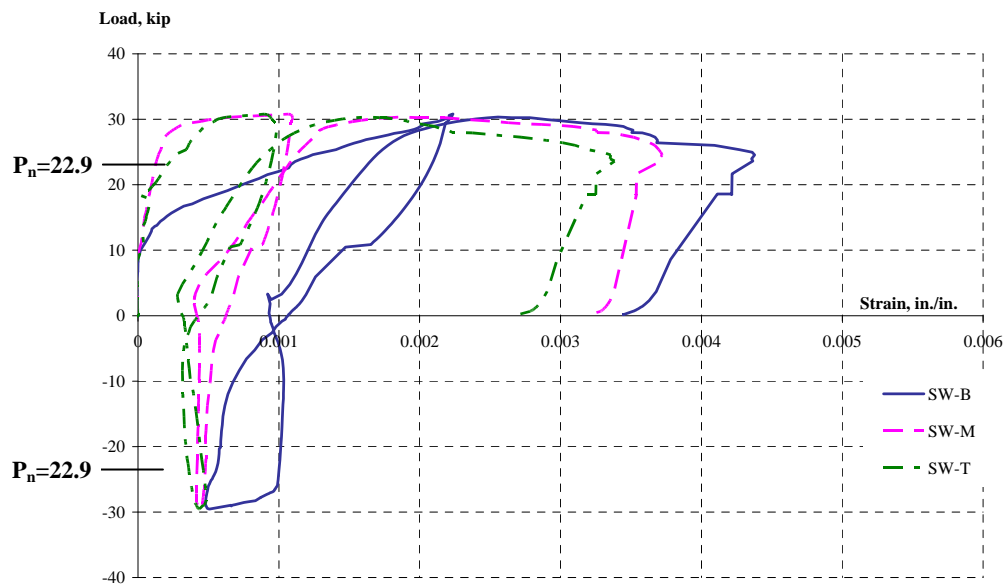*Figure 4.46   CFRP strains at location of splitting cracking, south-east, 2-A-S8-M*
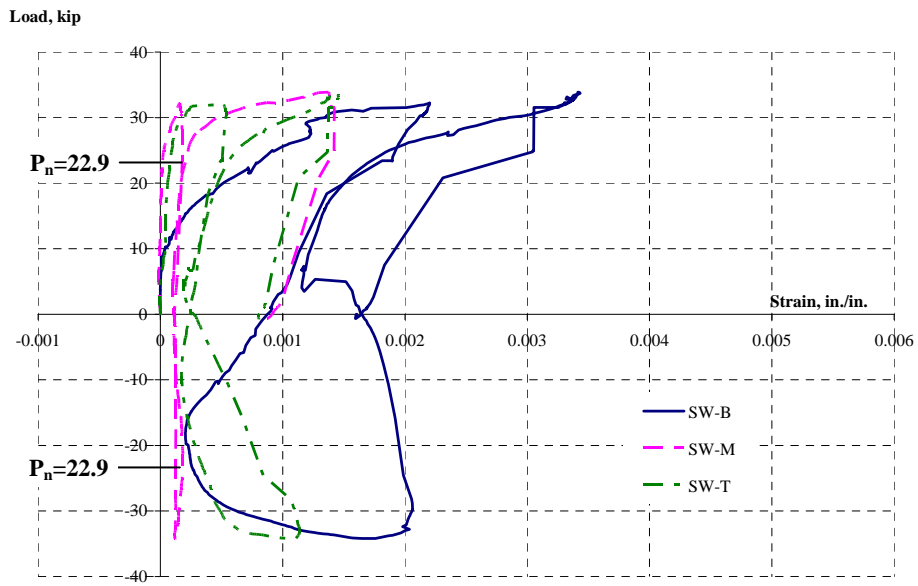
Figure 4.47   CFRP strains at location of splitting cracking, south-west, 2-A-S8-M
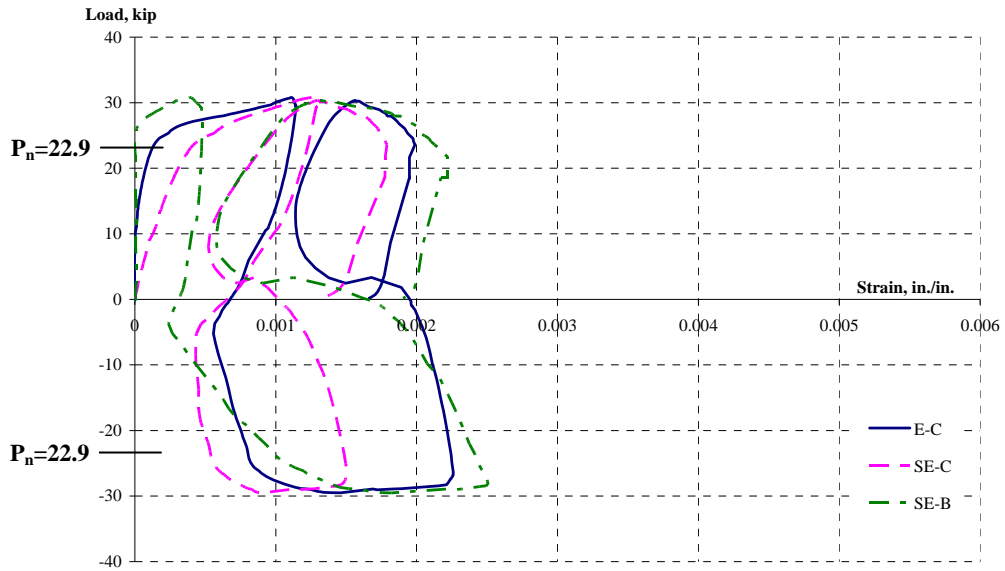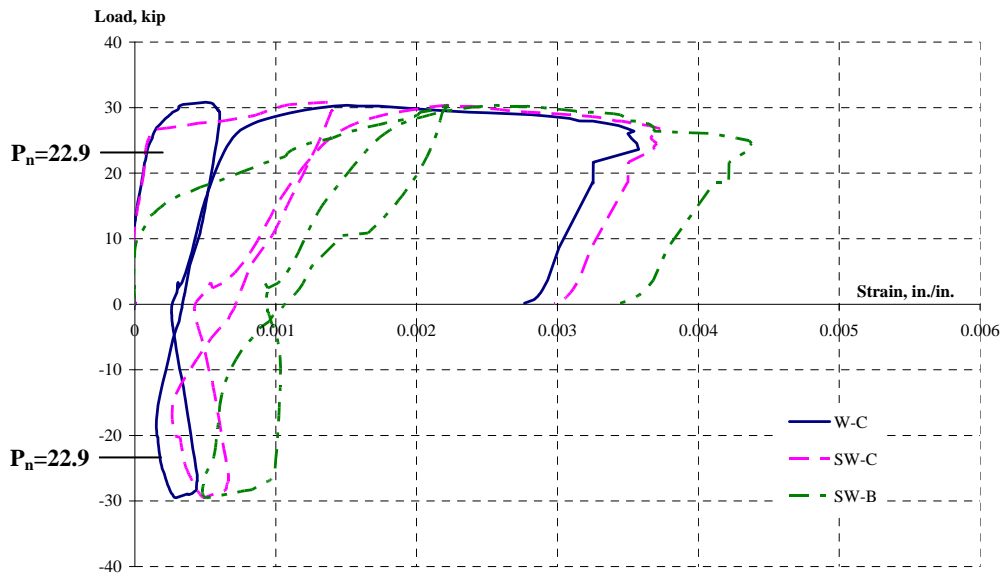
251

Table 4.6   Summary of test results, 2-A-S8-M

Face	Effective width of CFRP jackets	No. of CFRP anchors	Effective width of CFRP anchors	Total effective width of CFRP	Measured peak strength (Max. Load) P/P_n	Drift ratio at measured peak strength	Strain in CFRP jackets at location of splice cracking expected
East (As-built)					1.10*	1.1 %	
West (Undamaged)	48 in.	4	28 in.	76 in.	1.48	4.8 %	0.0015 ~ 0.0035
East (Damaged)	48 in.	4	28 in.	76 in.	1.49	4.5 %	0.0020 ~ 0.0030

* : splice failure

Computed: Nominal Strength (P_n): 22.9 kip; Yield strength: 24.8 kip; Ultimate Strength: 39.2 kip

4.5.3   Comparison of 1-A-S8-M and 2-A-S8-M

Contribution of CFRP Jackets and CFRP Anchors

The response of 1-A-S8-M and 2-A-S8-M after rehabilitation is shown in Figure 4.48.   1-A-S8-M and 2-A-S8-M were Type A column with 8 lap splices and their nominal strength was the same. 2-A-S8-M, which was rehabilitated by a combination of a CFRP jacket and CFRP anchors, showed better performance than 1-A-S8-M, which was rehabilitated only by a CFRP jacket. After rehabilitation, the strength of 2-A-S8-M was around 50 % more than the nominal strength while strength of 1-A-S8-M was around 30% more than the nominal strength. Because of the limitation in the stroke of the actuator, 2-A-S8-M was not tested up to its full deformation capacity. However, the response of 2-A-S8-M showed a larger drift ratio at the maximum lateral load than the drift ratio at the maximum lateral load of 1-A-S8-M. In addition, a decrease of strength was not observed in the undamaged side of 2-A-S8-M up to 5 % drift ratio.

In the spliced bars away from the corner, larger strain was observed in 2-A-S8-M than in 1-A-S8-M. The strain gage of a middle bar in the undamaged side (B-2-W) of 2-A-S8-M reached higher strain than in 1-A-S8-M (Figure 4.49).

252
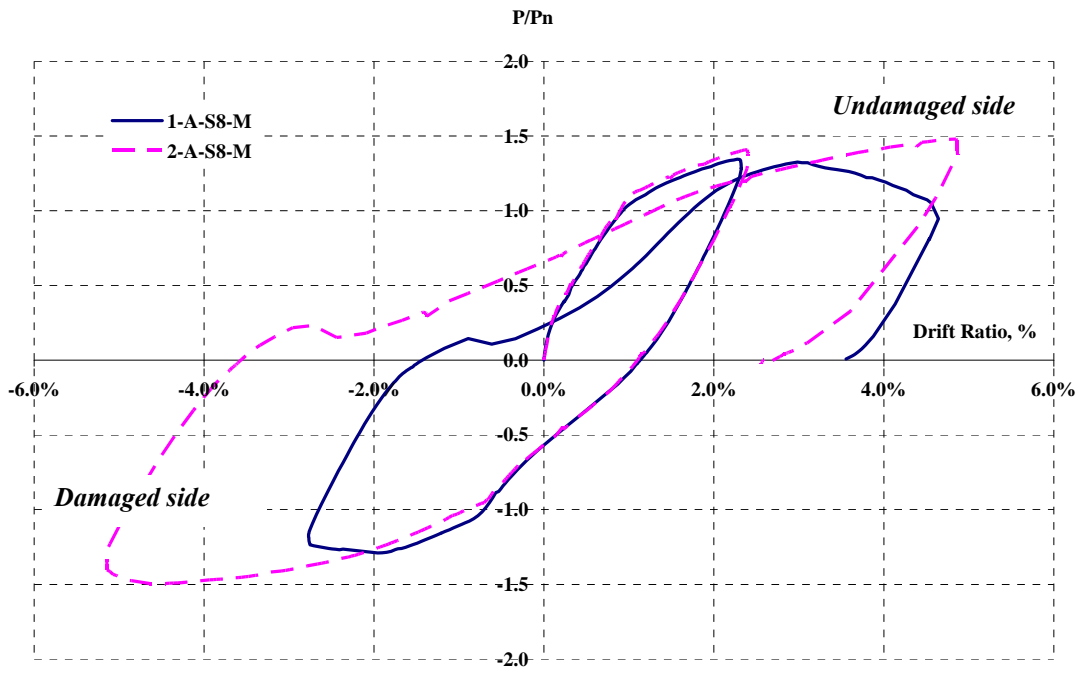
Figure 4.48   Response of 1-A-S8-M and 2-A-S8-M after rehabilitation
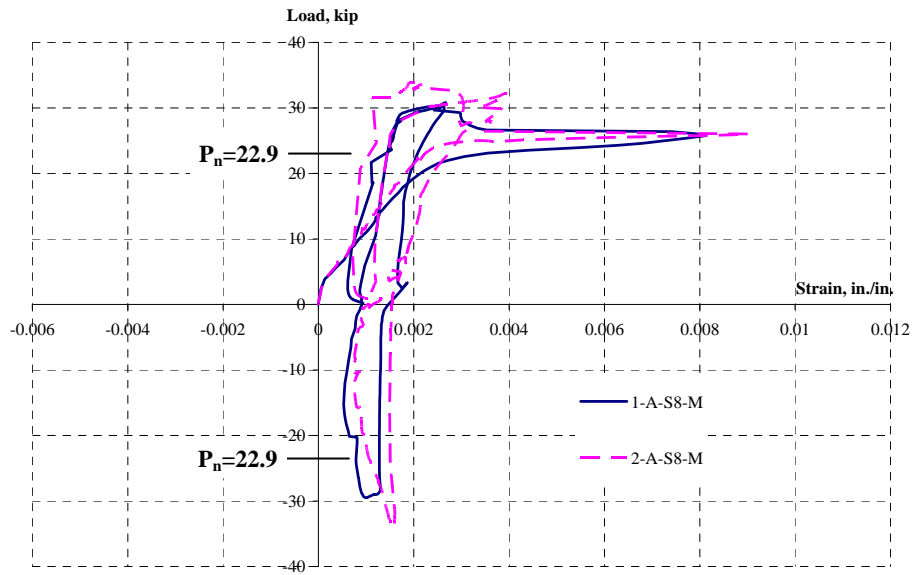
Figure 4.49   response of gage B-2-W in 1-A-S8-M and 2-A-S8-M

253

4.5.4   3-B-S10-M

A summary of the test results of 3-B-S10-M is shown in Table 4.7 at the end of this section.

4.5.4.1   *Drift Ratio VS Normalized Lateral Load*

Figure 4.50 shows drift ratio vs normalized lateral load response of 3-B-S10-M as-built and after rehabilitation. The actual yield strength ($P/P_n = 1.06$) and ultimate strength ($P/P_n = 1.68$) based on measured strength of the concrete and reinforcement are also provided. The measured compressive strength of the concrete was 4,500 psi and the measured yield and ultimate strength of the reinforcement were 63 ksi and 106 ksi.

Although the nominal strength was realized in this column as-built ($P/P_n = 1.01$), the load dropped once splitting of the concrete occurred at the splice. However, significant improvement of strength and deformation capacity was observed in 3-B-S10-M after rehabilitation with CFRP on both the damaged and undamaged sides of the column. The strength increased by 56 % for the damaged and by 54 % for the undamaged side after rehabilitation compared with the as-built strength. The drift ratio of 3-B-S10-M as-built was 1.0 % at the maximum load. The drift ratio corresponding to the peak strength was 5.5 % in the damaged side and 8.6 % in the undamaged side after rehabilitation. On the undamaged side, there was a gradual reduction in strength up to the stroke limit of the load actuator while on damaged side, no reduction of strength was observed.
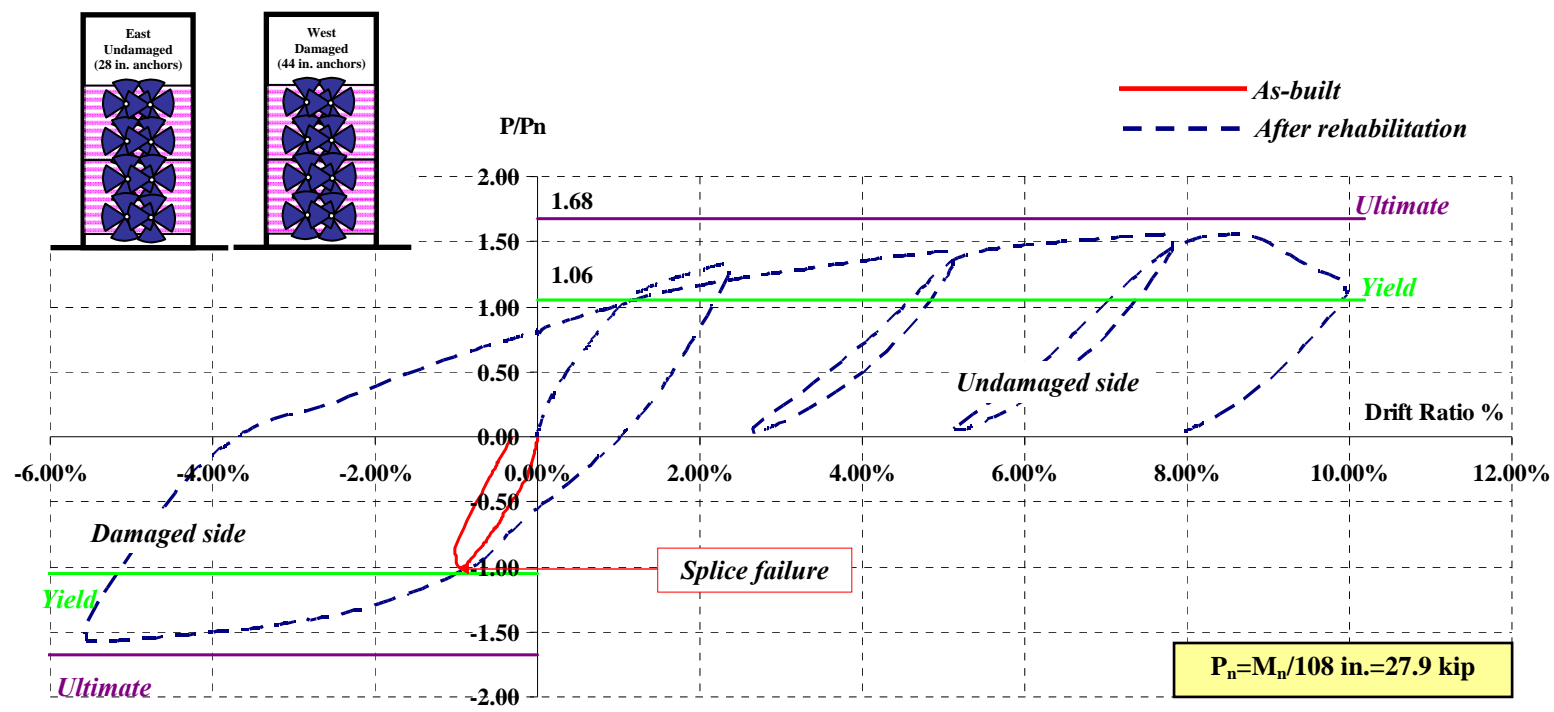
Figure 4.50   Drift ratio vs normalized lateral load, 3-B-S10-M

The failure mode of 3-B-S10-M as-built was a brittle splice failure (Figure 4.51). A sudden drop of load was observed at the peak load during the test of this column as-built (Figure 4.50). The use of the CFRP jackets and anchors effectively confined lap splices and changed the failure mode of 3-B-S10-M from a brittle splice failure to yielding of tension steel indicated by measured strains in the steel reinforcement presented in the next section.
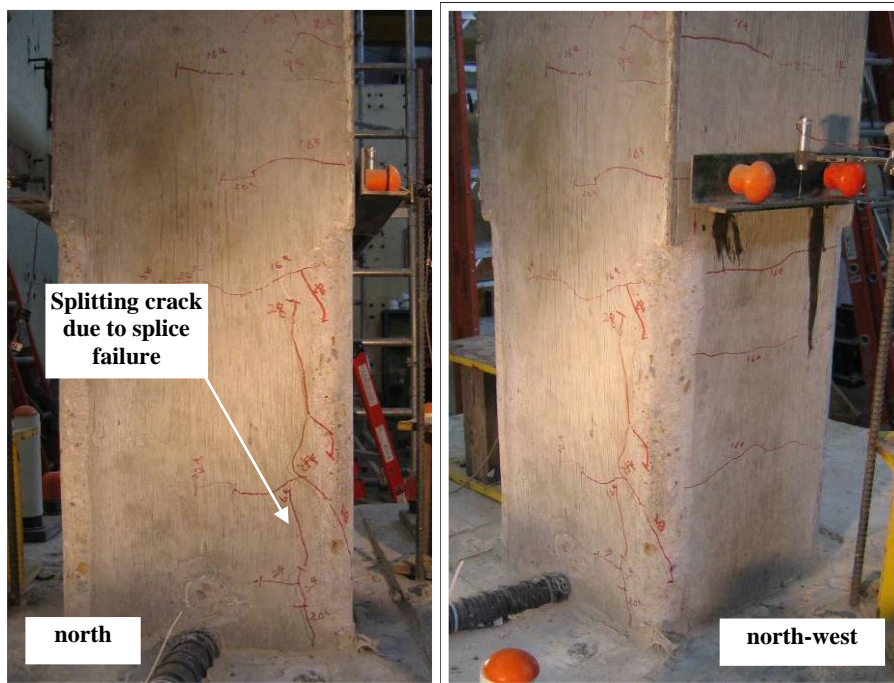
Figure 4.51   Splice failure of 3-B-S10-M before rehabilitation

4.5.4.2 Steel Reinforcement Strain

Layout of steel reinforcement strain gages in 3-B-S10-M is shown in Figure 4.52.
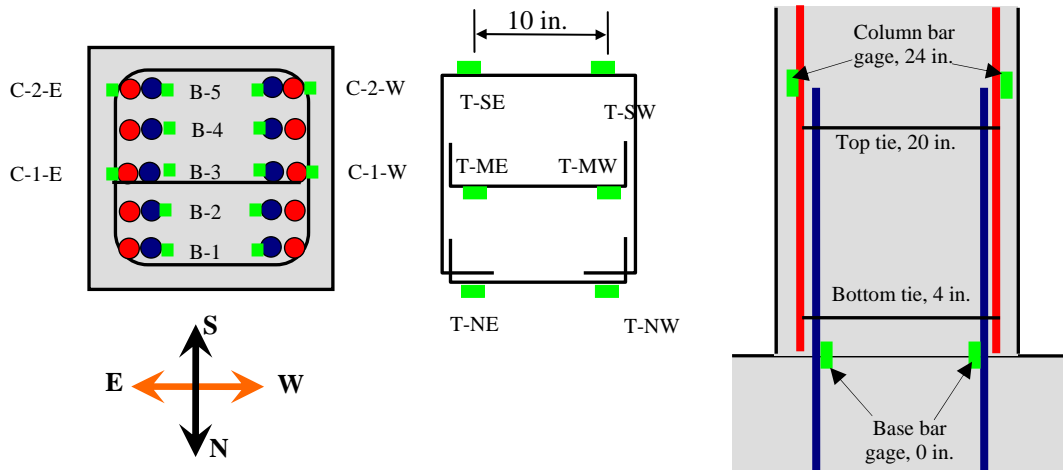
- **Base bar gages (B - # - Direction):** at the top of the footing
- **Column bar gages (C - # - Direction):** 24 in. from the top of the footing
- **Tie bar gages (T-Top or Bottom- Direction):**

  Top-tie at 20 in. from the top of the footing

  Bottom- tie at 4 in. from the top of the footing

Figure 4.52   Layout of steel reinforcement strain gages, 3-B-S10-M

4.5.4.2.1 Base Bar Strain, As-Built Test

Tensile strains in the base bars during the initial test are shown in Figure 4.53. Strain gages were installed on the base bars at the same level as the top of the footing. All the base bars yielded but only one bar (B-5-W) exhibited inelastic response. A brittle splice failure occurred right after the base bars reached yield and significant ductility was not realized. The actual yield strain of the bars was 0.0022 and the maximum strain measured in the gages except B-5-W was about 0.0025.
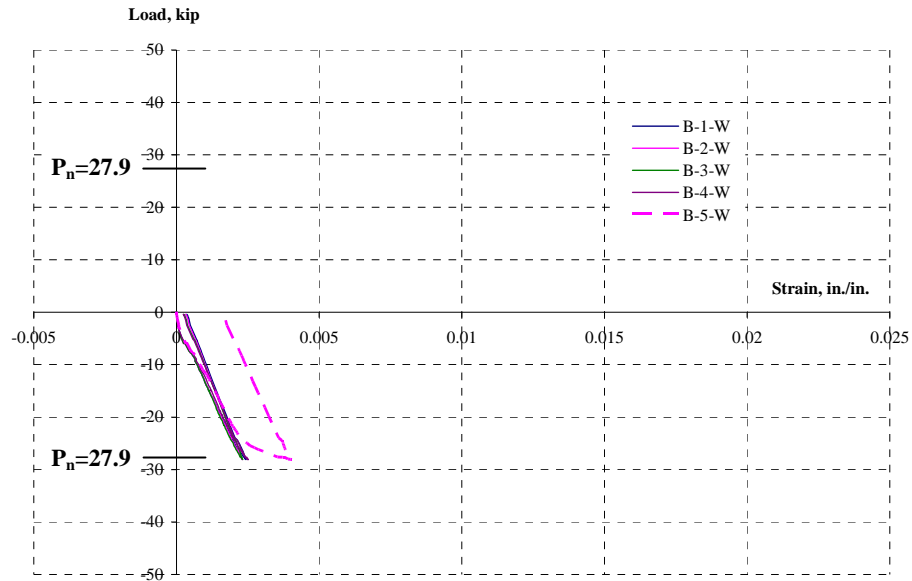
Figure 4.53   Base bar strains, as-built test, 3-B-S10-M

4.5.4.2.2 Base Bar Strain, Test after Rehabilitation

Base bar strains during the test after rehabilitation are shown in Figure 4.54 and Figure 4.55. The bars on the west face (damaged) of 3-B-S10-M were initially in compression while the bars on the east face (undamaged) of 3-B-S10-M were in tension. When the load was reversed the bars on the west face were in tension. All the bars yielded during tension loading. After the base bars reached large tensile strains the gages on the bars were damaged during loading reversal. However, strain hardening of the bars could be observed before the gages were damaged and the lateral draft and load response of 3-B-S10-M indicated strain hardening was reached.

258
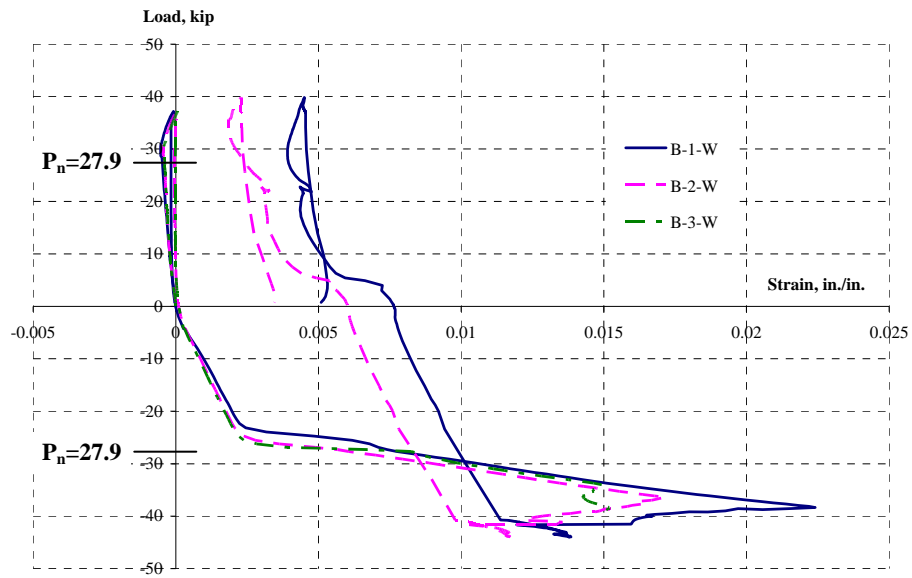
Figure 4.54   Base bar strains, test after rehabilitation, west face, 3-B-S10-M
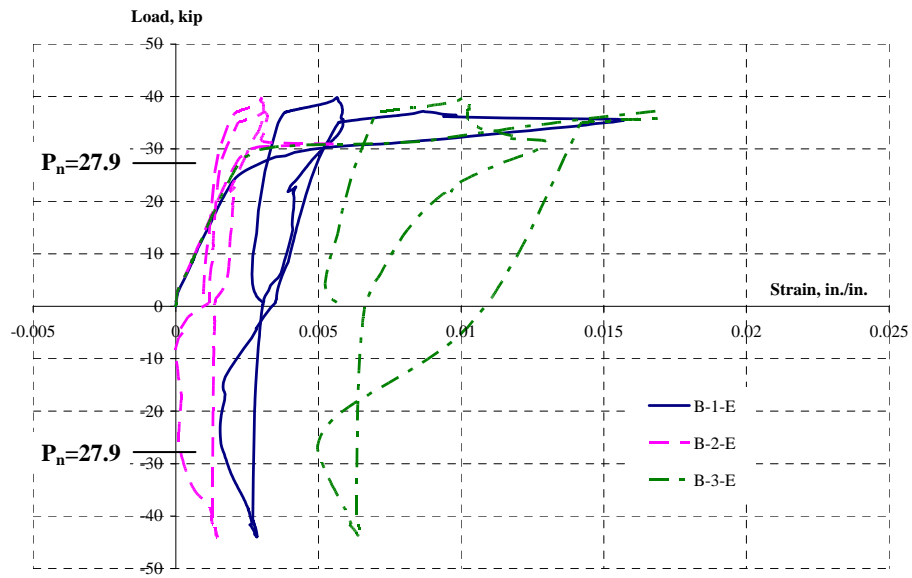
Figure 4.55   Base bar strains, test after rehabilitation, east face, 3-B-S10-M

259

4.5.4.3 CFRP Strain

The layout of strain gages on the CFRP jackets in 3-B-S10-M is shown in Figure 4.56. On the north and south face of 3-B-S10-M, six gages are installed on each face at the location where splitting cracking was expected. Gages NE-B, M and T and NW-B, M and T were installed at location where splitting cracking was expected on the north face, and gages SE-B, M and T and SW-B, M and T were installed at location where splitting cracking was expected on the south face. Strain in CFRP jackets were measured at three levels on the north and south face (B: bottom, M: middle and T: top). Strain gages were also installed at the bottom corners on the south face to observe strain transition around the corners (SE-C and SW-C). Two strain gages were installed on the east (E-B and E-T) and west (W-B and W-T) face in the CFRP jackets. These strain gages could be installed at a few locations in the CFRP jackets because the fan-portion of the CFRP anchors covered much of the sheet.

 In this section, measured strains on the south face and at the corners of 3-B-S10-M are provided. Additional strain data are shown in Appendix C.

Strain vs lateral load for strain gages at the location of expected splitting cracking is shown in Figure 4.57 and Figure 4.58. The maximum measured strain was between 0.0015 and 0.0030 (15~ 30 % of ultimate tensile strain of the CFRP) on the south-west side and between 0.0015 and 0.0035 (15 ~ 35 % of ultimate tensile strain of the CFRP) on the south-east side. In the south-west side, the highest strain was observed in the gage closest to the footing which was the bottom gage (SW-B) while the highest strain was observed in the top gage in the south-east side (SE-T).

Strain vs lateral load for strain gages at the corners of 3-B-S10-M is shown in Figure 4.59 and Figure 4.60. From the data of the distribution of CFRP strains at the corners, a smooth transition of strains was observed around the corner. The measured strain in the gage at the corner on the west face (W-B) was close to that in the gage at the arc of the south-west corner (SW-C). The measured strain at the arc of the south-east

260

corner (SE-C) showed a similar response as the strain at the corner on the south face (SE-B).
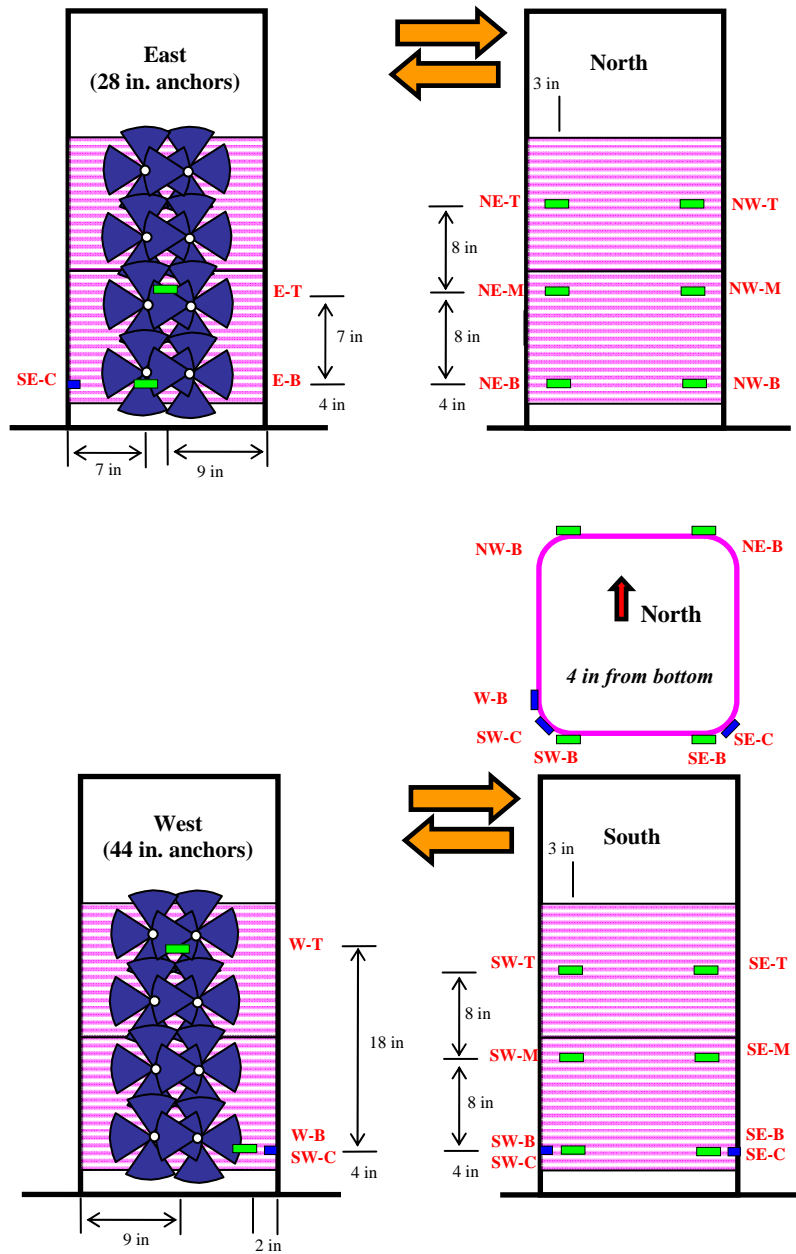
Figure 4.56   Layout of CFRP strain gages, 3-B-S10-M
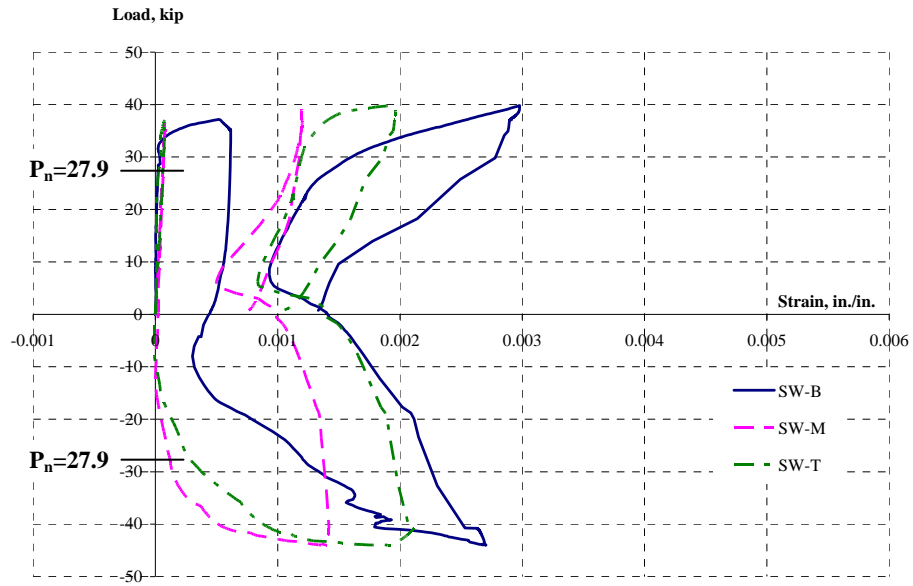
Figure 4.57   CFRP strains at location of splitting cracking, south-west, 3-B-S10-M
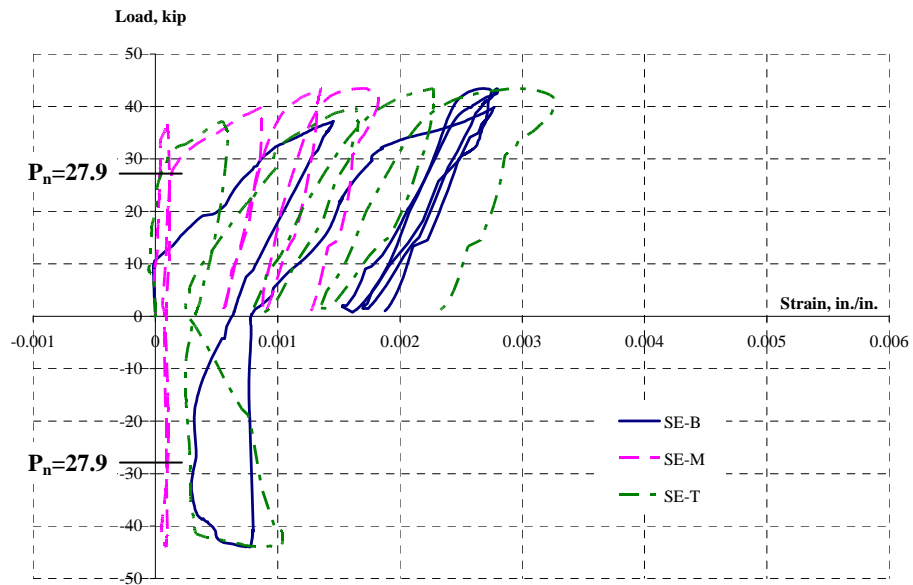
Figure 4.58   CFRP strains at location of splitting cracking, south-east, 3-B-S10-M

262
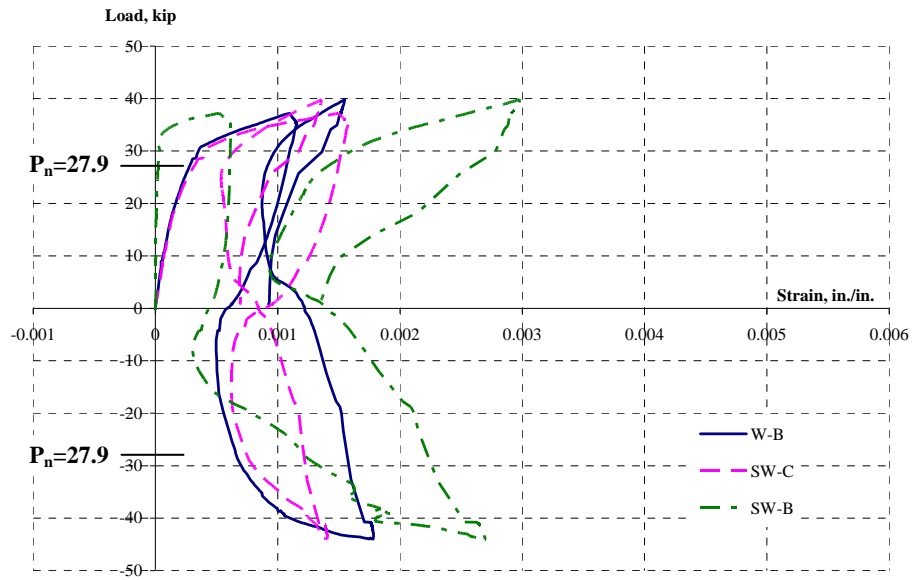
Figure 4.59   CFRP strains at south-west corner, 3-B-S10-M
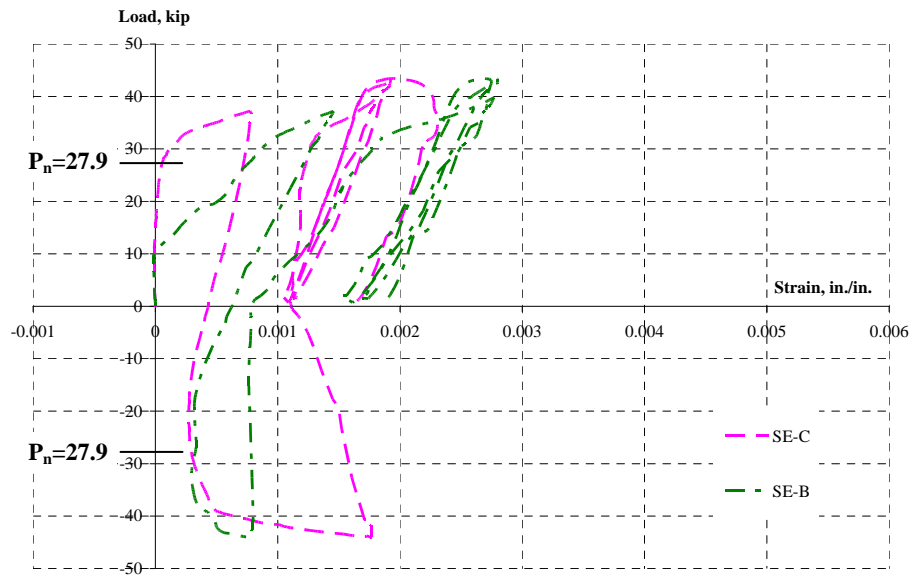
Figure 4.60   CFRP strains at south-east corner, 3-B-S10-M

263

Table 4.7   ***Summary of test results,*** *3-B-S10-M*

Face	Effective width of CFRP jackets	No. of CFRP anchors	Effective width of CFRP anchors	Total effective width of CFRP	Measured peak strength (Max. Load) P/P_n	Drift ratio at measured peak strength	Strain in CFRP jackets at location of splice cracking expected
West (As-built)					1.01*	.0 %	
East (Undamaged)	48 in.	8	28 in.	76 in.	1.56	8.6 %	0.0015 ~ 0.0035
West (Damaged)	48 in.	8	44 in.	92 in.	1.58	5.5 %	0.0015 ~ 0.0030

* : splice failure

Computed: Nominal Strength (P_n): 27.9 kip;   Yield strength: 29.5 kip;   Ultimate Strength: 46.9 kip

4.5.5   Comparison of the East and West Sides of 3-B-S10-M

Effect of Width of CFRP per CFRP Anchor

On the west face of 3-B-S10-M, the total width of CFRP sheet used in CFRP anchors was 44 in. (Design using the shear friction equation) while that on the east face was 28 in (designed using the test results of 2-A-S8-M). Only 64 % of CFRP required by the shear friction calculation was applied to the east side of 3-B-S10-M. However, as indicated by the response plotted in Figure 4.50, the performance of the east face of 3-B-S10-M was comparable to that of the west face of 3-B-S10-M. The strength increased by 54 % and the drift ratio at the maximum load increased by a factor of 8 on the east face of 3-B-S10-M after the rehabilitation. Therefore, the design procedure based on the shear friction mechanism provided a conservative estimation of material needed for CFRP anchors.

4.5.6 4-C-R20-M

A summary of the test results of 4-C-R20-M is shown in Table 4.8 in the end of this section.

4.5.6.1 Drift Ratio VS Normalized Lateral Load

Figure 4.61 shows drift ratio vs normalized lateral load response of 4-C-R20-M as-built and after rehabilitation. The actual yield strength (P/P_n = 1.06) and ultimate strength (P/P_n = 1.69) based on measured strength of the concrete and reinforcement are also provided. The measured compressive strength of the concrete was 4,600 psi and the measured yield and ultimate strength of the reinforcement were 63 ksi and 106 ksi.

The nominal capacity and significant deformation capacity was not realized in 4-C-R20-M in the as-built test (P/P_n = 0.96 at 1.1 % drift ratio). However, improvement of strength and deformation capacity was observed in 4-C-R20-M after rehabilitation with CFRP both on damaged and undamaged sides of the column. The strength increased by 20 % for the damaged and by 35 % for the undamaged side after rehabilitation compared with the as-built strength. The drift ratio corresponding to the peak strength was 2.1 % in the damaged side and 2.3 % in the undamaged side after rehabilitation. In both directions, there was a gradual reduction in strength up to the stroke limit of the load actuator.

The failure mode of 4-C-R20-M as-built was a brittle splice failure (Figure 4.62). A sudden drop of load was observed at the peak load during the test of this column as-built (Figure 4.61). The use of the CFRP jackets and anchors effectively confined lap splices and changed the failure mode of 4-C-R20-M from a brittle splice failure to yielding of tension steel indicated by measured strains in the steel reinforcement presented in the next section.
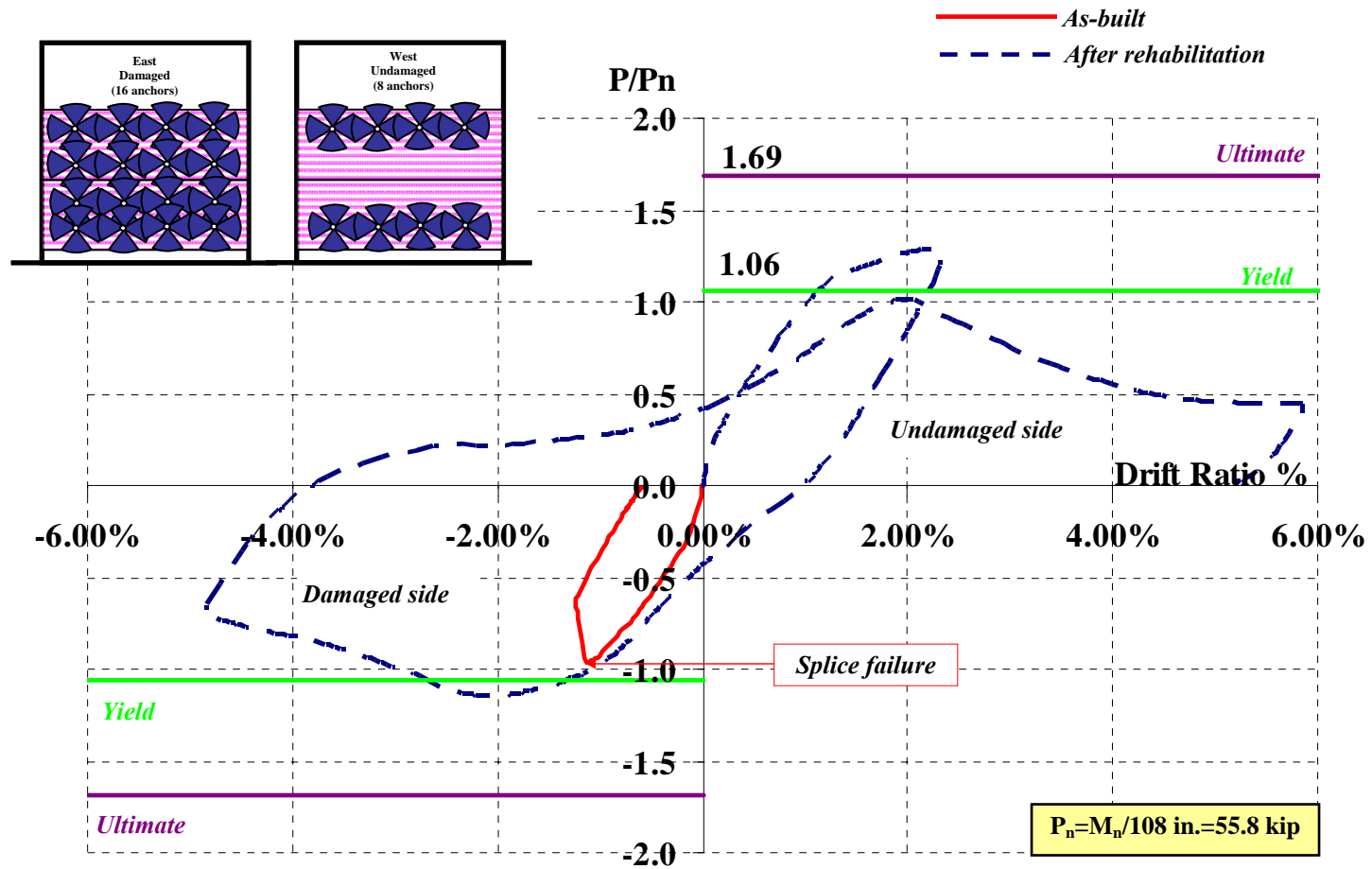
Figure 4.61   Drift ratio vs normalized lateral load, 4-C-R20-M
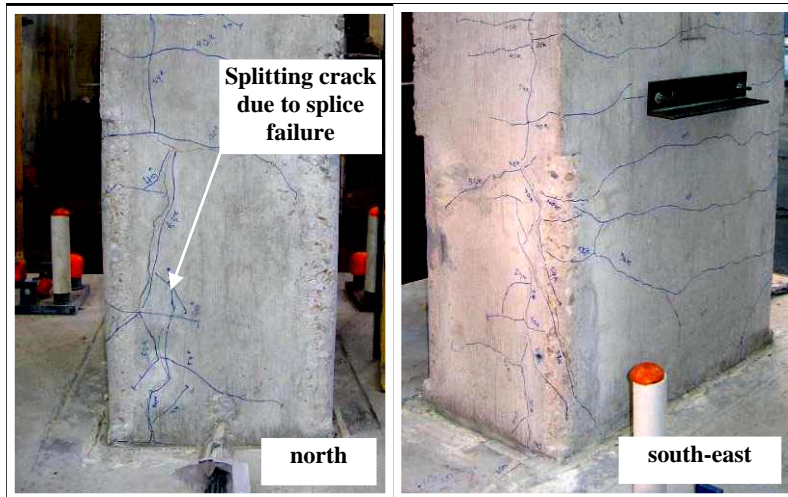
Figure 4.62   Splice failure of 4-C-R20-M before rehabilitation

4.5.6.2   Steel Reinforcement Strain

Layout of steel reinforcement strain gages in 4-C-R20-M is shown in Figure 4.63.

4.5.6.2.1 Base Bar Strain, As-Built Test

Tensile strains in the base bars during the initial test are shown in Figure 4.64. Strain gages were installed on the base bars at the same level as the top of the footing. Two base bars (B-2-E and B-4-E) out of 5 base bars with strain gages just reached yield but did not exhibited inelastic response because a brittle splice failure occurred right before the bars developed ductility. The actual yield strain of steel reinforcement was 0.0022 and the maximum strain measured in the base bar gages was also 0.0022.
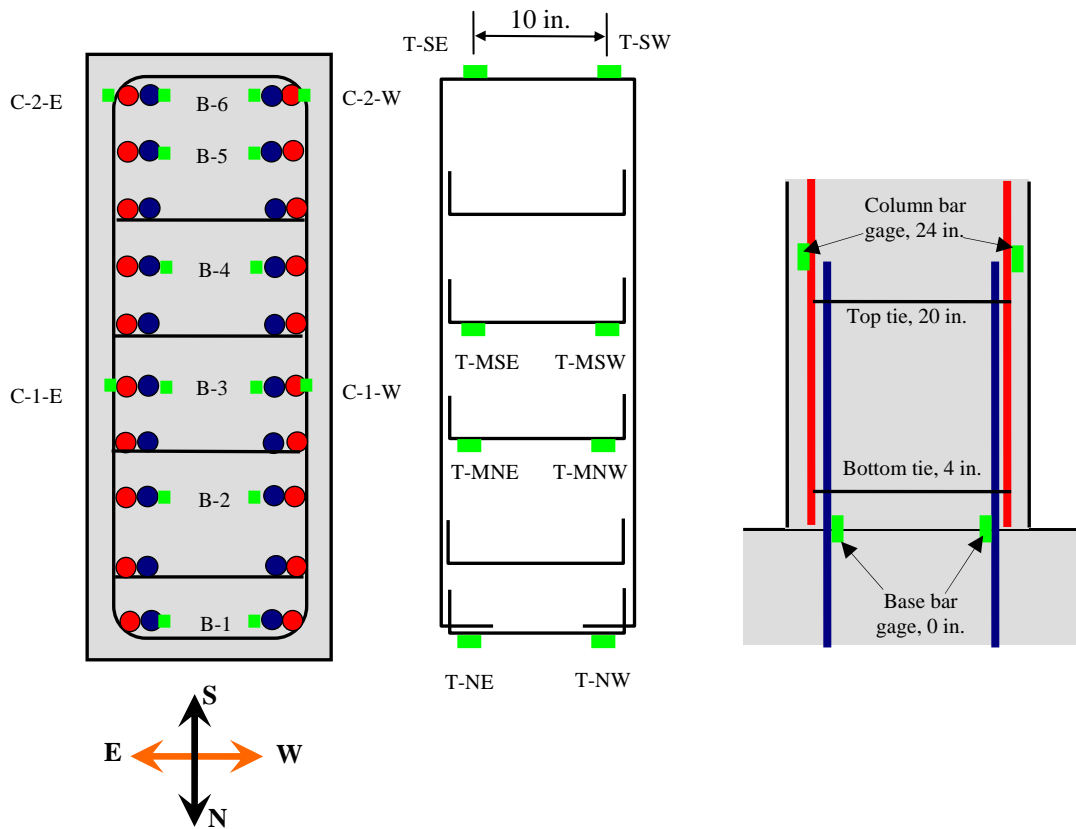
267

- **Base bar gages (B - # - Direction):** at the top of the footing
- **Column bar gages (C - # - Direction)**: 24 in. from the top of the footing
- **Tie bar gages (T-Top or Bottom- Direction):**

    Top-tie at 20 in. from the top of the footing

    Bottom- tie at 4 in. from the top of the footing

Figure 4.63   Layout of steel reinforcement strain gages, 4-C-R20-M
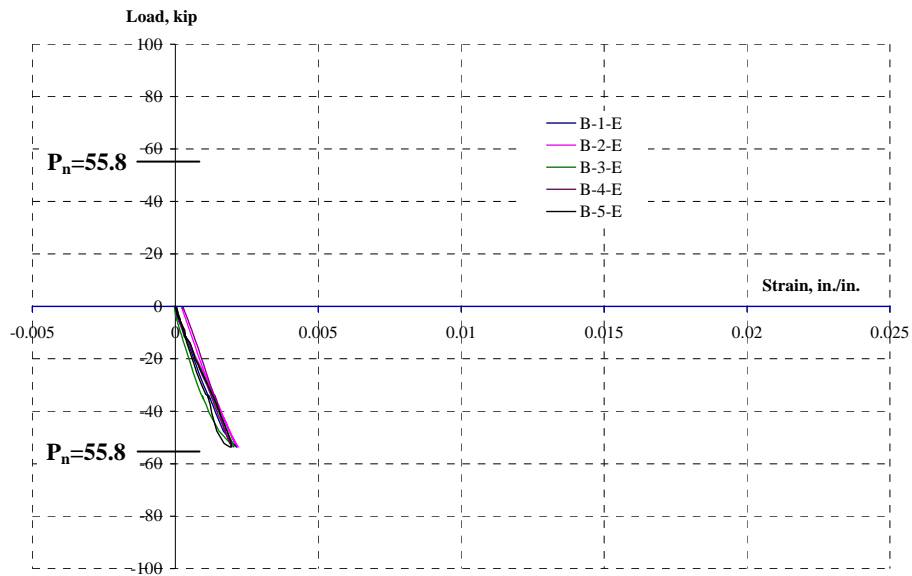
Figure 4.64   Base bar strains, as-built test, 4-C-R20-M

4.5.6.2.2 Base Bar Strain, Test after Rehabilitation

Base bar strains during the test after rehabilitation are shown in Figure 4.65 and Figure 4.66.   The bars on the east face (damaged) of 4-C-R20-M were initially in compression while the bars on the west face (undamaged) of 4-C-R20-M were in tension. When the load was reversed, the bars on the east face were in tension. All the bars yielded during tension loading. After the base bars reached large tensile strains, the gages on the bars were damaged during loading reversal. Therefore, strain hardening of the bars could not be observed although the lateral deformation of the column was significant and measured lateral load reflected strain hardening of the bars.

269
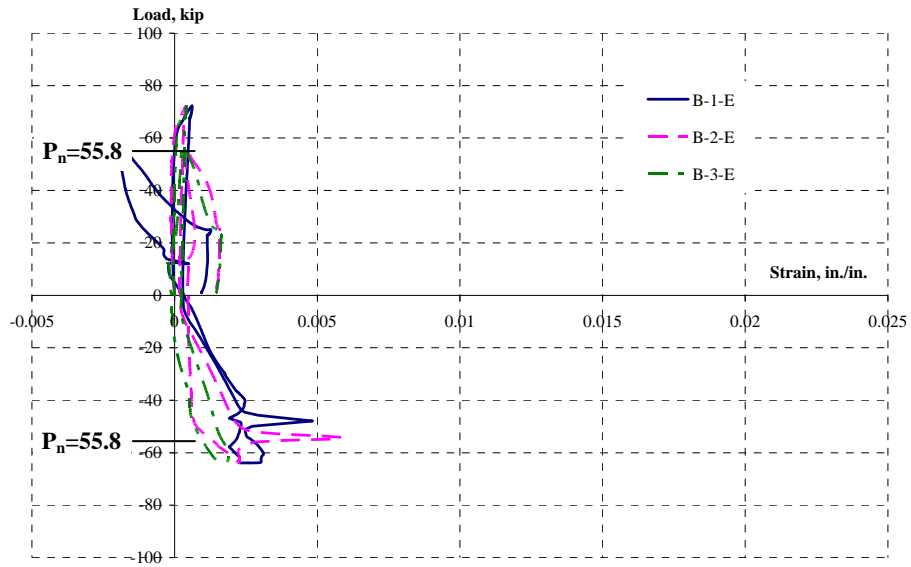
Figure 4.65   Base bar strains, test after rehabilitation, east face, 4-C-R20-M
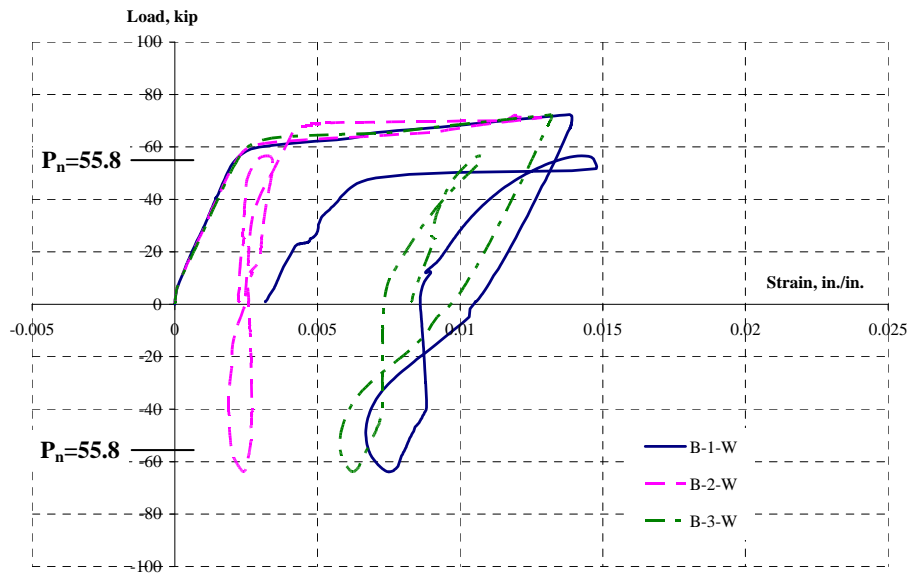
Figure 4.66   Base bar strains, test after rehabilitation, west face, 4-C-R20-M

270

4.5.6.3 CFRP Strain

The strain data on the CFRP jackets were could not be measured because of an error in the data acquisition system. However, the rehabilitation method used in 4-C-R20-M was also used in 5-C-R20-C, and the CFRP strain data on 5-C-R20-C showed the effectiveness of the CFRP jackets in confining the lap spliced region of a rectangular column.

Table 4.8   Summary of test results, 4-C-R20-M

Face	Effective width of CFRP jackets	No. of CFRP anchors	Effective width of CFRP anchors	Total effective width of CFRP	Measured peak strength (Max. Load) P/P_n	Drift ratio at measured peak strength	Strain in CFRP jackets at location of splice cracking expected
East (As-built)					0.96*	1.1 %	
West (Undamaged)	48 in.	8	56 in.	104 in.	1.30	2.3 %	
East (Damaged)	48 in.	16	56 in.	104 in.	1.15	2.1 %	

* : splice failure

Computed: Nominal Strength (P_n): 55.8 kip; Yield strength: 59.2 kip; Ultimate Strength: 94.1 kip

4.5.7 5-C-R20-C

A summary of the test results of 5-C-R20-C is shown in Table 4.9 at the end of this section.

4.5.7.1 Drift Ratio VS Normalized Lateral Load

Figure 4.67 shows drift ratio vs normalized lateral load response of 5-C-R20-C after rehabilitation. Different colors are used in different portions of the cyclic loading in the plot. 5-C-R20-C was not damaged before rehabilitation. In Figure 4.67, the drift ratio vs normalized lateral load response of 4-C-R20-M before rehabilitation was provided as a reference. The actual yield strength (P/P_n = 1.08) and ultimate strength (P/P_n = 1.71) based on measured strength of the concrete and reinforcement are also provided. The measured compressive strength of the concrete was 5,300 psi and the measured yield and ultimate strength of the reinforcement were 63 ksi and 106 ksi.

Significant improvement of strength and deformation capacity was observed in 5-C-R20-C after rehabilitation with CFRP under cyclic loading on the east (16 anchors) and west (8 anchors) faces of 5-C-R20-C. The strength increased by 42 % for the east face and by 41 % for the west face after rehabilitation compared with the as-built strength of 4-C-R20-M. The drift ratio of 4-C-R20-M as-built was 1.1 % at the maximum load. In 5-C-R20-C, the drift ratio corresponding to the peak strength was 3.6 % on the east face and 2.4 % on the west face after rehabilitation.

The west face of 5-C-R20-C showed rapid degradation cyclic loading to 3.6% drift while the east face showed degradation cyclic loading to 4.8 % drift.

The final failure mode of 5-C-R20-C was a splice failure. The splitting cracks due to splice failure were observed after cutting the column from the footing (Figure 4.68). However, the column developed significant ductility before it failed.

272

East
(16 anchors)

West
(8 anchors)

P/Pn

---- **4-C-R20-M, as-built**

2.00

1.71 — *Ultimate*

1.50

1.08 — *Yield*

8 anchors, west

1.00

0.50

0.00 — **Drift ratio %**

-8.0%   -6.0%   -4.0%   -2.0%   0.0%   2.0%   4.0%   6.0%   8.0%

-0.50

16 anchors, east

Splice failure

-1.00

Yield

-1.50

Ultimate

$P_n = M_n/108$ in.=55.8 kip

-2.00
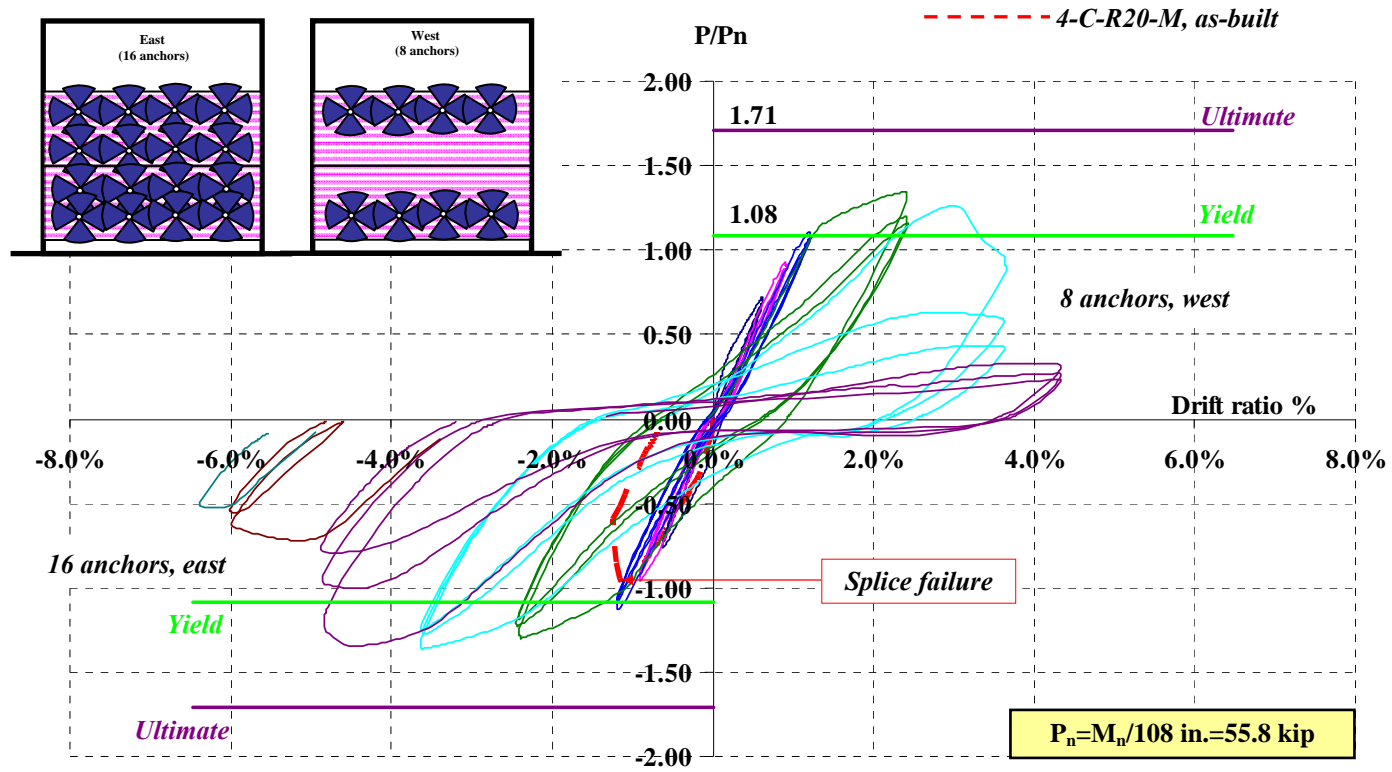
Figure 4.67   Drift ratio vs normalized lateral load, 5-C-R20-C

273
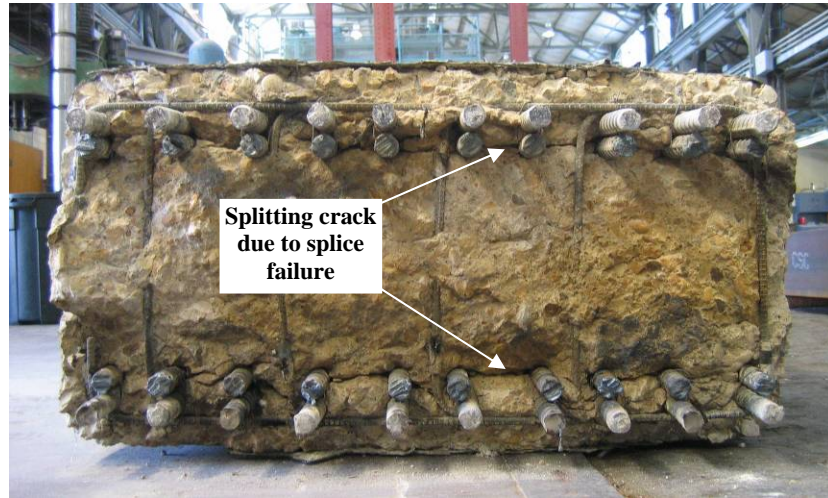
Figure 4.68   Splice failure of 5-C-R20-C

4.5.7.2   Steel Reinforcement Strain

Layout of steel reinforcement strain gages in 5-C-R20-C is shown in Figure 4.69.

4.5.7.2.1 Base Bar Strain

Base bar strains of 5-C-R20-C under cyclic loading are shown in Figure 4.70 and Figure 4.71. The bars on the east face (16 anchors) of 5-C-R20-C were initially in compression while the bars on the west face (8 anchors) were in tension. All the bars yielded during tension loading. The bars on the east face developed more ductility than those on the west face, and this result agreed with the drift ratio vs normalized lateral load response.
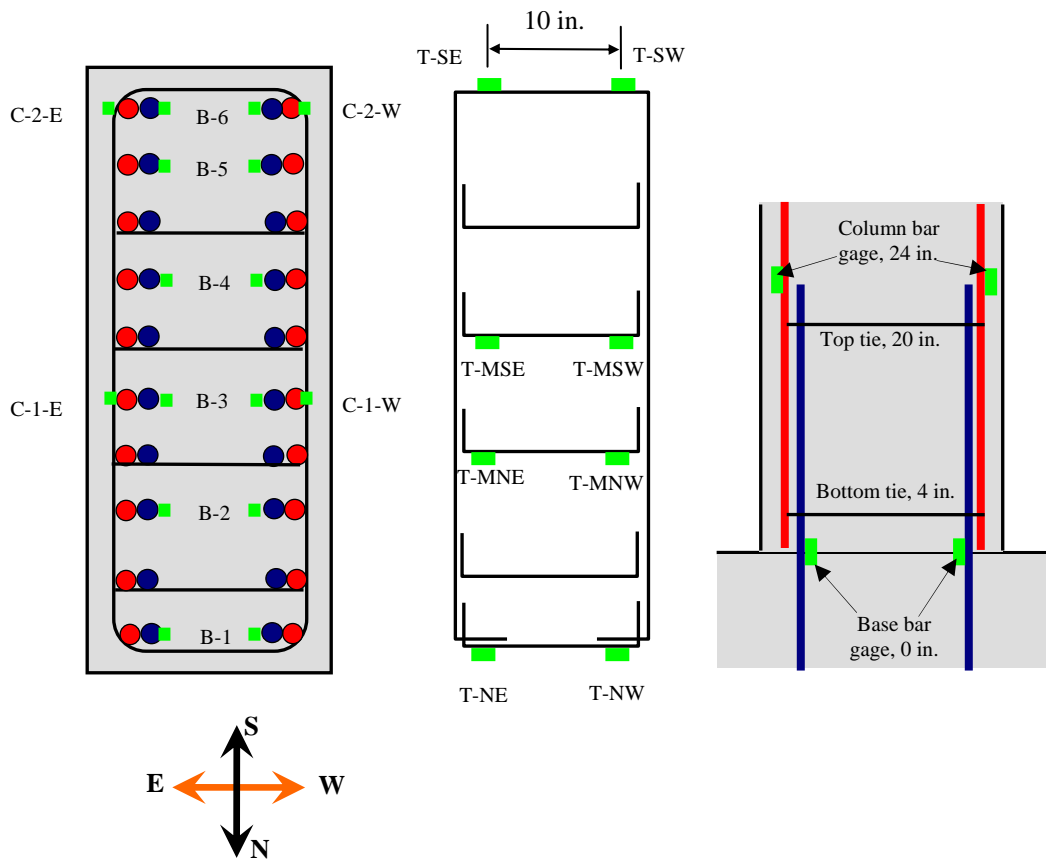
- **Base bar gages (B - # - Direction):** at the top of the footing
- **Column bar gages (C - # - Direction)**: 24 in. from the top of the footing
- **Tie bar gages (T-Top or Bottom- Direction):**

  Top-tie at 20 in. from the top of the footing

  Bottom- tie at 4 in. from the top of the footing

*Figure 4.69   Layout of steel reinforcement strain gages, 5-C-R20-C*
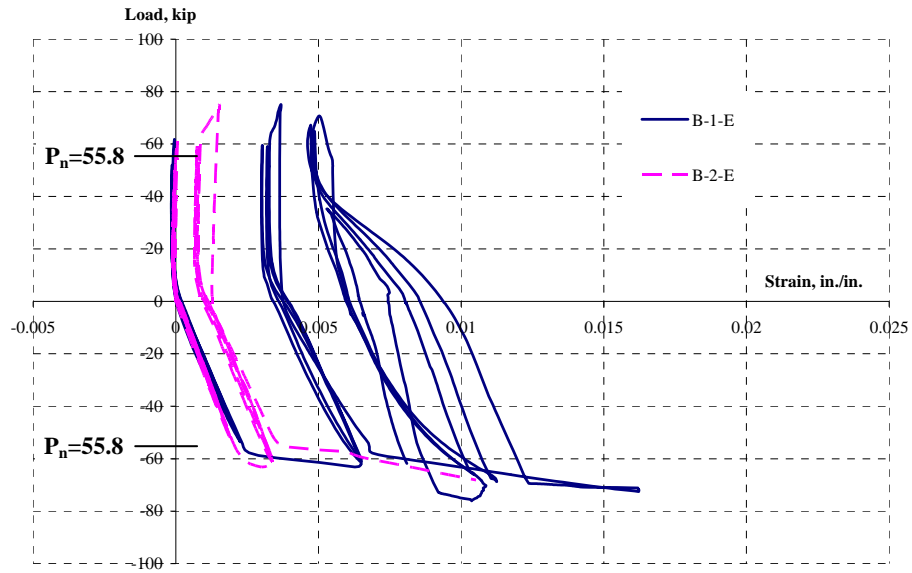
Figure 4.70   Base bar strains, east face, 5-C-R20-C
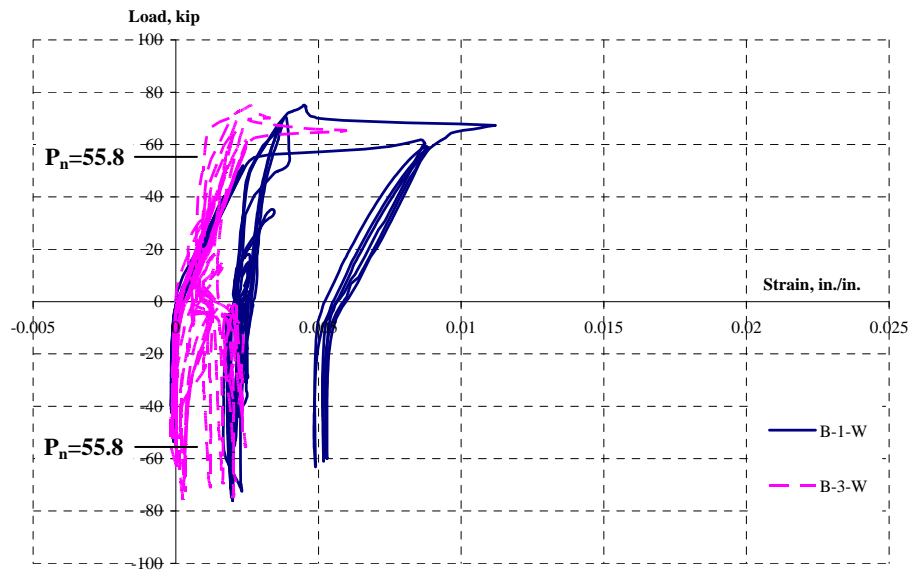
Figure 4.71   Base bar strains, west face, 5-C-R20-C

276

4.5.7.3   CFRP Strain

The layout of strain gages on the CFRP jackets in 5-C-R20-C is shown in Figure 4.72. On the north and south face of 5-C-R20-C, six gages were installed on each face at the location where splitting cracking was expected. Gages NE-B, M and T and NW-B, M and T were installed at location where splitting cracking was expected on the north face, and gages SE-B, M and T and SW-B, M and T were installed at location where splitting cracking was expected on the south face. Strain in CFRP jackets were measured at three levels on the north and south face (B: bottom, M: middle and T: top). Strain gages were also installed at the bottom corners on the south face to observe strain transition around the corners (SE-C and SW-C). Two strain gages were installed on the east (E-B and E-T) and west (W-B and W-T) face in the CFRP jackets. These strain gages were able to install only at the limited locations in the CFRP jackets because of the fan-portion of the CFRP anchors.

In this section, measured strains on the south face and at the corners of 5-C-R20-C are provided. Additional strain data are shown in Appendix C.

Strain vs lateral load for strain gages at the location of expected splitting cracking is shown in Figure 4.73 and Figure 4.74. The maximum measured strain was between 0.0020 and 0.0040 (20~ 40 % of ultimate tensile strain of the CFRP) on the south-east side and between 0.0025 and 0.0040 (25 ~ 40 % of ultimate tensile strain of the CFRP) on the south-west side. In the south-west side, the highest strain was observed in the gage closest to the footing which was the bottom gage (SW-B) while the highest strain was observed in the top gage in the south-east side (SE-T).

Strain vs lateral load for strain gages at the corners of 5-C-R20-C is shown in Figure 4.75 and Figure 4.76. From the data of the distribution of CFRP strains at the corners, a smooth transition of strains was observed around the corner. The measured strain in the gage at the corner on the east face (E-B) was close to that at the corner on the south face (SE-B). The measured strain at the arc of the south-west corner (SW-C)

277

showed a similar response as the strain at the corner on the west (W-B) and south (SW-B) faces.
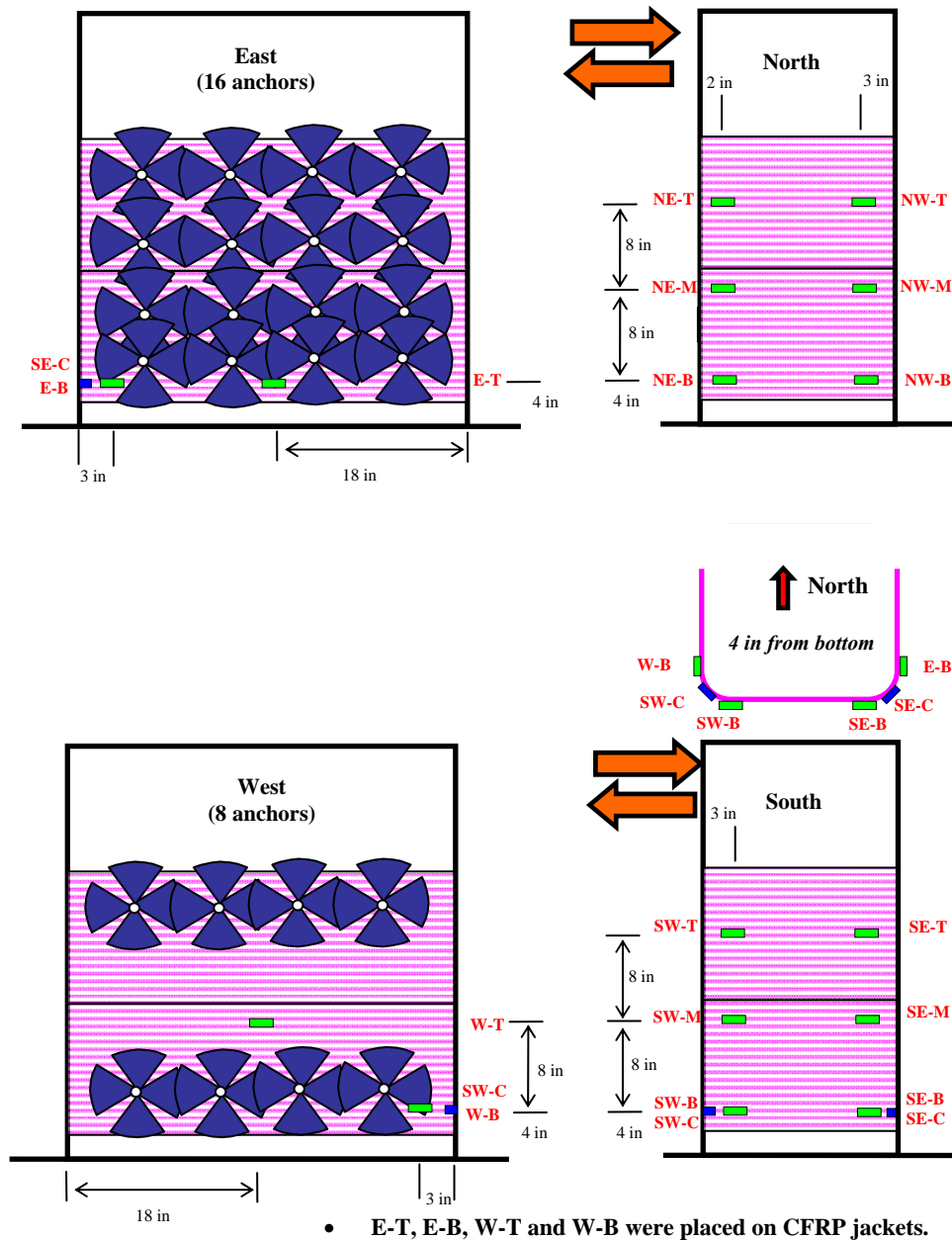
Figure 4.72   Layout of CFRP strain gages, 5-C-R20-C
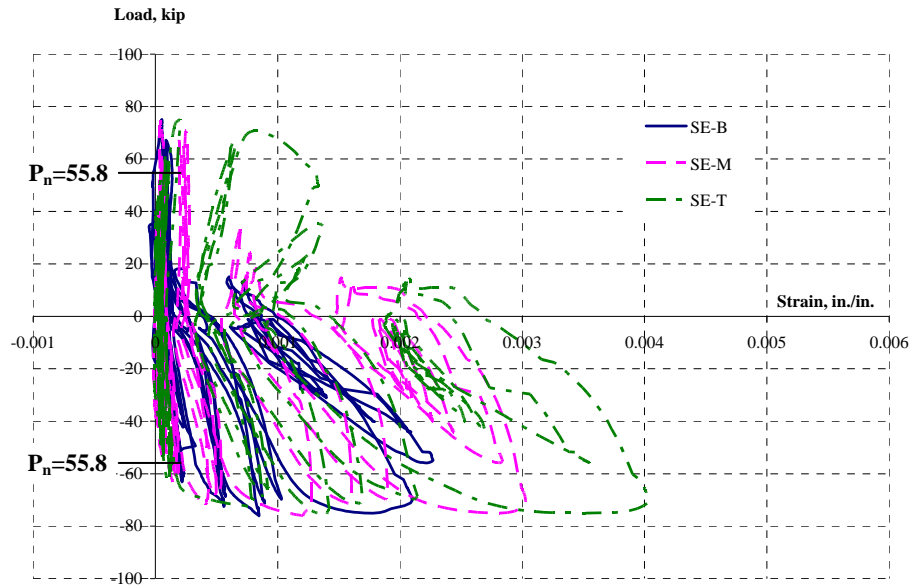
Figure 4.73   CFRP strains at location of splitting cracking, south-east, 5-C-R20-C
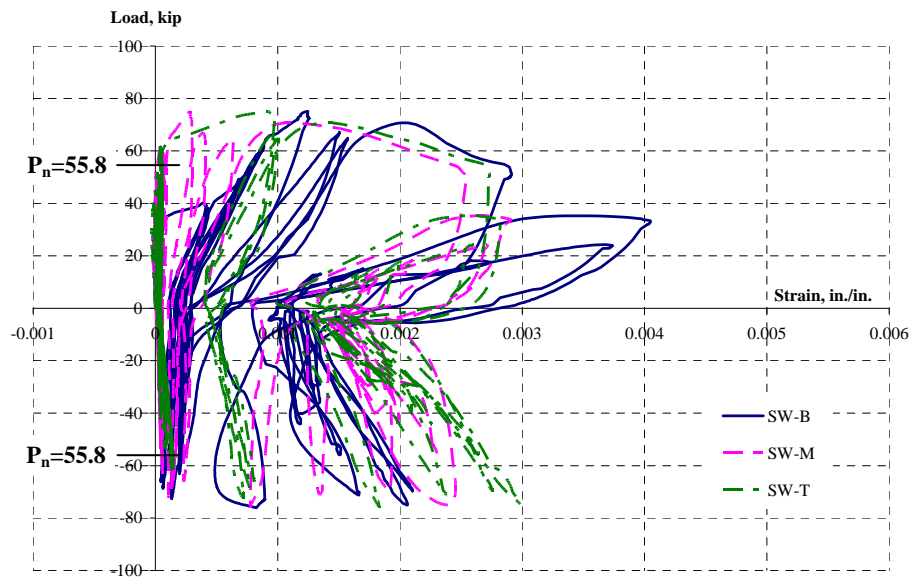
Figure 4.74   CFRP strains at location of splitting cracking, south-west, 5-C-R20-C

279
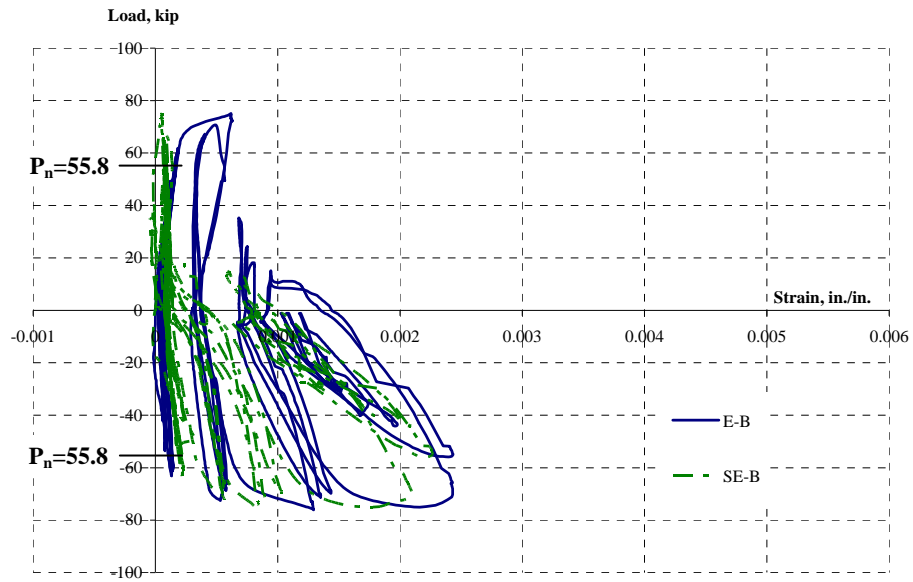
Figure 4.75   CFRP strains at south-east corner, 5-C-R20-C
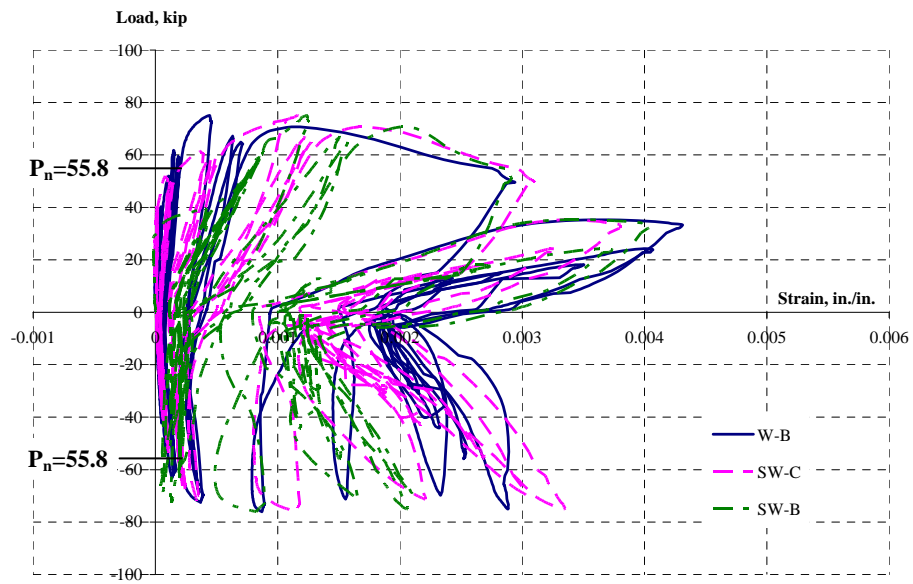
Figure 4.76   CFRP strains at south-west corner, 5-C-R20-C

280

Table 4.9   Summary of test results, 5-C-R20-C

Face	Effective width of CFRP jackets	No. of CFRP anchors	Effective width of CFRP anchors	Total effective width of CFRP	Measured peak strength (Max. Load) P/P_n	Drift ratio at measured peak strength	Strain in CFRP jackets at location of splice cracking expected
West (Undamaged)	48 in.	8	56 in.	104 in.	1.35	2.4 %	0.0025 ~ 0.0040
East (Undamaged)	48 in.	16	56 in.	104 in.	1.36	3.6 %	0.0020 ~ 0.0040

Computed: Nominal Strength (P_n): 55.8 kip; Yield strength: 60.3 kip; Ultimate Strength: 95.5 kip

4.5.8   Comparison of the East and West Sides of 5-C-R20-C

Effect of Number of CFRP Anchors

Sixteen CFRP anchors were used on the east and 8 on the west faces of 5-C-R20-C. The width of sheet used in a CFRP anchor on the east and west face was 3.5 in. and 7 in. so the total width of CFRP used in the anchors maintained the same, 56 in. Neither of the faces was damaged before rehabilitation so the only difference between the east and west face of 5-C-R20-C was the number of CFRP anchors. The layout of CFRP anchors in 5-C-R20-C is shown in Figure 4.23. Envelope of the cyclic response of 5-C-R20-C is shown in Figure 4.77. During the cyclic loading test, improvement of strength on both faces was similar (Figure 4.78). The east and west face of 5-C-R20-C reached about 135 % of the nominal strength. However, the east face of 5-C-R20-C (16 anchors) showed more deformation capacity than the west face (8 anchors). The draft ratio corresponding to the calculated yield strength was 4.8 % on the east face and 3.3 % on the west face (Figure 4.78). In addition, the east face showed rapid degradation cyclic loading to 4.8 % drift while the west face showed degradation cyclic loading to 3.6 % drift.

281

This test results indicate that the number of CFRP anchors does not effect the strength of a column rehabilitated by CFRP jackets and anchors but does influence the deformation capacity.
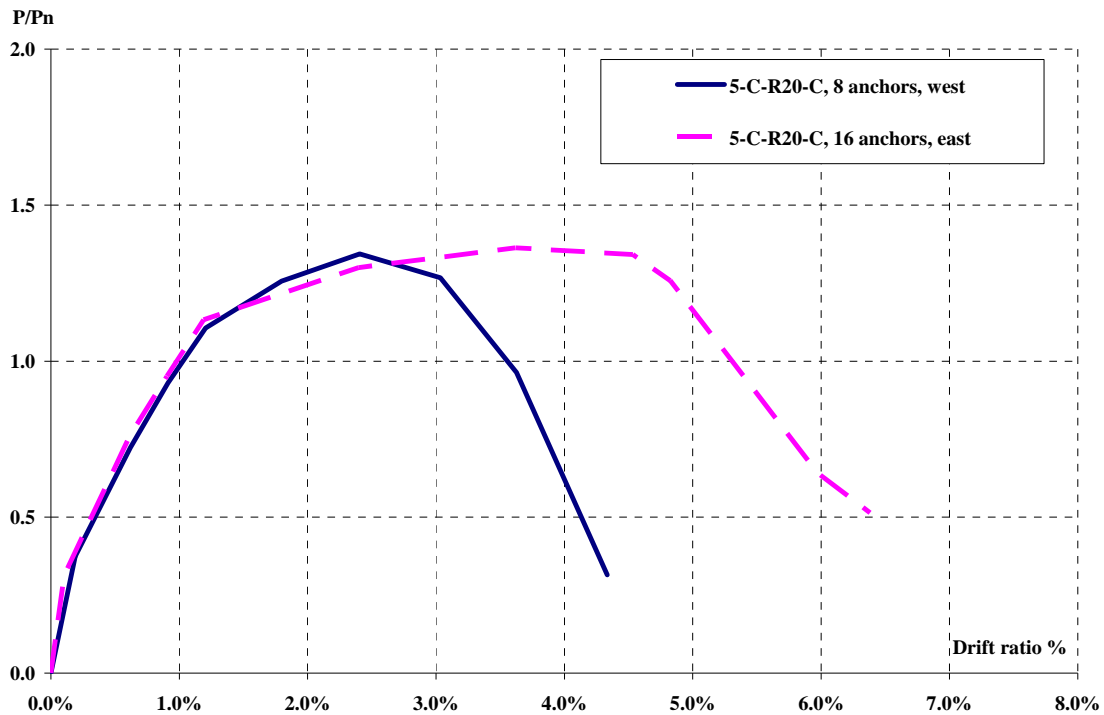
Figure 4.77   Envelope of cyclic response, 5-C-R20-C

4.5.9   Comparison of 4-C-R20-M and 5-C-R20-C

Monotonic Loading VS Cyclic Loading

The geometry of CFRP jackets and anchors in 4-C-R20-M and 5-C-R20-C was identical but 4-C-R20-M was tested under the monotonic loading while 5-C-R20-C was tested under cyclic loading. The east side of 4-C-R20-M was damaged before applying CFRP while 5-C-R20-C was undamaged.

As indicated by the responses plotted in Figure 4.78, 4-C-R20-M and 5-C-R20-C showed a similar response up to 2.5 % drift ratio while the east side of 4-C-R20-M

showed less strength than that of 5-C-R20-C because of damage before rehabilitation. After reaching 2.5 % drift ratio, 4-C-R20-M and 5-C-R20-C showed different responses due to different level of degradation.
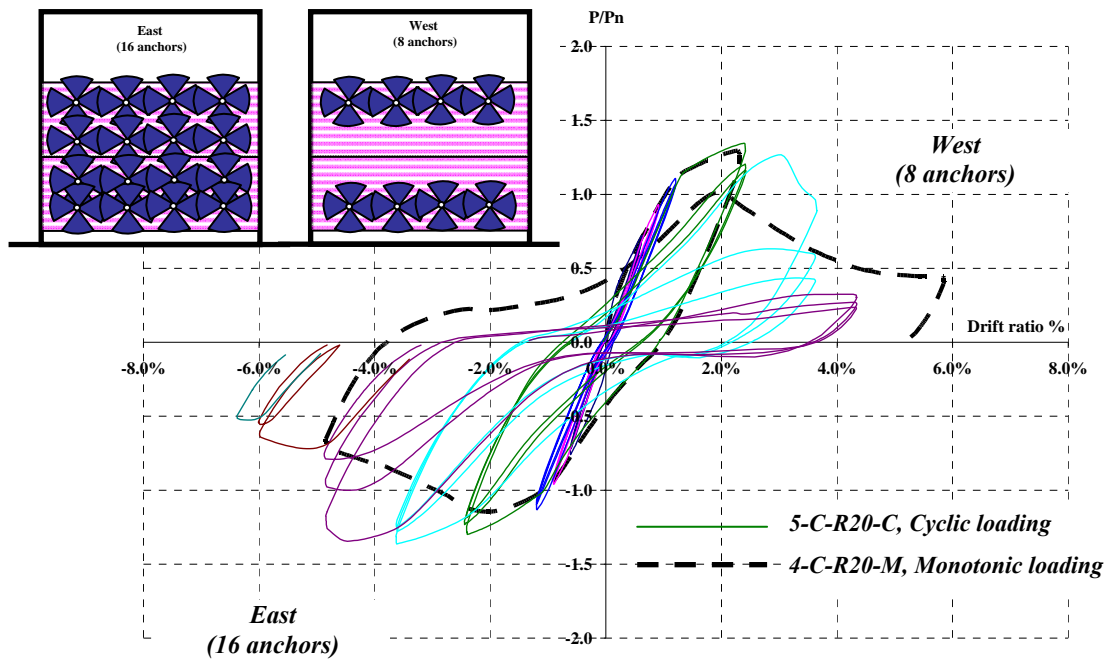
Figure 4.78   Drift ratio vs normalized lateral load, 4-C-R20-M and 5-C-R20-C

4.5.10 Comparison of 3-B-S10-M, 4-C-R20-M and 5-C-R20-C

Effect of Shape of Column Section, Square or Rectangle

Comparing the east face of 3-B-S10-M, 4-C-R20-M and 5-C-R20-C, the same width and geometry of CFRP anchors were used on one face of the column. However, the strength and deformation capacity in 4-C-R20-M and 5-C-R20-C (rectangular column) improved less than in 3-B-S10-M (square column). Eight spliced bars out of 10 spliced bars were away from the corners in 4-C-R20-M and 5-C-R20-C while 3 bars were away from the corners in 3-B-S10-M. The measured peak strength on the east face of 3-B-S10-M was 56 % more than the nominal capacity while that on the east face of 4-C-R20-M and 5-C-R20-C was 35% more than the nominal capacity. The longitudinal reinforcement

used in 3-B-S10-M, 4-C-R20-M, and 5-C-R20-C had the same strength but the compressive strength of concrete in 3-B-S10-M was the lowest among these 3 columns. The draft ratio corresponding to the calculated yield strength on the east face was 10.0% in 3-B-S10-M and 2.7 % and 4.8 % in 4-C-R20-M and 5-C-R20-C.

The rehabilitation method using CFRP jackets and anchors was not as effective as in the rectangular column (8 splice bars were away from the corners) as in the square columns (3 splice bars were away from the corners) because CFRP jackets did not confine lap splices of longitudinal bars away from the corner as effectively. However, considerable increase of strength and deformation capacity was still observed in the rehabilitated rectangular column compared to that before rehabilitation.

4.5.11 6-C-R20-C

A summary of the test results of 6-C-R20-C is shown in Table 4.10 in the end of this section.

4.5.11.1 Drift Ratio VS Normalized Lateral Load

Figure 4.79 shows drift ratio vs normalized lateral load response of 6-C-R20-C after rehabilitation. 6-C-R20-C was not damaged before rehabilitation. In Figure 4.79, the drift ratio vs normalized lateral load response of 4-C-R20-M as-built was provided as a reference. The actual yield strength (P/P_n = 1.08) and ultimate strength (P/P_n = 1.72) based on measured strength of the concrete and reinforcement are also provided. The measured compressive strength of the concrete was 5,400 psi and the measured yield and ultimate strength of the reinforcement were 63 ksi and 106 ksi.

Improvement of strength and deformation capacity was observed in 6-C-R20-C after rehabilitation with CFRP under cyclic loading on the east (16 anchors) and west (20 anchors) faces of 6-C-R20-C. The strength increased by 42 % for the east face and by 44 % for the west face after rehabilitation compared with the as-built strength of 4-C-R20-M. The drift ratio of 4-C-R20-M as-built was 1.1 % at the maximum load. The drift ratio corresponding to the peak strength was 3.6 % for the east face and 2.4 % for the west face after rehabilitation.

Both the east and west faces of 5-C-R20-C showed rapid degrading under cyclic loading to 3.6% drift.

The final failure mode of 6-C-R20-C was a splice failure after yield of the spliced longitudinal bars was reached (Figure 4.80). Ductility of the column was developed before failure. Splice cracks were observed in the column section after cutting the column from the footing. The use of the CFRP jackets and anchors effectively confined lap splices.

285

East
(16 anchors)

West
(20 anchors)

P/Pn

- - - - - *4-C-R20-M, as-built*

1.72 ———————————————— *Ultimate*

1.08 ———————————————— *Yield*

20 anchors, west

Drift ratio %

-8.0% -6.0% -4.0% -2.0% 0.0% 2.0% 4.0% 6.0% 8.0%

16 anchors, east

Splice failure

Yield

Ultimate

Pₙ=Mₙ/108"=55.8 kip
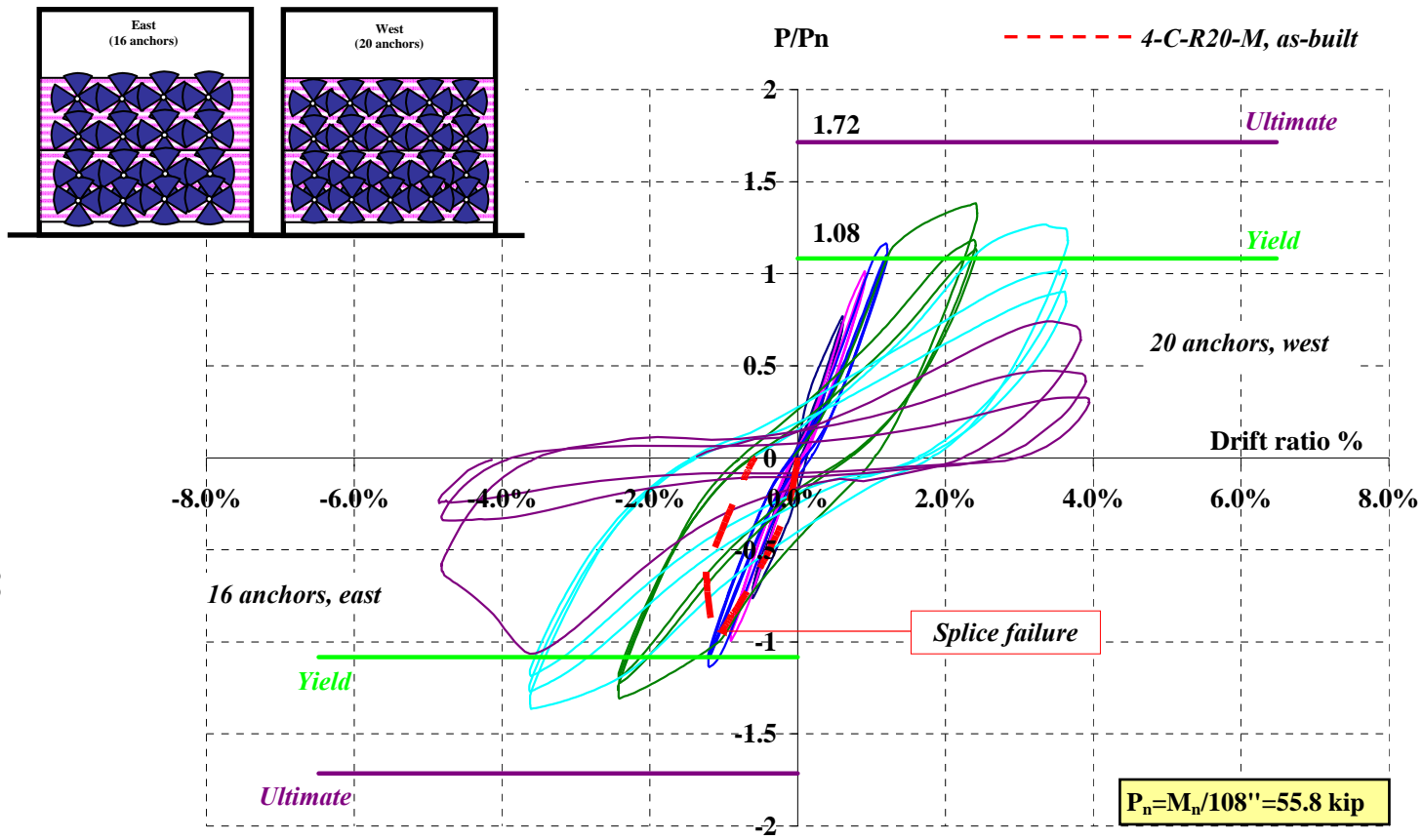
Figure 4.79   Drift ratio vs normalized lateral load, 6-C-R20-C
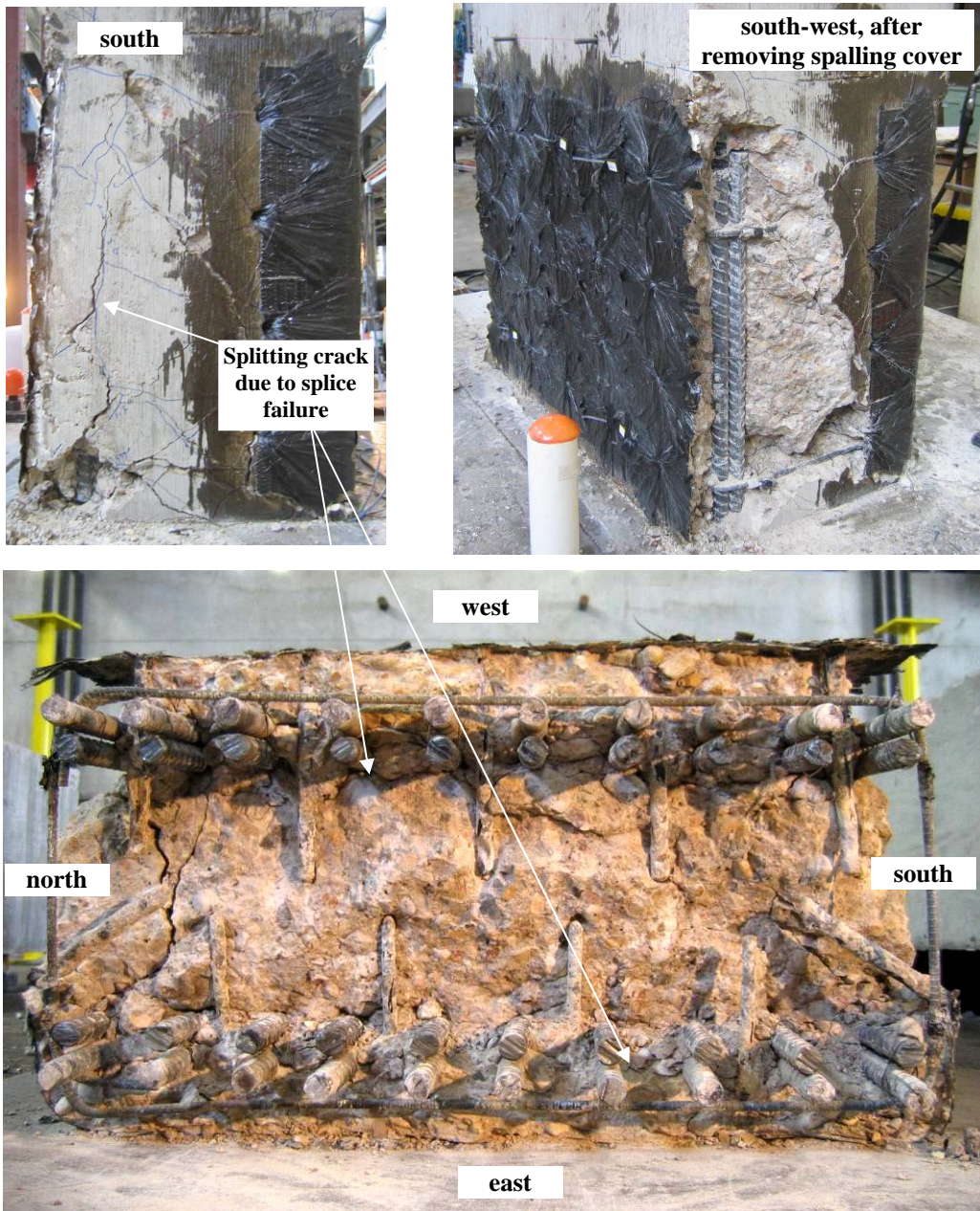
Figure 4.80   Splice failure of 6-C-R20-C

4.5.11.2 Steel Reinforcement Strain

Layout of steel reinforcement strain gages in 6-C-R20-C is shown in Figure 4.81.

4.5.11.2.1   Base Bar Strain

Base bar strains of 6-C-R20-C under cyclic loading are shown in Figure 4.82 and Figure 4.83.   The bars on the east face (16 anchors) of 6-C-R20-C were initially in compression while the bars on the west face (20 anchors) were in tension. All the bars yielded during tension loading. The bars on both faces developed inelastic strain, and this result agreed with the drift ratio vs normalized lateral load response.
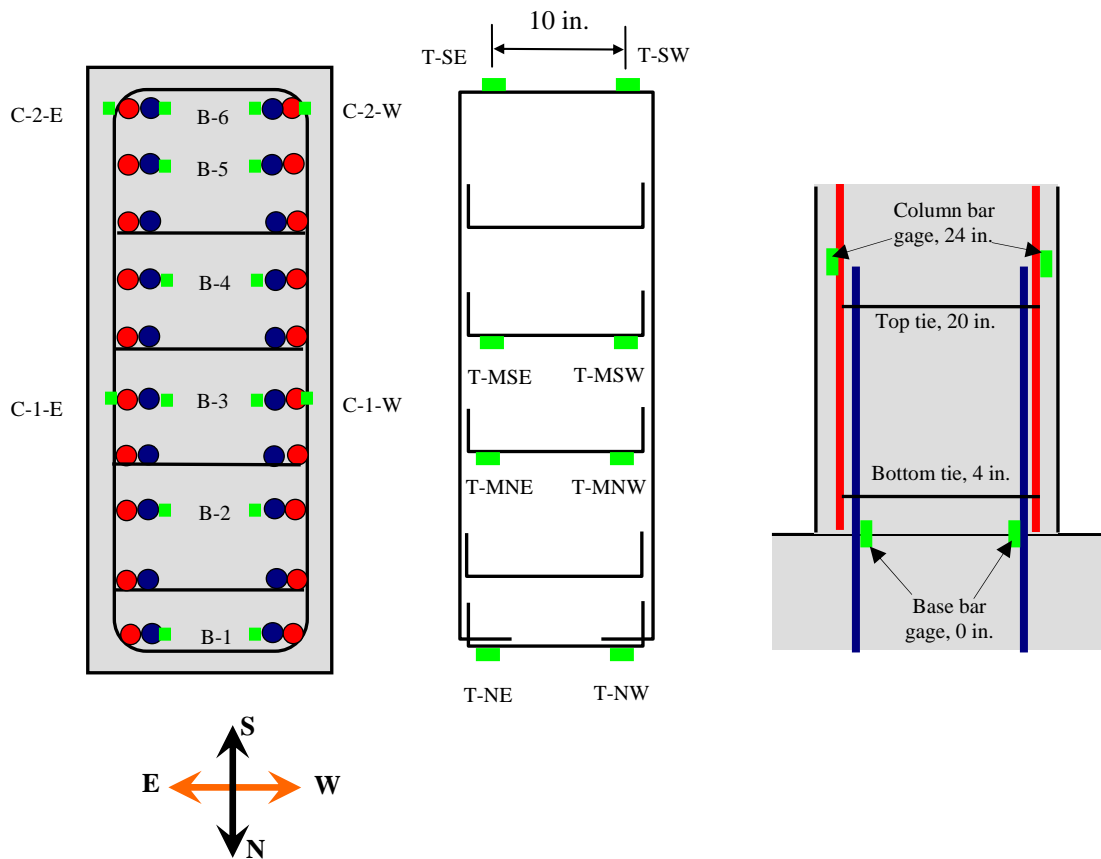
C-2-E   B-6   C-2-W
B-5
C-1-E   B-4
C-1-W   B-3
B-2
B-1

S
E ⟷ W
N

10 in.
T-SE   T-SW

T-MSE   T-MSW
T-MNE   T-MNW

T-NE   T-NW

Column bar gage, 24 in.
Top tie, 20 in.
Bottom tie, 4 in.
Base bar gage, 0 in.

- **Base bar gages (B - # - Direction):** at the top of the footing
- **Column bar gages (C - # - Direction):** 24 in. from the top of the footing
- **Tie bar gages (T-Top or Bottom- Direction):**

   Top-tie at 20 in. from the top of the footing

   Bottom- tie at 4 in. from the top of the footing

Figure 4.81   Layout of steel reinforcement strain gages, 6-C-R20-C

289
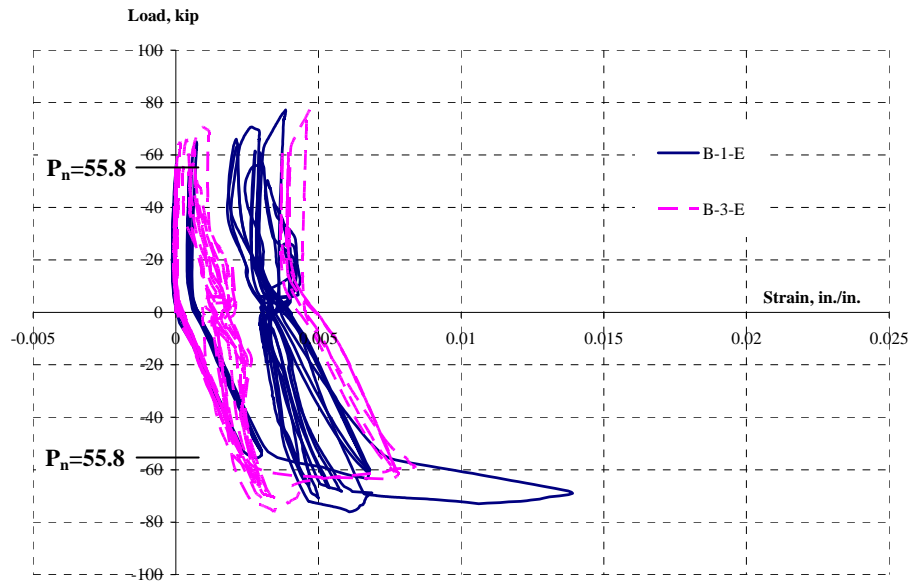
Figure 4.82   Base bar strains, east face, 6-C-R20-C
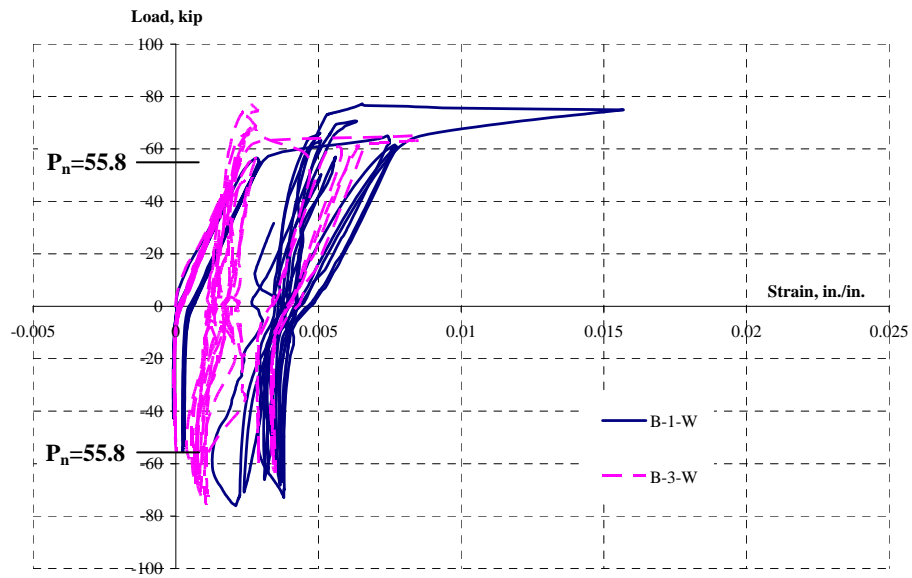
Figure 4.83   Base bar strains, west face, 6-C-R20-C

290

4.5.11.3 CFRP Strain

The layout of strain gages on the CFRP jackets in 6-C-R20-C is shown in Figure 4.84. On the north and south face of 6-C-R20-C, no strain gage was installed because the fan portion of the CFRP anchors covered the CFRP jackets. Five gages were installed on the east face and four gages were installed on the west face in the CFRP jackets. Strain gages were also installed at the north-east corner to observe strain transition around corners (EN-B and EN-C).

In this section, measured strains on the east and west face and at the corners of 6-C-R20-C are provided. Additional strain gage data installed in the east and west faces are shown in Appendix C.

Strain vs lateral load for strain gages on the east and west face is shown in Figure 4.85 and Figure 4.86. The maximum measured strain was between 0.0010 and 0.0025 (10~ 25 % of ultimate tensile strain of the CFRP) on the east side and between 0.0010 and 0.0015 (10 ~ 15 % of ultimate tensile strain of the CFRP) on the west face.

Strain vs lateral load for strain gages at the corners of 6-C-R20-C is shown in Figure 4.87. From the CFRP strains at the corners, a smooth transition of strains was observed. The measured strain at the arc of the north-east corner (EN-C) showed a similar response as the strain at the corner on the east face (EN-B). However, the maximum measured strain of CFRP jacket at the corner of 6-C-R20-C was smaller than that of 5-C-R20-C.

East
(16 anchors)

3 in

E-T

3 in

ES-T

EN-T

ES-B

EN-B
EN-C

16 in

4 in

18 in

North

6 in

EN-C

West
(20 anchors)

W-T   WS-T

WN-B

WS-B

18 in

5 in

7 in   7 in   9 in

South
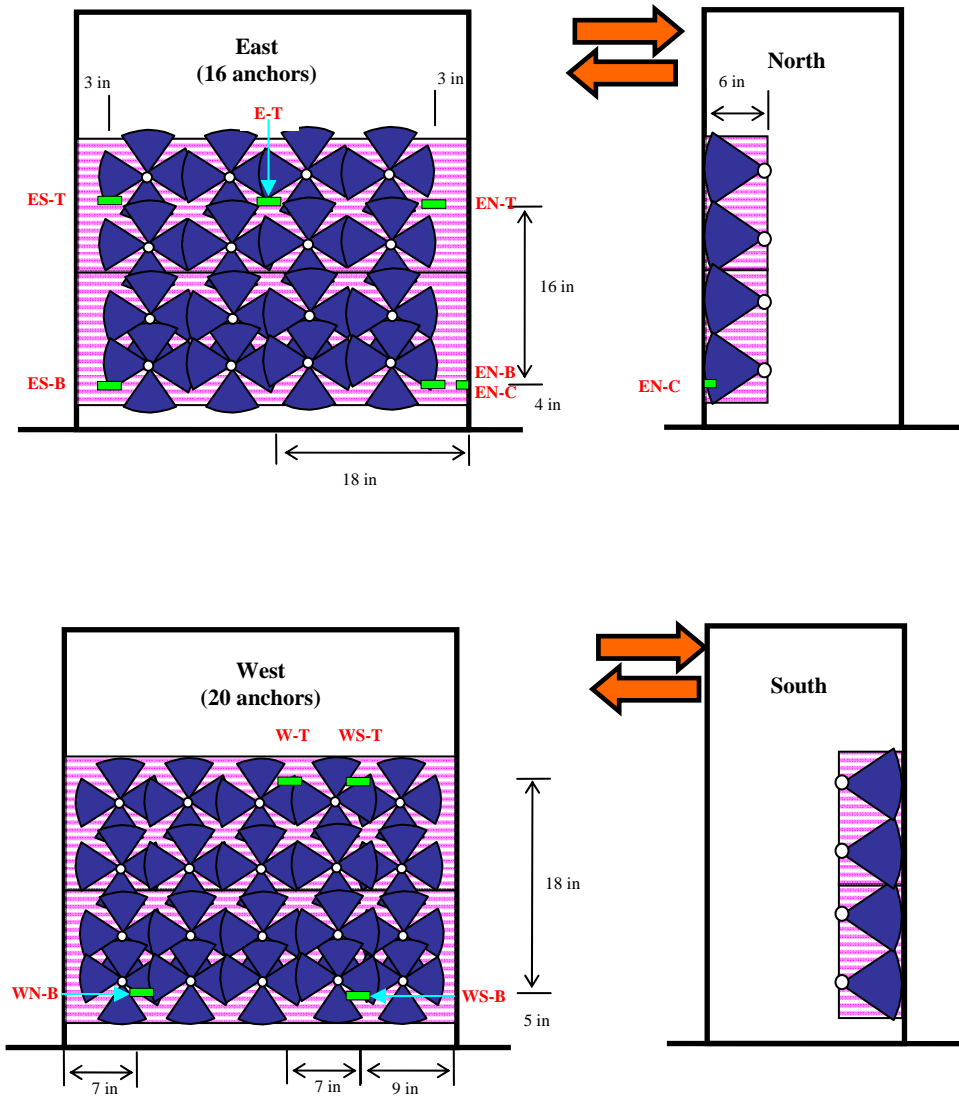
- **All gages were placed on CFRP jackets.**

Figure 4.84   Layout of CFRP strain gages, 6-C-R20-C
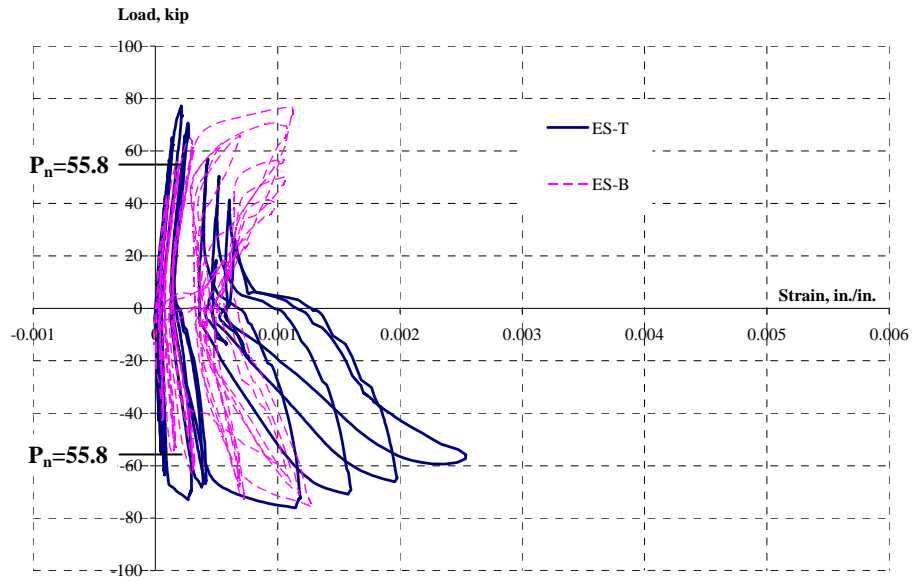
Figure 4.85   CFRP strains, east face, 6-C-R20-C
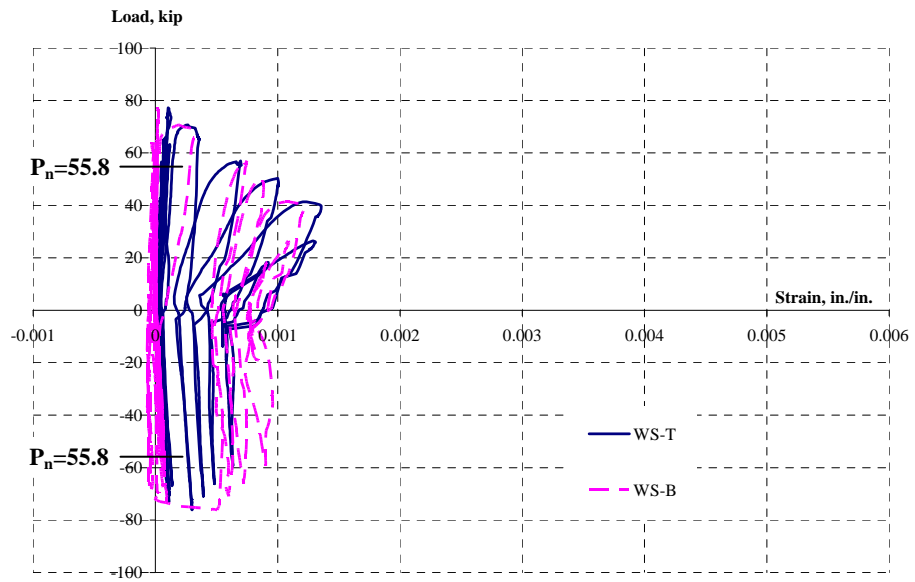
Figure 4.86   CFRP strains, west face, 6-C-R20-C

293
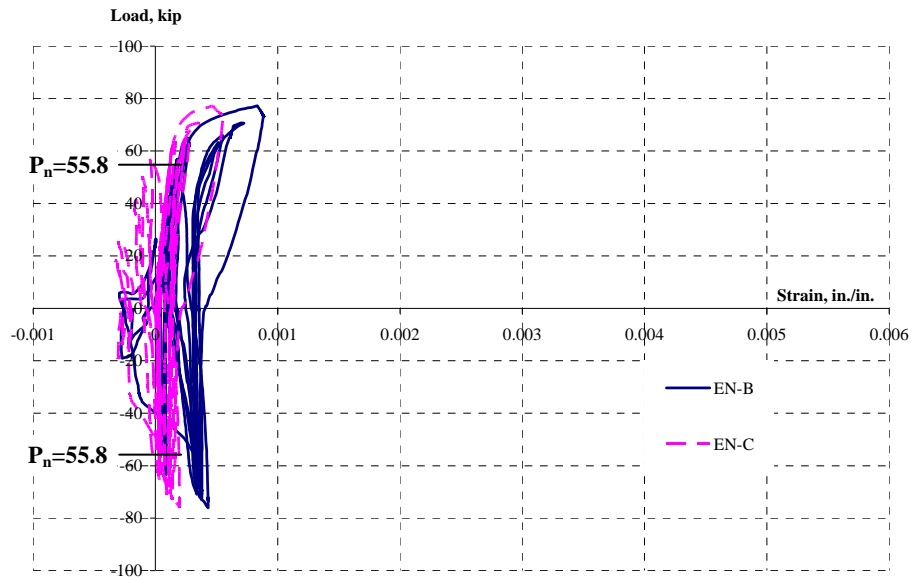
Figure 4.87   CFRP strains at north-east corner, 6-C-R20-C

Table 4.10   Summary of test results, 6-C-R20-C

Face	Effective width of CFRP jackets	No. of CFRP anchors	Effective width of CFRP anchors	Total effective width of CFRP	Measured peak strength (Max. Load) P/P_n	Drift ratio at measured peak strength	Strain in CFRP jackets at location of splice cracking expected
West (Undamaged)		20	104 in.	104 in.	1.38	2.4 %	
East (Undamaged)	48 in.	16	56 in.	104 in.	1.36	3.6 %	

Computed: Nominal Strength (P_n): 55.8 kip; Yield strength: 60.4 kip; Ultimate Strength: 95.7 kip

4.5.12 Comparison of 5-C-R20-C and 6-C-R20-C

Performance of a Column with Walls after CFRP Rehabilitation

In 6-C-R20-C, 16 CFRP anchors with the partial CFRP jackets were used on the east face, and 20 CFRP anchors without a CFRP jacket were used on the west face. The total width of CFRP across the plane of splitting cracking was the same (104 in. width). The layout of CFRP in 6-C-R20-C is shown in Figure 4.25.

The rehabilitation method of 6-C-R20-C was comparable to that of the east face of 5-C-R20-C. 5-C-R20-C and 6-C-R20-C were tested under cyclic loading and had the same total width of CFRP across the pane of splitting cracking. The number of CFRP anchors (4) in each column of anchors in 6-C-R20-C was also the same as that on the east face of 5-C-R20-C. Envelopes of the cyclic response of both faces of 6-C-R20-C and the east face of 5-C-R20-C are shown in Figure 4.88.

The strength of both faces of 6-C-R20-C was similar to the east face of 5-C-R20-C but the east face of 5-C-R20-C showed more deformation capacity than 6-C-R20-C. The measured peak strength of the east and west face of 6-C-R20-C was 36 % and 38% more than the nominal strength while that of the east face of 5-C-R20-C was 36%. The draft ratio corresponding to the calculated yield strength on the east and west face of 6-C-R20-C was 3.6 % while that on the east face of 5-C-R20-C was 4.8% (Figure 4.78 and Figure 4.79).

The rehabilitation methods using CFRP anchors with partial CFRP jackets or without CFRP jackets was as effective as the rehabilitation method using CFRP anchors with fully wrapped CFRP jackets in improving strength. However, they were less effective in improving deformation capacity.

In addition, drift ratio at the measured peak strength on the east face of 6-C-R20-C was 3.6% while that on the west face was 2.4 %. Therefore, the rehabilitation method using the partial CFRP jackets may be a more efficient use of CFRP than that using no CFRP jackets.

295
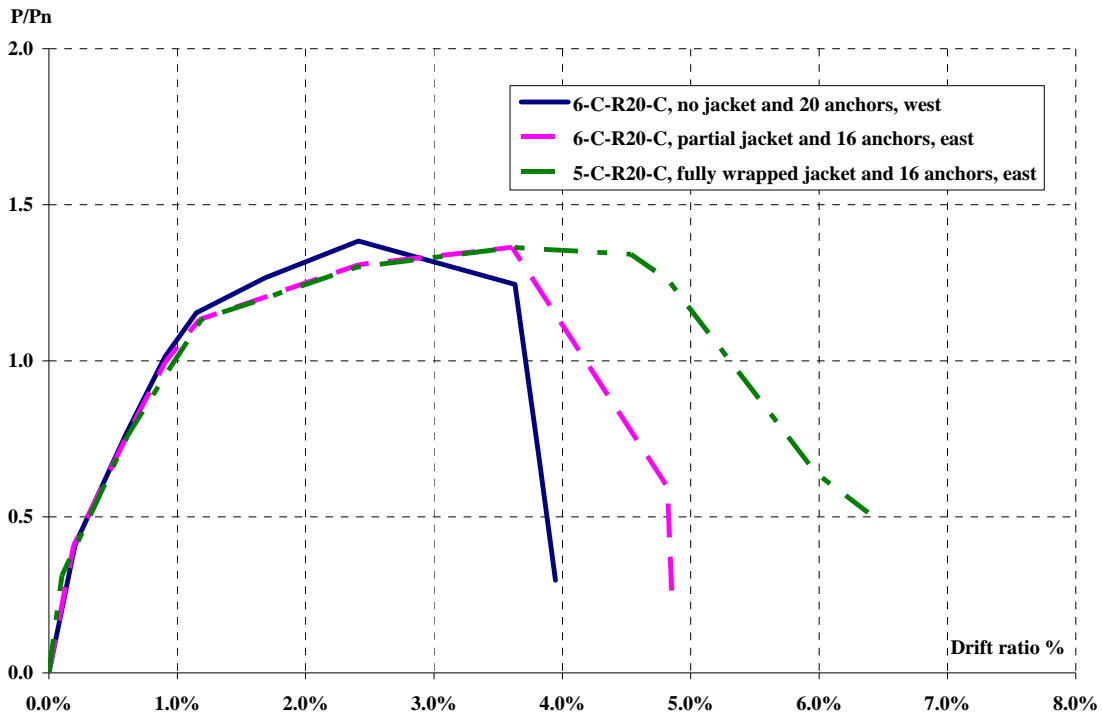
Figure 4.88   Envelope of cyclic response, 5-C-R20-C and 6-C-R20-C

4.5.13 Comparison of Rehabilitations Using CFRP and Steel

The rehabilitation using CFRP jackets and anchors is comparable to the rehabilitation using steel jackets and adhesive anchor bolts. Two columns, one square and one rectangular column, were selected from the study of Aboutaha (1994) to compare the effectiveness of the rehabilitation using CFRP and steel.

Square column FC 17 was identical to the Type A (1-A-S8-M and 2-A-S8-M) column in this study. FC 17 was strengthened as-built using a steel jacket only on the west face and a steel jacket and anchor bolts on the east face (Figure 4.89). FC 17 was tested under cyclic loading and an envelope of the cyclic response of FC 17 was used for comparison with the response of 1-A-S8-M and 2-A-S8-M which were tested under

monotonic loading. The lateral load was normalized using the computed nominal strength of FC 17. The nominal strength was calculated using the design strength of concrete (4,000 psi) and steel (60 ksi).

The rehabilitation on the west face of FC 17 was comparable to that of 1-A-S8-M because only jackets were used in these columns without anchor bolts or CFRP anchors. The envelope of the cyclic response on the west face of FC 17 is plotted with the monotonic response of the undamaged face (west) of 1-A-S8-M in Figure 4.90. The strength of the west face of FC 17 was similar to the undamaged face of 1-A-S8-M, but the west face of FC 17 showed more deformation capacity than the undamaged face of 1-A-S8-M without strength degradation. However, the difference in the deformation capacity may be influenced by the width of the jackets. While the width of the CFRP jacket was 24 in., which was the same as the splice length, the width of the steel jackets was 34.5 in.

The rehabilitation on the east face of FC 17 was comparable to that of 2-A-S8-M because a combination of steel jackets and anchor bolts and a combination of CFRP jackets and anchors were used in these columns. The envelope of the cyclic response on the east face of FC 17 is plotted with the monotonic response of the undamaged face (west) of 2-A-S8-M in Figure 4.91. The strength of the east face of FC 17 was similar to the undamaged face of 2-A-S8-M, but the undamaged face of 2-A-S8-M showed more deformation capacity than the east face of FC 17 without strength degradation. A larger number of CFRP anchors (4 anchors) were used on the undamaged face of 2-A-S8-M than the number of anchor bolts on the east face of FC 17 (2 anchor bolts).
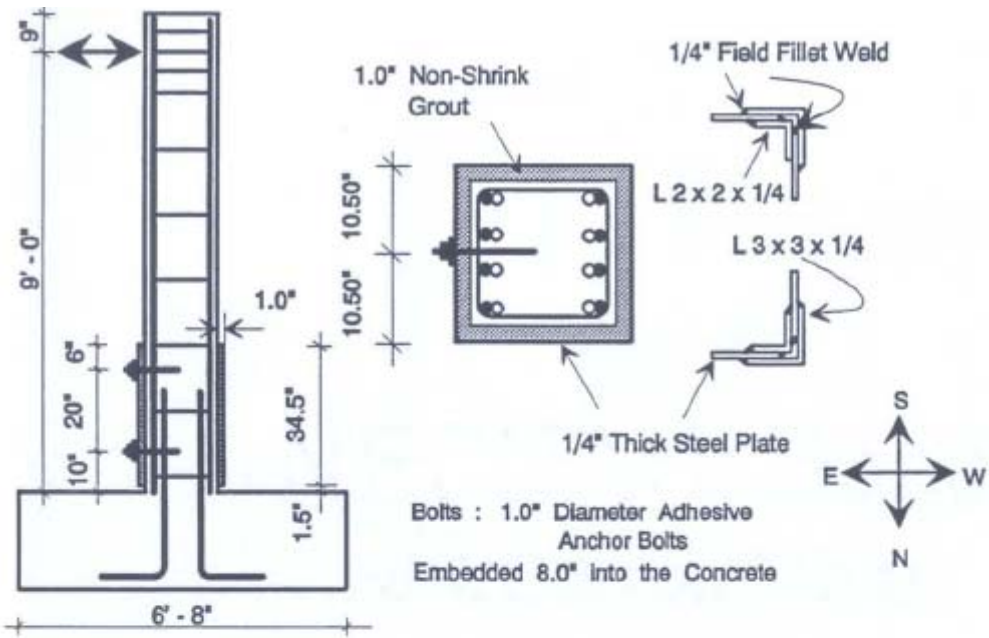
(a) Details of Column FC17
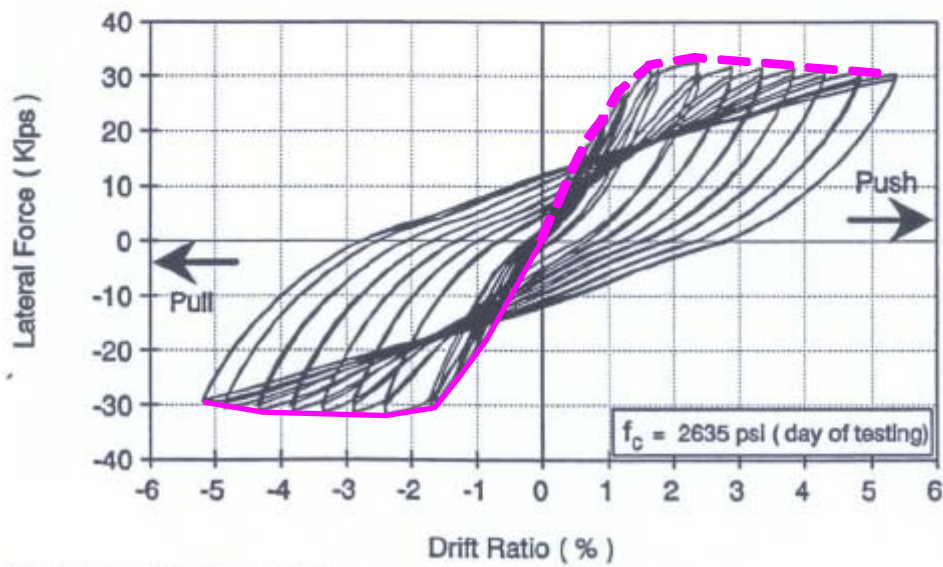
(b) Hysteretic Response

Figure 4.89   Square column with steel jackets and anchor bolts,
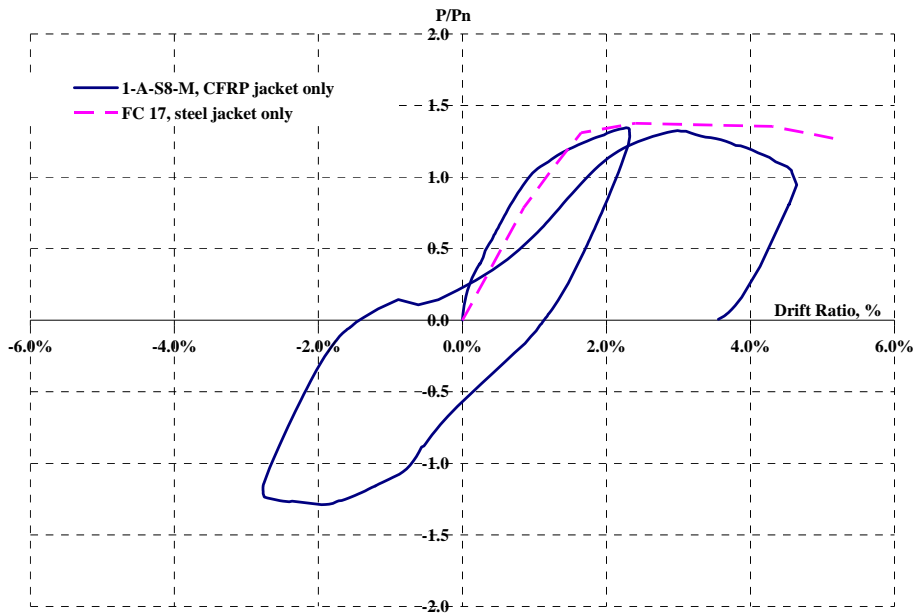*FC 17, (Aboutaha, 1994)*

298

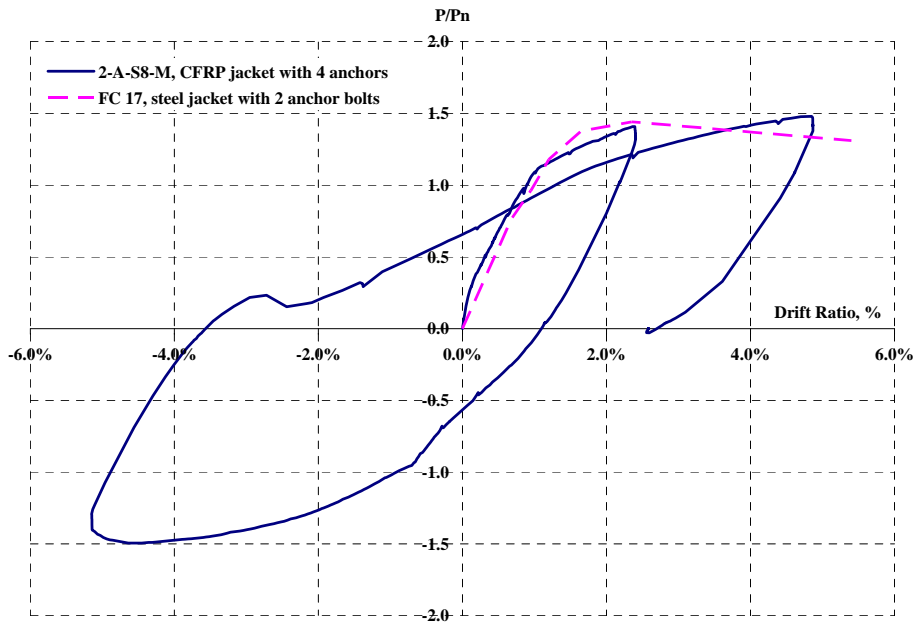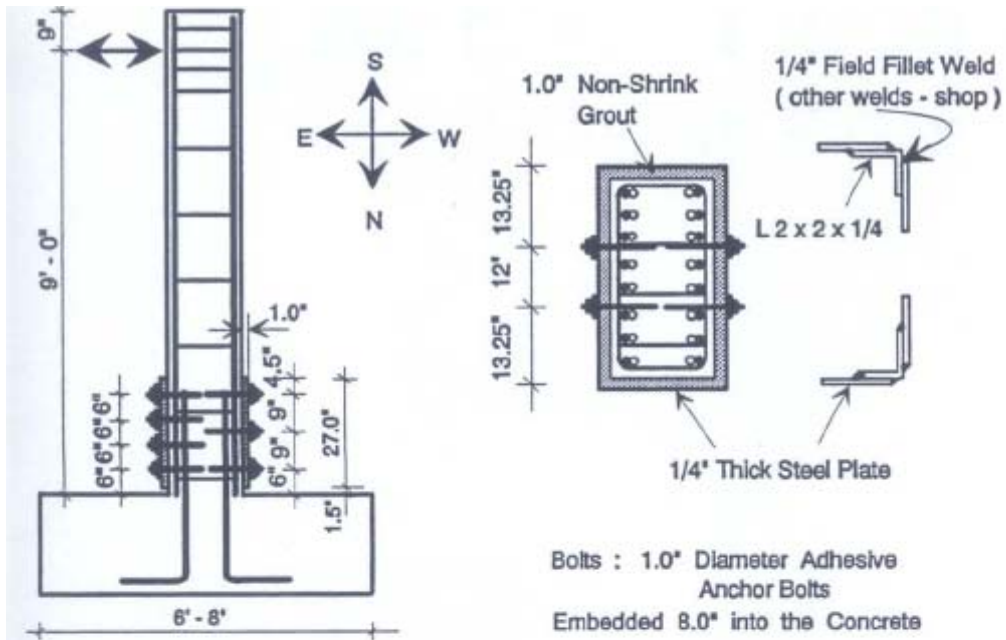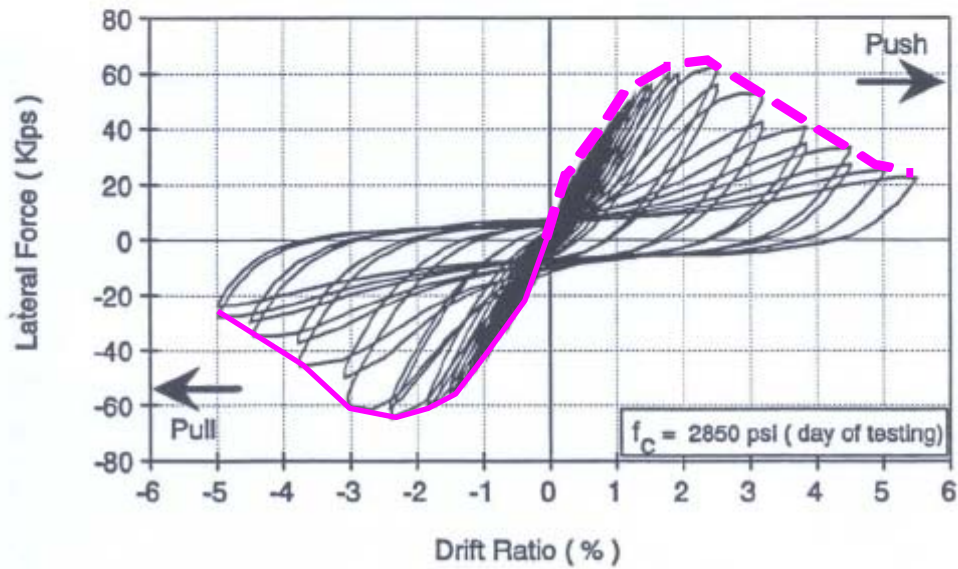***Figure 4.90   Comparison of CFRP and steel jackets in square columns***

Figure 4.91   Comparison of CFRP jackets with anchors and steel jackets with anchor bolts in square columns

In Figure 4.92, the rehabilitation of a rectangular column FC 11 using steel jackets and anchor bolts is shown. Dimensions of FC 11 were identical to 5-C-R20-C although the number of lap splices in FC 11 was 16 while 20 bars are spliced in 5-C-R20-C. FC 11 was strengthened as-built using steel jackets with 6 anchor bolts on the west face and with 8 anchor bolts on the east face. 5-C-R20-C was also strengthened as-built using CFRP jackets with 8 anchors on the west face and with 16 anchors on the east face. The width of the jackets in theses columns was similar (steel jacket: 27 in.; CFRP jacket: 24 in.). Both FC 11 and 5-C-R20-C were tested under cyclic loading and envelopes of the cyclic response were used to compare the two columns (Figure 4.93). The lateral load was normalized using the computed nominal strength of the columns. The nominal strength was calculated using the design strength of concrete (4,000 psi) and steel (60 ksi).

Envelopes of the cyclic response on each face of two columns are shown in Figure 4.93. The effect of the number of anchor bolts or CFRP anchors were evaluated using these columns. The strength of both faces of FC 11 and 5-C-R20-C was similar, but the east face of 5-C-R20-C (16 anchors) showed more deformation capacity than both faces of FC 11 and the west face of 5-C-R20-C without degrading of the strength. The west face of 5-C-R20-C (8 anchors) exhibited a response similar to that of both faces of FC 11 until a drift ratio of about 3.5 % was reached. At that drift, the splices were still carrying a force equal to their nominal capacity. At larger drift, there was a rapid strength degradation of the west face of 5-C-R20-C compared with FC 11. The number of anchor bolts had little influence on the behavior of FC 11.

(a) Details of Column FC11

(b) Hysteretic Response

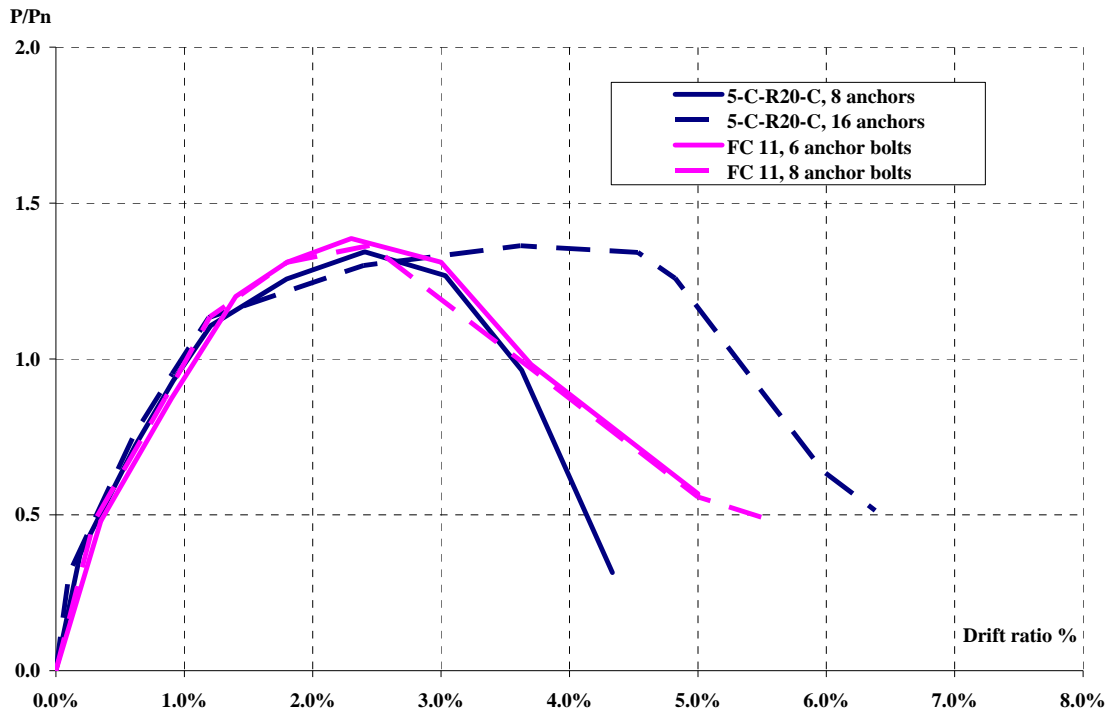*Figure 4.92   Rectangular column with steel jackets and anchor bolts,*
FC 11 (Aboutaha, 1994)

301

Figure 4.93 ***Comparison of CFRP jackets with anchors and steel jackets with anchor bolts in rectangular columns***

For both a square and a rectangular column, rehabilitation using the CFRP jackets and anchors was as effective as that using the steel jackets and anchor bolts. A similar level of strength improvement was achieved in the rehabilitated columns. However, deformation capacity depended on the rehabilitation details. Larger deformation capacity was achieved using CFRP than steel jackets but a larger number of the CFRP anchors were required than steel anchor bolts. When CFRP or steel jackets were used without CFRP anchors or steel bolts, a column with steel jackets maintained strength over a larger deformation range than a column with the CFRP jackets.

4.6   SUMMARY OF BEHAVIOR

A summary of the column test results is shown in Table 4.11. The nominal strength (P_n) was calculated using the design strength of concrete (4,000 psi) and steel (60 ksi). The calculated yield strength was based on measured strength of the concrete and reinforcement. The actual compressive strength of concrete is provided in Table 4.1 and the tensile strength of longitudinal reinforcement is provided in Section 4.2.1. The measured peak strength is the normalized value of the maximum applied lateral load using the nominal capacity of the column. Drift ratio at the measured peak strength and drift ratio at the calculated yield strength were also provided in Table 4.11. The drift ratio at the calculated yield strength is a drift corresponding to a measured load which is equal to the calculated yield load during the reduction of strength after the peak strength was reached. This drift is presented if it is within the stroke limit of the load actuator.

A brittle splice failure occurred in all the as-built columns which were designed based on provisions of the ACI 318-63. The as-built columns exhibited little or no ductility before splice failure occurred. However, the columns rehabilitated with CFRP showed a significant increase in deformation capacity under both monotonic and cyclic loading. CFRP jackets and anchors effectively confined lap splices and changed the failure mode of square and rectangular columns from brittle splice failure to yielding of column reinforcement.

The measured peak strength of the columns increased by 13 ~ 56 % after rehabilitation with respect to the as-built strength (Figure 4.94). The measured peak strength was larger than calculated yield strength in all the columns after rehabilitation. Drift at splice failure of the as-built column was about 1 %. However, after rehabilitation, drifts of 1.9 ~ 8.6 % were reached before the columns strength began to degrade (drift at the measured peak strength, Figure 4.95) and drifts of 2.7 ~ 10.0 % were exhibited at the yield load after the column strength began to degrade (drift at the calculated yield strength, Figure 4.96). The improvement was observed for both damaged and undamaged

303

faces of the column. The test results indicate that the rehabilitation methods using CFRP jackets and anchors were effective in improving deformation capacity and strength of poorly detailed reinforced concrete columns.

Table 4.11   Summary of Test Results

Specimen	Test condition		CFRP jacket	No. of CFRP anchors	Measured peak strength (Max. Load) P/P_n	Drift at measured peak strength	Drift at calculated yield strength
1-A-S8-M	As-built				1.14[***]	1.1 %	
	Repair and strengthening	Undamaged side (West)	x		1.34	2.3 %	4.3 %
		Damaged side (East)	x		1.29	1.9 %	
2-A-S8-M	As-built				1.10[***]	1.1 %	
	Repair and strengthening	Undamaged side (West)	x	4	1.48	4.8 %	
		Damaged side (East)	x	4	1.49	4.5 %	
3-B-S10-M	As-built				1.01[***]	1.0 %	
	Repair and strengthening	Undamaged side (East)	x	8	1.56	8.6 %	10.0 %
		Damaged side[*] (West)	x	8	1.58	5.5 %	
4-C-R20-M	As-built				0.96[***]	1.1 %	
	Repair and strengthening	Undamaged side (West)	x	8	1.30	2.3 %	
		Damaged side (East)	x	16	1.15	2.1 %	2.7 %
5-C-R20-C	Strengthening	West	x	8	1.35	2.4 %	3.3 %
		East	x	16	1.36	3.6 %	4.8 %
6-C-R20-C	Strengthening	West		20	1.38	2.4 %	3.6 %
		East	x[**]	16	1.36	3.6 %	3.6 %

* East side was damaged under monotonic loading except 3-B-S10-M.

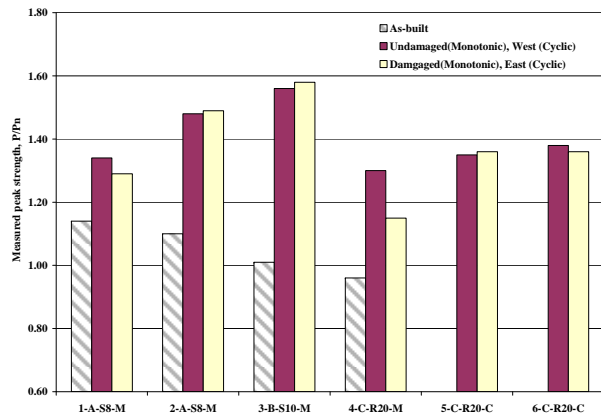******Partial jacket with anchors were used on the east side of 6-C-R20-C.

[***]Splice failure

304

Figure 4.94   Measured peak strength
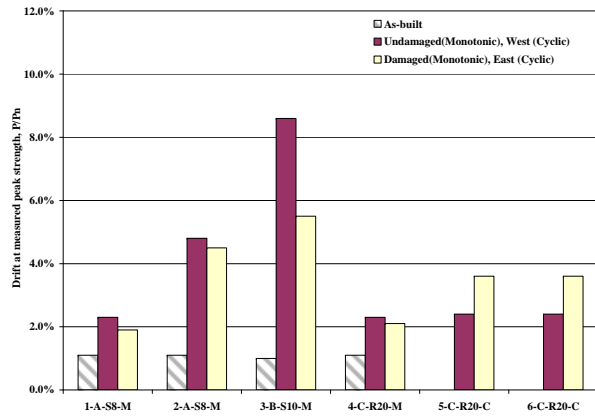

Figure 4.95   Drift ratio at measured peak strength
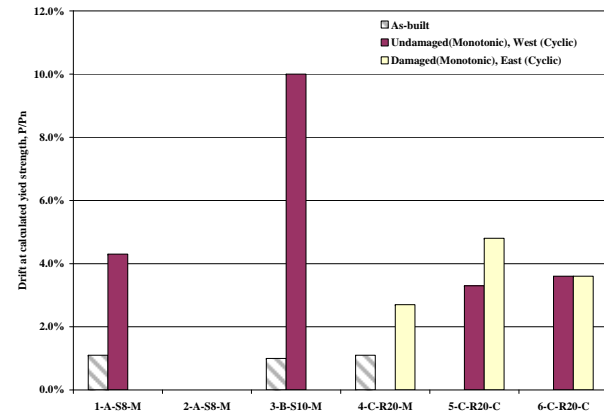

Figure 4.96   Drift ratio at calculated yield strength

Findings from the column splice tests can be summarized as follows:

1. Strength and deformation capacity improved more when the column was rehabilitated by a combination of CFRP jackets and anchors than when rehabilitated by CFRP jackets only or CFRP anchors only.

2. Rehabilitation was more effective for a square column (4 or 5 spliced bars on a face) than for a rectangular column (10 spliced bars on a face). However, rectangular columns exhibited good performance after rehabilitation.

3. The width of CFRP anchors can be calculated conservatively using shear friction.

4. A decrease in the number of CFRP anchors improved the strength of the splice if total width of CFRP material was maintained. However, deformation capacity was improved by using more anchors.

5. The rehabilitation method using partial CFRP jackets or a CFRP sheet on one face can be applied to a column with walls. Such rehabilitation improved the deformation capacity less than when using fully wrapped CFRP jackets. However, the same improvement in the strength was achieved using partial jackets.

6. The rehabilitation using CFRP jackets and anchors was as effective as that using steel jackets and adhesive anchor bolts.

CHAPTER 5

Design Guidelines

5.1 OVERVIEW

Based on the test results, design guidelines for CFRP rehabilitation for existing reinforced concrete structures with poor detailing for continuity of reinforcement subjected to extreme loads such as loss of support due to blast or impact, wind or earthquake loads were developed. In previous studies use of CFRP for strengthening or repair of structures subjected to static loads has been discussed. Design guidelines for CFRP rehabilitation for two critical members, beams and columns, that are important for structural integrity under extreme loading are presented.

5.2 USE OF CFRP TO PROVIDE CONTINUITY IN BOTTOM REINFORCEMENT OF BEAMS

In this section, guidelines for bottom face application of CFRP with CFRP anchors are provided for situations requiring continuity of reinforcement. Although rehabilitation using CFRP U-wraps was studied, the dynamic performance of U-wraps was inferior to anchors. Design guidelines for rehabilitation using side faces of a beam are not presented because proof-of-concept tests using Type C beams (development of flexural hinges) were not conducted.

The width of beam sheets needs to be selected based on the tensile capacity of the bottom reinforcement that will be developed at the hinge. When designing the test specimens, the typical test value of the tensile strength of the CFRP (143 ksi) was used rather than the design value (121 ksi). In the guidelines, the design value is used. The width of connection sheets and CFRP anchors are based on the width of the beam sheets. In the test program, 33 % more CFRP was used in the connection sheets and anchors than the beam sheets but the use of 50 % more CFRP is recommended in the guideline. The location of column hole, through which the connection sheets passes, is assumed to be located at less than 2 in. from the bottom face of the beam. A height transition ramp with

1:4 slope is assumed to be used regardless of geometry of beams and columns. The anchors are should be placed at least two locations in a beam sheet. The first set of anchors should be located at the toe of the ramp where ramp meets the beam and the second set of anchors should be located a point that is at least equal to the development length of the bottom reinforcement from the column face. Detailing requirements for anchors are discussed in the next section.

5.2.1 Design Procedure

1. Determine width of beam sheets based on tensile strength of the bottom reinforcement. Use at least 50 % more materials than the materials needed to develop tensile strength of the bottom reinforcement. Select the number of layers based on the available width of the bottom face which is at least 2 in. less than the width of the beam.

$$T_b = 1.25 f_y A_s \qquad\qquad \textbf{\textit{Equation 5-1}}$$

$$T_f = f_{fu} w_f t_f \qquad\qquad \textbf{\textit{Equation 5-2}}$$

$$T_f / T_b \geq 1.5 \qquad\qquad \textbf{\textit{Equation 5-3}}$$

$$w_f = \frac{1.5 \times (1.25 f_y A_s)}{f_{fu} t_f} \qquad\qquad \textbf{\textit{Equation 5-4}}$$

T_b: expected tensile strength of the bottom reinforcement, lb

T_f: tensile strength of CFRP sheet, lb

f_y : yield strength of reinforcement, psi

f_c' : compressive strength of concrete, psi

A_s: area of the bottom reinforcement, in^2

f_{fu}: tensile strength of CFRP, psi

t_f: thickness of CFRP sheet, in.

w_f : width of CFRP beam sheet, in.

2. Calculate width for CFRP anchors and connection sheets

 - Width of a set of CFRP anchors = Width of connection sheets: $1.5\,w_f$

3. Determine length of the connection sheets

- Length of Connection sheet=

Length of height transition regions, 2×8 in. + Width of the column passed through, b_c

(2 in. : 8 in. height transition ramp was assumed to be used)

4. Determine length of the beam sheets and location of the second set of anchors based on development length, l_d (ACI 318-08, Section 12.2) of the bottom reinforcement.

- Location of the second set of anchors: $1.1 l_d$ from the column face

(location of the anchors / #3 bar development length = 13 in /11.6 in.=1.1, C-BC-A-6G-02)

- Length of beam sheets: $L_s=1.2 l_d$

(10 % increase for the height transition and length beyond the second set of anchors)

5. Distribute the anchors based on the detailing requirements

A. First anchor should be located at the toe of the ramp where ramp meets the beam.

B. The center to center spacing of anchors at the same distance from the column face should be larger than $2d_h$ (d_h = diameter of a hole) and 1.5 in.

C. Area of an anchor hole needs to be at least 40% larger than area of an anchor (Section 5.2.1.3)

D. The anchor should be inserted at least 4 in. into the core

E. The angle of the fan portion of an anchor should be less than 90 degree. At least 0.5 in. overlap is required between anchors. The fan portion of anchors should cover entire width of the beam sheets and be placed on the concrete surface at least 0.5 in. from the edge of the beam sheet.

F. Based on D and E, select length of an anchor

6. Column hole needs to be located at less than 2 in. from the beam face. If connection sheets needs to be distributed, use following requirements:

A. The center to center spacing of anchors at the same distance from the column face should be larger than $2d_h$ and 1.5 in.

B. Area of an column hole needs to be at least 40% larger than area of an connection sheet

(Section 5.2.1.3)

C. the angle of the fan portion of connection sheet should be less than 90 degrees.
At least 0.5 in. overlap is required between anchors. The fan portion of anchors should cover entire width of the beam sheets and be placed on the concrete surface at least 0.5 in. from the edge of the beam sheet.

It is unlikely that moment along the CFRP-strengthened region will exceed the flexural capacity of the strengthened section because the tensile strength provided by beam sheets is 50 % more than that of the bottom reinforcement. However, if length of the CFRP-strengthened region is long with respect to span length of the beam or large moment occurs at the ends of the CFRP-strengthened region, a check should be made to ensure that the moment does not cause premature fracture of CFRP.

Because half scale specimens were tested under dynamic loading in the experimental program, the tests with the specimens reflecting actual geometry of structural members may be needed before applying this guideline to practice. Distribution of multiple connection sheets was not studied so tests for verifying performance of multiple connection sheets may also be needed. Above requirements for distribution of connection sheets are based on the test results of the anchors.

5.2.2 Design Example

Design for loss an interior column in a perimeter frame

Typical beam and girder detail diagram with EXTERIOR, INTERIOR sections and SECTION view.

MARK	SIZE		BOTTOM		TOP	STIRRUPS	
	W	D	"A" BARS	"B" BARS	TOP	NO.- SIZE	SPACING FROM FACE OF SUPPORT
GI	14	32	3 #9	3 #8 *	3 #9 @NON-CONTINUOUS ENDS 3 #9} @ COLS. 1 TO 6 ¢ 3 #8} 19 TO 24 (2 LAYERS #9 BARS IN TOP LAYER)	22 #3	1@2, 3@6, 3@9, 2@10 2@12
G2	14	32	3 #8	2 #6 *	3 #11 @ COLS. 7 TO 18	14 #3	1@2, 3@12, 3@18
BI	12	22	3 #8	3 #7 *	3 #7 EACH END	8 #3	1@2, 1@8, 2@12
B2	12	22	3 #7	2 #8 *	2 #8 NON-CONT. END 4 #9 CONT. END	14 #3	1@2, 2@5, 2@8, 2@12

BEAM AND GIRDER SCHEDULE
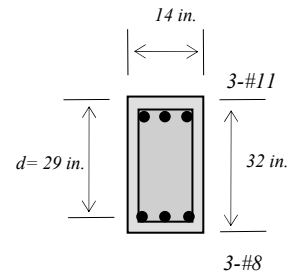
* GR 60 reinforcement; f_c' =4,000 psi

Figure 5.1 Example Girder (ACI 315-74)

1. Determine width of beam sheets based on tensile strength of the bottom reinforcement. Use at least 50 % more materials than the materials needed to develop tensile strength of the bottom reinforcement. Select the number of layers based on the available width of the bottom face which is at least 2 in. less than the width of the beam.

$$T_b = 1.25 f_y A_s = 1.25 \times 60,000 \times (3 \times 0.79) = 177,750 \, lb$$

$$w_f = \frac{1.5 \times (1.25 f_y A_s)}{f_{fu} t_f} = \frac{1.5(1.25 \times 60,000 \times (3 \times 0.79))}{121,000 \times 0.04} = 55.1 \, in.$$

- Available width for the beam sheet =14 in. -2 in. =12 in.

- *Use 5 layers of 11 in. wide beam sheets* (5 ×11=55 in.)

$$T_f = f_{fu} w_f t_f = 121,000 \times 55 \times 0.04 = 266,200 \, lb$$

311

2. Calculate width for CFRP anchors and connection sheets

       - Width of a set of CFRP anchors or connection sheet: 1.5 w_f = 1.5×55 =82.5 in.

3. Determine length of the connection sheets

       - Length of Connection sheet= 2×8 +18.5 = 34.5 in.

4. Determine length of the beam sheets and location of the second set of anchors based on development length, l_d (ACI 318-08, Section 12.2) of the bottom reinforcement.

$$l_d = \left[\frac{f_y \psi_t \psi_e}{20\lambda\sqrt{f_c'}} \right] d_b = \left[\frac{60,000 \times 1.0 \times 1.0}{20 \times 1.0 \times \sqrt{4000}} \right] \times 1.0 = 47.4 \ in.$$

       - Location of the second set of anchors: 1.1 l_d = 1.1×47.4= 52.1 in., Use 52 in.

       - Length of beam sheets: L_s=1.2 l_d = 1.2×47.4= 56.9 in., Use 57 in.

5. *Distribute anchors based on the detailing requirements*

    - Try two 20 in. width anchor and two 22 in. anchor

    - 2.5 in. spacing and 60 degree fan

    - 1.25 in. diameter and 9 in. depth anchor hole
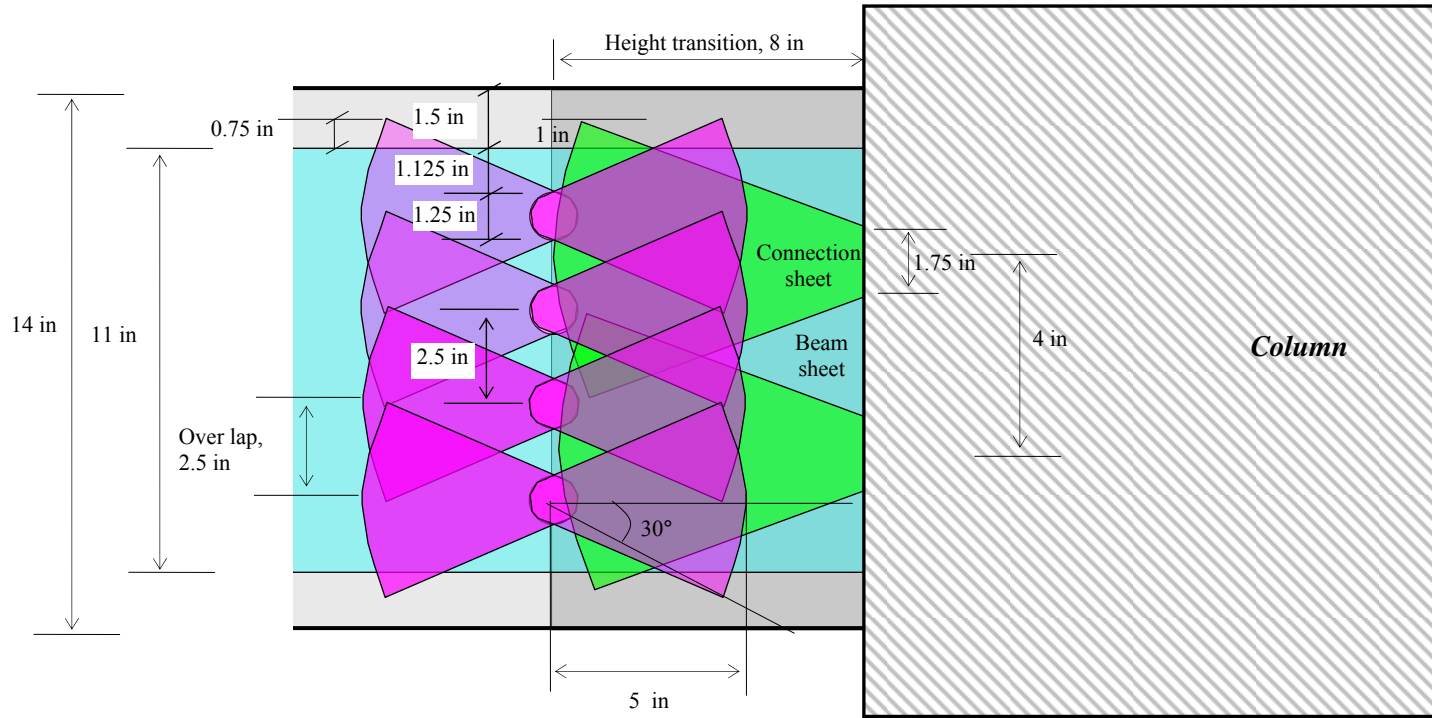
Figure 5.2   **Layout of the first set of anchors**

A. A. First anchor should be located at the toe of the ramp where ramp meets the beam.

O.K.

B. The center to center spacing of anchors at the same distance from the column face should be larger than $2d_h$ and 1.5 in.

spacing of anchor, 2.5 in. $\geq 2\,d_h$= 2.5 in. O.K.

C. Area of an anchor hole needs to be at least 40% larger than area of an anchor (Section 5.2.1.3)

$$\frac{\pi(1.25)^2/4}{22\times 0.04}=1.39\approx 1.40$$ O.K.

D. The anchor should be inserted at least 4 in. into the core

depth of hole, 9 in. – cover, 3 in. = 6 in. O.K.

E. The angle of the fan portion of an anchor should be less than 90 degrees.

At least 0.5 in. overlap is required between anchors. The fan portion of anchors should cover entire width of the beam sheets and be placed on the concrete surface at least 0.5 in. from the edge of the beam sheet.

See Figure 5.2 O.K.

F. Based on D and E, select length of an anchor

depth of hole, 9 in + fan portion, 5 in. =14 in. O.K.

6. *Column hole needs to be located at less than 2 in. from the beam face. If connection sheets needs to be distributed, use following requirements:*

> *- Try two 42 in. width connection sheets*
> *- 4 in. spacing and 53 degree fan*
> *- 1.75 in. diameter*

A. The center to center spacing of connection sheet should be larger than $2d_h$ or 1.5 in.

spacing of anchor, 4 in. $\geq 2\,d_h$= 3.5 in. O.K.

B. Area of a column hole needs to be at least 40% larger than area of an connection sheet

$$\frac{\pi(1.75)^2/4}{42\times 0.04}=1.43>1.40$$ O.K.

314

C. the angle of the fan portion of connection sheet should be less than 90 degrees.

At least 0.5 in. overlap is required between anchors. The fan portion of anchors should cover entire width of the beam sheets and be placed on the concrete surface at least 0.5 in. from the edge of the beam sheet.

See Figure 5.2   *O.K*

5.3 **USE OF CFRP TO REHABILITATE POORLY DETAILED LAP SPLICES**

5.3.1 **Design of CFRP Jackets and Anchors Using Shear Friction**

CFRP jackets and anchors used in the rehabilitation were initially designed using shear friction equation. The test results indicated that the design procedure provided a conservative estimation of the CFRP needed to develop the splice strength. In this section, design guidelines based on the test results are presented.

5.3.1.1 Minimum Required Splice Length for Rehabilitation

Effectiveness of confinement using rehabilitation was evaluated to find the minimum of the existing splice length needed for rehabilitation. Required splice length of the steel reinforcement in tension can be calculated using ACI 318-08, Section 12.2.3.

$$l_d = \left[\frac{3}{40} \frac{f_y}{\sqrt{f_c'}} \frac{\psi_t \psi_e \psi_s}{\left(\dfrac{c_b + K_{tr}}{d_b} \right)} \right] d_b \quad ACI\,318 - 08\ Section\,12.2.3 \qquad \textbf{\textit{Equation 5-5}}$$

l_d : development length for deformed bar in tension, in.

d_b : diameter of bar, in.

f_c' : compressive strength of concrete, psi

f_y : yield strength of reinforcement, psi

ψ_t , ψ_e , ψ_s : modification factor based on bar location, coating and size

c_b : a factor represents smallest of the side cover

K_{tr} : a factor represents the contribution of confining reinforcement across potential splitting planes.

The term $\left(\dfrac{c_b + K_{tr}}{d_b} \right)$ in Equation 5-5 represents contribution of confining reinforcement and the concrete around the spliced bars that restrain against splitting cracks. This term should not be greater than 2.5 in the code. However, using the test

316

results, $\left(\dfrac{c_b + K_{tr}}{d_b}\right)$ could be calculated according to the strength of the lap splices in the specimens and the calculated value of this term represents the effectiveness of the CFRP confinement for rehabilitating the lap splices. Equation 5-5 can be rearranged as Equation 5-6 if the values of ψ_t, ψ_e, and ψ_s were assumed to be 1.0.

$$\left(\frac{c_b + K_{tr}}{d_b}\right) = \left[\frac{3}{40}\frac{f_y}{\sqrt{f_c'}}\frac{1}{l_d}\right]d_b \qquad\qquad \textbf{\textit{Equation 5-6}}$$

The values used or measured in the tests can be substituted for the terms in Equation 5-6. For all the columns, l_d was equal to 24 in. and d_b was equal to 1 in. (#8 bar). In the calculation, measured compressive strength was used for f_c' (3rd column of Table 5.1) and the peak normalized strength (4th column of Table 5.1) multiplied by 60,000 psi was used instead of f_y to reflect the actual stress level in the bars because the strength was normalized by nominal strength which was based on GR60 reinforcement. The modified stresses in the bars are shown in 5th column of Table 5.1. The calculated values of $\left(\dfrac{c_b + K_{tr}}{d_b}\right)$ are presented in 6th column of Table 5.1 and are between 3.2 and 4.4 which are larger than the code specified value, 2.5. Those large values indicate that actual effectiveness of the CFRP confinement can be larger than the code allows.

Another way of expressing the effectiveness of the CFRP confinement for rehabilitating lap splices is the use of a factor α which is derived in Equation 5-7. Calculated value of α for the splices in the specimens are presented in 7th column of Table 5.1

$$l_d = \alpha\left[\frac{f_y}{\sqrt{f_c'}}\right]d_b \;, \qquad \alpha = \frac{3}{40}\frac{1}{\left(\dfrac{c_b + K_{tr}}{d_b}\right)} \qquad\qquad \textbf{\textit{Equation 5-7}}$$

317

The effectiveness of the CFRP confinement also can be expressed by a multiplier to bar diameter, d_b. This value can be determined using the calculated value α and the normal strength of the concrete (f_c'=4,000 psi) and steel (f_y=60,000 psi.) in Equation 5-7. The required length, l_d in terms of d_b is shown in the last column of Table 5.1.

Table 5.1   *Summary of calculation results of minimum required lap splice length*

1	2	3	4	5	6	7	8
Specimen	Face	f_c', psi	P_{peak}/P_n	$(P_{peak}/P_n)f_y$, f_y= 60,000 psi	$(c_b+K_{tr})/db$	α for mimimum required lap splice length	Minimum required splice length, fc'=4,000psi, fy=60,000psi
1-A-S8-M	West	5,600	1.34	80,400	3.36	0.022	21.2d_b
	East		1.29	77,400	3.23	0.023	22.0d_b
2-A-S8-M	West	5,300	1.48	88,800	3.81	0.020	18.7d_b
	East		1.49	89,400	3.84	0.020	18.5d_b
3-B-S10-M	West	4,500	1.58	94,800	4.42	0.017	16.1d_b
	East		1.56	93,600	4.36	0.017	16.3d_b
4-C-R20-M	West	4,600	1.30	78,000	3.59	0.021	19.8d_b
	East		1.15	69,000	3.18	0.024	22.4d_b
5-C-R20-C	West	5,600	1.35	81,000	3.38	0.022	21.0d_b
	East		1.36	81,600	3.41	0.022	20.9d_b
6-C-R20-C	West	5,600	1.38	82,800	3.46	0.022	20.6d_b
	East		1.36	81,600	3.41	0.022	20.9d_b

The α factor and the bar diameter multiplier were used in the previous codes to determine the lap splice length in compression. ACI 318-63, Section 805 requires using a lap splice length of $24\,d_b$ for GR 60 reinforcement in compression and this length is linearly proportional to f_y. However, the largest value of the minimum required splice length is $22.4\,d_b$ (the east face of 4-C-R20-M) which is less than $24\,d_b$ and the minimum required splice length is also linearly proportional to f_y. Therefore, if a structure was designed according to ACI 318-63, it is possible to strengthen or repair the lap splices for tensile load using CFRP.

ACI 318-71, Section 7.7 requires using α=0.02 to calculate the length of a lap splice in compression. The test results indicate that α is not more than 0.02 for the square columns (4 or 5 spliced bars on a face) rehabilitated using a combination of the CFRP

318

jackets and anchors (2-A-S8-M and 3-B-S10-M). This means that the minimum lap splice length required for rehabilitation is less than the length of a lap splice in compression based on ACI 318-71. The test results indicate that α is larger than 0.02 for the lap splices on all the faces of the rectangular columns (10 spliced bars on a face). However, α is close to 0.02 (α=0.021 ~ 0.022) when the lap splices of 5-C-R20-C, 6-C-R20-C and the west face of 4-C-R20-M were strengthened. Considering conservatism in the development length equation, the calculated α's are close enough to 0.02 so that it can be recommended that lap splices designed using α=0.02 can be strengthened using CFRP rehabilitation. In contrast, when the lap splices were repaired, α was 0.024 and was 20 % larger than the code requirement for compression lap splices (the east face of 4-C-R20-M). Therefore, strengthening of the lap splices in a column which contains 10 spliced bars on a face and was designed according to ACI 318-71 is possible but repair of the lap splices in a damaged column may not result in development of the splice in tension. However, if the actual length of the lap splices is longer than the length calculated using α=0.024, lap splices can be repaired. A summary of lap splices that can be rehabilitated according to various codes is shown in Table 5.2 based on the results of this report. Another method to check the applicability of the rehabilitation is comparison of the actual spice length with the length calculated using α=0.024 (lap splice in a damaged column containing between 5 and 10 spliced bars on a face) or α=0.020 (all the other cases).

Table 5.2   *Summary of lap splice conditions needed for rehabilitation*

Design code	ACI 318- 63		ACI 318- 71	
Number of spliced bars on a column face	Less than 5 spliced bars	Between 5 and 10 spliced bars	Less than 5 spliced bars	Between 5 and 10 spliced bars
Strengtheing (As-built column)	Yes	Yes	Yes	Yes
Repair (Damaged column)	Yes	Yes	Yes	No

5.3.1.2 Contribution of CFRP Jackets, CFRP Anchors and Transverse Reinforcement

In the rehabilitated column, CFRP jackets, CFRP anchors and transverse reinforcement contributed to the force perpendicular to the shear plane where splitting cracking was expected. In the initial shear-friction design equation, it was assumed that 1/3 of the ultimate strength of the CFRP jackets and anchors and the yield strength of the transverse reinforcement can be developed.

The strain in the CFRP jackets and transverse reinforcement at the expected location of the splitting cracks were measured. Although strain gages were located at the cracked section, the measure strain in the CFRP jackets was 0.0015 ~ 0.0045 (15~ 45 % of the ultimate strain) and in the transverse reinforcement was 0.0005 ~ 0.005 (yield strain = 0.0021). Therefore, the design assumptions regarding the contribution of the CFRP jackets and transverse reinforcement were reasonable. The strain data for the CFRP jackets and transverse reinforcement were presented in Section 4.5 and Appendix C. Strain in the CFRP anchors could not be measured but failure of the CFRP anchors was not observed in any specimens.

5.3.1.3 Details of CFRP anchors

Distribution of CFRP anchors was based on the detailing requirements presented in Section 4.2.3. The vertical spacing of CFRP anchors in the lap splice region needed to be less than 6 in. In the west faces of 4-C-R20-M and 5-C-R20-C, vertical spacing was 18 in. (1/2 of the lap splice length) while the spacing was 6 in. (1/4 of the lap splice length) in the other columns. The lap splices with the anchors at 18 in. vertical spacing exhibited the least deformation capacity of all the columns although the strength was comparable. Therefore, vertical spacing of the CFRP anchors in the lap splice region smaller than 6 in. or 1/4 of the lap splice length appears to be a reasonable detailing requirement.

For the horizontal spacing, the CFRP anchors were placed at the middle of the lap splices on at least one side of every lap spliced longitudinal bar except corner bars. No other spacing was examined but the splices performed well using this spacing.

320

In addition, it was found that clear spacing between a CFRP anchor and #8 lap spliced bars was less than 1.25 in. for all the CFRP anchors tested (Table 5.3). It should be noted that anchors must be located close to the spliced bars to effectively restrain splitting and as shown in Figure 5.3 . The effectiveness of an anchor may be factor of cover and bar size also.
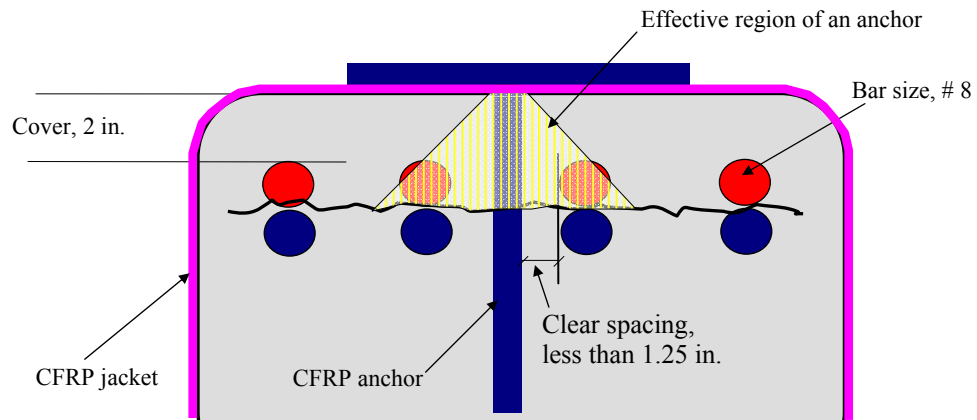
Figure 5.3   **Spacing between CFRP anchor and lap spliced bars**

Table 5.3   ***Ratio of hole area to CFRP anchor area and clear spacing between CFRP anchor and lap spliced bars***

Specimen	Face	Width of anchor, in.	Area of anchor, in.^{2}	Diameter of Hole, in.	Area of hole, in.^{2}	Area of hole/ Area of anchor	Clear spacing between lap splice and anchor, in.
2-A-S8-M	West	7	0.28	0.750	0.44	1.58	1.25
	East	7	0.28	0.750	0.44	1.58	1.25
3-B-S10-M	West	5.5	0.22	0.625	0.31	1.39	0.84
	East	3.5	0.14	0.500	0.20	1.40	0.91
4-C-R20-M	West	7	0.28	0.750	0.44	1.58	0.88
	East	3.5	0.14	0.500	0.20	1.40	1.00
5-C-R20-C	West	7	0.28	0.750	0.44	1.58	0.88
	East	3.5	0.14	0.500	0.20	1.40	1.00
6-C-R20-C	West	5.2	0.21	0.625	0.31	1.47	1.00
	East	3.5	0.14	0.500	0.20	1.40	0.93
Pendulum test		2.7	0.11	0.500	0.20	1.82	
		3	0.12	0.500	0.20	1.64	
		2	0.08	0.375	0.11	1.38	

Diameter and depth of anchor hole were selected to prevent bond failure of a CFRP anchor (Equation 4-10). No bond failure of the anchors was observed during the tests and this equation was a reasonable estimate of the tensile strength of the CFRP anchors. However, when size of an anchor hole is selected, area of a hole must be large enough to insert a CFRP anchor. This is a practical requirement for selecting size of an anchor hole. The ratios of the hole area to the CFRP anchor area are shown in Table 5.3. The smallest value of the ratios is 1.38. Therefore, area of an anchor hole should be 40 % greater than that of the CFRP anchor. This detailing requirement can be used with Equation 4-10 to select size of an anchor hole. Equation 4-10 (= Equation 5-17) and the detailing requirements are summarized in the next section.

5.3.1.4 Design Procedure

The shear friction equation and detailing requirements initially used to design the CFRP jackets and anchors for the specimens provided a conservative estimation of CFRP materials. The rehabilitation based on this design procedure improved the strength and deformation capacity of the columns with poorly detailed lap splices. In this section, a modified design procedure is proposed based on the test results. The design equations are basically the same as the equations presented in Section 4 but several requirements are added based on the findings in this study.

1. Determine if the lap splice can be rehabilitated using Table 5.2 or compare of the actual spice length with the length calculated using α=0.024 (lap splice in a damaged column containing between 5 and 10 spliced bars on a face) or α=0.02 (all the other cases).

$$l_d = \left[\alpha \frac{f_y}{\sqrt{f_c'}} \right] d_b \le actual\ splice\ length$$

2. Calculate tensile force in the longitudinal bars, T_b and check T_b with the upper limit on shear-friction strength, $V_{n,max}$

$$T_b = 1.25 f_y A_s \qquad\qquad \text{\textit{Equation 5-8}}$$

$$V_{n,max} = vbL_s \qquad\qquad \text{\textit{Equation 5-9}}$$

$$V_{n,max} \ge T_b \qquad\qquad \text{\textit{Equation 5-10}}$$

T_b: expected tensile force in the longitudinal bars, lb

f_y : yield strength of reinforcement, psi

f_c' : compressive strength of concrete, psi

A_s: area of longitudinal bars, in^2

$V_{n,max}$: upper limit on shear friction strength, lb(ACI 318-08,11.6.5)

v: maximum stress transferred by shear friction smaller of $0.2 f_c'$ or 800 psi

(ACI318-08, Section 11.6.5)

b: width of column

3. Determine the total effective width of CFRP anchors using one layer of CFRP jackets and $V_n > T_b$ (Assume 1/3 of f_{fu} is effective)

$$V_n = \mu(V_j + V_a + V_s) \geq T_b \qquad \text{Equation 5-11}$$

$$V_j = (f_{fu}/3)t_f(2L_j) \qquad \text{Equation 5-12}$$

$$V_a = n_a(f_{fu}/3)A_a \qquad \text{Equation 5-13}$$

$$V_s = f_y A_{vf} \qquad \text{Equation 5-14}$$

$$\frac{n_a A_a}{t_f} \geq \frac{1}{t_f}\frac{3}{f_{fu}}\left[\frac{T_b}{\mu} - (f_{fu}/3)t_f(2L_j) - f_y A_{vf}\right] \qquad \text{Equation 5-15}$$

μ : coefficient of friction =1.4 (ACI 318-08,11.6.4.3)

V_n: nominal shear strength, lb

V_j: force perpendicular to shear plane contributed by CFRP jackets, lb

V_a: force perpendicular to shear plane contributed by CFRP anchors, lb

V_s: force perpendicular to shear plane contributed by transverse steel reinforcement, lb

f_{fu}: tensile strength of CFRP, psi

t_f: thickness of CFRP sheet, in.

L_j: width of CFRP jacket, in.

n_a: number of CFRP anchors

A_a: area of a CFRP anchor, in^2

A_{vf}: area of steel shear-friction reinforcement, in^2

$\dfrac{n_a A_a}{t_f}$: effective width of total CFRP anchors, *in^2*

4. Determine the number of CFRP anchors using the following detailing requirements

- Vertical spacing of CFRP anchors in the lap spliced region should be smaller than *6 in. or 1/4 of the lap splice length.*
- Horizontal distribution of CFRP anchors: *at the middle of lap splices on at least one side of every lap spliced longitudinal bar except corner bars*
- Diameter and depth of anchor hole to prevent bond failure of a CFRP anchor:

$$(f_{fu}/3)A_a \leq P_n \qquad \textbf{\textit{Equation 5-16}}$$

$$P_n = 4\sqrt{f_c'} \times h_c \times (d_h + h_c) \times \pi + 22\sqrt{f_c'} \times h_c \times (L_a - h_c)$$

$$\textbf{\textit{Equation 5-17}}$$

P_n : tensile strength of CFRP anchor, lb

h_c : concrete cone depth, 2 in. *(Ozdemir et al,. 2005)*

d_h: diameter of anchor hole, in.

L_a: depth of anchor hole from the shear plane, in,. > 4 in. (Ozdemir et al,. 2005)

- Clear spacing between CFRP anchor and lap spliced bars ≤ 1.25 in.
- Area of an anchor hole needs to be at least 40% larger than area of a anchor

5.3.1.5 Design Example, the West Face of 3-B-S10-M

1. Determine if the lap splice is possible to rehabilitate using Table 5.2.

The West face of 3-B-S10-M: 24 in. long 5 spliced bars in a damaged
column designed according to ACI 318-63

Design code	ACI 318- 63		ACI 318- 71	
Number of spliced bars on a column face	Less than 5 spliced bars	Between 5 and 10 spliced bars	Less than 5 spliced bars	Between 5 and 10 spliced bars
Strengtheing (As-built column)	Yes	Yes	Yes	Yes
Repair (Damaged column)	Yes	Yes	Yes	No

OR

$$l_d = \left[\alpha \frac{f_y}{\sqrt{f_c'}} \right] d_b = \left[0.020 \frac{60,000}{\sqrt{4000}} \right] \times 1 = 19.0 \ in. \leq 24 \ in. \qquad \textbf{\textit{O.K.}}$$

2. Calculate tensile force in the longitudinal bars, T_b and check T_b with the upper
limit on shear-friction strength, $V_{n,max}$

$$T_b = 1.25 f_y A_s = 1.25 \cdot 60,000 \cdot (5 \cdot 0.79) = 296,250 \ lb$$

$$V_{n,max} = vbL_s = 800 \cdot 18 \cdot 24 = 345,600 \ lb$$

$$A_s = \text{5-\#8(5x0.79 in}^2\text{)}, \quad b=18 \ in.$$

$$V_{n,max} \geq T_b \qquad \qquad \textbf{\textit{O.K.}}$$

2. Determine the total effective width of CFRP anchors using one layer of CFRP
jackets and $V_n > T_b$

$$V_n = \mu(V_j + V_a + V_s) \geq T_b$$

$$V_j = (f_{fu}/3)t_f(2L_j) = (143,000/3) \cdot 0.04 \cdot 24 = 91,520 \; lb$$

$$V_s = f_y A_{vf} = 60,000 \cdot (6 \cdot 0.11) = 39,600 \; lb$$

$$\frac{n_a A_a}{t_f} \geq \frac{1}{t_f} \frac{3}{f_{fu}} \left[\frac{T_b}{\mu} - (f_{fu}/3)t_f(2L_j) - f_y A_{vf} \right]$$

$$\frac{n_a A_a}{t_f} \geq \frac{1}{0.04} \frac{3}{143,000} \left[\frac{296,250}{1.4} - 91,520 - 396,000 \right] = 42.2 \; in.$$

$$\mu = 1.4, \quad f_{fu} = 143,000 \; psi, \quad t_f = 0.04 \; in.$$

$$L_j = 24 \; in., \quad A_{vf} = 6 \times 0.66 \; in^2, \; (6\text{-}\#3 \; ties \; across \; the \; shear \; plane)$$

4. Determine the number of CFRP anchors using the detailing requirements

- Vertical distribution: *24 in./6 in. = 4 rows of anchors (*Figure 5.4)
- Horizontal distribution: *2 columns of anchors (*Figure 5.4)
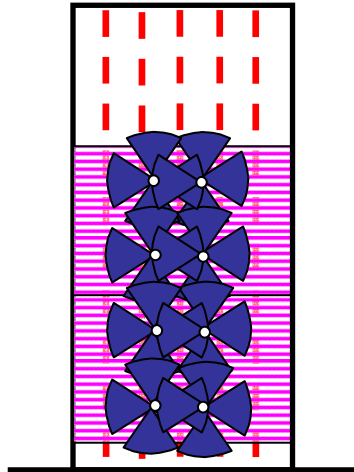
Figure 5.4   Distribution of CFRP anchors

- Total number of anchor, n_a= *4x2=8 anchors*

$$\frac{42.2 \; in}{8 \; anchors} = 5.275 \; in. \; per \; anchor \rightarrow Use \; 5.5 \; in. \; anchor$$

- Diameter and depth of anchor hole:

Try d_h=5/8 in. and L_a= 6 in. > 4 in.

$(f_{fu}/3)A_a = (143,000/3)(0.04 \cdot 5.5) = 10,487 \; lb$

$$P_n = 4\sqrt{f_c'} \times h_c \times (d_h + h_c) \times \pi + 22\sqrt{f_c'} \times h_c \times (L_a - h_c)$$
$$= 4\sqrt{4,000} \times 2 \times (5/8 + 2) \times \pi + 22\sqrt{4,000} \times 2 \times (6 - 2) = 15,304 \, lb$$

$(f_{fu}/3)A_a \le P_n$ **O.K.**

- Clear spacing between CFRP anchor and lap spliced bars:

0.84 in. $\le$ 1.25 in.   **O.K.**

- Area of an anchor hole needs to be at least 40% larger than area of an anchor

$$\frac{\pi(5/8)^2/4}{5.5 \times 0.04} = 1.39$$ **O.K.**

5.3.2   Backbone Curves for the Rehabilitated Columns

In FEMA 365, *Prestandard and Commentary for the Seismic Rehabilitation of Buildings* (2000), procedures to evaluate capacity of existing buildings under seismic loading are discussed. Nonlinear static analysis is one of the procedures and reflects nonlinear behavior of structural components through component force vs deformation curves which consist of a series of linear segments (Figure 5.5).
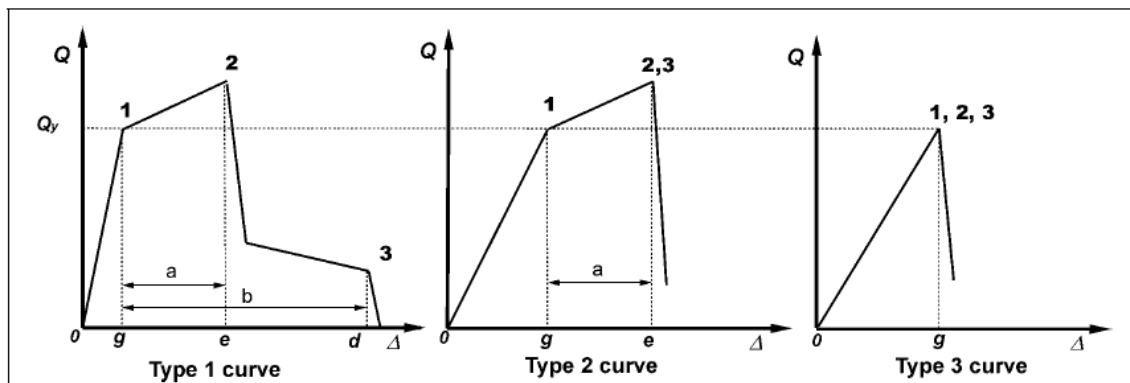
Figure 5.5   Component force vs deformation curves (FEMA 356, 2000)

A component force vs deformation curve is an approximate curve of a backbone curve which is developed from the results of a structural component test under cyclic loading. Backbone curves of the columns tested under cyclic loading (5-C-R20-C and 6-C-R20-C) were developed based on the experimental data of cyclic lading tests according to FEMA 356, Section 2.8 (2000). The backbone curves were drawn through the intersection of the first cycle curve of the (*i*)th deformation step with the second cycle curve of the (*i-1*)th deformation step, for all *i* steps. This procedure is indicated in Figure 5.6 and Figure 5.8.

The backbone curves were approximated by a series of linear segments conforming to a Type 2 curve shown in Figure 5.5. A Type 2 curve was selected because of a lack of information about the residual strength of the splice. Backbone curves were normalized by the calculated yield strength of the columns based on the measured strength of the concrete and the steel reinforcement. Development of Type 2 curves from the backbone

329

curves is described in Figure 5.7 and Figure 5.9. Three deformation parameters, *g*, *e* and *a* are used to characterize Type 2 curves. Parameters *g* and *e* are deformations corresponding to the end of the elastic and plastic ranges. The deformation range corresponding to the plastic range is denoted as *a*. A summary of these parameters for the columns are shown in Table 5.4.

Table 5.4   Summary of Type 2 curves for different rehabilitation methods

Specimen	Rehabilitation method		a	g	e	e ≥ 2g ?
	CFRP jacket	No. of anchors				
5-C-R20-C	Full	8	1.20 %	1.20 %	2.40 %	Yes
	Full	16	2.05 %	1.55 %	3.60 %	Yes
6-C-R20-C		20	1.20 %	1.20 %	2.40 %	Yes
	Partial	16	1.70 %	1.70 %	3.40 %	Yes

According to FEMA 356 all structural behavior can be classified either deformation-controlled or force-controlled using component force vs deformation curves. If a structural component exhibits deformation capacity without losing strength, the behavior is classified as a deformation-controlled otherwise it is classified force-controlled. For structural behavior following a Type 2 curve, *e* must not be less than *2g* to be classified as deformation-controlled behavior. Response of all the strengthened columns using CFRP satisfied this requirement and could be classified as deformation-controlled.

Type 2 curves for the different rehabilitation methods are shown in Figure 5.10. The column face with a CFRP jacket and 16 anchors (the east face of 5-C-R20-C) exhibited the largest strength and deformation capacity. For this case, *a* was 2.0 % which was equal to *a* for a column with conforming transverse reinforcement, 2.0 % indicated in Table 5.5 (For all test columns, axial load, *P* was 0 and $\dfrac{V}{b_w d\sqrt{f_c'}} \le 3$). A component has conforming transverse reinforcement if hoops are spaced at not more than d/3 within the

plastic hinge region. Rehabilitation with a CFRP jacket and 16 anchors provided the same level of confinement as the conforming transverse reinforcement.

The Type 2 curve for the column face with a CFRP jacket and 8 anchors (the west face of 5-C-R20-C) exhibited the least deformation capacity (a = 1.2%). Although a at the column face was less than 2.0 %, it was twice as large as the specified a of a column with nonconforming transverse reinforcement, 0.6% indicated in Table 5.5.

The Type 2 curves derived from the test program provide a conservative estimation of the strength and deformation capacity of a column with CFRP rehabilitation because residual strength and deformation were not considered. In addition, the curve for the rectangular column with a CFRP jacket and 16 anchors (the east face of 5-C-R20-C) can be safely applied to a CFRP rehabilitated column with a fewer spliced bars away from corners such as the square specimens (1-A-S8-M, 2-A-S8-M, and 3-B-S10-M). Eight spliced bars out of 10 spliced bars were away from the corners in 5-C-R20-C while 2 or 3 bars were away from the corners in the square columns. The test results indicate that rehabilitation was more effective in the square columns than in rectangular columns. Therefore, the backbone curve presented can be used in CFRP rehabilitated columns which contain less than 10 splices on a face if the rehabilitation is designed according to the design method discussed in the previous section.
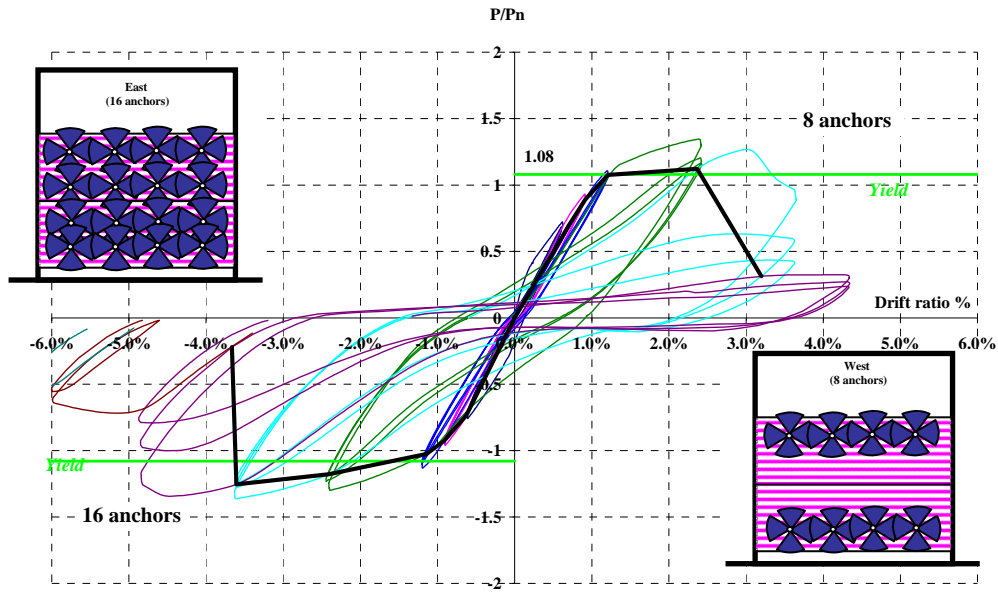
Figure 5.6   Development of backbone curve, 5-C-R20-C
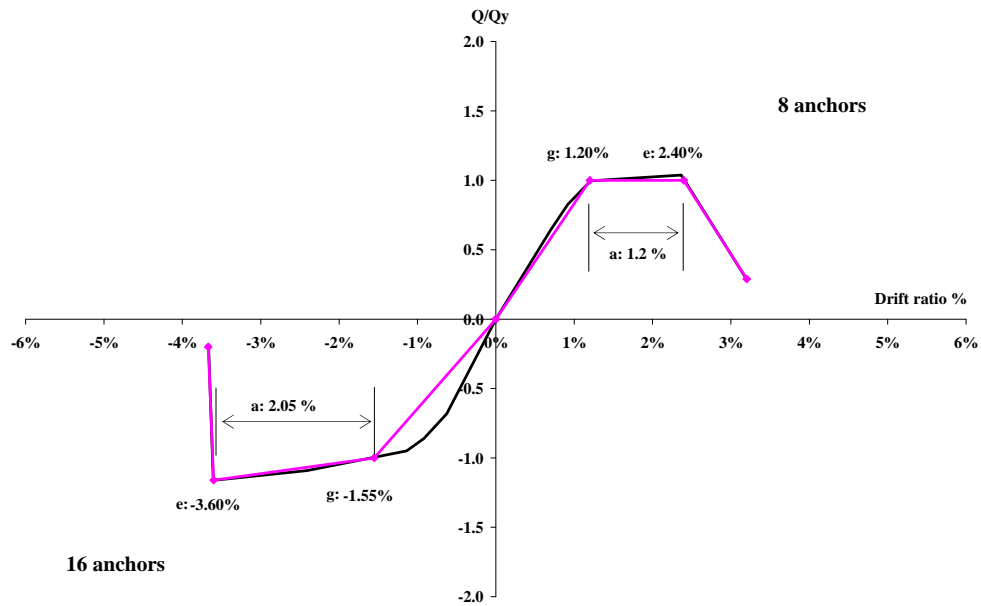
Figure 5.7   Development of Type 2 curve, 5-C-R20-C

332
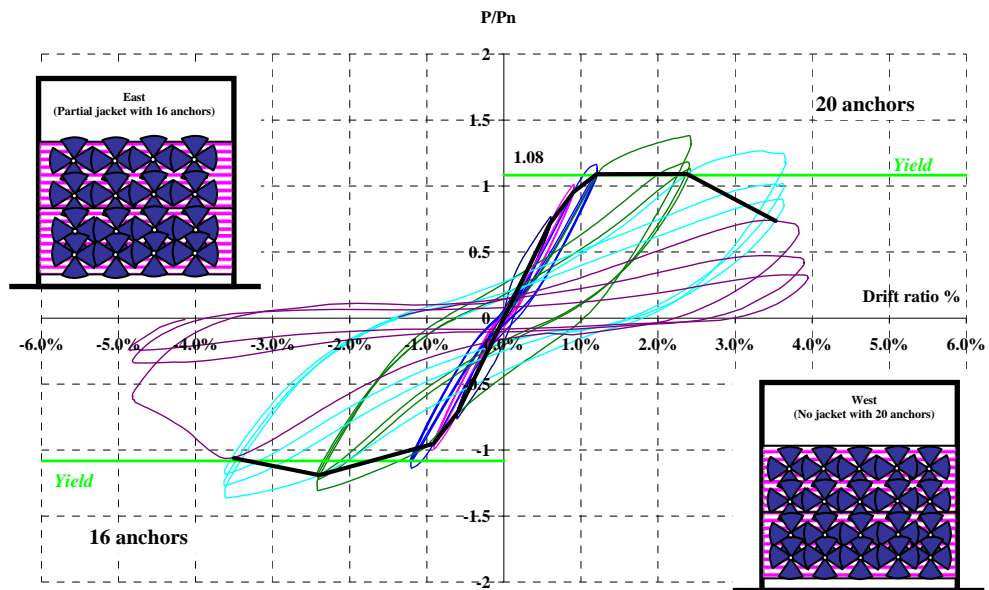
Figure 5.8   Development of backbone curve, 6-C-R20-C
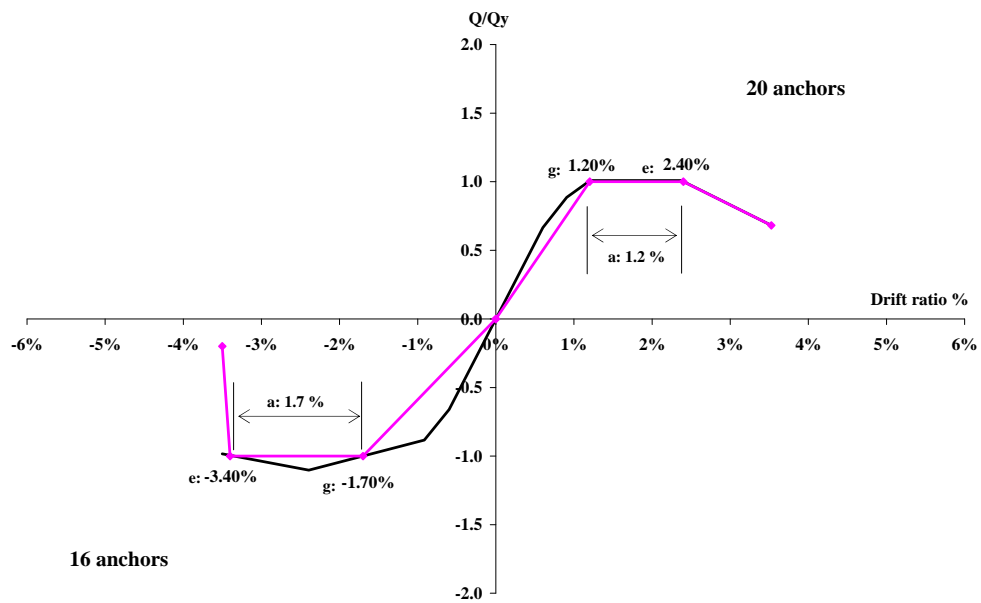
Figure 5.9   Development of Type 2 curve, 6-C-R20-C

333
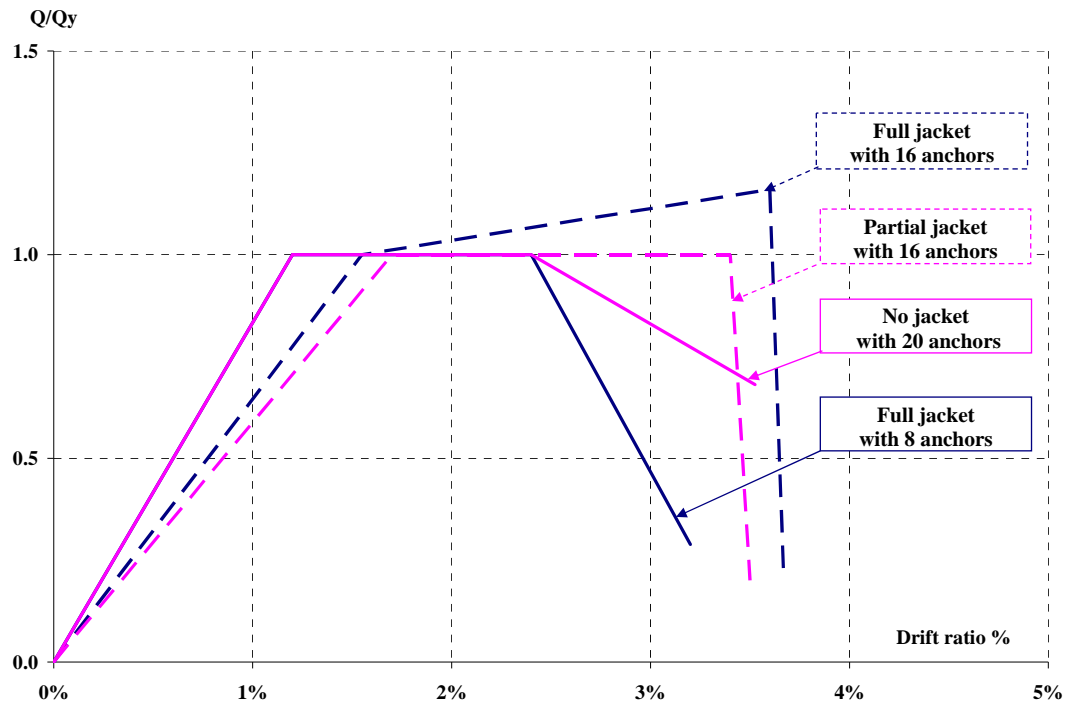
Figure 5.10   Type 2 curves for different rehabilitation methods

The chart contains the following labels:

- **Q/Qy** (vertical axis)
- **Drift ratio %** (horizontal axis)
- **Full jacket with 16 anchors**
- **Partial jacket with 16 anchors**
- **No jacket with 20 anchors**
- **Full jacket with 8 anchors**

Vertical axis values: 1.5, 1.0, 0.5, 0.0

Horizontal axis values: 0%, 1%, 2%, 3%, 4%, 5%

Table 5.5   Modeling parameters for reinforced concrete columns (FEMA 356, 2000)

Table 6-8   Modeling Parameters and Numerical Acceptance Criteria for Nonlinear Procedures— Reinforced Concrete Columns

			Modeling Parameters[4]			Acceptance Criteria[4]					
						Plastic Rotation Angle, radians					
							Performance Level				
								Component Type			
			Plastic Rotation Angle, radians		Residual Strength Ratio		Primary			Secondary	
Conditions			a	b	c	IO	LS	CP	LS	CP
i. Columns controlled by flexure[1]											
$\dfrac{P}{A_g f'_c}$	Trans. Reinf.[2]	$\dfrac{V}{b_w d \sqrt{f'_c}}$									
≤ 0.1	C	≤ 3	0.02	0.03	0.2	0.005	0.015	0.02	0.02	0.03
≤ 0.1	C	≥ 6	0.016	0.024	0.2	0.005	0.012	0.016	0.016	0.024
≥ 0.4	C	≤ 3	0.015	0.025	0.2	0.003	0.012	0.015	0.018	0.025
≥ 0.4	C	≥ 6	0.012	0.02	0.2	0.003	0.01	0.012	0.013	0.02
≤ 0.1	NC	≤ 3	0.006	0.015	0.2	0.005	0.005	0.006	0.01	0.015
≤ 0.1	NC	≥ 6	0.005	0.012	0.2	0.005	0.004	0.005	0.008	0.012
≥ 0.4	NC	≤ 3	0.003	0.01	0.2	0.002	0.002	0.003	0.006	0.01
≥ 0.4	NC	≥ 6	0.002	0.008	0.2	0.002	0.002	0.002	0.005	0.008
ii. Columns controlled by shear[1,3]											
All cases [5]			—	—	—	—	—	—	.0030	.0040
iii. Columns controlled by inadequate development or splicing along the clear height[1,3]											
Hoop spacing ≤ d/2			0.01	0.02	0.4	0.005	0.005	0.01	0.01	0.02
Hoop spacing > d/2			0.0	0.01	0.2	0.0	0.0	0.0	0.005	0.01
iv. Columns with axial loads exceeding 0.70P$_o$[1,3]											
Conforming hoops over the entire length			0.015	0.025	0.02	0.0	0.005	0.01	0.01	0.02
All other cases			0.0	0.0	0.0	0.0	0.0	0.0	0.0	0.0

1. When more than one of the conditions i, ii, iii, and iv occurs for a given component, use the minimum appropriate numerical value from the table.

2. "C" and "NC" are abbreviations for conforming and nonconforming transverse reinforcement. A component is conforming if, within the flexural plastic hinge region, hoops are spaced at ≤ $d/3$, and if, for components of moderate and high ductility demand, the strength provided by the hoops (V_s) is at least three-fourths of the design shear. Otherwise, the component is considered nonconforming.

3. To qualify, columns must have transverse reinforcement consisting of hoops. Otherwise, actions shall be treated as force-controlled.

4. Linear interpolation between values listed in the table shall be permitted.

5. For columns controlled by shear, see Section 6.5.2.4.2 for acceptance criteria.

CHAPTER 6
Summary and Conclusions

6.1 SUMMARY

CFRP materials were used to rehabilitate existing reinforced concrete structures that had inadequate reinforcement details to withstand the effects of extreme loading that could lead to collapse or progressive collapse. The deficient details involve discontinuity in bottom reinforcement in beams (horizontal discontinuity) and poorly detailed lap splices in columns (vertical discontinuity). Two separate experimental studies were conducted using CFRP materials to rehabilitate beam and column specimens.

Use of CFRP to Provide Continuity in Bottom Reinforcement in Beams

The CFRP rehabilitation techniques to provide continuity in bottom reinforcement under static loading conditions were developed by Kim (2006) and Orton (2007). The techniques needed to be verified under dynamic loading conditions because of the nature of loading which caused progressive collapse. The use of CFRP anchors and U-wraps were investigated under dynamic loading. After verifying that these methods resulted in the CFRP reaching full strength under dynamic loading, rehabilitation methods to produce ductile response (or energy absorbing hinging regions) in regions of bottom reinforcement discontinuity were studied. CFRP sheets were anchored to effectively transfer stress from CFRP to bottom reinforcement under dynamic loading. So the strength of CFRP was utilized and large rotational capacity of the beam was developed by yielding of the bottom reinforcement. The CFRP rehabilitation techniques, which were effective under static loading, were found to be acceptable under dynamic loading as well.

Use of CFRP to Rehabilitate Poorly Detailed Lap Splices in Columns

Square and rectangular column specimens were designed based on provisions of the ACI 318-63 and tested as-built or after rehabilitation. A brittle splice failure occurred in the as-built columns. However, after rehabilitating the columns using CFRP jackets and anchors, the failure mode changed from a brittle splice failure to yield of column reinforcement and the strength and deformation capacity were improved under both monotonic and cyclic loading. The improvement was observed in damaged splices that had failed and were repaired as in undamaged splices that were strengthened using a combination of CFRP jackets and anchors.

Design Guidelines

Based on the test results of beams and columns, design guidelines for CFRP rehabilitations were proposed. For the rehabilitation to provide continuity in bottom reinforcement in beams, The width of CFRP sheets to provide continuity were selected based on tensile strength of bottom reinforcement. The width of CFRP anchors were selected based on the width of the anchored sheets. The length of CFRP sheets and locations of CFRP anchors were selected according to required code development lengths of the bottom reinforcement.

CFRP jackets and anchors to rehabilitate poorly detailed lap splices in columns were designed using shear friction equations. The test results indicated that the design procedure provided a conservative estimation of CFRP materials needed to restrain concrete splitting along a plane through the splices. Based on the results of cyclic loading tests, backbone curves for the response of columns rehabilitated using CFRP were developed. The backbone curves can be used in nonlinear static analysis of reinforced concrete columns with CFRP rehabilitation.

6.2 CONCLUSIONS

Horizontal and vertical continuities can be provided through the use of CFRP for rehabilitating existing reinforced concrete structures that were designed prior to the introduction of codes that require continuous reinforcement along members and between adjacent members. The vulnerability of such structures to collapse can be reduced through rehabilitation. Key findings are listed below.

1. CFRP rehabilitation techniques that produced failure (full strength of the CFRP material) under static loading performed satisfactorily under dynamic (impact) loading.

2. By designing the CFRP rehabilitation to provide a continuous tensile force path in regions where bars were discontinuous under earlier codes, it was possible to develop yielding in the existing beam reinforcement and flexural hinging to absorb energy under extreme loading (impact or earthquake).

3. A splice region in columns designed for compression only can be detailed to prevent premature splice failure before inelastic strains are developed in the longitudinal reinforcement.

4. Design procedure using shear friction provided a conservative estimation of CFRP materials needed to restrain concrete splitting along a plane through the splices in columns.

5. The rehabilitation using CFRP jackets and anchors was as effective as that using steel jackets and adhesive anchor bolts to rehabilitate poorly detailed lap splices in columns.

338

6.3 FUTURE RESEARCH

6.3.1 Qualification Test for CFRP Anchors

As discussed in Section 3.8, although the performance of CFRP anchors has received considerable attention, a reliable test method for qualifying of CFRP anchors in reinforced concrete structures does not exist. Therefore, development of a simple test method for evaluating effectiveness of CFRP anchors is necessary. In addition, this test method may be used in quality control of CFRP anchors in practice. Research on qualification test methods for CFRP anchors is continuing at the University of Texas at Austin.

6.3.2 Rehabilitation of Poorly Detailed Reinforced Concrete Beams under Dynamic Loading

The dynamic loading condition used in this study was an impact load which was applied at the center point of a beam. In this loading condition, continuity was successfully provided through a rehabilitation method using CFRP, and the strength and deformation capacity of rehabilitated beams was evaluated under dynamic loading. The tests results of this study indicate that it was possible to select the quantity of CFRP materials to provide required strength for a beam. It was assumed that the maximum required strength due to dynamic loading is already known. GSA and DOD require using a dynamic amplification factor of 2 which means applying 2 times the static load to a structure to reflect effect of dynamic loading (GSA, 2003; DOD, 2005). This guideline may provide a target strength for designing CFRP materials.

However, in this study, the characteristics of dynamic loading were not investigated when a column was removed. When a column is removed, the applied load is distributed over a floor area while the applied load in this study was an impact point load. Effect of a dynamic load in a condition of column removal may not be as large as 2 times the static load due to the characteristics of the loading and the geometry of a

339

structure such as support conditions, transverse beams and slabs. The effect of loading should be verified using a more realistic test structure with multiple bays and stories under distributed and sustained dynamic loading after the column removal. Such a study may allow using lower dynamic amplification factor and reduced quantities of CFRP for rehabilitation.

Another way to provide continuity in a beam in an existing structure is to provide CFRP transverse reinforcement that confines the region where the top and bottom reinforcement overlap. The development of continuous load path consisting of transverse CFRP sheets and anchors should be studied

6.3.3   Rehabilitation of Poorly Detailed Reinforced Concrete Columns

Shear friction equation were used to design CFRP jackets and anchors. The test results shows that the design of CFRP materials based on shear friction provide a conservative estimation. Design guidelines, which provide more efficient use of the materials, can be developed through further research. The effectiveness of CFRP anchors depending on variables such as concrete cover, size of spliced bars, spacing between an anchor and spliced bars, and spacing of the anchors needs to be studied to use CFRP more efficiently. The effect of extension of CFRP jackets along a member and multiple layers CFRP in jackets combined with anchors also needs to be studied.

APPENDIX A

Additional Experimental Data –Beam Tests under Dynamic Loading
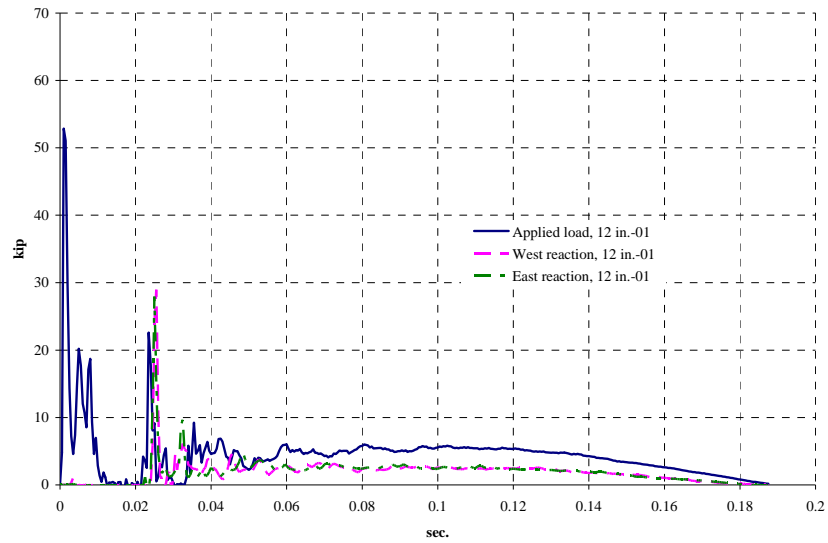
A.1 A-BF-A-5S

A.1.1 Drop Height: 1 in.
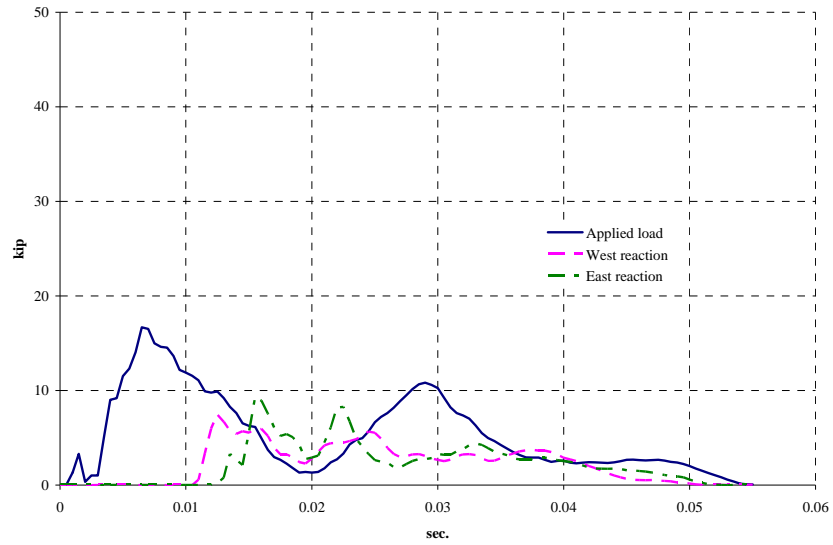
Figure A.1   Measured applied load and reactions, A-BF-A-5S, 1 in.
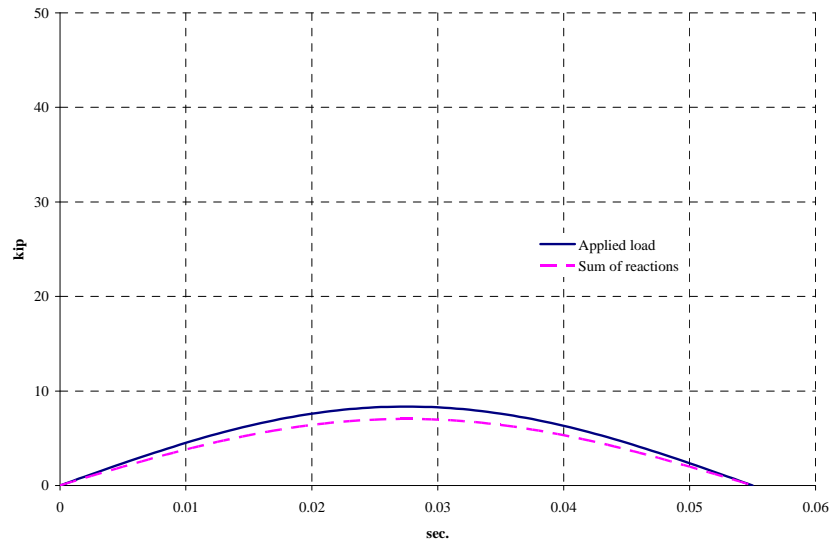
***Figure A.2   Normalized applied load and sum of reactions, A-BF-A-5S, 1 in.***

342
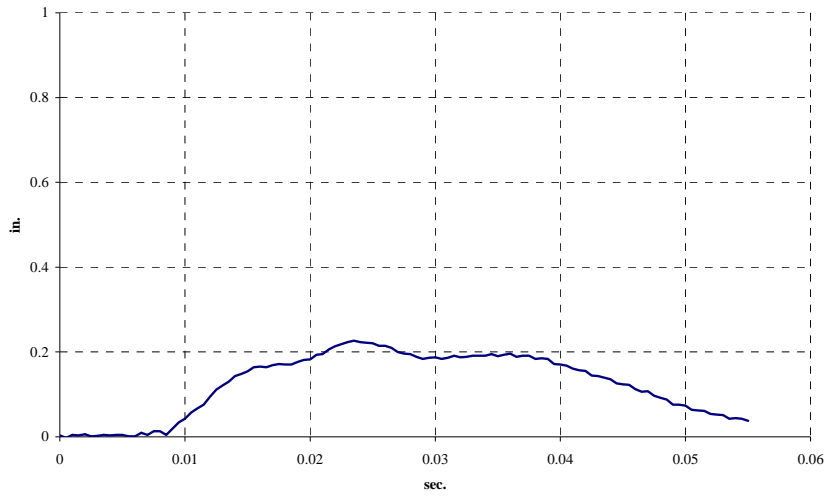
Figure A.3 Displacement in the center, A-BF-A-5S, 1 in.
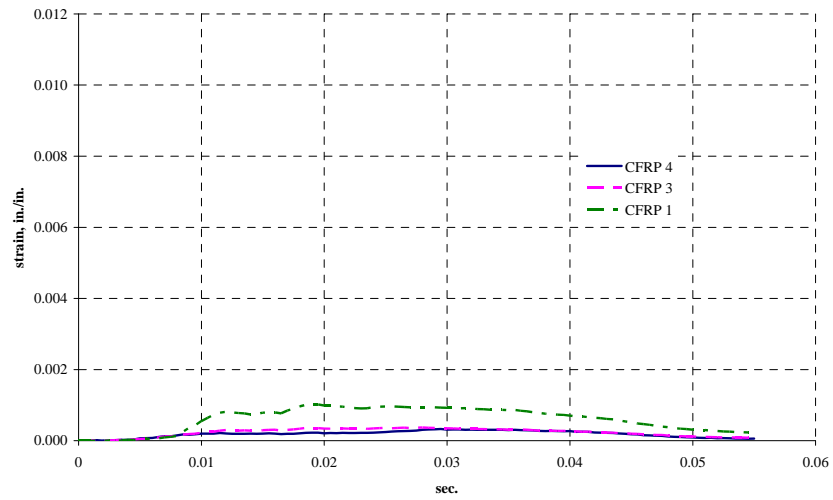
Figure A.4 CFRP strain, A-BF-A-5S, 1 in.

343
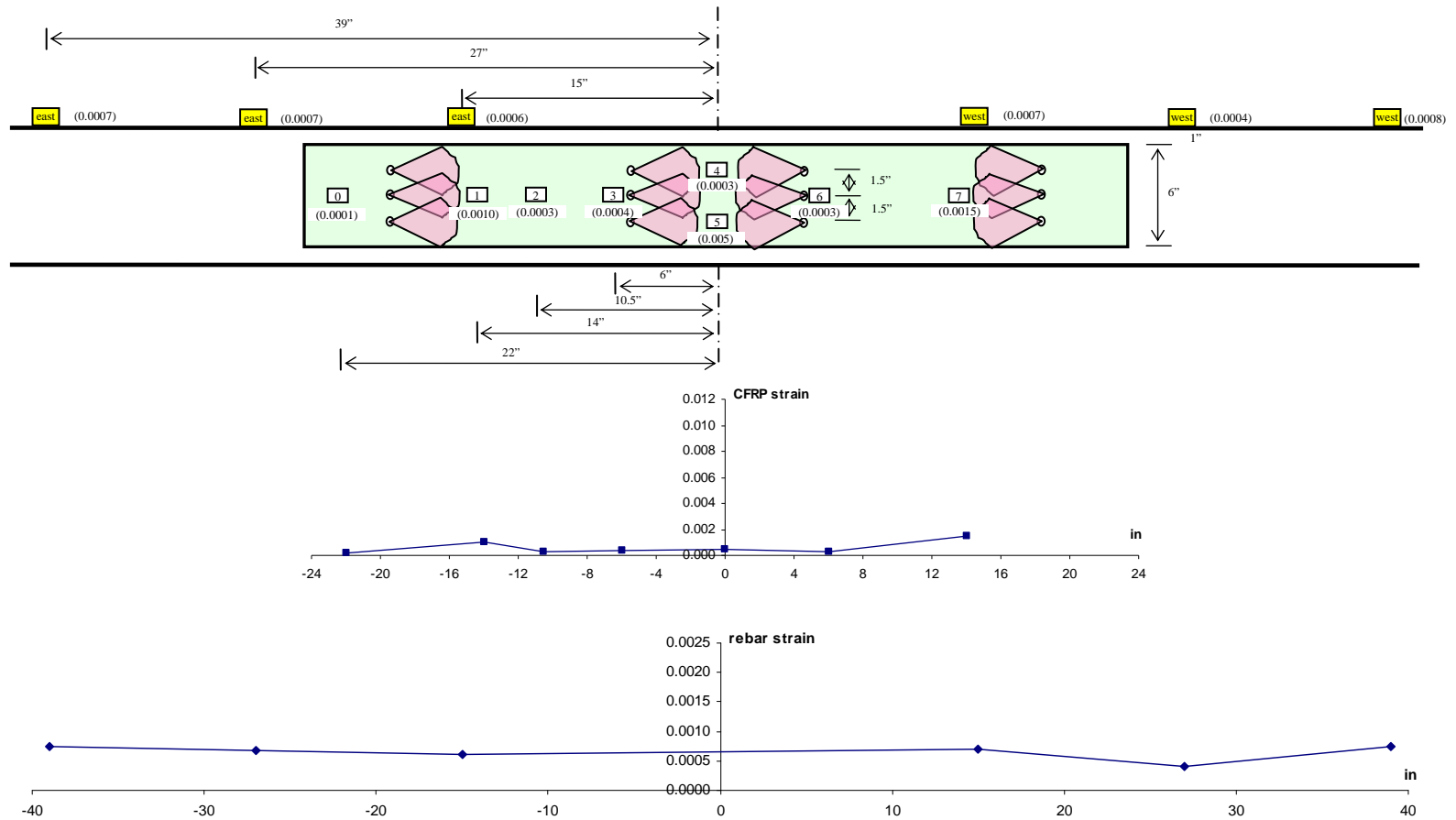
Figure A.5   ***Location of strain gages and distribution of strain in CFRP and bars, A-BF-A-5S, 1 in.***

A.1.2 Drop Height: 3 in.-01
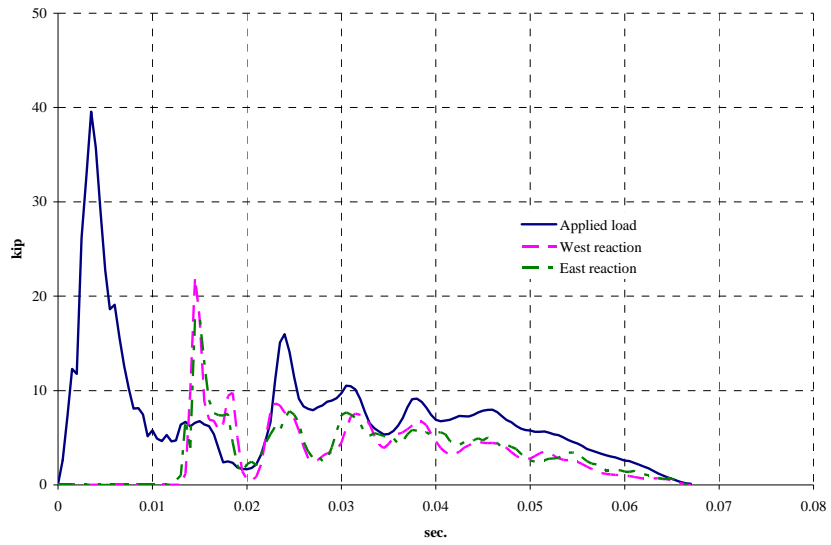
Figure A.6   Measured applied load and reactions, A-BF-A-5S, 3 in.-01
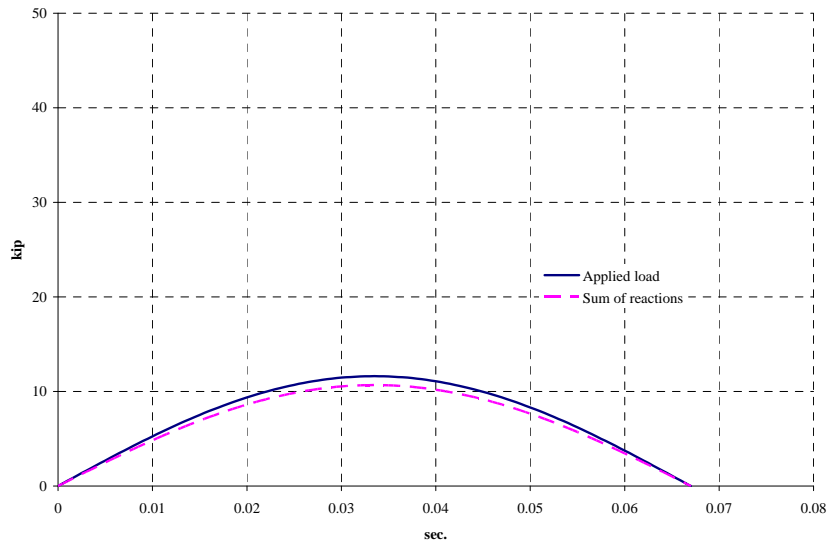
Figure A.7   Normalized applied load and sum of reactions, A-BF-A-5S, 3 in.-01

345
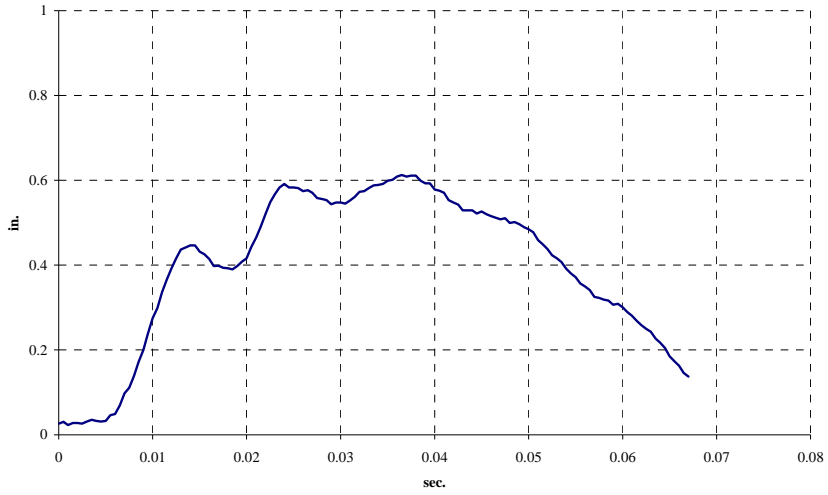
Figure A.8   Displacement in the center, A-BF-A-5S, 3 in.-01
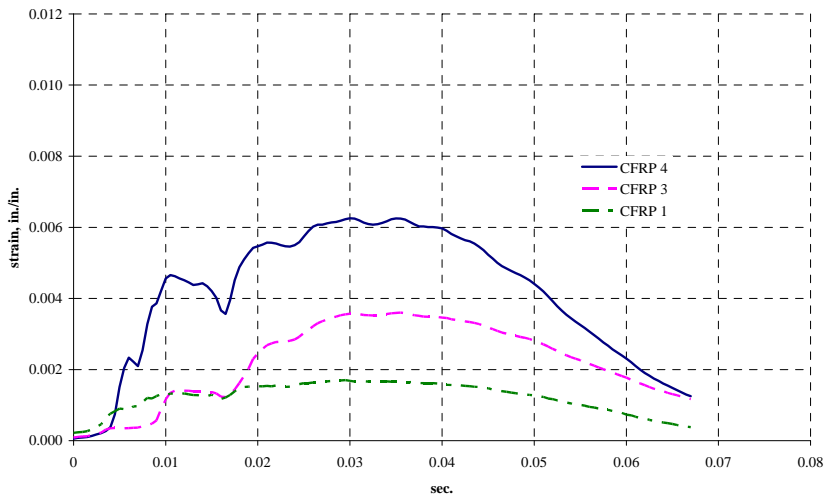
Figure A.9   CFRP strain, A-BF-A-5S, 3 in.-01

346
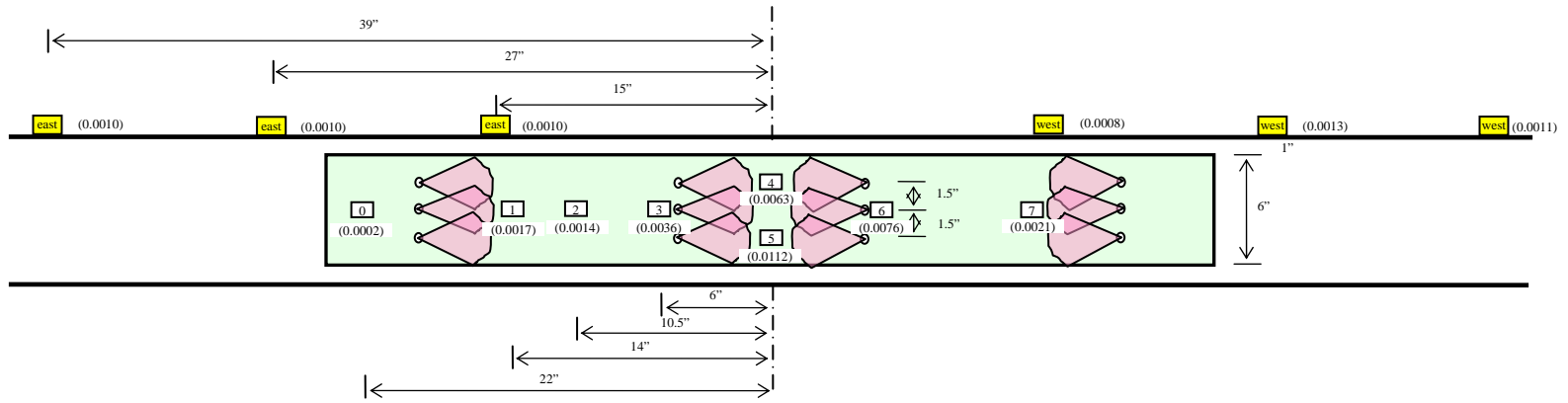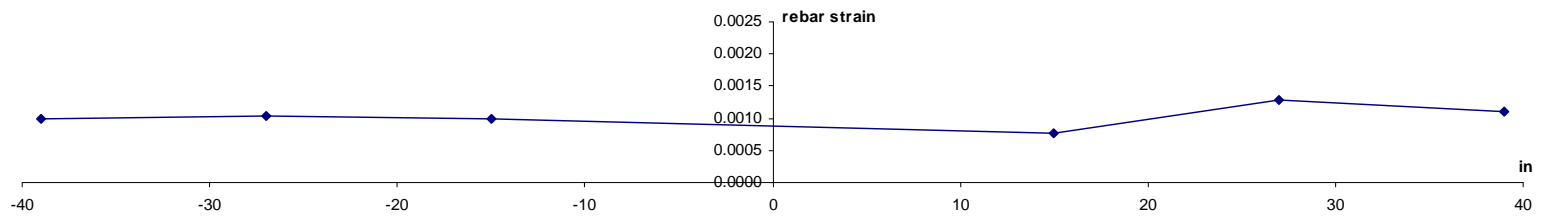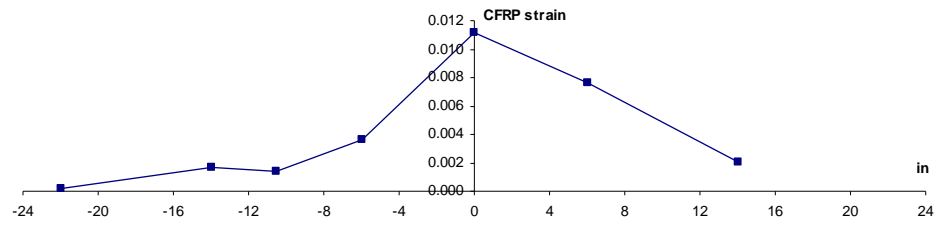
Figure A.10   Location of strain gages and distribution of strain in CFRP and bars, A-BF-A-5S, 3 in.-01

A.1.3 Drop Height: 3 in.-02
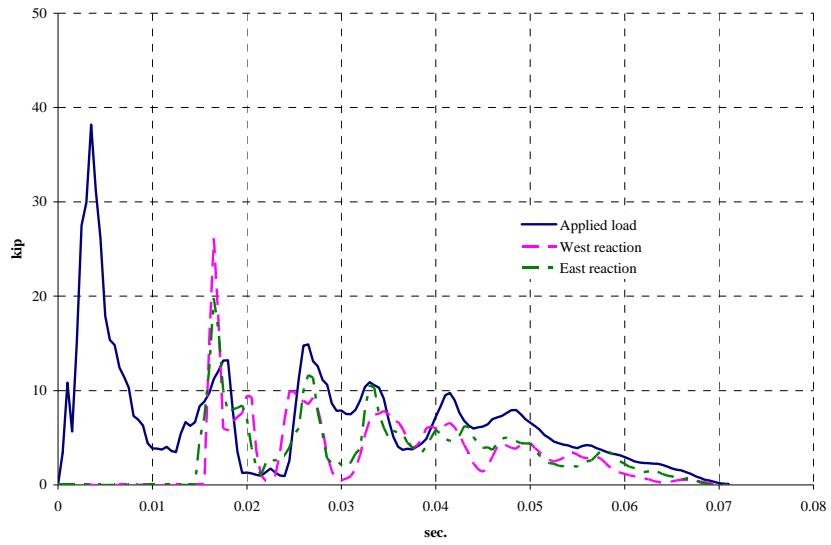
Figure A.11   Measured applied load and reactions, A-BF-A-5S, 3 in.-02
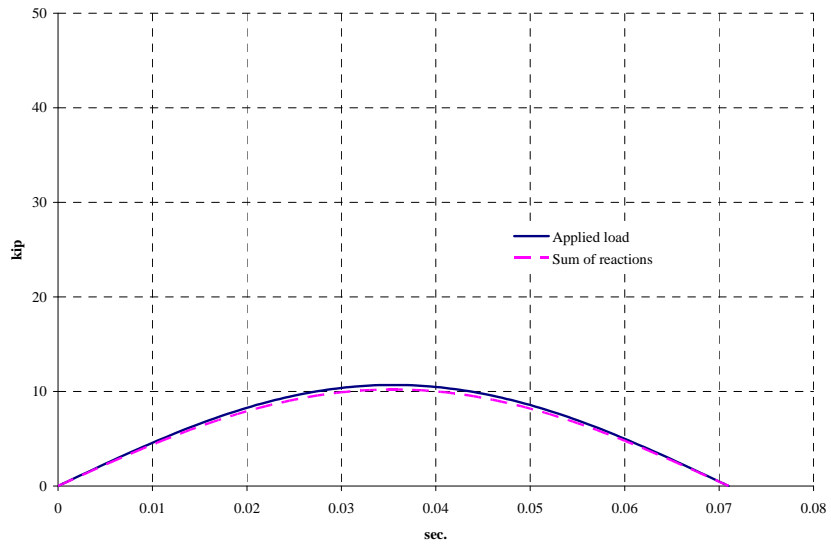
Figure A.12   Normalized applied load and sum of reactions, A-BF-A-5S, 3 in.-02
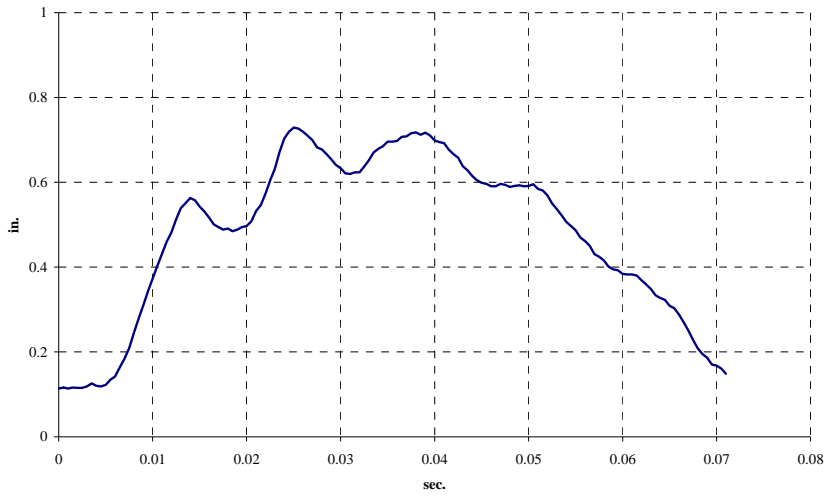
Figure A.13   Displacement in the center, A-BF-A-5S, 3 in.-02
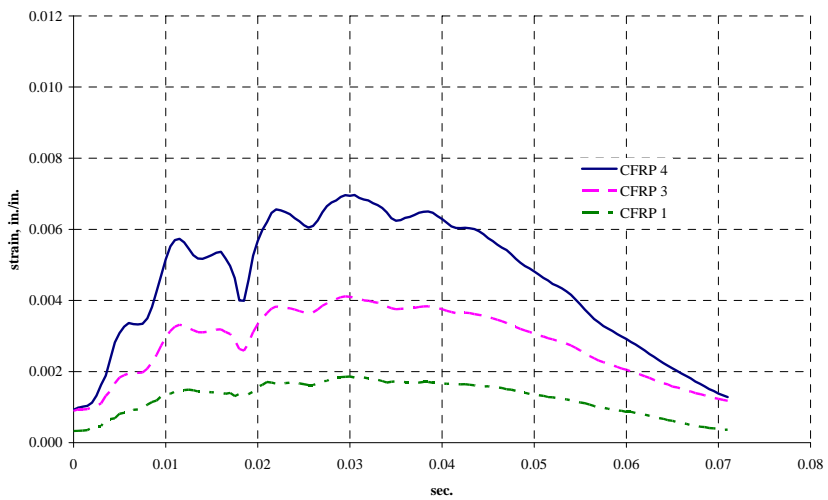
Figure A.14   CFRP strain, A-BF-A-5S, 3 in.-02

349
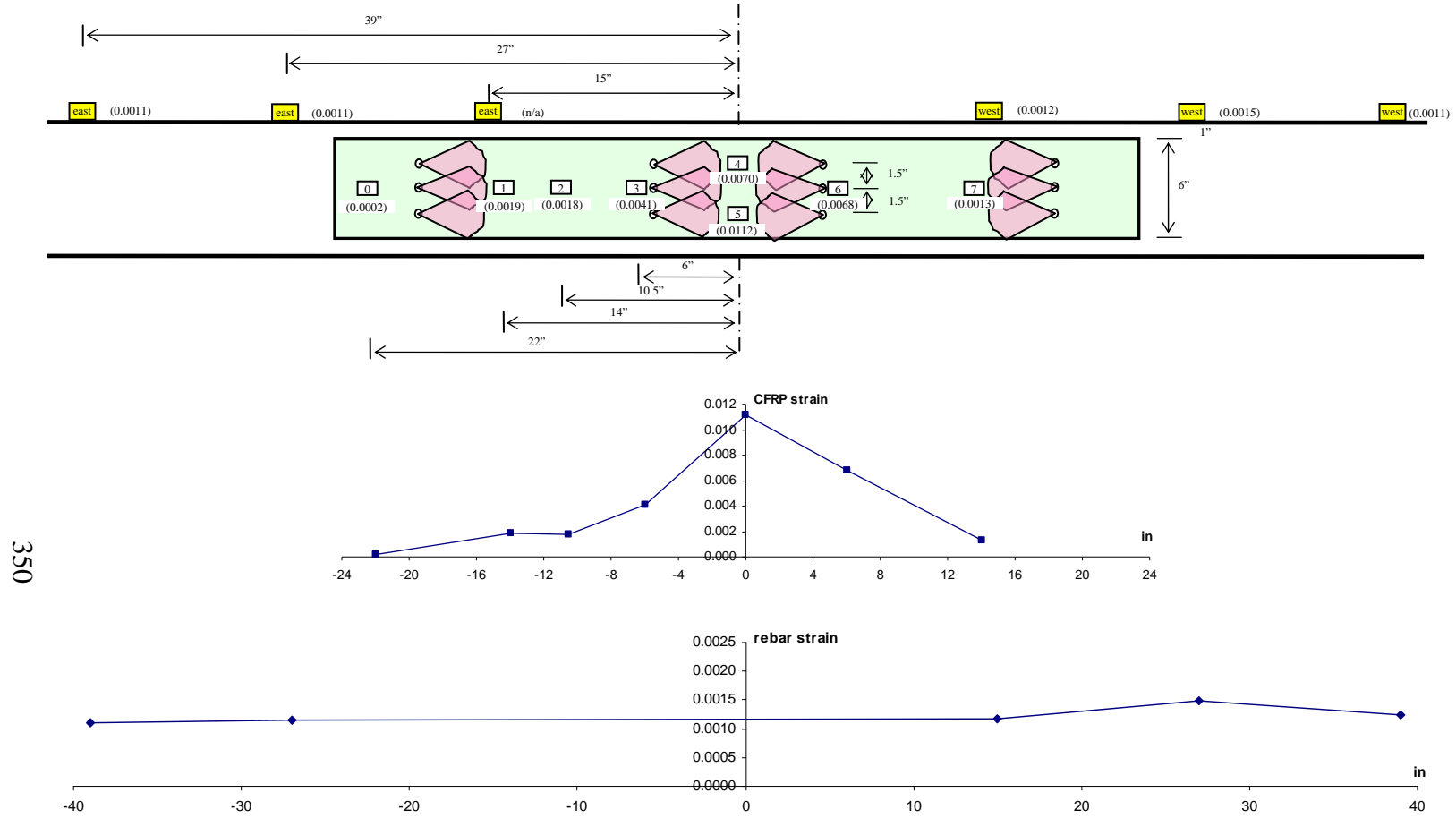
Figure A.15   Location of strain gages and distribution of strain in CFRP and bars, A-BF-A-5S, 3 in.-02

A.2   A-BF-U-5S

A.2.1   Drop Height: 1 in.
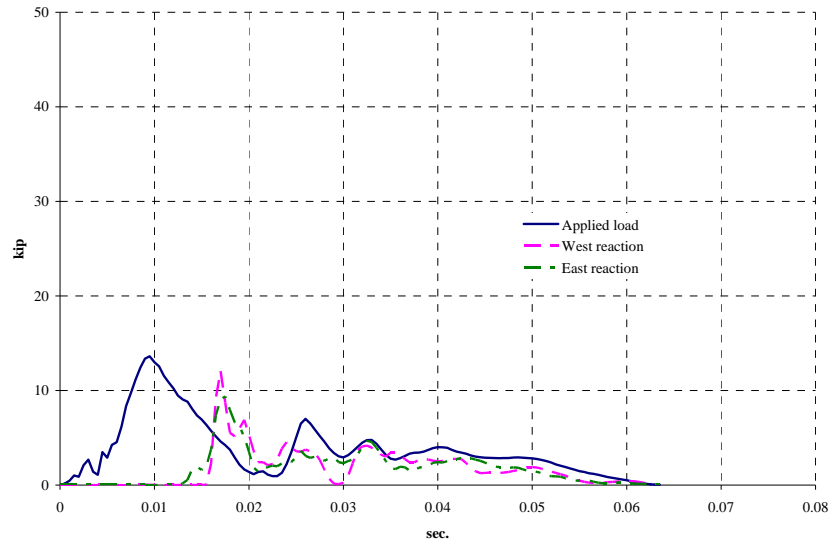
Figure A.16   Measured applied load and reactions, A-BF-U-5S, 1 in.
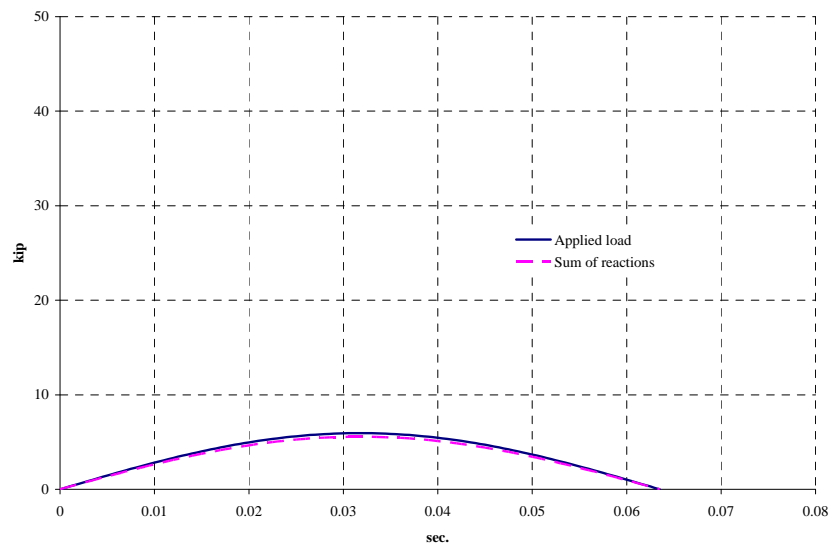
Figure A.17   Normalized applied load and sum of reactions, A-BF-U-5S, 1 in.

351
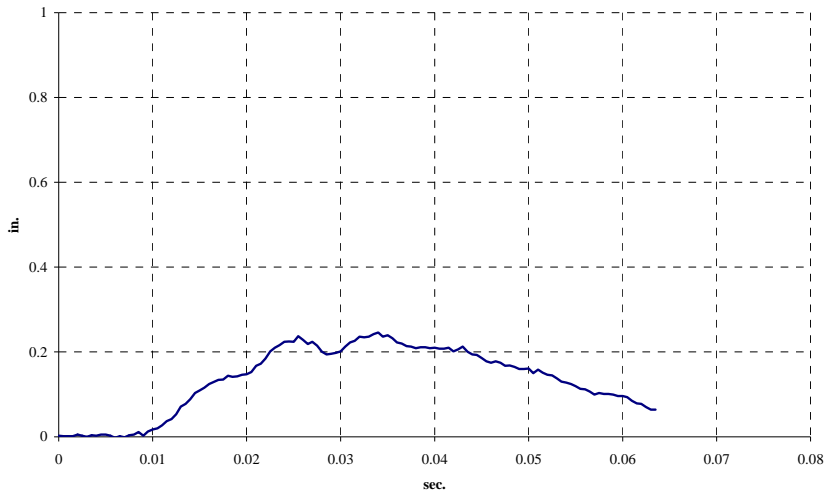
Figure A.18   Displacement in the center, A-BF-U-5S, 1 in.
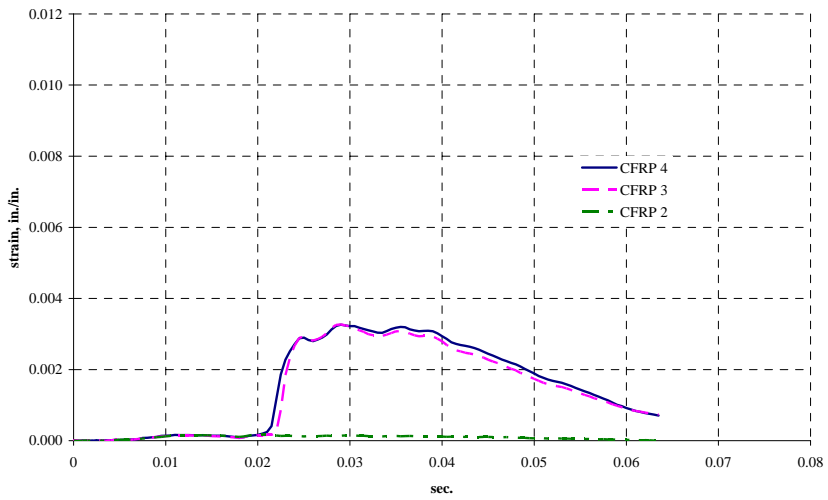
Figure A.19   CFRP strain, A-BF-U-5S, 1 in.

352
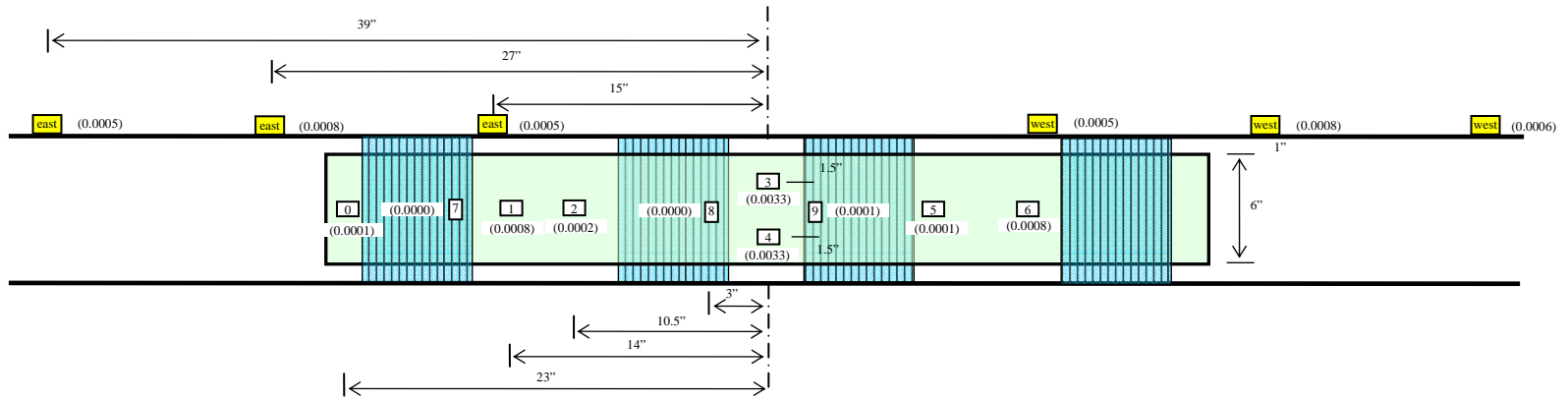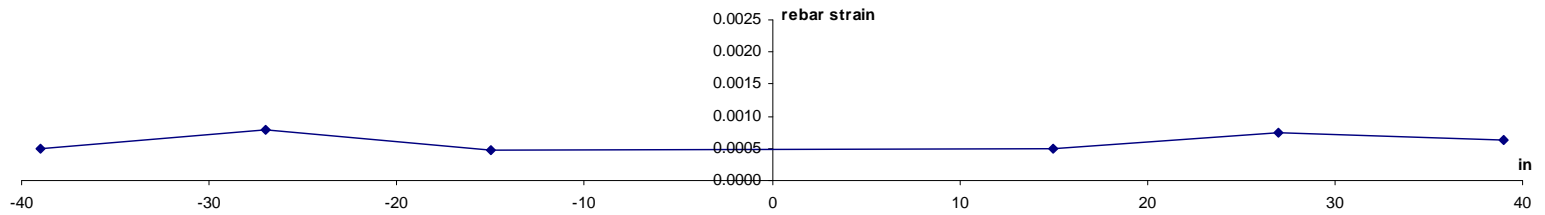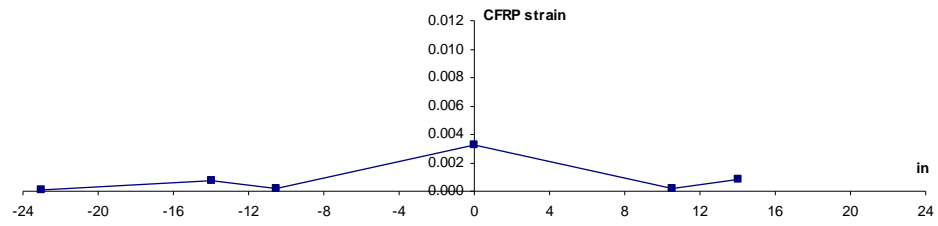
Figure A.20   Location of strain gages and distribution of strain in CFRP and bars, A-BF-U-5S, 1 in.

A.2.2 Drop Height: 1.5 in.
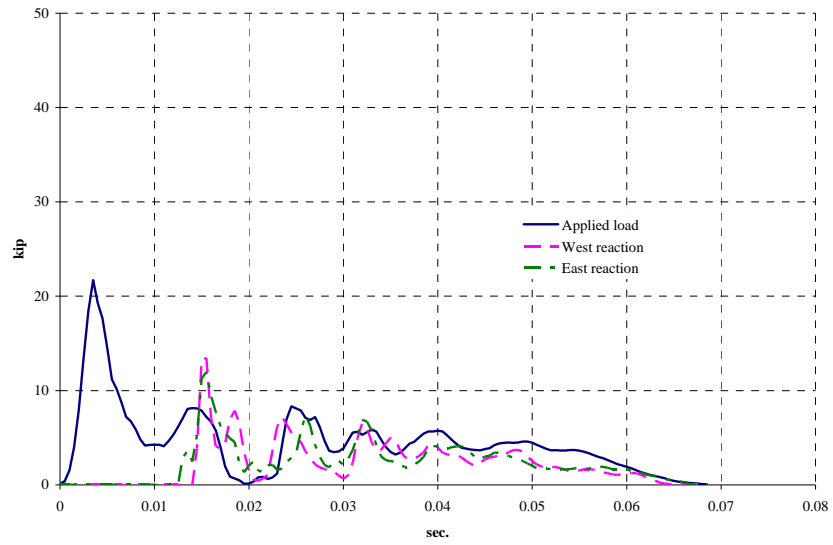
Figure A.21   Measured applied load and reactions, A-BF-U-5S, 1.5 in.
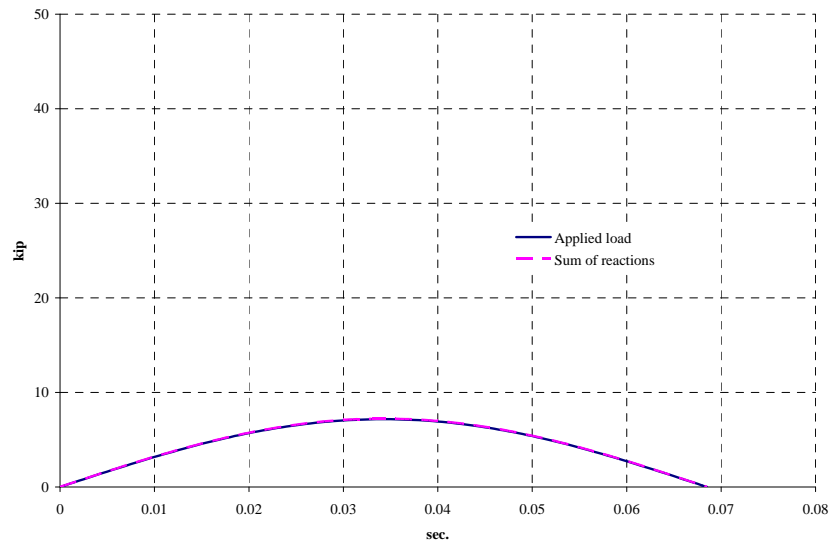
Figure A.22   Normalized applied load and sum of reactions, A-BF-U-5S, 1.5 in.

354
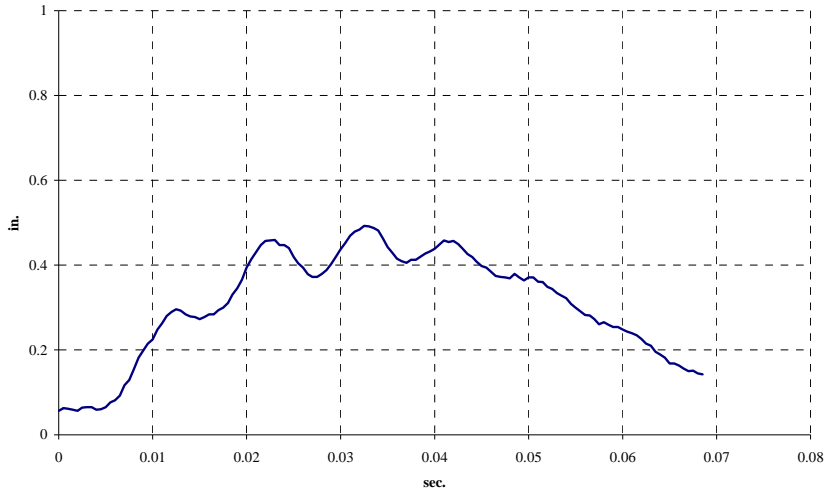
Figure A.23   Displacement in the center, A-BF-U-5S, 1.5 in.
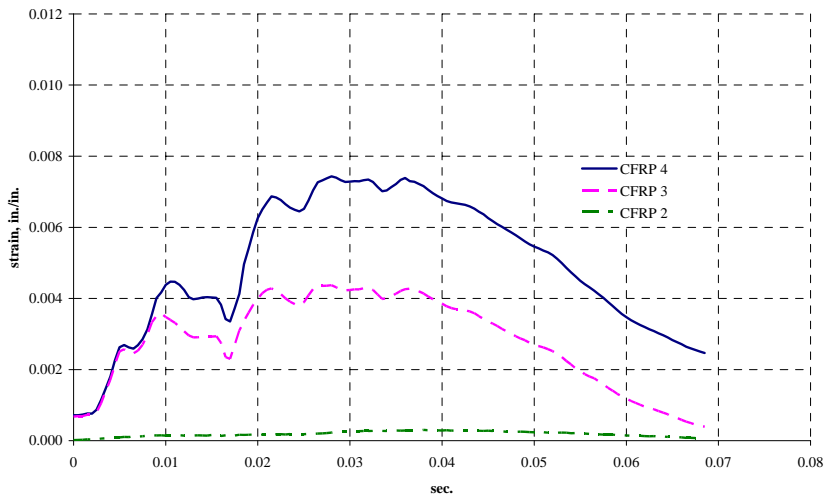
Figure A.24   CFRP strain, A-BF-U-5S, 1.5 in.

355
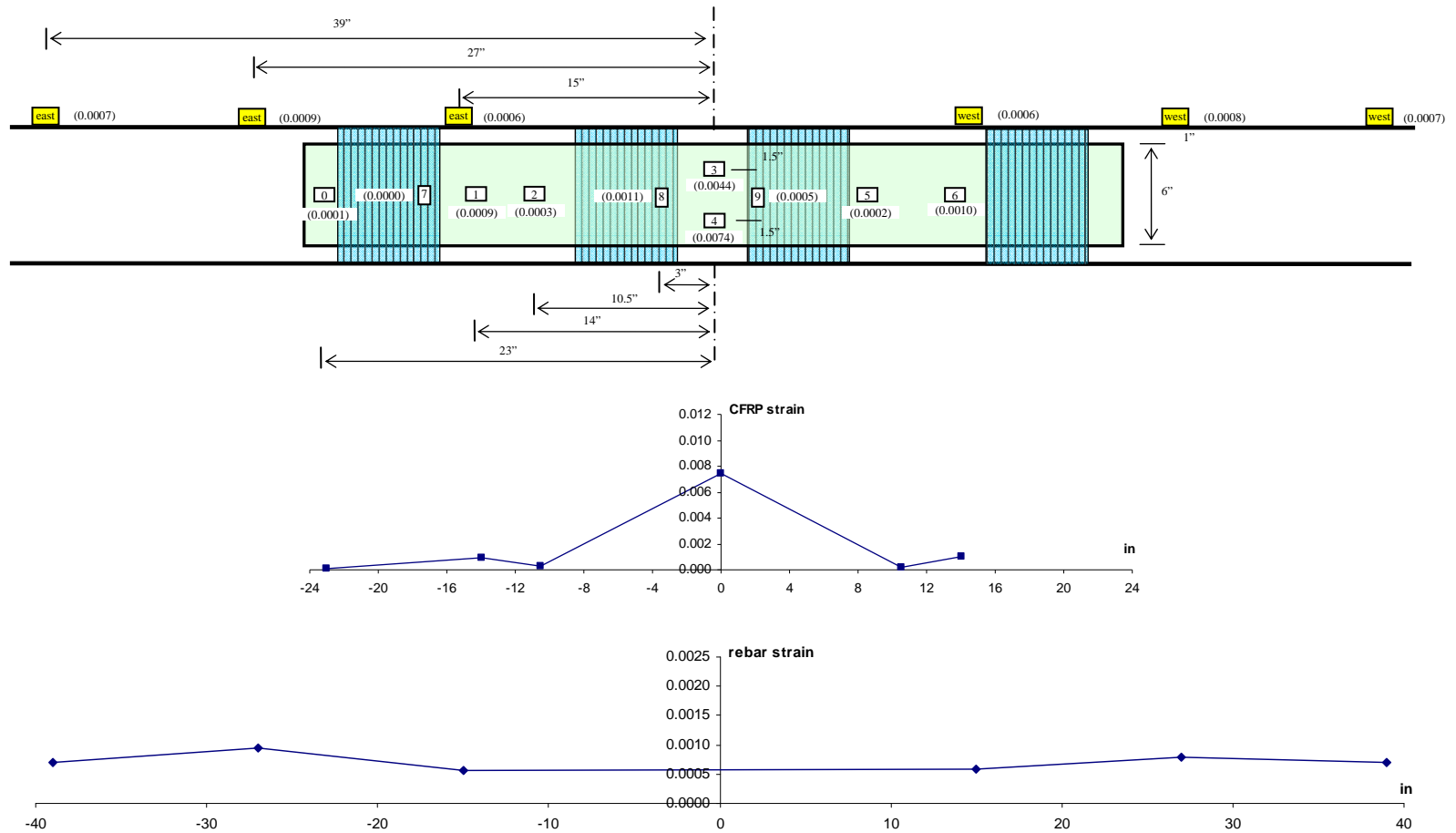
Figure A.25   Location of strain gages and distribution of strain in CFRP and bars, A-BF-U-5S, 1.5 in.

A.3 B-BH-A -6S

A.3.1 Drop Height: 3 in.
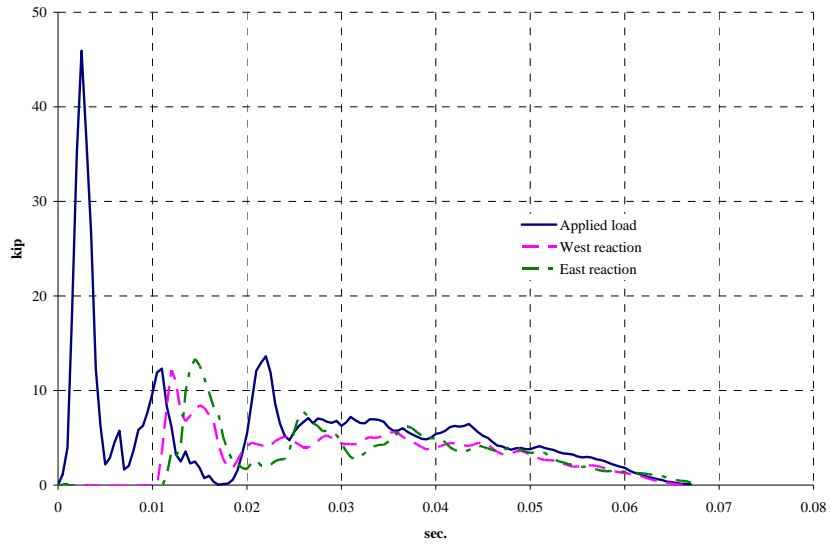
Figure A.26   Measured applied load and reactions, B-BH-A-6S, 3 in.
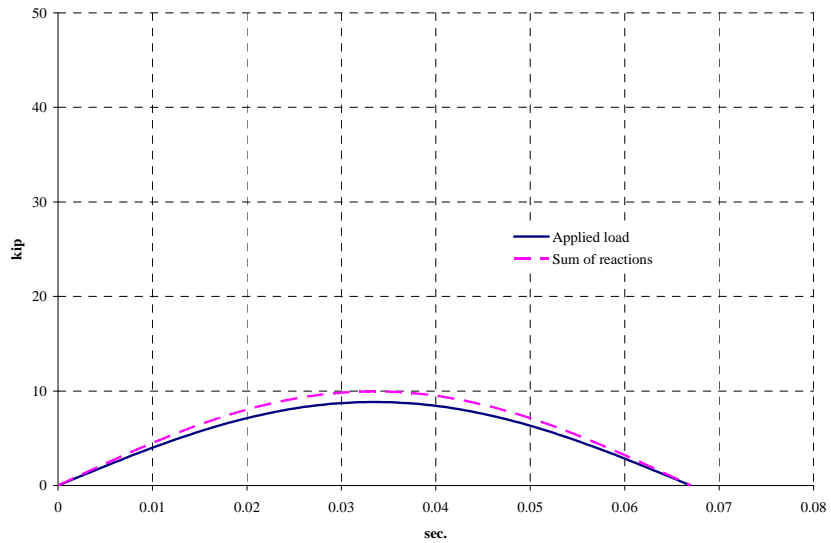
Figure A.27   Normalized applied load and sum of reactions, B-BH-A-6S, 3 in.

357
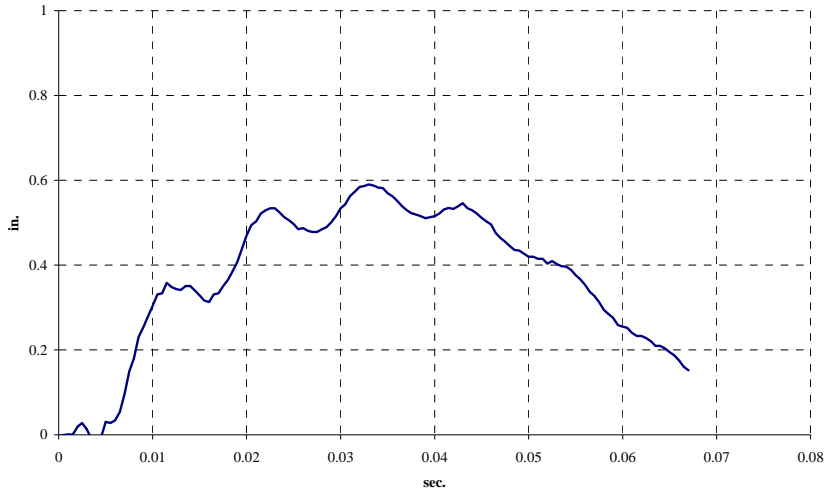
Figure A.28   Displacement in the center, B-BH-A-6S, 3 in.
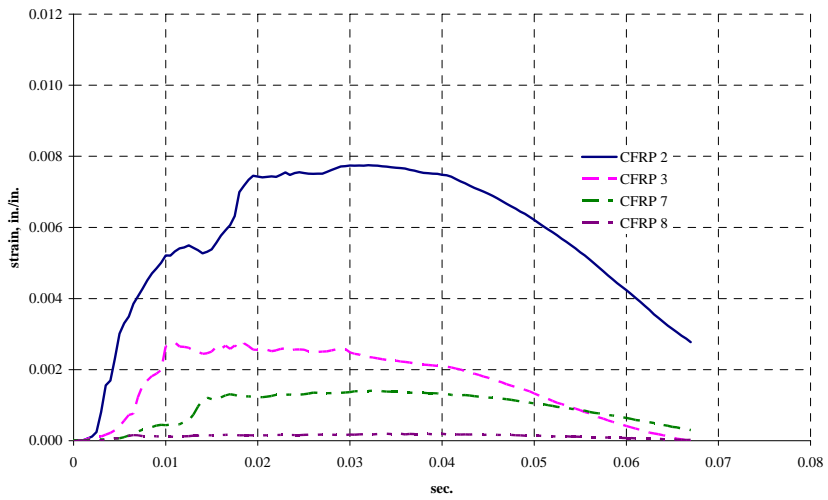
Figure A.29   CFRP strai , B-BH-A-6S, 3 in.

358
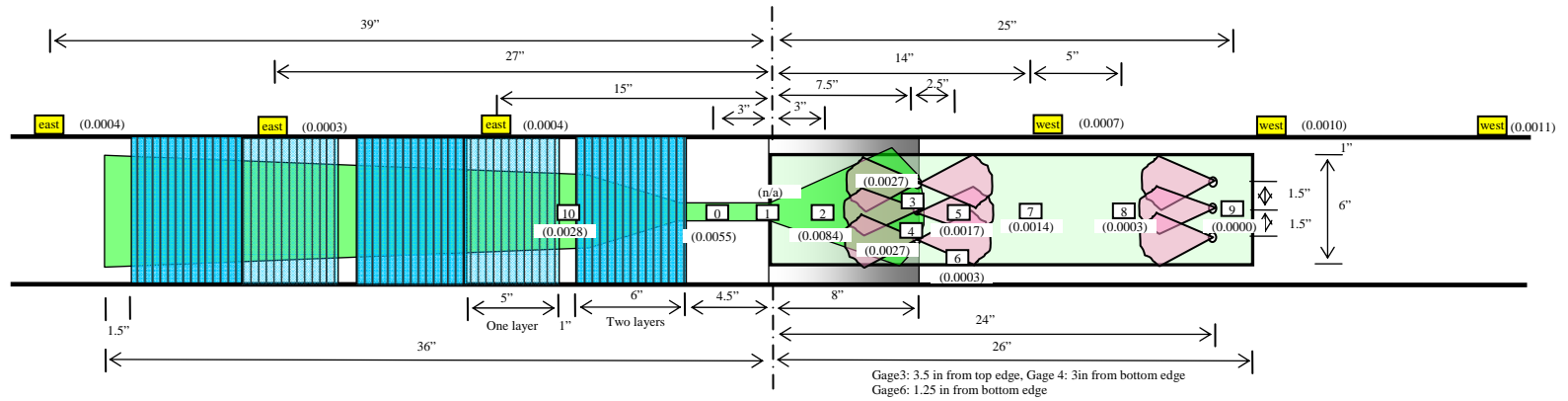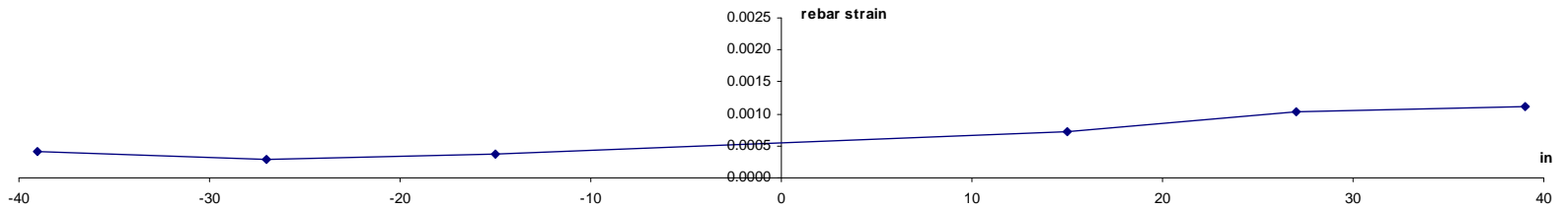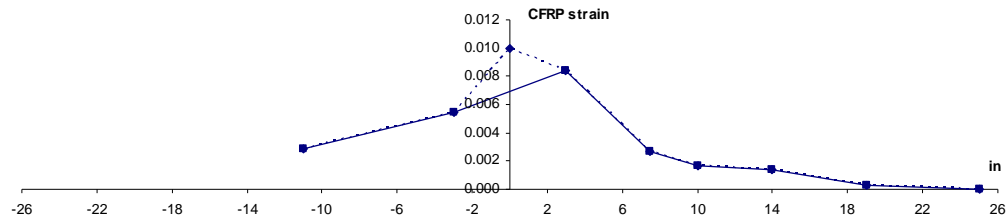
Figure A.30   Location of strain gages and distribution of strain in CFRP and bars, B-BH-A-6S, 3 in.

359

A.4   A-S-A-6G

A.4.1   Drop Height: 6 in.
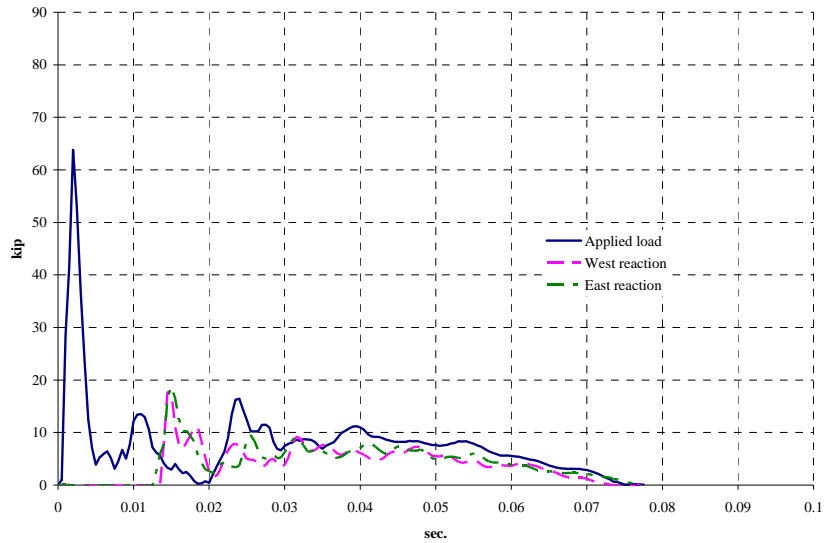
Figure A.31   Measured applied load and reactions, A-S-A-6G, 6 in.
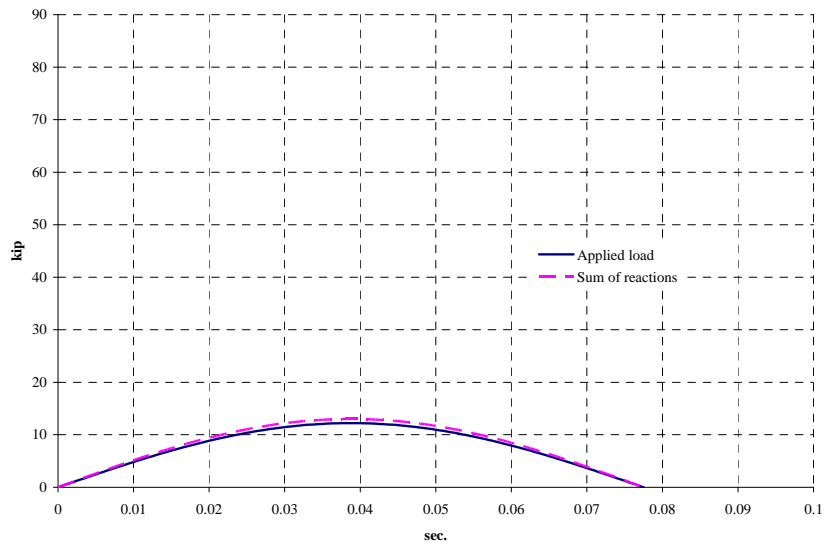
Figure A.32   Normalized applied load and sum of reactions, A-S-A-6G, 6 in.

360
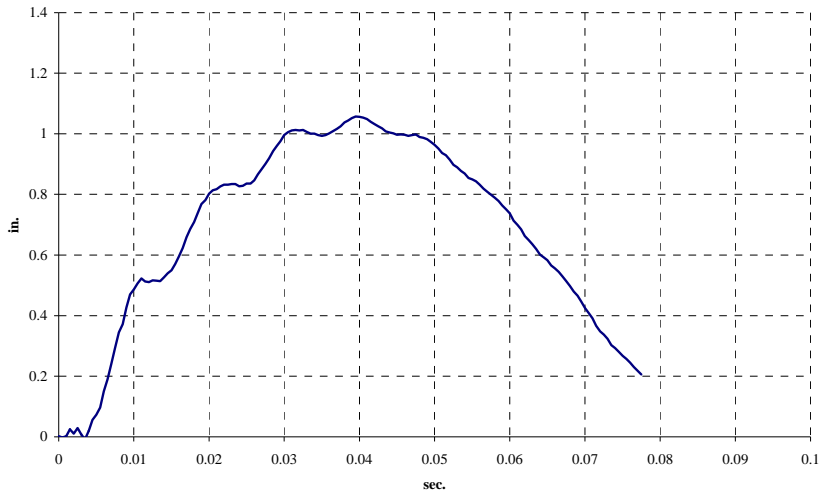
Figure A.33   Displacement in the center, A-S-A-6G, 6 in.
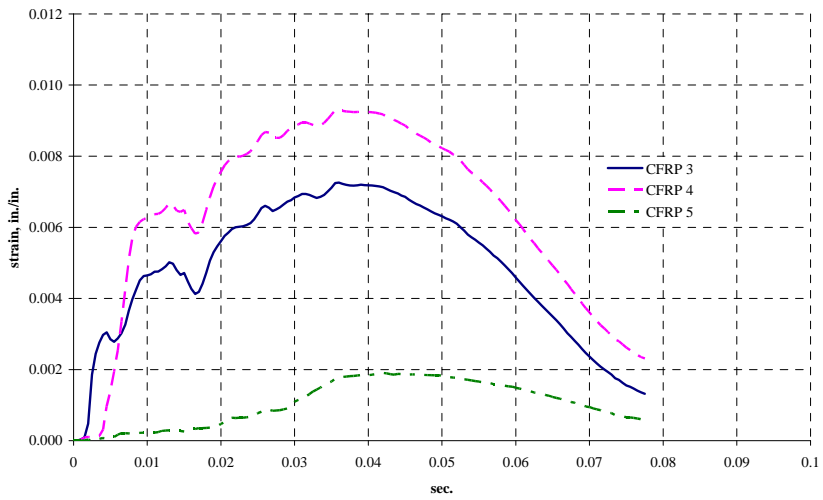
Figure A.34   CFRP strain, A-S-A-6G, 6 in.
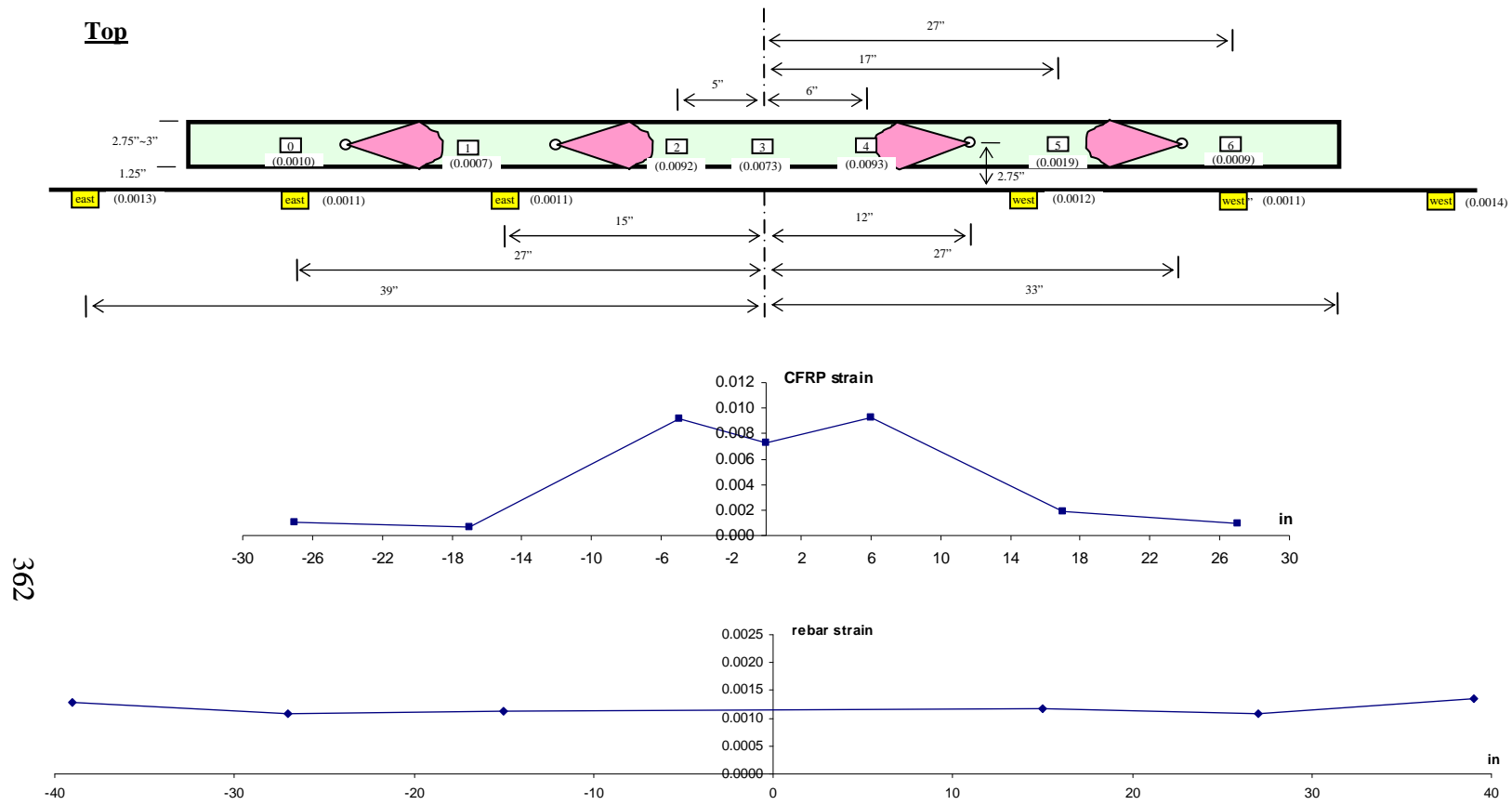
Figure A.35   Location of strain gages and distribution of strain in CFRP and bars, A-S-A-6G, 6 in.

A.5 A-S-AU-2S

A.5.1 Drop Height: 6 in.
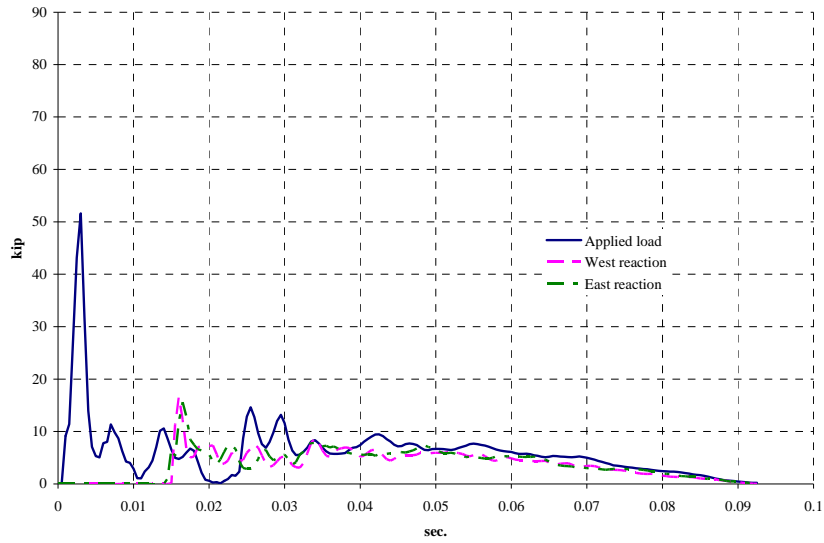
Figure A.36   Measured applied load and reactions, A-S-AU-2S, 6 in.
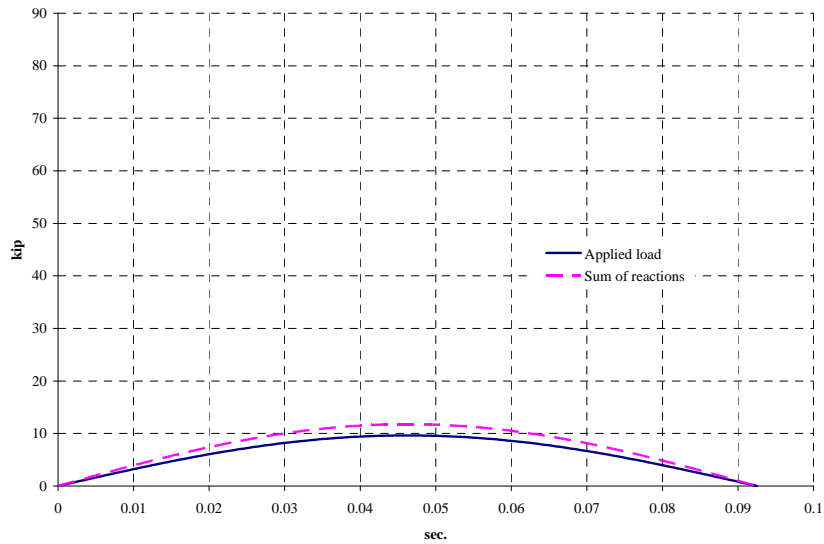
Figure A.37   Normalized applied load and sum of reactions, A-S-AU-2S, 6 in.

363
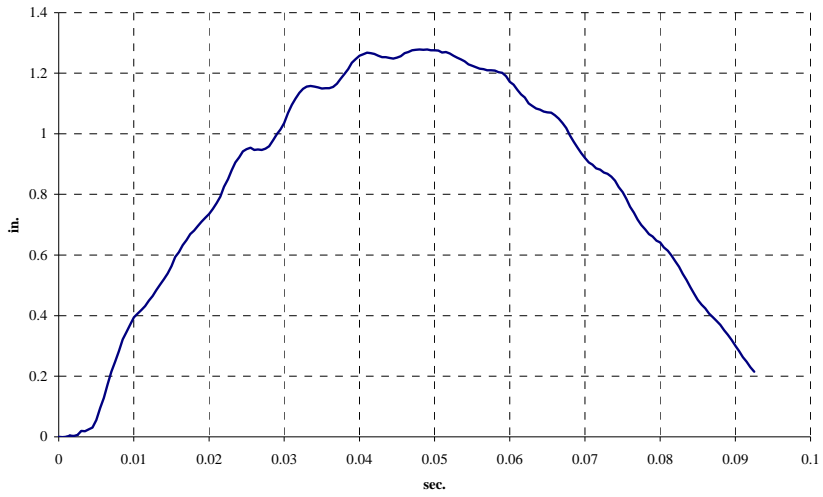
Figure A.38   Displacement in the center, A-S-AU-2S, 6 in.
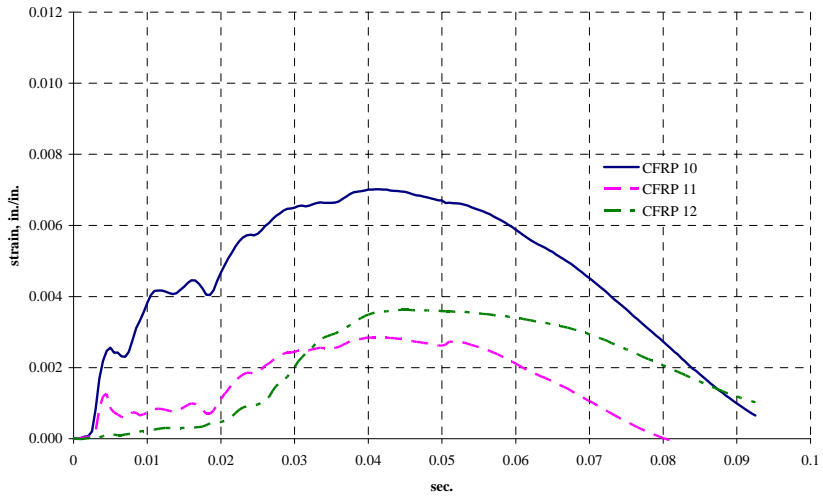
Figure A.39   CFRP strain, A-S-AU-2S, 6 in.

364

Bottom

| 0 (0.0010) | 1 (0.0039) | 2 (0.0069) | 3 (0.0082) | 4 (0.0053) | 5 (0.0044) | 6 (0.0011) |

1.5" 12" 6" 11" 10"

6" 66"

Top

| 7 (0.0011) | 8 (0.0032) | 9 (0.0070) | 10 (0.0070) | 11 (0.0029) | 12 (0.0036) | 13 (0.0012) |

1.5" 12" 6" 11" 10"

6" 66"
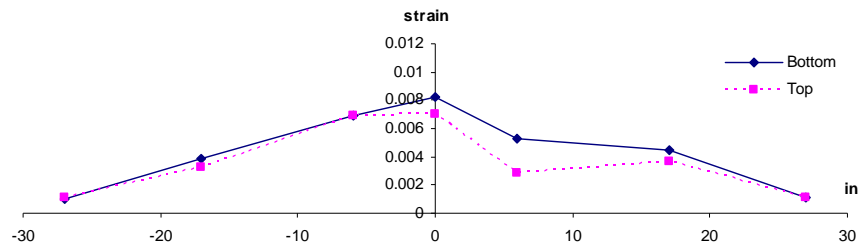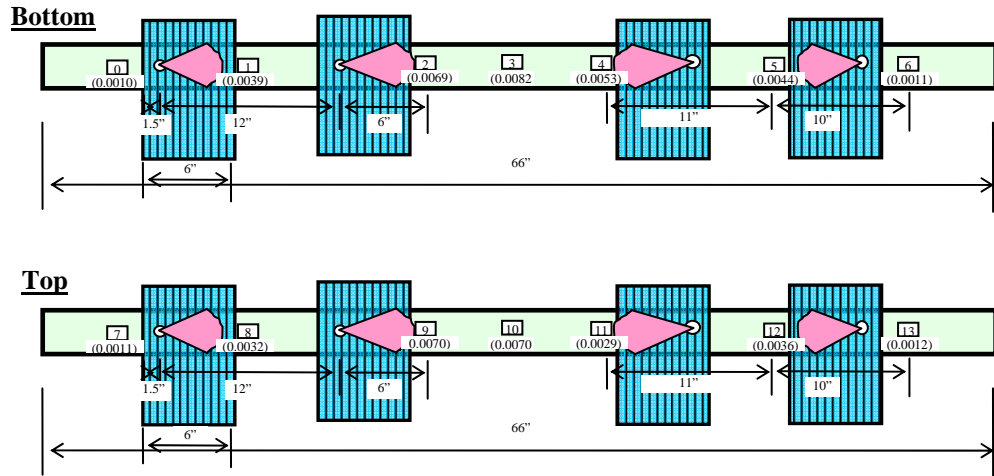
strain

Figure A.40   Location of strain gages and distribution of strain in CFRP, A-S-AU-2S, 6 in.

365

A.6 C-BC-A-6G-01

A.6.1 Drop Height: 2 in.
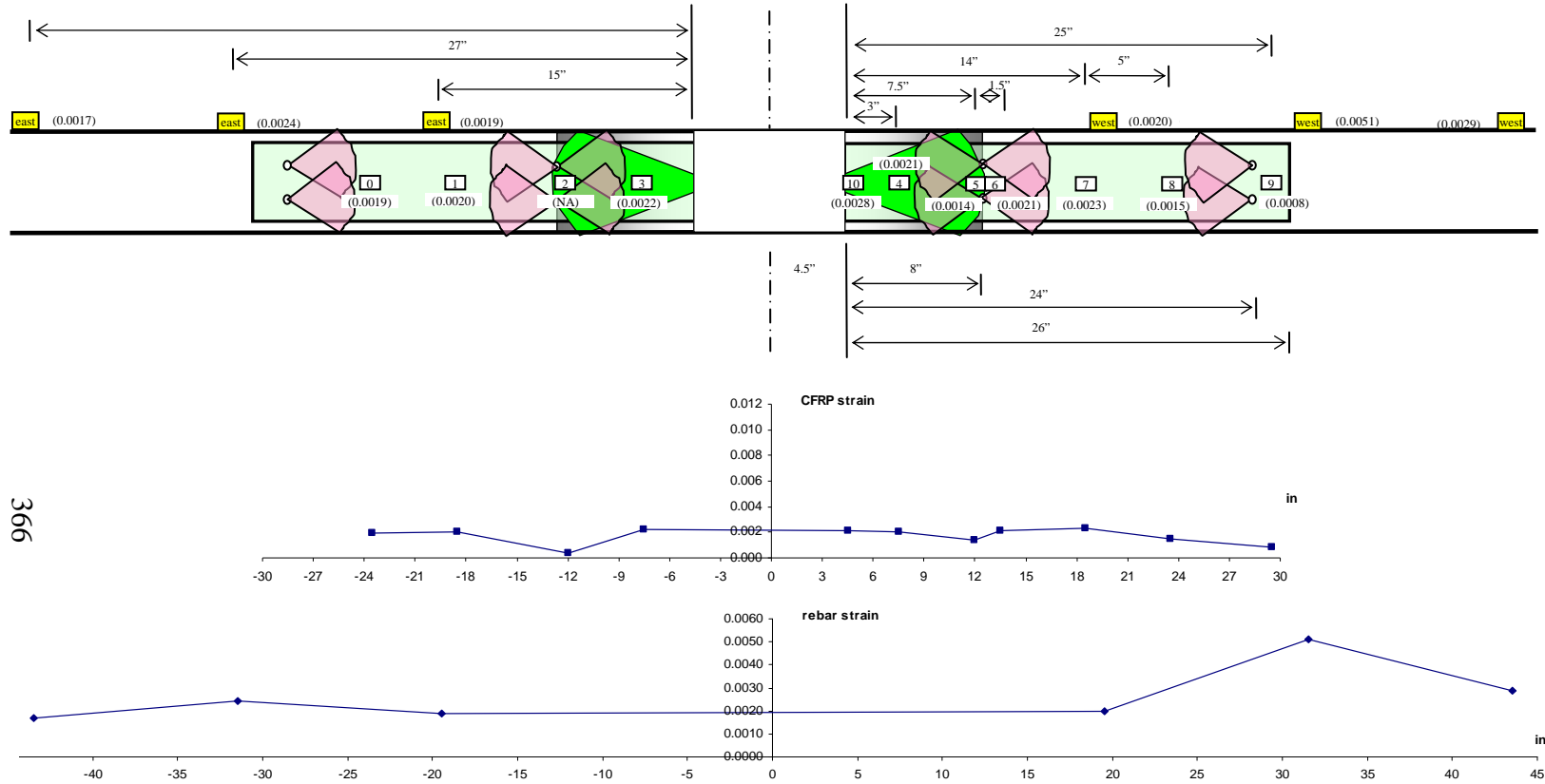
Figure A.41 Location of strain gages and distribution of strain in CFRP and bars, C-BC-A-6G-01, 2 in.

A.6.2   Drop Height: 4.5 in.
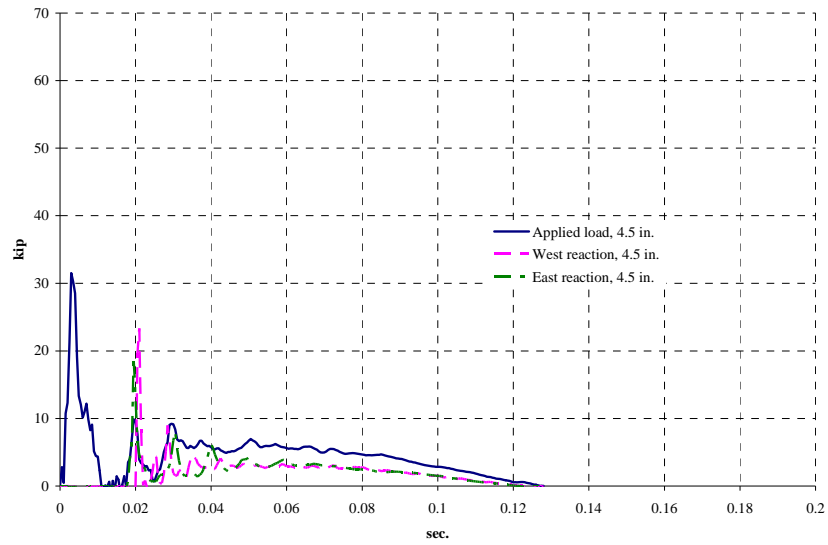
Figure A.42   Measured applied load and reactions, C-BC-A-6G-01, 4.5 in.
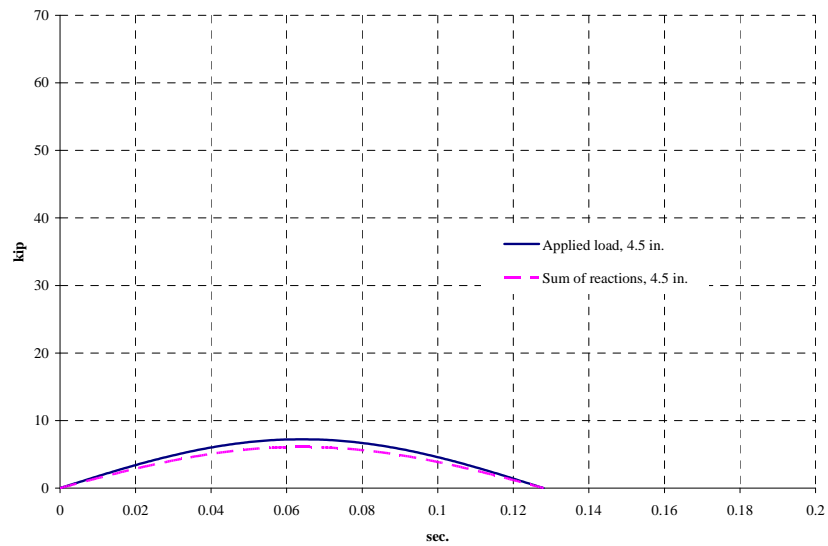
Figure A.43   Normalized applied load and sum of reactions, C-BC-A-6G-01, 4.5 in.

367
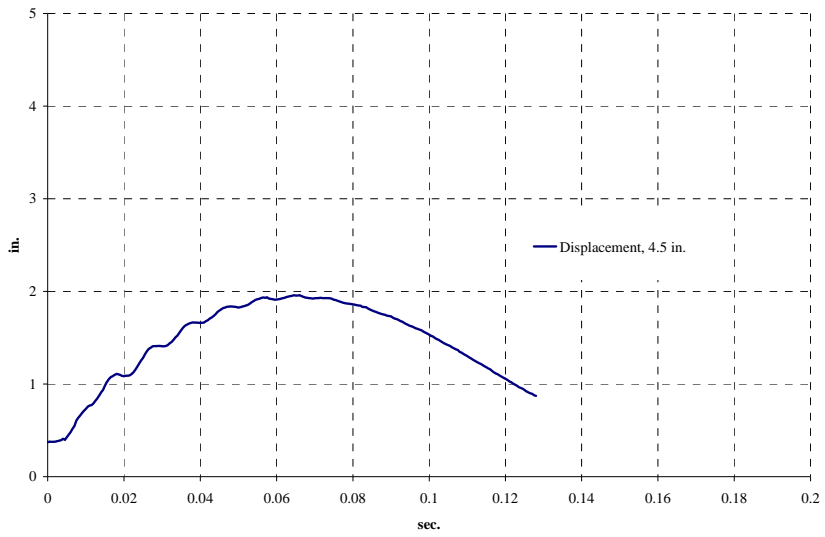
Figure A.44   Displacement in the center, C-BC-A-6G-01, 4.5 in.
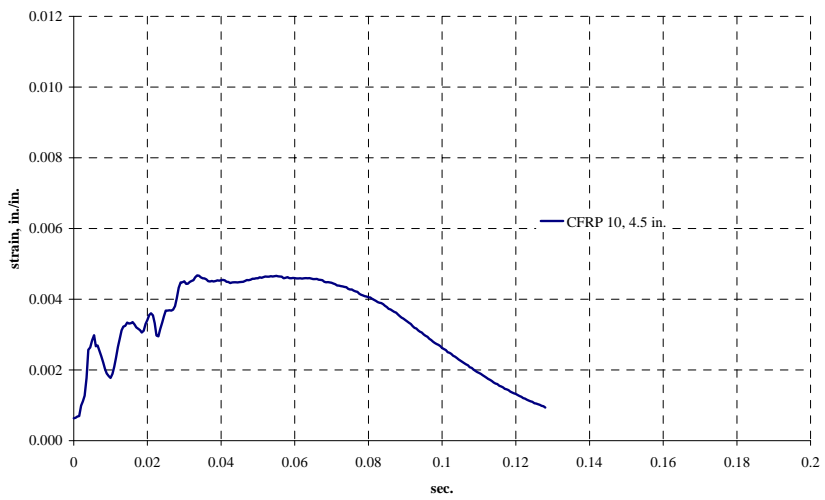
Figure A.45   CFRP strain, C-BC-A-6G-01, 4.5 in.

368
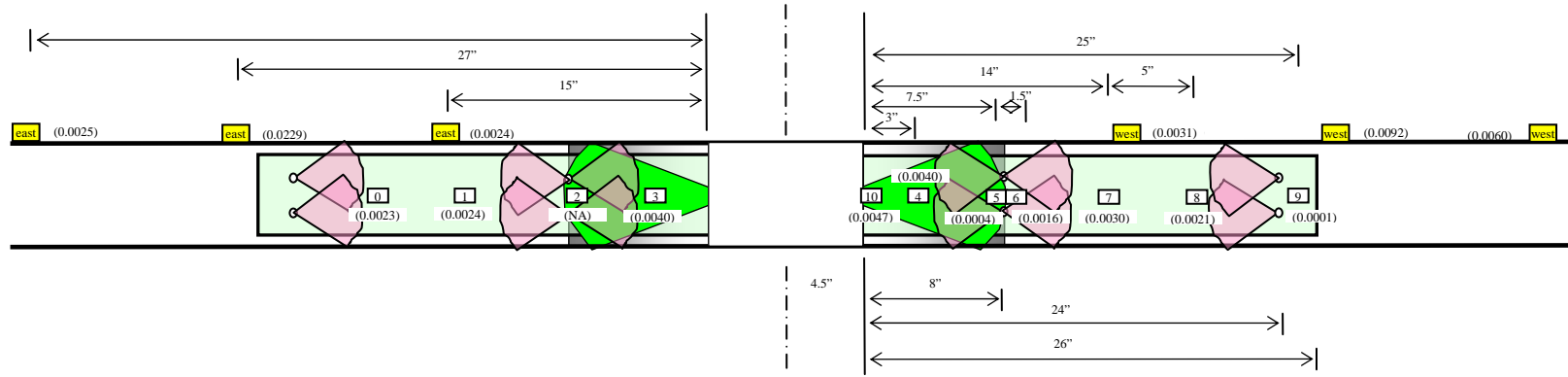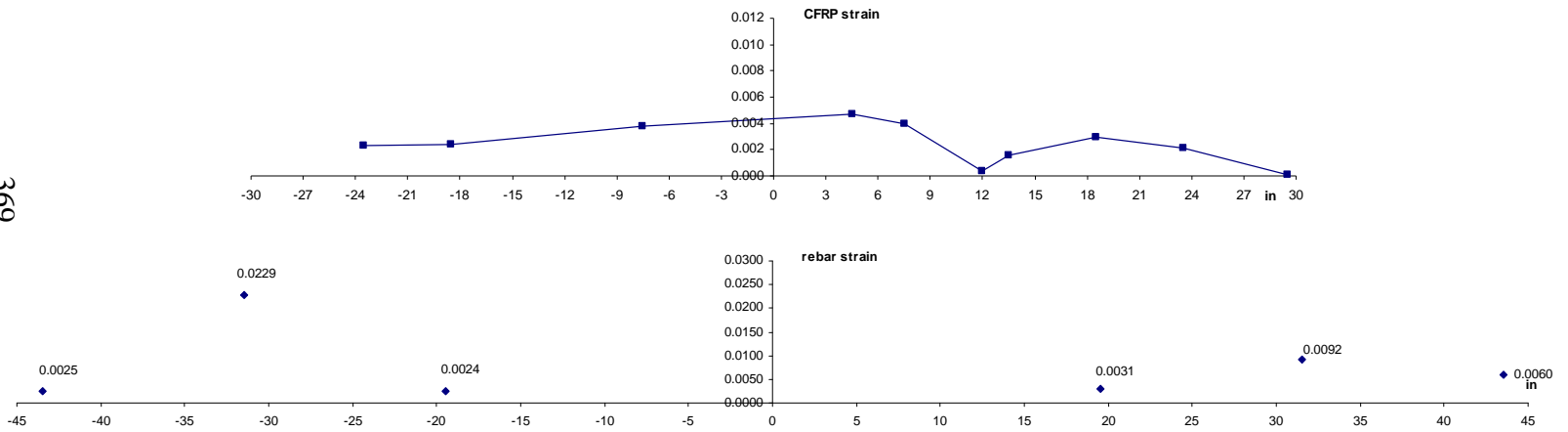
Figure A.46   Location of strain gages and distribution of strain in CFRP and bars, C-BC-A-6G-01, 4.5 in.
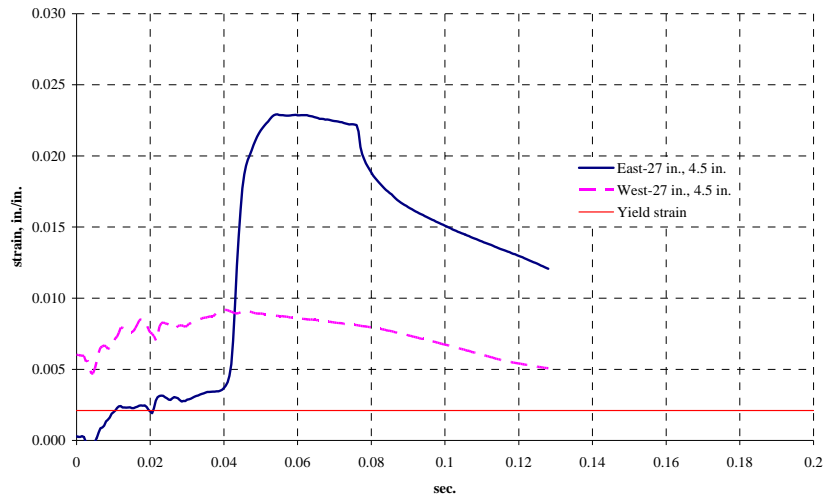
Figure A.47   Steel reinforcement strain, C-BC-A-6G-01, 4.5 in.

A.6.3 Drop Height: 9 in.
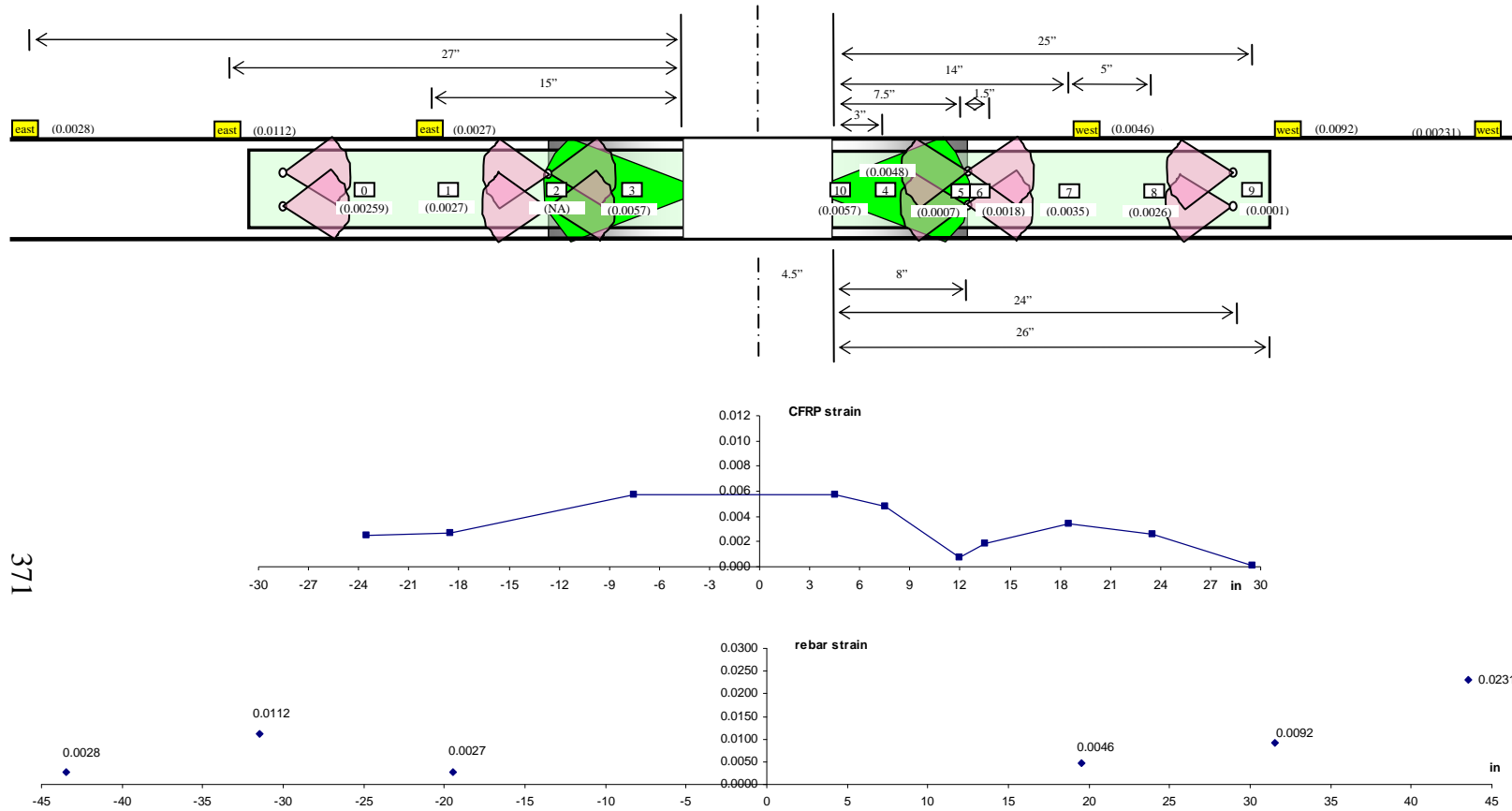
Figure A.48   Location of strain gages and distribution of strain in CFRP and bars, C-BC-A-6G-01, 9 in.

A.7 C-BC-A-6G-02

A.7.1 Drop Height: 2 in.
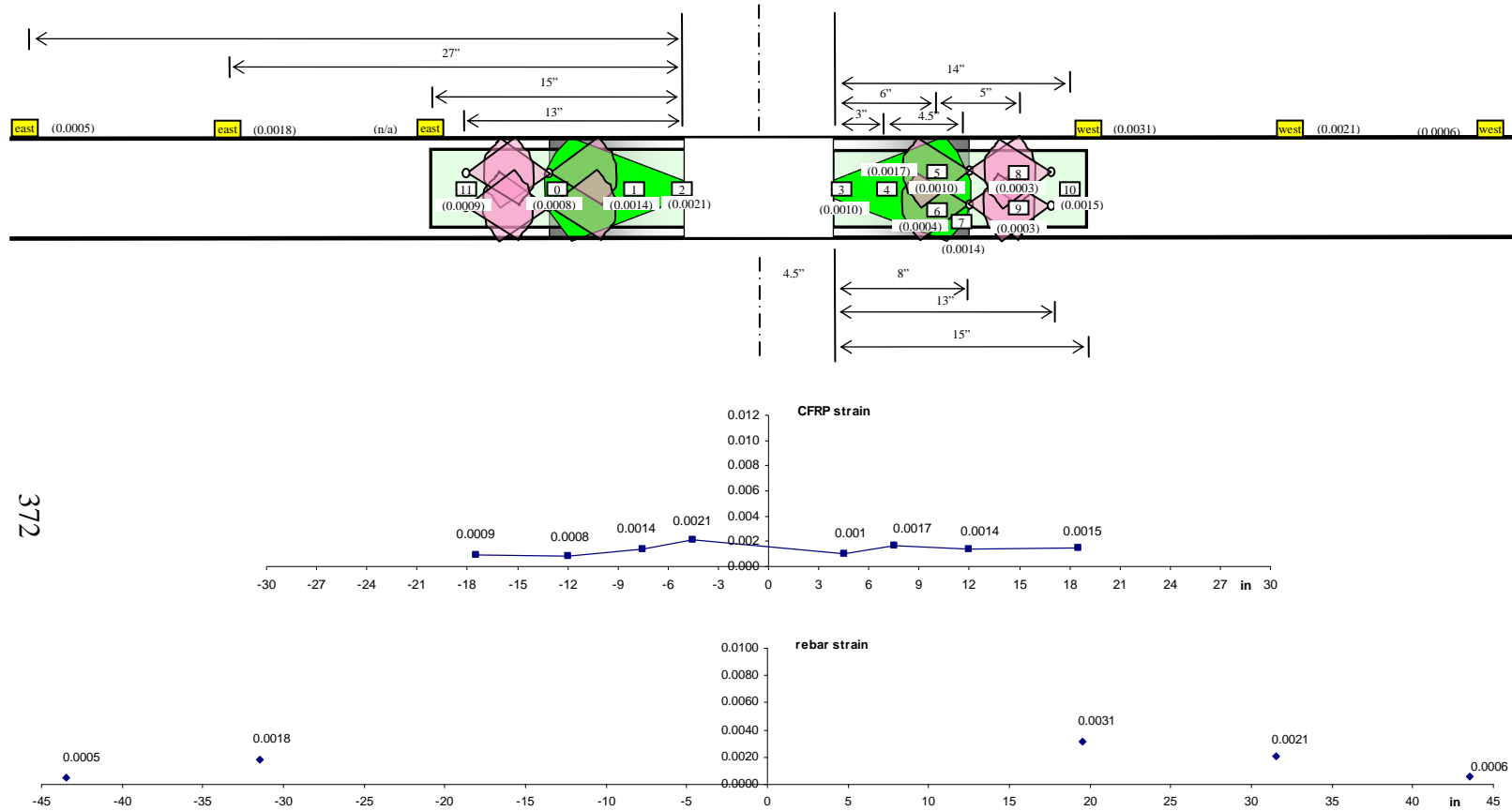
Figure A.49   Location of strain gages and distribution of strain in CFRP and bars, C-BC-A-6G-02, 2 in.

A.7.2 Drop Height: 4.5 in.
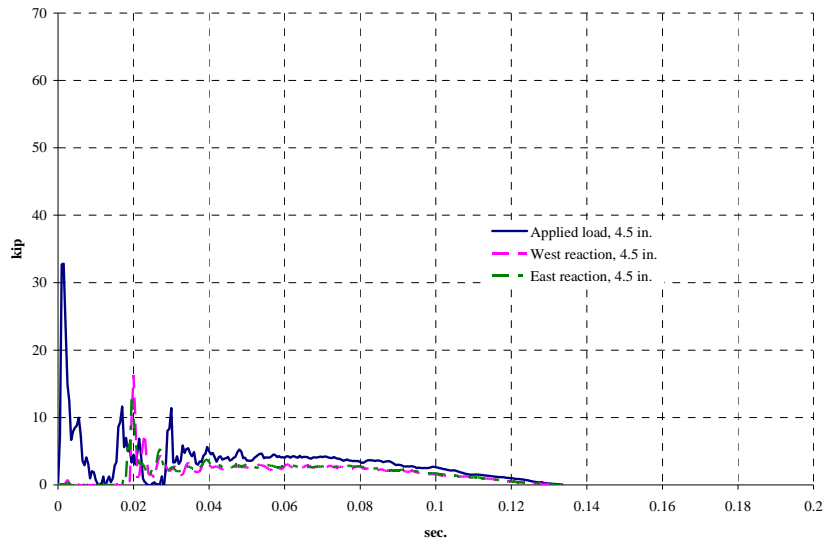
Figure A.50   Measured applied load and reactions, C-BC-A-6G-02, 4.5 in.
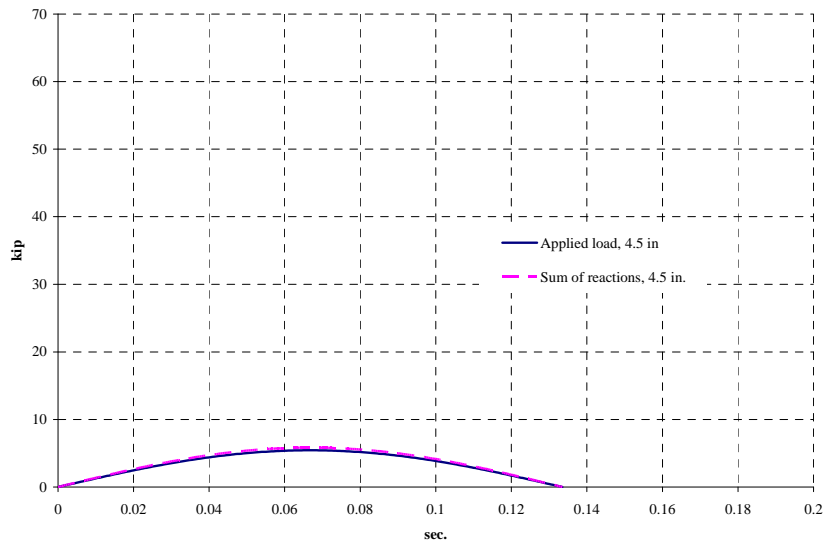
Figure A.51   Normalized applied load and sum of reactions, C-BC-A-6G-02, 4.5 in.

373
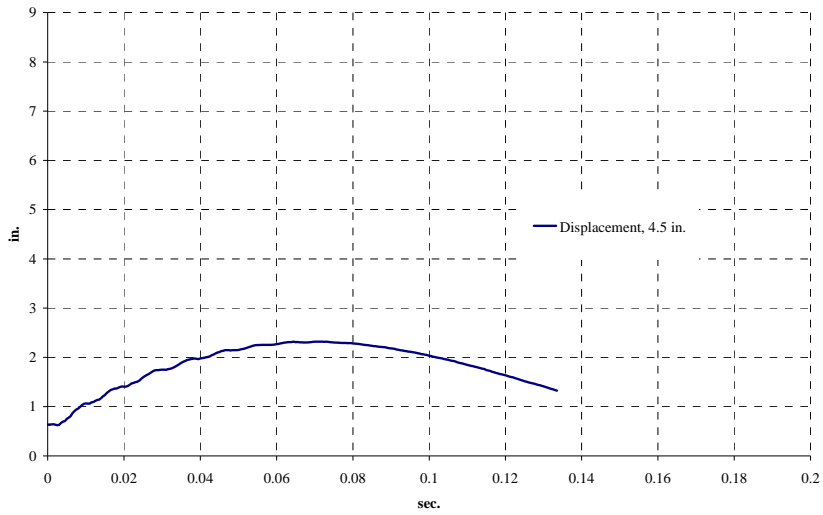
Figure A.52   Displacement in the center, C-BC-A-6G-02, 4.5 in.
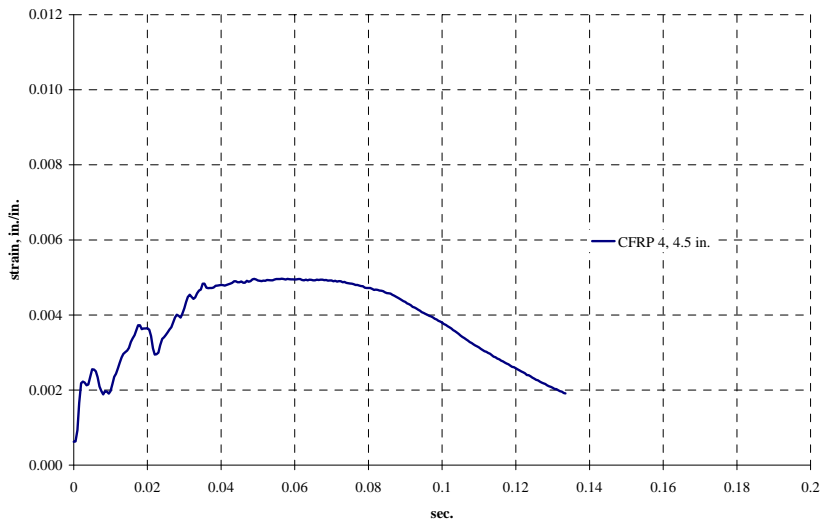
Figure A.53   CFRP strain, C-BC-A-6G-02, 4.5 in.

374
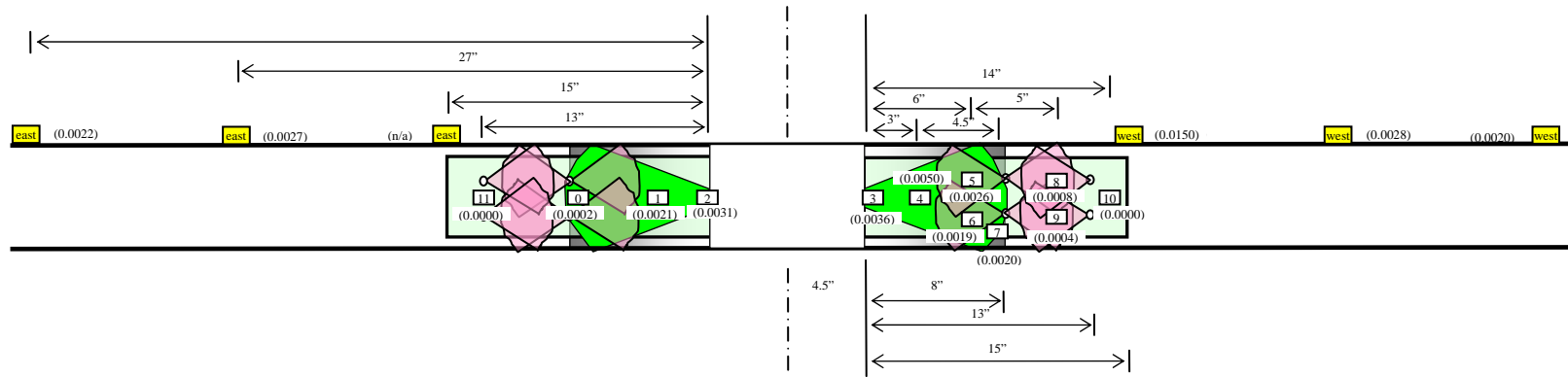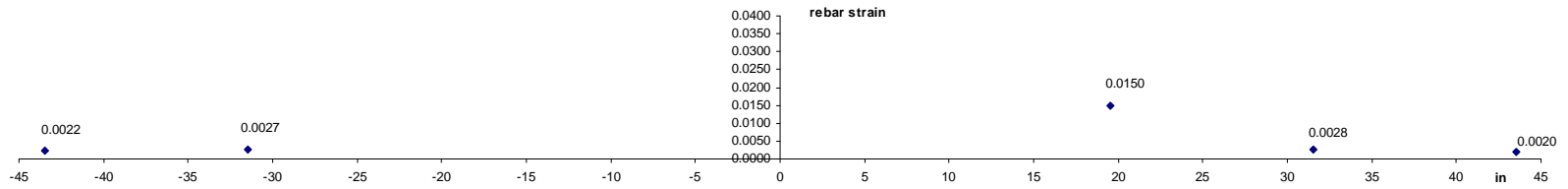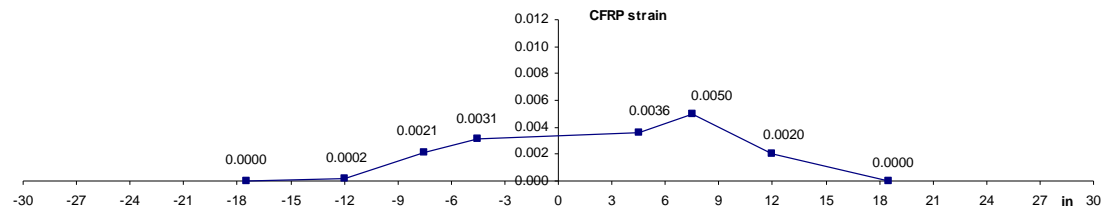
Figure A.54   Location of strain gages and distribution of strain in CFRP and bars, C-BC-A-6G-02, 4.5 in.
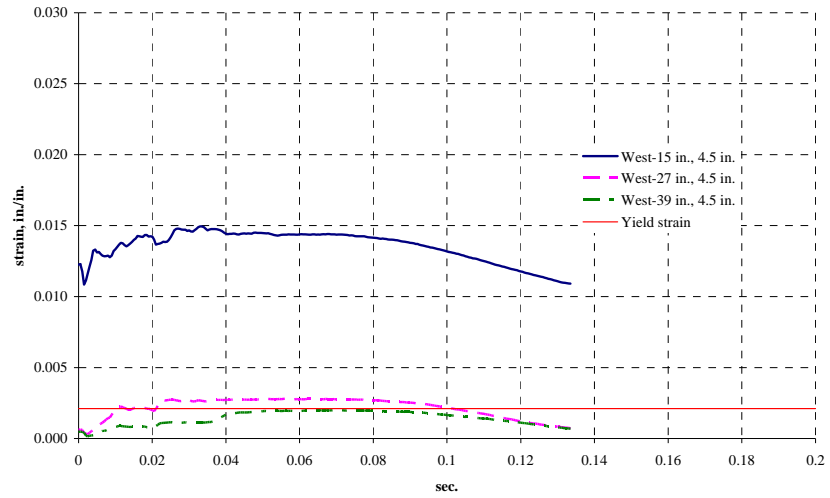
Figure A.55   Steel reinforcement strain, C-BC-A-6G-02, 4.5 in.

A.7.3   Drop Height: 9 in.
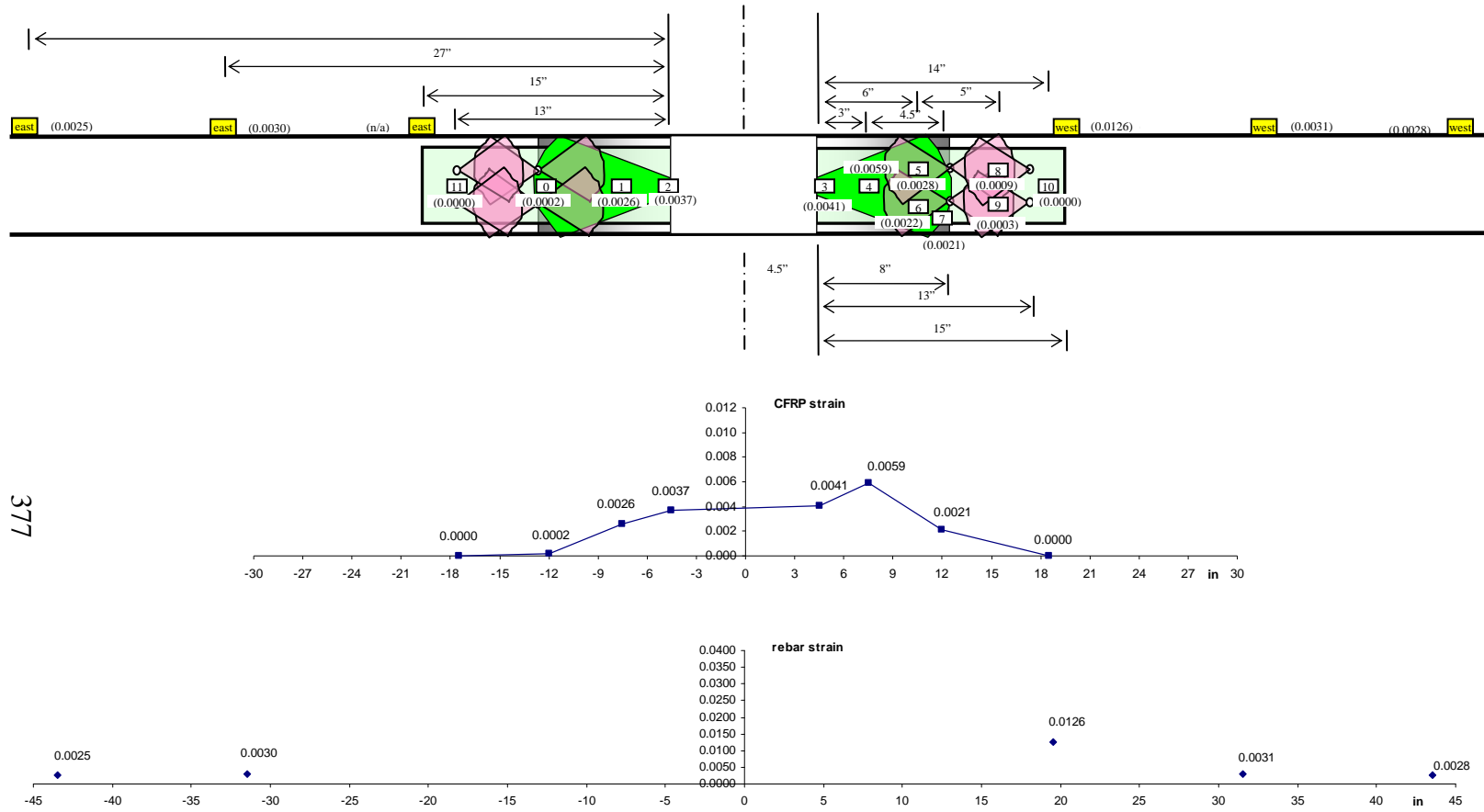
Figure A.56   Location of strain gages and distribution of strain in CFRP and bars, C-BC-A-6G-02, 9 in.

A.7.4 Drop Height: 12 in.-01

Figure A.57   *Measured applied load and reactions, C-BC-A-6G-02, 12 in.-01*
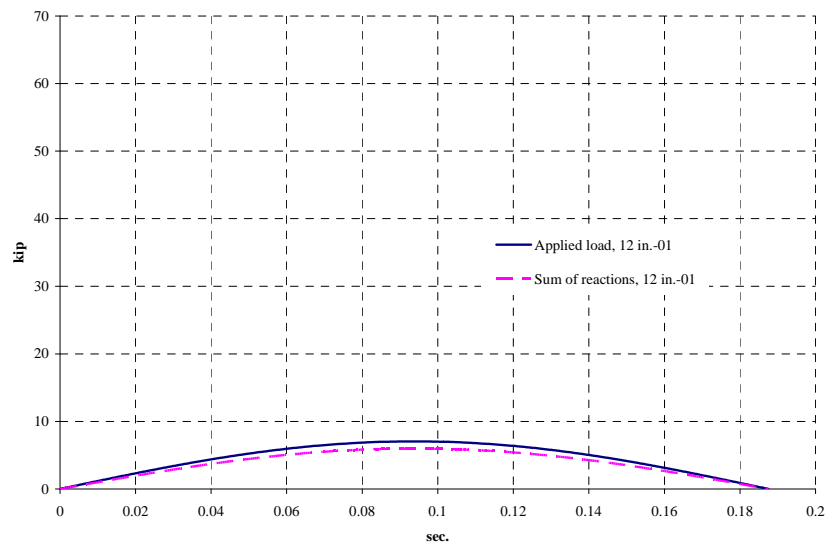
Figure A.58   *Normalized applied load and sum of reactions, C-BC-A-6G-02, 12 in.-01*

378
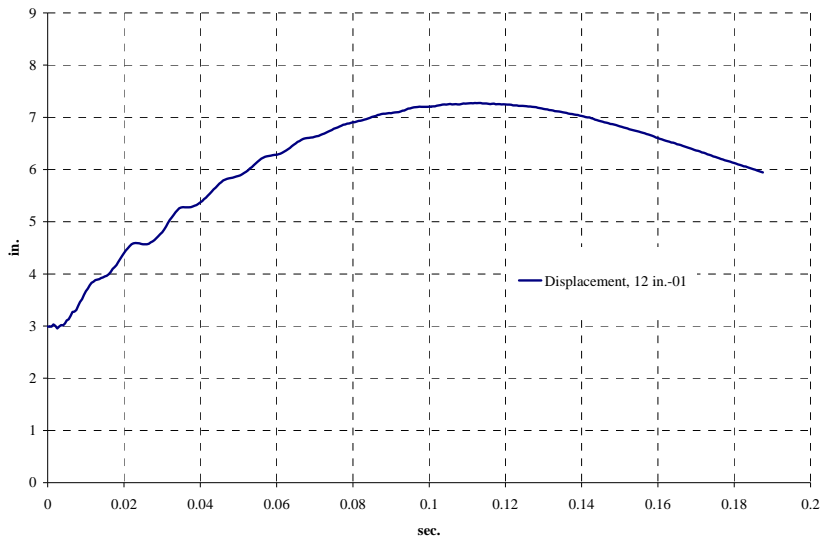
Figure A.59   Displacement in the center, C-BC-A-6G-02, 12 in.-01
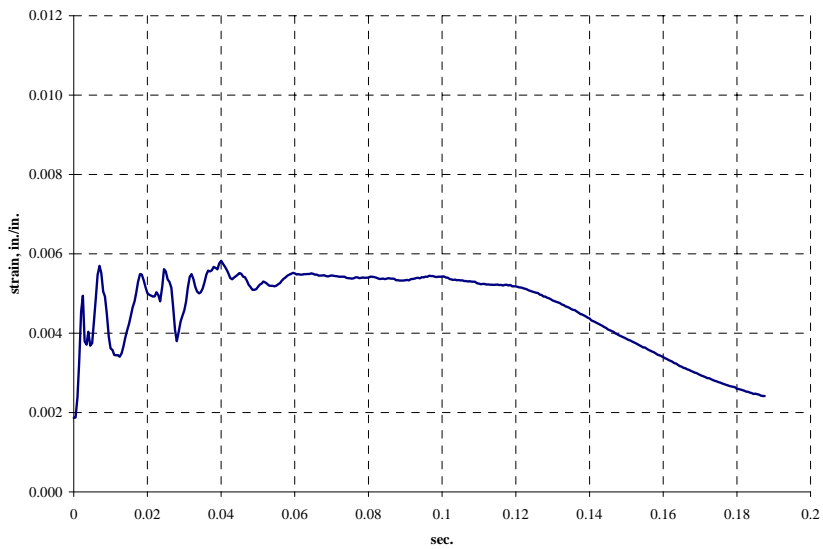
Figure A.60   CFRP strain, C-BC-A-6G-02, 12 in.-01

CFRP strain

0.0000 0.0002 0.0026 0.0036 0.0039 0.0058 0.0016 0.0000

rebar strain

0.0027 0.0031 0.0086 0.0030 0.0028
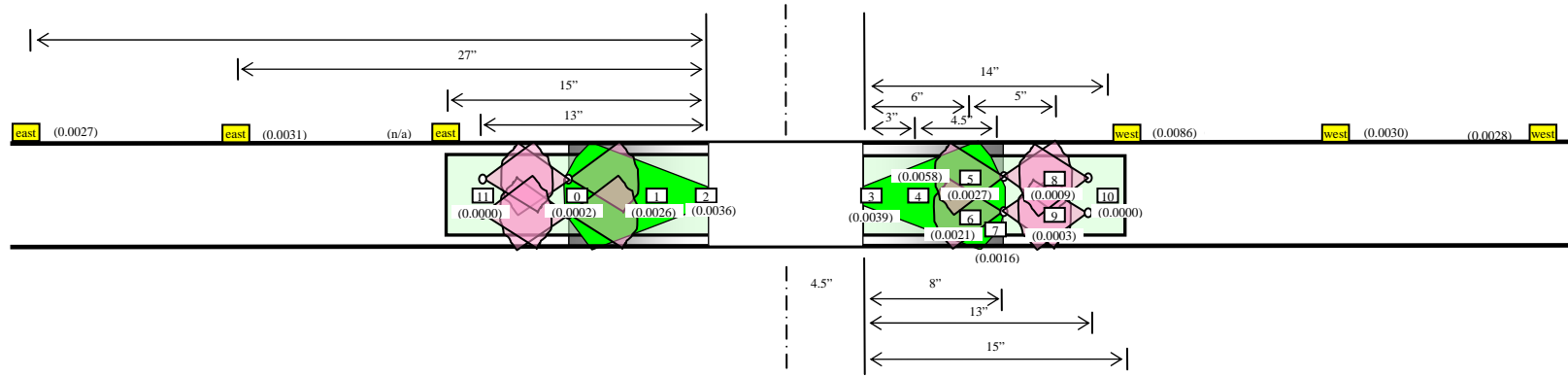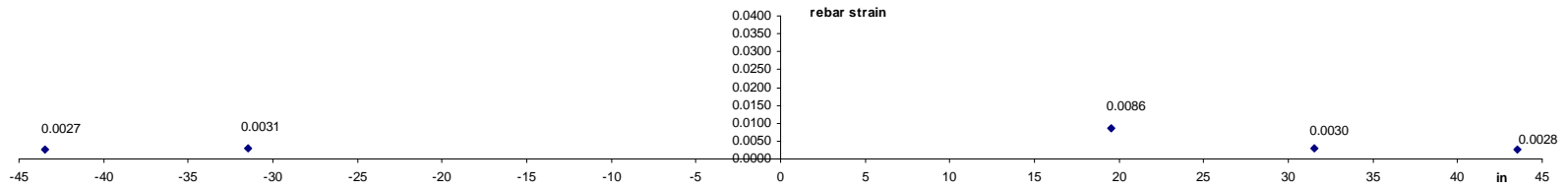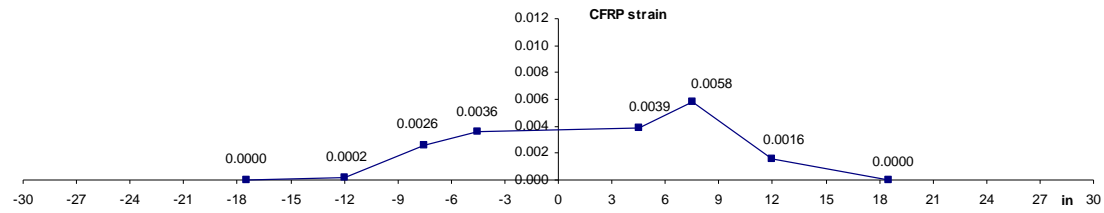
Figure A.61   Location of strain gages and distribution of strain in CFRP and bars, C-BC-A-6G-02, 12 in.-01
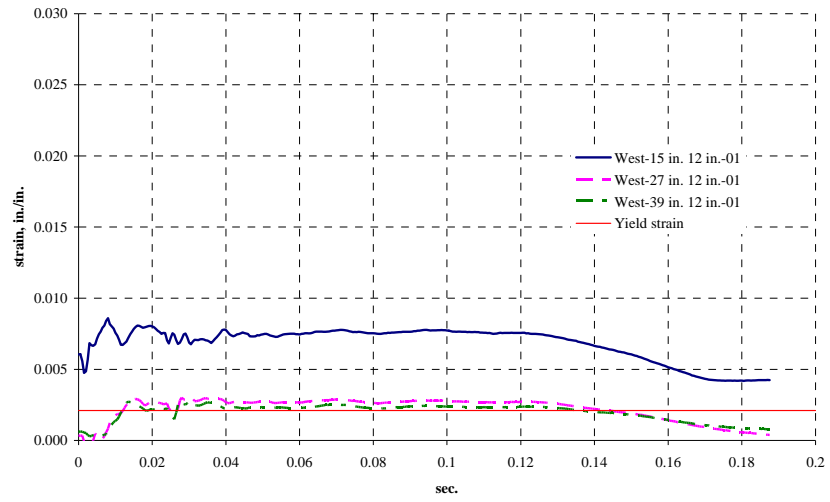
Figure A.62   Steel reinforcement strain, C-BC-A-6G-02, 12 in.-01

A.8   C-BC-U-6G

A.8.1   Drop Height: 2 in.
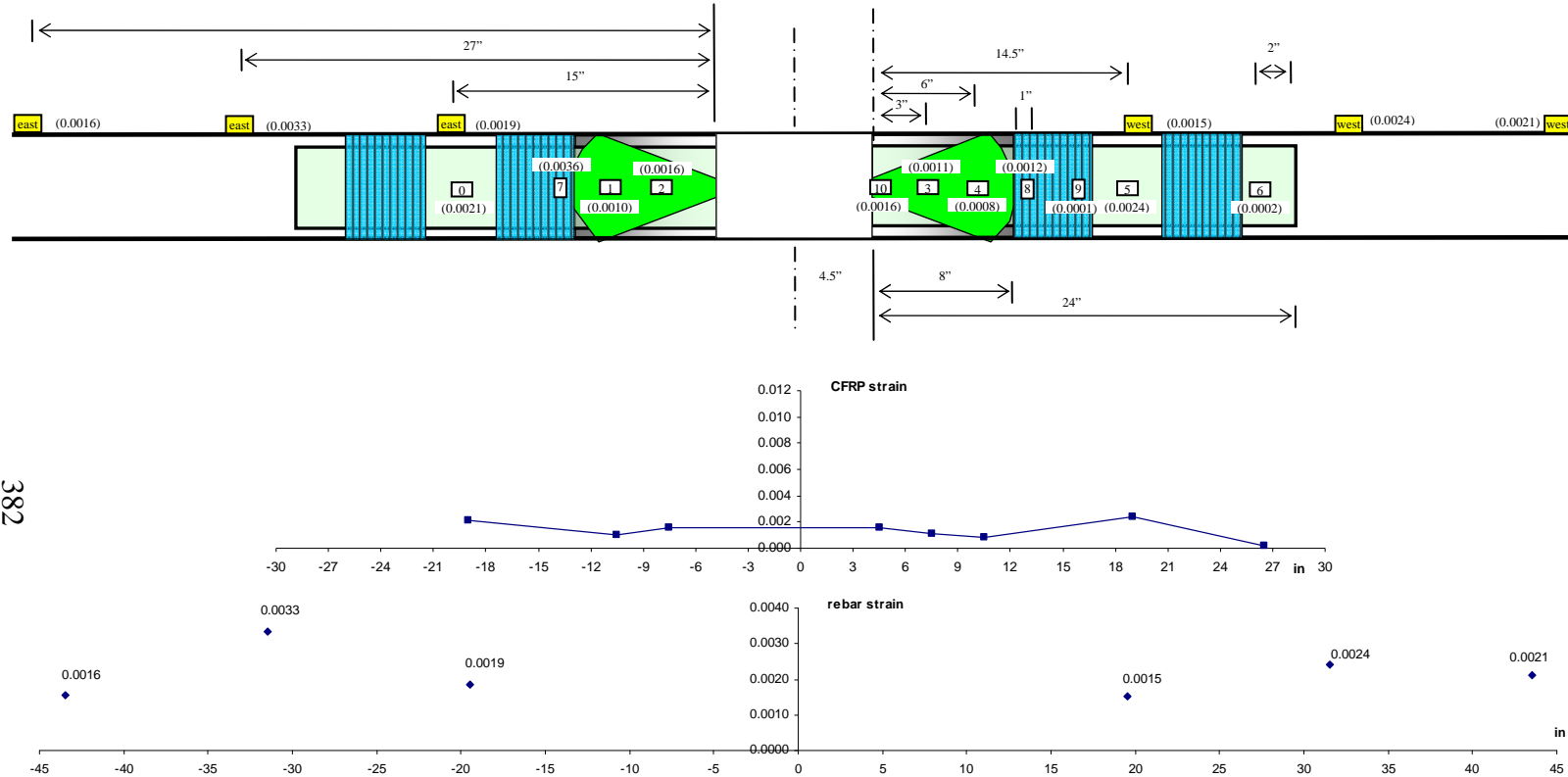
Figure A.63   Location of strain gages and distribution of strain in CFRP and bars, C-BC-U-6G, 2 in.

APPENDIX B

Crack Injection and Installation Procedure of CFRP in Reinforced Concrete Columns

B.1 CRACK INJECTION PROCEDURE

1. Clean surface along the crack. Blow out crack with dry and oil-free compressed air.

2. Bond injection ports with CI 070 EP Crack Sealing Compound. Port spacing approximately 6" to 12" with wider spacing for thinner slabs.

3. Seal the crack with CI 070 EP surface sealing compound in strips of minimum 2" wide, 1/8" deep. (Seal both sides if crack goes completely through concrete.)

4. A light tap with a hammer to the rear end of the CI 060 EP cartridge breaks the internal glass cylinder, releasing the hardener. Mix by see-saw motion for approximately 30 motions. Do not shake.

5. Puncture the seal of the cartridge tip. Then screw on connection hose.

6. Plug connection hose to bottom port. Place air relief stopper in next port above.

7. Inject CI 060 EP resin until it appears visibly in the next port above. Remove air relief stopper (non-return valve is now closed) and insert into next port. Continue injecting into original port until the port accepts no more resin (when normal hand pressure is used on the dispenser).

8. Detach connection hose from port and plug to the next higher port. Repeat operating steps 6 and 7 up to the end of the crack.

9. After the injection resin has set, generally over night, the ports and the sealing compound can be removed with a flat chisel. If required, the surface can be ground even.

http://www.us.hilti.com/data/techlib/docs/installation%20instructions/construction%20chemicals/CI060.pdf

B.2 CFRP INSTALLATION PROCEDURE

The installation procedure of CFRP in reinforced concrete columns is as follows.

1) Drill holes and grind edge of holes for CFRP anchors

2) Grind to roughen the concrete surface

3) Grind to round the corners

4) Clean the holes and surfaces with air compressed

5) Prepare epoxy resin

6) Saturate the concrete surface and holes with the epoxy resin

7) Saturate CFRP jackets with the epoxy resin and remove excess epoxy

8) Place the CFRP jackets on the column

9) Saturate CFRP anchors with the epoxy resin

10) Place the CFRP anchors on the column

11) Cure

Figure B.2.1   Drill holes for CFRP anchors

Figure B.2.2   Grind edge of the holes for CFRP anchors

385

Figure B.2.3   Grind to roughen the concrete surface

Figure B.2.4   Grind to round the corners

Figure B.2.5   Clean the holes with air compressed

Figure B.2.6   Clean the surfaces with air compressed

387

Figure B.2.7   Prepare epoxy resin

Figure B.2.8   Saturate the concrete surface with the epoxy resin

Figure B.2.9   Saturate the holes with the epoxy resin

Figure B.2.10 Saturate the holes with the epoxy resin

Figure B.2.11 Saturate CFRP jackets with the epoxy resin

Figure B.2.12 Remove excess epoxy

Figure B.2.13 Place the CFRP jackets on the column

Figure B.2.14 Place the CFRP jackets on the column

Figure B.2.15 Saturate CFRP anchors with the epoxy resin

Figure B.2.16 Place the CFRP anchors on the column

Figure B.2.17 Place the CFRP anchors on the column

Figure B.2.18 Inject epoxy to fill all voids in anchor hole

393

Figure B.2.19 Complete column

APPENDIX C

Additional Experimental Data – Column Tests

In APPENDIX C, additional experimental data of the column test which are not shown in CHAPTER 4 is provided. Data from damaged instruments are removed.

C.1 1-A-S8-M

C.1.1 Lateral Displacement VS Lateral Load
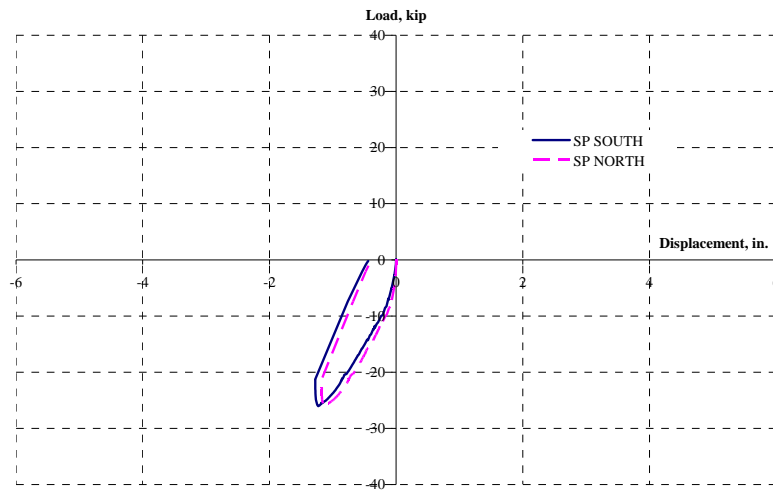
Figure C.1   Lateral displacement vs lateral load, test <u>as built</u>, 1-A-S8-M
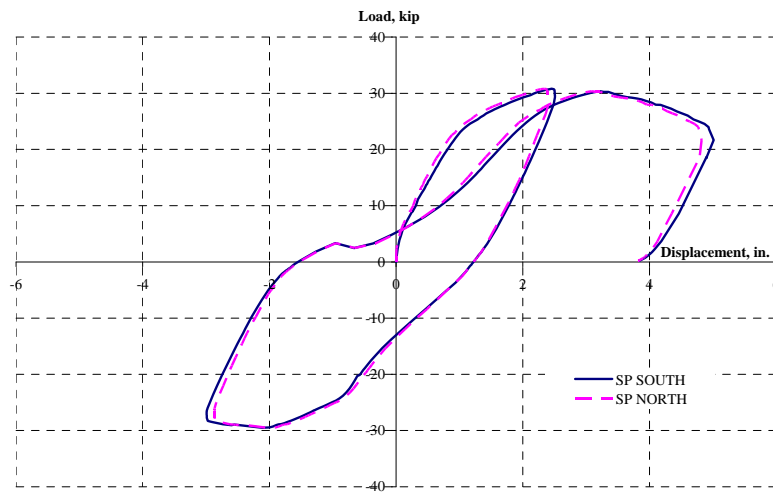
Figure C.2   Lateral displacement vs lateral load, test <u>after rehabilitation</u>, 1-A-S8-M

C.1.2   Vertical Displacement at 30 in. from Top of the Footing VS Lateral Load
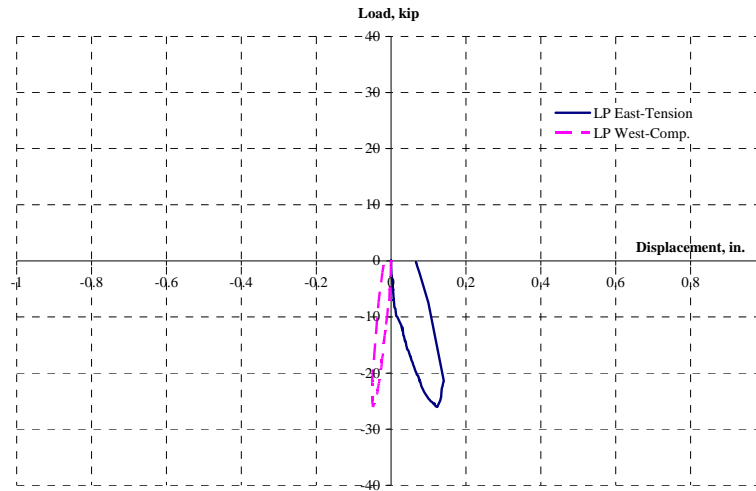
*Figure C.3   Vertical displacement at 30 in. from top of the footing vs lateral load,
test <u>as built</u>, 1-A-S8-M*
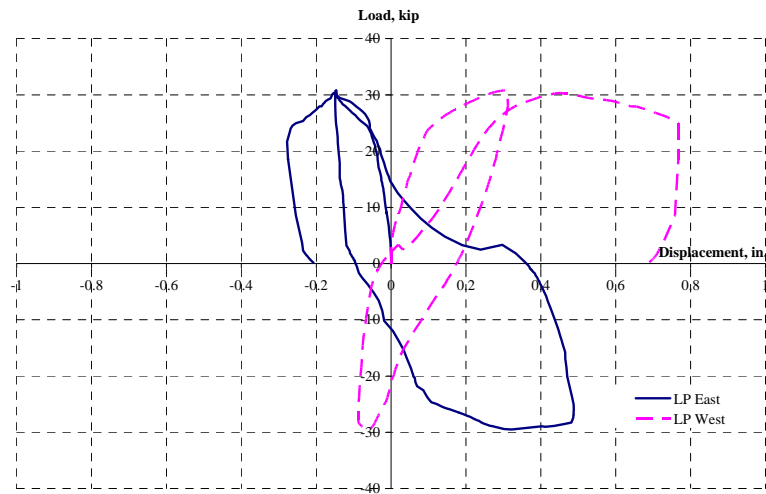
*Figure C.4   Vertical displacement at 30 in. from top of the footing vs lateral load,
test <u>after rehabilitation</u>, 1-A-S8-M*

C.1.3 Steel Reinforcement Strain
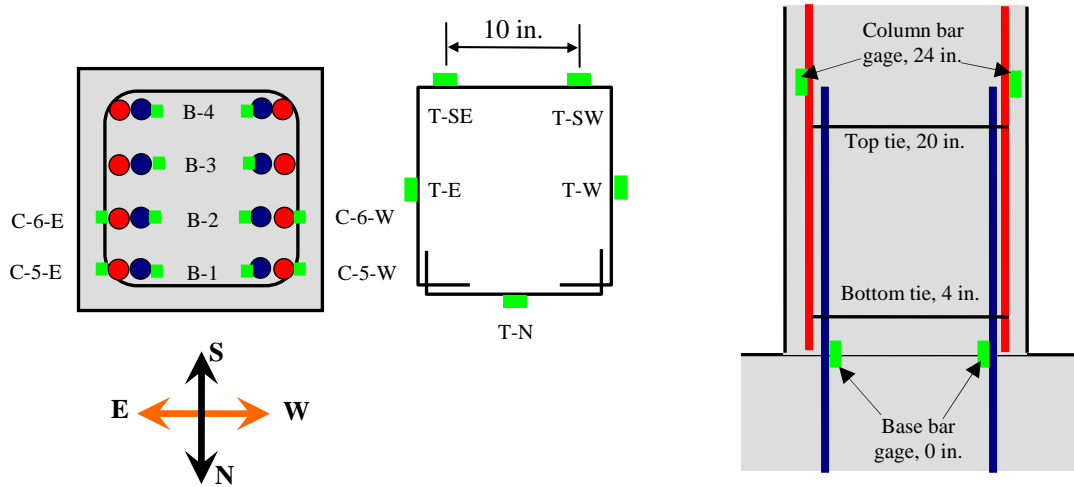
- **Base bar gages (B - # - Direction):** at the top of the footing
- **Column bar gages (C - # - Direction):** 24 in. from the top of the footing
- **Tie bar gages (T-Top or Bottom- Direction):**

> **Top-**tie at 20 in. from the top of the footing
>
> **Bottom-** tie at 4 in. from the top of the footing

Figure C.5   Layout of steel reinforcement strain gages, 1-A-S8-M

C.1.3.1 Base Bar Strain

C.1.3.1.1 Test as Built
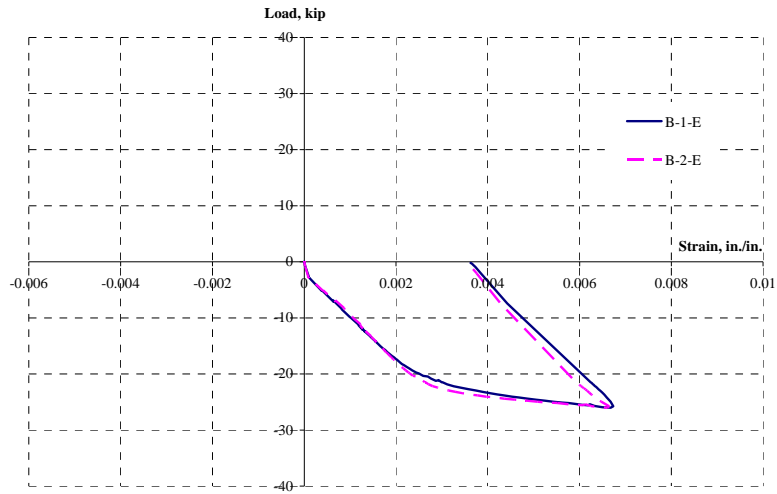
Figure C.6   Base bar strains, east side, 1-A-S8-M
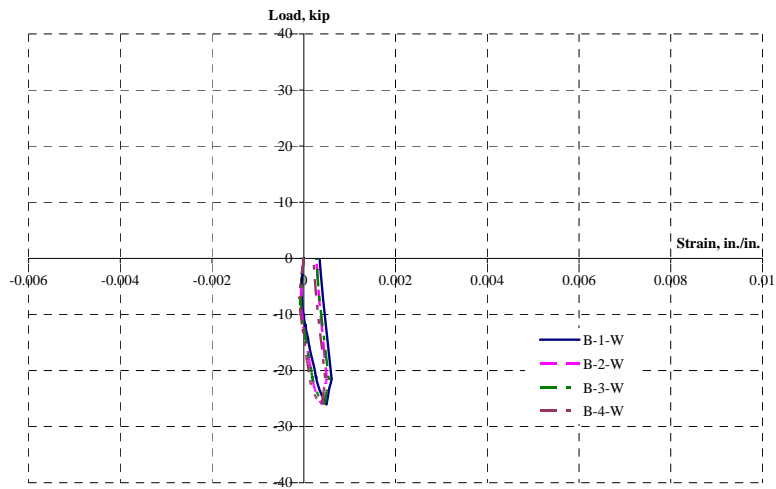
Figure C.7   Base bar strains, west side, 1-A-S8-M

399

C.1.3.1.2 Test after Rehabilitation
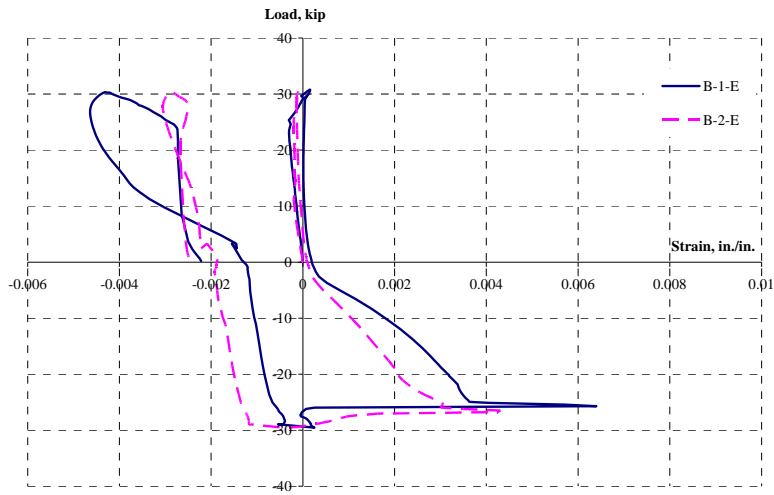
Figure C.8   Base bar strains, east side, 1-A-S8-M
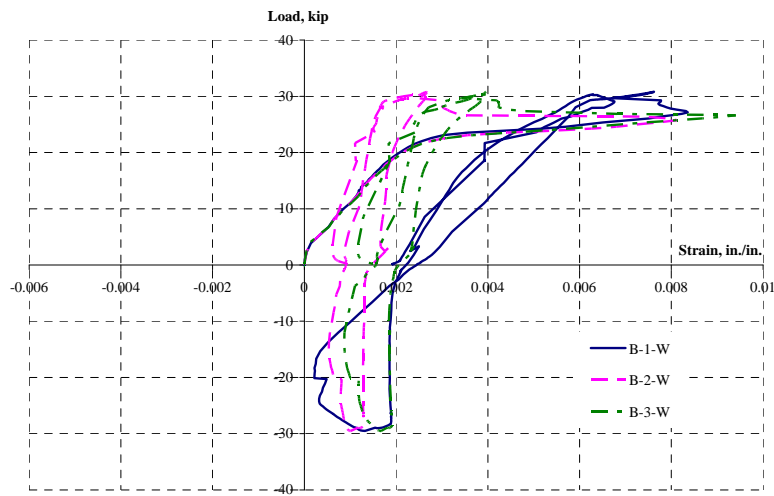
Figure C.9   Base bar stain, west side, 1-A-S8-M

C.1.3.2 Column Bar Strain

C.1.3.2.1 Test as Built
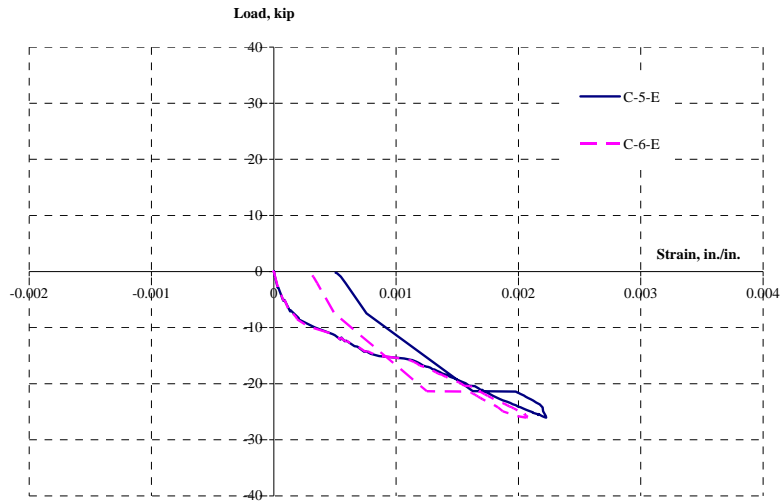
Figure C.10   Column bar strains, east side, 1-A-S8-M
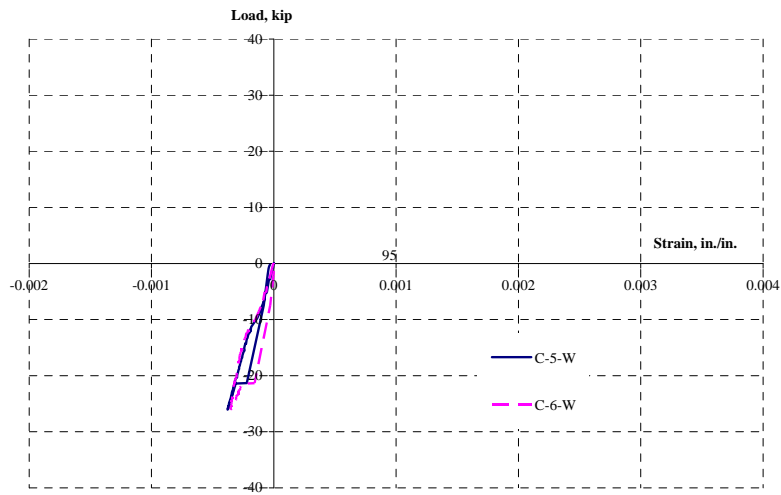
Figure C.11   Column bar strains, west side, 1-A-S8-M

C.1.3.2.2 Test after Rehabilitation
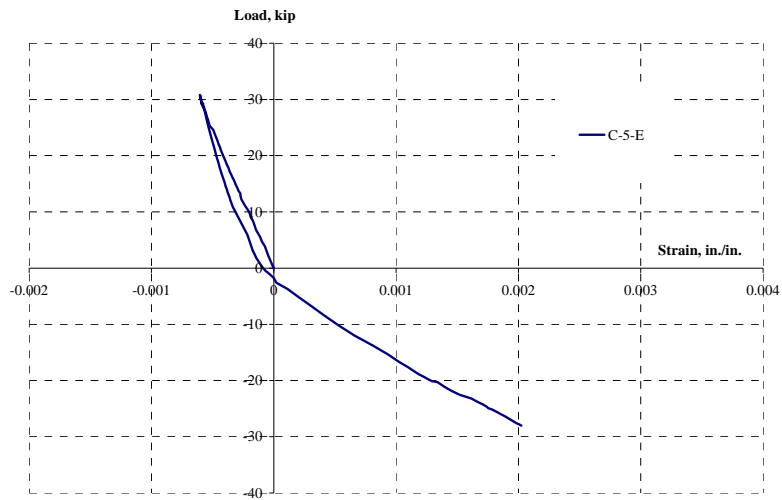
Figure C.12   Column bar strains, east side, 1-A-S8-M
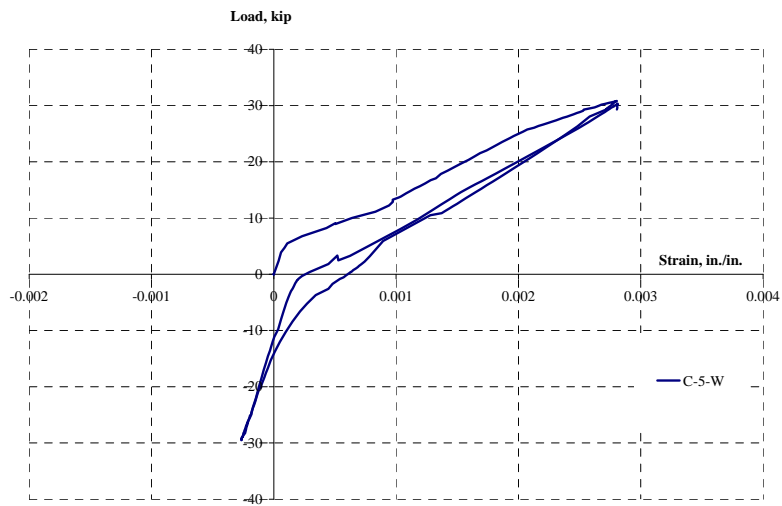
Figure C.13   Column bar strains, west side, 1-A-S8-M

C.1.3.3   Tie Strain

C.1.3.3.1 Test as Built
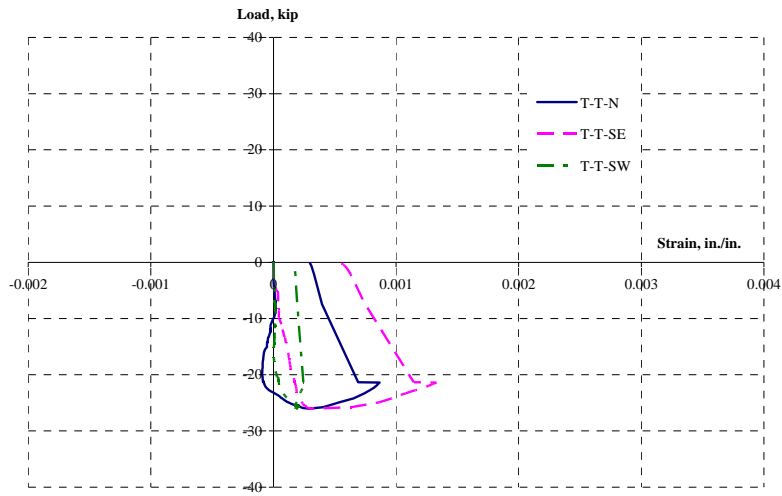
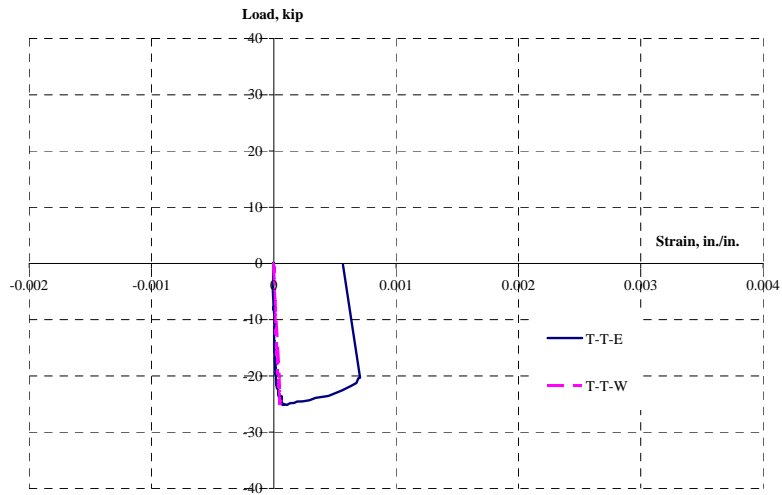*Figure C.14   Top tie strains, north and south face, 1-A-S8-M*
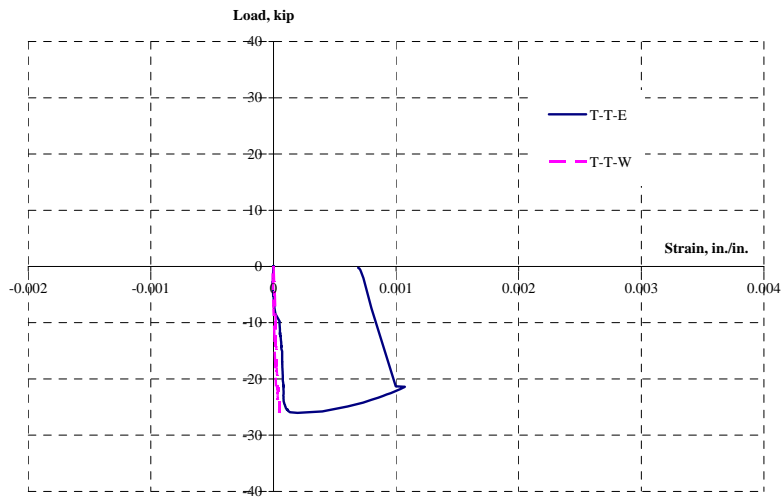
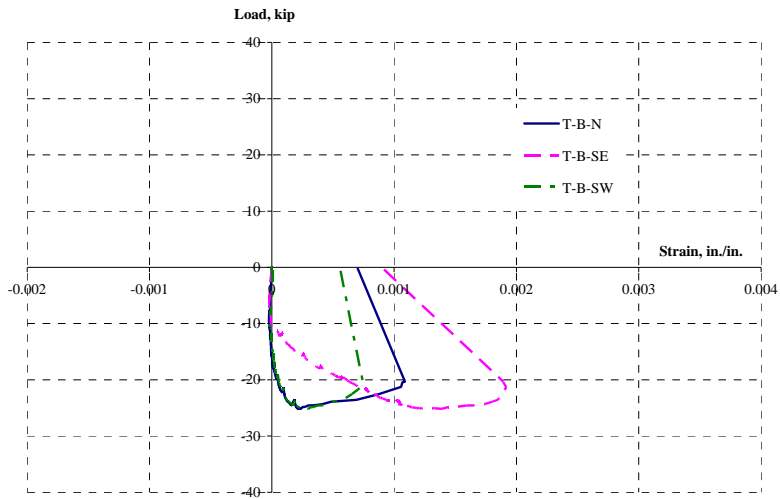*Figure C.15   Top tie strains, east and west face, 1-A-S8-M*

403
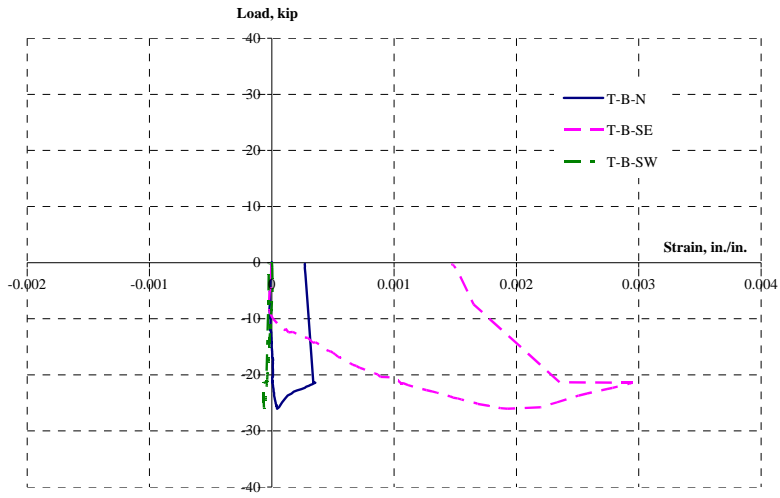
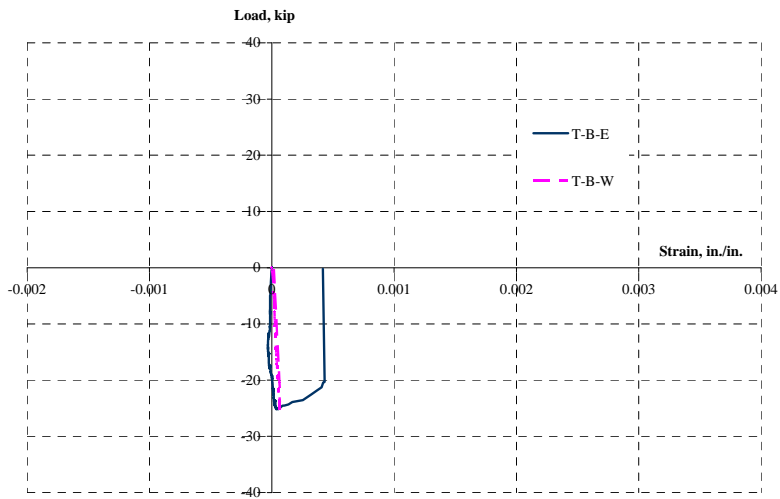*Figure C.16   Bottom tie strains, north and south face, 1-A-S8-M*
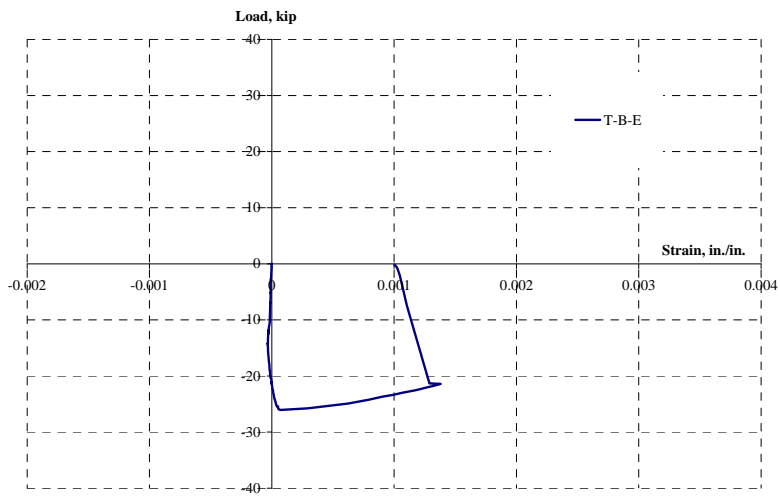
Figure C.17   Bottom tie strains, east face, 1-A-S8-M

C.1.3.3.2 Test after Rehabilitation
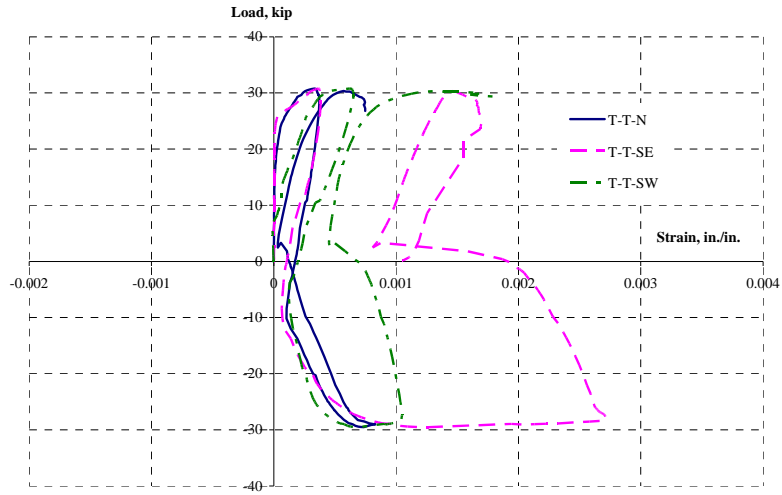
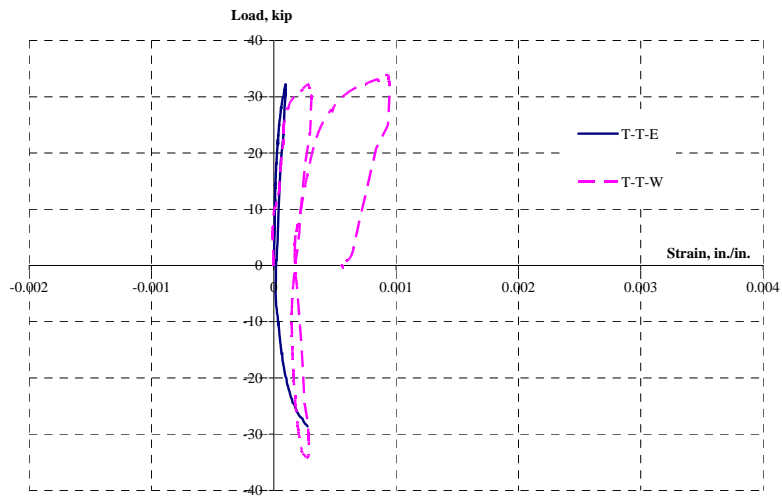*Figure C.18   Top tie strains, north and south face, 1-A-S8-M*
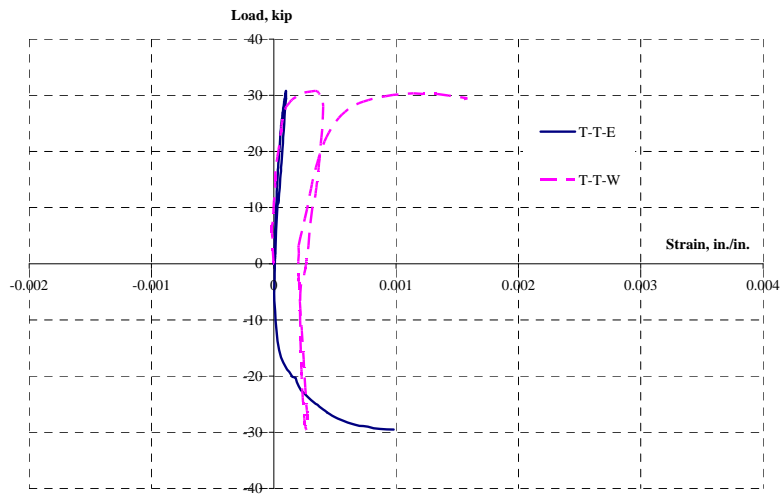
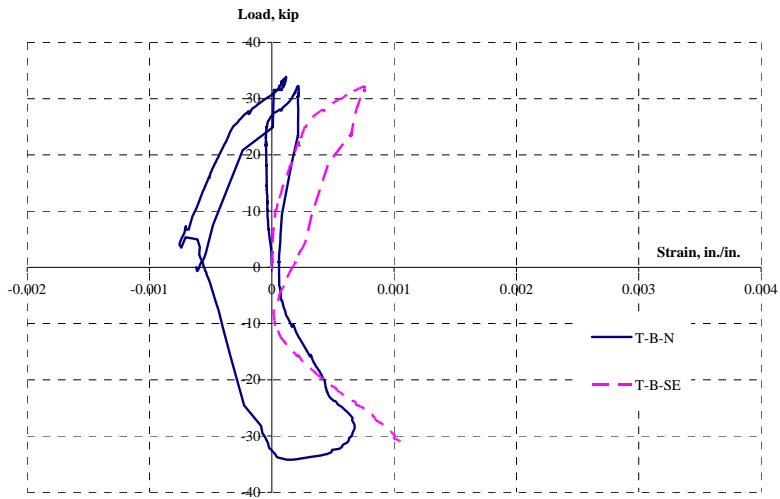*Figure C.19   Top tie strains, east and west face, 1-A-S8-M*

405
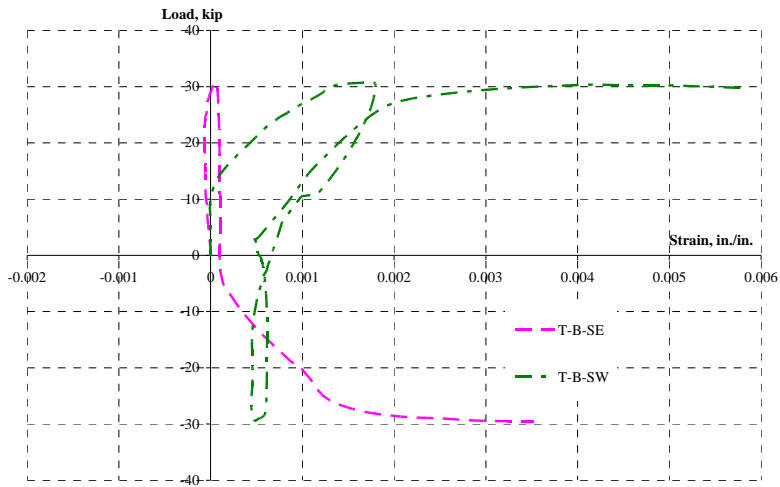
Figure C.20 Bottom tie strains, north and south face, 1-A-S8-M
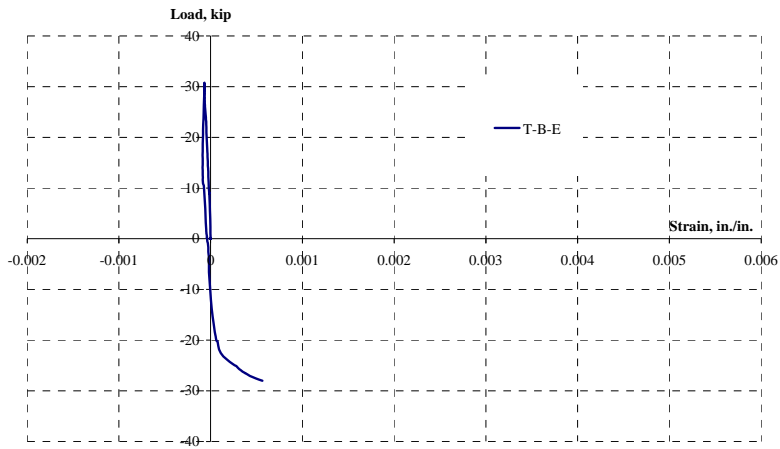
Figure C.21   Bottom tie strains, east face, 1-A-S8-M

406

C.1.4 CFRP Strain Gage
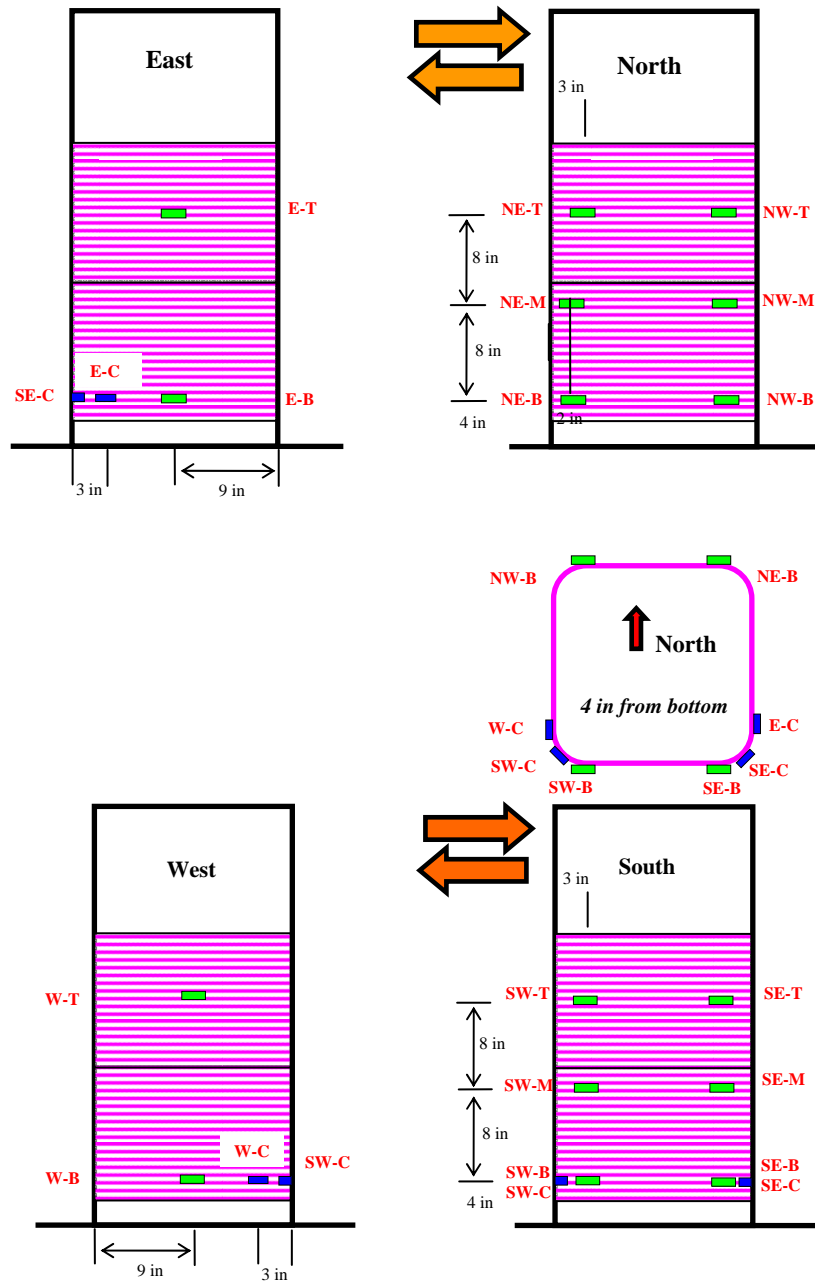
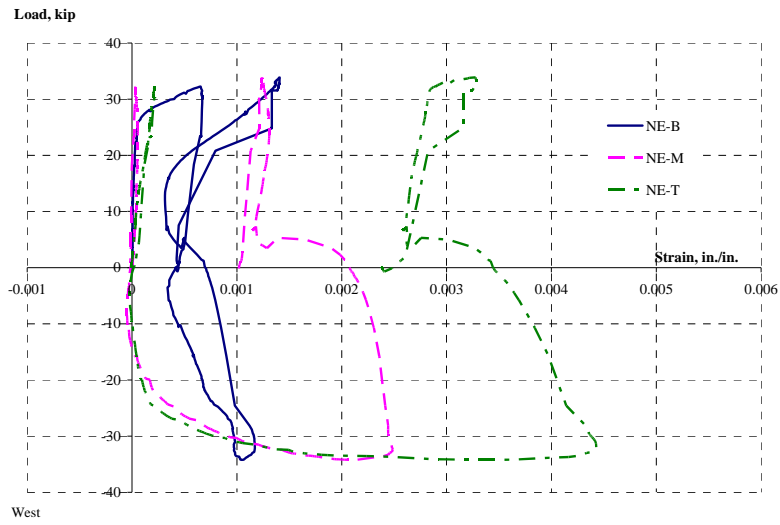*Figure C.22   Layout of CFRP strain gages, 1-A-S8-M*
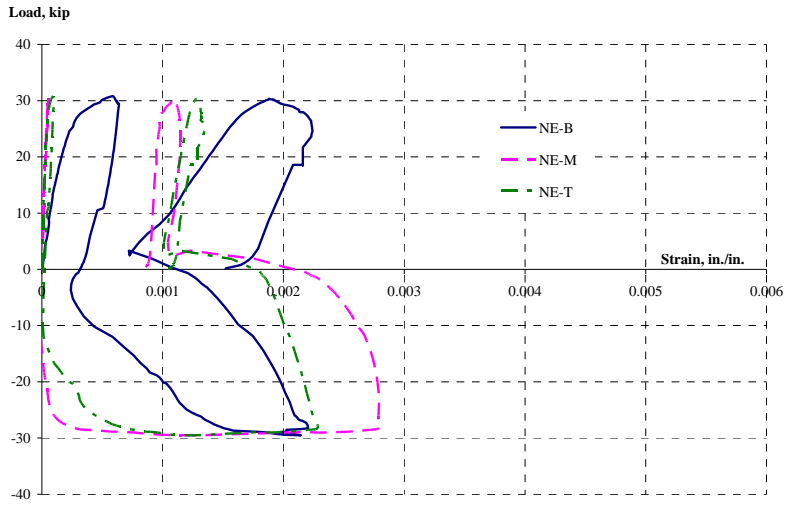
Figure C.23   CFRP strains at location of splitting cracking, north-east, 1-A-S8-M
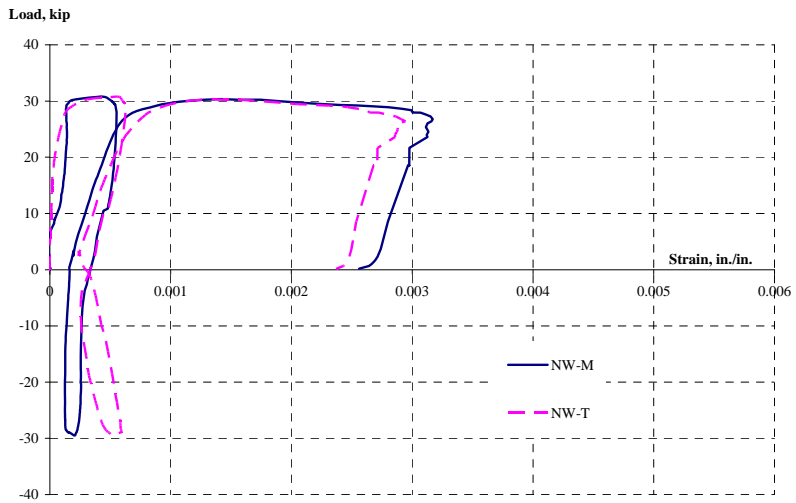
Figure C.24   CFRP strains at location of splitting cracking, north-west, 1-A-S8-M

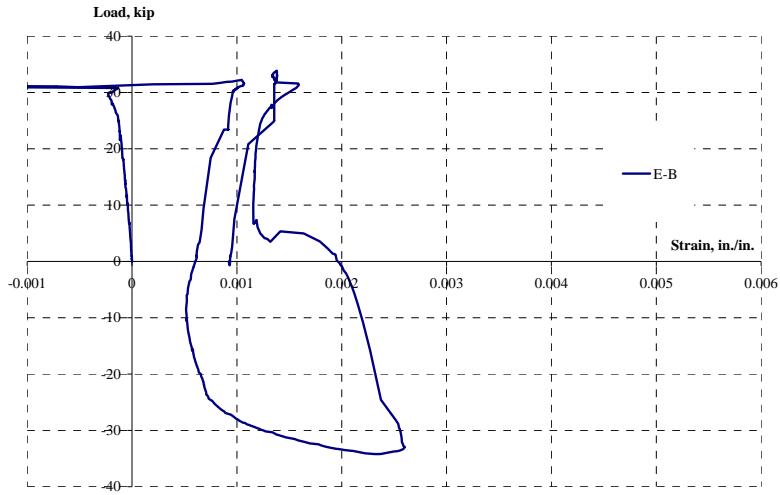408
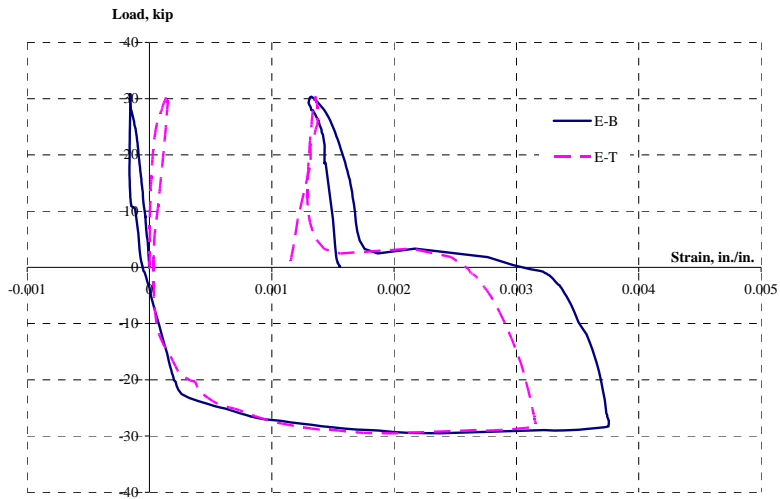
Figure C.25   CFRP strains, east face, 1-A-S8-M
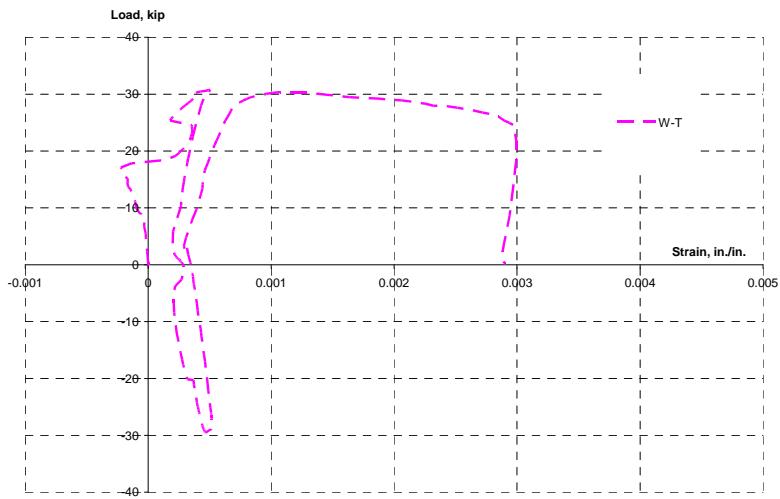
Figure C.26   CFRP strains, west face, 1-A-S8-M

409

C.2   2-A-S8-M

C.2.1   Lateral Displacement VS Lateral Load
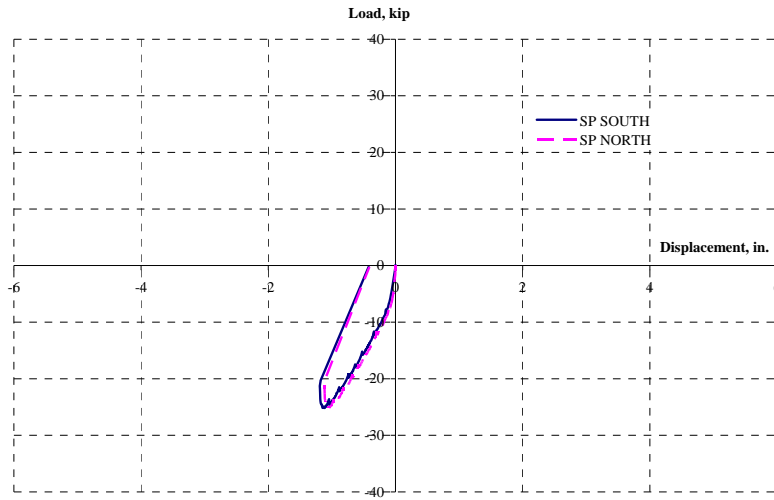
Figure C.27   Lateral displacement vs lateral load, test __as built__, 2-A-S8-M
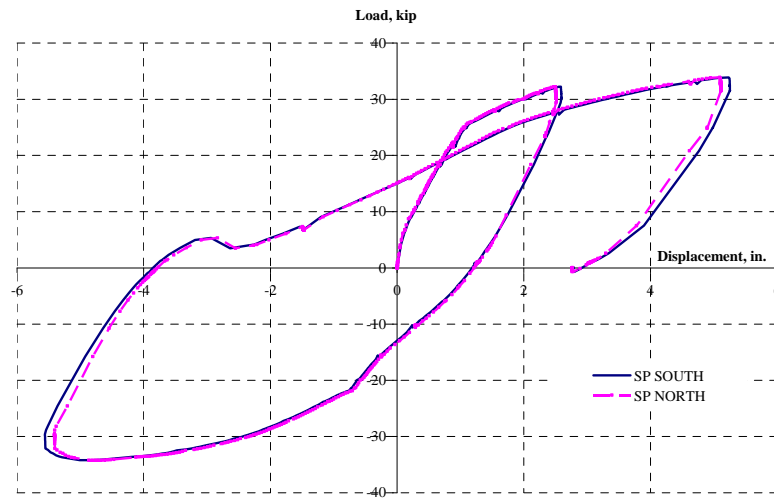
Figure C.28   Lateral displacement vs lateral load, test __after rehabilitation__, 2-A-S8-M

C.2.2 Vertical Displacement at 30 in. from Top of the Footing VS Lateral Load
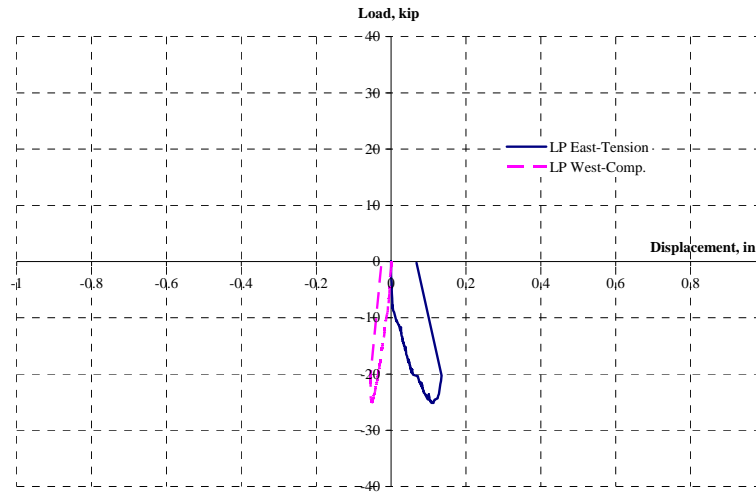
Figure C.29   Vertical displacement at 30 in. from top of the footing vs lateral load, test as built, 2-A-S8-M
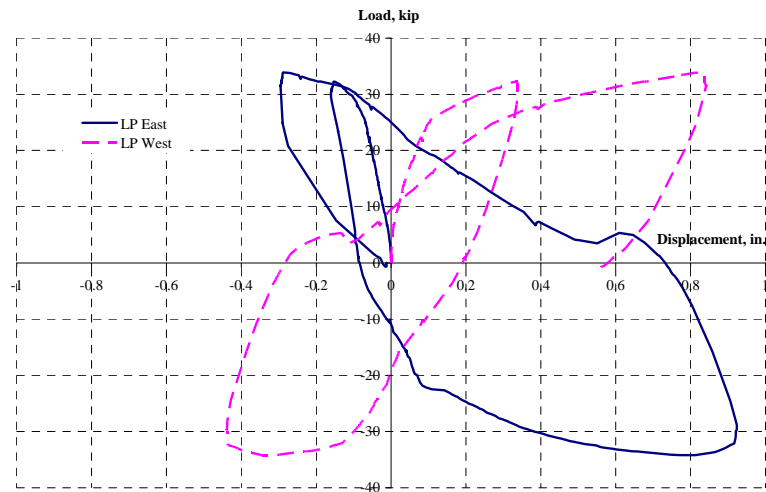
Figure C.30   Vertical displacement at 30 in. from top of the footing vs lateral load, test after rehabilitation, 2-A-S8-M

411

C.2.3 Steel Reinforcement Strain
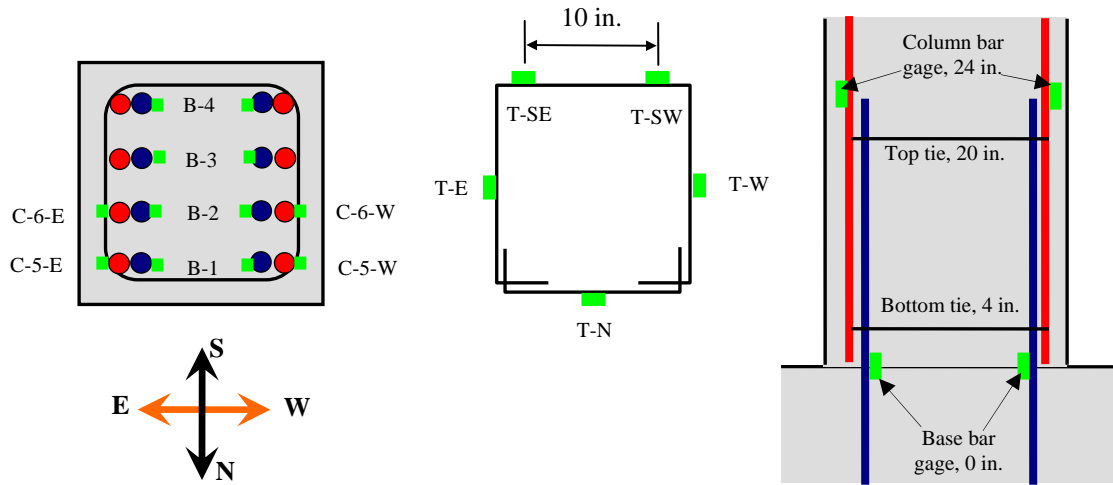
- **Base bar gages (B - # - Direction):** at the top of the footing
- **Column bar gages (C - # - Direction)**: 24 in. from the top of the footing
- **Tie bar gages (T-Top or Bottom- Direction):**

  Top-tie at 20 in. from the top of the footing

  Bottom- tie at 4 in. from the top of the footing

Figure C.31   Layout of steel reinforcement strain gages, 2-A-S8-M

C.2.3.1 Base Bar Strain

C.2.3.1.1 Test as Built
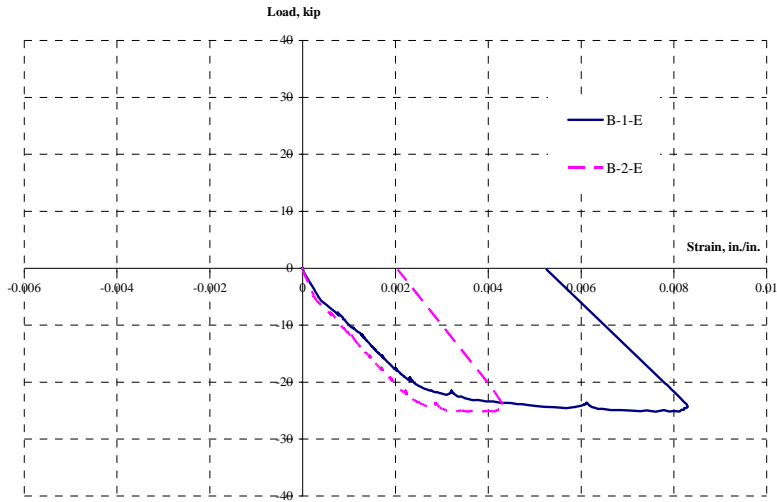
Figure C.32   Base bar strains, east side, 2-A-S8-M
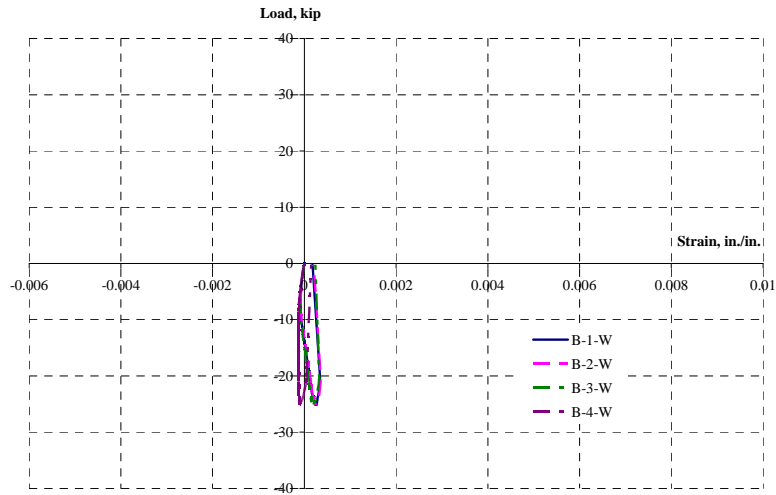
Figure C.33   Base bar strains, west side, 2-A-S8-M

413

C.2.3.1.2 Test after Rehabilitation
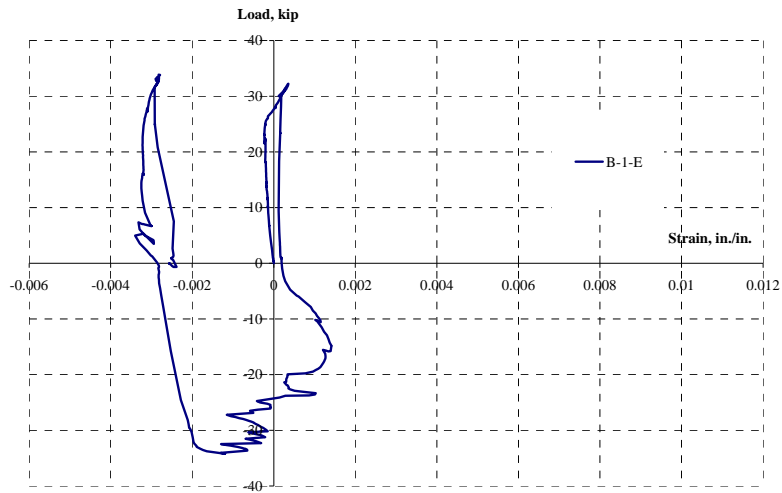
Figure C.34   Base bar strains, east side, 2-A-S8-M
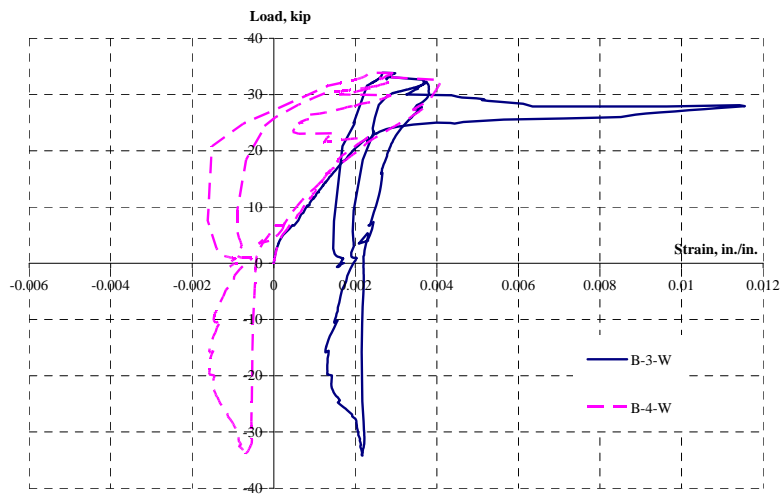
Figure C.35   Base bar stain, west side, 2-A-S8-M

414

C.2.3.2 Column Bar Strain

C.2.3.2.1 Test as Built
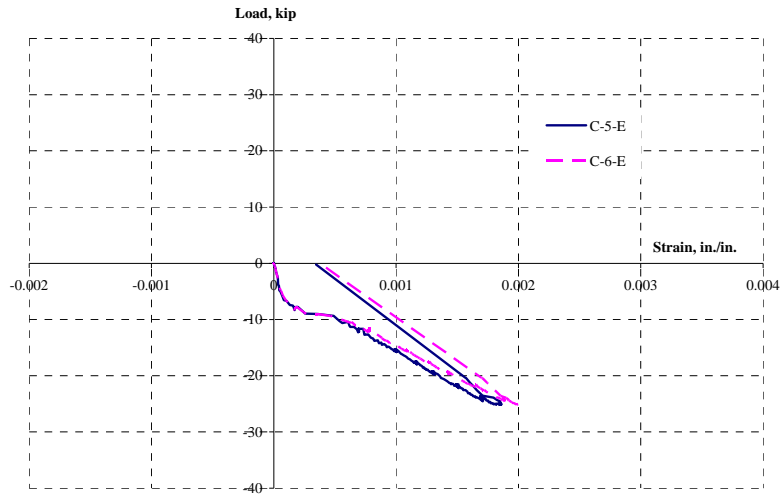
Figure C.36   Column bar strains, east side, 2-A-S8-M
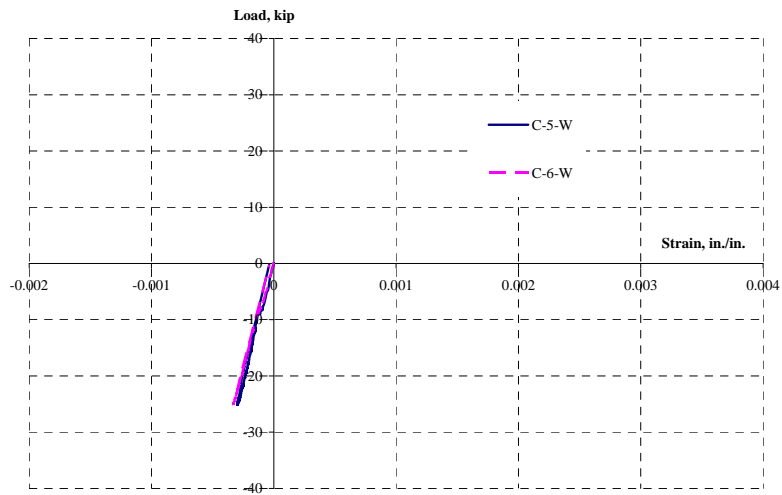
Figure C.37   Column bar strains, west side, 2-A-S8-M

415

C.2.3.2.2 Test after Rehabilitation
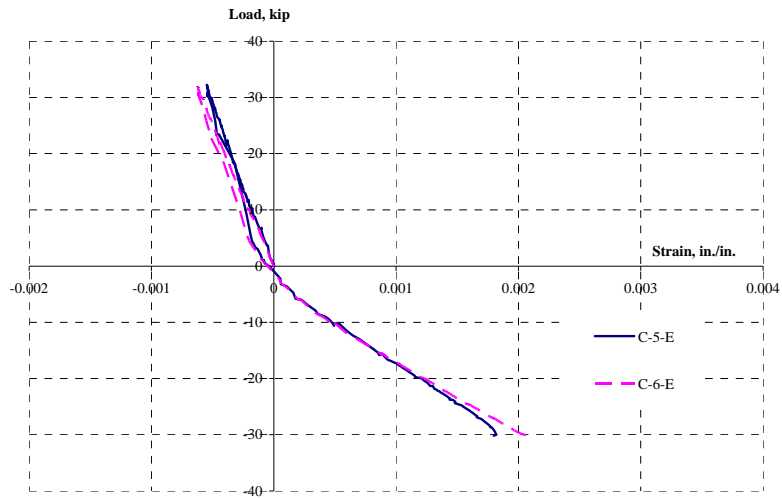
Figure C.38   Column bar strains, east side, 2-A-S8-M
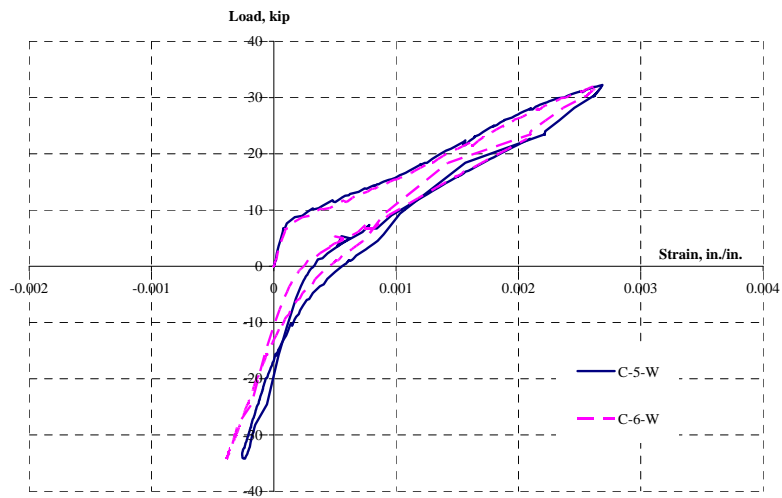
Figure C.39   Column bar strains, west side, 2-A-S8-M

416

C.2.3.3 Tie Strain

C.2.3.3.1 Test as Built
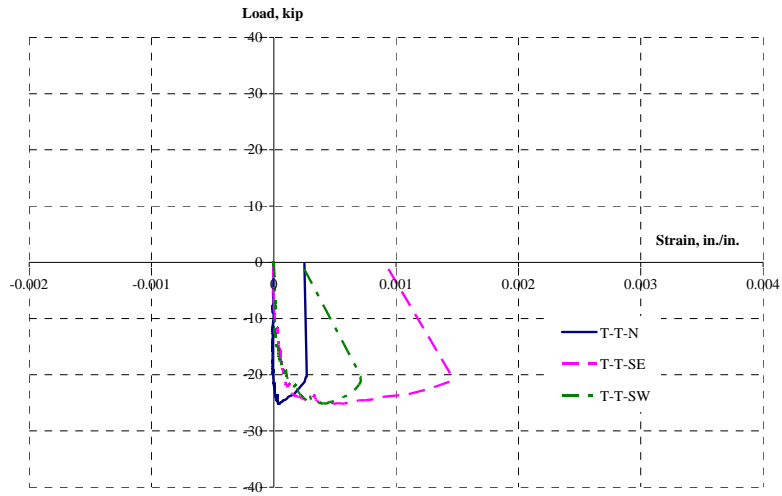
Figure C.40   Top tie strains, north and south face, 2-A-S8-M

Figure C.41   Top tie strains, east and west face, 2-A-S8-M

417

Figure C.42   Bottom tie strains, north and south face, 2-A-S8-M

Figure C.43   Bottom tie strains, east and west face, 2-A-S8-M

418

C.2.3.3.2 Test after Rehabilitation
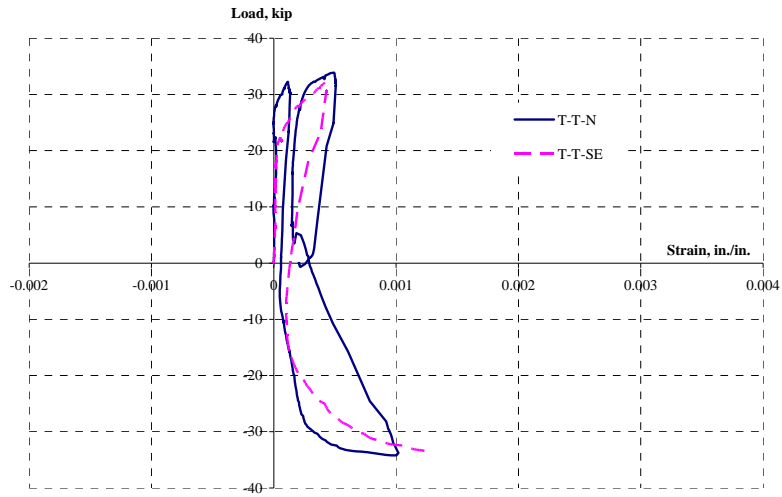
Figure C.44   Top tie strains, north and south face, 2-A-S8-M

Figure C.45   Top tie strains, east and west face, 2-A-S8-M

Figure C.46 Bottom tie strains, north and south face, 2-A-S8-M
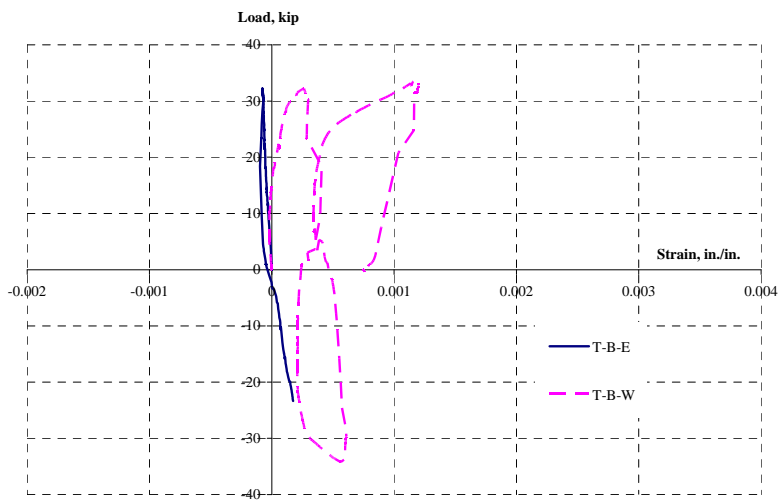
Figure C.47   Bottom tie strains, east and west face, 2-A-S8-M

420

C.2.4 CFRP Strain Gage
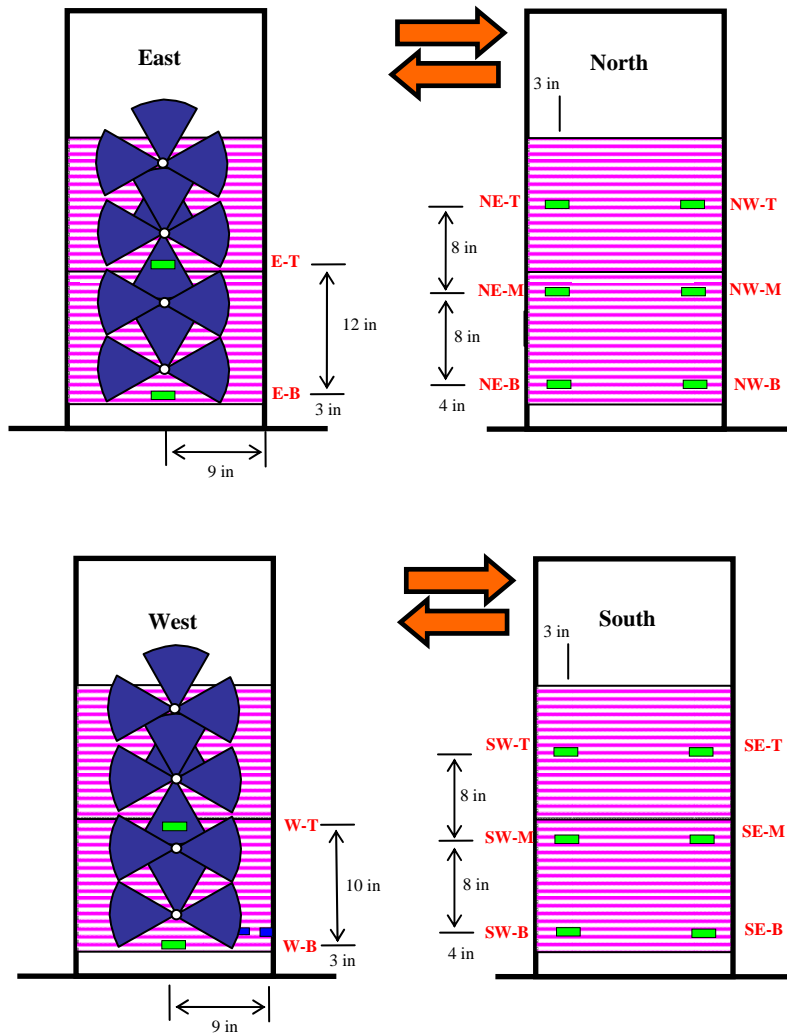
- **E-T, E-B, W-T and W-B were placed on CFRP jackets.**

Figure C.48   Layout of CFRP strain gages, 2-A-S8-M

Figure C.49   CFRP strains at location of splitting cracking, north-east, 2-A-S8-M
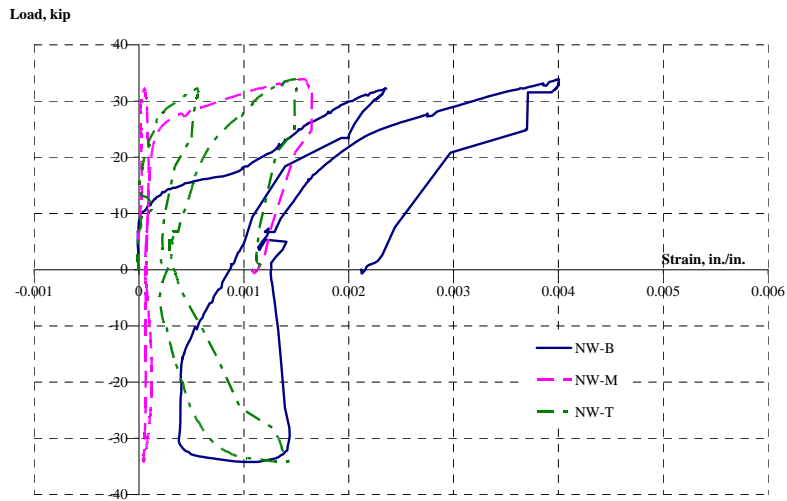
Figure C.50   CFRP strains at location of splitting cracking, north-west, 2-A-S8-M

422

Figure C.51   CFRP strains, east face, 2-A-S8-M
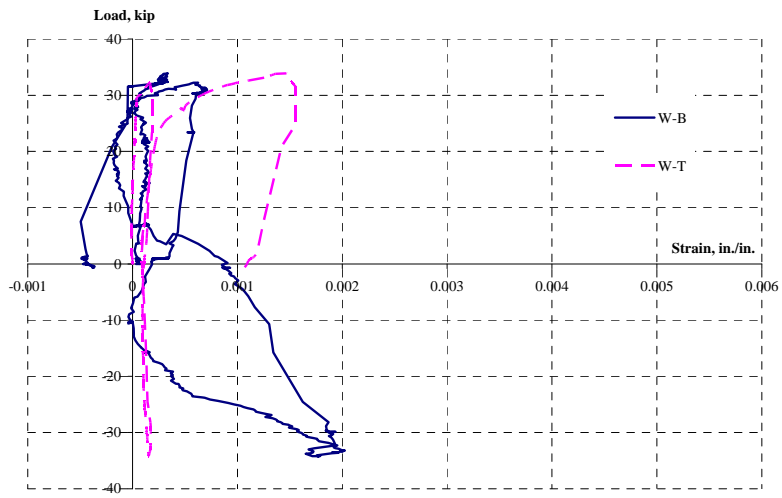
Figure C.52   CFRP strains, west face, 2-A-S8-M

423

C.3   3-B-S10-M

C.3.1   Lateral Displacement VS Lateral Load
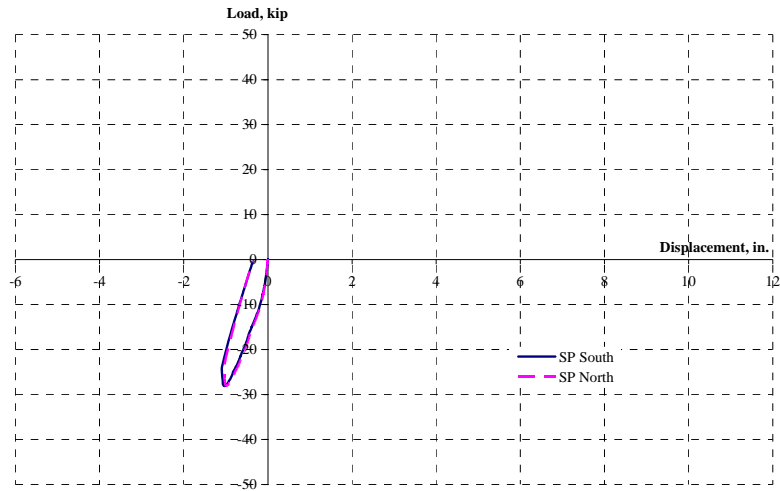
Figure C.53   Lateral displacement vs lateral load, test <u>as built</u>, 3-B-S10-M
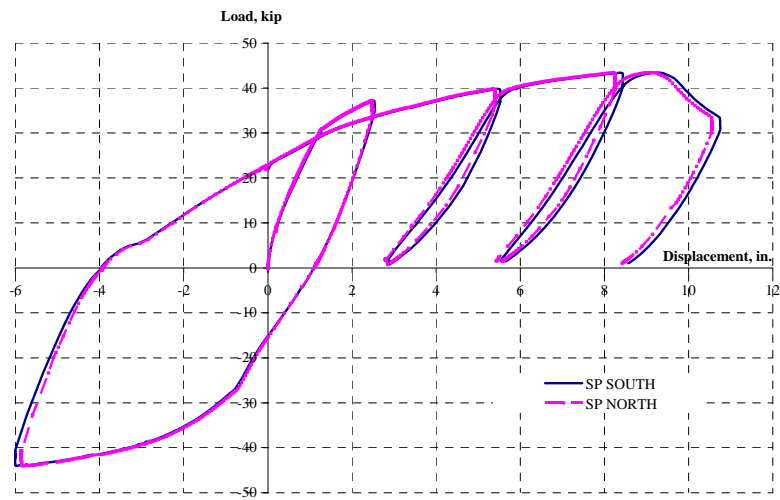
Figure C.54   Lateral displacement vs lateral load, test <u>after rehabilitation</u>, 3-B-S10-M

424

C.3.2 Vertical Displacement at 30 in. from Top of the Footing VS Lateral Load
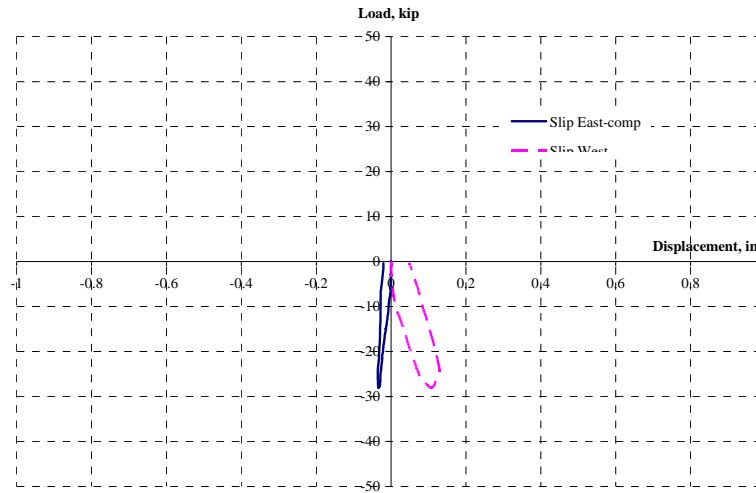
Figure C.55   Vertical displacement at 30 in. from top of the footing vs lateral load,

test <u>as built</u>, 3-B-S10-M
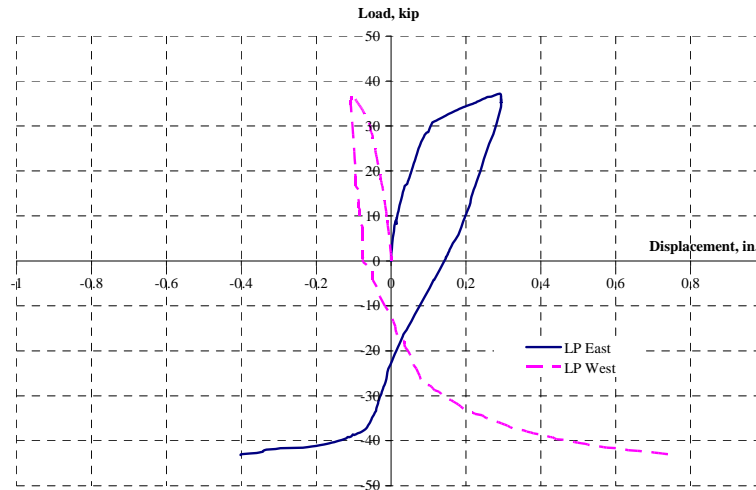
Figure C.56   Vertical displacement at 30 in. from top of the footing vs lateral load,

test <u>after rehabilitation</u>, 3-B-S10-M

425

C.3.3 Steel Reinforcement Strain
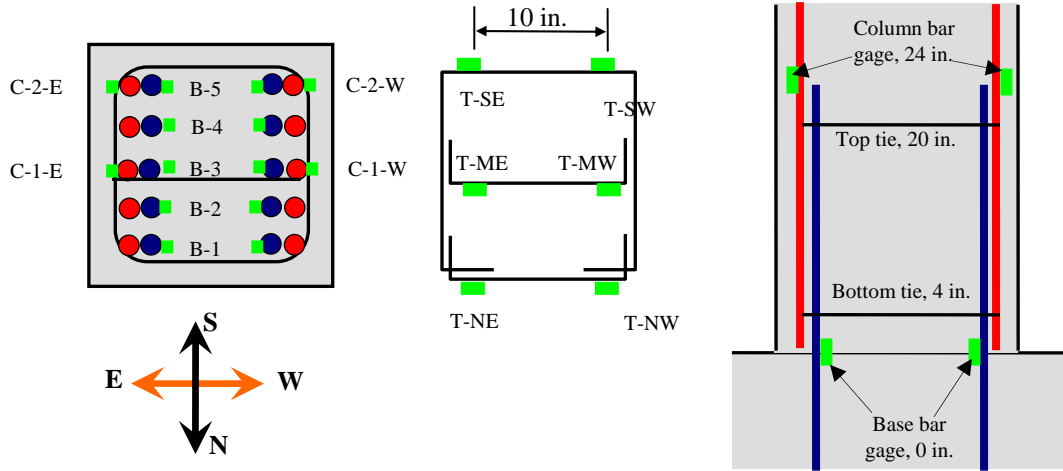
- **Base bar gages (B - # - Direction):** at the top of the footing

- **Column bar gages (C - # - Direction):** 24 in. from the top of the footing

- **Tie bar gages (T-Top or Bottom- Direction):**

  Top-tie at 20 in. from the top of the footing

  Bottom- tie at 4 in. from the top of the footing

Figure C.57   Layout of steel reinforcement strain gages, 3-B-S10-M

C.3.3.1 Base Bar Strain

C.3.3.1.1 Test as Built

Load, kip

Legend:
- B-1-E
- B-2-E
- B-3-E
- B-4-E
- B-5-E

Strain, in./in.
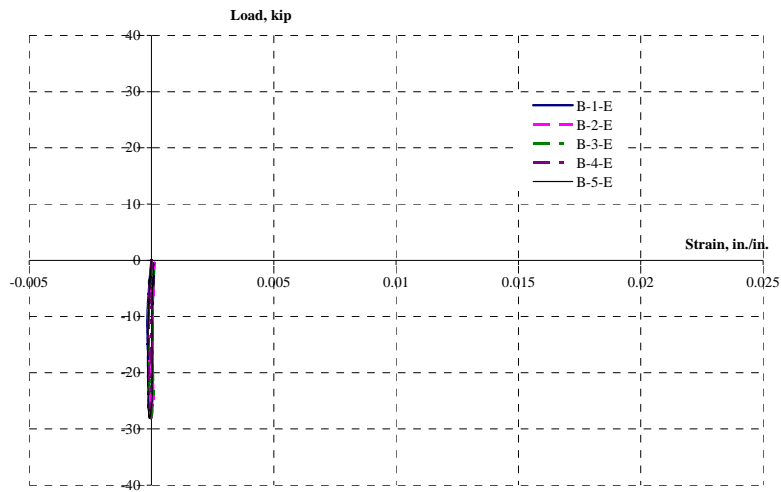
Figure C.58   Base bar strains, east side, 3-B-S10-M

Load, kip

Legend:
- B-1-W
- B-2-W
- B-3-W
- B-4-W
- B-5-W

Strain, in./in.
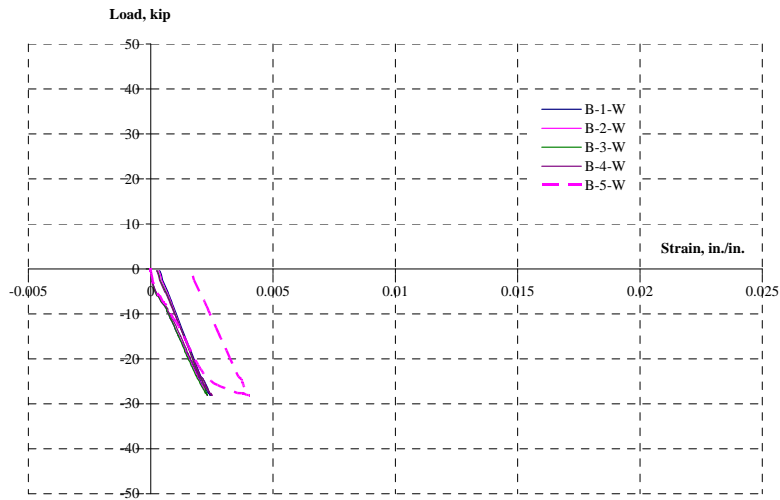
Figure C.59   Base bar strains, west side, 3-B-S10-M

427

C.3.3.1.2 Test after Rehabilitation
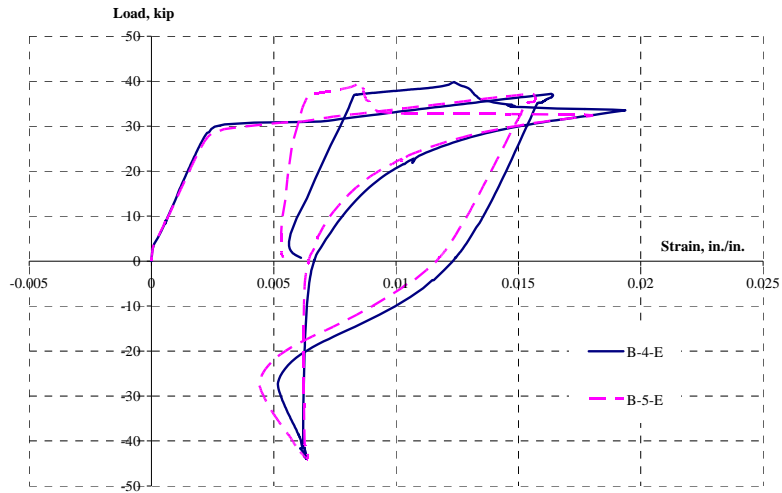
Figure C.60   Base bar strains, east side, 3-B-S10-M
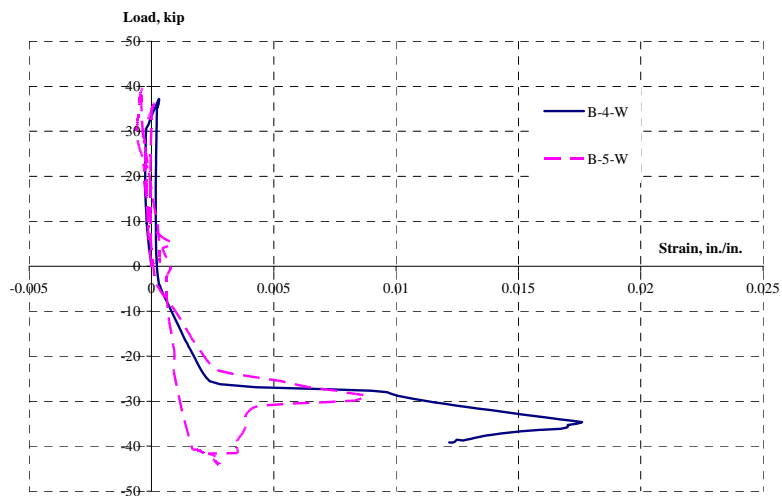
Figure C.61   Base bar stain, west side, 3-B-S10-M

428

C.3.3.2 Column Bar Strain

C.3.3.2.1 Test as Built
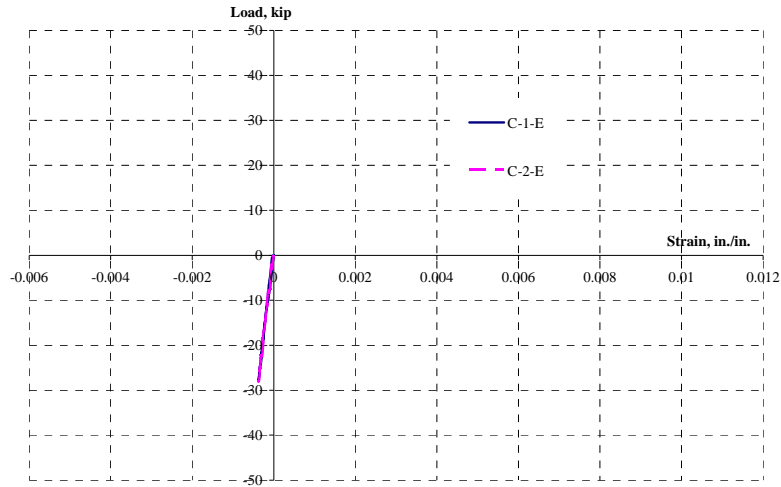
Figure C.62   Column bar strains, east side, 3-B-S10-M
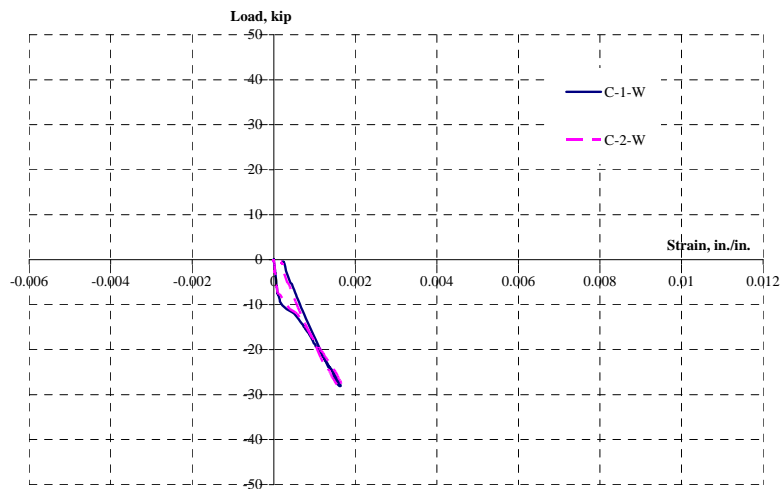
Figure C.63   Column bar strains, west side, 3-B-S10-M

429

C.3.3.2.2 Test after Rehabilitation
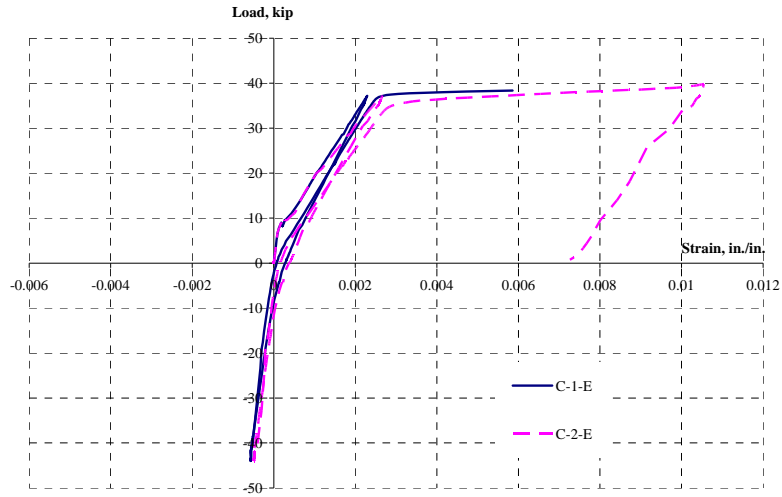
Figure C.64   Column bar strains, east side, 3-B-S10-M
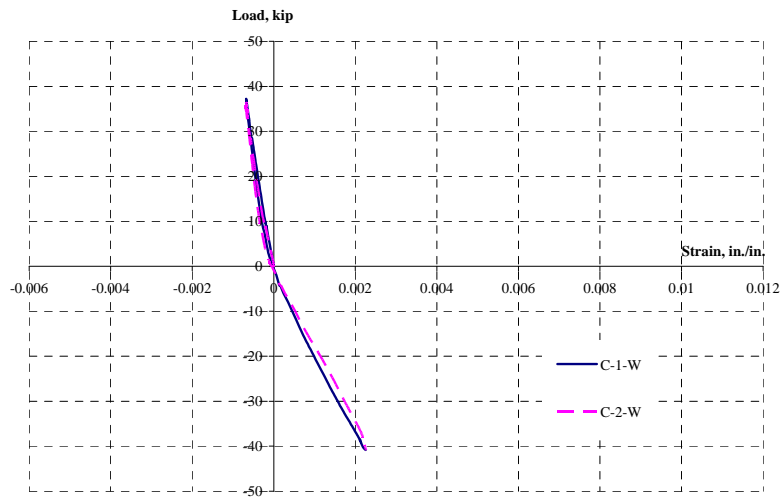
Figure C.65   Column bar strains, west side, 3-B-S10-M

C.3.3.3 Tie Strain

C.3.3.3.1 Test as Built
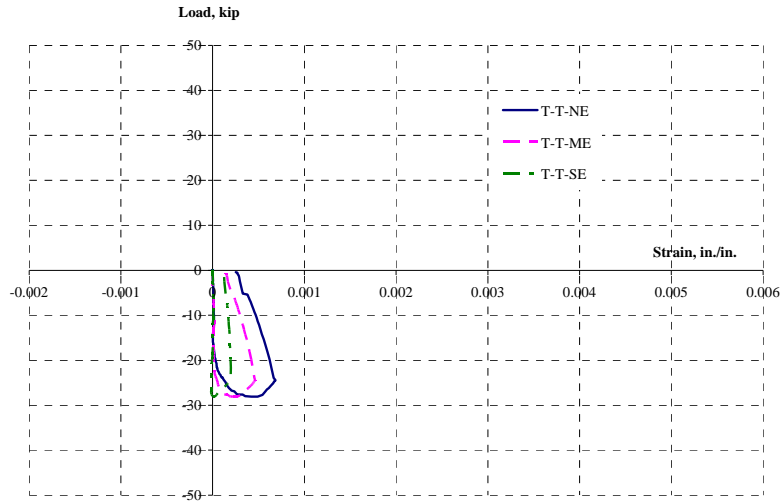
Figure C.66   Top tie strains, east, 3-B-S10-M
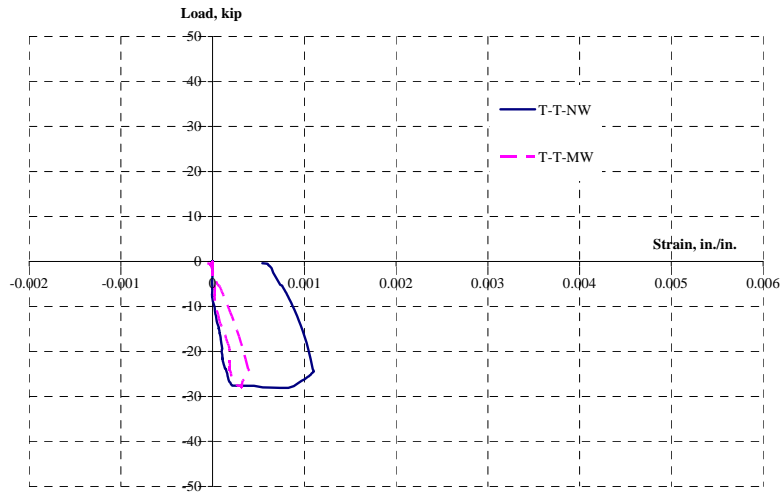
Figure C.67   Top tie strains, west, 3-B-S10-M

431
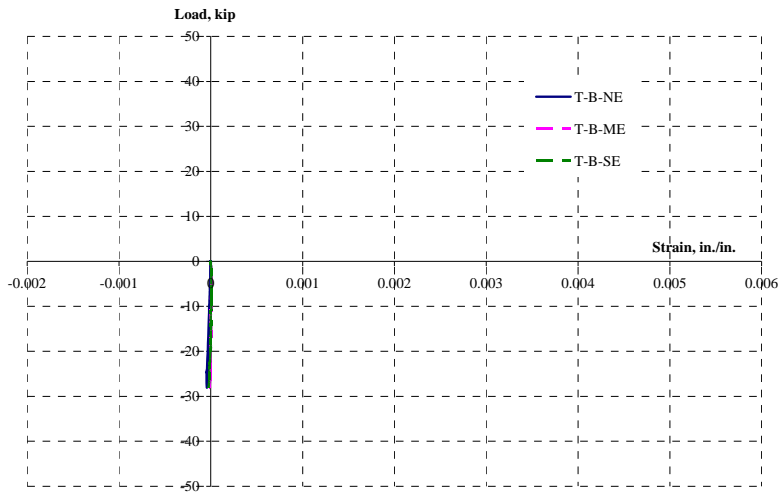
Figure C.68   Bottom tie strains, east, 3-B-S10-M
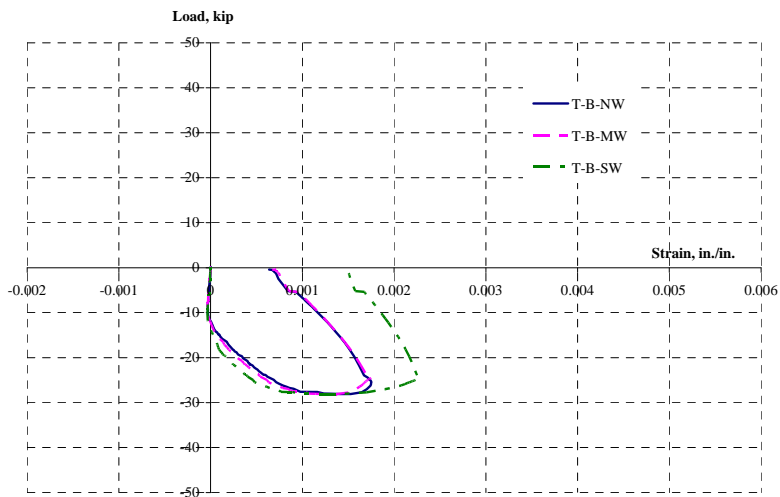
Figure C.69   Bottom tie strains, west, 3-B-S10-M
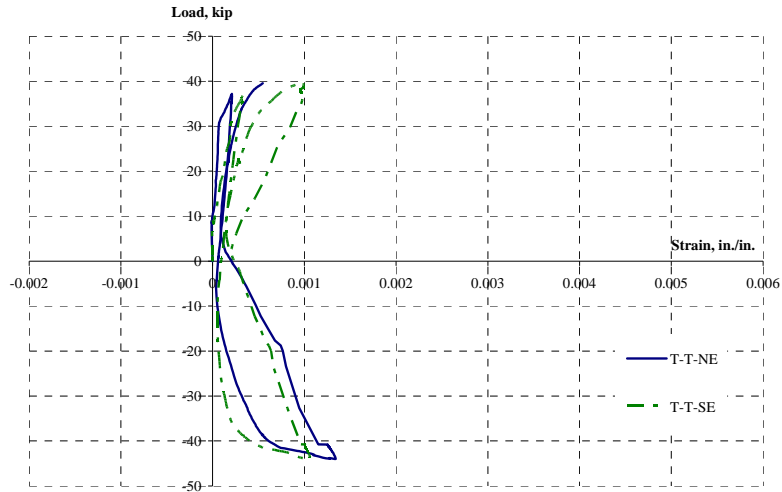
C.3.3.3.2 Test after Rehabilitation
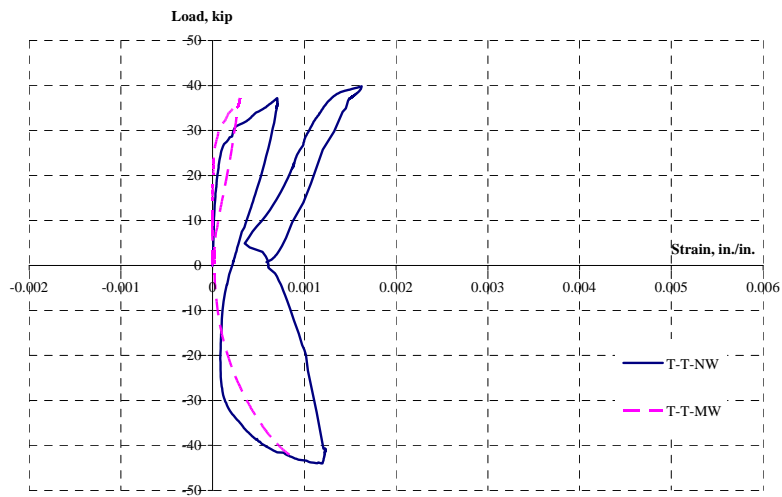

Figure C.70   Top tie strains, east, 3-B-S10-M
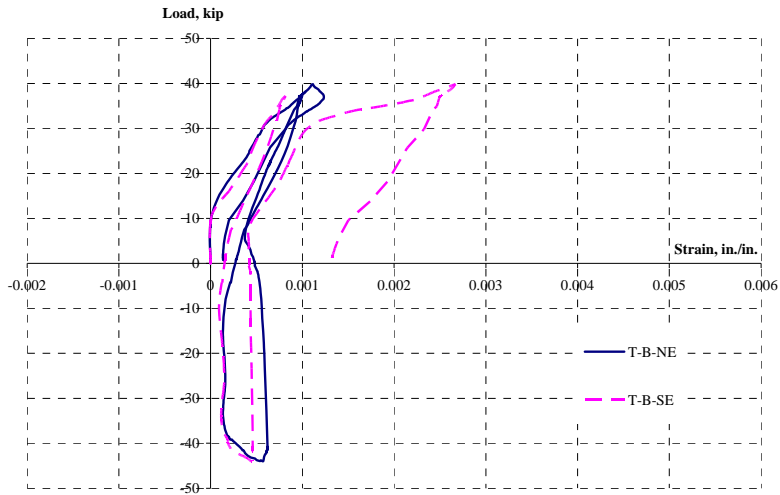

Figure C.71   Top tie strains, west, 3-B-S10-M
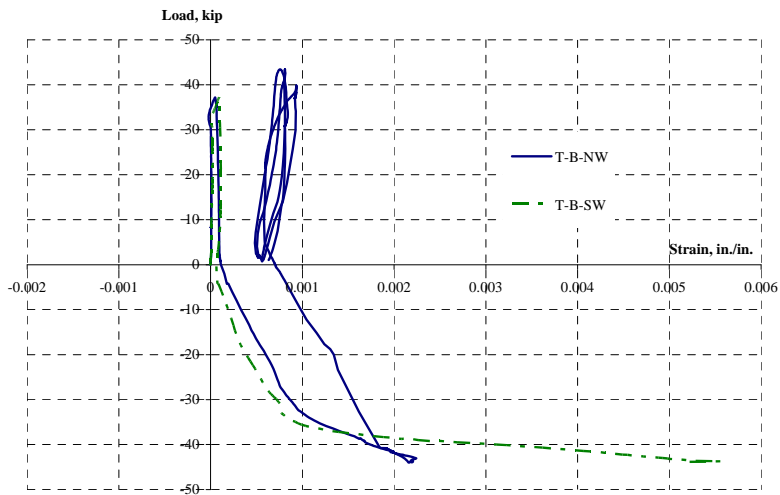
Figure C.72 Bottom tie strains, east, 3-B-S10-M

Figure C.73   Bottom tie strains, west, 3-B-S10-M

434

C.3.4 CFRP Strain Gage

East (28 in. anchors)
E-T
SE-C   E-B
7 in
4 in
7 in   9 in

North
3 in
NE-T   NW-T
8 in
NE-M   NW-M
8 in
NE-B   NW-B
4 in   4 in

NW-B   NE-B
North
4 in from bottom
W-B
SW-C   SE-C
SW-B   SE-B

West (44 in. anchors)
W-T
18 in
W-B
SW-C
4 in
9 in   2 in

South
3 in
SW-T   SE-T
8 in
SW-M   SE-M
8 in
SW-B   SE-B
SW-C   SE-C
4 in   4 in
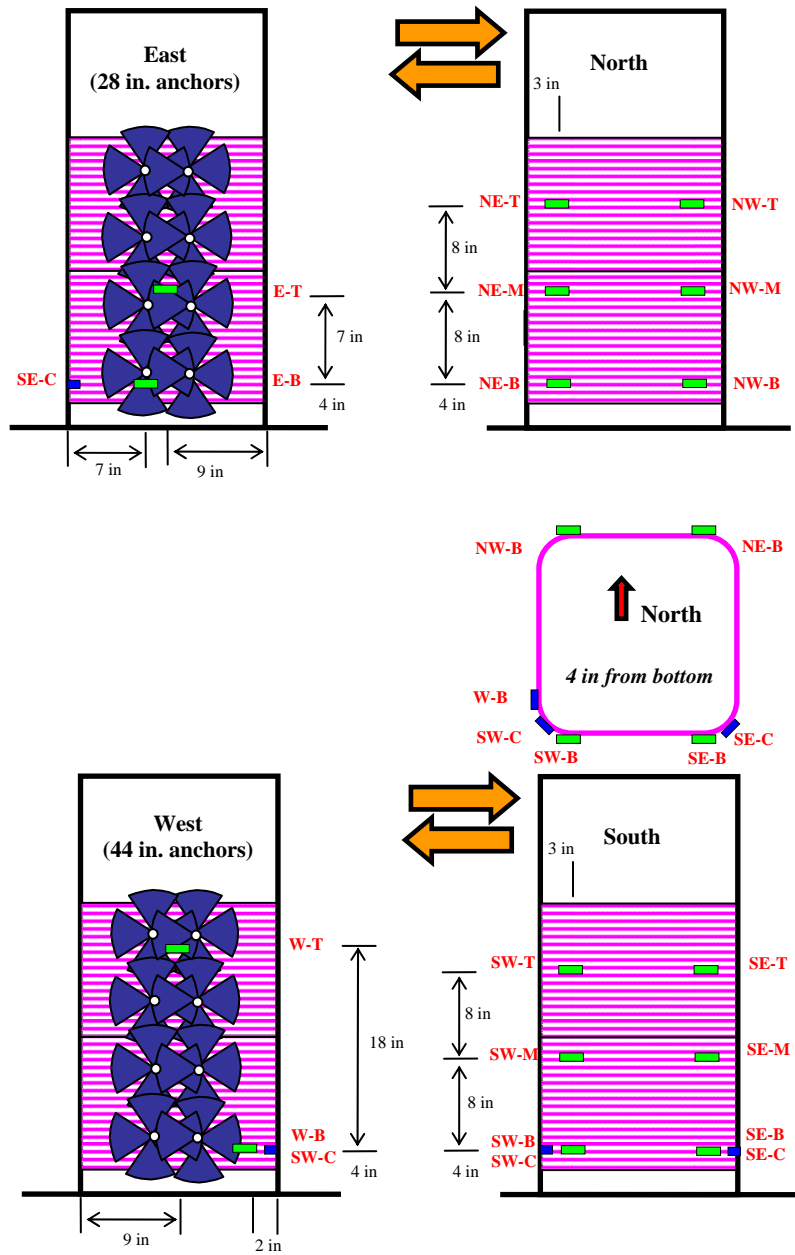
- **E-T, E-B, W-T and W-B were placed on CFRP jackets.**

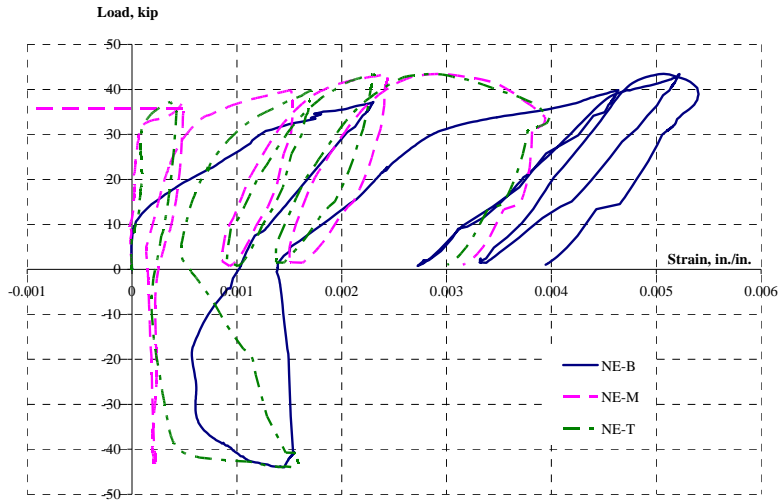*Figure C.74   Layout of CFRP strain gages, 3-B-S10-M*

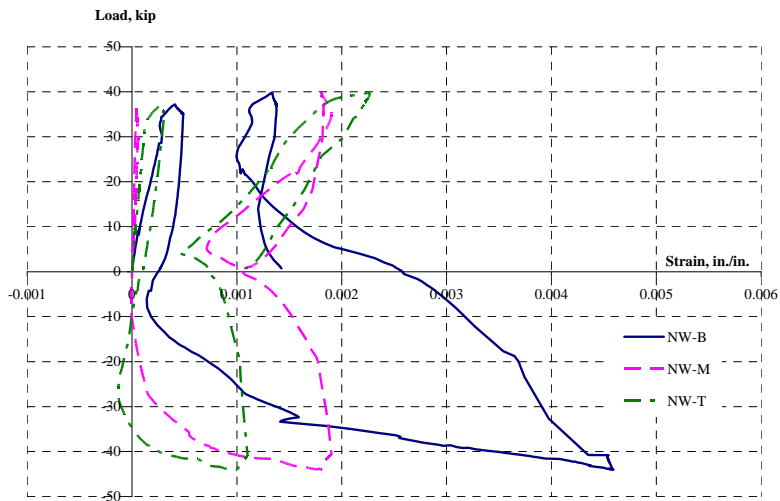*Figure C.75   CFRP strains at location of splitting cracking, north-east, 3-B-S10-M*

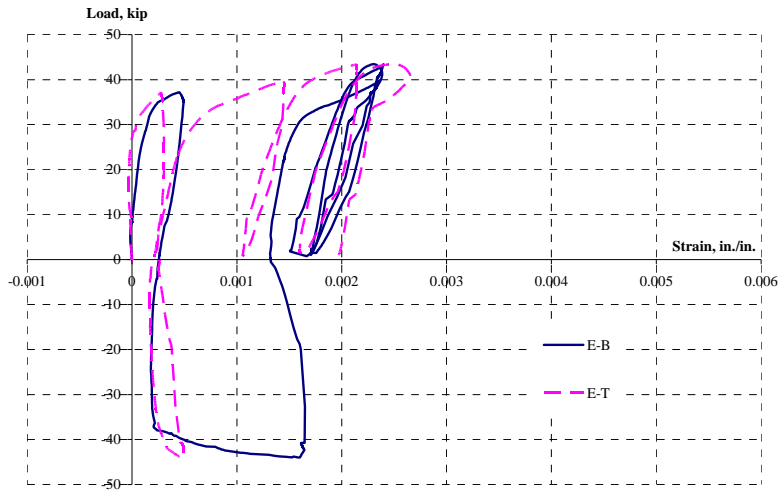*Figure C.76   CFRP strains at location of splitting cracking, north-west, 3-B-S10-M*
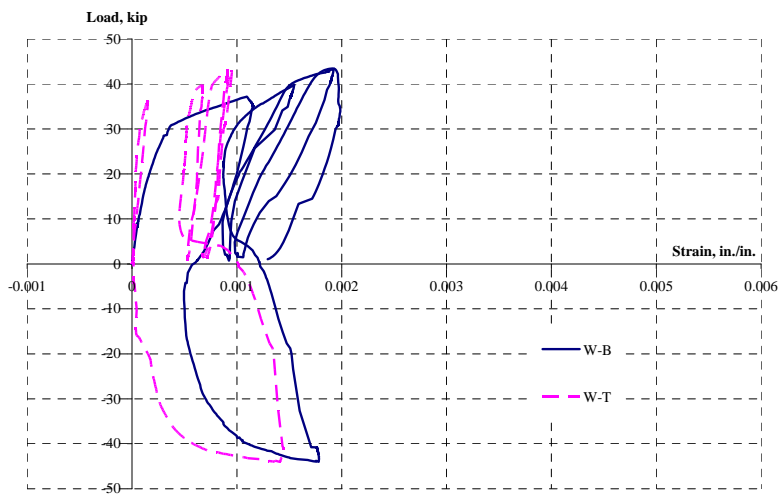
436

Figure C.77   CFRP strains, east face, 3-B-S10-M

Figure C.78   CFRP strains, west face, 3-B-S10-M

437

C.4 4-C-R20-M

C.4.1 Lateral Displacement VS Lateral Load
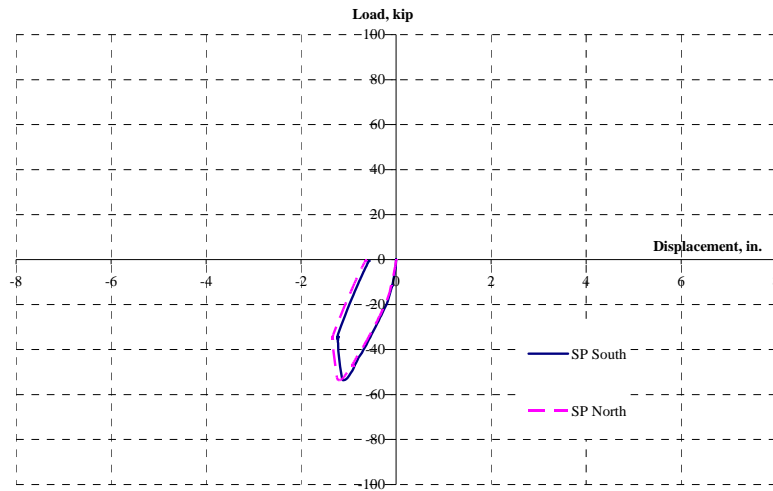

Figure C.79   Lateral displacement vs lateral load, test <u>as built</u>, 4-C-R20-M
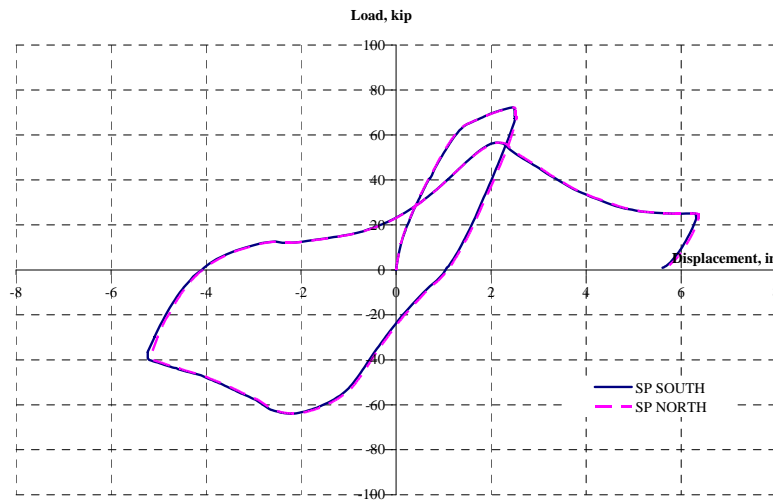

Figure C.80   Lateral displacement vs lateral load, test <u>after rehabilitation</u>, 4-C-R20-M

438

C.4.2 Vertical Displacement at 30 in. from Top of the Footing VS Lateral Load
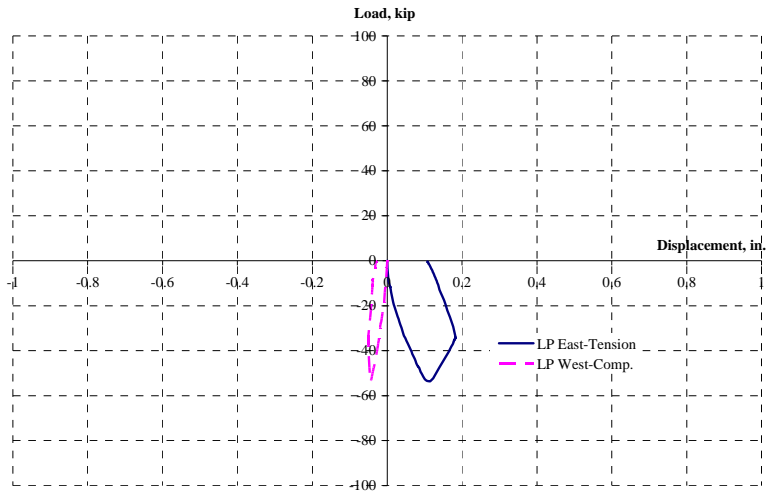

Figure C.81   Vertical displacement at 30 in. from top of the footing vs lateral load, test __as built__, 4-C-R20-M
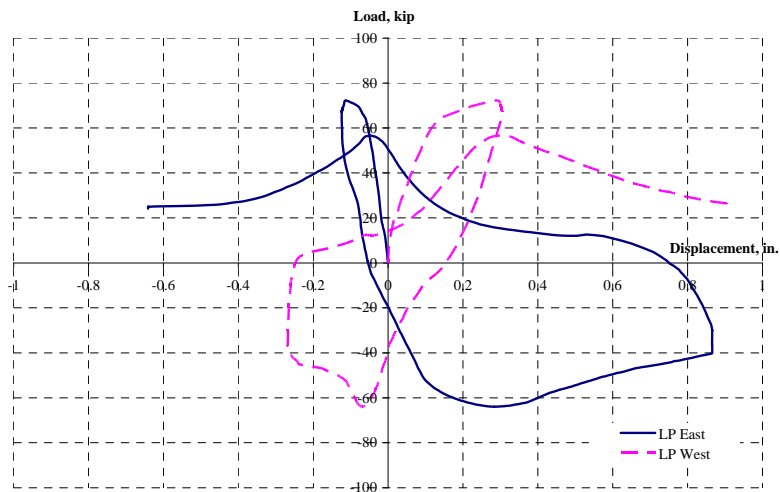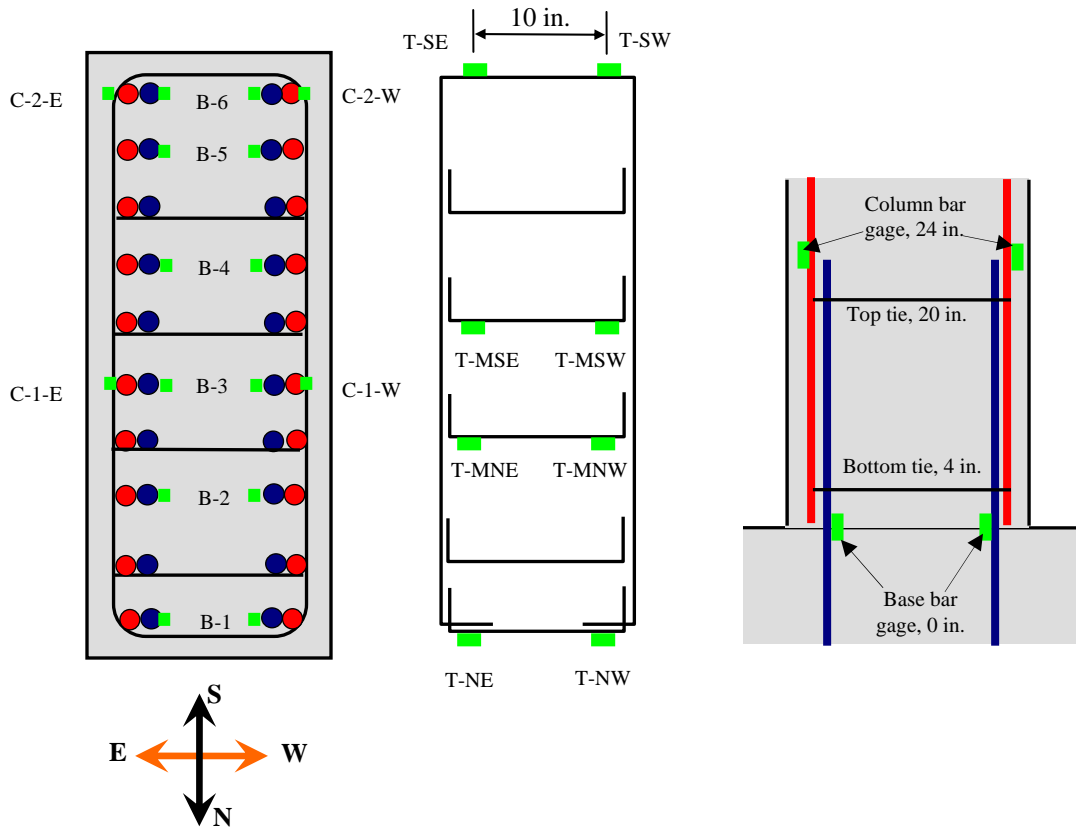

Figure C.82   Vertical displacement at 30 in. from top of the footing vs lateral load, test __after rehabilitation__, 4-C-R20-M

C.4.3 Steel Reinforcement Strain

- **Base bar gages (B - # - Direction):** at the top of the footing
- **Column bar gages (C - # - Direction)**: 24 in. from the top of the footing
- **Tie bar gages (T-Top or Bottom- Direction):**

  Top-tie at 20 in. from the top of the footing

  Bottom- tie at 4 in. from the top of the footing

Figure C.83   Layout of steel reinforcement strain gages, 4-C-R20-M

C.4.3.1 Base Bar Strain

C.4.3.1.1 Test as Built

Load, kip
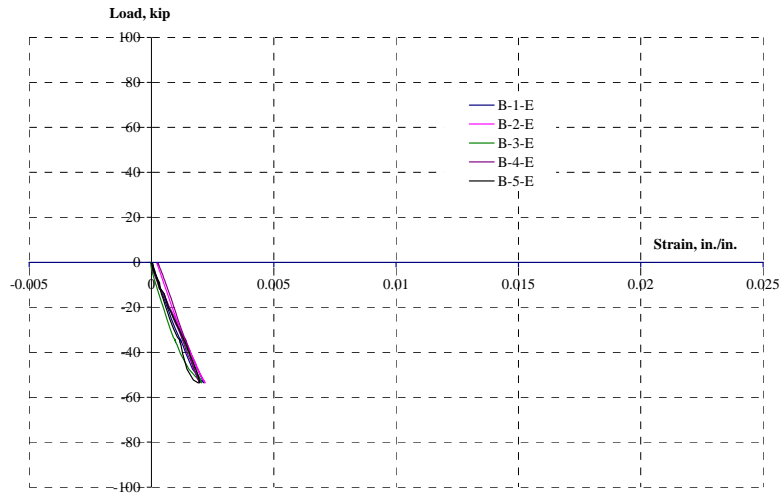
B-1-E
B-2-E
B-3-E
B-4-E
B-5-E

Strain, in./in.

Figure C.84   Base bar strains, east side, 4-C-R20-M

Load, kip

Strain, in./in.

B-1-W
B-2-W
B-3-W
B-4-W
B-5-W
B-6-W

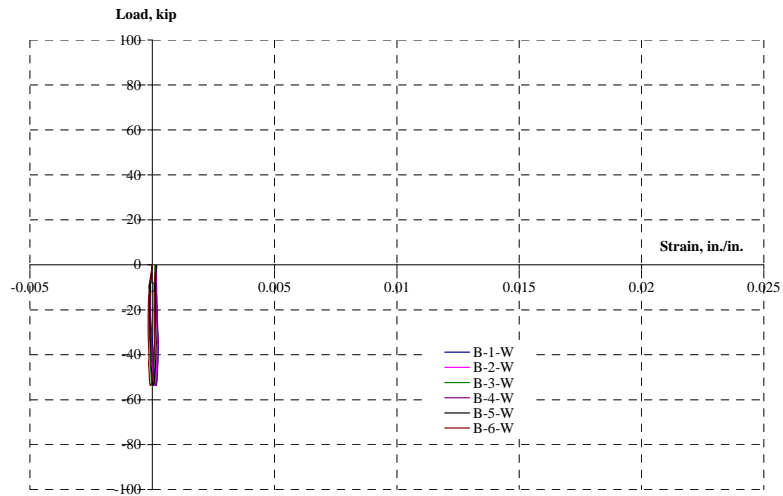*Figure C.85   Base bar strains, west side, 4-C-R20-M*

441

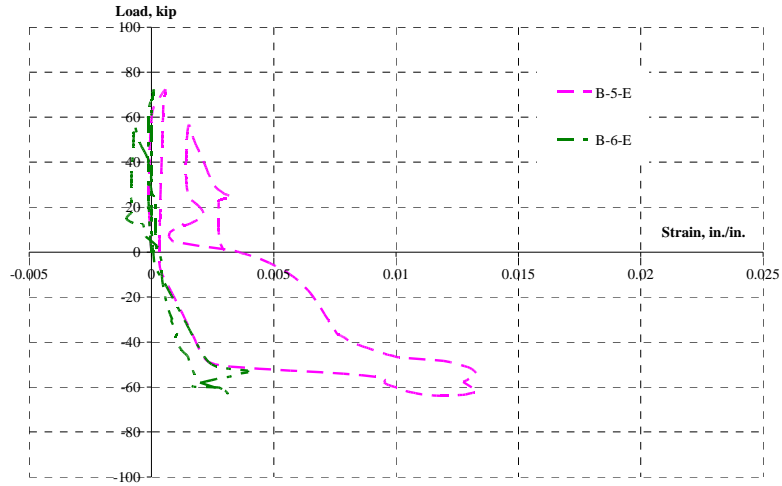## C.4.3.1.2 Test after Rehabilitation

Figure C.86   Base bar strains, east side, 4-C-R20-M

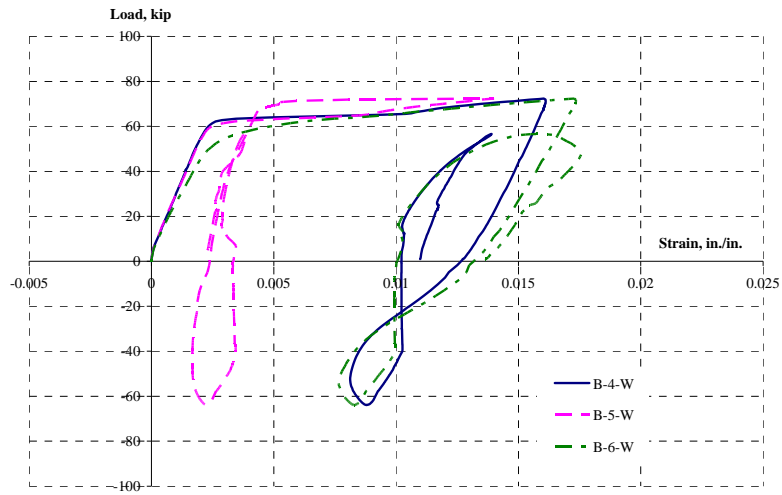**Figure C.87   Base bar stain, west side, 4-C-R20-M**

C.4.3.2 Column Bar Strain

C.4.3.2.1 Test as Built
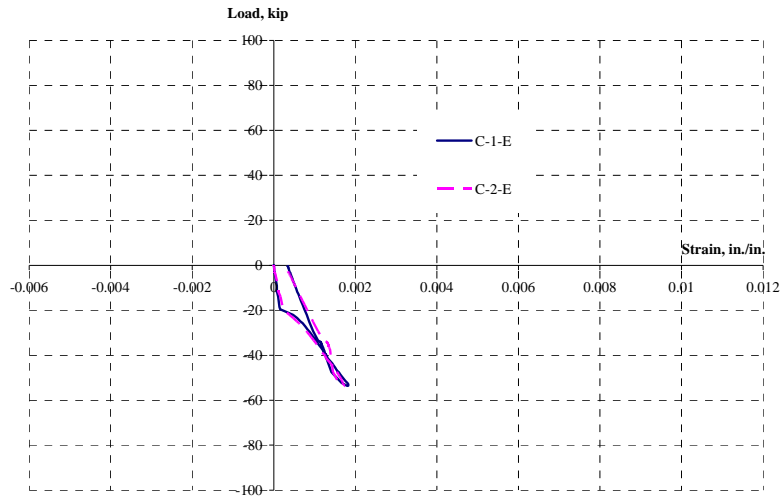
Figure C.88   Column bar strains, east side, 4-C-R20-M
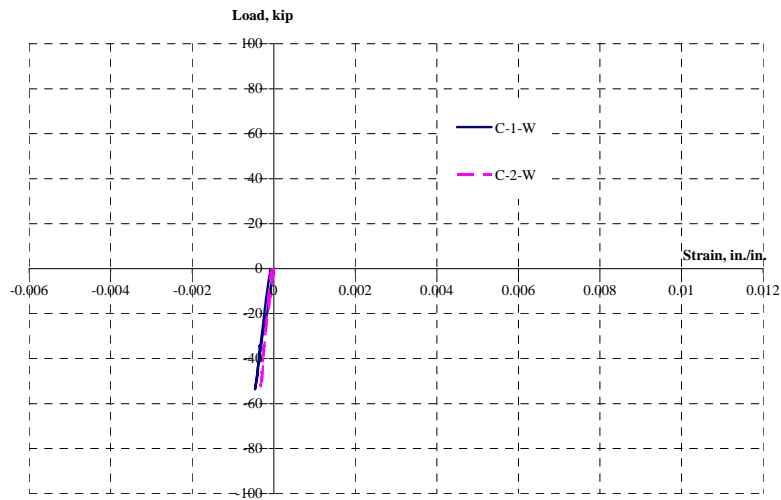
Figure C.89   Column bar strains, west side, 4-C-R20-M

C.4.3.2.2 Test after Rehabilitation
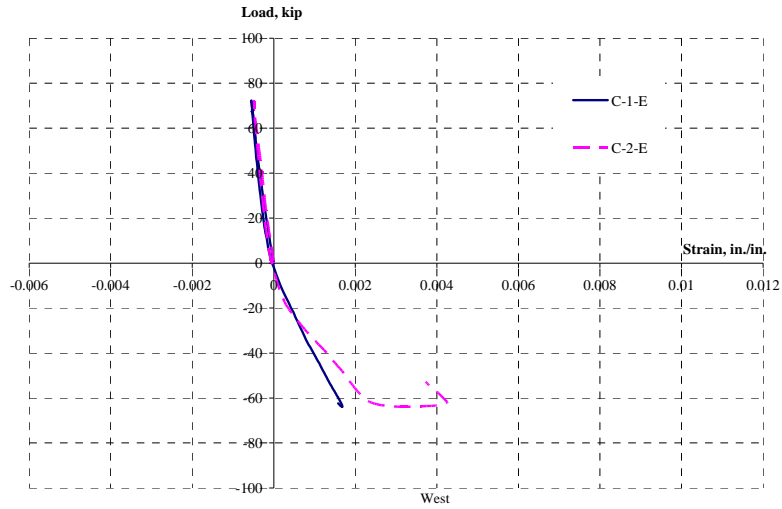
Figure C.90   Column bar strains, east side, 4-C-R20-M
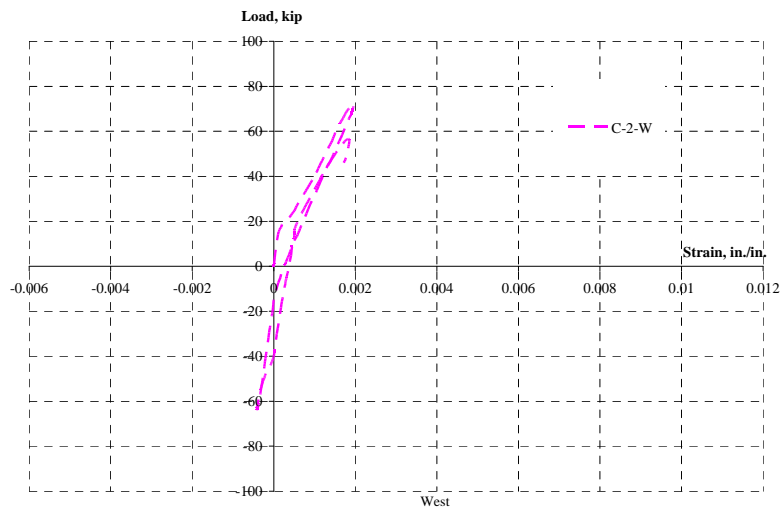
Figure C.91   Column bar strains, west side, 4-C-R20-M

444

C.4.3.3 Tie Strain

C.4.3.3.1 Test as Built
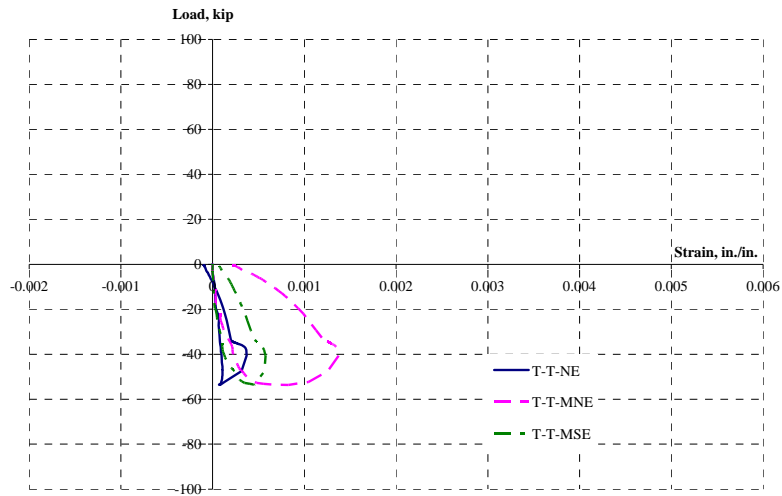
Figure C.92   Top tie strains, east, 4-C-R20-M
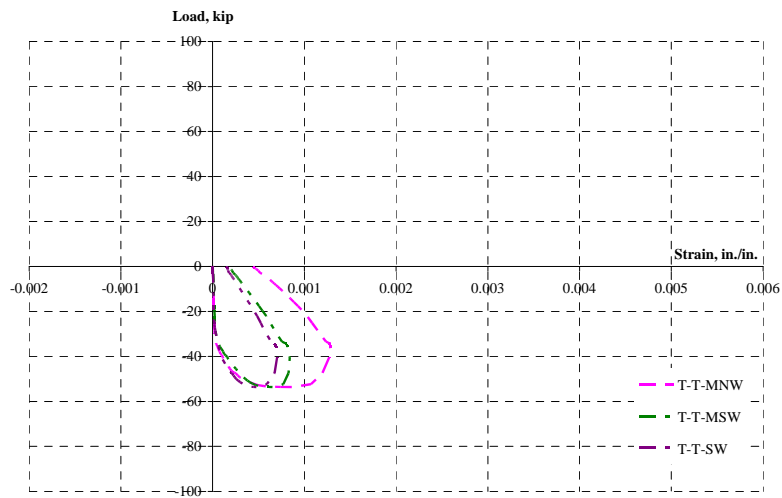
Figure C.93   Top tie strains, west, 4-C-R20-M
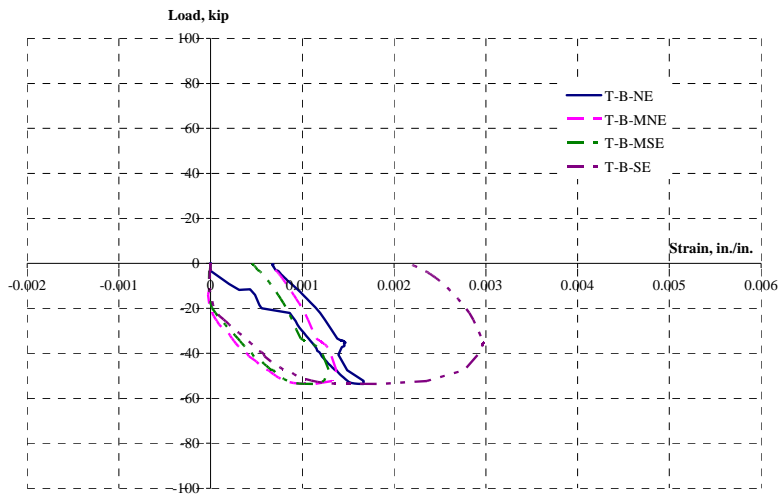
Figure C.94   Bottom tie strains, east, 4-C-R20-M

Figure C.95   Bottom tie strains, west, 4-C-R20-M

C.4.3.3.2 Test after Rehabilitation

Figure C.96   Top tie strains, east, 4-C-R20-M

Figure C.97   Top tie strains, west, 4-C-R20-M

447
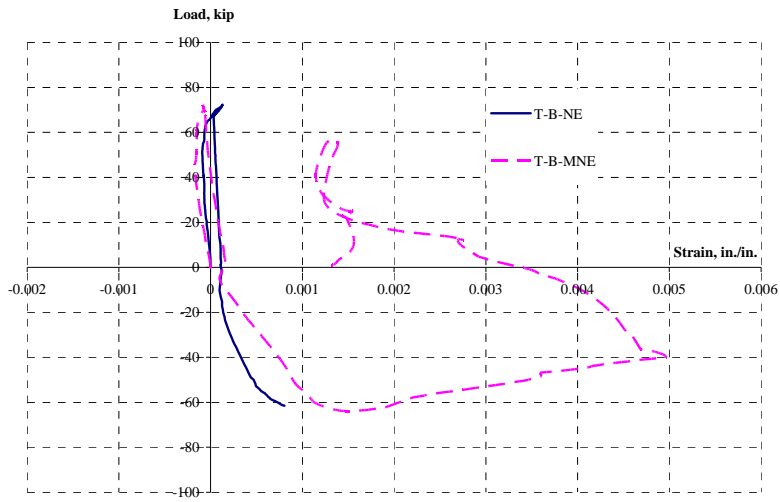
Figure C.98 Bottom tie strains, east, 4-C-R20-M
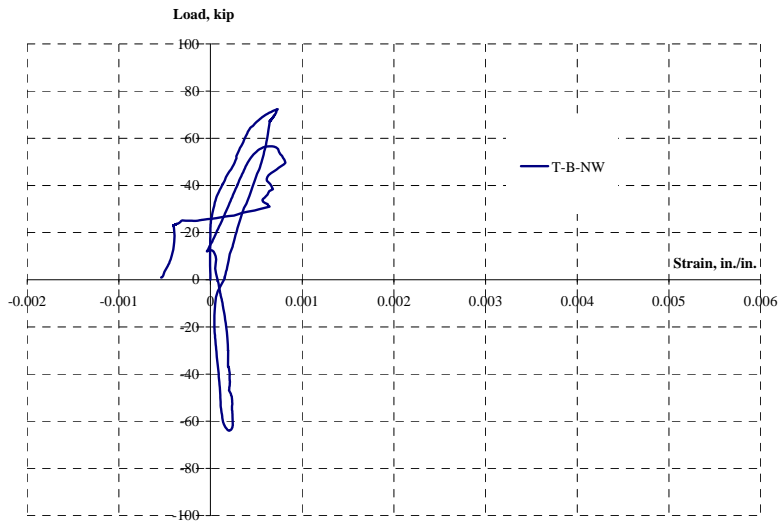
Figure C.99   Bottom tie strains, west, 4-C-R20-M

448

C.5   5-C-R20-C

C.5.1   Lateral Displacement VS Lateral Load

Figure C.100 Lateral displacement vs lateral load, 5-C-R20-C

C.5.2   Vertical Displacement at 30 in. from Top of the Footing VS Lateral Load

Figure C.101 Vertical displacement at 30 in. from top of the footing vs lateral load, 5-C-R20-C

449

C.5.3 Steel Reinforcement Strain
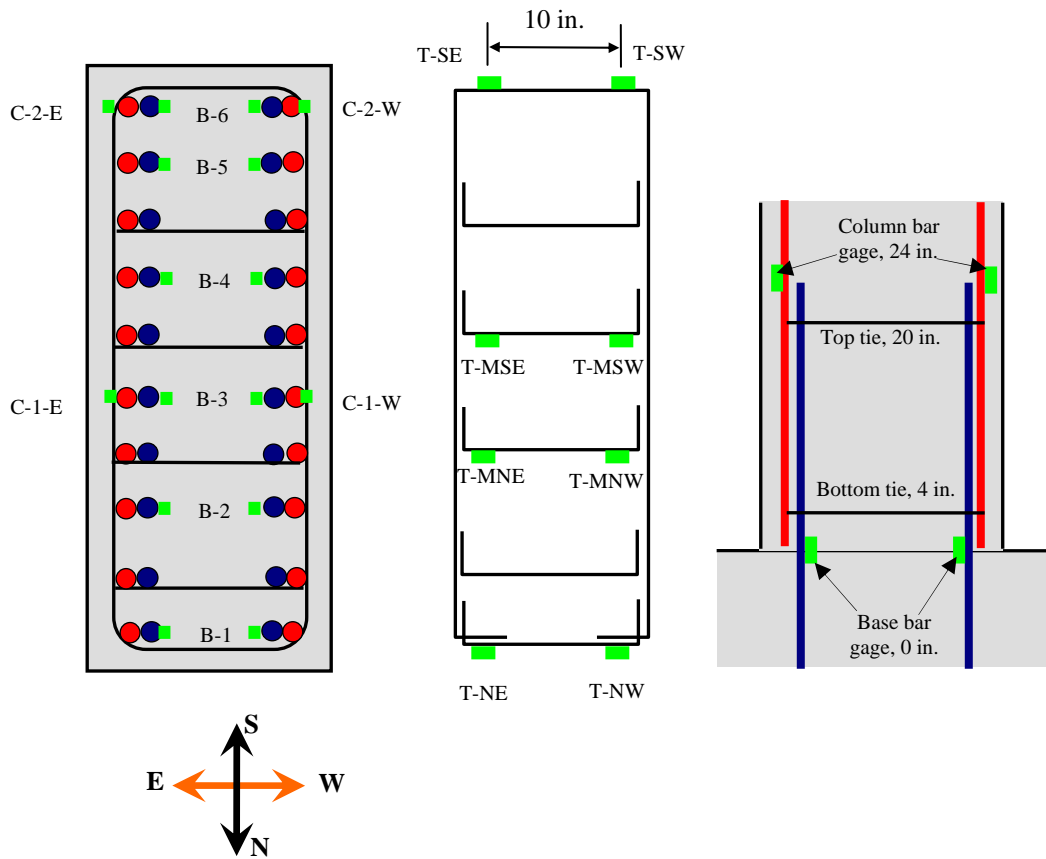
- **Base bar gages (B - # - Direction):** at the top of the footing
- **Column bar gages (C - # - Direction)**: 24 in. from the top of the footing
- **Tie bar gages (T-Top or Bottom- Direction):**

> **Top-**tie at 20 in. from the top of the footing

> **Bottom-** tie at 4 in. from the top of the footing

Figure C.102 Layout of steel reinforcement strain gages, 5-C-R20-C

C.5.3.1 Base Bar Strain

Figure C.103 Base bar strains, east side, 5-C-R20-C

Figure C.104 Base bar strains, west side, 5-C-R20-C

451

C.5.3.2 Column Bar Strain
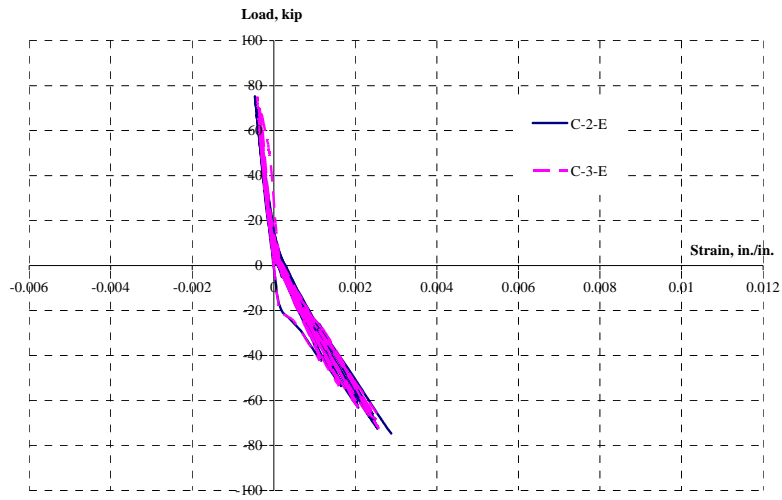
Figure C.105 Column bar strains, east side, 5-C-R20-C
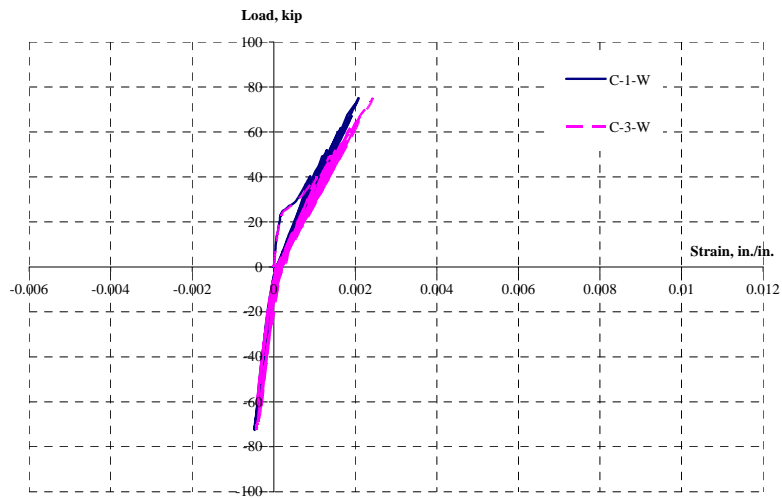
Figure C.106 Column bar strains, west side, 5-C-R20-C

452
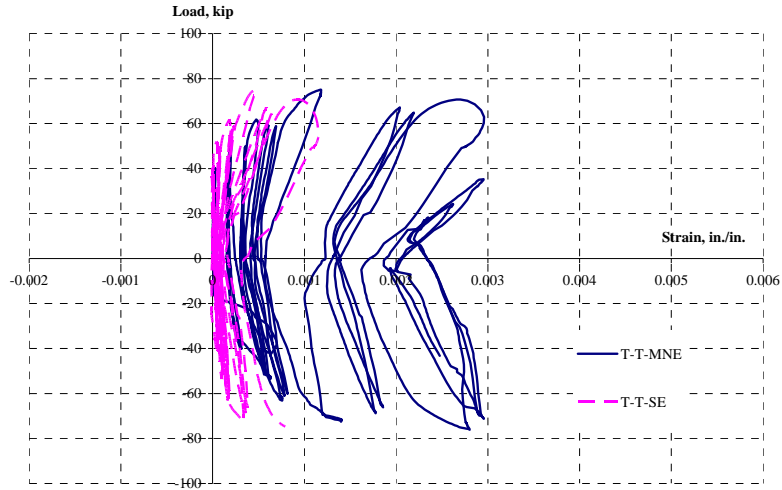
C.5.3.3   Tie Strain

Figure C.107 Top tie strains, east, 5-C-R20-C
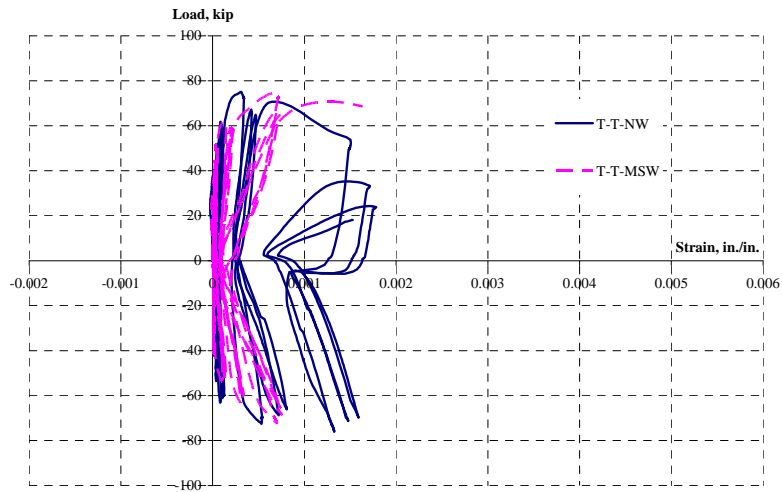
Figure C.108 Top tie strains, west, 5-C-R20-C

453
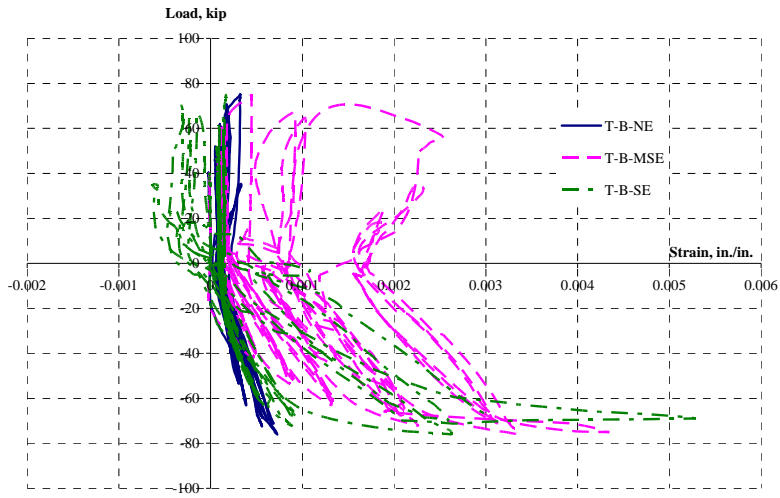
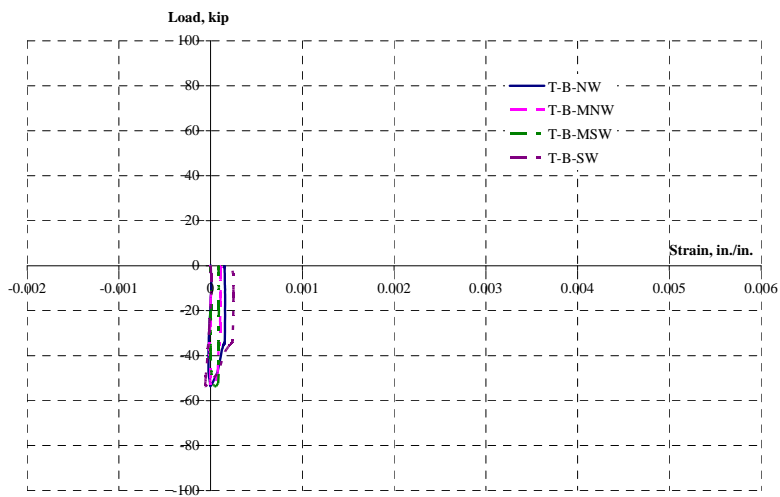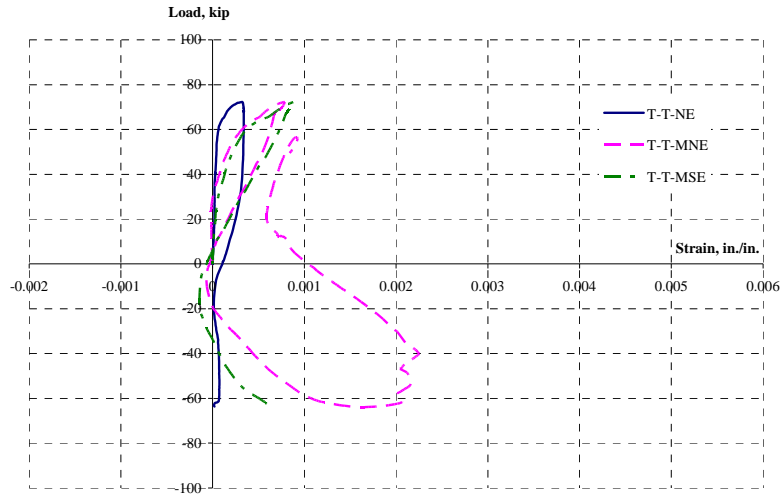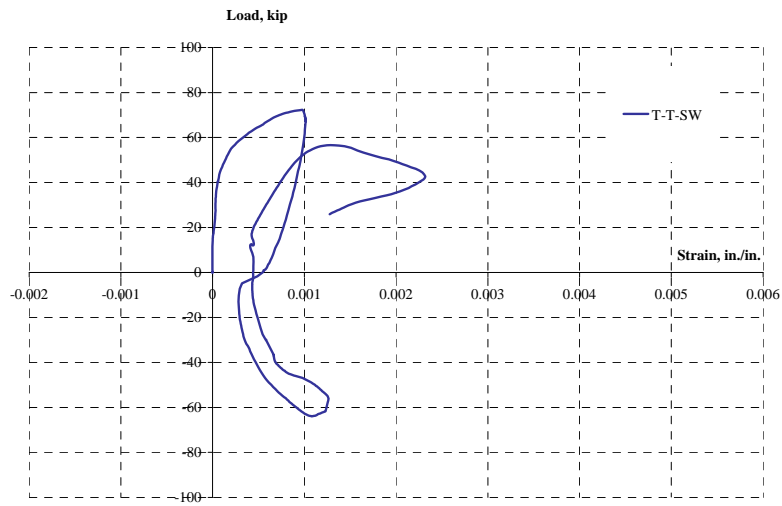*Figure C.109 Bottom tie strains, east, 5-C-R20-C*
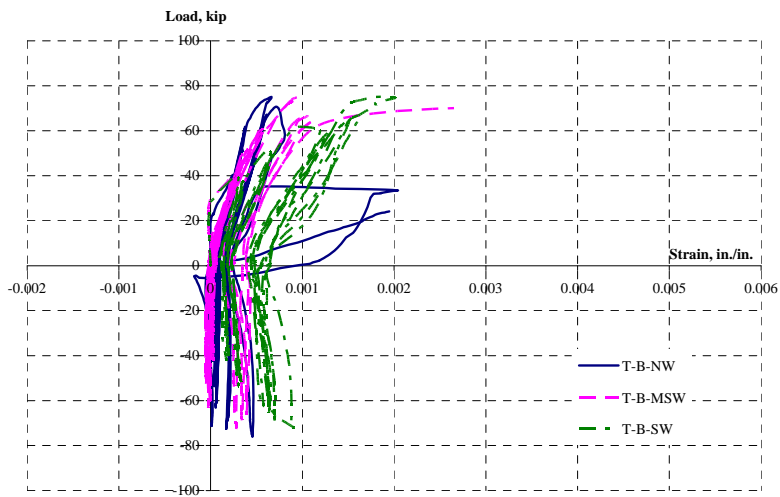
Figure C.110 Bottom tie strains, west, 5-C-R20-C

454

C.5.4 CFRP Strain Gage
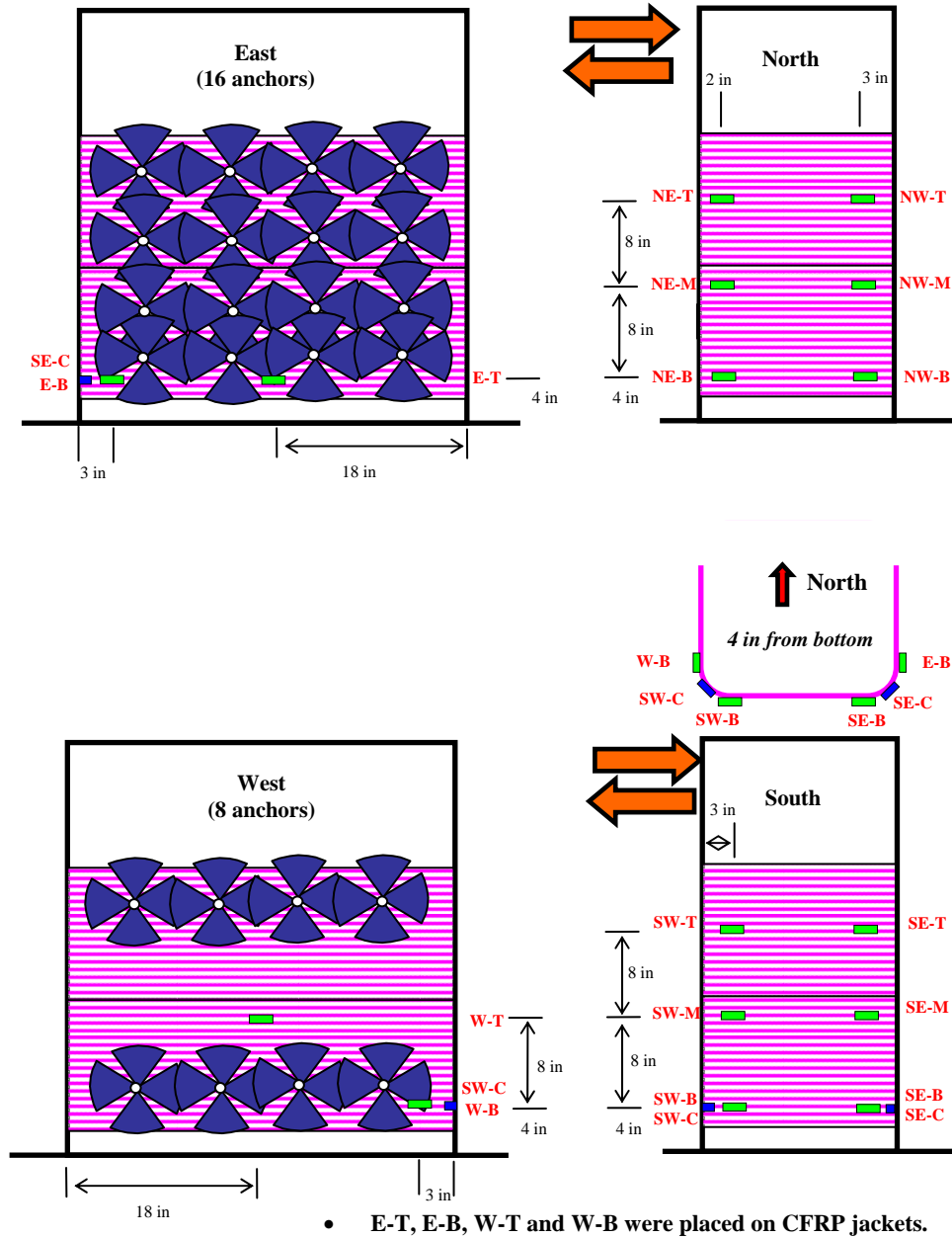
Figure C.111 Layout of CFRP strain gages, 5-C-R20-C

- E-T, E-B, W-T and W-B were placed on CFRP jackets.
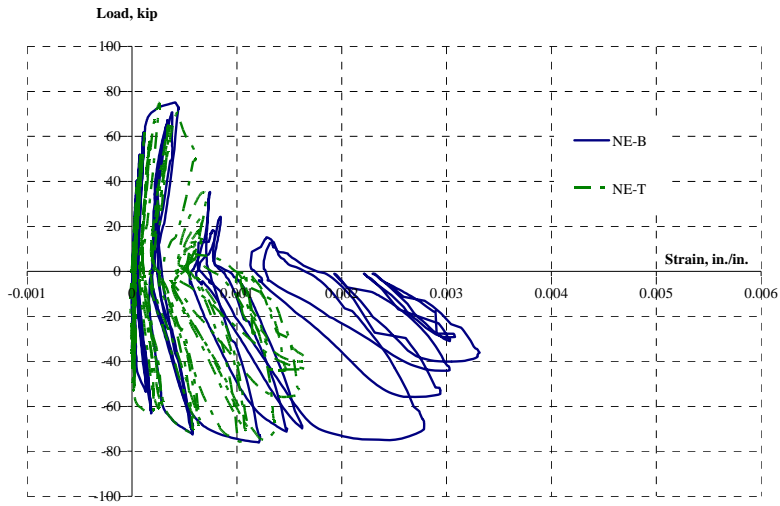
Figure C.112 CFRP strains at location of splitting cracking, north-east, 5-C-R20-C
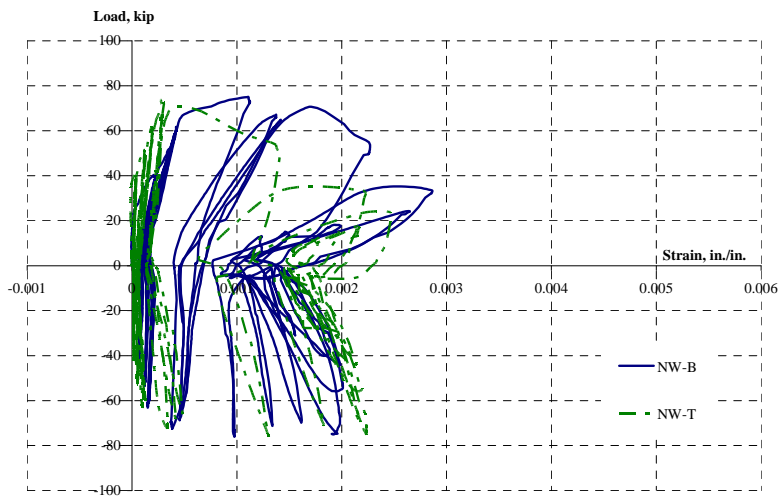
Figure C.113 CFRP strains at location of splitting cracking, north-west, 5-C-R20-C

456
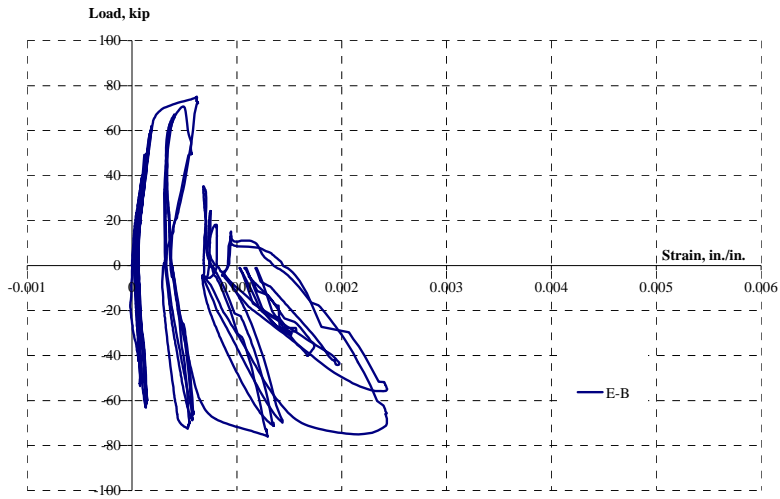
Figure C.114 CFRP strains, east face, 5-C-R20-C
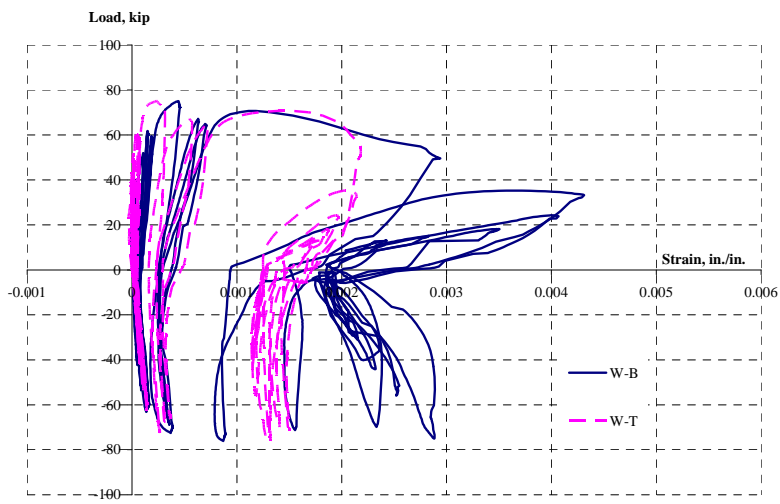
Figure C.115 CFRP strains, west face, 5-C-R20-C

457

C.6   6-C-R20-C

C.6.1   Lateral Displacement VS Lateral Load
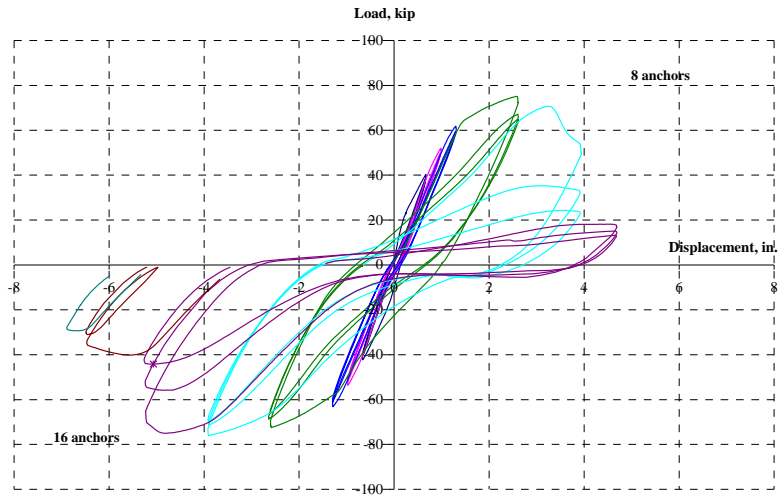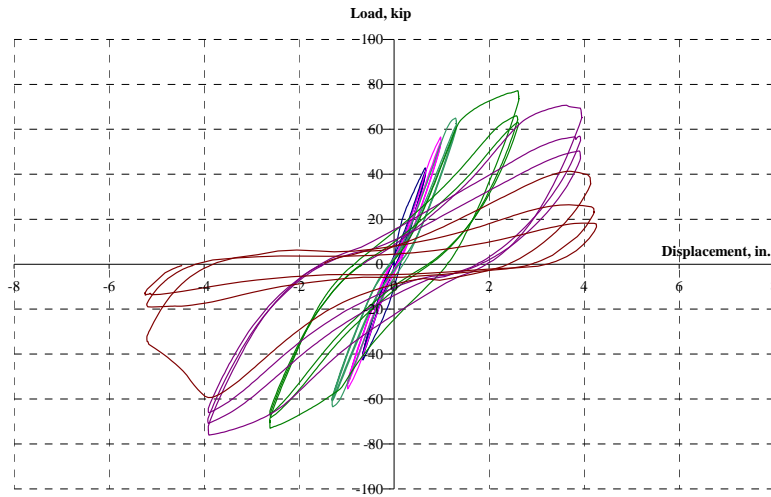

Figure C.116   Lateral displacement vs lateral load, 6-C-R20-C

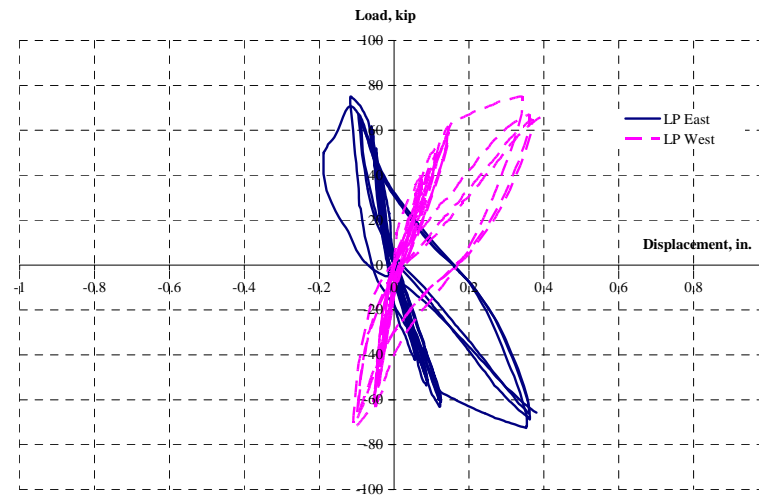### C.6.2   Vertical Displacement at 30 in. from Top of the Footing VS Lateral Load
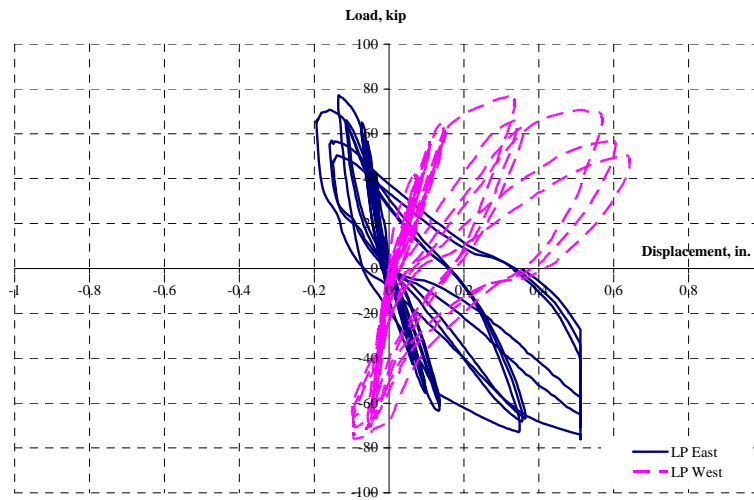
Figure C.117   Vertical displacement at 30 in. from top of the footing vs lateral load, 6-C-R20-C

458

C.6.3 Steel Reinforcement Strain
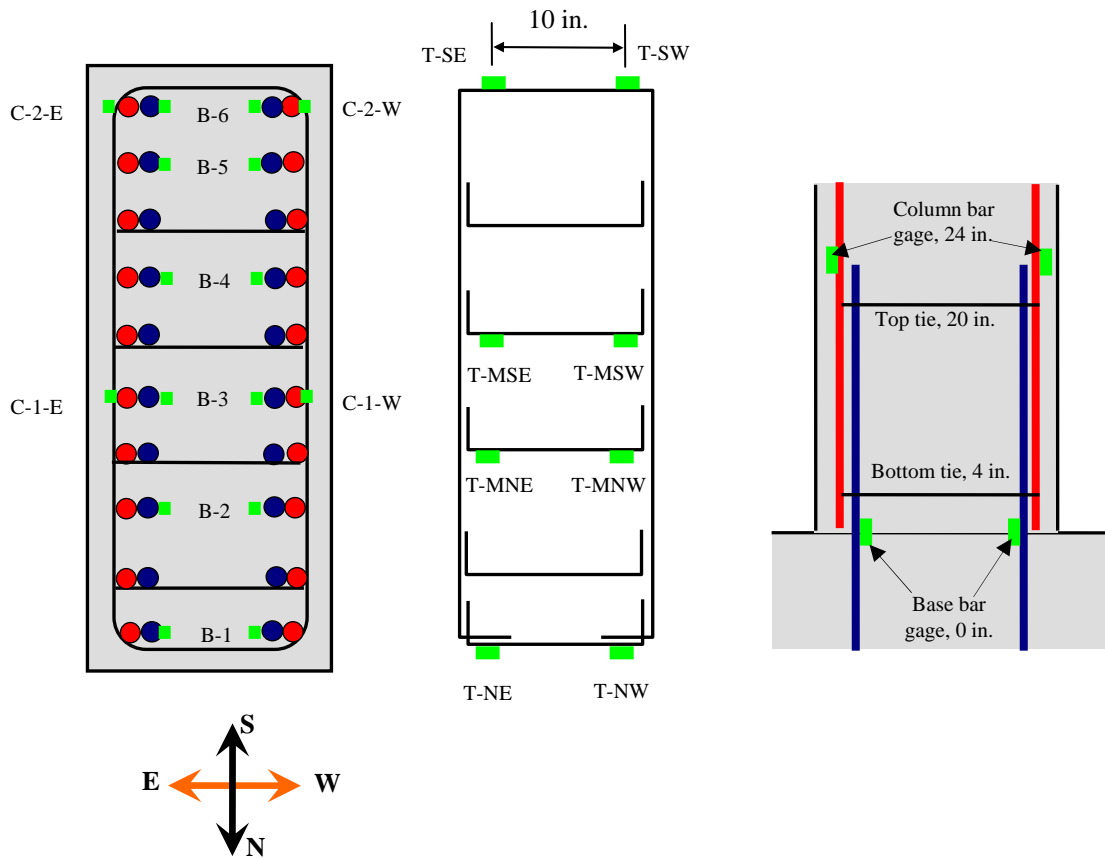
- **Base bar gages (B - # - Direction):** at the top of the footing
- **Column bar gages (C - # - Direction)**: 24 in. from the top of the footing
- **Tie bar gages (T-Top or Bottom- Direction):**

  Top-tie at 20 in. from the top of the footing

  Bottom- tie at 4 in. from the top of the footing

Figure C.118 Layout of steel reinforcement strain gages, 6-C-R20-C

459

C.6.3.1   Base Bar Strain
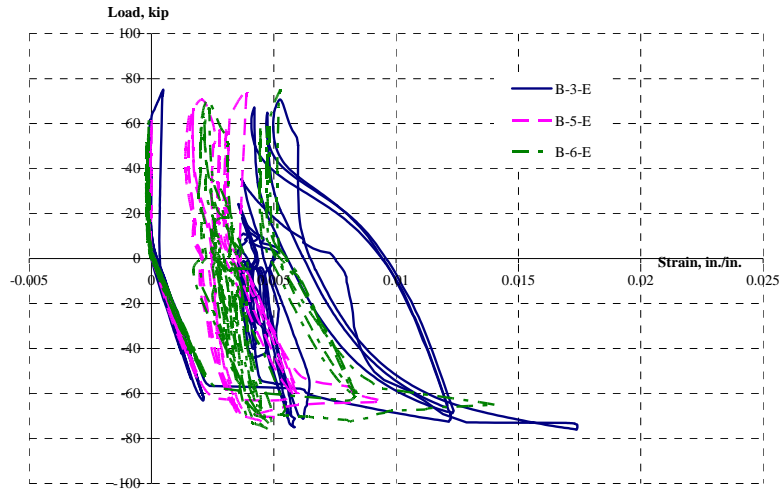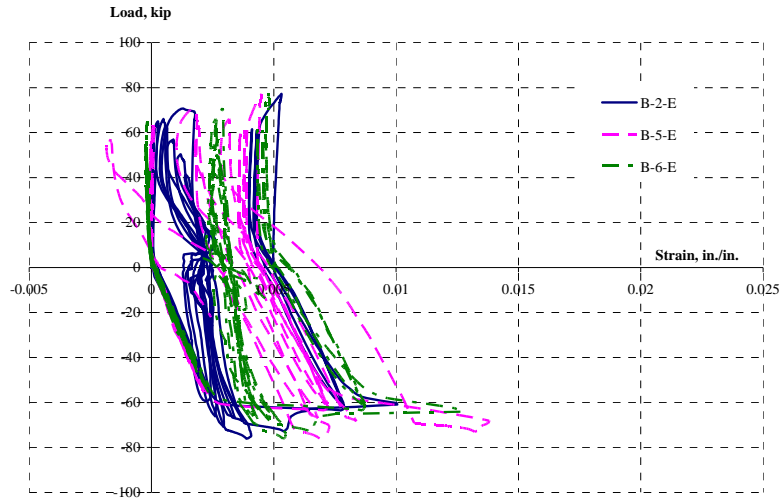

Figure C.119 Base bar strains, east side, 6-C-R20-C

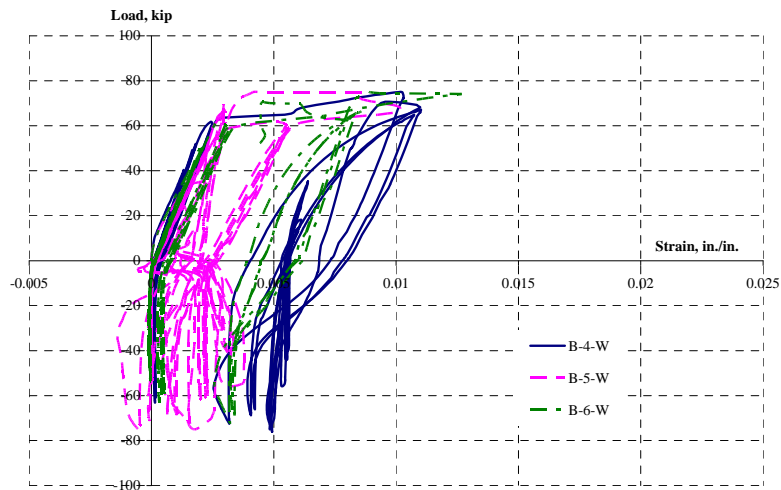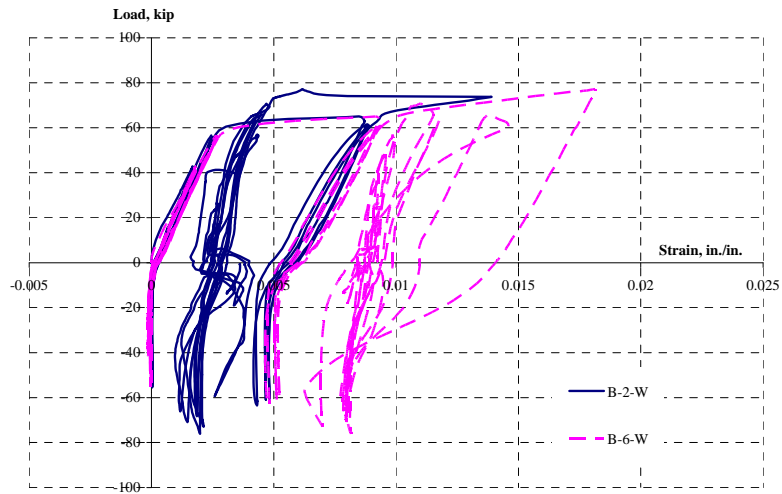***Figure C.120 Base bar strains, west side, 6-C-R20-C***

C.6.3.2 Column Bar Strain
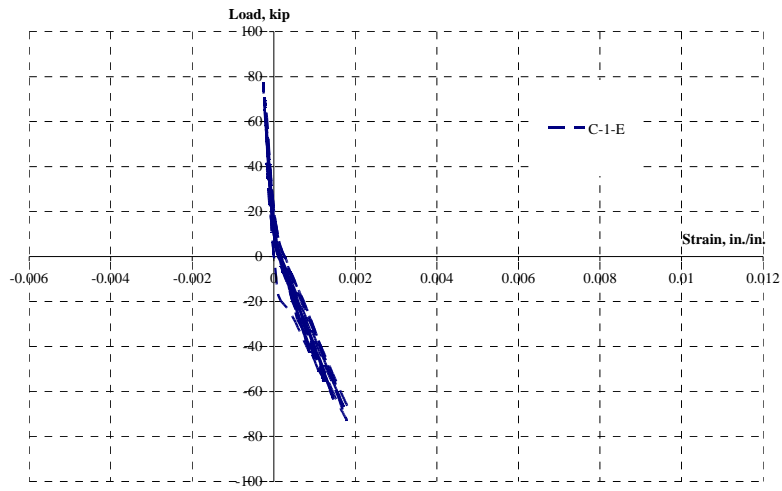
Figure C.121 Column bar strains, east side, 6-C-R20-C

C.6.3.3 Tie Strain
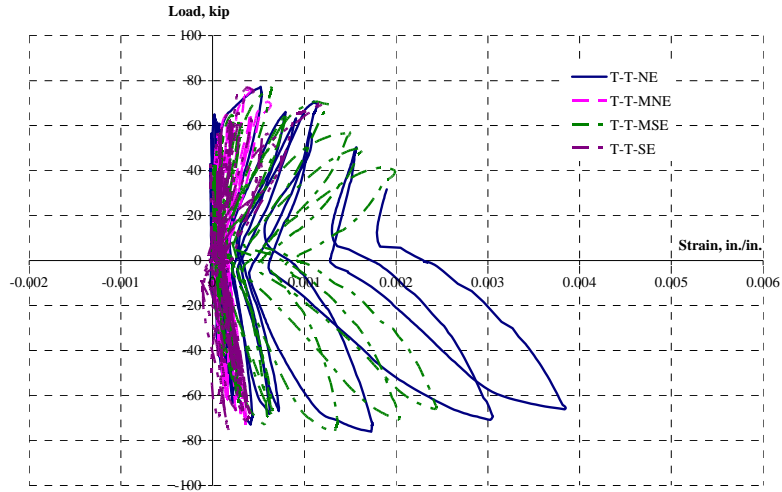
Figure C.122 Top tie strains, east, 6-C-R20-C
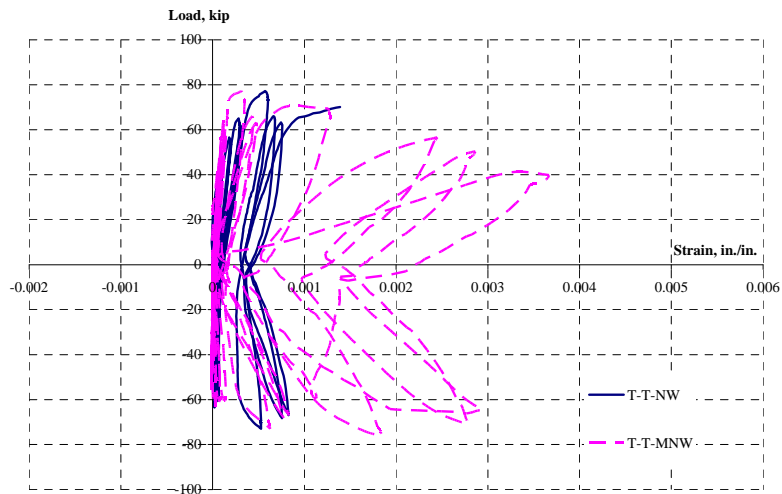
Figure C.123 Top tie strains, west, 6-C-R20-C
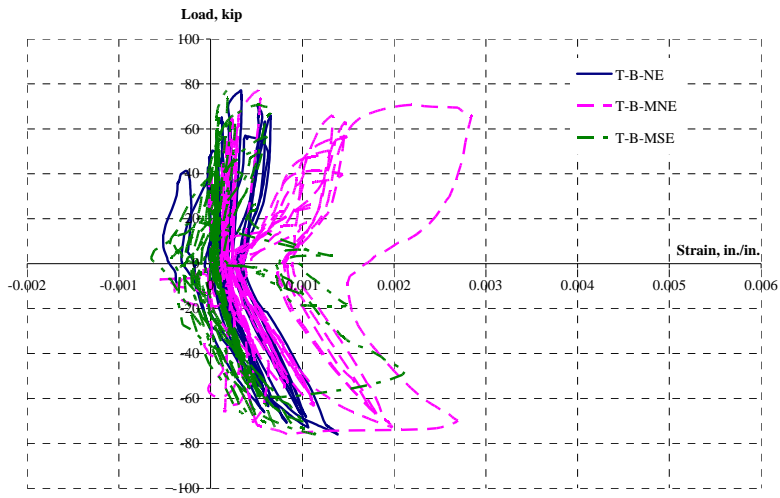
Figure C.124 Bottom tie strains, east, 6-C-R20-C
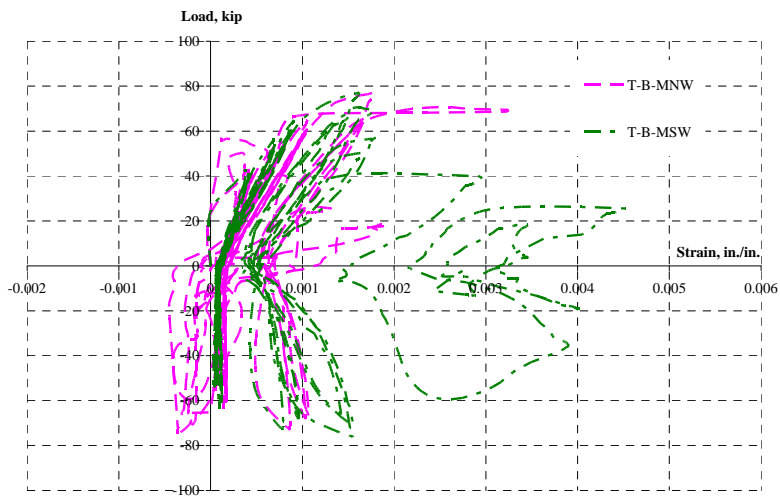
Figure C.125 Bottom tie strains, west, 6-C-R20-C

463

C.6.4 CFRP Strain Gage
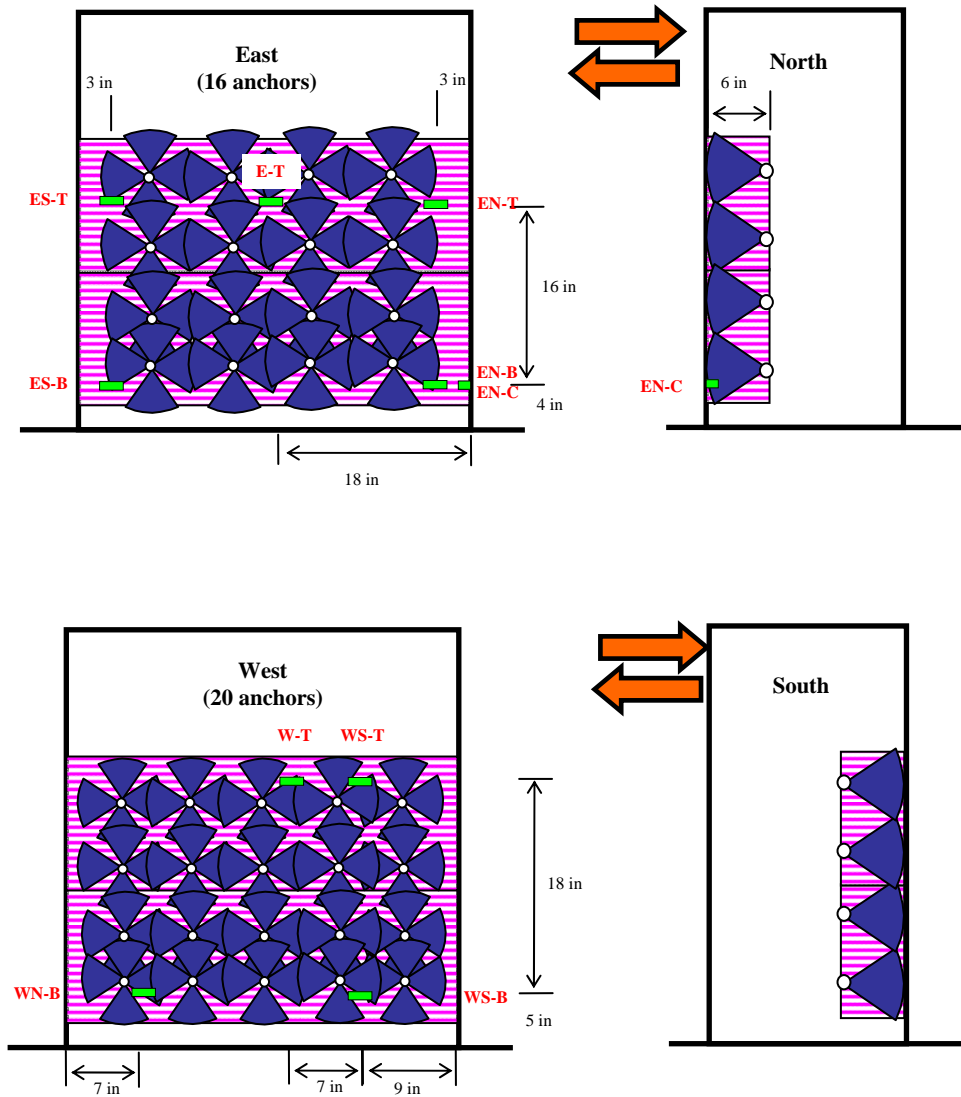
Figure C.126 Layout of CFRP strain gages, 6-C-R20-C, 6-C-R20-C
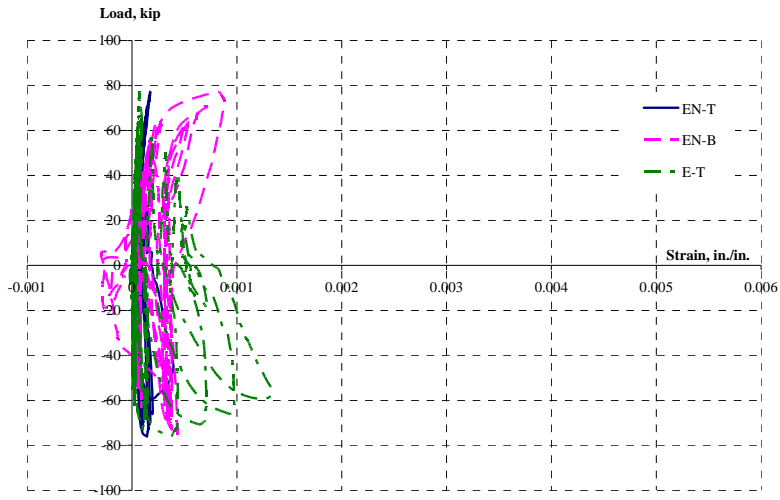
Figure C.127 CFRP strains, east face, 6-C-R20-C
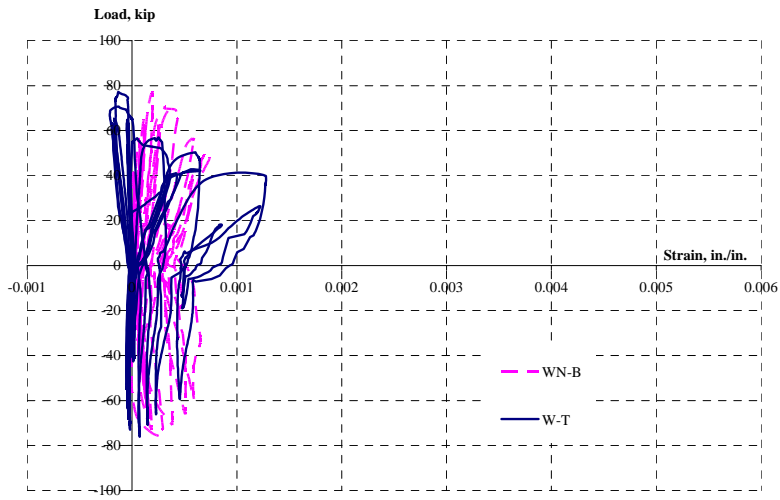
Figure C.128 CFRP strains, west face, 6-C-R20-C

465

APPENDIX D

Construction of Specimens

D.1   BEAM TEST

467

D.2 Column Test

468
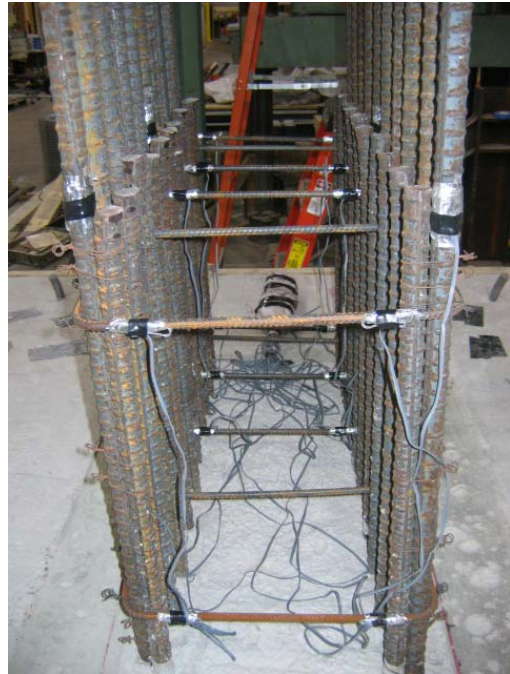
REFERENCES

1. Aboutaha, R. S., 1994, "Seismic Retrofit of Non-Ductile Reinforced Concrete Columns Using Rectangular Steel Jackets," Ph.D. Dissertation, University of Texas at Austin, USA, 374 pp.

2. Aboutaha, R. S.; Engelhardt, M. D.; Jirsa, J. O.; and Kreger, M. E., 1999, "Rehabilitation of Shear Critical Concrete Columns by Use of Rectangular Steel Jackets," *ACI Structural Journal*, V. 96 No. 1, Jan.-Feb. pp. 68-78.

3. Aboutaha, R. S.; Engelhardt, M. D.; Jirsa, J. O.; and Kreger, M. E., 1999, "Experimental Investigation of Seismic Repair of Lap Splice Failures in Damaged Concrete Columns," *ACI Structural Journal*, V. 96, No. 2, Mar.-Apr. pp. 297-306.

4. ACI Committee 315, 1974, "Manual of Standard Practice for Detailing Reinforced Concrete Structures (ACI 315-74)," American Concrete Institute, Detroit, MI, USA, pp. 167.

5. ACI Committee 318, 1956, "Building Code Requirements for Reinforced Concrete (ACI 318-56)," American Concrete Institute, Detroit, MI, USA, pp. 916-985.

6. ACI Committee 318, 1963, "Building Code Requirements for Reinforced Concrete (ACI 318-63)," American Concrete Institute, Detroit, MI, USA, 143 pp.

7. ACI Committee 318, 1971, "Building Code Requirements for Reinforced Concrete (ACI 318-71)," American Concrete Institute, Detroit, MI, USA, 78 pp.

8. ACI Committee 318, 2002, "Building Code Requirements for Structural Concrete (ACI 318-02) and Commentary (318R-02)," American Concrete Institute, Farmington Hills, MI, USA, 443 pp.

9. ACI Committee 318, 2005, "Building Code Requirements for Structural Concrete (ACI 318-05) and Commentary (318R-05)," American Concrete Institute, Farmington Hills, MI, USA, 430 pp.

10. ACI Committee 318, 2008, "Building Code Requirements for Structural Concrete (ACI 318-08) and Commentary (318R-08)," American Concrete Institute, Farmington Hills, MI, USA, 465 pp.

11. ACI Committee 440, 2002, "Guide for the Design and Construction of Externally Bonded FRP Systems for Strengthening Concrete Structures (ACI 440.2R-02)," American Concrete Institute, Farmington Hills, MI, USA, 45 pp.

12. ACI Committee 440, 2002, "Report on Fiber-Reinforced Polymer (FRP) Reinforcement for Concrete Structures," American Concrete Institute, Farmington Hills, MI, USA, 100 pp.

13. Ali, Mir M., 2002, "Protective Design of Concrete Buildings under Blast Loading," *Structures and Materials*, V. 11, Structures under Shock and Impact VII, pp. 23-33.

14. Antonopoulos, C. P and Triantafillou, T. C., 2003, "Experimental Investigation of FRP-Strengthened RC Beam-Column Joints," *Journal of Composites for Construction*, V. 7, No. 1, February, pp. 39-49.

15. Arduini, M.; Di Tommaso, A.; and Nanni, A., 1997, "Brittle Failure in FRP Plate and Sheet Bonded Beams," *ACI Structural Journal*, V. 94, No. 4, Jul.-Aug., pp. 363-370.

16. ASCE, Structural Engineering Institute, 2006, "Minimum Design Loads for Buildings and Other Structures (ASCE 7-05)," American Society of Civil Engineers, Structural Engineering Institute, Reston, VA, USA, 388 pp.

17. ASCE and FEMA, 2000, "Prestandard and Commentary for the Seismic Rehabilitation of Building (FEMA 356)," Federal Emergency Management Agency, Washington D.C., USA

18. ASCE and FEMA, 1998, "Handbook for the Seismic Evaluation of Buildings (FEMA 310)," Federal Emergency Management Agency, Washington D.C., USA

19. Astaneh-Asl, A., 2003, "Progressive Collapse Prevention in New and Existing Buildings," *Proceeding of the 9th Arab Structural Engineering Conference*, Emerging Technologies in Structural Engineering, Abu Dhabi, UAE, pp 1001-1008.

20. ASTM International, 2007, "Standard Test Method for Flexural Strength of Concrete Using Simple Beam With Center-Point Loading, (C293-07)," ASTM International, West Conshohocken, PA, USA, 3 pp.

21. Biggs, J. M., 1964, "Introduction to Structural Dynamics," McGraw-Hill, New York, NY, USA, 341 pp.

22. Binici, B. and Mosalam, K. M., 2007, "Analysis of Reinforced Concrete Columns Retrofitted with Fiber Reinforced Polymer Lamina," *Composites Part B: Engineering*, V. 38, No. 2, pp. 265-276.

23. Blaszak, G.; Gold, W.; and Kliger, H. S., 2000, "Proposed Qualification Criteria for FRP Systems Used for Infrastructure Applications," *International SAMPE Symposium and Exhibition (Proceedings)*, V. 45 (II), pp. 1832-1839.

24. Bonacci J. F. and Jaalej, F., 2001, "Behavioral Trends of RC Beams Strengthened with Externally Bonded FRP." *Journal of Composite for Construction*, V. 5, No. 2, pp. 102 -113.

25. Brena, S., 2000, "Strengthening Reinforced Concrete Bridges Using Carbon Fiber Reinforced Polymer Composite," Ph.D. Dissertation, University of Texas at Austin, USA, 437 pp.

26. Cantwell, W. J. and Smith, K., 1999, "Static and Dynamic Response of CFRP-Strengthened Concrete Structures," *Journal of Materials Science Letters*, V. 18, No. 4, Feb., pp. 309-310.

27. Chopra, A. K., 2001, "Dynamic of Structures: Theory and Applications to Earthquake Engineering," Prentice Hall, Upper Saddle River, NJ, USA, 844 pp.

28. Chowdhury, E. U.; Bisby, L. A.; Green, M. F.; Kodur, V. K. R., 2007, "Investigation of Insulated FRP-Wrapped Reinforced Concrete Columns in Fire," *Fire Safety Journal*, V. 42, No. 6-7, Sep./Oct., pp. 452-460.

29. Cook, R. A.; Kunz, J.; Fuchs, W.; and Konz, R. C., 1998, "Behavior and Design of Single Adhesive Anchors under Tensile Load in Uncracked Concrete Source," *ACI Structural Journal*, V. 95, No. 1, Jan.-Feb., pp. 9-26.

30. Department of Defense, 2005, "Design of Buildings to Resist Progressive Collapse (UFC 4-023-03)," Department of Defense, USA.

31. Ellingwood. B.R.; Smilowitz R.; et al., 2007, "Best Practice for Reducing the Potential for Progressive Collapse in Buildings (NISTIR 7396)," National Institute of Standard and Technology (NIST), Feb., 2007.

32. Elsanadedy, H. M. and Haraoun, M. A., 2005, "Seismic Design Criteria for Circular Lap-Spliced Reinforced Concrete Bridge Columns Retrofitted with Fiber-Reinforced Polymer Jackets," *ACI Structural Journal*, V. 102, No. 3, May-Jun., pp. 354-362.

33. Erki, M. A. and Meier, U., 1999, "Impact Loading of Concrete Beams Externally Strengthened with CFRP Llaminates," *Journal of Composites for Construction*, V. 3, No. 3, pp. 117-124

34. Ferguson, P. M. and Krishnaswamy, C. N., 1971, "Tensile Lap Splices, Part 2: Design Recommendations for Retaining Wall Splices and Large Bar Splices," Center for Highway Research, University of Texas at Austin, USA, 60 pp.

35. Fib Task Group 9.3, 2001, "Externally Bonded FRP Reinforcement for RC Structures," The International Federation for Structural Concrete, Lausanne, Switzerland, 130 pp.

36. Fuchs, W.; Eligehausen, R.; and Breen, J. E., 1995, "Concrete Capacity Design (CCD) Approach for Fastening to Concrete," *ACI Structural Journal*, V. 92, No. 1, Jan.-Feb., pp. 73-94.

37. GangaRao, H. V. S. and Vijay, P. V., 1998, "Bending Behavior of Concrete Beams Wrapped with Carbon Fabric," *Journal of Structural Engineering*, V. 124, No. 1, Jan., pp. 3-10.

38. Ghosh, K. K. and Sheikh, S. A., 2007, "Seismic Upgrade with Carbon Fiber-Reinforced Polymer of Columns Containing Lap-Spliced Reinforcing Bars," *ACI Structural Journal,* V. 104, No. 2, Mar.- Apr., pp. 227-236.

39. Grace, N. F.; Abdel-Sayed, G.; and Ragheb, W. F., 2002, "Strengthening of Concrete Beams Using Innovative Ductile Fiber-Reinforced Polymer Fabric," *ACI Structural Journal*, V. 99, No. 5, Sep.-Oct., pp. 692-700.

40. GSA, 2003, "Progressive Collapse Analysis and Design Guidelines for New Federal Office Buildings and Major Modernization Projects," General Service Administration, USA.

41. Harajli, M. H., and Rteil, A. A., 2004, "Effect of Confinement Using Fiber-Reinforced Polymer or Fiber-Reinforced Concrete on Seismic Performance of Gravity Load-Designed Columns." *ACI Structural Journal*, V. 101, No. 1, pp. 47-56.

42. Harajli, M. H., 2005, "Behavior of Gravity Load-Designed Rectangular Concrete Columns Confined with Fiber Reinforced Polymer Sheets," *Journal of Composites for Construction*, V. 9, No. 1, pp. 4-14.

43. Harajli, M. H. and Dagher, F., 2008, "Seismic Strengthening of Bond-Critical Regions in Rectangular Reinforced Concrete Columns Using Fiber-Reinforced Polymer Wraps," *ACI Structural Journal*, V. 105, No. 1, Jan.-Feb., pp. 68-77.

44. Haroun, M. A. and Elsanadedy, H. M., 2005, "Fiber-Reinforced Plastic Jackets for Ductility Enhancement of Reinforced Concrete Bridge Columns with Poor Lap-Splice Detailing," *Journal of Bridge Engineering*, V.10, No. 6, pp. 749-757.

45. Harries, K. A.; Ricles, J. R.; Pessiki, S.; and Sause, R., 2006, "Seismic Retrofit of Lap splices in Nonductile Square Columns Using Carbon Fiber-Reinforced Jackets," *ACI Structural Journal*, V. 103, No. 6, Nov.-Dec., pp. 874-884.

46. Hughes, B. P. and Al-Dafiry, H., 1995, "Impact Energy Absorption at Contact Zone and Supports of Reinforced Plain and Fibrous Concrete Beams," *Construction and Building Materials*, V. 9, No. 4, Aug, pp. 239-244.

47. Ishikawa, N.; Katsuki, S.; and Takemoto, K. 2002, "Incremental Impact Test and Simulation of Prestressed Concrete Beam," *Structures and Materials*, V. 11, Structures under Shock and Impact VII, pp. 489-498.

48. Jerome, D. M. and Ross, C. A., 1996, "Dynamic response of concrete beams externally reinforced with carbon fiber reinforced plastic (CFRP) subjected to impulsive loads," American Society of Mechanical Engineers, Pressure Vessels and Piping Division (Publication) PVP, V. 325, Structures Under Extreme Loading Conditions, pp. 83-94.

49. Johnson A., 2004, "Behavior of CFRP Wrapped Concrete Compression Members with Circular and Square Cross-Sections," M.S. Department Report, University of Texas at Austin, USA, 44 pp.

50. Khalifa, A.; Alkhrdaji, T.; Nanni, A.; and Lansburg, S., 1999, "Anchorage of Surface Mounted FRP Reinforcement," *Concrete international: Design and Construction*, V. 21, No. 10, Oct, pp. 49-54.

51. Kim, I. S, 2006, "Rehabilitation of Poorly Detailed RC Structures Using CFRP Materials," M.S. Theses, University of Texas at Austin, USA, 144 pp

52. Kim, I.; Jirsa, J. O.; and Bayrak, O., 2006, "Use of CFRP to Strengthening Poorly Detailed Reinforced Concrete beams," *Third International Conference on FRP Composites in Civil Engineering (CICE 2006)*, Miami, FL, USA, pp. 563-566.

53. Kim, I.; Jirsa, J. O.; and Bayrak, O., 2007, "Use of CFRP to Strengthen Poorly Detailed Reinforced Concrete Beams under Dynamic Loading," *Proceeding of the 8th International Symposium on Fiber-Reinforced Polymer Reinforcement for Concrete Structure (FRPRCS-8)*, Patras, Greece, pp. 172-173.

54. Kishi, N.; Mikami, H.; and Ando, T., 2002, "Impact-Resistant Behavior of Shear-Failure-Type RC Beams under Falling-Weight Impact Loading," *Structures and Materials*, V. 11, Structures under Shock and Impact VII, pp. 499-508.

55. Kobayashi, K.; Fujii, S.; Yabe, Y.; Tsukagoshi, H.; and Sugiyama T, 2001, "Advanced Wrapping System with CF-Anchor", *Proceedings of the 5th International Conference on Fibre Reinforced Plastics for Reinforced Concrete Structures*, Cambridge, United Kingdom, Volume 1, pp. 379-388.

56. Kodur, V. K. R.; Bisby, L. A.; and Green, M. F., 2007, "Preliminary Guidance for the Design of FRP-Strengthened Concrete Members Exposed to Fire," *Journal of Fire Protection Engineering*, V. 17, No. 1, Feb., pp. 5-26.

57. Krawinkler, H., 1996, "Cyclic Loading Histories for Seismic Experimentation on Structural Components," *Earthquake Spectra*, V. 12, No. 1, Feb., pp. 1-11.

58. Lamanna, A. J., 2002, "Flexural Strengthening of Reinforced Concrete Beams with Mechanically Fastened Fiber Reinforced Polymer Strips." The University of Wisconsin at Madison, USA.

59. MacGregor, J. G. and Wight, J. K., 2005, "Reinforced Concrete Mechanics and Design," Prentice Hall, Upper Saddle River, NJ, USA, 1132 pp.

60. Meirovitch, L., 2001, "Fundamentals of Vibrations," McGraw-Hill, New York, NY, USA, 806 pp.

61. Mitchell, G, T., 2005, "Pendulum Simulation of Vehicular Impact on Retrofit Bridge Barriers," M.S. Theses, University of Texas at Austin, USA, 144 pp.

62. Nofal, N.M. and Hamdy, G. A., 2005, "Effect of Fire Protection Materials on FRP Strengthened Concrete Axial Compression Members," *Journal of Engineering and Applied Science*, V. 52, No. 6, Dec., pp. 1123-1141.

63. Norris, T.; Saadatmanesh, H.; and Ehsani, M. R., 1997, "Shear and Flexural Strengthening of R/C Beams with Carbon Fiber Sheets," *Journal of Structural Engineering*, V. 123, No. 7, Jul., pp. 903-911.

64. Orangun, C. O.; Jirsa, J. O.; and Breen, J. E., 1977, "Revaluation of Test Data on Development Length and Splices," *Journal of The American Concrete Institute*, V. 74, No. 3, Mar, pp. 114-122.

65. Orozco, L. A., 2006, "Development of an Experimental Setup for Testing Scaled Versions of AASHTO Type IV Girder under Dynamic Impact Loadings," M.S. Department Report, University of Texas at Austin, USA, 113 pp.

66. Orton, S., 2007, "Development of a CFRP system to Provide Continuity in Existing Reinforced Concrete Buildings Vulnerable to Progressive Collapse," Ph.D. Dissertation, University of Texas at Austin, USA, 363 pp.

67. Orton, S.; Jirsa, J. O.; and Bayrak, O., 2006, "Anchorage of Carbon Fiber Reinforced Polymer sheets with and without Height Transition," *Third International Conference on FRP Composites in Civil Engineering (CICE 2006)*, Miami, FL, USA, pp. 665-668.

68. Ozdemir, G. and Akyuz, U., 2006, "Tensile Capacities of CFRP Anchors", Advances in Earthquake Engineering for Urban Risk Reduction (*Proceedings of the NATO Science for Peace Workshop on Advances in Earthquake Engineering for Urban Risk Reduction, Istanbul, Turkey*), Springer, pp. 471-488.

69. Park, R. and Paulay, T., 1975, "Reinforced Concrete Structures," Wiley & Sons, New York, NY, USA, 769 pp.

70. Parker, H., 1976, "Simplified Design of Reinforced Concrete," Wiley & Sons, New York, NY, USA, 303 pp.

71. Paulay, T. and Priestley, M. J. N., 1992, "Seismic Design of Reinforced Concrete and Masonry Buildings," Wiley & Sons, New York, NY, USA, 744 pp.

72. Regan P., 1975, "Catenary Action in Damaged Concrete Structures," Industrialization in Concrete Building Construction (ACI publication SP-48), American Concrete Institute, Detroit, MI, USA, pp. 191-224.

73. Ritchie, P. A.; Thomas, D. A.; Lu, L.-W.; and Connelly, G. M., 1991, "External Reinforcement of Concrete Beams using Fiber Reinforced Plastics," *ACI Structural Journal*, V. 88, No. 4, Jul.-Aug., pp. 490-500.

74. Ross, C. A.; Jerome, D. M.; Tedesco, J. W.; and Hughes, M. L., 2000, "Strengthening of Reinforced Concrete Beams with Externally Bonded Composite Laminates," *ACI Structural Journal*, V. 97, No. 1, Jan-Feb., pp. 204-205.

75. Rutherford & Chekene Consulting Engineers and National Institute of Standard and Technology, 2006, "Techniques for the Seismic Rehabilitation of Existing Buildings (FEMA 547)," Federal Emergency Management Agency, National Institute of Standard and Technology, USA.

76. Sasani, M.; Bazan, M. and Sagiroglu, S., 2007, "Experimental and analytical progressive collapse evaluation of actual reinforced concrete structure," *ACI Structural Journal*, V.104, No. 6, Nov.-Dec., pp 731-739.

77. Sasani, M. and Sagiroglu, S., 2008, "Progressive Collapse of Reinforced Concrete Structures: A Multihazard Perspective," *ACI Structural Journal*, V. 105, No. 1, Jan.-Feb., pp. 96-103.

78. Shannag, M. J. and Alhassan, M. A., 2005, "Seismic Upgrade of Interior Beam-Column Subassemblages with High-Performance Fiber-Reinforced Concrete Jackets." *ACI Structural Journal*, V. 102, No. 1, Jan.-Feb., pp. 131-138.

79. Sheng, L.-H., 2001, "Summary of CALTRANS' FRP Composite Pre-Qualification Program," *International SAMPE Symposium and Exhibition (Proceedings),* V. 46 I, pp. 923-930.

80. SR-CF 工法 研究會 (SR-CF Construction Method Research Council), 2001, 既存建設物の 耐震改修設計施工指針 (Seismic Rehabilitation Design Procedures of Existing Structures), 建設物等防災技術平價委員會, pp. 146-155 (In Japanese).

81. Tastani, S. P. and Pantazopoulou, S. J., 2008. "Detailing Procedures for Seismic Rehabilitation of Reinforced Concrete Members with Fiber Reinforced Polymers," *Engineering Structures*, V. 30, No. 2, pp. 450-461.

82. Teng, J. G.; Chen, J. F.; et al., 2002, "FRP Strengthened RC Structures," Wiley & Sons, New York, NY, USA, 266 pp.

83. Toutanji, H.; Saxena, P.; and Zhao, L., 2006, "Prediction of Bond Failure of Concrete Prisms Bonded with FRP Composites," *Third International Conference on FRP Composites in Civil Engineering (CICE 2006)*, Miami, FL, USA, pp. 63-66.

84. Triantafillou, T. C.; et al., 2006, "Retrofitting of Concrete Structures by Externally bonded FRPs with Emphasis on Seismic Application," Course Material Prepared by the Austhors of the 2005 fib short courses held in Istanbul and Ankara, The International Federation for Structural Concrete, Lausanne, Switzerland, 217 pp.

85. Uzumeri, S., 1977, "Strength and Ductility of Cast-In-Place Beam-Column Joints," ACI publication SP-53, American Concrete Institute, Detroit, MI, USA, pp. 293-350.

86. Xiao, J.; Li, J.; and Zha, Q., 2004, "Experimental Study on Bond Behavior between FRP and Concrete," Construction and Building Materials," V 18, No. 10, Dec., pp. 745-752.

87. Youssef, M. N.; Haroun, M.; Feng, M.; and Mosallam, A., 2000, "Experimental Study on RC Bridge Columns Retrofitted Using Fiber Composite Materials," *International SAMPE Symposium and Exhibition (Proceedings)*, 45 (II), pp. 1803-1812.

VITA

In Sung Kim was born in Seoul, Republic of Korea on November 1, 1978, the son of Yeo Keun Kim and Soon Hee Kim. After completing his work at Chosun University High School, Kwangju, Korea, in 1997, he entered Yonsei University in Seoul, Korea. He received the degree of Bachelor of Science in Civil Engineering from Yonsei University in February of 2001. During the following years, he was employed as an engineer at Seohae Construction Co. LTD., Incheon, Korea. In August of 2004, he entered The Graduate School at The University of Texas at Austin. After completing his Master of Science degree in Engineering in May of 2006, he began work on his Ph.D. under the supervision of James O. Jirsa. Upon completion of his doctoral work, he accepted a position at Degenkolb Engineers at San Francisco.

Permanent Address: Greentown 1304-103,
                   Jung2dong, Wonmi-Gu, 420-721
                   Republic of Korea

This thesis was typed by the author.

478